

GEOPHYSICAL FLUID MECHANICS

VOLUME 4

VERTICAL COORDINATES, SCALAR FIELDS, AND HAMILTON'S PRINCIPLE

Stephen.M.Griffies@gmail.com

Princeton University Atmospheric and Oceanic Sciences

Draft from January 12, 2026



COPYRIGHT ©2025 BY STEPHEN M. GRIFFIES
ALL RIGHTS RESERVED
GRIFFIES, STEPHEN M., 1962-
GEOPHYSICAL FLUID MECHANICS
THIS BOOK WAS TYPESET USING LATEX.

CONTENTS

	Page
PREFACE	vii
GUIDE TO THIS BOOK	xvii
Part I. Generalized vertical coordinates	1
1 FOUNDATIONS IN TENSOR CALCULUS	5
2 MECHANICAL EQUATIONS	31
3 CONTINUOUS AND LAYERED ISOPYCNAL MODELS	69
Part II. Scalar fields	105
4 DIFFUSIVE PROCESSES	109
5 TRACER ADVECTION AND DIFFUSION	141
6 EDDY-MEAN INTERACTION FOR SCALARS	189
7 PARAMETERIZED OCEAN TRACER TRANSPORT	221
8 OCEAN DENSITY AND SEA LEVEL	255
9 WATER MASS TRANSFORMATION THEORY	285
Part III. Hamilton's principle for fluid mechanics	333
10 SCALAR FIELD THEORY IN GALILEAN SPACE-TIME	337
11 HAMILTON'S PRINCIPLE FOR PERFECT FLUIDS	363
12 APPROXIMATE THEORIES FROM HAMILTON'S PRINCIPLE	389
Part IV. End matter	393
A GLOSSARY OF CONCEPTS AND TERMS	395
B LIST OF ACRONYMS	421
C LIST OF SYMBOLS	423
BIBLIOGRAPHY	433
INDEX	447

CONTENTS

PREFACE

Geophysical fluid mechanics (GFM) is a branch of theoretical physics concerned with natural fluid motion on a rotating and gravitating planet or star. The subject makes use of concepts from classical continuum mechanics and thermodynamics, along with the corresponding methods of mathematical physics. The primary inspiration for our study comes from the motion of fluids in the earth's atmosphere and ocean, though the principles and methods are also applicable to extra-terrestrial fluid flows. Geophysical fluids are in near rigid-body motion with the rotating planet, thus prompting a description from the rotating (non-inertial) planetary reference frame. Body forces from gravity plus planetary rotation (Coriolis and centrifugal) are fundamental features of the motion, as are contact forces from stresses (pressure and friction). In this book, we limit attention to the motion of a single phase of matter (gas or liquid), with the study of multiphase geophysical fluid mechanics, which is relevant to a moist atmosphere, outside our scope. Electromagnetic forces, important for the study of astrophysical fluid motions, are also ignored. We also ignore chemical reactions (which transform matter from one form to another), and nuclear reactions (which convert between matter and nuclear energy).

Geophysical fluid flows manifest over a huge range of space and time scales, with linear and nonlinear interactions transferring information across these scales. Physical insights into such flows typically result from examining a hierarchy of conceptual models using a variety of methods and perspectives. Some of the models we consider are formulated within the context of a **perfect fluid** comprising a single material constituent with fundamental processes limited to the reversible and mechanical. Other models are posed using a **real fluid** that is comprised of multiple matter constituents exposed to an **irreversible process** such as mixing of momentum through viscous friction, mixing of matter through matter diffusion, and/or the mixing of enthalpy through conduction. Some models consider constant density fluids, as commonly considered in classical **hydrodynamics**. And some models ignore rotation, thus tacitly applying to flows with length scales too short to feel the planetary Coriolis acceleration, whereas others ignore buoyancy to thus focus on the dynamics of a homogeneous fluid in a rotating reference frame.

We develop geophysical fluid mechanics from a mathematical physics perspective, with a grounding in fundamentals offering a robust and versatile framework for exploring a gamut of special cases and approximations. Topics are approached by establishing general principles prior to the examination of case studies. Consistent with this approach, our treatment focuses on developing the mechanics of geophysical fluid motion, with that focus supporting theoretical explorations that often extend beyond that required for phenomenological purposes. Correspondingly, we embrace the opportunity to examine physics through multiple lenses that render a variety of complementary insights. In a nutshell, if a physical system can be formulated and analyzed in more than one way, then we do so if it enhances pedagogy and exposes layers of understanding. As a result, brevity is sacrificed to support exposition and exploration, with this perspective leading to a book with multiple volumes.

The presentation is based on the premise that skills in theoretical physics are optimally taught by nurturing physical reasoning, with physical reasoning supported by mathematical precision coupled to the elucidation of concepts using words and pictures. Correspondingly, the presentation is both deductive and descriptive. The deductive approach supports a precise understanding through the use of elementary physical notions that are expressed mathematically. The descriptive approach builds skills in reasoning along with the ability to articulate physical ideas using words and pictures that complement the maths. Readers are supported by development of salient physical concepts and mathematical methods in the process of building understanding. With sufficient study, the material in this book should be accessible to the advanced undergraduate student or entering graduate student in fields such as applied mathematics, astrophysics, atmospheric physics, engineering, geophysics, ocean physics, planetary physics, and theoretical physics.

We generally offer details to mathematical derivations. Doing so nurtures the mathematical skills required for the budding theorist, with the reader strongly encouraged to work through the various derivations and exercises to fully embrace each detail and concept. Exposing mathematical details also helps to unpack many of the physical concepts encapsulated by equations. It is notable that the concepts encountered in this book generally accord with common experience (we are doing classical physics), thus affording a means to check on the validity of the maths. Even so, it does take time to wrap one's head around the physics of large-scale ocean and atmosphere circulations, so patience and persistence are required. Furthermore, as we are studying physics, all mathematical equations must satisfy dimensional consistency, with this constraint offering the physicist a powerful tool for exposing spurious mathematical statements.

We consider this book to be an intellectual journey taken together by the author and reader, thus motivating use of the first person plural pronouns *we* and *us*. Furthermore, we cultivate the deductive and descriptive approaches by embracing the synergism between physics and maths, whereby physics informs the maths and maths reveals the physics. This synergism is facilitated by a presentation style inspired by [Mermin \(1989\)](#), who identified the following characteristics for clear presentations of mathematical physics.

- RULE 1: All displayed equations are given numbers to facilitate cross-referencing. Additionally, any equation supporting another equation or a discussion is itself afforded an equation number.
- RULE 2: Cross-referenced equations are referred to by their equation number as well as descriptive phrases or names (e.g., “as seen by the vector-invariant velocity equation XX.YY” rather than just “as seen by equation XX.YY”). Coupling maths to words supports learning and reduces the need to flip pages to view the cited equation.
- RULE 3: Equations are part of the prose and are thus subject to punctuation.

Concerning the book's title

The study of rotating and stratified geophysical fluid motion largely started in the first half of the 20th century. During recent decades, the study has seen particular evolution through deepening physical foundations, refining mathematical formulations, increasing the intellectual and predictive value of numerical simulations, extending applications across terrestrial and planetary systems, and expanding observational and laboratory measurements and techniques.

What has emerged is a recognition that a fruitful study of rotating and stratified fluid flows makes use of ideas that go beyond the traditional notions of **geophysical fluid dynamics** (GFD). Rather, the contemporary practitioner develops insights by weaving together concepts and tools from mathematics, Newtonian mechanics, analytical mechanics, fluid mechanics, thermodynamics, classical scalar field theory, numerical simulations, laboratory experiments, field measurements, and data science. Acknowledging this broadening of the practice motivates the term *mechanics* in this book’s title, rather than the more focused *dynamics*. It is a minor change in verbiage that reflects a broadening of the perspectives and goals pursued here.

Two pillars of theoretical geophysical fluid mechanics

We conceive of two pillars to theoretical geophysical fluid mechanics that are synergistic, thus offering lessons, guidance, and feedback to the other. The **elements pillar** of geophysical fluid mechanics comprises the physical and mathematical formulation of conceptual models used to garner insight into rotating and stratified fluid motion. This pillar is concerned with setting the stage by deductively and descriptively exposing how physical concepts are mathematically expressed to describe geophysical fluid flows. We provide a thorough treatment of the element pillar given its foundational importance, and since it is commonly offered only a terse treatment in other presentations. We emphasize that the elements pillar is far more than equation manipulation, although one certainly must become adept at that task. Instead, at its core, the elements pillar allows the physicist to reveal the fundamental physical concepts in a precise mathematical manner. Doing so supports understanding while building the foundations for the **emergent phenomena pillar**. The emergent phenomena pillar of geophysical fluid mechanics studies solutions to equations that describe phenomena, such as waves, instabilities, turbulence, and general circulation, all of which emerge from the fundamental equations. Phenomena can emerge in manners that are far from simple to understand deductively, particularly when considering nonlinear behavior such as turbulence. Our treatment of the emergent pillar is limited to waves and instabilities, whereas turbulence and general circulation are beyond our scope, though we do touch upon these topics where suited to the discussion.¹

Some themes found in this book

This multi-volume book covers a number of topics in theoretical geophysical fluid mechanics. Throughout, we encounter a number of themes that appear in various guises, with the following offering a brief survey.

Causation and budgets

A great deal of this book is concerned with deriving and understanding equations that describe the evolution of fluid properties, with such equations (differential or integral) derived from physical principles such as Newton’s laws of motion, Hamilton’s principle of stationary action, Noether’s theorem, thermodynamic laws, mass conservation, and vorticity mechanics. These **budget equations** form the theoretical foundation of continuum mechanics. As part of this development we often seek information about what *causes* fluid motion, making use of a variety of kinematic and mathematical frameworks. The causality question is nicely posed by Newton’s

¹The further one moves along the axis of nonlinearity, the more Sisyphean the task of connecting fundamental processes to emergent phenomena. This perspective is lucidly discussed by [Anderson \(1972\)](#).

equation of motion, which says that acceleration (motion) arises from a net force (the cause of motion). Even though seemingly a clear decomposition of cause and effect, this fundamental statement of Newtonian mechanics offers little more than the definition of a force. We break the self-referential loop, and thus make physical progress, after specifying the nature of the force (e.g., gravitational, frictional), as well as by offering properties of these forces as per Newton's third law (the action/reaction law).²

In geophysical fluid mechanics, we sometimes refer to a time evolving budget equation as an **evolution equation** or, more commonly, a **prognostic equation**, with each term in the prognostic equation referred to as a **time tendency**.³ For prognostic equations, knowledge of the processes contributing to the net time tendency enables a prediction of flow properties. The question arises how to practically determine the tendencies acting in the fluid, particularly when tendencies are generally dependent on the flow itself. This question is often very difficult to answer. Such is the complexity and beauty inherent in nonlinear field theories such as fluid mechanics, where cause and effect are intrinsically coupled.

We can sometimes make progress by turning the problem around, whereby kinematic knowledge of the motion offers inferential knowledge of the dynamical processes contributing to the motion. This situation is exemplified by pressure forces acting within a non-divergent flow whereby pressure provides the force that acts, instantaneously and globally, to maintain the constraint that the velocity is non-divergent.⁴ We may also make use of constraints that restrict the flow in manners that assist in prediction and understanding.

Constraints

Determining the forces, either directly or indirectly, provides physical insight into the cause of fluid flow and its changes. This approach is sometimes referred to a **momentum based viewpoint** since it is based on working directly with the momentum equation (i.e., Newton's second law of motion). However, we are commonly unable to deduce the forces due to complexities inherent in nonlinear field theories. Furthermore, there are many occasions when we are simply uninterested in the forces. In these cases, we are motivated to use constraints that can allow us to sidestep forces but still garner insights into the motion.

One example of a constraint concerns the inability of fluid to flow through a solid static material boundary, such as the solid-earth boundary encountered by geophysical flows. To understand how this constraint impacts the macroscopic fluid motion, we do not need to understand details of the atomic forces that underlie the resistance to macroscopic motion. Instead, we simply impose the kinematic boundary condition whereby the component of the velocity that is normal to the boundary vanishes at the boundary. The forces active within the fluid, no matter what flavor they may take, are constrained to respect the kinematic boundary condition. Another example concerns the study of vorticity. A variety of vorticity constraints offer the means to deduce flow properties without determining forces. Indeed, the **vorticity based viewpoint** often provides a framework that is more versatile in practice than the momentum-based approach, thus prompting the importance of vortex mechanics in the study of geophysical fluid flows.

²For more on this perspective of Newton's laws, see Chapter 1 of *Symon* (1971) or Chapter 2 of *Marion and Thornton* (1988).

³This language has its origins in weather forecasting.

⁴For non-divergent flow, pressure acts as the *Lagrange multiplier* enforcing flow non-divergence.

Associations and balances

Besides seeking causal relations pointing toward the future, many basic questions of fluid mechanics arise either instantaneously, as in the constraints maintaining non-divergent flows, or when the flow is steady, in which case properties at each point in space have no time dependence. In steady flows, the net acceleration, and hence the net force, vanish at each point within the fluid, although the fluid itself can still be moving (steady flows are not necessarily static). For steady flows we are unconcerned with causality since time changes have been removed. In this manner, a steady state equation is a [diagnostic equation](#) rather than a [prognostic equation](#). Diagnostic equations thus provide mechanical statements about associations between physical processes that manifest as balances. The [geostrophic balance](#) is the canonical association in geophysical fluid mechanics, where the horizontal Coriolis force is balanced by the horizontal pressure gradient force. Another balance concerns the vertical pressure gradient and its near balance with the weight of fluid above a point in the fluid, with this [hydrostatic balance](#) approximately maintained at the large scale even for moving geophysical fluids. Further associations arise when studying steady vorticity balances, with the [Sverdrup balance](#) a key example that is commonly used in ocean circulation theory.

We summarize the above by saying that diagnostic equations are concerned with the way things are, whereas prognostic equations point to how things will be. So although a predictive theory requires prognostic equations that manifest causal relations, an understanding of how fluid motion appears, and in particular how it is constrained, is revealed by studying diagnostic relations that expose associations through balances.

Mathematical transformations between kinematic perspectives

Geophysical fluid flows are complex. Hence, it proves useful to avail ourselves of a variety of methods and perspectives that support a mechanistic description of the motion. Many methods are associated with distinct kinematic lenses that reveal particular facets of the flow that might be less visible using alternative lenses. Examples include the Eulerian (spatial) and Lagrangian (material) kinematics used throughout fluid mechanics; the dual position space (x -space) and wavevector space (k -space) used for wave mechanics; the variety of vertical coordinates used for vertically stratified flows; and the analysis of motion in property spaces exemplified by watermass or thermodynamic analysis. We make use of these perspectives throughout this book, and offer the mathematical tools (e.g., tensor methods) needed to transform between them.

Newtonian mechanics and Hamilton's principle

Throughout this book we pursue the maxim

PURSUE ALL WAYS TO FORMULATE AND TO SOLVE A PROBLEM.

A canonical example concerns the complementary perspectives available from Newtonian mechanics and Hamilton's principle of stationary action. Each offers logically consistent results yet approaches mechanics from fundamentally distinct conceptual and operational perspectives. In a Newtonian approach to fluid mechanics, governing differential equations are formulated using a continuum version of Newton's law of motion, in which forces (causes) and accelerations (effects) are articulated as a means to understand and predict the flow. The alternative approach of Hamilton's principle of stationary action approaches mechanics via a variational formulation involving the [action](#). Hamilton's principle says that the action functional is extremized by

the physically realized system. The action is the space-time integral of the difference between kinetic and potential/internal energies, and by extremizing the action we reveal the governing Euler-Lagrange differential equations. The Euler-Lagrange equations are identical to Newton's equations for those cases where Newton's equations are available,⁵ and yet the route to deriving these equations is very distinct. It is by pursuing these distinct paths that we uncover new insights and develop distinct tools for analysis.

Hamilton's principle is not typically covered in fluid mechanics books. This absence contrasts to the ubiquity of Hamilton's principle in other areas of physics. We include facets of Hamilton's principle in this book with the hope that doing so partially remedies the disconnect.⁶ Furthermore, we include Hamilton's principle since it provides novel perspectives on the fundamental equations of geophysical fluid mechanics, and renders insights and tools for the study of emergent phenomena such as waves and instabilities. The reader interested in a serious pursuit of theoretical mechanics should, at some point, make friends with Hamilton's principle. The effort is nontrivial as it requires brain muscles not exercised when studying Newtonian mechanics. But the conceptual and technical payoff is significant.

Non-dimensionalization and scale analysis

Mathematical symbols describing a physical system generally have physical dimensions. Examining the physical dimensions of an equation supports an understanding of the physical content of the equation, and provides a powerful means to identify errors in mathematical manipulations. It is for this reason that we prefer to expose physical dimensions throughout this book, rather than the alternative approach of working predominantly with non-dimensional equations. Even so, scale analysis, as realized through [non-dimensionalization](#), offers an essential tool for deriving mathematical equations used to describe particular flow regimes.

There are two general types of dimensional scales that we use to non-dimensionalize a mathematical physics equation. The first is the [external scale](#), with examples in this book being the gravitational acceleration, Coriolis parameter, and specified properties of the background state such as the buoyancy frequency or prescribed flow. External scales are set by the geophysical parameter regime in which the flow occurs, and as such they are under direct control of the theorist or experimentalist. The second is the [emergent scale](#), which emerges from the flow itself. Emergent scales, such as the length scale and velocity scale of the flow, are specified by the subjective interest of the theorist though these scales are not under direct control. That is, we choose to focus on flows with a particular scale for purposes of examining the corresponding equations that describe that flow regime. A key example concerns our study of planetary geostrophy and quasi-geostrophy, where we choose to focus on flows of a particular scale where the Coriolis acceleration is of leading order importance.

We thus consider the operational aspects of scale analysis to be largely subjective in nature. Namely, we approach the analysis with a subjective bias towards the flow regime of interest, which in turn affects choices for non-dimensional parameters that lead to the corresponding

⁵Hamilton's principle yields the Maxwell's equations of electromagnetism, and yet Maxwell's equations are distinct from Newton's equations. Indeed, Hamilton's principle is used throughout modern physics in areas far beyond Newtonian mechanics.

⁶There certainly are examples where Hamilton's principle is discussed in fluid mechanics books, with [Salmon \(1998\)](#), [Olbers et al. \(2012\)](#), and [Badin and Crisciani \(2018\)](#) notable examples that have inspired this author. Even so, these books remain the exception rather than the norm. As a result, the broader geophysical fluid mechanics community, even those pursuing theoretical aspects, are largely unaware of the beauty and power of Hamilton's principle. This situation contrasts to nearly every other area of mechanics, in which Hamilton's principle is central to both theory and application.

asymptotic equations that describe the regime. Hence, scale analysis is deductive while being strongly guided by our subjective interests.

Geophysical Fluid Mechanics and Climate Science

Fluid mechanics has a history of applications that span science and engineering, from blood flow to the evolution of galaxies. A key 21st century application of geophysical fluid mechanics concerns the questions of earth system science associated with the uncontrolled greenhouse gas experiment pursued by industrialized civilization's carbon centered energy use. Leading order science questions about climate warming have been sufficiently addressed to recognize that the planet has reached a crisis point threatening many features of the biosphere. Even so, mechanistic answers to a number of questions remain at the cutting edge of research. What will happen to the atmospheric jet stream and storm tracks in a world without summer Arctic sea ice? Will tropical storms be more powerful in a warmer world? What are the patterns for coastal sea level rise and their connections to large-scale ocean circulation? What are the key processes acting to bring relatively warm ocean waters to the base of high latitude ice shelves? How stable are the ocean and atmosphere's large-scale overturning circulations and their associated heat transport? Are there feasible and sustainable climate intervention options that equitably reduce the negative impacts of climate warming without introducing new problems? These questions, and countless others, constitute key intellectual challenges of climate science in particular and Earth system science more generally.

Numerical circulation models, observational field campaigns (both *in situ* and remote), and laboratory experiments, are core platforms for Earth system science. Many of these platforms have reached a level of maturity allowing them to vividly reveal details of the complex and multi-scaled nature of planetary fluid flow. Geophysical fluid mechanics is key to the design of observational field campaigns and novel laboratory and numerical experiments, and it provides the intellectual framework for developing mechanistic analyses and robust interpretations of measurements and simulations. In this way, geophysical fluid mechanics furthers predictive capability for weather and climate forecast systems and it enhances confidence in projections for future climate. In a world of increasingly large volumes of simulated and measured data, we conjecture that the marriage of fundamental physical theory to data science tools will enable the significant science and engineering advances needed to address key questions of Earth system science.

About the cover

I took the cover photo of an iceberg, ocean, clouds, and sea bird (can you find the bird?) in the Orkney Passage region of the Southern Ocean during a research cruise from March-May 2017 aboard the British ship James Clark Ross. I am grateful to Alberto Naveira Garabato, the chief scientist on this cruise, for taking me to this amazing part of the planet. Although I largely pursue theoretical research, experiences with seagoing field research have greatly enhanced my scientific viewpoint and profoundly deepened a connection to the natural forces and phenomena that are in part described by geophysical fluid mechanics.

Gratitudes

This book greatly benefited from interactions with students in the Princeton University Atmospheric and Oceanic Sciences Program. In particular, parts of this book served as the basis for my teaching, over many years, a two-semester graduate course, AOS 571 and AOS 572. It also supported a variety of special topic classes (AOS/GEO 585) and lecture series. Further inspiration was offered by students, postdocs, and fellow researchers and scholars encountered on my path. I also thank those who provided specific suggestions, corrections, and comments on various drafts of this book, whose names are too many to list.

I am grateful for having been part of the unique research and learning environment cultivated by three of the world's best examples of scientific enterprises. First and foremost, I am the product of NOAA's Geophysical Fluid Dynamics Laboratory (GFDL), where I worked as a research physicist from 1996 until 2025. As part of my life as a US federal research scientist, I was fortunate to also be associated with Princeton University's Atmospheric and Oceanic Sciences (AOS) program, where I was a postdoc from 1993-1996 and then a faculty member from 2014-2026. As of 2026, I entered the most recent (hopefully not the final!) part of my career journey as a CNRS research scientist in Paris, a position offering an amazing, and humbling, level of intellectual freedom. Throughout my career, I have focused research concerns on ocean physics and the ocean's role in climate, and I have pursued this research from the perspective garnered from the theoretical physics, applied maths, and chemical engineering training of my undergraduate and graduate education.

The communities at GFDL, Princeton AOS, and CNRS provide an ideal setting for those interested in broadening scientific perspectives while diving deep into particular research areas. As part of my research and mentoring in this community, I have encountered thinkers whose style, questions, and insights have taken root in my work. This work has also afforded me the opportunity to travel the world to interact with colleagues whose wisdom and love of the scientific endeavor are infectious and inspiring. Throughout these interactions, I have entered into trusting and non-judgmental spaces where deep learning and understanding arise. Partaking in these spaces, where heart and mind meld, has been among the most fulfilling experiences of my life.

Developing a book of this nature is not a simple endeavor. It starts modestly, grows over time, and eventually becomes a passion and obsession. I was particularly drawn to writing during the COVID-19 pandemic that kept the world largely sequestered at home, and I am grateful that my life situation allowed for this work to safely flourish during what were otherwise very difficult times for civilization. Writing this book has been an exercise in rational thought that exemplifies the maxim "to write is to learn", as articulated by [Zinnser \(1993\)](#). It was furthermore fed by spiritual food from meditation, yoga, family, and community. In particular, each step was supported by my wife, Adi, and our son, Francisco. I am deeply grateful for their patience and trust as I satisfied the goal of writing this book through countless nights, weekends, and holidays. I treasure being part of our family and I dedicate this work to you two amazing human beings.

Caveats and limitations

This book remains a work in progress that is not yet ready for publication. There are many loose threads detailed at the start of various chapters. In addition, here are items targeted for completion prior to release of this book to a publisher.

-
- Wave mechanics
 - equatorial shallow water waves
 - Rossby wave packets and motion in non-homogeneous background
 - Shallow water waves on a rotating sphere, including Laplace's tidal equations, Hough functions, and spherical harmonics
 - Ray theory using Hamilton's principle as in [Tracy et al. \(2014\)](#)
 - Flow stability
 - Charney problem of baroclinic instability
 - Arnold's stability theorem
 - Rayleigh-Benard convection
 - Application of Hamilton's principle
 - Referential flow using Hamilton's principle
 - shallow water and Hamilton's principle
 - semi-geostrophy and Hamilton's principle
 - quasi-geostrophy and Hamilton's principle
 - waves and mean flow interactions
 - Mathematical topics
 - Lie derivative following Section F.3 of [Tromp \(2025\)](#)



GUIDE TO THIS BOOK

No book is an island, with this book generously making use of other books, review articles, research papers, and online tutorials. Many readers find value in studying a subject from a variety of perspectives and voices, thus justifying the proliferation of books with overlapping subject matter. Sometimes it is merely one or two sentences that allow for an idea or concept to click within the reader's brain, whereas other topics require the full gamut of detailed derivations and discussions coming from multiple voices. For these reasons we provide pointers to written and/or video presentations that offer supportive views on material in this book. Many further resources are available through a quick internet search or consultation with artificial intelligence (AI).

There is no pretense that any reader will study all topics in this multi-volume book. This recognition is particularly apparent in a world where research and educational agendas often spread rather than focus attention. Hence, an attempt has been made to facilitate picking up each book at a variety of starting points. For that purpose, each chapter is written in a reasonably self-contained manner and with a brief guide at the start of each chapter listing pre-requisite material. As such, some equations and derivations are reproduced in more than one place, thus obviating the need to back reference. Certainly each chapter cannot be fully self-contained, since this is a book with material building from other chapters across the volumes. We thus make generous use of cross-referencing to point out allied material treated elsewhere. We also make extensive use of the glossary to help define concepts accessed in one volume that might be more thoroughly treated in another volume.



Organization

This book contains five volumes, each of which comprises parts that have multiple chapters. Parts and chapters start with a brief guide to the material along with pointers to dependencies. The book's end matter includes a glossary of key concepts and terms. Items highlighted within the text identify terms with a glossary entry. The glossary also serves as an annotated index, with page numbers pointing to where the terms and concepts are examined within a particular volume. Indeed, the glossary is an essential means to navigate this multi-volume book, reducing (though not eliminating) the need to have more than one volume open at a time. The glossary is then followed by a list of acronyms⁷ and then by a list of symbols. A bibliography follows, with pages listed for where the book or paper is cited. We close the book with an index.

Not all topics are treated equally, with some probed deeply whereas others are given relatively superficial treatment. Indeed, there are many topics omitted that arguably should

⁷We generally try to avoid acronyms, but some are inevitable.

find a home here. Each shortcoming reflects on the author's limited energy and experience rather than a judgement of relative importance.

Cross-referencing to specific sections and equations is provided when pointing to material within the same volume. Cross-referencing material in other volumes is less specific. In many cases, a cross-reference concerns an item in the glossary and/or index, which can be consulted across volumes to help make the connection.



Volume 1

VOLUME 1 establishes foundations in mathematical physics and classical mechanics.

Mathematical physics

We start the book with a suite of mathematical methods chapters. Many readers can skim these chapters without sacrificing too much from later chapters, assuming they have a working knowledge of Cartesian tensors as well as vector differential and integral calculus. Where unfamiliar mathematics topics arise in later chapters, the reader is encouraged to return to this part of the book to help develop the necessary skills.

Classical mechanics

We here survey salient topics from classical mechanics with a geophysical perspective, and in turn develop concepts and methods that have direct relevance to the continuum physics of geophysical fluid flows. Of particular note, this part develops an understanding of physics as viewed from a rotating reference frame. Doing so allows for the sometimes non-intuitive results of rotating physics to be developed within the context of a particle system as a pedagogical preface to later developments for geophysical fluid motion.



Volume 2

VOLUME 2 treats the fundamentals of fluid mechanics with an emphasis on geophysical fluid mechanics.

Kinematics of fluid flow

Mechanics is comprised of kinematics (the study of intrinsic properties of motion) and dynamics (the study of forces and energies causing motion). In the fluid kinematics part of this book, we initiate a study of fluid mechanics by focusing on the kinematics of fluid flow and matter transported by that flow. Our treatment exposes both the Eulerian and Lagrangian viewpoints and emphasizes the variety of kinematic notions and tools key to describing fluid motion. We also encounter facets of material transport as described by the tracer equation. We emphasize that fluid flow, and the transport of matter within that flow, have many features that are fundamentally distinct from point particle and rigid body motion. It takes practice to intellectually digest these differences.

Some kinematic topics can seem esoteric on first encounter, particularly the study of Lagrangian kinematics. However, an incomplete understanding of fluid kinematics can lead to difficulties appreciating facets of fluid dynamics. The reader is thus encouraged to fully study the kinematics chapters, and to revisit the material as the needs arise in later chapters.

Thermodynamics

We study the rudiments of thermodynamics with a focus on topics arising in the study of geophysical fluids. We pay particular attention to the role of gravity in modifying the treatment of thermodynamic equilibrium states, with gravity an essential facet of geophysical fluids and yet a force that is commonly ignored in standard treatments of thermodynamics. We ignore phase transitions, which is a notable limitation of our treatment, thus making this part of the book a mere introduction to the study of a moist atmosphere or an ocean with sea ice.

Dynamics of geophysical fluid flow

In this lengthy part of the book, we study how Newton's laws of mechanics and the principles of thermodynamics are applied to continuum fluid motion on a rotating and gravitating planet. We approach the subject by focusing on how forces that act on fluid elements lead to accelerations and thus to motion. In particular, we examine **body forces** that act throughout the volume of a fluid element (e.g., planetary gravity, planetary Coriolis, and planetary centrifugal) as well as **contact forces** that act on the boundary of a fluid element (e.g., pressure and friction).



Volume 3

Shallow water mechanics

A shallow water fluid is comprised of hydrostatically balanced homogeneous fluid layers. The layers are also typically assumed to be immiscible, so that interactions between layers occur only via mechanical forces from pressure acting at the layer interfaces. The shallow water fluid allows us to focus on planetary rotation and vertical stratification without the complexities of vertically continuous stratification and thermodynamics. Many physical insights garnered by studying shallow water fluids extend to more realistic fluids, thus making the shallow water model very popular among theorists and teachers. Indeed, [Zeitlin \(2018\)](#) provides an example of just how far one can go in understanding geophysical fluids with shallow water theory.

Vorticity

Vorticity plays a role in the motion of all geophysical fluids since motion on a rotating planet provides a nonzero **planetary vorticity** even to fluids at rest on the planet. This feature of geophysical fluids contrasts to many other areas of fluid mechanics, where irrotational flows are commonly encountered. **Potential vorticity** is a strategically chosen component of the vorticity vector that melds mechanics (vorticity) to thermodynamics (stratification). Material conservation properties of potential vorticity are striking and render important constraints on fluid motion. Indeed, perhaps the most practical reason to study vorticity concerns the various constraints imposed on the flow moving on a rotating and gravitating planet. These constraints provide conceptual insights and predictive power.

Nearly geostrophic balanced flows

Balanced models generally remove the horizontally divergent motions associated with gravity waves, thus allowing a focus on the large-scale vortical motions. Balanced models have a rich history among theoretical geophysical fluid studies, providing insights into both laminar oceanic flows through planetary geostrophy, and wave-turbulent atmospheric and oceanic flows through quasi-geostrophy. When studying balanced models, we focus on the shallow water and continuously stratified versions of quasi-geostrophy and planetary geostrophy.



Volume 4

Generalized vertical coordinates

The chapters on **generalized vertical coordinate (GVC)s (GVC)** dive into the maths, kinematics, dynamics, and applications of such coordinates for the study of geophysical fluid mechanics. This material is central to many current research activities, including subgrid scale parameterizations and the design of numerical atmosphere and ocean models. The mathematics in this part leans heavily on the general tensors studied in **VOLUME 1**. Even so, many readers can make the most of these chapter without the full gamut of general tensors.

Scalar fields

Many chapters target the mechanics of scalar fields with a focus mostly on the ocean. Here we consider active tracers (temperature and salinity), passive tracers, and buoyancy. Much of this study forms the basis of tracer mechanics, which has proven very important for the ocean since it is generally very difficult to measure vector fields such as velocity and vorticity, whereas tracer distributions are far more readily measured. We also consider facets of sea level analysis in this part of the book.

Hamilton's principle for geophysical flows

We study the analytical mechanics of geophysical flows using Hamilton's principle. This material forms the heart of field theory, both classical and quantum. It requires a different set of techniques than used in the study of Newtonian fluid mechanics used elsewhere in this book. Hence, it offers complementary insights that deepen our understanding of geophysical fluid flows in particular.



Volume 5

Linear wave mechanics

We study a variety of geophysical waves and associated mathematical methods used for their characterization. Notably, we consider waves not commonly included in a book on geophysical fluids, such as sound and capillary waves, with these waves included due to their ubiquity in the natural environment as well as their pedagogical value. Most focus, however, is given to waves arising from the Coriolis acceleration (inertial waves, planetary Rossby waves, topographic

Rossby waves) and gravitational acceleration (surface gravity waves, internal gravity waves). Furthermore, we study linear waves and their corresponding wave packets, first studying their behavior in a homogeneous background environment where Fourier methods are available. Thereafter, we introduce methods needed to study linear waves on a gently varying background, including the methods of geometrical optics and wave action, with these methods of use particularly when Fourier methods are not suited.

Flow instabilities

We study instabilities that arise in geophysical fluid motions, distinguishing two classes of fluid instabilities: **local instabilities** or **parcel instabilities** versus **global instabilities** or **wave instabilities**. Local instabilities are afforded a local necessary and sufficient condition to determine whether the fluid base state is unstable to perturbations. In contrast, global instabilities arise from the constructive interference of waves and so involve the solution of an eigenvalue problem to determine properties of unstable waves. At most, a necessary condition can be derived to determine whether a global instability exists. Our study of fluid instabilities introduces a suite of case studies that foster analysis and conceptual methods to establish a foundation for further study. Geophysical fluid instability analysis remains an active area of research, with insights into the suite of primary and secondary instabilities providing compelling stories for how the ocean and atmosphere work.



Pointers on written and spoken communication

To thrive in research and teaching requires one to master elements of both written and spoken communication. Here are a few pointers for the student interested in furthering these skills.

CLEAR THINKING LEADS TO CLEAR COMMUNICATION

Clear communication is the sign of clear thinking. Some people communicate better in writing, where one has the opportunity to carefully organize thoughts and refine the writing. Others are better at speaking, where spontaneous and interactive reflections and experiences can bolster the clarity of a presentation.

As inspiration for both the clear and obscure, pick up a textbook or lecture notes and analyze the presentation for clarity. Where is the presentation confusing? Where is the material crystal clear? Then pick up a journal article and perform the same analysis. What is appealing? What is unappealing? Then go to the internet and find a science or engineering lecture, old or new. What makes the speaker engaging and clear, or boring and obscure?

EMPATHY IS KEY

Empathy is a basic facet of effective communication and teaching, where the writer, speaker, or teacher places their mind inside that of an interested and smart reader or listener. Identify with their quest to understand new ideas and to comprehend the foundations and assumptions. Are the assumptions justified based on the audience? How compelling is the scientific story? Are missing steps crucial to understanding or easily dispensed with for streamlining the presentation?

Although poor communication hinders our ability to digest new ideas and concepts, it is also important to appreciate that some material is tough no matter how well it is communicated. We should aim to make a subject matter as simple as possible, but not simpler (paraphrasing Einstein). Furthermore, it sometimes takes a few generations of teaching before some scientific material can be sufficiently digested to allow for the core conceptual nuggets to be revealed. As an example, try reading Newton or Maxwell's original works as compared to a modern presentation of Classical Mechanics or Electromagnetism. So as we strive for clear communication, we cannot presume that clarity is sufficient to remove the struggles everyone experiences when learning.

Additionally, it is essential to recognize that everyone makes mistakes, either in fundamentals or practices. The toughest part of making mistakes is often the self-imposed shame and embarrassment. However, mistakes offer significant opportunities for learning and advancing, with honesty and humility critical for identifying weaknesses, both in our own work and those of others.



Pointers on physics problem solving

We conclude each chapter with a suite of exercises. Working through these exercises, in full detail, is an integral part of learning and doing physics. Indeed, there is no replacement for struggle and head-scratching to support the physics problem-solving brain muscle. However, with the advent of AI tools, one can readily access AI generated solutions. It goes without saying that over-reliance on AI tools greatly compromises one's ability to develop the skills necessary to know whether the AI solution is correct. In light of this situation, we provide some worked solutions, which generally go beyond what is expected from a student learning the material for the first time, as we aim for the solutions to be instructional as well as utilitarian. For this reason, we expose many of the intermediate steps needed to derive a solution, further supporting an in-depth learning of how to independently solve physics problems. Additionally, it helps to identify when an incorrect result follows from a physical/conceptual error (e.g., incorrect setup of the problem solution) or a mathematical error (e.g., sign error).

We observe that most people are not born with *a priori* physics problem solving skills. Rather, it takes extensive practice to develop the necessary brain muscle. The student who values the ability to solve physics problems should resist the temptation to quickly flip pages to read solutions. Time pondering an exercise is time well spent learning how to do theoretical physics in a manner needed to pursue novel research. In the remainder of this section we offer specific pointers of use when diving into a physics problem.

CHECK FOR DIMENSIONAL CONSISTENCY

The symbols we use in mathematical physics correspond to geometrical objects (e.g., points, vectors, tensors) describing a physical concept (e.g., position in space, velocity, temperature, angular momentum, stress). Hence, the symbols generally carry physical dimensions. The physical dimensions we are concerned with in this book are length (L), time (T), mass (M), and temperature. We do not consider electromagnetism or the quantum mechanical world. Physical dimensions of the equations must be self-consistent. For example, if one writes an equation $A = B$, where A and B have different physical dimensions, then the equation makes no physical

sense. Something is wrong. Although not always sufficient to uncover errors, dimensional analysis is an incredibly powerful necessary step in debugging the maths.

CHECK FOR TENSORIAL CONSISTENCY

In the same way that mathematical equations in physics need to maintain dimensional consistency, they must also respect tensor rules. For example, the equation $A = B$ makes mathematical sense if A and B are both scalars. Likewise, $\mathbf{A} = \mathbf{B}$ makes sense if \mathbf{A} and \mathbf{B} are both vectors. However, if both \mathbf{A} and \mathbf{B} are vectors, then the equation $\mathbf{A} = \nabla \cdot \mathbf{B}$ does not make sense because the left hand side is a vector and the right hand side is a scalar. A more subtle example is when \mathbf{A} is a vector yet \mathbf{B} is an axial vector. In this case, \mathbf{A} remains invariant under a change from right hand to left hand coordinates whereas \mathbf{B} flips sign. Maintaining basic tensorial rules can be considered the next level of sophistication beyond dimensional analysis.

USE WORDS AND PICTURES

Words and pictures are important elements in explaining a physical concept and/or a problem in physics. Hence, it is good practice to liberally sprinkle sentences in between the key equations for the purpose of explaining what the maths means using clear English. Here are some practical payoffs to the student for this style of presentation.

- The process of explaining the maths using words and pictures requires one to dive deeper into the logic of a physics problem. Doing so often reveals weak points, incomplete or unmentioned assumptions, and errors. This process is a very important learning stage in preparing to stand in front of an audience to present results and to answer questions. It is a key facet of research and teaching.
- Physics teachers are often more forgiving of math errors if you convince the teacher that you have a sensible physical understanding of the problem. Plain English and pictures are very useful means for this purpose.

THERE IS OFTEN MORE THAN ONE PATH TO A SOLUTION

In physics, there is often more than one path to a problem solution or to the formulation of a concept. Pursuing distinct paths offers novel physical and mathematical insights, exposes otherwise hidden assumptions, and allows one to double-check the veracity of a solution. Some of the most profound advances in physics came from pursuing distinct formulations. One example concerns the distinct formulation of mechanics offered by Newton (1642-1746), and then later by Lagrange (1736-1813) and then Hamilton (1805-1865). Had Lagrange or Hamilton rested on the merits of their predecessors, we may well have had a very different intellectual evolution of 19th and 20th century physics.



Part I

Generalized vertical coordinates

The flow of geophysical fluids is affected by the Coriolis acceleration arising from planetary rotation, the gravitational stratification arising in a fluid with non-homogeneous density, and interactions with the solid-earth boundaries that introduces form stresses and boundary layer turbulent processes. In describing geophysical fluid flows, we can be motivated to choose coordinates designed to simplify theoretical analyses and/or enhance the fidelity of numerical simulations. A **GVC** (**GVC**) offers a mathematical framework with these motivations in mind. Specifically, a **GVC** is suited to describing fluid mechanics according to monotonically stacked coordinate surfaces defined by the generalized vertical coordinate, $\sigma = \sigma(x, y, z, t)$. The introduction of generalized vertical coordinates originates from [Starr \(1945\)](#) for atmospheric modeling and [Bleck \(1978\)](#) for ocean modeling. There is a growing use of **GVC**-based numerical ocean (e.g., [Griffies et al. \(2020\)](#)) and atmospheric models. This usage prompts the need to master their use in theoretical studies as well as the formulation of numerical models, thus motivating this part of the book.

There are two key mathematical features of generalized vertical coordinates that require extra mathematical precision beyond the geopotential vertical coordinate. First, surfaces of constant generalized vertical coordinate are space and time dependent, so that observers on a fixed σ -surface are non-inertial, and the lateral directions on these surfaces are not strictly horizontal. Second, generalized vertical coordinates are non-orthogonal, with one of its basis vectors aligned with the gravity field whereas two basis vectors are aligned along the undulating σ -surface (we illustrate this property in Figure 1.3). The time dependent and non-orthogonal properties of generalized vertical coordinates contrast to the static and locally orthogonal coordinates, such as Cartesian, polar-cylindrical, or spherical). To handle such generality, we find it useful to employ the general tensor machinery from **VOLUME 1**.

By aligning one of its basis vectors with the gravitational acceleration (as well as the local vertical component of planetary rotation), generalized vertical coordinates allow for the mathematical treatment of gravity and planetary rotation in a manner directly analogous to geopotential coordinates. This orientation is a great advantage of generalized vertical coordinates. However, one might question whether this benefit is worth the cost of having to learn how to handle non-orthogonal coordinates. For large-scale geophysical fluid mechanics, we contend that the benefit greatly outweighs the cost. However, many ocean theorists studying the physics of ocean boundary layers next to a constant sloping bottom have chosen to use orthogonal slope-normal coordinates ([Phillips \(1970\)](#), [Wunsch \(1970\)](#), [Garrett et al. \(1993\)](#), [Callies \(2018\)](#), and [Holmes et al. \(2019a\)](#), others). In Exercise 1.7 we derive the planetary geostrophic equations in the rotated orthogonal coordinate, thus illustrating how the gravitational acceleration and locally vertical planetary rotation vector are projected onto more than a single basis vector.⁸ Although the use of slope-normal coordinates is widespread for idealized theoretical studies of boundary layer flows, [Peterson and Callies \(2022\)](#) illustrate the utility of a particular terrain following generalized vertical coordinate as a contrast to the slope-normal coordinate.

Taking the perspective that generalized vertical coordinates are valuable for geophysical fluid mechanics, our goal in this part of the book is to develop their mathematics and to use these coordinates in formulating the kinematics and dynamics of stratified geophysical fluid flows. The following provides a summary of the chapters where this work is presented.

- **MATHEMATICAL FOUNDATIONS:** In Chapter 1 we establish the mathematics of generalized vertical coordinates, with particular attention given to identifying aspects arising from

⁸There is another case where locally orthogonal coordinate are useful. Namely, for the study of anisotropic tracer diffusion within the ocean interior, in which diffusive fluxes from mesoscale turbulence is suitably oriented according to neutral directions. A full study of neutral diffusion provided in Section 7.4.

their time dependence and non-orthogonality. Notably, the non-orthogonality makes it crucial to distinguish covariant from contravariant representations of vector fields.

- GEOPHYSICAL FLUID MECHANICS: We then focus in Chapter 2 on developing the kinematics of generalized vertical coordinates. Dia-surface transport plays a central role in the kinematics, thus warranting a deep dive into its many facets. We then study the suite of geophysical fluid dynamical equations using generalized vertical coordinates.
- CONTINUOUS AND LAYERED ISOPYCNAL EQUATIONS: In Chapter 3 we focus on the hydrostatic ocean Boussinesq equations as formulated using buoyancy as the vertical coordinate. This work provides a mathematical and physical basis for *isopycnal* models of the ocean and isentropic models of the atmosphere. We then specialize the continuous equations to their vertically discrete (layered) form and explore **thickness weighted averaging (TWA)** within the perfect fluid stacked shallow water model.

MATHEMATICS IN THIS PART

The mathematics in this chapter rely extensively on the tensor analysis from VOLUME 1, including Cartesian tensors and general tensors.

Chapter 1

FOUNDATIONS IN TENSOR CALCULUS

In this chapter we present the tensor calculus foundations for describing fluid flow using a GVC (GVC). Figure 1.1 offers a schematic of how these coordinates monotonically partition the vertical direction. Such coordinates are of particular use for stratified fluid mechanics, where it is often convenient to use a vertical coordinate that is distinct from, but uniquely and invertibly related to, the geopotential vertical coordinate, z . To allow us to focus on the vertical coordinate, we here make use of Cartesian coordinates for the lateral/vertical directions.¹

CHAPTER GUIDE

We make use of the general tensor analysis detailed in VOLUME 1, with the maths here forming the foundations for subsequent chapters on generalized vertical coordinates.

1.1	Loose threads	6
1.2	Cartesian and generalized vertical coordinates	6
1.2.1	Notation conventions	7
1.2.2	Notation for the vertical position of a GVC surface	7
1.3	Example generalized vertical coordinates	8
1.3.1	Pressure coordinates	8
1.3.2	Terrain following coordinates	8
1.3.3	Rescaled geopotential and pressure coordinates	9
1.3.4	Bottom slope oriented coordinates	10
1.3.5	Isopycnal or buoyancy coordinates	10
1.4	Spatial basis vectors	10
1.4.1	An important detail regarding the transformation matrix	11
1.4.2	Expressions for the basis vectors	11
1.5	Basis one-forms	11
1.5.1	More on the inverse transformation matrix	12
1.5.2	Basis one-forms	12
1.5.3	Verifying the bi-orthogonality relation	13
1.6	Triple product identities	13
1.7	Position of a point in space	14
1.8	Transforming components of a vector	16
1.9	Representing the velocity vector	16
1.9.1	Contravariant components	17
1.9.2	Covariant components	17

¹A coordinate transformation to general orthogonal curvilinear coordinates, such as spherical coordinates, is straightforward relative to the niceties arising from the non-orthogonal nature of generalized vertical coordinates.

1.9.3	Introducing the material time derivative	17
1.9.4	Equivalence to the Cartesian velocity representation	18
1.10	Metric tensor using generalized vertical coordinates	18
1.10.1	Representation of the metric tensor and its inverse	18
1.10.2	Jacobian of transformation	19
1.10.3	Covariant and contravariant representations	19
1.10.4	Metric tensor for points living on a constant σ -surface	20
1.11	Volume element and the Levi-Civita tensor	20
1.12	Partial derivative operators	21
1.12.1	Analytical derivation	21
1.12.2	Geometrical derivation	21
1.12.3	The gradient as a tensor operator	22
1.13	Material time derivative	23
1.14	Divergence of a vector and the divergence theorem	23
1.15	The diffusion operator	24
1.15.1	Continuous expression	24
1.15.2	Layer thickness weighted diffusion operator	25
1.16	Vorticity	25
1.16.1	Contravariant components	26
1.16.2	Transforming from Cartesian coordinates	26
1.17	Circulation	27
1.18	Exercises	28

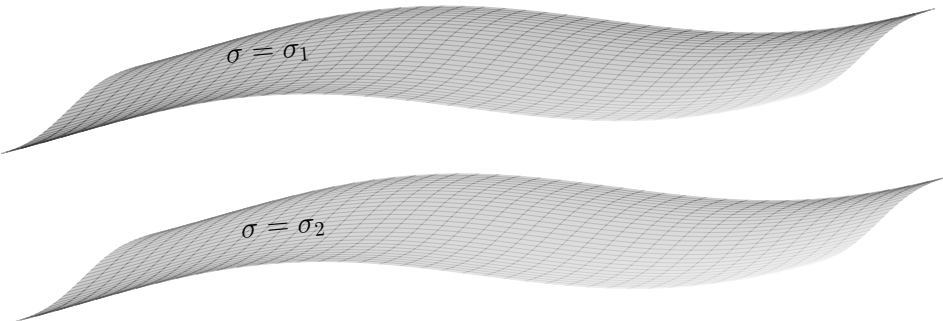


FIGURE 1.1: Schematic to illustrate the geometry of two surfaces of constant GVC with values, $\sigma(x, y, z, t) = \sigma_1$ and $\sigma(x, y, z, t) = \sigma_2$. The surfaces undulate in space and time and are assumed to layer the fluid in a manner that the surface normal, $\hat{\mathbf{n}} = \nabla\sigma/|\nabla\sigma|$, always has a non-zero projection onto the vertical: $\hat{\mathbf{n}} \cdot \hat{\mathbf{z}} = \partial_z\sigma/|\nabla\sigma| \neq 0$. That is, the surfaces never become vertical nor do they overturn. It also means that there is a 1-to-1 invertible relation between σ and geopotential, so that there is a monotonic relation in which specifying $(x, y, \sigma(x, y, z, t))$ is sufficient to yield a unique z .

1.1 Loose threads

- Compute geodesics for motion restricted to an isopycnal, using the metric from Section 1.10.4. Will need to compute the Christoffel symbols; could be a bunch of work but one question is whether there is a relation to neutral directions that appears.

1.2 Cartesian and generalized vertical coordinates

In this section we establish some of the basic notational conventions for Cartesian coordinates and generalized vertical coordinates.

1.2.1 Notation conventions

We make use of the symbol, σ , for a generalized vertical coordinate (GVC) as in Figure 1.1. The coordinate triad, (x, y, σ) , is *not* orthogonal, with lack of orthogonality the central property of GVCs that influences nearly all aspects of their calculus. To help develop the mathematics for transforming between Cartesian coordinates and GVCs, it is important to distinguish the two coordinate systems, and we make use of a few options that are motivated by the usage. Namely, we write the time coordinate and spatial Cartesian coordinates according to

$$\xi^\alpha = (\xi^0, \xi^a) = (\xi^0, \xi^1, \xi^2, \xi^3) = (t, x, y, z) \text{ with } \alpha = 0, 1, 2, 3, \text{ and } a = 1, 2, 3. \quad (1.1)$$

The Latin coordinate label, a , runs over the spatial coordinates 1, 2, 3, whereas the Greek label, α , also includes the time coordinate that has $\alpha = 0$. The corresponding generalized vertical coordinates are denoted with an overbar

$$\xi^{\bar{\alpha}} = (\xi^{\bar{0}}, \xi^{\bar{1}}, \xi^{\bar{2}}, \xi^{\bar{3}}) = (\bar{t}, \bar{x}, \bar{y}, \sigma). \quad (1.2)$$

The 1-to-1 coordinate transformation between Cartesian and GVC coordinates is written

$$\xi^{\bar{0}} = \xi^0 \iff \bar{t} = t \quad (1.3a)$$

$$\xi^{\bar{1}} = \xi^1 \iff \bar{x} = x \quad (1.3b)$$

$$\xi^{\bar{2}} = \xi^2 \iff \bar{y} = y \quad (1.3c)$$

$$\xi^{\bar{3}} = \sigma(x, y, z, t), \quad (1.3d)$$

with the final relation expressing the generalized vertical coordinate as a function of space and time. We ordered the coordinates appearing in $\sigma(x, y, z, t)$ with time in the last position, which is the conventional ordering in this book for functions of space and time. We continue this ordering even though the zeroth coordinate is time.

The coordinate transformation between Cartesian space-time and GVC space-time is invertible so that we can write

$$\xi^0 = \xi^{\bar{0}} \quad (1.4a)$$

$$\xi^1 = \xi^{\bar{1}} \quad (1.4b)$$

$$\xi^2 = \xi^{\bar{2}} \quad (1.4c)$$

$$\xi^3 = \xi^3(\bar{x}, \bar{y}, \sigma, \bar{t}) = \xi^3(x, y, \sigma, t). \quad (1.4d)$$

The relation

$$\xi^3 = \xi^3(\xi^{\bar{a}}) = \xi^3(x, y, \sigma, t) \quad (1.5)$$

provides the vertical position of a given σ surface.

1.2.2 Notation for the vertical position of a GVC surface

Since $\xi^3 = z$, one commonly writes

$$z = z(x, y, \sigma, t). \quad (1.6)$$

However, this expression is prone to confusion since the meaning of z is overloaded.² Namely, one meaning ascribes to z a particular value of the vertical position; say $z = -100$ m. The other meaning, as on the right hand side of equation (1.6), is for z as the geopotential position of a particular σ surface, with this position determined by setting the horizontal position, (x, y) , the generalized vertical coordinate, σ , and the time. It takes practice to routinely distinguish when z refers to a particular vertical position or refers to a coordinate function. The distinction is important for both fundamentals and practices.

Those who routinely work with generalized vertical coordinates typically have no problem with the overloaded meaning for z . Indeed, after reading this chapter we should be able to hold the two meanings in our mind without confusion. Even so, to help build the necessary brain muscle, we commonly write the vertical position of a generalized vertical coordinate as

$$z = \eta(x, y, \sigma, t). \quad (1.7)$$

The symbol, η , is used throughout this book to represent the vertical position of a surface, such as the ocean free surface ($z = \eta(x, y, t)$), solid-earth topography ($z = \eta_b(x, y)$), or, as used here, for the vertical position of a specific generalized vertical coordinate surface labeled by σ . Hence, for example, the vertical position of a pressure surface of chosen value p is given by the functional relation

$$\xi^3 = z = \eta(\bar{x}, \bar{y}, p, \bar{t}) = \eta(x, y, p, t). \quad (1.8)$$

We make use of the η nomenclature where it seems useful, but gradually sprinkle in more use of the $z(x, y, \sigma, t)$ notation since it is natural for many of the formulations.

1.3 Example generalized vertical coordinates

Before further diving into the maths, we here offer some examples of generalized vertical coordinates commonly used to study geophysical fluid flows. Figure 1.2 displays three of the coordinates described below.

1.3.1 Pressure coordinates

For hydrostatic compressible fluids, such as the large-scale atmosphere, pressure is a convenient choice since it absorbs the appearance of density in many formula, such as mass continuity as discussed in Section 2.10.2. Hence, a natural expression of the compressible hydrostatic equations of motion makes use of pressure rather than geopotential for the vertical coordinate, in which case we set $\sigma = p(x, y, z, t)$.

1.3.2 Terrain following coordinates

The terrain following coordinate used in Boussinesq ocean studies is given by

$$\sigma = \frac{z - \eta_s}{-\eta_b + \eta_s} \quad \text{terrain following Boussinesq coordinate,} \quad (1.9)$$

where $z = \eta_s(x, y, t)$ is the vertical position of the ocean free surface. We illustrate these coordinates in Figure 1.2. The terrain following coordinate is non-dimensional and extends from

²We use the term *overloaded* as in computer programming, where one often finds an operator given more than one usage depending on the inputs.

$\sigma = 0$ at the ocean surface ($z = \eta_s(x, y, t)$) to $\sigma = -1$ at the ocean bottom ($z = \eta_b(x, y)$). For rigid lid ocean models with $\eta_s = 0$, the terrain following coordinate becomes time independent

$$\sigma = -\frac{z}{\eta_b} \quad \text{terrain following rigid lid ocean.} \quad (1.10)$$

Finally, for a non-Boussinesq fluid it is more convenient to use pressure to define the terrain following coordinate so that

$$\sigma = \frac{p - p_a}{p_b - p_a} \quad \text{terrain following pressure coordinate.} \quad (1.11)$$

In this equation, p_a is the pressure applied at the ocean surface and p_b is the pressure at the ocean bottom. For use in studying the atmosphere we might set p_a as the top of the atmosphere pressure, which is typically assumed to be zero as in [Phillips \(1957\)](#).

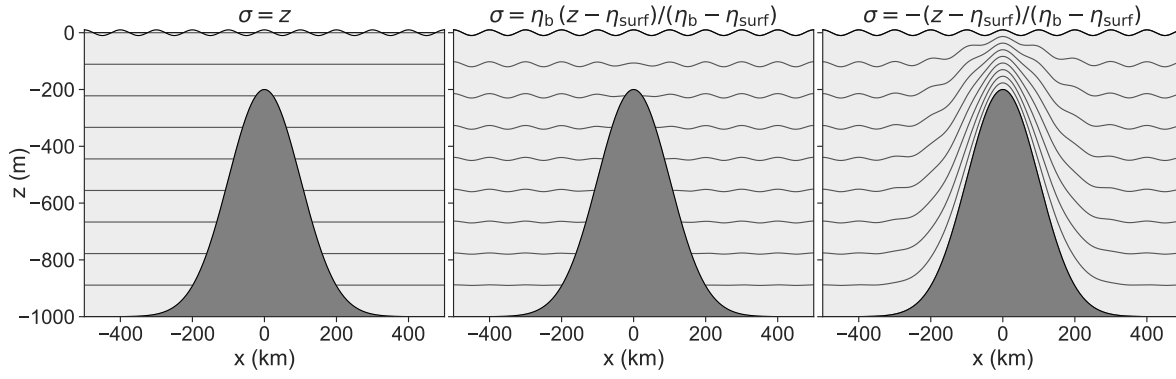


FIGURE 1.2: Three examples of generalized vertical coordinates in the presence of a Gaussian hill and a free surface, with a highly exaggerated free surface amplitude of 20 m allowing for its visualization (2 m is a more physically realistic amplitude for large-scale ocean flows). Left panel: geopotential coordinates, which are horizontal throughout the domain. Middle panel: $\sigma = z^* = \eta_b(z - \eta_s)/(\eta_b - \eta_s)$, which ranges from $\eta_b \leq z^* \leq 0$ and is quasi-horizontal and yet incorporates motion of the free surface. Right panel: terrain following coordinate, $\sigma = -(z - \eta_s)/(\eta_b - \eta_s)$, which ranges from $-1 \leq \sigma \leq 0$ and incorporates undulations of the bottom topography and free surface. Note that near the ocean surface there can be regions where the free surface undulations cause water to fall outside of the domain of the geopotential vertical coordinate domain, with such situations problematic for a numerical model.

1.3.3 Rescaled geopotential and pressure coordinates

Numerical models making use of terrain-following coordinates from Section 1.3.2 can suffer from nontrivial errors in the horizontal pressure gradient calculation, which we discuss in Section 2.14. To partially remedy this problem, it is common to follow [Adcroft and Campin \(2004\)](#) (see [Black \(1994\)](#) for the atmosphere analog) by working with a nearly horizontal coordinate that absorbs the free surface motion

$$\sigma = z^* = \frac{\eta_b(z - \eta_s)}{\eta_b - \eta_s} \quad \text{rescaled geopotential ocean coordinate,} \quad (1.12)$$

where z^* is the symbol used in the literature. We illustrate these coordinates in Figure 1.2. Like the terrain following coordinate (1.9), z^* has a time-independent range, only here it is given by the dimensional range

$$\eta_b \leq z \leq \eta_s \implies \eta_b \leq z^* \leq 0. \quad (1.13)$$

The corresponding coordinate for a non-Boussinesq hydrostatic fluid is

$$\sigma = p^* = \frac{p_{\text{bo}} (p - p_{\text{a}})}{p_{\text{b}} - p_{\text{a}}} \quad \text{rescaled pressure coordinate,} \quad (1.14)$$

where p_{bo} is the bottom pressure for a resting fluid.

1.3.4 Bottom slope oriented coordinates

For their studies of ocean mixing along a constant sloped bottom, [Peterson and Callies \(2022\)](#) make use of an alternative to the traditional terrain following coordinates from Section 1.3.2, here defining a bottom slope oriented coordinate (recall $\eta_{\text{b}} = \eta_{\text{b}}(x, y)$)

$$\sigma = z - \mathbf{x} \cdot \nabla \eta_{\text{b}} = z - x \partial \eta_{\text{b}} / \partial x - y \partial \eta_{\text{b}} / \partial y, \quad (1.15)$$

with $\nabla \eta_{\text{b}}$ the slope of the bottom topography.

1.3.5 Isopycnal or buoyancy coordinates

Buoyancy surfaces are material when there is no mixing. Hence, for the study of perfect fluid mechanics it is quite convenient to use the Archimedian buoyancy, b , as the vertical coordinate, $\sigma = b(x, y, z, t)$. Equivalently, one may choose the potential density as the vertical coordinate. We have much more to say about isopycnal vertical coordinates in Chapter 3 when developing the equations for isopycnal ocean models.

1.4 Spatial basis vectors

Write the three Cartesian basis vectors, \mathbf{e}_a , as

$$(\mathbf{e}_1, \mathbf{e}_2, \mathbf{e}_3) = (\hat{\mathbf{x}}, \hat{\mathbf{y}}, \hat{\mathbf{z}}). \quad (1.16)$$

We now consider the transformation of these basis vectors into their corresponding GVC (GVC) representation. This transformation is given by

$$\mathbf{e}_{\bar{a}} = \Lambda^a_{\bar{a}} \mathbf{e}_a, \quad (1.17)$$

where the transformation matrix is³

$$\Lambda^a_{\bar{a}} = \begin{bmatrix} \partial x / \partial \bar{x} & \partial x / \partial \bar{y} & \partial x / \partial \sigma \\ \partial y / \partial \bar{x} & \partial y / \partial \bar{y} & \partial y / \partial \sigma \\ \partial z / \partial \bar{x} & \partial z / \partial \bar{y} & \partial z / \partial \sigma \end{bmatrix} = \begin{bmatrix} 1 & 0 & 0 \\ 0 & 1 & 0 \\ \partial \eta / \partial \bar{x} & \partial \eta / \partial \bar{y} & \partial \eta / \partial \sigma \end{bmatrix}, \quad (1.18)$$

where the second equality wrote $z = \eta(x, y, \sigma, t)$ for the vertical position of a σ surface (see Section 1.2). The diagonal unit values for the space-space components arise since a horizontal position is the same for Cartesian coordinates and generalized vertical coordinates, and the horizontal directions are orthogonal. Likewise, the time coordinate does not change when changing \bar{x} , \bar{y} , or σ . Additionally, $\partial x / \partial \sigma = \partial y / \partial \sigma = 0$ since the horizontal position remains

³Equation (1.18) makes use of a common overloaded meaning for $\Lambda^a_{\bar{a}}$. First, it can mean the element in the a -row and \bar{a} -column of the transformation matrix, Λ . Second, it can be the matrix itself, with the exposed indices useful to reveal how the matrix is used within tensorial manipulations. It is this second meaning that is used for equation (1.18).

unchanged when moving across a **GVC** surface. In contrast, non-zero values for $\partial\eta/\partial\bar{x}$ and $\partial\eta/\partial\bar{y}$ arise since we generally change vertical position when moving horizontally along a sloped σ surface. Finally, the element $\partial\eta/\partial\sigma$ is nonzero due to vertical coordinate stratification of the fluid when represented using generalized vertical coordinates.

1.4.1 An important detail regarding the transformation matrix

To further detail how to produce elements of the transformation matrix (1.18), it is crucial to ensure that the proper variables are held fixed when performing the partial derivatives. For example, consider the top row

$$\Lambda^1_{\bar{x}} = \begin{bmatrix} [\partial x/\partial\bar{x}]_{\bar{y},\sigma} & [\partial x/\partial\bar{y}]_{\bar{x},\sigma} & [\partial x/\partial\sigma]_{\bar{x},\bar{y}} \end{bmatrix} \quad (1.19)$$

Since $x = \bar{x}$, all elements vanish except for the first. Namely, $[\partial x/\partial\bar{y}]_{\bar{x},\sigma} = 0$ since x cannot change when \bar{x} is fixed. The same idea leads to the results for y derivatives.

1.4.2 Expressions for the basis vectors

Use of the transformation matrix (1.18) renders the spatial components of the **GVC** basis vectors

$$\mathbf{e}_{\bar{1}} = \hat{\mathbf{x}} + \hat{\mathbf{z}} (\partial\eta/\partial\bar{x}) \quad (1.20a)$$

$$\mathbf{e}_{\bar{2}} = \hat{\mathbf{y}} + \hat{\mathbf{z}} (\partial\eta/\partial\bar{y}) \quad (1.20b)$$

$$\mathbf{e}_{\bar{3}} = \hat{\mathbf{z}} (\partial\eta/\partial\sigma). \quad (1.20c)$$

The basis vectors $\mathbf{e}_{\bar{1}}$ and $\mathbf{e}_{\bar{2}}$ have a vertical component due to sloping **GVC** surfaces. These basis vectors lie within the tangent plane of the **GVC** surface. The basis vector $\mathbf{e}_{\bar{3}}$ is purely vertical and has a non-unit magnitude due to the inverse vertical stratification,

$$\partial\eta/\partial\sigma = (\partial\sigma/\partial\eta)^{-1}. \quad (1.21)$$

The left panel of Figure 1.3 illustrates the basis vectors.

As an example, consider the rigid lid terrain following vertical coordinate (1.10), where $\sigma = -z/\eta_b$. In this case, the vertical position of a generalized vertical surface is given by $\eta = -\sigma\eta_b$ so that the basis vectors are

$$\mathbf{e}_{\bar{1}} = \hat{\mathbf{x}} - \hat{\mathbf{z}}\sigma(\partial\eta_b/\partial\bar{x}) \quad \text{and} \quad \mathbf{e}_{\bar{2}} = \hat{\mathbf{y}} - \hat{\mathbf{z}}\sigma(\partial\eta_b/\partial\bar{y}) \quad \text{and} \quad \mathbf{e}_{\bar{3}} = -\hat{\mathbf{z}}\eta_b. \quad (1.22)$$

Notice how $\mathbf{e}_{\bar{3}}$ has physical dimensions of length, whereas $\mathbf{e}_{\bar{1}}$ and $\mathbf{e}_{\bar{2}}$ are non-dimensional. For the bottom slope oriented coordinate (1.15), with $\sigma = z - \mathbf{x} \cdot \nabla\eta_b$, we have $\eta = \sigma + \mathbf{x} \cdot \nabla\eta_b$ and the corresponding basis vectors

$$\mathbf{e}_{\bar{1}} = \hat{\mathbf{x}} + \hat{\mathbf{z}}(\partial\eta_b/\partial\bar{x}) \quad \text{and} \quad \mathbf{e}_{\bar{2}} = \hat{\mathbf{y}} + \hat{\mathbf{z}}(\partial\eta_b/\partial\bar{y}) \quad \text{and} \quad \mathbf{e}_{\bar{3}} = \hat{\mathbf{z}}. \quad (1.23)$$

1.5 Basis one-forms

In addition to basis vectors, we make use of *one-forms*, which are dual to vectors. The basis one-forms are obtained by transforming from Cartesian into **GVCs** through use of the inverse

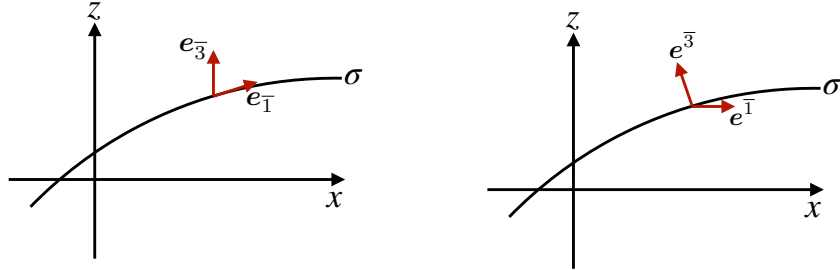


FIGURE 1.3: Illustrating the basis vectors (left panel) and basis one-forms (right panel) for generalized vertical coordinates. The $e_{\bar{3}}$ basis vector is vertical whereas $e_{\bar{1}}$ and $e_{\bar{2}}$ lie within the tangent plane to the σ surface. As a complement, the basis one-form, $e^{\bar{3}}$, is normal to the σ surface whereas the basis one-forms, $e^{\bar{1}}$ and $e^{\bar{2}}$, are horizontal.

transformation matrix

$$e^{\bar{a}} = \Lambda^{\bar{a}}_a e^a, \quad (1.24)$$

where the inverse transformation matrix takes the form

$$\Lambda^{\bar{a}}_a = \begin{bmatrix} \partial \bar{x} / \partial x & \partial \bar{x} / \partial y & \partial \bar{x} / \partial z \\ \partial \bar{y} / \partial x & \partial \bar{y} / \partial y & \partial \bar{y} / \partial z \\ \partial \sigma / \partial x & \partial \sigma / \partial y & \partial \sigma / \partial z \end{bmatrix} = \begin{bmatrix} 1 & 0 & 0 \\ 0 & 1 & 0 \\ \partial \sigma / \partial x & \partial \sigma / \partial y & \partial \sigma / \partial z \end{bmatrix}. \quad (1.25)$$

As for the transformation matrix (1.18), the unit diagonal values arise since a horizontal position in Cartesian and GVCs is the same and the horizontal directions are orthogonal. Likewise, $\partial \bar{x} / \partial z = \partial \bar{y} / \partial z = 0$ since the horizontal position on a GVC surface remains unchanged when moving across a depth surface. The nonzero values for $\partial \sigma / \partial x$, $\partial \sigma / \partial y$, and $\partial \sigma / \partial z$, arise in the presence of horizontal and vertical stratification of the generalized vertical coordinate.

1.5.1 More on the inverse transformation matrix

When computing elements of the inverse transformation matrix (1.25), it is crucial to ensure that the proper variables are held fixed. For example, consider the top row where we compute

$$\Lambda^{\bar{1}}_a = [[\partial \bar{x} / \partial x]_{y,z} \quad [\partial \bar{x} / \partial y]_{x,z} \quad [\partial \bar{x} / \partial z]_{x,y}]. \quad (1.26)$$

Just as for the transformation matrix (1.19), since $x = \bar{x}$, all but the first element vanish in equation (1.26). Namely, $[\partial \bar{x} / \partial y]_{x,z} = 0$ since the \bar{x} cannot change when x is fixed. The same idea holds for the \bar{y} row.

1.5.2 Basis one-forms

Use of the inverse transformation matrix (1.25) renders the spatial components of the GVC basis one-forms

$$e^{\bar{1}} = \hat{x} \quad (1.27a)$$

$$e^{\bar{2}} = \hat{y} \quad (1.27b)$$

$$e^{\bar{3}} = e^a \partial_a \sigma = \hat{x} (\partial \sigma / \partial x) + \hat{y} (\partial \sigma / \partial y) + \hat{z} (\partial \sigma / \partial z) = \nabla \sigma. \quad (1.27c)$$

The left panel of Figure 1.3 illustrates the basis one-forms.

As an example, consider again the rigid lid terrain following coordinate (1.10), $\sigma = -z/\eta_b$, in which case

$$\mathbf{e}^{\bar{3}} = \nabla\sigma = -(1/\eta_b) [\hat{\mathbf{z}} - (z/\eta_b) \nabla\eta_b]. \quad (1.28)$$

Similarly, the bottom slope oriented coordinate (1.15), with $\sigma = z - \mathbf{x} \cdot \nabla\eta_b$, has

$$\mathbf{e}^{\bar{3}} = \hat{\mathbf{z}} - \nabla\eta_b - \hat{\mathbf{x}} (\mathbf{x} \cdot \partial_x \nabla\eta_b) - \hat{\mathbf{y}} (\mathbf{x} \cdot \partial_y \nabla\eta_b) = \hat{\mathbf{z}} - \nabla\eta_b - (\mathbf{x} \cdot \nabla) \nabla\eta_b. \quad (1.29)$$

In the case where the bottom slope is constant in both directions then this result simplifies to

$$\mathbf{e}^{\bar{3}} = \hat{\mathbf{z}} - \nabla\eta_b. \quad (1.30)$$

1.5.3 Verifying the bi-orthogonality relation

The basis one-forms satisfy the bi-orthogonality relation with the basis vectors

$$\mathbf{e}^{\bar{a}} \cdot \mathbf{e}_{\bar{b}} = \delta^{\bar{a}}_{\bar{b}}. \quad (1.31)$$

This identity is trivial to verify for all $\bar{a} = 1, 2, 3$.

1.6 Triple product identities

We find various occasions to make use of a suite of triple product identities that hold for generalized vertical coordinates. For this purpose we write σ as a composite function

$$\sigma = \sigma(x, y, z, t) = \sigma[x, y, z(\bar{t}, \bar{x}, \bar{y}, \sigma), t], \quad (1.32)$$

with $\eta(\bar{x}, \bar{y}, \sigma, \bar{t})$ written as $z(\bar{x}, \bar{y}, \sigma, \bar{t})$ as it here eases the manipulations. Use of the chain rule leads to the space-time differential increment

$$d\sigma = dt \left[\frac{\partial \sigma}{\partial t} \right]_{x,y,z} + dx \left[\frac{\partial \sigma}{\partial x} \right]_{t,y,z} + dy \left[\frac{\partial \sigma}{\partial y} \right]_{t,x,z} + dz \left[\frac{\partial \sigma}{\partial z} \right]_{t,x,y}. \quad (1.33)$$

Likewise, writing $z = z[\bar{t}, \bar{x}, \bar{y}, \sigma]$ leads to the space-time differential increment dz

$$dz = d\bar{t} \left[\frac{\partial z}{\partial \bar{t}} \right]_{\bar{x}, \bar{y}, \sigma} + d\bar{x} \left[\frac{\partial z}{\partial \bar{x}} \right]_{\bar{t}, \bar{y}, \sigma} + d\bar{y} \left[\frac{\partial z}{\partial \bar{y}} \right]_{\bar{t}, \bar{x}, \sigma} + d\sigma \left[\frac{\partial z}{\partial \sigma} \right]_{\bar{t}, \bar{x}, \bar{y}}. \quad (1.34)$$

We note the identities

$$\left[\frac{\partial \sigma}{\partial z} \right]_{t,x,y} \left[\frac{\partial z}{\partial \sigma} \right]_{\bar{t}, \bar{x}, \bar{y}} = 1 \quad d\bar{t} = dt \quad d\bar{x} = dx \quad d\bar{y} = dy, \quad (1.35)$$

which follow since $t = \bar{t}$, $x = \bar{x}$, and $y = \bar{y}$. Substituting equation (1.34) into equation (1.33) and making use of the identities (1.35) yields

$$\begin{aligned} 0 = & dt \left[\left[\frac{\partial \sigma}{\partial t} \right]_{x,y,z} + \left[\frac{\partial \sigma}{\partial z} \right]_{t,x,y} \left[\frac{\partial z}{\partial \bar{t}} \right]_{\bar{x}, \bar{y}, \sigma} \right] \\ & + dx \left[\left[\frac{\partial \sigma}{\partial x} \right]_{t,y,z} + \left[\frac{\partial \sigma}{\partial z} \right]_{t,x,y} \left[\frac{\partial z}{\partial \bar{x}} \right]_{\bar{t}, \bar{y}, \sigma} \right] + dy \left[\left[\frac{\partial \sigma}{\partial y} \right]_{t,x,z} + \left[\frac{\partial \sigma}{\partial z} \right]_{t,x,y} \left[\frac{\partial z}{\partial \bar{y}} \right]_{\bar{t}, \bar{x}, \sigma} \right]. \end{aligned} \quad (1.36)$$

For this equation to hold with general increments dt , dx , and dy requires that each bracketed term vanish, which in turn leads to the following set of triple product identities

$$\left[\frac{\partial \sigma}{\partial z} \right]_{t,x,y} \left[\frac{\partial z}{\partial \bar{t}} \right]_{\bar{x},\bar{y},\sigma} = - \left[\frac{\partial \sigma}{\partial t} \right]_{x,y,z} \quad (1.37a)$$

$$\left[\frac{\partial \sigma}{\partial z} \right]_{t,x,y} \left[\frac{\partial z}{\partial \bar{x}} \right]_{\bar{t},\bar{y},\sigma} = - \left[\frac{\partial \sigma}{\partial x} \right]_{t,y,z} \quad (1.37b)$$

$$\left[\frac{\partial \sigma}{\partial z} \right]_{t,x,y} \left[\frac{\partial z}{\partial \bar{y}} \right]_{\bar{t},\bar{x},\sigma} = - \left[\frac{\partial \sigma}{\partial y} \right]_{t,x,z} \quad (1.37c)$$

If the vertical stratification, $\partial\sigma/\partial z$, is non-zero, the triple product identities are equivalent to

$$\left[\frac{\partial z}{\partial \bar{t}} \right]_{\bar{x},\bar{y},\sigma} = - \frac{[\partial\sigma/\partial t]_{x,y,z}}{[\partial\sigma/\partial z]_{t,x,y}} = - \left[\frac{\partial \sigma}{\partial t} \right]_{x,y,z} \left[\frac{\partial z}{\partial \sigma} \right]_{t,x,y} \quad (1.38a)$$

$$\left[\frac{\partial z}{\partial \bar{x}} \right]_{\bar{t},\bar{y},\sigma} = - \frac{[\partial\sigma/\partial x]_{t,y,z}}{[\partial\sigma/\partial z]_{t,x,y}} = - \left[\frac{\partial \sigma}{\partial x} \right]_{t,y,z} \left[\frac{\partial z}{\partial \sigma} \right]_{t,x,y} \quad (1.38b)$$

$$\left[\frac{\partial z}{\partial \bar{y}} \right]_{\bar{t},\bar{x},\sigma} = - \frac{[\partial\sigma/\partial y]_{t,x,z}}{[\partial\sigma/\partial z]_{t,x,y}} = - \left[\frac{\partial \sigma}{\partial y} \right]_{t,x,z} \left[\frac{\partial z}{\partial \sigma} \right]_{t,x,y} \quad (1.38c)$$

Since $t = \bar{t}$, $x = \bar{x}$, and $y = \bar{y}$ we can write these identities in the more succinct form

$$\left[\frac{\partial z}{\partial \bar{t}} \right]_{\sigma} = \left[\frac{\partial \eta}{\partial \bar{t}} \right]_{\sigma} = - \frac{[\partial\sigma/\partial t]_z}{[\partial\sigma/\partial z]} \quad (1.39a)$$

$$\left[\frac{\partial z}{\partial \bar{x}} \right]_{\sigma} = \left[\frac{\partial \eta}{\partial \bar{x}} \right]_{\sigma} = - \frac{[\partial\sigma/\partial x]_z}{[\partial\sigma/\partial z]} \quad (1.39b)$$

$$\left[\frac{\partial z}{\partial \bar{y}} \right]_{\sigma} = \left[\frac{\partial \eta}{\partial \bar{y}} \right]_{\sigma} = - \frac{[\partial\sigma/\partial y]_z}{[\partial\sigma/\partial z]}, \quad (1.39c)$$

where we reintroduced the notation $\eta(x, y, \sigma, t) = z(x, y, \sigma, t)$. These identities are quite useful for manipulating equations involving GVCs. In particular, equations (1.39b) and (1.39c) provide alternate expressions for the slope of σ isosurfaces relative to the horizontal plane (see Section 1.12).

1.7 Position of a point in space

We are familiar with locating a point in space using Cartesian coordinates. We can also specify the position using generalized vertical coordinates by making use of the basis vectors (1.20a)-(1.20c)

$$\mathcal{P} = \xi^{\bar{a}} e_{\bar{a}} \quad (1.40a)$$

$$= \bar{x} [\hat{\mathbf{x}} + (\partial\eta/\partial\bar{x}) \hat{\mathbf{z}}] + \bar{y} [\hat{\mathbf{y}} + (\partial\eta/\partial\bar{y}) \hat{\mathbf{z}}] + \sigma (\partial\eta/\partial\sigma) \hat{\mathbf{z}} \quad (1.40b)$$

$$= \hat{\mathbf{x}} \bar{x} + \hat{\mathbf{y}} \bar{y} + \hat{\mathbf{z}} [\bar{x} (\partial\eta/\partial\bar{x}) + \bar{y} (\partial\eta/\partial\bar{y}) + \sigma (\partial\eta/\partial\sigma)] \quad (1.40c)$$

$$= \hat{\mathbf{x}} \bar{x} + \hat{\mathbf{y}} \bar{y} + \hat{\mathbf{z}} \xi^{\bar{a}} \partial_{\bar{a}} \eta. \quad (1.40d)$$

We identify the following properties as a means to help understand these expressions, with Figure 1.4 offering a schematic.

- The expression (1.40b) has horizontal positions, \bar{x} and \bar{y} , multiplying the basis vectors, $e_{\bar{x}}$

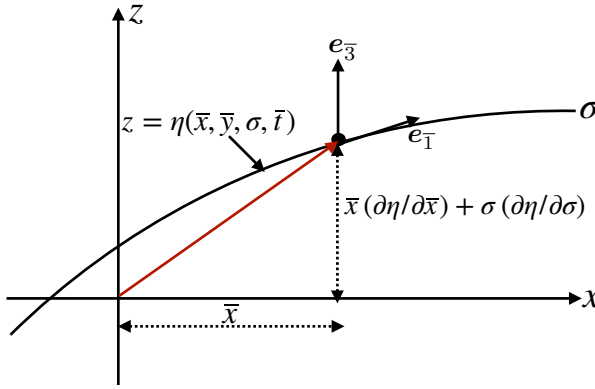


FIGURE 1.4: The position of a point in space as represented using a generalized vertical coordinate following equation (1.41a). For this example, $\bar{y} = 0$ so that the horizontal position is determined by the coordinate $\bar{x} = x$, whereas the vertical position is determined by $\bar{x}(\partial z / \partial \bar{x}) + \sigma(\partial z / \partial \sigma) = \bar{x}(\partial \eta / \partial \bar{x}) + \sigma(\partial \eta / \partial \sigma)$.

and $e_{\bar{y}}$, with these vectors tangent to a surface of constant generalized vertical coordinate (σ -surface) as in Figure 1.4. Likewise, the third term, $\sigma(\partial \eta / \partial \sigma) \hat{z}$, positions the point vertically according to the value of σ , along with its inverse stratification, $\partial \eta / \partial \sigma = \partial z / \partial \sigma$.

- Consider the case of $y = \bar{y} = 0$ so that the position is given by

$$\mathcal{P} = \bar{x} \hat{x} + \hat{z} [\bar{x}(\partial \eta / \partial \bar{x}) + \sigma(\partial \eta / \partial \sigma)] \quad (1.41a)$$

$$= \bar{x} \hat{x} + \hat{z} (\partial \eta / \partial \sigma) [\bar{x}(\partial \sigma / \partial z)_x (\partial \eta / \partial \bar{x})_\sigma + \sigma] \quad (1.41b)$$

$$= \bar{x} \hat{x} + \hat{z} (\partial \eta / \partial \sigma) [-\bar{x}(\partial \sigma / \partial x)_z + \sigma], \quad (1.41c)$$

where we used the triple product identity (1.39b) for the final equality. Consequently, a horizontal position vector is realized using generalized vertical coordinates with $\sigma = \bar{x}(\partial \sigma / \partial x)$. That is, a horizontal position vector crosses surfaces of constant generalized vertical coordinate when the σ -surface has a nonzero horizontal slope.

- The projection of the position vector onto the basis one-forms leads to

$$\mathcal{P} \cdot e^{\bar{b}} = \xi^{\bar{a}} e_{\bar{a}} \cdot e^{\bar{b}} = \xi^{\bar{b}}. \quad (1.42)$$

This result follows from the bi-orthogonality relation (1.31). So the projection of the position vector onto a basis one-form picks out the corresponding coordinate value.

- Equation (1.7) provides the spatial dependence for the vertical position of the surface of constant generalized vertical coordinate

$$z = z(\xi^{\bar{a}}) = \eta(\xi^{\bar{a}}). \quad (1.43)$$

At any particular time instance we can perform a Taylor series about a reference geopotential $z_0 = \eta_0$, so that

$$\eta(\xi^{\bar{a}}) \approx \eta_0 + \xi^{\bar{a}} \partial_{\bar{a}} \eta. \quad (1.44)$$

We can thus write the position (1.40d) in the form

$$\mathcal{P} = \hat{x} \bar{x} + \hat{y} \bar{y} + \hat{z} [\eta - \eta_0]. \quad (1.45)$$

Taking the reference geopotential as $\eta_0 = 0$ recovers the Cartesian expression. Since

the position vector is a geometric object, it is reassuring that the generalized vertical coordinate representation is the same as the Cartesian representation; it is merely a reorganization of the basis vectors and corresponding coordinates.

1.8 Transforming components of a vector

Consider a vector field, \mathbf{F} , with Cartesian representation

$$\mathbf{F} = F^a \mathbf{e}_a = F^x \hat{\mathbf{x}} + F^y \hat{\mathbf{y}} + F^z \hat{\mathbf{z}}. \quad (1.46)$$

The corresponding generalized vertical coordinate components are related through the transformation matrix

$$F^{\bar{a}} = \Lambda^{\bar{a}}_a F^a. \quad (1.47)$$

Making use of the transformation matrix (1.25) yields the relations between **GVC** components and Cartesian components

$$F^{\bar{1}} = F^1 \quad \text{and} \quad F^{\bar{2}} = F^2 \quad \text{and} \quad F^{\bar{3}} = \nabla \sigma \cdot \mathbf{F}, \quad (1.48)$$

where we wrote

$$\nabla \sigma \cdot \mathbf{F} = (\partial \sigma / \partial x) F^1 + (\partial \sigma / \partial y) F^2 + (\partial \sigma / \partial z) F^3. \quad (1.49)$$

The vector field thus can be represented in generalized vertical coordinates as

$$\mathbf{F} = F^{\bar{a}} \mathbf{e}_{\bar{a}} = F^1 \mathbf{e}_{\bar{1}} + F^2 \mathbf{e}_{\bar{2}} + (\nabla \sigma \cdot \mathbf{F}) \mathbf{e}_{\bar{3}}. \quad (1.50)$$

Similarly, the covariant components transform as $F_{\bar{a}} = \Lambda^a_{\bar{a}} F_a$, where use of the inverse transformation matrix (1.25) renders

$$F_{\bar{1}} = F_1 + (\partial z / \partial \bar{x}) F_3 = F_1 + (\partial \eta / \partial \bar{x}) F_3 \quad (1.51a)$$

$$F_{\bar{2}} = F_2 + (\partial z / \partial \bar{y}) F_3 = F_2 + (\partial \eta / \partial \bar{y}) F_3 \quad (1.51b)$$

$$F_{\bar{3}} = (\partial z / \partial \sigma) F_3 = (\partial \eta / \partial \sigma) F_3, \quad (1.51c)$$

and the expression for the vector field

$$\mathbf{F} = F_{\bar{a}} \mathbf{e}^{\bar{a}} = [F_1 + (\partial \eta / \partial \bar{x}) F_3] \mathbf{e}^{\bar{1}} + [F_2 + (\partial \eta / \partial \bar{y}) F_3] \mathbf{e}^{\bar{2}} + (\partial \eta / \partial \sigma) F_3 \mathbf{e}^{\bar{3}}. \quad (1.52)$$

Recall also that for Cartesian coordinates the contravariant and covariant components to a vector are identical: $F^a = F_a$.

1.9 Representing the velocity vector

As an example of the results from Section 1.8, we here represent the velocity vector, \mathbf{v} , considering both covariant and contravariant representations. As for the position of a point in space as detailed in Section 1.7, we are assured that both the Cartesian and **GVC** representations lead to the same velocity vector since the velocity is an objective geometric object. In Section 1.9.4 we verify that the transformation formalism indeed respects this equivalence, with the **GVC** representation equivalent to the Cartesian representation

$$\mathbf{v} = u \hat{\mathbf{x}} + v \hat{\mathbf{y}} + w \hat{\mathbf{z}}. \quad (1.53)$$

1.9.1 Contravariant components

Following Section 1.8, we have the contravariant velocity components using generalized vertical coordinates

$$v^{\bar{1}} = u \quad \text{and} \quad v^{\bar{2}} = v \quad \text{and} \quad v^{\bar{3}} = v^a \partial_a \sigma = \mathbf{v} \cdot \nabla \sigma. \quad (1.54)$$

Use of the basis vectors (1.20a)-(1.20c) then leads to

$$\mathbf{v} = v^{\bar{a}} \mathbf{e}_{\bar{a}} \quad (1.55a)$$

$$= u \mathbf{e}_{\bar{x}} + v \mathbf{e}_{\bar{y}} + (v^a \partial_a \sigma) \mathbf{e}_{\sigma} \quad (1.55b)$$

$$= u [\hat{\mathbf{x}} + (\partial \eta / \partial \bar{x}) \hat{\mathbf{z}}] + v [\hat{\mathbf{y}} + (\partial \eta / \partial \bar{y}) \hat{\mathbf{z}}] + (\mathbf{v} \cdot \nabla \sigma) (\partial \eta / \partial \sigma) \hat{\mathbf{z}}. \quad (1.55c)$$

We emphasize that the contravariant representation of the horizontal velocity is the same for both geopotential vertical coordinates and generalized vertical coordinates. This fundamental property is often missed in the literature.

1.9.2 Covariant components

The covariant velocity components are given by

$$v_{\bar{1}} = u + (\partial \eta / \partial \bar{x}) w \quad \text{and} \quad v_{\bar{2}} = v + (\partial \eta / \partial \bar{y}) w \quad \text{and} \quad v_{\bar{3}} = (\partial \eta / \partial \sigma) w. \quad (1.56)$$

The one-form basis (1.27a)–(1.27c) thus leads to the velocity vector

$$\mathbf{v} = v_{\bar{a}} \mathbf{e}^{\bar{a}} = [u + (\partial \eta / \partial \bar{x}) w] \hat{\mathbf{x}} + [v + (\partial \eta / \partial \bar{y}) w] \hat{\mathbf{y}} + w (\partial \eta / \partial \sigma) \nabla \sigma. \quad (1.57)$$

1.9.3 Introducing the material time derivative

The material time derivative of the generalized vertical coordinate is

$$\frac{D\sigma}{Dt} = \frac{\partial \sigma}{\partial t} + \mathbf{v} \cdot \nabla \sigma = \dot{\sigma}, \quad (1.58)$$

with $\dot{\sigma}$ symbolizing any process contributing to motion across σ isosurfaces (as fully explained in Section 2.4). Using the expression (1.58) in the velocity vector expression (1.55c) leads to

$$\mathbf{v} = u [\hat{\mathbf{x}} + (\partial \eta / \partial \bar{x}) \hat{\mathbf{z}}] + v [\hat{\mathbf{y}} + (\partial \eta / \partial \bar{y}) \hat{\mathbf{z}}] + (\mathbf{v} \cdot \nabla \sigma) (\partial \eta / \partial \sigma) \hat{\mathbf{z}} \quad (1.59a)$$

$$= u [\hat{\mathbf{x}} + (\partial \eta / \partial \bar{x}) \hat{\mathbf{z}}] + v [\hat{\mathbf{y}} + (\partial \eta / \partial \bar{y}) \hat{\mathbf{z}}] + (\dot{\sigma} - \partial \sigma / \partial t) (\partial \eta / \partial \sigma) \hat{\mathbf{z}} \quad (1.59b)$$

$$= u \hat{\mathbf{x}} + v \hat{\mathbf{y}} + [\partial \eta / \partial \bar{t} + \mathbf{u} \cdot \nabla_{\sigma} z + (\partial \eta / \partial \sigma) \dot{\sigma}] \hat{\mathbf{z}}, \quad (1.59c)$$

where the final equality made use of the triple product (1.38a): $(\partial \sigma / \partial t) (\partial \eta / \partial \sigma) = -\partial \eta / \partial \bar{t}$. In the steady state and in the absence of material changes to σ , the three dimensional flow lies within a surface of constant σ , whereby $\mathbf{v} \cdot \nabla \sigma = 0$ and

$$\mathbf{v} = u [\hat{\mathbf{x}} + (\partial \eta / \partial \bar{x}) \hat{\mathbf{z}}] + v [\hat{\mathbf{y}} + (\partial \eta / \partial \bar{y}) \hat{\mathbf{z}}] \quad \text{if } \partial_t \sigma = 0 \text{ and } \dot{\sigma} = 0. \quad (1.60)$$

However, in general there are transient fluctuations and material changes so that $\mathbf{v} \cdot \nabla \sigma \neq 0$.

1.9.4 Equivalence to the Cartesian velocity representation

Use of the triple product identities (1.39b)-(1.39c) allows us to manipulate both expressions (1.55c) and (1.57) to recover the Cartesian expression

$$\mathbf{v} = u \hat{\mathbf{x}} + v \hat{\mathbf{y}} + w \hat{\mathbf{z}}. \quad (1.61)$$

Another way to see this identity is to note that in equation (1.59c), the vertical component is an expression for the material time derivative of the vertical position

$$w = \frac{Dz}{Dt} = \frac{\partial \eta}{\partial t} + \mathbf{u} \cdot \nabla_{\mathbf{r}} \eta + \frac{\partial \eta}{\partial \sigma} \dot{\sigma}. \quad (1.62)$$

We derive this identity in Section 2.5 where we discuss further kinematic results using generalized vertical coordinates.

1.10 Metric tensor using generalized vertical coordinates

The metric tensor provides the means to measure the distance between two points in space. One can represent the metric using any variety of coordinates, and here we examine its representation using generalized vertical coordinates. We are interested in two metric tensors, one for points living in three dimensional Euclidean space and the second for points restricted to a particular surface of constant generalized vertical coordinate.

1.10.1 Representation of the metric tensor and its inverse

For three dimensional Euclidean space, the generalized vertical coordinate representation of the metric tensor is given by

$$g_{\bar{a}\bar{b}} = \mathbf{e}_{\bar{a}} \cdot \mathbf{e}_{\bar{b}} = \begin{bmatrix} 1 + (\partial z / \partial \bar{x})^2 & (\partial z / \partial \bar{x})(\partial z / \partial \bar{y}) & (\partial z / \partial \bar{x})(\partial z / \partial \sigma) \\ (\partial z / \partial \bar{x})(\partial z / \partial \bar{y}) & 1 + (\partial z / \partial \bar{y})^2 & (\partial z / \partial \bar{y})(\partial z / \partial \sigma) \\ (\partial z / \partial \bar{x})(\partial z / \partial \sigma) & (\partial z / \partial \bar{y})(\partial z / \partial \sigma) & (\partial z / \partial \sigma)^2 \end{bmatrix}, \quad (1.63)$$

with the triple product identities (1.39b) and (1.39c) bringing the metric tensor into the form

$$g_{\bar{a}\bar{b}} = \begin{bmatrix} 1 + [(\partial \sigma / \partial x)(\partial z / \partial \sigma)]^2 & (\partial \sigma / \partial x)(\partial \sigma / \partial y)(\partial z / \partial \sigma)^2 & -(\partial \sigma / \partial x)(\partial z / \partial \sigma)^2 \\ (\partial \sigma / \partial x)(\partial \sigma / \partial y)(\partial z / \partial \sigma)^2 & 1 + [(\partial \sigma / \partial y)(\partial z / \partial \sigma)]^2 & -(\partial \sigma / \partial y)(\partial z / \partial \sigma)^2 \\ -(\partial \sigma / \partial x)(\partial z / \partial \sigma)^2 & -(\partial \sigma / \partial y)(\partial z / \partial \sigma)^2 & (\partial z / \partial \sigma)^2 \end{bmatrix}. \quad (1.64)$$

The representation of the inverse metric tensor is given by the somewhat simpler expression

$$g^{\bar{a}\bar{b}} = \mathbf{e}^{\bar{a}} \cdot \mathbf{e}^{\bar{b}} = \begin{bmatrix} 1 & 0 & \partial \sigma / \partial x \\ 0 & 1 & \partial \sigma / \partial y \\ \partial \sigma / \partial x & \partial \sigma / \partial y & |\nabla \sigma|^2 \end{bmatrix}, \quad (1.65)$$

where we used the basis one-forms given by equations (1.27a)-(1.27c). Proof that

$$g^{\bar{a}\bar{b}} g_{\bar{b}\bar{c}} = \delta^{\bar{a}}_{\bar{c}} \quad (1.66)$$

requires use of the triple product identities (1.39b) and (1.39c). Note that an additional means to derive the metric tensor (1.63) is given by writing the squared line element as⁴

$$ds^2 = dx^2 + dy^2 + dz^2 \quad (1.67a)$$

$$= dx^2 + dy^2 + [(\partial z / \partial \bar{x}) dx + (\partial z / \partial \bar{y}) dy + (\partial z / \partial \sigma) d\sigma]^2, \quad (1.67b)$$

from which the metric tensor (1.63) is revealed upon expanding the quadratic term and then rearranging.

1.10.2 Jacobian of transformation

The determinant of the generalized vertical coordinate representation of the three-dimensional metric tensor (1.63) is

$$\det(g_{\bar{a}\bar{b}}) = (\partial z / \partial \sigma)^2 = (\partial \eta / \partial \sigma)^2, \quad (1.68)$$

so that the Jacobian of transformation is the *specific thickness*

$$\frac{\partial(x, y, z)}{\partial(\bar{x}, \bar{y}, \sigma)} = \frac{\partial z}{\partial \sigma} = \frac{\partial \eta}{\partial \sigma}. \quad (1.69)$$

The coordinate transformation from Cartesian coordinates to generalized vertical coordinates is invertible only so long as the Jacobian remains nonzero and single-signed, meaning the fluid retains a monotonic vertical stratification of the σ -surfaces. The invertible relation between z and σ means that each point in the vertical can be uniquely specified by either of the two vertical coordinates. For example, using pressure as the generalized vertical coordinate in a hydrostatic fluid yields the Jacobian

$$\frac{\partial z}{\partial \sigma} = \frac{\partial z}{\partial p} = -\frac{1}{\rho g}, \quad (1.70)$$

which is indeed single-signed since the gravitational acceleration, $g > 0$, and the mass density is also positive, $\rho > 0$.

1.10.3 Covariant and contravariant representations

In addition to providing the means to measure distances between two points in space, the metric tensor allows us to convert between the covariant and contravariant representations of a tensor; i.e., to raise and lower tensor indices. For a vector we have the identity

$$F_{\bar{a}} = g_{\bar{a}\bar{b}} F^{\bar{b}}. \quad (1.71)$$

Through the metric tensor, we are afforded the ability to work with either the covariant or contravariant representation of a tensor as determined by convenience.

⁴The traditional notation in physics writes the squared line element as $ds^2 = (ds)^2$. Likewise, $dx^2 = (dx)^2$, etc.

1.10.4 Metric tensor for points living on a constant σ -surface

In some cases we are interested in describing motion restricted to a constant σ -surface, with points on this surface determined by

$$\sigma(x, y, z) = \sigma_0, \quad (1.72)$$

for some constant, σ_0 . Taking the differential of this identity leads to

$$d\sigma = 0 = (\partial_a \sigma) dx^a. \quad (1.73)$$

Introducing the slope of the σ -surface relative to the horizontal plane (recall that $\partial_z \sigma \neq 0$)

$$S = \nabla_{\mathbf{v}} z = -\nabla_h \sigma / \partial_z \sigma, \quad (1.74)$$

allows us to eliminate the vertical increment via

$$dz = S_x dx + S_y dy. \quad (1.75)$$

This identity provides the vertical distance between two infinitesimally close points that live on a constant σ -surface.

To find the metric tensor we write the distance in three dimensional space between two infinitesimally close points that live a constant σ -surface

$$d\mathbf{x} \cdot d\mathbf{x} = dx^a \delta_{ab} dx^b \quad (1.76a)$$

$$= (dx)^2 + (dy)^2 + (S_x dx + S_y dy)^2 \quad (1.76b)$$

$$= (dx \quad dy) \begin{pmatrix} 1 + S_x^2 & S_x S_y \\ S_x S_y & 1 + S_y^2 \end{pmatrix} \begin{pmatrix} dx \\ dy \end{pmatrix}, \quad (1.76c)$$

which then leads to the metric tensor

$$\tilde{g}_{ab} = \begin{pmatrix} 1 + S_x^2 & S_x S_y \\ S_x S_y & 1 + S_y^2 \end{pmatrix}, \quad (1.77)$$

where the tensor labels extend over $a, b = 1, 2$. It is straightforward to show that the inverse metric is given by

$$\tilde{g}^{ab} = \frac{1}{1 + S_x^2 + S_y^2} \begin{pmatrix} 1 + S_y^2 & -S_x S_y \\ -S_x S_y & 1 + S_x^2 \end{pmatrix}. \quad (1.78)$$

1.11 Volume element and the Levi-Civita tensor

As noted in Section 1.10.2, when represented using generalized vertical coordinates, the square root of the metric tensor determinant (1.63) provides the Jacobian of transformation

$$\sqrt{\det(g_{\bar{a}\bar{b}})} = \partial z / \partial \sigma = \partial \eta / \partial \sigma. \quad (1.79)$$

In turn, the volume element is

$$dV = dx dy dz = (\partial z / \partial \sigma) dx dy d\sigma. \quad (1.80)$$

The covariant Levi-Civita tensor has the representation using generalized vertical coordinates

$$\varepsilon_{\bar{a}\bar{b}\bar{c}} = (\partial z / \partial \sigma) \epsilon_{\bar{a}\bar{b}\bar{c}} \quad \varepsilon^{\bar{a}\bar{b}\bar{c}} = (\partial z / \partial \sigma)^{-1} \epsilon^{\bar{a}\bar{b}\bar{c}}, \quad (1.81)$$

where ϵ is the permutation symbol with its components independent of coordinate representation.

1.12 Partial derivative operators

We here consider the partial derivative operators and their transformation between coordinate systems. These identities are used throughout GVC calculus. Given the importance of these expressions, we offer two derivations, with the geometric derivation in Section 1.12.2 requiring minimal use of tensor formalism.

1.12.1 Analytical derivation

The partial derivative operators in generalized vertical coordinates is determined via $\partial_{\bar{a}} = \Lambda^a_{\bar{a}} \partial_a$. Including also the time derivative leads to the relations

$$\partial_{\bar{t}} = \partial_t + (\partial z / \partial \bar{t}) \partial_z = \partial_t + (\partial \eta / \partial \bar{t}) \partial_z \quad (1.82a)$$

$$\partial_{\bar{x}} = \partial_x + (\partial z / \partial \bar{x}) \partial_z = \partial_x + (\partial \eta / \partial \bar{x}) \partial_z \quad (1.82b)$$

$$\partial_{\bar{y}} = \partial_y + (\partial z / \partial \bar{y}) \partial_z = \partial_y + (\partial \eta / \partial \bar{y}) \partial_z \quad (1.82c)$$

$$\partial_{\sigma} = (\partial z / \partial \sigma) \partial_z = (\partial \eta / \partial \sigma) \partial_z. \quad (1.82d)$$

We can make use of the triple product identities (1.39b) and (1.39c) to express the slope of a constant GVC surface in the equivalent manners

$$\mathbf{S} = \nabla_{\sigma} \eta = \nabla_{\sigma} z = -(\partial \sigma / \partial z)^{-1} \nabla_z \sigma \quad (1.83)$$

where we introduced the standard shorthand notation

$$\nabla_{\sigma} = \hat{\mathbf{x}} \partial / \partial \bar{x} + \hat{\mathbf{y}} \partial / \partial \bar{y} \quad \text{and} \quad \nabla_z = \hat{\mathbf{x}} \partial / \partial x + \hat{\mathbf{y}} \partial / \partial y. \quad (1.84)$$

It is common to transform between the horizontal gradient operators, in which case we write

$$\nabla_{\sigma} = \nabla_z + (\nabla_z z) \partial_z \equiv \nabla_z + \mathbf{S} \partial_z. \quad (1.85)$$

We emphasize that ∇_{σ} is merely a shorthand for the two partial derivative operators and that it only has components in the horizontal directions. Furthermore, the σ subscript is not a tensor index.

1.12.2 Geometrical derivation

We now complement the previous analytical derivation of the lateral derivative operator by offering a geometric derivation. As we see, this operator is computed by taking the difference of a function along surfaces of constant generalized vertical coordinate, but with the lateral distance computed in the horizontal direction as shown in Figure 1.5. This particular feature of the horizontal derivative operator is a key aspect of the non-orthogonality property of generalized vertical coordinates.

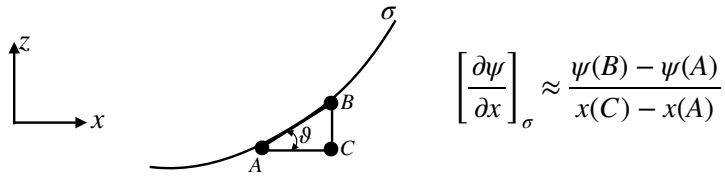


FIGURE 1.5: A surface of constant generalized vertical coordinate, σ , along with a local tangent plane with a slope $\tan \vartheta$ with respect to the horizontal plane. This figure illustrates the identities (1.87a)-(1.87d), with these identities relating a lateral derivative taken along the GVC surface to horizontal and vertical derivatives taken along orthogonal Cartesian axes.

Consider the geometry shown in Figure 1.5, which shows a generalized vertical coordinate surface (constant σ surface) along with a sample tangent plane with a slope

$$S^x = \frac{\text{rise}}{\text{run}} = \tan \vartheta = \frac{z(B) - z(C)}{x(C) - x(A)} \approx \left[\frac{\partial z}{\partial x} \right]_{\sigma} = -\frac{(\partial \sigma / \partial x)_z}{(\partial \sigma / \partial z)} \quad (1.86)$$

relative to the horizontal. We readily verify the following identities based on finite difference operations for an arbitrary function

$$\left[\frac{\partial \psi}{\partial x} \right]_{\sigma} \approx \frac{\psi(B) - \psi(A)}{x(C) - x(A)} \quad (1.87a)$$

$$= \frac{\psi(C) - \psi(A)}{x(C) - x(A)} + \frac{\psi(B) - \psi(C)}{x(C) - x(A)} \quad (1.87b)$$

$$= \frac{\psi(C) - \psi(A)}{x(C) - x(A)} + \left[\frac{z(B) - z(C)}{x(C) - x(A)} \right] \frac{\psi(B) - \psi(C)}{z(B) - z(C)} \quad (1.87c)$$

$$= \left[\frac{\partial \psi}{\partial x} \right]_z + S^x \left[\frac{\partial \psi}{\partial z} \right]_x. \quad (1.87d)$$

Taking the continuum limit then leads to the relations between horizontal derivatives computed on constant σ surfaces to those computed on constant z surfaces

$$\left[\frac{\partial}{\partial x} \right]_{\sigma} = \left[\frac{\partial}{\partial x} \right]_z + \left[\frac{\partial z}{\partial x} \right]_{\sigma} \frac{\partial}{\partial z} = \left[\frac{\partial}{\partial x} \right]_z + \left[\frac{\partial \eta}{\partial x} \right]_{\sigma} \frac{\partial}{\partial z} \quad (1.88a)$$

$$\left[\frac{\partial}{\partial y} \right]_{\sigma} = \left[\frac{\partial}{\partial y} \right]_z + \left[\frac{\partial z}{\partial y} \right]_{\sigma} \frac{\partial}{\partial z} = \left[\frac{\partial}{\partial y} \right]_z + \left[\frac{\partial \eta}{\partial y} \right]_{\sigma} \frac{\partial}{\partial z}, \quad (1.88b)$$

which can be written in the shorthand vector notation

$$\nabla_{\text{hr}} = \hat{x} \left[\frac{\partial}{\partial x} \right]_{\sigma} + \hat{y} \left[\frac{\partial}{\partial y} \right]_{\sigma} = \nabla_h + (\nabla_{\text{hr}} z) \partial_z = \nabla_h + (\nabla_{\text{hr}} \eta) \partial_z. \quad (1.89)$$

1.12.3 The gradient as a tensor operator

The gradient is given by the equivalent expressions

$$\nabla = e^a \partial_a = e^{\bar{a}} \partial_{\bar{a}}. \quad (1.90)$$

The gradient has the following Cartesian coordinate expression

$$\nabla = \hat{x} \partial_x + \hat{y} \partial_y + \hat{z} \partial_z, \quad (1.91)$$

and the equivalent generalized vertical coordinate expression

$$\nabla = \hat{\mathbf{x}} \partial_{\bar{x}} + \hat{\mathbf{y}} \partial_{\bar{y}} + (\nabla \sigma) \partial_{\sigma}. \quad (1.92)$$

In Exercise 1.3 we verify the equality between equations (1.91) and (1.92) by making use of equations (1.82b)-(1.82d) for the partial derivatives and equations (1.27a)-(1.27c) for the one-form basis.

1.13 Material time derivative

Making use of the relations for the partial derivative operators in Section 1.12 allows us to write the material time derivative in the following equivalent forms

$$\frac{D}{Dt} = \left[\frac{\partial}{\partial t} \right]_z + \mathbf{u} \cdot \nabla_h + w \frac{\partial}{\partial z} \quad (1.93a)$$

$$= \left[\frac{\partial}{\partial t} \right]_{\sigma} - (\partial \eta / \partial \bar{t}) \partial_z + \mathbf{u} \cdot [\nabla_{\sigma} - (\nabla_{\sigma} \eta) \partial_z] + w \partial / \partial z \quad (1.93b)$$

$$= \left[\frac{\partial}{\partial t} \right]_{\sigma} + \mathbf{u} \cdot \nabla_{\sigma} + [w - \mathbf{u} \cdot \nabla_{\sigma} \eta - \partial \eta / \partial \bar{t}] (\partial \sigma / \partial z) \partial / \partial \sigma \quad (1.93c)$$

$$= \left[\frac{\partial}{\partial t} \right]_{\sigma} + \mathbf{u} \cdot \nabla_{\sigma} + \frac{D\sigma}{Dt} \frac{\partial}{\partial \sigma} \quad (1.93d)$$

$$= \left[\frac{\partial}{\partial t} \right]_{\sigma} + \mathbf{u} \cdot \nabla_{\sigma} + \frac{\partial z}{\partial \sigma} \frac{D\sigma}{Dt} \frac{\partial}{\partial z}. \quad (1.93e)$$

The equality (1.93d) made use of the identity (1.62), which is itself derived in Section 2.5 where we discuss further kinematic results using generalized vertical coordinates. Besides differences in the spatial operators, it is important to note that the time derivative operators are computed on constant geopotential surfaces and constant σ -surfaces, respectively. However, the horizontal velocity component is the *same* for both forms of the material time derivative

$$(u, v) = \frac{D(x, y)}{Dt}. \quad (1.94)$$

1.14 Divergence of a vector and the divergence theorem

Making use of the general expression from VOLUME 1 for the covariant divergence of a vector renders the generalized vertical coordinate expression

$$\nabla_{\bar{a}} F^{\bar{a}} = [\det(g_{\bar{a}\bar{b}})]^{-1/2} \partial_{\bar{a}} \left[[\det(g_{\bar{a}\bar{b}})]^{1/2} F^{\bar{a}} \right] = (\partial z / \partial \sigma)^{-1} \partial_{\bar{a}} [(\partial z / \partial \sigma) F^{\bar{a}}]. \quad (1.95)$$

Recall that the GVC vector components, $F^{\bar{a}}$, are related to the Cartesian components in equation (1.48), and the GVC components of the partial derivative operator, $\partial_{\bar{a}}$, are related to the Cartesian operator in equation (1.84).

When making use of the [divergence theorem](#), we require the product of the volume element and the covariant divergence. For generalized vertical coordinates we make use of the volume element (1.80) so that

$$(\nabla_{\bar{a}} F^{\bar{a}}) dV = \partial_{\bar{a}} [(\partial z / \partial \sigma) F^{\bar{a}}] d\bar{x} d\bar{y} d\sigma, \quad (1.96)$$

which reduces to a boundary integral when integrating over a volume.

1.15 The diffusion operator

As an explicit example of the covariant divergence operator (1.95), we here consider the diffusion operator discussed in Chapter 5. The derivation here recovers much of what we just discussed in Section 1.14, yet we make use of a bit less tensor formalism though at the cost of more algebra.

1.15.1 Continuous expression

The diffusion operator is the convergence of the diffusive flux

$$\mathcal{R} = -\nabla \cdot \mathbf{J}, \quad (1.97)$$

where \mathbf{J} is the tracer flux vector. We here convert the pieces of this operator from Cartesian coordinates into generalized vertical coordinates, making use of the transformation of partial derivative operators given in Section 1.12. Also, we make use of the shorthand $z(x, y, \sigma, t)$ rather than $\eta(x, y, \sigma, t)$

$$-\mathcal{R} = \nabla \cdot \mathbf{J} \quad (1.98a)$$

$$= \nabla_h \cdot \mathbf{J}^h + \partial_z J^z \quad (1.98b)$$

$$= (\nabla_{\sigma} - \nabla_{\sigma} z \partial_z) \cdot \mathbf{J}^h + (\sigma_z) \partial_{\sigma} J^z \quad (1.98c)$$

$$= \sigma_z [z_{\sigma} \nabla_{\sigma} \cdot \mathbf{J}^h + (\hat{z} \partial_{\sigma} - \nabla_{\sigma} z \partial_{\sigma}) \cdot \mathbf{J}] \quad (1.98d)$$

$$= \sigma_z [\nabla_{\sigma} \cdot (z_{\sigma} \mathbf{J}^h) - \mathbf{J}^h \cdot \nabla_{\sigma} (z_{\sigma}) + \partial_{\sigma} J^z - \partial_{\sigma} (\nabla_{\sigma} z \cdot \mathbf{J}) + \mathbf{J} \cdot \partial_{\sigma} (\nabla_{\sigma} z)] \quad (1.98e)$$

$$= \sigma_z [\nabla_{\sigma} \cdot (z_{\sigma} \mathbf{J}^h) + \partial_{\sigma} J^z - \partial_{\sigma} (\nabla_{\sigma} z \cdot \mathbf{J}^h)] \quad (1.98f)$$

$$= \sigma_z (\nabla_{\sigma} \cdot (\partial_{\sigma} z \mathbf{J}^h) + \partial_{\sigma} [(\hat{z} - \nabla_{\sigma} z) \cdot \mathbf{J}]) \quad (1.98g)$$

$$= \sigma_z [\nabla_{\sigma} \cdot (z_{\sigma} \mathbf{J}^h) + \partial_{\sigma} (z_{\sigma} \nabla \sigma \cdot \mathbf{J})], \quad (1.98h)$$

where we used

$$z_{\sigma} \nabla \sigma = \hat{z} - \nabla_{\sigma} z \quad (1.99)$$

to reach the final equality, and made use of the shorthand

$$z_{\sigma} = \partial z / \partial \sigma \quad \text{and} \quad \sigma_z = \partial \sigma / \partial z = (z_{\sigma})^{-1}. \quad (1.100)$$

The coordinate transformations in Section 1.8 for vector components reveal that the expression (1.98h) is identical to equation (1.95) derived using formal tensor methods. Likewise, multiplying by the volume element

$$dV = dx dy dz = dx dy z_{\sigma} d\sigma, \quad (1.101)$$

leads to

$$-\mathcal{R} dV = [\nabla_{\sigma} \cdot (z_{\sigma} \mathbf{J}^h) + \partial_{\sigma} (z_{\sigma} \nabla \sigma \cdot \mathbf{J})] dx dy d\sigma, \quad (1.102)$$

which is identical to the expression (1.96).

1.15.2 Layer thickness weighted diffusion operator

Consider a prescribed increment, $\delta\sigma$, separating two σ isosurfaces. This increment commutes with the horizontal operator $\nabla_{\mathbf{h}}$, acting within the layer. We can thus formally consider the following layer-integrated or thickness weighted form of the diffusion operator

$$-\mathcal{R} \delta V = [\nabla_{\mathbf{h}} \cdot (\delta\sigma z_{\sigma} \mathbf{J}^h) + \delta\sigma \partial_{\sigma} (z_{\sigma} \nabla\sigma \cdot \mathbf{J})] \delta x \delta y \quad (1.103a)$$

$$= \frac{1}{\delta z} [\nabla_{\mathbf{h}} \cdot (\delta\sigma z_{\sigma} \mathbf{J}^h) + \delta\sigma \partial_{\sigma} (z_{\sigma} \nabla\sigma \cdot \mathbf{J})] \delta x \delta y \delta z \quad (1.103b)$$

$$= \frac{1}{h} [\nabla_{\mathbf{h}} \cdot (h \mathbf{J}^h) + \Delta_{\sigma} (z_{\sigma} \nabla\sigma \cdot \mathbf{J})] \delta x \delta y h, \quad (1.103c)$$

where we introduced the infinitesimal layer thickness

$$h = \delta z = z_{\sigma} \delta\sigma \quad (1.104)$$

and the non-dimensional differential operator

$$\Delta_{\sigma} \equiv \delta\sigma \frac{\partial}{\partial\sigma}. \quad (1.105)$$

Cancelling the volume element on both sides leads to the diffusion operator

$$\mathcal{R} = -\frac{1}{h} [\nabla_{\mathbf{h}} \cdot (h \mathbf{J}^h) + \Delta_{\sigma} (z_{\sigma} \nabla\sigma \cdot \mathbf{J})]. \quad (1.106)$$

This form is commonly found in the numerical modeling literature when considering generalized vertical coordinate models.

We make the following comments concerning the diffusion operator in equation (1.106).

- Our introduction of the layer thickness $h = z_{\sigma} \delta\sigma$ is treated a bit more formally in Sections 2.10 and 2.11 by considering a vertical integral over a coordinate layer. Even so, the resulting diffusion operator is the same as that derived here.
- The thickness weighted flux, $h \mathbf{J}^h$, is oriented within the horizontal plane. However, its contribution to the diffusion operator is computed by taking its convergence using the operator $\nabla_{\mathbf{h}}$ rather than the horizontal operator $\nabla_{\mathbf{h}}$. This distinction is fundamental to how operators, such as advection and diffusion, appear using generalized vertical coordinates.
- The flux $z_{\sigma} \nabla\sigma \cdot \mathbf{J}$ is commonly referred to as the dia-surface subgrid scale flux.
- For the special case of a diffusive flux with zero component parallel to $\nabla\sigma$, the diffusion operator reduces to

$$\mathcal{R} = -\frac{1}{h} [\nabla_{\mathbf{h}} \cdot (h \mathbf{J}^h)] \quad \text{if } \nabla\sigma \cdot \mathbf{J} = 0. \quad (1.107)$$

The neutral diffusion operator of Section 7.4.4 is an example of such an operator, with σ in that case given by the locally referenced potential density.

1.16 Vorticity

Vorticity is the curl of the velocity

$$\omega = \text{curl}(\mathbf{v}) = \mathbf{e}_a \varepsilon^{abc} \partial_b v_c = \mathbf{e}_{\bar{a}} \varepsilon^{\bar{a}\bar{b}\bar{c}} \partial_{\bar{b}} v_{\bar{c}}, \quad (1.108)$$

where we made use of the expression for the curl from VOLUME 1. In this section we unpack this expression to write the vorticity using generalized vertical coordinates.

1.16.1 Contravariant components

The contravariant components of the vorticity are given by via

$$\omega^{\bar{a}} = \varepsilon^{\bar{a}\bar{b}\bar{c}} \partial_{\bar{b}} v_{\bar{c}} = (\partial z / \partial \sigma)^{-1} \epsilon^{\bar{a}\bar{b}\bar{c}} \partial_{\bar{b}} v_{\bar{c}}, \quad (1.109)$$

where we made use of equation (1.81) to introduce the permutation symbol. Expanding the components leads to

$$\omega^{\bar{1}} = (\partial \sigma / \partial z) (\partial_{\bar{2}} v_{\bar{3}} - \partial_{\bar{3}} v_{\bar{2}}) \quad (1.110a)$$

$$\omega^{\bar{2}} = (\partial \sigma / \partial z) (\partial_{\bar{3}} v_{\bar{1}} - \partial_{\bar{1}} v_{\bar{3}}) \quad (1.110b)$$

$$\omega^{\bar{3}} = \omega^{\sigma} = (\partial \sigma / \partial z) (\partial_{\bar{1}} v_{\bar{2}} - \partial_{\bar{2}} v_{\bar{1}}), \quad (1.110c)$$

so that the curl is given by

$$\omega = \mathbf{e}_{\bar{a}} \omega^{\bar{a}} = (\partial \sigma / \partial z) [\mathbf{e}_{\bar{1}} (\partial_{\bar{2}} v_{\bar{3}} - \partial_{\bar{3}} v_{\bar{2}}) + \mathbf{e}_{\bar{2}} (\partial_{\bar{3}} v_{\bar{1}} - \partial_{\bar{1}} v_{\bar{3}}) + \mathbf{e}_{\bar{3}} (\partial_{\bar{1}} v_{\bar{2}} - \partial_{\bar{2}} v_{\bar{1}})], \quad (1.111)$$

where equations (1.20a)-(1.20c) provide expressions for the basis vectors written using generalized vertical coordinates.

1.16.2 Transforming from Cartesian coordinates

Equation (1.111) is written solely with the generalized vertical coordinates. An alternative approach connects performs a transformation from the Cartesian vorticity components using the transformation matrix

$$\omega^{\bar{a}} = \Lambda^{\bar{a}}_a \omega^a, \quad (1.112)$$

where ω^a are the Cartesian components

$$\omega = \hat{\mathbf{x}} \left[\frac{\partial w}{\partial y} - \frac{\partial v}{\partial z} \right] + \hat{\mathbf{y}} \left[\frac{\partial u}{\partial z} - \frac{\partial w}{\partial x} \right] + \hat{\mathbf{z}} \left[\frac{\partial v}{\partial x} - \frac{\partial u}{\partial y} \right]. \quad (1.113)$$

Making use of the transformation matrix $\Lambda^{\bar{a}}_a$ from equation (1.25) yields (just as in Section 1.8)

$$\omega^{\bar{x}} = \omega^x = \frac{\partial w}{\partial y} - \frac{\partial v}{\partial z} \quad \text{and} \quad \omega^{\bar{y}} = \omega^y = \frac{\partial u}{\partial z} - \frac{\partial w}{\partial x} \quad \text{and} \quad \omega^{\sigma} = \boldsymbol{\omega} \cdot \nabla \sigma. \quad (1.114)$$

Note that for isopycnal coordinates in a Boussinesq fluid, ω^{σ} equals to the potential vorticity when the vorticity is the absolute vorticity (Section 3.3). That is, the potential vorticity is the isopycnal component of the absolute vorticity.

1.17 Circulation

The velocity circulation (VOLUME 3) is given by the closed oriented path integral of the velocity projected into the direction of the path

$$\mathcal{C} \equiv \oint_{\partial\mathcal{S}} \mathbf{v} \cdot d\mathbf{x} \quad (1.115)$$

where $d\mathbf{x}$ is the vector line element along the path and $\partial\mathcal{S}$ is the closed path defining the boundary to a two-dimensional surface, \mathcal{S} . [Stokes' theorem](#) leads to the identity

$$\mathcal{C} = \oint_{\partial\mathcal{S}} \mathbf{v} \cdot d\mathbf{x} = \int_{\mathcal{S}} (\nabla \times \mathbf{v}) \cdot \hat{\mathbf{n}} d\mathcal{S} = \int_{\mathcal{S}} \boldsymbol{\omega} \cdot \hat{\mathbf{n}} d\mathcal{S}, \quad (1.116)$$

where $\hat{\mathbf{n}}$ is the outward normal vector orienting the area element $d\mathcal{S}$ according to the right-hand rule applied to the bounding circuit. These results manifest Galilean space-time [covariance](#), so that they hold for an arbitrary coordinate representation.

As a particular case, consider the circulation around a closed path on a constant σ surface, in which

$$\hat{\mathbf{n}} = \frac{\nabla\sigma}{|\nabla\sigma|} \quad (1.117)$$

is the outward normal and

$$\boldsymbol{\omega} \cdot \hat{\mathbf{n}} = \frac{\omega^\sigma}{|\nabla\sigma|} \quad (1.118)$$

where $\omega^\sigma = \boldsymbol{\omega} \cdot \nabla\sigma$ (equation (1.114)). So long as the vertical stratification remains non-zero ($\partial\sigma/\partial z \neq 0$) we can write the area factor in the form

$$\frac{d\mathcal{S}}{|\nabla\sigma|} = \frac{d\mathcal{S}}{\sqrt{(\partial\sigma/\partial x)^2 + (\partial\sigma/\partial y)^2 + (\partial\sigma/\partial z)^2}} \quad (1.119a)$$

$$= \frac{d\mathcal{S}}{|\partial\sigma/\partial z| \sqrt{[(\partial\sigma/\partial x)/(\partial\sigma/\partial z)]^2 + [(\partial\sigma/\partial y)/(\partial\sigma/\partial z)]^2 + 1}} \quad (1.119b)$$

$$= \frac{d\mathcal{S}}{|\partial\sigma/\partial z| \sqrt{1 + \tan^2 \vartheta}} \quad (1.119c)$$

$$= \left| \frac{\partial z}{\partial \sigma} \right| |\cos \vartheta| d\mathcal{S} \quad (1.119d)$$

$$= \left| \frac{\partial z}{\partial \sigma} \right| dA. \quad (1.119e)$$

The equality (1.119c) introduces the angle, ϑ , between the boundary surface and the horizontal plane as in Figure 1.5. The squared slope of this surface given by

$$\tan^2 \vartheta = \frac{\nabla_h \sigma \cdot \nabla_h \sigma}{(\partial\sigma/\partial z)^2} = \nabla_h z \cdot \nabla_h z. \quad (1.120)$$

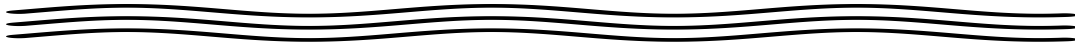
The equality (1.119d) made use of a trigonometric identity, and the equality (1.119e) introduced the horizontal projection of the area,

$$dA = |\cos \vartheta| d\mathcal{S}. \quad (1.121)$$

Bringing these results together leads to the expression for circulation around a closed loop on a

constant σ surface

$$\mathcal{C}_{\sigma-\text{surface}} = \int_{\mathcal{S}} (\boldsymbol{\omega} \cdot \nabla \sigma) |\partial z / \partial \sigma| \, dA. \quad (1.122)$$



1.18 Exercises

EXERCISE 1.1: TRIPLE PRODUCT AND TRANSFORMATION MATRIX

Use the triple product identities (1.39b)-(1.39c) to verify that equation (1.71) agrees with the transformation matrix approach detailed in Section 1.8. It is sufficient to show the agreement with just $F_{\bar{1}}$.

EXERCISE 1.2: VECTOR CROSS PRODUCT OF BASIS VECTORS

Verify the following relation (VOLUME 1) for the cross product of two basis vectors using generalized vertical coordinates

$$\mathbf{e}_{\bar{a}} \times \mathbf{e}_{\bar{b}} = \epsilon_{\bar{a}\bar{b}\bar{c}} \mathbf{e}^{\bar{c}} \implies \mathbf{e}_{\bar{a}} \times \mathbf{e}_{\bar{b}} = (\partial z / \partial \sigma) \epsilon_{\bar{a}\bar{b}\bar{c}} \mathbf{e}^{\bar{c}}. \quad (1.123)$$

EXERCISE 1.3: CHECKING THE REPRESENTATIONS OF THE GRADIENT OPERATOR

Confirm that the two Cartesian expression (1.91) for the gradient operator is indeed identical to the generalized vertical coordinate representation (1.92). Hint: make use of equations (1.82b)-(1.82d) for the partial derivatives and equations (1.27a)-(1.27c) for the one-form basis. Hint: also make use of the triple product identities from Section 1.10.3.s

EXERCISE 1.4: CHECKING THE GVC REPRESENTATION OF THE METRIC TENSOR

We here verify the identity (1.66) through use of the generalized vertical coordinate representation of the metric tensor and its inverse as given in Section 1.10.1.

- (a) Show that $g^{\bar{1}\bar{b}} g_{\bar{b}\bar{1}} = 1$.
- (b) Show that $g^{\bar{1}\bar{b}} g_{\bar{b}\bar{2}} = 0$.

EXERCISE 1.5: TRANSFORMATION OF THE METRIC TENSOR

We computed the inverse metric tensor in equation (1.65) through the identity

$$g^{\bar{a}\bar{b}} = \mathbf{e}^{\bar{a}} \cdot \mathbf{e}^{\bar{b}}, \quad (1.124)$$

and used the basis one-forms for generalized vertical coordinates given by equations (1.27a)-(1.27c). Here we make use of the transformation matrix and verify the identity

$$g^{\bar{a}\bar{b}} = (\Lambda^{\bar{a}}_a \mathbf{e}^a) \cdot (\Lambda^{\bar{b}}_b \mathbf{e}^b), \quad (1.125)$$

where $\Lambda^{\bar{a}}_a$ is the inverse transformation matrix (1.25) and \mathbf{e}^b are the Cartesian basis one-forms.

- (a) Show that $g^{\bar{1}\bar{1}} = 1$.
- (b) Show that $g^{\bar{1}\bar{3}} = \partial \sigma / \partial x$.

EXERCISE 1.6: METRIC TENSOR FOR RIGID LID TERRAIN FOLLOWING COORDINATES

Consider the specific case of rigid lid terrain following coordinates from Section 1.3.2, for which the generalized vertical coordinate is $\sigma = -z/\eta_b$. Hint: see Appendix B from *Callies and Ferrari (2018)*.

- (a) Write the metric tensor (1.64).
 (b) Write the inverse metric tensor (1.65).

EXERCISE 1.7: RIGIDLY ROTATED EQUATIONS FOR PLANETARY GEOSTROPHY

On page 2 we identified a key reason to favor generalized vertical coordinates, which are non-orthogonal, rather than rigidly rotated orthogonal coordinates. Namely, the problem with rotated orthogonal coordinates is that the hydrostatic pressure gradient appears in more than a single component equation of motion. Here we illustrate the mathematics of this rotation by considering the unforced perfect fluid planetary geostrophic equations from VOLUME 2. In fact, our only concern is with the velocity equation, here written as

$$\rho_0 f (\hat{z} \times \mathbf{u}) = -\nabla p' - \rho' g \hat{z}, \quad (1.126)$$

where

$$p' = p - p_0 \quad \text{and} \quad \rho' = \rho - \rho_0 \quad \text{with} \quad dp_0/dz = -\rho_0 g \quad \text{and} \quad \partial p'/\partial z = -\rho' g. \quad (1.127)$$

Our goal in this exercise is to examine the planetary geostrophic momentum equation after performing a rigid coordinate rotation as in Figure 1.6. That is, we perform a rotation of the Cartesian coordinate system in a counter-clockwise direction through an angle, φ , relative to the \hat{x} axis.

A version of the rotated equations (with friction included) are sometimes used to study bottom boundary layer physics next to a sloped bottom, such as [Phillips \(1970\)](#), [Garrett et al. \(1993\)](#), [Callies \(2018\)](#), [Holmes et al. \(2019a\)](#), and [Wenegrat and Thomas \(2020\)](#). Notably, these studies generally drop certain terms in the rotated equations based on specifics of the dynamical regime under consideration. For this exercise we keep all terms arising from the rotation since the goal here is mathematical. That is, we wish to see the full rotated equation set so that it can be examined prior to making any dynamical assumptions that target a specific application.

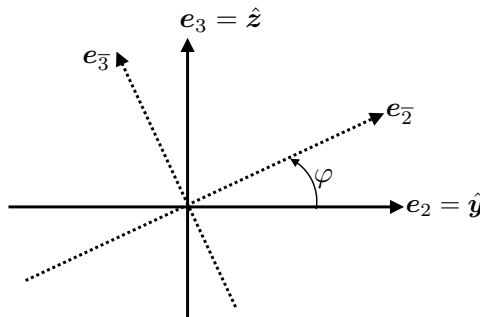
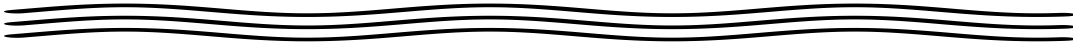


FIGURE 1.6: A schematic for Exercise 1.7 to illustrate the rigid rotation of the Cartesian coordinate system in an counter-clockwise sense around the \hat{x} direction (which points out of the page) through an angle φ . The unrotated basis vectors are written $\mathbf{e}_a = (\hat{x}, \hat{y}, \hat{z})$, and the rotated basis vectors are $\mathbf{e}_{\bar{a}}$.

- (a) Write the basis vectors, $\mathbf{e}_{\bar{a}}$, for the rotated Cartesian coordinate system in terms of the unrotated basis vectors, $\mathbf{e}_a = (\hat{x}, \hat{y}, \hat{z})$.
 (b) Write the transformation matrix, $\Lambda^a_{\bar{a}}$, and inverse transformation matrix, $\Lambda^{\bar{a}}_a$, that give rise to this rotation.
 (c) Write the representation of the velocity vector using the rotated basis, and express this representation in terms of the unrotated velocity components, $v^a = (u, v, w)$. That is, compute $v^{\bar{a}} = \Lambda^{\bar{a}}_a v^a$.
 (d) Write the unrotated basis vectors, \mathbf{e}_a , in terms of the rotated basis vectors, $\mathbf{e}_{\bar{a}}$, according

to the transformation $\mathbf{e}_a = \Lambda^{\bar{a}}_a \mathbf{e}_{\bar{a}}$.

- (e) Write the representation of the velocity vector using the unrotated basis, and express this representation in terms of the rotated velocity components, $v^{\bar{a}}$. That is, compute $v^a = \Lambda^a_{\bar{a}} v^{\bar{a}}$.
- (f) Write $\hat{\mathbf{z}} \times \mathbf{u}$ using the rotated coordinates.
- (g) Write $\nabla p'$ using the rotated coordinates.
- (h) Write the equation of motion (1.126) in the rotated coordinate system.
- (i) Comment on the potential problems with this approach, as relates to the form of the hydrostatic balance.



Chapter 2

MECHANICAL EQUATIONS

In this chapter we develop the kinematical and dynamical equations for a moving geophysical fluid as formulated using generalized vertical coordinates. The key part of the kinematic formulation concerns the *dia-surface*, which measures the motion of fluid through a surface. The discussion here unifies ideas developed for [kinematic boundary conditions](#) with transport across an arbitrary surface in the fluid interior, and we do so within the context of a [GVC \(GVC\)](#), whose mathematics was studied in Chapter 1. In particular, we make use of the dia-surface transport formulation to express the material time derivative operator using generalized vertical coordinates. This form for the material time derivative allows us to decompose the vertical velocity into motion relative to a moving [GVC](#) surface. In turn, we are afforded a means to reinterpret the velocity vector and corresponding particle trajectories.

Once we have explored the kinematic description of motion using generalized vertical coordinates, we then work through derivations of the [GVC](#) version of mass continuity as well as the tracer equation, and derive their layer integrated versions appropriate for vertically discrete layered models. Thereafter, we derive the dynamical equations for momentum, vorticity, and potential vorticity using generalized vertical coordinates. The suite of mechanical equations provide the foundations for many numerical models of the atmosphere and ocean. Besides being essential for developing methods for numerical simulations, understanding the physical and mathematical basis of these equations supports the analysis of simulations.

CHAPTER GUIDE

We introduced mathematical properties of a [GVC \(GVC\)](#) in Chapter 1, including the calculus using these time dependent non-orthogonal coordinates. Following the treatment in Chapter 1, we here use the symbol σ to denote a generalized vertical coordinate, where σ has functional dependence $\sigma(x, y, z, t)$.

2.1	Loose threads	32
2.2	Example generalized vertical coordinate surfaces	33
2.2.1	Ocean free surface	33
2.2.2	Solid earth boundary	33
2.2.3	Ocean mixed layer base	34
2.2.4	Interior generalized vertical coordinate surfaces	34
2.3	Specific thickness	34
2.4	The dia-surface transport	36
2.4.1	Flow normal to the GVC surface	36
2.4.2	Accounting for movement of the surface	36

2.4.3	We only care about divergent surface motion	37
2.4.4	Dia-surface transport in terms of $D\sigma/Dt$	38
2.4.5	Defining the dia-surface transport	38
2.4.6	Expressions for the dia-surface velocity component	39
2.4.7	Relating w and $w^{(\delta)}$	40
2.4.8	Dia-surface velocity component for water mass analysis	40
2.4.9	Area integrated dia-surface transport for non-divergent flows	40
2.5	Material time derivative	42
2.6	Vertical velocity and dia-surface velocity	43
2.6.1	Decomposing the vertical velocity	43
2.6.2	Another form of the vertical velocity decomposition	43
2.7	The velocity vector and fluid particle trajectories	45
2.7.1	Coordinate representations of the velocity vector	45
2.7.2	Fluid particle trajectories	46
2.8	Subduction across the mixed layer base	47
2.9	Mass continuity	48
2.9.1	Cartesian coordinates	48
2.9.2	Generalized vertical coordinates	49
2.10	Layer integrated mass continuity	50
2.10.1	Non-Boussinesq (compressible) fluids	50
2.10.2	Mass continuity using pressure coordinates	52
2.10.3	Boussinesq ocean (non-divergent flow)	53
2.10.4	Rescaled geopotential coordinates	53
2.11	Layer integrated tracer equation	54
2.12	Overturning circulation in the meridional-σ plane	55
2.12.1	Overturning streamfunction	55
2.12.2	Proving that $\Psi(y, \sigma, t)$ is a streamfunction	56
2.13	Equations of motion	57
2.13.1	Mass and tracer equations	58
2.13.2	Momentum equation	58
2.13.3	Flux-form horizontal momentum equation	59
2.13.4	Vector-invariant horizontal momentum equation	59
2.13.5	Hydrostatic flow with constant gravitational acceleration	60
2.14	Concerning the pressure force	60
2.14.1	Computing the horizontal pressure gradient	61
2.14.2	Integrated pressure contact stress on the cell faces	62
2.14.3	Net vertical pressure force	63
2.14.4	Net horizontal pressure force	63
2.14.5	Comments	64
2.15	Hydrostatic vorticity and potential vorticity	64
2.15.1	Basic manipulations	64
2.15.2	Vorticity and potential vorticity equation	65
2.15.3	Potential vorticity for the Boussinesq ocean	66
2.15.4	Comments	67
2.16	Exercises	67

2.1 Loose threads

- Compare to the slope orthogonal coordinates of [Holmes et al. \(2019a\)](#).

2.2 Example generalized vertical coordinate surfaces

In Section 1.3 we provided some specific examples of a generalized vertical coordinates used to partition the ocean domain. Here we offer further examples as illustrated in Figure 2.1, focusing on aspects of specific coordinate surfaces that prove of use for the kinematics of this chapter.

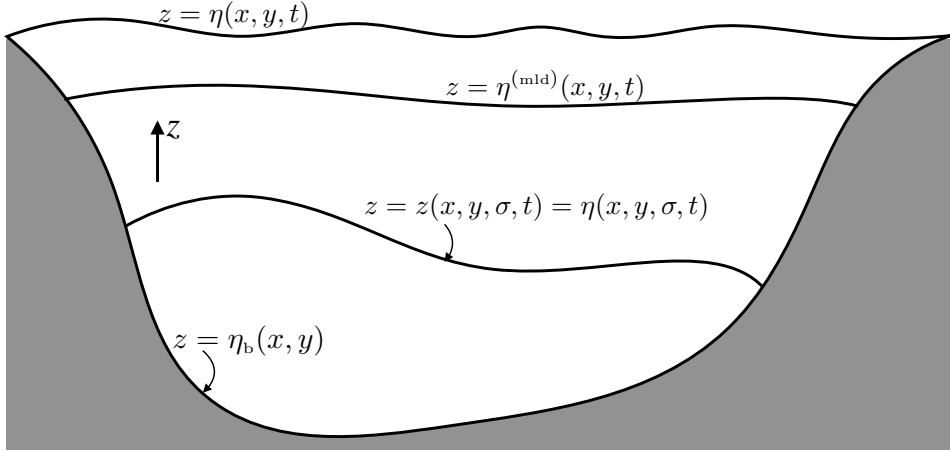


FIGURE 2.1: Example surfaces of a constant generalized vertical coordinate, $\sigma(x, y, z, t)$, in an ocean basin. Each of these surfaces is assumed to be smooth and to not overturn. The ocean free surface can be represented mathematically by $\sigma(x, y, z, t) = z - \eta(x, y, t) = 0$; the ocean mixed layer base can be written $\sigma(x, y, z, t) = z - \eta^{\text{mld}}(x, y, t) = 0$; and the solid earth bottom $\sigma(x, y, z) = z - \eta_b(x, y) = 0$. Likewise, the vertical position of an interior generalized vertical coordinate surface can be written $z - \eta(x, y, \sigma, t) = \text{constant}$, where $\eta(x, y, \sigma, t)$ is a function of horizontal position and time for the surface defined by a particular value of the generalized vertical coordinate.

2.2.1 Ocean free surface

We considered the [kinematic boundary condition](#) at the ocean free surface in [VOLUME 2](#), across which water and tracer can cross via precipitation, evaporation, river runoff, and sea ice melt. Momentum exchange across the boundary arises from stresses between the ocean and atmosphere or ice. The ocean free surface can be represented mathematically by the identity

$$\sigma(x, y, z, t) = z - \eta(x, y, t) = 0 \quad \text{ocean free surface.} \quad (2.1)$$

This identity holds so long as we assume the surface height, η , is a smooth and well defined surface that contains no overturns at the scales of interest. This assumption requires the filtering of breaking surface waves from the mathematical description.

2.2.2 Solid earth boundary

We may mathematically describe the solid Earth lower boundary by using the time independent generalized vertical coordinate

$$\sigma(x, y, z) = z - \eta_b(x, y) = 0 \quad \text{ocean bottom.} \quad (2.2)$$

We typically assume that there is no fluid mass transport through the solid Earth. However, in the case of geothermal heating, we may consider an exchange of heat between the ocean and

the solid Earth. Momentum is exchanged between the solid Earth and ocean fluid through the action of stresses.

2.2.3 Ocean mixed layer base

Let

$$\sigma = z - \eta^{\text{mld}}(x, y, t) = 0 \quad (2.3)$$

represent the vertical position of the ocean mixed layer base, with the corresponding normal vector

$$\hat{\mathbf{n}}^{(\text{mld})} = \frac{\nabla(z - \eta^{\text{mld}})}{|\nabla(z - \eta^{\text{mld}})|} = \frac{\nabla(\hat{z} - \nabla\eta^{\text{mld}})}{\sqrt{1 + |\nabla\eta^{\text{mld}}|^2}}. \quad (2.4)$$

This example is relevant for the study of ocean ventilation, whereby we are interested in measuring the transport of fluid that enters the ocean interior across the mixed layer base (see Section 2.8).

2.2.4 Interior generalized vertical coordinate surfaces

Within the fluid interior, transport across surfaces of constant generalized vertical coordinate, $\sigma = \sigma(x, y, z, t)$, constitutes the dia-surface transport affecting budgets of mass, tracer, and momentum within layers bounded by two generalized vertical coordinate surfaces. A canonical example is provided by isopycnal layers formed by surfaces of constant potential density (equivalently, constant buoyancy surfaces) as used in isopycnal ocean models as well as theoretical descriptions of perfect fluid dynamics. The vertical position of this surface is written in one of two equivalent manners

$$z = z(x, y, \sigma, t) = \eta(x, y, \sigma, t). \quad (2.5)$$

The first expression exposes the functional dependence of the vertical position of the σ surface at a horizontal position and time. In Section 1.2 we discussed the potential for confusion between writing z as a particular vertical position versus a function, thus motivating $z = \eta(x, y, \sigma, t)$. However, by now we should have sufficient experience with generalized vertical coordinates so that we can well distinguish when z refers to a particular vertical position versus $z(x, y, \sigma, t)$ as a coordinate function. For this reason we only infrequently use the nomenclature $z = \eta(x, y, \sigma, t)$ in this chapter.

2.3 Specific thickness

As mentioned in Section 1.10.2, a surface of constant generalized vertical coordinate can be successfully used to partition the vertical so long as the transformation between the generalized vertical coordinate and the geopotential coordinate is invertible. The Jacobian of transformation is given by

$$\frac{\partial z}{\partial \sigma} = z_{,\sigma}, \quad (2.6)$$

which must be single signed for suitable generalized vertical coordinates. This constraint means that we do not allow the surfaces to overturn, which is the same assumption made about the ocean surface, $z = \eta(x, y, t)$, and solid earth bottom, $z = \eta_b(x, y)$. This restriction places a limitation on the ability of certain GVC models (e.g., isopycnal models) to describe non-hydrostatic processes, such as the overturning common in Kelvin-Helmholtz billows and

gravitational convection. Note that for both the solid earth bottom and ocean free surface

$$\frac{\partial z}{\partial \sigma} = 1, \quad (2.7)$$

with this relation also holding for the geopotential coordinate, $\sigma = z$.

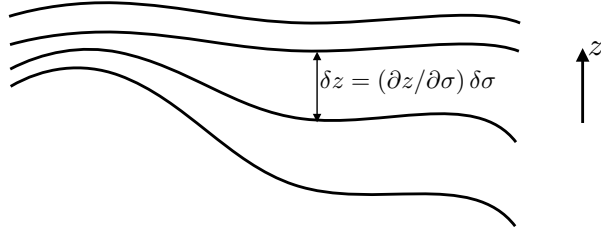


FIGURE 2.2: Illustrating the thickness between surfaces of constant generalized vertical coordinates, $\delta z = (\partial z / \partial \sigma) \delta \sigma$. In regions with larger magnitude for the specific thickness, $\partial z / \partial \sigma$, or equivalently smaller vertical stratification of the σ surfaces, $\partial \sigma / \partial z$, the layers are thicker so that isolines of constant σ are further apart. The converse holds where $\partial z / \partial \sigma$ is small (equivalently $\partial \sigma / \partial z$ is large).

We refer to the Jacobian of transform as the *specific thickness* and sometimes find it useful to write it in one of the following manners

$$\langle = z_{,\sigma} = \frac{\partial z}{\partial \sigma}. \quad (2.8)$$

This name is motivated by noting that the vertical thickness of an infinitesimal layer of coordinate thickness $\delta \sigma$ is given by

$$\delta z = \frac{\partial z}{\partial \sigma} \delta \sigma = \langle \delta \sigma, \quad (2.9)$$

with Figure 2.2 providing an example with finitely thick layers. For example, if $\sigma = b(x, y, z, t)$ (buoyancy or potential density as in isopycnal models), then the thickness of a buoyancy layer is given by

$$\delta z = \frac{\partial z}{\partial b} \delta b = N^{-2} \delta b, \quad (2.10)$$

with

$$N^2 = \frac{\partial b}{\partial z} \quad (2.11)$$

the squared **buoyancy frequency** in a **Boussinesq ocean**. For a hydrostatic flow using pressure as the vertical coordinate, the thickness of a pressure layer is

$$\delta z = \frac{\partial z}{\partial p} \delta p = -\frac{1}{\rho g} \delta p \quad (2.12)$$

where we used the hydrostatic relation

$$\frac{\partial p}{\partial z} = -\rho g \quad (2.13)$$

with g the constant acceleration due to effective gravity. Note that we assume the layer thickness is positive, $\delta z > 0$. For this purpose, with hydrostatic pressure we might choose to consider negative pressure increments, $\delta p < 0$, as this corresponds to vertically upward movement in a

fluid column.

2.4 The dia-surface transport

In this section we develop the concept of dia-surface transport and derive its expression in terms of the material time derivative of the generalized vertical coordinate.

2.4.1 Flow normal to the GVC surface

At an arbitrary point on a surface of constant generalized vertical coordinate (see Figure 2.3), the rate at which fluid moves in the direction normal to the surface is given by

$$\text{RATE OF FLUID FLOW IN DIRECTION } \hat{\mathbf{n}} = \mathbf{v} \cdot \hat{\mathbf{n}}, \quad (2.14)$$

where

$$\hat{\mathbf{n}} = \frac{\nabla \sigma}{|\nabla \sigma|}, \quad (2.15)$$

is the surface unit normal pointing in a direction of increasing σ . Two examples are useful to ground this expression in common experience. For the ocean free surface, $\sigma = z - \eta(x, y, t) = 0$, the unit normal takes the form

$$\hat{\mathbf{n}} = \frac{\nabla(z - \eta)}{|\nabla(z - \eta)|} = \frac{\hat{\mathbf{z}} - \nabla \eta}{\sqrt{1 + |\nabla \eta|^2}}, \quad (2.16)$$

whereas at the solid Earth bottom, $\sigma = z - \eta_b(x, y) = 0$,

$$\hat{\mathbf{n}} = -\frac{\nabla(z - \eta_b)}{|\nabla(z - \eta_b)|} = \frac{-\hat{\mathbf{z}} + \nabla \eta_b}{\sqrt{1 + |\nabla \eta_b|^2}}. \quad (2.17)$$

Use of the material time derivative

$$\frac{D\sigma}{Dt} = \frac{\partial \sigma}{\partial t} + \mathbf{v} \cdot \nabla \sigma \quad (2.18)$$

in equation (2.14) leads to the identity

$$\mathbf{v} \cdot \hat{\mathbf{n}} = \frac{1}{|\nabla \sigma|} \left[\frac{D\sigma}{Dt} - \frac{\partial \sigma}{\partial t} \right]. \quad (2.19)$$

Hence, the component to the velocity of a fluid particle that is normal to a generalized vertical coordinate surface is proportional to the difference between the material time derivative of the surface coordinate and its partial time derivative.

2.4.2 Accounting for movement of the surface

A generalized vertical coordinate surface is generally moving. So to diagnose the net transport of fluid penetrating the surface requires us to subtract the velocity of the surface, $\mathbf{v}^{(\sigma)}$, from the velocity of a fluid particle. We are thus led to

$$\text{RATE THAT FLUID CROSSES A MOVING GVC SURFACE} = \hat{\mathbf{n}} \cdot (\mathbf{v} - \mathbf{v}^{(\sigma)}). \quad (2.20)$$

We next develop a kinematic property of the surface velocity, or more precisely the normal

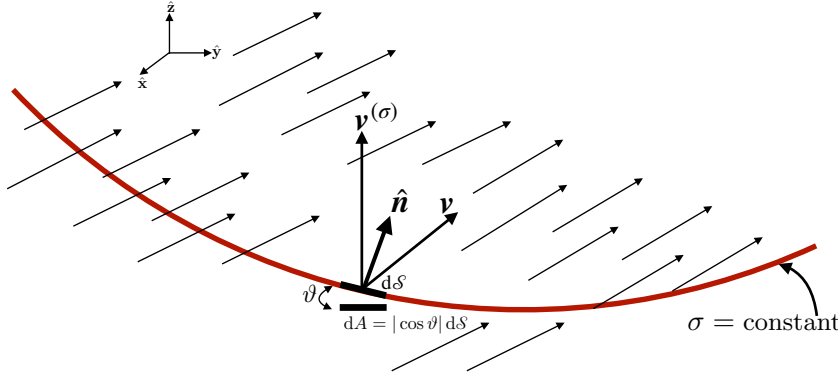


FIGURE 2.3: A surface of constant generalized vertical coordinate, $\sigma = \text{constant}$, within a fluid. The normal direction, $\hat{\mathbf{n}} = \nabla\sigma/|\nabla\sigma|$, points in the direction of increasing σ . We show an example velocity vector for a fluid particle, \mathbf{v} , at a point on the surface as well as the velocity, $\mathbf{v}^{(\sigma)}$, of a point that lives on the surface. Note that kinematics is only concerned with the normal component to the surface velocity, $\mathbf{v}^{(\sigma)} \cdot \hat{\mathbf{n}}$, as per equation (2.25). We require dynamical information to obtain information about the tangential component of $\mathbf{v}^{(\sigma)}$, but such information is not required for this chapter. Following equation (2.30), the horizontal projection of the surface area element is given by $dA = |\cos \vartheta| dS$, where ϑ is the angle between the surface and the horizontal and $dA = dx dy$.

component to that velocity. For that purpose, consider an infinitesimal increment in both space and time under which σ undergoes an infinitesimal change

$$\delta\sigma = \delta\mathbf{x} \cdot \nabla\sigma + \delta t \partial_t\sigma. \quad (2.21)$$

Now restrict attention to a point fixed on a constant σ surface, in which

$$\delta\sigma = \delta\mathbf{x}^{(\sigma)} \cdot \nabla\sigma + \delta t \partial_t\sigma = 0, \quad (2.22)$$

where $\delta\mathbf{x}^{(\sigma)}$ is a differential increment following the moving surface. We define the velocity of that point as

$$\mathbf{v}^{(\sigma)} = \frac{\delta\mathbf{x}^{(\sigma)}}{\delta t}, \quad (2.23)$$

in which case equation (2.22) implies that at each point within the fluid,

$$\frac{\partial\sigma}{\partial t} + \mathbf{v}^{(\sigma)} \cdot \nabla\sigma = 0. \quad (2.24)$$

We can likewise write this equation as one for the normal component of the surface velocity

$$\mathbf{v}^{(\sigma)} \cdot \hat{\mathbf{n}} = -\frac{1}{|\nabla\sigma|} \frac{\partial\sigma}{\partial t}. \quad (2.25)$$

Evidently, the normal component to the surface velocity vanishes when the surface is locally static.

2.4.3 We only care about divergent surface motion

For the kinematics of fluid motion relative to a surface of constant generalized vertical coordinates, we are only concerned with the normal component to the surface velocity, $\mathbf{v}^{(\sigma)} \cdot \hat{\mathbf{n}}$. That is, we are only concerned with divergent motion of the surface, defined as motion parallel

to the surface normal direction, $\hat{\mathbf{n}}$. We have no concern for rotational or tangential motion, which is motion perpendicular to $\hat{\mathbf{n}}$. Even so, some authors, by fiat, choose to set to zero the tangential component of the surface motion. In fact, specification of the tangential surface velocity component is generally not available without extra information about the surface motion, nor is its specification necessary for developing kinematic properties of fluid motion relative to arbitrary generalized vertical coordinate surfaces. Hence, we make no assumption about tangential motion of the surface.

2.4.4 Dia-surface transport in terms of $D\sigma/Dt$

Using expression (2.25) in equation (2.20) leads to the net flux of fluid crossing the surface of constant generalized vertical coordinate

$$\hat{\mathbf{n}} \cdot (\mathbf{v} - \mathbf{v}^{(\sigma)}) = \frac{1}{|\nabla\sigma|} \frac{D\sigma}{Dt} \iff \nabla\sigma \cdot (\mathbf{v} - \mathbf{v}^{(\sigma)}) = \frac{D\sigma}{Dt}. \quad (2.26)$$

Hence, if the material time derivative of a generalized vertical coordinate vanishes, then there is zero fluid crossing the surface with the *barycentric velocity*. That is, this result holds for motion of the fluid as defined by the barycentric velocity, \mathbf{v} (VOLUME 2). Hence, for multi-component fluids, $D\sigma/Dt = 0$ can still, in principle, be associated with tracer exchange or heat exchange across the surface via diffusion, so long as the net matter crossing the surface is zero.

2.4.5 Defining the dia-surface transport

The area normalizing the volume flux in equation (2.26) is the area $d\mathcal{S}$ of an infinitesimal patch on the surface of constant generalized vertical coordinate with outward unit normal $\hat{\mathbf{n}}$. We now follow the trigonometry discussed in Section 1.17 to introduce the horizontal projection of this area, dA , which is more convenient to work with for many purposes. So long as the vertical stratification remains non-zero ($\partial\sigma/\partial z \neq 0$) we can write the area factor in the form

$$\frac{d\mathcal{S}}{|\nabla\sigma|} = \frac{d\mathcal{S}}{\sqrt{(\partial\sigma/\partial x)^2 + (\partial\sigma/\partial y)^2 + (\partial\sigma/\partial z)^2}} \quad (2.27a)$$

$$= \frac{d\mathcal{S}}{|\partial\sigma/\partial z| \sqrt{[(\partial\sigma/\partial x)/(\partial\sigma/\partial z)]^2 + [(\partial\sigma/\partial y)/(\partial\sigma/\partial z)]^2 + 1}} \quad (2.27b)$$

$$= \frac{d\mathcal{S}}{|\partial\sigma/\partial z| \sqrt{1 + \tan^2 \vartheta}} \quad (2.27c)$$

$$= \left| \frac{\partial z}{\partial \sigma} \right| |\cos \vartheta| d\mathcal{S} \quad (2.27d)$$

$$= \left| \frac{\partial z}{\partial \sigma} \right| dA. \quad (2.27e)$$

The equality (2.27c) introduced the angle, ϑ , between the boundary surface and the horizontal plane (Figure 2.3). The squared slope of this surface given by (see Section 1.12)

$$\tan^2 \vartheta = \frac{\nabla_h \sigma \cdot \nabla_h \sigma}{(\partial\sigma/\partial z)^2} = \nabla_{\mathbf{v}} z \cdot \nabla_{\mathbf{v}} z. \quad (2.28)$$

The equality (2.27d) made use of a trigonometric identity so that

$$|\cos \vartheta|^{-1} = |z_{,\sigma} \nabla \sigma|. \quad (2.29)$$

Furthermore, the equality (2.27e) introduced the horizontal projection of the area,

$$dA = |\cos \vartheta| d\mathcal{S}. \quad (2.30)$$

We now introduce the *dia-surface velocity component* for the GVC coordinate

$$w^{(\dot{\sigma})} = \frac{\partial z}{\partial \sigma} \frac{D\sigma}{Dt} = z_{,\sigma} \dot{\sigma}, \quad (2.31)$$

which measures the volume of fluid passing through the surface, per unit horizontal area, per unit time

$$w^{(\dot{\sigma})} \equiv \hat{\mathbf{n}} \cdot (\mathbf{v} - \mathbf{v}^{(\sigma)}) \frac{d\mathcal{S}}{dA} \quad (2.32)$$

$$= \frac{(\text{VOLUME/TIME}) \text{ FLUID THROUGH SURFACE}}{\text{HORIZONTAL AREA OF SURFACE}}, \quad (2.33)$$

so that

$$w^{(\dot{\sigma})} dA \equiv \hat{\mathbf{n}} \cdot (\mathbf{v} - \mathbf{v}^{(\sigma)}) d\mathcal{S}. \quad (2.34)$$

We refer to $w^{(\dot{\sigma})}$ as the dia-surface velocity component since it measures flow rate of fluid through the surface. We can think of $w^{(\dot{\sigma})}$ as the “vertical” velocity which, when multiplied by the horizontal area element, measures the transport of fluid that crosses the surface in the normal direction.

2.4.6 Expressions for the dia-surface velocity component

Making use of various identities derived above, as well as the transformation of partial derivative operators in Section 1.12, allows us to write the dia-surface velocity component in the following equivalent forms

$$w^{(\dot{\sigma})} = \frac{\partial z}{\partial \sigma} \frac{D\sigma}{Dt} \quad (2.35a)$$

$$= z_{,\sigma} |\nabla \sigma| \hat{\mathbf{n}} \cdot (\mathbf{v} - \mathbf{v}^{(\sigma)}) \quad (2.35b)$$

$$= z_{,\sigma} \nabla \sigma \cdot \mathbf{v} - z_{,\sigma} |\nabla \sigma| \hat{\mathbf{n}} \cdot (\mathbf{v} - \mathbf{v}^{(\sigma)}) \quad (2.35c)$$

$$= (\hat{\mathbf{z}} - \nabla_{\mathbf{h}} z) \cdot \mathbf{v} + z_{,\sigma} \partial_t \sigma \quad (2.35d)$$

$$= (\hat{\mathbf{z}} - \nabla_{\mathbf{h}} z) \cdot \mathbf{v} - \frac{\partial z}{\partial t} \quad (2.35e)$$

$$= w - (\partial_t + \mathbf{u} \cdot \nabla_{\mathbf{h}}) z, \quad (2.35f)$$

where $\partial z / \partial t = (\partial z / \partial t)_{\sigma}$ is the time derivative for the depth of the σ surface. We also made use of the identity (see equations (1.39b) and (1.39c))

$$\nabla_{\mathbf{h}} z = -z_{,\sigma} \nabla_{\mathbf{h}} \sigma = -\nabla_{\mathbf{h}} \sigma / \partial_z \sigma \quad (2.36)$$

to express the slope of the σ surface as projected onto the horizontal direction plane, as well as the triple product identity (1.39a) for the time derivative

$$\left[\frac{\partial z}{\partial t} \right]_{\sigma} = - \frac{[\partial \sigma / \partial t]_z}{[\partial \sigma / \partial z]}. \quad (2.37)$$

2.4.7 Relating w and $w^{(\dot{\sigma})}$

Equation (2.35f) directly relates the dia-surface velocity component to the vertical component of the fluid particle velocity

$$w = \frac{Dz}{Dt} \longleftrightarrow w^{(\dot{\sigma})} = \frac{\partial z}{\partial \sigma} \frac{D\sigma}{Dt} = w - (\partial_t + \mathbf{u} \cdot \nabla_{\mathbf{r}})z. \quad (2.38)$$

When the σ -surface is static, so that it occupies a constant vertical position, $\partial z / \partial t = 0$, then the dia-surface velocity component reduces to

$$w^{(\dot{\sigma})} = w - \mathbf{u} \cdot \nabla_{\mathbf{r}} z \quad \text{static } \sigma\text{-surface}, \quad (2.39)$$

whereas if the σ -surface is flat, then the dia-surface velocity component measures the flux of fluid moving vertically relative to the motion of the generalized vertical coordinate surface. Finally, if the surface is flat and static, the dia-surface velocity component becomes the vertical velocity component

$$w^{(\dot{\sigma})} = w = \frac{Dz}{Dt} \quad \sigma\text{-surface static and flat}, \quad (2.40)$$

which is the case for the geopotential vertical coordinate.

2.4.8 Dia-surface velocity component for water mass analysis

In some literature presentations, the dia-surface velocity component is taken to be

$$w^{\text{dia}} = \hat{\mathbf{n}} \cdot (\mathbf{v} - \mathbf{v}^{(\sigma)}) = \frac{1}{|\nabla \sigma|} \frac{D\sigma}{Dt}. \quad (2.41)$$

As seen in Chapter 9, the reason to prefer equation (2.41) for watermass transformation analysis is that avoids the need to assume vertically stable stratification for surfaces of constant σ . Dropping that assumption allows us to consider water mass transformation between arbitrarily oriented elements of seawater, even those that are gravitationally unstable, with w^{dia} the appropriate object to measure flow across such arbitrarily oriented surfaces.

2.4.9 Area integrated dia-surface transport for non-divergent flows

We close this section by further emphasizing the distinction, in time dependent flows, between dia-surface transport and flow normal to a surface. For this purpose consider a non-divergent flow whereby $\nabla \cdot \mathbf{v} = 0$. Non-divergence means that for any closed surface within the fluid interior, the following identity holds via the divergence theorem

$$0 = \int_{\mathcal{R}} \nabla \cdot \mathbf{v} dV = \oint_{\partial \mathcal{R}} \hat{\mathbf{n}} \cdot \mathbf{v} dS. \quad (2.42)$$

Notably, only in the case of a static surface can we conclude that there is no net flow across the surface. For surfaces that move, there is generally a nonzero net dia-surface transport.

As a specific example, consider a fluid region such as shown in Figure 2.4, which is bounded below by the solid-earth bottom and above by a constant σ -surface. Since the solid-earth bottom is static and there is no-normal flow through the bottom, the identity (2.42) means

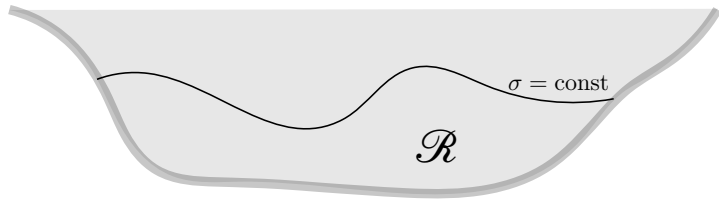


FIGURE 2.4: A constant generalized vertical coordinates surface, $\sigma = \text{constant}$, within a fluid region that intersects the bottom. The region, \mathcal{R} , is bounded above by the σ -surface and below by the solid-earth. Along the constant σ -surface a non-divergent flow satisfies $\int_{\sigma=\text{const}} \hat{\mathbf{n}} \cdot \mathbf{v} \, dS = 0$.

that the area integrated flow normal to the GVC vanishes

$$\int_{\sigma=\text{const}} \hat{\mathbf{n}} \cdot \mathbf{v} \, dS = 0. \quad (2.43)$$

But what does this identity imply about the area integrated dia-surface velocity? For the case of a geopotential vertical coordinate, $\sigma = z$, it means that the area integrated vertical velocity vanishes across any geopotential surface below the ocean free surface, $\int_{z=\text{const}} w \, dA = 0$ (see VOLUME 2). What about other generalized vertical coordinates?

To address this question consider the general result

$$\int_{\sigma=\text{const}} \hat{\mathbf{n}} \cdot (\mathbf{v} - \mathbf{v}^{(\sigma)}) \, dS = \int_{\sigma=\text{const}} w^{\text{dia}} \, dS = \int_{\sigma=\text{const}} w^{(\dot{\sigma})} \, dA, \quad (2.44)$$

where again $dA = dx \, dy$. Now make use of the property (2.43) for non-divergent flows as well as the identity (2.25) to render

$$\int_{\sigma=\text{const}} w^{(\dot{\sigma})} \, dA = - \int_{\sigma=\text{const}} \hat{\mathbf{n}} \cdot \mathbf{v}^{(\sigma)} \, dS \quad (2.45a)$$

$$= \int_{\sigma=\text{const}} \frac{\partial_t \sigma}{|\nabla \sigma|} \, dS \quad (2.45b)$$

$$= \int_{\sigma=\text{const}} \frac{\partial \sigma}{\partial t} \left| \frac{\partial z}{\partial \sigma} \right| \, dA \quad (2.45c)$$

$$= - \int_{\sigma=\text{const}} \left[\frac{\partial z}{\partial t} \right]_{\sigma} \, dA. \quad (2.45d)$$

The final equality holds if $\partial z / \partial \sigma > 0$, whereas we swap signs when the vertical stratification is $\partial z / \partial \sigma < 0$. We can go one further step by noting that the time derivative is computed with σ constant, as is the horizontal area integral. Hence, we can pull the time derivative outside the integral to render

$$\int_{\sigma=\text{const}} w^{(\dot{\sigma})} \, dA = - \left[\frac{\partial}{\partial t} \right]_{\sigma} \int_{\sigma=\text{const}} z \, dA. \quad (2.46)$$

Evidently, for a non-divergent flow the integrated dia-surface transport across a σ -surface equals to minus the time tendency for the area integrated vertical position of that surface. Hence, there is an area integrated dia-surface transport across the σ -surface so long as there is a volume change for the region beneath the surface.

For the case of an isopycnal surface in a perfect fluid, there is no change in the volume beneath any interior isopycnal surface since no flow crosses the isopycnal, in which case we recover the expected result $\int_{\sigma=\text{const}} w^{(\dot{\sigma})} \, dA = 0$. However, this result does not hold for other

coordinates, such as the rescaled vertical coordinate discussed in Sections 1.3.3 and 2.10.4, in which case

$$z^* = H \frac{z - \eta}{H + \eta} \quad (2.47a)$$

$$\frac{\partial z}{\partial z^*} = 1 + H/\eta > 0 \quad (2.47b)$$

$$\left[\frac{\partial z}{\partial t} \right]_{z^*} = \frac{\partial \eta}{\partial t} (1 + z^*/H), \quad (2.47c)$$

so that

$$\int_{z^*=\text{const}} w^{(z^*)} dA = \int_{z^*=\text{const}} (\partial \eta / \partial t) (1 + z^*/H) dA, \quad (2.48)$$

which is generally nonzero. For example, consider a flat bottom so that

$$\int_{z^*=\text{const}} w^{(z^*)} dA = (1 + z^*/H) \int_{z^*=\text{const}} (\partial \eta / \partial t) dA = (1 + z^*/H) \int_{z^*=\text{const}} (Q_m / \rho_0) dA, \quad (2.49)$$

where Q_m is the surface mass flux and we made use of the free surface equation

$$\partial_t \eta = Q_m / \rho_0 - \nabla \cdot \mathbf{U}, \quad (2.50)$$

holding for a non-divergent flow (VOLUME 2). In this case the area integrated dia-surface transport across a z^* surface is proportional to the area integrated surface mass flux.

2.5 Material time derivative

The expression (2.31) for $w^{(\dot{\sigma})}$ brings the material time derivative operator into the following equivalent forms

$$\frac{D}{Dt} = \left[\frac{\partial}{\partial t} \right]_z + \mathbf{u} \cdot \nabla_h + w \frac{\partial}{\partial z} \quad (2.51a)$$

$$= \left[\frac{\partial}{\partial t} \right]_\sigma + \mathbf{u} \cdot \nabla_\sigma + \frac{D\sigma}{Dt} \frac{\partial}{\partial \sigma} \quad (2.51b)$$

$$= \left[\frac{\partial}{\partial t} \right]_\sigma + \mathbf{u} \cdot \nabla_\sigma + w^{(\dot{\sigma})} \frac{\partial}{\partial z}. \quad (2.51c)$$

Note that the chain-rule means that

$$\frac{\partial}{\partial \sigma} = \frac{\partial z}{\partial \sigma} \frac{\partial}{\partial z}, \quad (2.52)$$

thus providing a relationship between the two vertical coordinate partial derivatives. Furthermore, recall that subscripts in the above derivative operators denote variables held fixed when taking the partial derivatives.

We highlight the special case of no fluid particles crossing the generalized coordinate surface. This situation occurs for a perfect fluid with σ equal to the buoyancy or isopycnal coordinate. For perfect fluid flow, the material time derivative in equation (2.51c) only has a horizontal two-dimensional advective component, $\mathbf{u} \cdot \nabla_\sigma$. This result does *not* mean that fluid particle motion in a perfect fluid is strictly horizontal. Indeed, it generally is not, as the form given by equation (2.51a) makes clear. Rather, it means that the advective transport of fluid properties

occurs along surfaces of constant buoyancy, and such transport is measured by the convergence of horizontal advective fluxes as measured along these constant buoyancy surfaces.

2.6 Vertical velocity and dia-surface velocity

Making use of the material time derivative operator in the form of equation (2.51c) affords us an opportunity to emphasize both the differences and similarities between the vertical velocity component and the dia-surface velocity component. Namely, the vertical velocity component takes on the equivalent forms

$$w = \frac{Dz}{Dt} = \left[\frac{\partial z}{\partial t} \right]_{\sigma} + \mathbf{u} \cdot \nabla_{\sigma} z + w^{(\dot{\sigma})} = \frac{\partial z}{\partial \sigma} \left[-\frac{\partial \sigma}{\partial t} - \mathbf{u} \cdot \nabla_{\sigma} \sigma + \frac{D\sigma}{Dt} \right], \quad (2.53)$$

and the corresponding expressions for the dia-surface velocity component are given by

$$w^{(\dot{\sigma})} = \frac{\partial z}{\partial \sigma} \frac{D\sigma}{Dt} = \frac{\partial z}{\partial \sigma} \left[\frac{\partial \sigma}{\partial t} + \mathbf{u} \cdot \nabla_{\sigma} \sigma + w \frac{\partial \sigma}{\partial z} \right] = - \left[\frac{\partial z}{\partial t} \right]_{\sigma} - \mathbf{u} \cdot \nabla_{\sigma} z + w. \quad (2.54)$$

Whereas the vertical velocity component, w , measures the transport crossing z surfaces, which are static and horizontal, the dia-surface velocity component, $w^{(\dot{\sigma})}$, measures the transport crossing σ surfaces, which are generally moving and sloped. It is notable that the area normalization used in equation (2.33) for the dia-surface velocity component means that it appears only in the expression for the vertical velocity (i.e., $w^{(\dot{\sigma})}$ is not in the expressions for the horizontal velocity components, u or v). However, as we see in the following, the appearance of $w^{(\dot{\sigma})}$ in the w equation does not necessarily mean that $w^{(\dot{\sigma})}$ corresponds to vertical particle motion. Instead, a nonzero $w^{(\dot{\sigma})}$ can arise from vertical motion of the σ -surface even while a fluid particle remains fixed in space.

2.6.1 Decomposing the vertical velocity

The expression

$$w = \left[\frac{\partial z}{\partial t} \right]_{\sigma} + \mathbf{u} \cdot \nabla_{\sigma} z + w^{(\dot{\sigma})} \quad (2.55)$$

decomposes the vertical velocity of a fluid particle into (i) time changes to the vertical position of the σ -surface at a particular horizontal point, (ii) lateral particle motion projected onto a sloped σ -surface, (iii) motion that crosses a σ -surface. Importantly, the three terms are coupled. For example, consider the case of σ defined by isopycnals, in which case irreversible mixing ($w^{(\dot{\sigma})} \neq 0$) changes the configuration of σ surfaces by changing both their height, $(\partial z / \partial t)_{\sigma}$, and their slope, $\nabla_{\sigma} z$.

2.6.2 Another form of the vertical velocity decomposition

Consider the velocity for a point on the surface, $\mathbf{v}^{(\sigma)}$, which satisfies (Section 2.4.2)

$$\frac{\partial \sigma}{\partial t} + \mathbf{v}^{(\sigma)} \cdot \nabla \sigma = 0. \quad (2.56)$$

Making use of the triple product identities from Section 1.6

$$\frac{\partial z}{\partial \sigma} \nabla \sigma = -\nabla_{\mathbf{v}} z + \hat{\mathbf{z}} \quad \text{and} \quad \frac{\partial z}{\partial \sigma} \left[\frac{\partial \sigma}{\partial t} \right]_z = - \left[\frac{\partial z}{\partial t} \right]_{\sigma} \quad (2.57)$$

brings equation (2.56) into the form

$$\left[\frac{\partial z}{\partial t} \right]_{\sigma} = (\hat{\mathbf{z}} - \nabla_{\mathbf{v}} z) \cdot \mathbf{v}^{(\sigma)} \implies \hat{\mathbf{z}} \cdot \mathbf{v}^{(\sigma)} = \left[\frac{\partial z}{\partial t} \right]_{\sigma} + \mathbf{u}^{(\sigma)} \cdot \nabla_{\mathbf{v}} z, \quad (2.58)$$

where $\mathbf{u}^{(\sigma)}$ is the horizontal component to the surface velocity, $\mathbf{v}^{(\sigma)}$. This equation shows that the vertical component to the σ -surface velocity is given by the sum of the changes to the vertical position of the surface, plus the projection of the horizontal motion of the surface onto the slope of the surface. Additionally, even if the σ -surface has no component of velocity in the vertical, the vertical position of the σ -surface, as measured at a horizontal point, generally changes if the surface is sloped and moves horizontally pass that point

$$\left[\frac{\partial z}{\partial t} \right]_{\sigma} = -\mathbf{u}^{(\sigma)} \cdot \nabla_{\mathbf{v}} z \quad \text{if } \hat{\mathbf{z}} \cdot \mathbf{v}^{(\sigma)} = 0. \quad (2.59)$$

Returning to the general result (2.58) allows us to write

$$\left[\frac{\partial z}{\partial t} \right]_{\sigma} + \mathbf{u} \cdot \nabla_{\mathbf{v}} z = \hat{\mathbf{z}} \cdot \mathbf{v}^{(\sigma)} + (\mathbf{u} - \mathbf{u}^{(\sigma)}) \cdot \nabla_{\mathbf{v}} z. \quad (2.60)$$

Furthermore, return to the fundamental definition of the dia-surface velocity component detailed in Section 2.4, in which we showed that

$$w^{(\dot{\sigma})} = \frac{\partial z}{\partial \sigma} \frac{D\sigma}{Dt} = \frac{\partial z}{\partial \sigma} \nabla \sigma \cdot (\mathbf{v} - \mathbf{v}^{(\sigma)}) = (-\nabla_{\mathbf{v}} z + \hat{\mathbf{z}}) \cdot (\mathbf{v} - \mathbf{v}^{(\sigma)}). \quad (2.61)$$

This expression, along with equation (2.60), leads to the rather elaborate decomposition of the vertical velocity component according to motion of a generalized vertical coordinate surface

$$w = \underbrace{\left[\hat{\mathbf{z}} \cdot \mathbf{v}^{(\sigma)} + (\mathbf{u} - \mathbf{u}^{(\sigma)}) \cdot \nabla_{\mathbf{v}} z \right]}_{(\partial_t + \mathbf{u} \cdot \nabla_{\mathbf{v}}) z} + \underbrace{\left[\hat{\mathbf{z}} \cdot (\mathbf{v} - \mathbf{v}^{(\sigma)}) - (\mathbf{u} - \mathbf{u}^{(\sigma)}) \cdot \nabla_{\mathbf{v}} z \right]}_{w^{(\dot{\sigma})}}. \quad (2.62)$$

Terms in the first bracket compute vertical particle motion relative to the σ -surface. The dia-surface contribution from the second bracket removes the contribution from σ -surface motion to leave just the vertical motion of the particle. All terms on the right hand side cancel, except for $\hat{\mathbf{z}} \cdot \mathbf{v} = w$, thus trivially revealing $w = w$. The decomposition of w is rather pedantic when viewed in the unpacked form of equation (2.62). Even so, let us consider some special cases to offer further interpretation.

- NO HORIZONTAL CONTRIBUTION: Consider the case where the horizontal velocity of a fluid particle matches that of the σ -surface: $\mathbf{u} = \mathbf{u}^{(\sigma)}$. Alternatively, consider the case with flat σ -surfaces so that $\nabla_{\mathbf{v}} z = 0$. In either case the vertical velocity is given by

$$w = \underbrace{\left[\hat{\mathbf{z}} \cdot \mathbf{v}^{(\sigma)} \right]}_{(\partial_t + \mathbf{u} \cdot \nabla_{\mathbf{v}}) z} + \underbrace{\left[\hat{\mathbf{z}} \cdot (\mathbf{v} - \mathbf{v}^{(\sigma)}) \right]}_{w^{(\dot{\sigma})}}. \quad (2.63)$$

The first contribution is from vertical motion of the σ -surface. The second contribution adjusts for the vertical motion of the particle relative to the σ -surface, leaving behind just the vertical motion of the particle. This rather trivial case exemplifies the contributions from the two pieces of the vertical velocity.

- **ZERO VERTICAL PARTICLE MOTION:** Consider the case where $w = 0$ so that

$$w = 0 \quad (2.64a)$$

$$= \left[\frac{\partial z}{\partial t} \right]_{\sigma} + \mathbf{u} \cdot \nabla_{\mathbf{h}\sigma} z + w^{(\dot{\sigma})} \quad (2.64b)$$

$$= \underbrace{\left[\hat{\mathbf{z}} \cdot \mathbf{v}^{(\sigma)} + (\mathbf{u} - \mathbf{u}^{(\sigma)}) \cdot \nabla_{\mathbf{h}\sigma} z \right]}_{(\partial_t + \mathbf{u} \cdot \nabla_{\mathbf{h}\sigma}) z} + \underbrace{\left[-\hat{\mathbf{z}} \cdot \mathbf{v}^{(\sigma)} - (\mathbf{u} - \mathbf{u}^{(\sigma)}) \cdot \nabla_{\mathbf{h}\sigma} z \right]}_{w^{(\dot{\sigma})}}. \quad (2.64c)$$

The final expression is trivial since each term in one bracket identically cancels terms in the other bracket. The penultimate expression reveals the balance between dia-surface transport and motion relative to the σ surface

$$-w^{(\dot{\sigma})} = \left[\frac{\partial z}{\partial t} \right]_{\sigma} + \mathbf{u} \cdot \nabla_{\mathbf{h}\sigma} z \quad \text{if } w = 0. \quad (2.65)$$

A particularly simple realization of this balance holds for σ given by isopycnals and where the isosurfaces are horizontal. In the presence of uniform mixing, the flat isopycnals stay flat and there is correspondingly no vertical motion of fluid particles even as the vertical stratification is modified. In contrast, the vertical position of an isopycnal surface changes according to the dia-surface velocity component $(\partial z / \partial t)_{\sigma} = -w^{(\dot{\sigma})} \neq 0$. This case illustrates that $w^{(\dot{\sigma})} \neq 0$ can still occur even when there is zero fluid particle motion since $w^{(\dot{\sigma})} \neq 0$ can arise from motion of a σ -surface alone.

2.7 The velocity vector and fluid particle trajectories

In this section we explore aspects of the velocity vector written using both Cartesian coordinates and generalized vertical coordinates. We complement that analytical discussion with a geometrical interpretation of fluid particle motion.

2.7.1 Coordinate representations of the velocity vector

Recall from Section 2.6 the vertical velocity component can be written in two forms given by equation (2.53). We focus on the expression

$$w = \left[\frac{\partial z}{\partial t} \right]_{\sigma} + \mathbf{u} \cdot \nabla_{\mathbf{h}\sigma} z + w^{(\dot{\sigma})}, \quad (2.66)$$

so that the full velocity vector can be written in the following equivalent manners

$$\mathbf{v} = u \hat{\mathbf{x}} + v \hat{\mathbf{y}} + w \hat{\mathbf{z}} \quad (2.67a)$$

$$= u \hat{\mathbf{x}} + v \hat{\mathbf{y}} + \left[(\partial z / \partial t)_{\sigma} + \mathbf{u} \cdot \nabla_{\mathbf{h}\sigma} z + w^{(\dot{\sigma})} \right] \hat{\mathbf{z}} \quad (2.67b)$$

$$= u [\hat{\mathbf{x}} + \hat{\mathbf{z}} (\partial z / \partial x)_{\sigma}] + v [\hat{\mathbf{y}} + \hat{\mathbf{z}} (\partial z / \partial y)_{\sigma}] + \left[(\partial z / \partial t)_{\sigma} + w^{(\dot{\sigma})} \right] \hat{\mathbf{z}}. \quad (2.67c)$$

$$= u [\hat{\mathbf{x}} + \hat{\mathbf{z}} (\partial z / \partial x)_\sigma] + v [\hat{\mathbf{y}} + \hat{\mathbf{z}} (\partial z / \partial y)_\sigma] + [(w - \nabla_{\mathbf{h}} z) \cdot \mathbf{v}] \hat{\mathbf{z}} \quad (2.67d)$$

$$= u [\hat{\mathbf{x}} + \hat{\mathbf{z}} (\partial z / \partial x)_\sigma] + v [\hat{\mathbf{y}} + \hat{\mathbf{z}} (\partial z / \partial y)_\sigma] + (\partial z / \partial \sigma) (\nabla \sigma \cdot \mathbf{v}) \hat{\mathbf{z}}. \quad (2.67e)$$

From Section 1.9, we can connect equation (2.67e) to the contravariant representation of the velocity vector using generalized vertical coordinates

$$\mathbf{v} = u \hat{\mathbf{x}} + v \hat{\mathbf{y}} + w \hat{\mathbf{z}} = v^{\bar{1}} \mathbf{e}_{\bar{1}} + v^{\bar{2}} \mathbf{e}_{\bar{2}} + v^{\bar{3}} \mathbf{e}_{\bar{3}}, \quad (2.68)$$

where we introduced the generalized vertical coordinate basis vectors, $\mathbf{e}_{\bar{\alpha}}$, given by equations (1.20a)-(1.20c)

$$\mathbf{e}_{\bar{1}} = \hat{\mathbf{x}} + \hat{\mathbf{z}} (\partial z / \partial x)_\sigma \quad \text{and} \quad \mathbf{e}_{\bar{2}} = \hat{\mathbf{y}} + \hat{\mathbf{z}} (\partial z / \partial y)_\sigma \quad \text{and} \quad \mathbf{e}_{\bar{3}} = \hat{\mathbf{z}} (\partial z / \partial \sigma), \quad (2.69)$$

and the contravariant components to velocity vector (equation (1.54))

$$v^{\bar{1}} = u \quad \text{and} \quad v^{\bar{2}} = v \quad \text{and} \quad v^{\bar{3}} = \nabla \sigma \cdot \mathbf{v} \quad (2.70)$$

2.7.2 Fluid particle trajectories

To help further understand the velocity as represented using generalized vertical coordinates, consider the following three cases as illustrated in Figure 2.5.

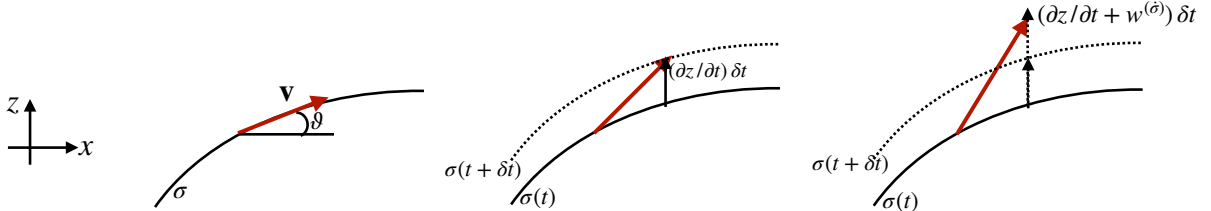


FIGURE 2.5: This schematic shows the various contributions to the fluid particle velocity (red vector) when written relative to motion of a particular generalized vertical coordinate surface. The fluid particle sits at the tail of the velocity vector at time t and at the head at time $t + \delta t$. The left panel is for the case of a static and material σ -surface so that the particle remains on the σ -surface and has a velocity vector given by equation (2.72). The slope of the σ -surface in the $\hat{\mathbf{x}}$ -direction is given by $\tan \vartheta = (\partial z / \partial x)_\sigma$. The middle panel is for a non-steady material σ -surface whereby the velocity of a particle takes on the form (2.73), with the particle remaining on the moving σ -surface. The right panel shows the case of a non-steady and non-material σ -surface with velocity (2.74). In this final case the particle position departs from the original σ -surface due to the nonzero dia-surface velocity component, $w^{(\dot{\sigma})} \neq 0$. It is not known *a priori* whether this departure is due to particle motion, motion of the surface, or both. Notably, the horizontal position of the particle remains identical for each of the three cases. It is only the vertical position that is modified according to the slope of the σ -surface (left panel), motion of the σ -surface (middle panel), and motion crossing the σ -surface (right panel).

- STEADY AND MATERIAL σ -SURFACE: The velocity vector is aligned with the instantaneous σ -surface ($\mathbf{v} \cdot \nabla \sigma = 0$) when the σ -surface is steady ($\partial \sigma / \partial t = 0$) and material ($D\sigma / Dt = 0$). Hence, we can diagnose the vertical velocity component in terms of the horizontal via

$$w \partial \sigma / \partial z = -\mathbf{u} \cdot \nabla_h \sigma \implies w = \mathbf{u} \cdot \nabla_h z, \quad (2.71)$$

where we used the triple product identities (1.39b) and (1.39c) for the final equality. The velocity vector thus takes on the form

$$\partial \sigma / \partial t = D\sigma / Dt = 0 \implies \mathbf{v} = u [\hat{\mathbf{x}} + \hat{\mathbf{z}} (\partial z / \partial x)_\sigma] + v [\hat{\mathbf{y}} + \hat{\mathbf{z}} (\partial z / \partial y)_\sigma]. \quad (2.72)$$

In this case, the fluid particle motion remains on the static σ -surface, so that the fluid velocity vector is determined by the horizontal velocity plus the slope of the σ surface.

- NON-STEADY AND MATERIAL σ -SURFACE: Next consider material σ surfaces ($D\sigma/Dt = 0$) that move ($\partial_t\sigma \neq 0$), in which case the velocity vector is

$$D\sigma/Dt = 0 \implies \mathbf{v} = u [\hat{\mathbf{x}} + \hat{\mathbf{z}} (\partial z/\partial x)_\sigma] + v [\hat{\mathbf{y}} + \hat{\mathbf{z}} (\partial z/\partial y)_\sigma] + (\partial z/\partial t)_\sigma \hat{\mathbf{z}}. \quad (2.73)$$

To remain on the moving surface, the fluid particle must move vertically by the extra amount $(\partial z/\partial t)_\sigma \delta t \hat{\mathbf{z}}$ relative to the case of a static σ -surface.

- NON-STEADY AND NON-MATERIAL σ -SURFACE: The general case with a non-material and non-steady σ also requires the dia-surface velocity component, $w^{(\dot{\sigma})}$, which is diagnosed based on the material time derivative of σ and the inverse stratification, $w^{(\dot{\sigma})} = (\partial z/\partial \sigma) D\sigma/Dt$:

$$\mathbf{v} = u [\hat{\mathbf{x}} + \hat{\mathbf{z}} (\partial z/\partial x)_\sigma] + v [\hat{\mathbf{y}} + \hat{\mathbf{z}} (\partial z/\partial y)_\sigma] + \left[(\partial z/\partial t)_\sigma + w^{(\dot{\sigma})} \right] \hat{\mathbf{z}}. \quad (2.74)$$

The contribution from $w^{(\dot{\sigma})}$ measures the vertical motion of the particle relative to the moving σ -surface. Hence, the sum, $(\partial z/\partial t)_\sigma + w^{(\dot{\sigma})}$, measures the vertical motion of the particle relative to a fixed origin. As emphasized in Section 2.6, a non-zero $w^{(\dot{\sigma})}$ arises from motion of the fluid particle relative to the σ -surface, and this relative motion does not necessarily mean that the particle moves; e.g., recall the example discussed in Section 2.6.2 with a static particle and moving σ -surface.

2.8 Subduction across the mixed layer base

As a brief example of the formalism, consider the generalized vertical coordinate defined according to the mixed layer base as in equation (2.3). The dia-surface mass transport across this surface leads us to define the subduction

$$-\mathcal{S}^{(\text{subduct})} \equiv \rho dA \left[\frac{D(z - \eta^{\text{mld}})}{Dt} \right] \quad \text{at } z = \eta^{\text{mld}}(x, y, t), \quad (2.75)$$

where the mass transport, $\mathcal{S}^{(\text{subduct})}$ (dimensions of mass per time), is positive for fluid moving downward beneath the mixed layer base into the pycnocline (subduction) and negative for water moving into the mixed layer (obduction). The area element, dA , is the horizontal projection of the area on the mixed layer base. Expanding the material time derivative leads to

$$\left[\frac{\mathcal{S}^{(\text{subduct})}}{\rho dA} \right] = -w + [\partial_t + \mathbf{u} \cdot \nabla] \eta^{\text{mld}} \quad \text{at } z = \eta^{\text{mld}}(x, y, t), \quad (2.76)$$

where again we define

$$\mathcal{S}^{(\text{subduct})} > 0 \quad \text{subduction (mixed layer loses mass)} \quad (2.77)$$

$$\mathcal{S}^{(\text{subduct})} < 0 \quad \text{obduction (mixed layer gains mass).} \quad (2.78)$$

We illustrate the kinematics of subduction in Figure 2.6. For the particular case of positive subduction (water moves from mixed layer to the interior), equation (2.76) reveals the following

three kinematic means for that to happen.

$$w < 0 \quad \text{vertically downward flow through mixed layer base} \quad (2.79a)$$

$$\partial_t \eta^{\text{mld}} > 0 \quad \text{mixed layer base shoals, thus decreasing MLD thickness} \quad (2.79b)$$

$$\mathbf{u} \cdot \nabla \eta^{\text{mld}} > 0 \quad \text{horizontal flow crossing sloped MLD boundary.} \quad (2.79c)$$

These pieces to the subduction provide kinematic answers to how water crossed the base of the mixed layer. We need dynamical information to determine why it crossed.

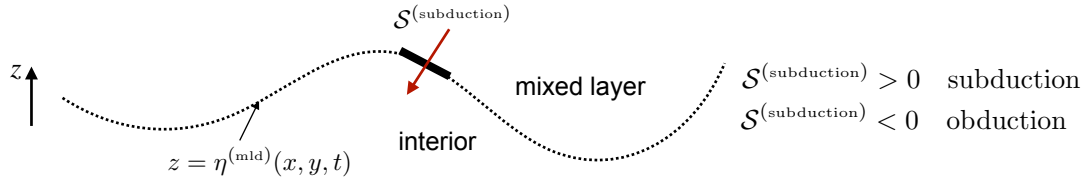


FIGURE 2.6: Illustrating the subduction as defined by equation (2.76), which measures the mass transport across the base of the ocean mixed layer. $S^{(\text{subduct})} > 0$ for water that enters the ocean interior, in which we say that water subducts from the mixed layer to the ocean interior, thus depleting the seawater mass contained in the mixed layer. Conversely, $S^{(\text{subduct})} < 0$ when water enters the mixed layer from below, in which we say that water is obducted from the interior into the mixed layer, thus adding seawater mass to the mixed layer. From equations (2.79a)-(2.79c) we see three kinematic means for water to cross $z = \eta^{\text{mld}}$: vertical flow, horizontal flow across a sloping mixed layer base, and vertical expansion or contraction of the mixed layer thickness.

2.9 Mass continuity

We here derive the Eulerian expression for mass continuity using generalized vertical coordinates. We then specialize to non-divergent flows, in which mass conservation is converted to volume conservation. To start, recall that mass conservation for a fluid element states that To develop the Eulerian expressions we first consider the case of Cartesian coordinates.

$$\rho \delta V = \rho \delta x \delta y \delta z = \rho \delta x \delta y z_{,\sigma} \delta \sigma \quad (2.80)$$

is constant following a fluid element.

2.9.1 Cartesian coordinates

Consider the expression

$$\frac{1}{\rho \delta V} \frac{D(\rho \delta V)}{Dt} = \frac{1}{\rho} \frac{D\rho}{Dt} + \frac{1}{\delta V} \frac{D(\delta V)}{Dt}. \quad (2.81)$$

Now make use of Cartesian coordinates to write the volume

$$\frac{1}{\delta V} \frac{D(\delta V)}{Dt} = \frac{1}{\delta x \delta y \delta z} \frac{D(\delta x \delta y \delta z)}{Dt} \quad (2.82a)$$

$$= \frac{1}{\delta x} \frac{D(\delta x)}{Dt} + \frac{1}{\delta y} \frac{D(\delta y)}{Dt} + \frac{1}{\delta z} \frac{D(\delta z)}{Dt} \quad (2.82b)$$

$$= \frac{\delta u}{\delta x} + \frac{\delta v}{\delta y} + \frac{\delta w}{\delta z} \quad (2.82c)$$

$$= \nabla \cdot \mathbf{v}. \quad (2.82d)$$

Setting $D(\rho \delta V)/Dt = 0$ leads to the expression from VOLUME 2 for the fluid mass continuity equation

$$\frac{D\rho}{Dt} = -\rho \nabla \cdot \mathbf{v}. \quad (2.83)$$

2.9.2 Generalized vertical coordinates

We follow the above procedure but now use generalized vertical coordinates so that

$$\frac{1}{\delta V} \frac{D(\delta V)}{Dt} = \frac{1}{\delta x \delta y z_{,\sigma} \delta \sigma} \frac{D(\delta x \delta y z_{,\sigma} \delta \sigma)}{Dt} \quad (2.84a)$$

$$= \frac{1}{\delta x} \frac{D(\delta x)}{Dt} + \frac{1}{\delta y} \frac{D(\delta y)}{Dt} + \frac{1}{z_{,\sigma}} \frac{D(z_{,\sigma})}{Dt} + \frac{1}{\delta \sigma} \frac{D(\delta \sigma)}{Dt} \quad (2.84b)$$

$$= \frac{\delta u}{\delta x} + \frac{\delta v}{\delta y} + \frac{1}{z_{,\sigma}} \frac{D(z_{,\sigma})}{Dt} + \frac{\delta(\dot{\sigma})}{\delta \sigma} \quad (2.84c)$$

$$= \nabla_{\mathbf{v}} \cdot \mathbf{u} + \frac{1}{z_{,\sigma}} \frac{D(z_{,\sigma})}{Dt} + \frac{\partial \dot{\sigma}}{\partial \sigma}, \quad (2.84d)$$

where we introduced the shorthand

$$\dot{\sigma} = D\sigma/Dt. \quad (2.85)$$

We also set

$$\frac{\delta u}{\delta x} + \frac{\delta v}{\delta y} = \nabla_{\mathbf{v}} \cdot \mathbf{u} \quad (2.86)$$

since we are working with generalized vertical coordinates so that we consider infinitesimal displacements occurring on constant σ surfaces. We are thus led to

$$\frac{1}{\rho \delta V} \frac{D(\rho \delta V)}{Dt} = \nabla_{\mathbf{v}} \cdot \mathbf{u} + \frac{1}{z_{,\sigma}} \frac{Dz_{,\sigma}}{Dt} + \frac{\partial \dot{\sigma}}{\partial \sigma} + \frac{1}{\rho} \frac{D\rho}{Dt} = 0. \quad (2.87)$$

Now use the material time derivative in the form (2.51b) to derive the flux-form expression of mass conservation

$$\frac{\partial(\rho z_{,\sigma})}{\partial t} + \nabla_{\mathbf{v}} \cdot (\rho z_{,\sigma} \mathbf{u}) + \frac{\partial(\rho z_{,\sigma} \dot{\sigma})}{\partial \sigma} = 0, \quad (2.88)$$

where the time derivative is computed holding σ fixed. We can furthermore introduce the dia-surface velocity component

$$w^{(\dot{\sigma})} = z_{,\sigma} \dot{\sigma} \quad (2.89)$$

so that mass continuity takes the form

$$\frac{\partial(\rho z_{,\sigma})}{\partial t} + \nabla_{\mathbf{v}} \cdot (\rho z_{,\sigma} \mathbf{u}) + \frac{\partial(\rho w^{(\dot{\sigma})})}{\partial \sigma} = 0. \quad (2.90)$$

Alternatively, we can reintroduce the material time derivative operator to write the mass continuity equation (2.88) in the form

$$\frac{1}{\rho z_{,\sigma}} \frac{D(\rho z_{,\sigma})}{Dt} = -(\nabla_{\mathbf{v}} \cdot \mathbf{u} + \partial \dot{\sigma} / \partial \sigma), \quad (2.91)$$

where we used equation (2.51b) to write

$$\frac{D}{Dt} = \left[\frac{\partial}{\partial t} \right]_{\sigma} + \mathbf{u} \cdot \nabla_{\sigma} + \dot{\sigma} \frac{\partial}{\partial \sigma}. \quad (2.92)$$

2.10 Layer integrated mass continuity

The formulation thus far has been continuous, with the only assumption made that the specific thickness, $\langle \rangle = \partial z / \partial \sigma$, is single signed. We here consider a discrete increment in the generalized vertical coordinate,

$$\sigma - \delta\sigma/2 \leq \sigma' \leq \sigma + \delta\sigma/2, \quad (2.93)$$

and formulate the mass budget over this layer whose thickness is given by

$$h \equiv \int_{z(\sigma - \delta\sigma/2)}^{z(\sigma + \delta\sigma/2)} dz = \int_{\sigma - \delta\sigma/2}^{\sigma + \delta\sigma/2} \frac{\partial z}{\partial \sigma} d\sigma, \quad (2.94)$$

and whose mass per horizontal area is

$$\delta m = \int_{z(\sigma - \delta\sigma/2)}^{z(\sigma + \delta\sigma/2)} \rho dz = \int_{\sigma - \delta\sigma/2}^{\sigma + \delta\sigma/2} \rho z_{,\sigma} d\sigma = \bar{\rho} h, \quad (2.95)$$

where $\bar{\rho}$ is the layer averaged density. Note that for a Boussinesq ocean the mass per area equals to the layer thickness times the reference density, ρ_0 ,

$$\delta m = \rho_0 h \quad \text{Boussinesq ocean.} \quad (2.96)$$

As defined by equation (2.94) and illustrated in Figure 2.2, the thickness of a layer is relatively large in regions where $\partial \sigma / \partial z$ is small; i.e., in regions where σ is weakly stratified in the vertical. Conversely, the layer thickness is relatively small where the vertical stratification is large. Furthermore, if the specific thickness is negative, then the layer thickness remains positive by choosing $\delta\sigma < 0$. For example, in a stably stratified fluid with σ given by potential density, $\partial \sigma / \partial z = -(g/\rho_0) N^2 < 0$ so that we take $\delta\sigma < 0$ to move vertically upward in the water column to regions of lower potential density. The same situation holds when σ is the hydrostatic pressure in which $\partial p / \partial z = -\rho g$ (Section 2.10.2).

The formulation in this section, and its companion for tracers in Section 2.11, holds across all generalized vertical coordinates, even incorporating the trivial case of geopotential coordinates ($\sigma = z$) whereby the specific thickness is unity. Application of the resulting layer integrated kinematics include the development of discrete equations for numerical layered models (see [Griffies et al. \(2020\)](#) for a review), as well as the shallow water models studied in VOLUME 3.

2.10.1 Non-Boussinesq (compressible) fluids

Performing a layer integral of the specific thickness equation (2.90) renders

$$\int_{\sigma - \delta\sigma/2}^{\sigma + \delta\sigma/2} \left[\frac{\partial(\rho z_{,\sigma})}{\partial t} + \nabla_{\sigma} \cdot (\rho z_{,\sigma} \mathbf{u}) + \frac{\partial(\rho w^{(\dot{\sigma})})}{\partial \sigma} \right] d\sigma = 0. \quad (2.97)$$

The dia-surface term integrates to a finite difference across the layer

$$\int_{\sigma-\delta\sigma/2}^{\sigma+\delta\sigma/2} \left[\frac{\partial(\rho z_{,\sigma})}{\partial t} + \nabla_{\mathbf{b}} \cdot (\rho z_{,\sigma} \mathbf{u}) \right] = -\Delta_{\sigma}(\rho w^{(\dot{\sigma})}), \quad (2.98)$$

where we introduced the dimensionless finite difference operator for properties defined at the layer interface

$$\Delta_{\sigma}(A) = A(\sigma + \delta\sigma/2) - A(\sigma - \delta\sigma/2). \quad (2.99)$$

The time derivative and horizontal space derivative commute with the layer integral, since the limits are specified fixed values for the layer increment, $\delta\sigma$, and the derivatives are computed with σ fixed. Hence, layer mass continuity takes the form

$$\left[\frac{\partial}{\partial t} \right]_{\sigma} \int_{\sigma-\delta\sigma/2}^{\sigma+\delta\sigma/2} \rho z_{,\sigma} d\sigma + \nabla_{\mathbf{b}} \cdot \int_{\sigma-\delta\sigma/2}^{\sigma+\delta\sigma/2} \rho \mathbf{u} z_{,\sigma} d\sigma = -\Delta_{\sigma}(\rho w^{(\dot{\sigma})}). \quad (2.100)$$

The first term involves the layer averaged density times the layer thickness as per equation (2.95). The second term involves the layer averaged density-weighted velocity, which is the layer averaged horizontal mass flux

$$\int_{\sigma-\delta\sigma/2}^{\sigma+\delta\sigma/2} \rho \mathbf{u} z_{,\sigma} d\sigma = h \bar{\rho} \bar{\mathbf{u}}. \quad (2.101)$$

We are thus led to the layer integrated continuity equation

$$\left[\frac{\partial(h \bar{\rho})}{\partial t} \right]_{\sigma} + \nabla_{\mathbf{b}} \cdot (h \bar{\rho} \bar{\mathbf{u}}) + \Delta_{\sigma}(\rho w^{(\dot{\sigma})}) = 0. \quad (2.102)$$

When evolving the fields in a discrete numerical model, we have direct access to information only about layer averaged fields. So how do we estimate the depth average of the horizontal advective flux, $\bar{\rho} \bar{\mathbf{u}}$, appearing in equation (2.102)? One method interprets all fields as their layer averaged values so that $\bar{\rho} \bar{\mathbf{u}} = \bar{\rho} \bar{\mathbf{u}}$, thus considering uncomputed sub-layer correlations $\bar{\rho}' \bar{\mathbf{u}'}$ as part of the truncation error. Alternately, we note that non-Boussinesq (compressible) hydrostatic flows can be described by a pressure-based vertical coordinate in which case the layer mass per horizontal area is proportional to a prescribed increment in pressure

$$\delta m = \int_{\sigma-\delta\sigma/2}^{\sigma+\delta\sigma/2} \rho z_{,\sigma} d\sigma = \bar{\rho} h = -g^{-1} \delta p. \quad (2.103)$$

Correspondingly, the layer integrated horizontal mass flux equals to the mass increment times the pressure-layer averaged velocity

$$\int_{\sigma-\delta\sigma/2}^{\sigma+\delta\sigma/2} \rho \mathbf{u} z_{,\sigma} d\sigma = -g^{-1} \int_{p-\delta p/2}^{p+\delta p/2} \mathbf{u} dp = -g^{-1} \bar{\mathbf{u}} \delta p = h \bar{\rho} \bar{\mathbf{u}}. \quad (2.104)$$

With either of the above two methods, we are led to the same layer integrated continuity equation, which we write in the generic form that drops overbars

$$\left[\frac{\partial(h \rho)}{\partial t} \right]_{\sigma} + \nabla_{\mathbf{b}} \cdot (h \rho \mathbf{u}) + \Delta_{\sigma}(\rho w^{(\dot{\sigma})}) = 0. \quad (2.105)$$

We illustrate contributions to this layer mass budget in Figure 2.7.

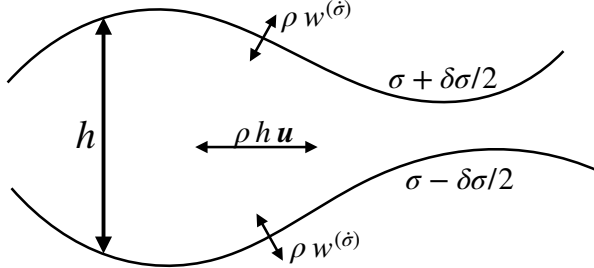


FIGURE 2.7: Illustrating the terms contributing to changes in layer mass according to the layer integrated continuity equation (2.105). The discrete layer is shown here with bounding interfaces at $\sigma - \delta\sigma/2$ and $\sigma + \delta\sigma/2$. Within a layer there is a horizontal redistribution due to horizontal advective transport. Additionally, matter can cross the layer due to dia-surface transport via $w^{(\delta)}$.

2.10.2 Mass continuity using pressure coordinates

Let us here consider in some detail the special case of pressure coordinates in a hydrostatic flow, and thus derive mass continuity using these coordinates.

Method I

The thickness of a hydrostatic pressure layer (equation (2.94)) takes on the following form

$$h = \int_{p-\delta p/2}^{p+\delta p/2} \frac{\partial z}{\partial p} dp = - \int_{p-\delta p/2}^{p+\delta p/2} \frac{dp}{\rho g}, \quad (2.106)$$

so that its mass per unit area is

$$\int_{p-\delta p/2}^{p+\delta p/2} \rho \frac{\partial z}{\partial p} dp = -\delta p/g. \quad (2.107)$$

The mass continuity equation (2.105) thus becomes

$$\frac{\partial(\delta p)}{\partial t} + \nabla_{hp} \cdot (\mathbf{u} \delta p) + \Delta_p (\dot{p}) = 0. \quad (2.108)$$

The partial time derivative vanishes since it is computed by holding pressure fixed so that the pressure increment has a zero time tendency

$$\left[\frac{\partial(\delta p)}{\partial t} \right]_p = 0. \quad (2.109)$$

Likewise, $\nabla_{hp}(\delta p) = 0$. Thus, we can divide by δp to render the continuity equation

$$\nabla_{hp} \cdot \mathbf{u} + \frac{\partial \dot{p}}{\partial p} = 0 \quad \text{compressible hydrostatic.} \quad (2.110)$$

This equation is isomorphic to the continuity equation for non-divergent flows written using geopotential coordinates

$$\nabla_h \cdot \mathbf{u} + \frac{\partial w}{\partial z} = \nabla_h \cdot \mathbf{u} + \frac{\partial w}{\partial z} = 0 \quad \text{non-divergent flow,} \quad (2.111)$$

where $w = \dot{z}$ is the vertical component to the velocity vector. For both pressure coordinates, describing non-Boussinesq fluids, and depth coordinates, describing Boussinesq fluids, the continuity equation is a diagnostic relation (i.e., no time derivatives) rather than prognostic (i.e., containing time derivatives).

Method II

For the second method we make use of the approach detailed in Section 2.9.2, which starts from

$$\frac{D(\rho \delta V)}{Dt} = 0. \quad (2.112)$$

In pressure coordinates the volume of the fluid element takes the form

$$\delta V = \delta x \delta y \delta z = \delta x \delta y \left[\frac{\partial z}{\partial p} \right] \delta p = -(\rho g)^{-1} \delta x \delta y \delta p. \quad (2.113)$$

Consequently,

$$0 = \frac{D(\rho \delta V)}{Dt} = g^{-1} \left(\frac{D(\delta x \delta y \delta p)}{Dt} \right), \quad (2.114)$$

so that

$$0 = \frac{1}{\delta x \delta y \delta p} \left(\frac{D(\delta x \delta y \delta p)}{Dt} \right) = \nabla_{hp} \cdot \mathbf{u} + \frac{\partial \dot{p}}{\partial p}. \quad (2.115)$$

The second step made use of the isomorphism between this result and that for equation (2.111) that holds for a geopotential vertical coordinate.

2.10.3 Boussinesq ocean (non-divergent flow)

Specializing to a non-divergent flow of the Boussinesq ocean, where fluid elements conserve their volume, yields the layer thickness equation

$$\frac{\partial h}{\partial t} + \nabla_b \cdot (h \mathbf{u}) + \Delta_\sigma w^{(\dot{\sigma})} = 0. \quad (2.116)$$

Further specializing to the case of zero dia-surface transport leads to

$$\frac{\partial h}{\partial t} + \nabla_b \cdot (h \mathbf{u}) = 0 \quad \text{no dia-surface transport.} \quad (2.117)$$

This case is commonly studied for stratified perfect fluids flows using isopycnal coordinates, in which isopycnal surfaces are material (Section 3.2).

2.10.4 Rescaled geopotential coordinates

In Section 1.3.3 we introduced the rescaled geopotential coordinate

$$z^* = \frac{H(z - \eta)}{H + \eta} = \frac{\eta_b(z - \eta)}{\eta_b - \eta} \quad \text{and} \quad \eta_b(x, y) \leq z^* \leq 0, \quad (2.118)$$

which is commonly used in Boussinesq ocean models, where $z = \eta(x, y, t)$ is the ocean free surface and $z = \eta_b(x, y) = -H(x, y)$ is the ocean bottom. The thickness of a coordinate layer is given by

$$h = dz = \frac{\partial z}{\partial z^*} dz^* = (1 + \eta/H) dz^* = (1 - \eta/\eta_b) dz^*. \quad (2.119)$$

The depth integrated column thickness and depth integrated coordinate thickness are given by

$$\int_{\eta_b}^{\eta} dz = \eta - \eta_b = \eta + H \quad \text{and} \quad \int_{z^*(\eta_b)}^{z^*(\eta)} dz^* = -\eta_b = H. \quad (2.120)$$

Correspondingly, the depth integrated thickness equation is given by the depth integrated volume budget

$$\frac{\partial \eta}{\partial t} + \nabla \cdot \mathbf{U} + [w_{z^*=0}^{(\dot{\sigma})} - w_{z^*=\eta_b}^{(\dot{\sigma})}] = 0. \quad (2.121)$$

We typically assume no fluid flow through the solid-earth bottom, so that $w_{z^*=\eta_b}^{(\dot{\sigma})} = 0$, whereas

$$-\rho_o w_{z^*=0}^{(\dot{\sigma})} = Q_m \quad (2.122)$$

is the mass flux crossing the ocean free surface as studied in VOLUME 2.

2.11 Layer integrated tracer equation

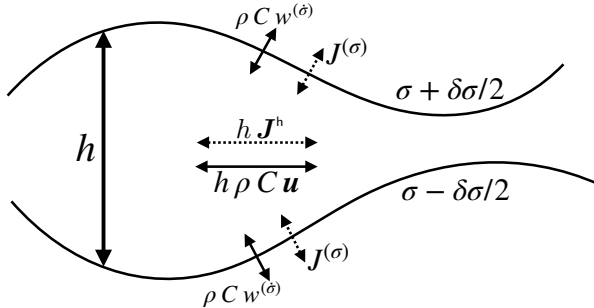


FIGURE 2.8: Illustrating the terms contributing to changes in layer tracer content according to the layer integrated tracer equation (2.127). The layer is shown here with bounding interfaces at $\sigma - \delta\sigma/2$ and $\sigma + \delta\sigma/2$. Within a layer there is a redistribution of tracer due to horizontal advective and subgrid scale tracer fluxes. Additionally, matter can cross the layer due to dia-surface transport via $\rho C w^{(\dot{\sigma})}$ and subgrid tracer transport $J^{(\sigma)}$.

The tracer equation is given by

$$\rho \frac{DC}{Dt} = -\nabla \cdot \mathbf{J}, \quad (2.123)$$

where \mathbf{J} is a subgrid scale flux. Now introduce the material time derivative operator in the form (2.51b) to have

$$\rho \left[\frac{\partial C}{\partial t} + \mathbf{u} \cdot \nabla_{\mathbf{v}} C + \dot{\sigma} \partial_{\sigma} C \right] = -\nabla \cdot \mathbf{J}, \quad (2.124)$$

Multiplying by the specific thickness and making use of the mass conservation equation (2.90)

renders the flux-form conservation equation

$$\frac{\partial(z_{,\sigma}\rho C)}{\partial t} + \nabla_{\mathbf{b}} \cdot (z_{,\sigma}\rho C \mathbf{u}) + \frac{\partial(\rho C w^{(\sigma)})}{\partial\sigma} = - \left[\nabla_{\mathbf{b}} \cdot (z_{,\sigma} \mathbf{J}^h) + \frac{\partial(z_{,\sigma} \nabla\sigma \cdot \mathbf{J})}{\partial\sigma} \right], \quad (2.125)$$

where we made use of expression (1.106) for the subgrid scale operator. Now perform a layer integral as detailed in Section 2.10 and use the layer mass continuity equation (2.105) to yield the layer integrated tracer equation

$$\frac{\partial(h\rho C)}{\partial t} + \nabla_{\mathbf{b}} \cdot (h\rho C \mathbf{u}) + \Delta_\sigma(\rho C w^{(\sigma)}) = - [\nabla_{\mathbf{b}} \cdot (h \mathbf{J}^h) + \Delta_\sigma(z_{,\sigma} \nabla\sigma \cdot \mathbf{J})]. \quad (2.126)$$

Alternatively, we can bring all terms to the left hand side to yield

$$\frac{\partial(h\rho C)}{\partial t} + \nabla_{\mathbf{b}} \cdot (h\rho C \mathbf{u} + h \mathbf{J}^h) + \Delta_\sigma(\rho C w^{(\sigma)} + J^{(\sigma)}) = 0 \quad (2.127)$$

where we wrote

$$J^{(\sigma)} = z_{,\sigma} \nabla\sigma \cdot \mathbf{J}. \quad (2.128)$$

We illustrate contributions to the layer tracer budget (2.127) in Figure 2.8. Note that we interpret these layer integrated fields and fluxes as per the discussion in Section 2.10.1.

2.12 Overturning circulation in the meridional- σ plane

In VOLUME 2 we studied the meridional-depth streamfunction. Here we introduce a streamfunction defined according to generalized vertical coordinate, $\sigma(x, y, z, t)$. This generalization is useful for studying the zonally integrated circulation partitioned according to σ surfaces rather than z surfaces, in particular when σ is potential density or specific entropy. We make use of Figure 2.9 in the following. We can make use of the Boussinesq ocean, where the flow field is non-divergent. Alternatively, we make use of a non-Boussinesq fluid when the flow is steady. As shown in this section, we are afforded a meridional- σ streamfunction only when σ is time independent.

2.12.1 Overturning streamfunction

Start from our discussion in VOLUME 2 for the meridional-depth streamfunction, here generalized to

$$\Psi(y, \sigma, t) = - \int_{x_1^{\text{rock}}}^{x_2^{\text{rock}}} \left[\int_{\eta_b(x', y)}^{z=\eta(x', y, \sigma, t)} v(x', y, z', t) dz' \right] dx'. \quad (2.129)$$

As defined, $\Psi(y, \sigma, t)$ makes use of $z = \eta(x', y, \sigma, t)$ for the upper bound on the vertical integral, where $\eta(x', y, \sigma, t)$ is the vertical position of a generalized vertical coordinate surface with value σ , such as depicted in Figure 2.9. In this manner, $\Psi(y, \sigma, t)$, is a function of latitude, σ , and time. Our job in the next subsection is to prove that $\Psi(y, \sigma, t)$ indeed serves as a streamfunction for the zonally integrated flow, with the zonal integral along constant σ surfaces rather than constant z surfaces.

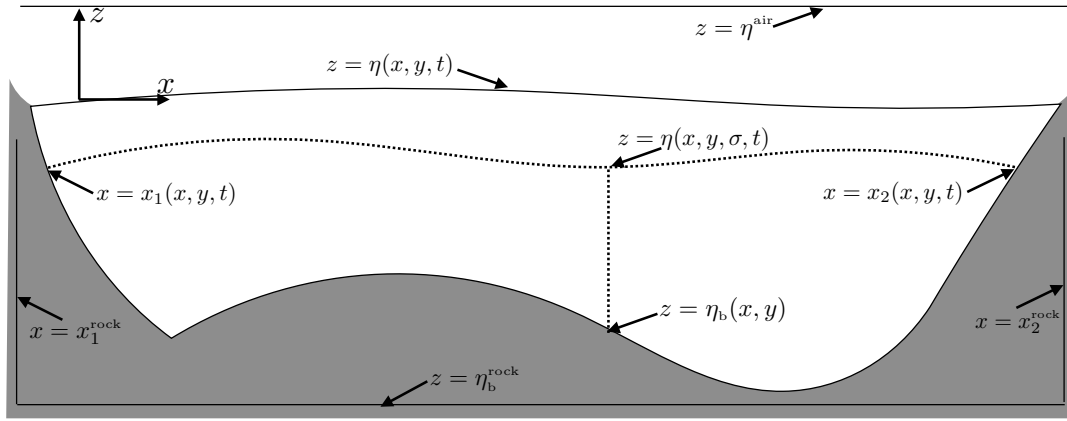


FIGURE 2.9: Geometry for computing the meridional streamfunction, here generalizing the meridional-depth streamfunction geometry from VOLUME 2 to meridional- σ . The zonal boundaries are written $x = x_1(y, z, t)$ and $x = x_2(y, z, t)$, which are generally functions of latitude and vertical position as well as time. The bottom is written as $z = \eta_b(x, y)$ and the vertical position of an arbitrary surface is written $z = \eta(x, y, \sigma, t)$, where we assume this surface is monotonic in the vertical as per the usual assumption for generalized vertical coordinates. Note that for shorthand, we often find it convenient to write $z = \eta_\sigma(x, y, t)$, particularly when suppressing the dependencies on horizontal position and time. We also display the constant zonal positions, $x_{1,2}^{\text{rock}}$, which are fully within the rock, as well as the bottom position, η_b^{rock} , which is also within the rock.

2.12.2 Proving that $\Psi(y, \sigma, t)$ is a streamfunction

To prove that $\Psi(y, \sigma, t)$ is indeed a streamfunction, we proceed much like in VOLUME 2 for the meridional-depth streamfunction, $\Psi(y, z, t)$, with the key new piece in the derivation concerning the space-time dependence of the $z = \eta(x, y, \sigma, t)$ surface. The vertical derivative of the streamfunction is given by

$$\frac{\partial \Psi}{\partial z} = -\frac{\partial}{\partial z} \int_{x_1^{\text{rock}}}^{x_2^{\text{rock}}} \left[\int_{\eta_b(x', y)}^{z=\eta(x', y, \sigma, t)} v(x', y, z', t) dz' \right] dx' \quad (2.130a)$$

$$= - \int_{x_1^{\text{rock}}}^{x_2^{\text{rock}}} \left[\frac{\partial}{\partial z} \int_{\eta_b(x', y)}^{z=\eta(x', y, \sigma, t)} v(x', y, z', t) dz' \right] dx' \quad (2.130b)$$

$$= - \int_{x_1^{\text{rock}}}^{x_2^{\text{rock}}} v(x', y, z = \eta(x', y, \sigma, t)) dx' \quad (2.130c)$$

$$= -V(y, \sigma, t). \quad (2.130d)$$

In these steps we used Leibniz's rule and noted that only the upper integration limit is a function of z . Furthermore, the upper limit on the vertical integral is evaluated at the vertical position of the σ surface. Hence, the zonal integral is defined while keeping the vertical position on the σ surface rather than on a constant geopotential surface.

For the meridional derivative we have

$$\frac{\partial \Psi}{\partial y} = - \int_{x_1^{\text{rock}}}^{x_2^{\text{rock}}} \left[\frac{\partial}{\partial y} \int_{\eta_b(x', y)}^{z=\eta(x', y, \sigma, t)} v(x', y, z', t) dz' \right] dx'. \quad (2.131)$$

Focusing on the vertical integral yields (dropping various coordinate dependencies when not

essential)

$$\frac{\partial}{\partial y} \int_{\eta_b(x',y)}^{z=\eta(x',y,\sigma)} v(x',y,z') dz' = v(\eta_\sigma) \partial_y \eta_\sigma - v(\eta_b) \partial_y \eta_b + \int_{\eta_b(x',y)}^{z=\eta(x',y,\sigma)} \partial_y v(x',y,z') dz'. \quad (2.132)$$

Focus again on the vertical integral and make use of the non-divergence condition to yield

$$\int_{\eta_b(x',y)}^{z=\eta(x',y,\sigma)} \partial_y v(x',y,z') dz' = - \int_{\eta_b(x',y)}^{z=\eta(x',y,\sigma)} [\partial_{x'} u(x',y,z') + \partial_{z'} w(x',y,z')] dz'. \quad (2.133)$$

Leibniz's rule on the $\partial_{x'} u(x',y,z')$ term then brings us to

$$\begin{aligned} \frac{\partial}{\partial y} \int_{\eta_b(x',y)}^{z=\eta(x',y,\sigma)} v(x',y,z') dz' &= -[w(\eta_\sigma) - \mathbf{u}(\eta_\sigma) \cdot \nabla \eta_\sigma] + [w(\eta_b) - \mathbf{u}(\eta_b) \cdot \nabla \eta_b] \\ &\quad - \frac{\partial}{\partial x} \int_{\eta_b(x',y)}^{z=\eta(x',y,\sigma)} u(x',y,z') dz'. \end{aligned} \quad (2.134)$$

Now $w(\eta_b) - \mathbf{u}(\eta_b) \cdot \nabla \eta_b = 0$ from the bottom no-flow **kinematic boundary condition**. Furthermore, from equation (2.35f) for the dia-surface velocity, we have

$$w(\eta_\sigma) - \mathbf{u}(\eta_\sigma) \cdot \nabla \eta_\sigma = w^{(\dot{\sigma})} + \partial_t \eta_\sigma. \quad (2.135)$$

Bringing these results together then renders

$$\frac{\partial \Psi}{\partial y} = \int_{x_1^{\text{rock}}}^{x_2^{\text{rock}}} [w^{(\dot{\sigma})}(x',y,z=\eta_\sigma) + \partial_t \eta_\sigma] dx', \quad (2.136)$$

where we set

$$u(x_1^{\text{rock}}) = u(x_2^{\text{rock}}) = 0. \quad (2.137)$$

We conclude that $\Psi(y, \sigma, t)$ is a streamfunction for the special case where σ is time independent, in which case

$$\frac{\partial \Psi}{\partial y} = \int_{x_1^{\text{rock}}}^{x_2^{\text{rock}}} w^{(\dot{\sigma})}(x',y,z=\eta_\sigma) dx' = W^{(\dot{\sigma})}(y, \sigma, t). \quad (2.138)$$

We can understand the need for time independence since that ensures that the flow underneath the σ surface is non-divergent, much like the case for a shallow water model in steady state (see VOLUME 3). In the literature, one can find $\Psi(y, \sigma, t)$ referred to as a streamfunction even when the flow has time dependence, in which case extra caution is needed if inferring the associated flow patterns.

2.13 Equations of motion

We here derive the equations of motion based on generalized vertical coordinates. The scalar equations were already discussed in Sections 2.9, 2.10, and 2.11, so we only summarize these equations here.

2.13.1 Mass and tracer equations

The mass and tracer equations were derived in Sections 2.9, 2.10, and 2.11, with their continuous vertical coordinate formulation given by

$$\frac{\partial(\rho \langle \cdot \rangle)}{\partial t} + \nabla_{\mathbf{v}} \cdot (\rho \langle \mathbf{u} \rangle + \partial_{\sigma}(\rho \langle \dot{\sigma} \rangle) = 0 \quad (2.139a)$$

$$\frac{\partial(\langle \rho C \rangle)}{\partial t} + \nabla_{\mathbf{v}} \cdot (\langle \rho C \mathbf{u} \rangle + \langle \mathbf{J}^h \rangle + \partial_{\sigma}(\rho \langle \dot{\sigma} C \rangle + \langle \nabla \sigma \cdot \mathbf{J} \rangle) = 0. \quad (2.139b)$$

Compatibility is maintained between the mass continuity equation (2.139a) and the tracer equation (2.139b) so long as the tracer equation reduces to the mass equation upon setting the tracer concentration to a spatial constant. Hence, for compatibility we must have the subgrid fluxes, \mathbf{J} , vanish when the tracer is a spatial constant. For example, diffusive fluxes, which are proportional to the tracer gradient, respect this constraint. These properties originate from our discussion of mass budgets and the **barycentric velocity** in VOLUME 2.

2.13.2 Momentum equation

From VOLUME 2, the horizontal and vertical components to the momentum equation are

$$\rho \frac{D\mathbf{u}}{Dt} + 2\rho \boldsymbol{\Omega} \times \mathbf{u} = -\rho \nabla_h \Phi - \nabla_h p + \rho \mathbf{F}^h \quad (2.140a)$$

$$\rho \frac{Dw}{Dt} = -\rho \frac{\partial \Phi}{\partial z} - \frac{\partial p}{\partial z} + \rho F^z. \quad (2.140b)$$

The simple form of the geopotential sets $\Phi = g z$, so that the horizontal gradient of the geopotential vanishes

$$\Phi = g z \implies \nabla_h \Phi = 0. \quad (2.141)$$

However, this gradient is nonzero in the presence of astronomical tide.

Horizontal momentum equation

We transform the horizontal derivatives from geopotential coordinates to generalized vertical coordinates according to (see equation (1.85))

$$\nabla_h = \nabla_{\mathbf{v}} - (\nabla_{\mathbf{v}} z) \partial_z, \quad (2.142)$$

thus leading to the horizontal momentum equation

$$\rho \frac{D\mathbf{u}}{Dt} + 2\rho \boldsymbol{\Omega} \times \mathbf{u} = -\rho [\nabla_{\mathbf{v}} - (\nabla_{\mathbf{v}} z) \partial_z] \Phi - [\nabla_{\mathbf{v}} - (\nabla_{\mathbf{v}} z) \partial_z] p + \rho \mathbf{F}^h. \quad (2.143)$$

In Section 2.13.5 we present some special cases for this equation that simplify the pressure and geopotential terms.

Vertical momentum equation

The vertical momentum equation is transformed into

$$\rho \frac{Dw}{Dt} = -\frac{\partial \sigma}{\partial z} \left[\rho \frac{\partial \Phi}{\partial \sigma} + \frac{\partial p}{\partial \sigma} \right] + \rho F^z, \quad (2.144)$$

with the hydrostatic form given by

$$\frac{\partial p}{\partial \sigma} = -\rho \frac{\partial \Phi}{\partial \sigma}. \quad (2.145)$$

2.13.3 Flux-form horizontal momentum equation

Using Cartesian horizontal coordinates and generalized vertical coordinates, the horizontal momentum equation includes a contribution from the acceleration that has a form similar to that for a tracer (Section 2.11)

$$\langle \rho \frac{Du}{Dt} \rangle = \left[\frac{\partial (\langle \rho u \rangle)}{\partial t} \right]_{\sigma} + \nabla_{\mathbf{v}} \cdot (\langle \rho u \mathbf{u} \rangle) + \partial_{\sigma} (\langle \rho u \dot{\sigma} \rangle) \quad (2.146a)$$

$$\langle \rho \frac{Dv}{Dt} \rangle = \left[\frac{\partial (\langle \rho v \rangle)}{\partial t} \right]_{\sigma} + \nabla_{\mathbf{v}} \cdot (\langle \rho v \mathbf{u} \rangle) + \partial_{\sigma} (\langle \rho v \dot{\sigma} \rangle). \quad (2.146b)$$

We provide a σ subscript on the time derivative operator to signal that this derivative is taken with σ held fixed. With spherical coordinates there are additional terms appearing on the right hand side (VOLUME 2). In particular, there is a metric term that contains the vertical velocity component, $w = Dz/Dt$. The appearance of w is awkward since the vertical velocity is not naturally computed using generalized vertical coordinates. This limitation is overcome through use of the vector-invariant velocity equation derived in Section 2.13.4.

2.13.4 Vector-invariant horizontal momentum equation

The **vector invariant** form of the velocity equation eliminates the metric terms that appear in the non-Cartesian flux-form equations. The vector-invariant form is also suited for deriving the vorticity equation considered in Section 2.15. Here, we start with the material time derivative in the form (2.51c) appropriate for generalized vertical coordinates, in which case the horizontal acceleration is given by

$$\frac{D\mathbf{u}}{Dt} = \left[\frac{\partial \mathbf{u}}{\partial t} \right]_{\sigma} + (\mathbf{u} \cdot \nabla_{\mathbf{v}}) \mathbf{u} + (\dot{\sigma} \partial_{\sigma}) \mathbf{u}. \quad (2.147)$$

Now make use of the vector identity (VOLUME 1)

$$(\mathbf{u} \cdot \nabla_{\mathbf{v}}) \mathbf{u} = \nabla_{\mathbf{v}} K + (\nabla_{\mathbf{v}} \times \mathbf{u}) \times \mathbf{u}, \quad (2.148)$$

where

$$K = \mathbf{u} \cdot \mathbf{u} / 2 \quad (2.149)$$

is the kinetic energy per mass of the horizontal flow. Introducing the generalized vertical coordinate version of the relative vorticity

$$\tilde{\zeta} \equiv \hat{\mathbf{z}} \cdot (\nabla_{\mathbf{v}} \times \mathbf{u}) = \left[\frac{\partial v}{\partial x} \right]_{\sigma} - \left[\frac{\partial u}{\partial y} \right]_{\sigma} \quad (2.150)$$

renders

$$\frac{D\mathbf{u}}{Dt} = \left[\frac{\partial \mathbf{u}}{\partial t} \right]_{\sigma} + \nabla_{\mathbf{v}} K + \tilde{\zeta} \hat{\mathbf{z}} \times \mathbf{u} + \dot{\sigma} \partial_{\sigma} \mathbf{u}, \quad (2.151)$$

so that the horizontal momentum equation takes the vector-invariant form

$$\left[\frac{\partial \mathbf{u}}{\partial t} \right]_{\sigma} + \dot{\sigma} \frac{\partial \mathbf{u}}{\partial \sigma} + (2\boldsymbol{\Omega} + \hat{\mathbf{z}} \tilde{\zeta}) \times \mathbf{u} = -\nabla_{\mathbf{v}} K - \nabla_{\mathbf{h}} \Phi - (1/\rho) \nabla_{\mathbf{h}} p + \mathbf{F}^h, \quad (2.152)$$

where again $\nabla_h = \nabla_{\mathbf{h}} - (\nabla_{\mathbf{h}} z) \partial_z$ as per equation (2.142). This equation is form-invariant regardless the horizontal coordinates, thus motivating the name *vector-invariant*.¹

2.13.5 Hydrostatic flow with constant gravitational acceleration

There are many special cases that simplify various terms in the momentum equation. For example, when considering a geopotential in the the simple form, $\Phi = g z$ with g assumed to be a constant effective gravitational acceleration, then the horizontal momentum equation (2.143) becomes

$$\rho \frac{D\mathbf{u}}{Dt} + 2\rho \boldsymbol{\Omega} \times \mathbf{u} = -[\nabla_{\mathbf{h}} - (\nabla_{\mathbf{h}} z) \partial_z] p + \rho \mathbf{F}^h. \quad (2.153)$$

Furthermore, assuming the flow maintains a hydrostatic balance (and corresponding simplification of the Coriolis acceleration as per the [traditional approximation](#)) allows us to write $\partial p / \partial z = -g \rho$ so that

$$\rho \frac{D\mathbf{u}}{Dt} + \rho f \hat{\mathbf{z}} \times \mathbf{u} = -[\nabla_{\mathbf{h}} p + \rho \nabla_{\mathbf{h}} \Phi] + \rho \mathbf{F}^h, \quad (2.154)$$

which also takes on the vector-invariant form

$$\left[\frac{\partial \mathbf{u}}{\partial t} \right]_{\sigma} + \dot{\sigma} \frac{\partial \mathbf{u}}{\partial \sigma} + (f + \tilde{\zeta}) \hat{\mathbf{z}} \times \mathbf{u} = -\nabla_{\mathbf{h}} (K + \Phi) - (1/\rho) \nabla_{\mathbf{h}} p + \mathbf{F}^h. \quad (2.155)$$

This form is commonly used for hydrostatic models of the ocean and atmosphere, such as discussed in [Griffies et al. \(2020\)](#).

2.14 Concerning the pressure force

As studied in [VOLUME 2](#), the pressure force acting on a fluid region is given by the integral

$$\mathbf{F}^{\text{press}} = - \oint_{\partial\mathcal{R}} p \hat{\mathbf{n}} d\mathcal{S} = - \int_{\mathcal{R}} \nabla p dV, \quad (2.156)$$

where the second equality follows from the [divergence theorem](#) applied to a scalar field. We refer to the right-most expression as the pressure gradient body force, and this expression is the basis for the discussion in [Sections 2.13.5](#) and [2.14.1](#). In this formulation, the pressure force at a point is oriented down the pressure gradient, so that the net pressure force acting on a region is the volume integral of the pressure gradient.

The middle expression in equation (2.156) formulates the pressure force acting on a region as the area integrated pressure contact stress acting on the region boundaries, with the orientation of the force determined by the inward normal at each point on the boundary. Much of this section is concerned with the contact stress expression as the basis for computing the pressure force acting on a finite region as shown in [Figure 2.11](#). The contact stress perspective was taken by [Lin \(1997\)](#) and [Adcroft et al. \(2008\)](#) in their finite volume approach to computing the pressure force acting on a finite numerical model grid cell.

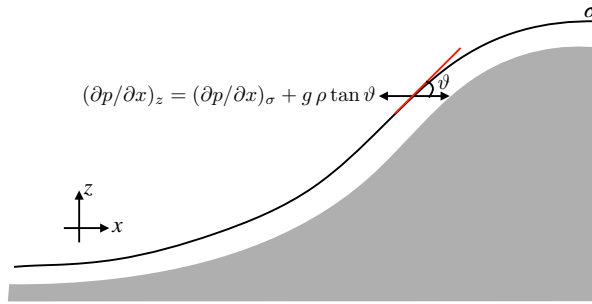


FIGURE 2.10: Illustrating how the horizontal pressure gradient is decomposed into two terms, one aligned with the surface of constant σ , and another associated with the slope of the σ -surface relative to the horizontal, $\tan \vartheta = (\partial z / \partial x)_\sigma$. We here consider the decomposition using terrain following vertical coordinates, where the vertical coordinate is aligned according to the solid-earth bottom (shaded region). Specifically, for terrain following Boussinesq ocean models we set $\sigma = (z - \eta) / (-\eta_b + \eta)$, where $z = \eta(x, y, t)$ is the ocean free surface and $z = \eta_b(x, y)$ is the ocean bottom topography. Terrain-following atmospheric models have a similar definition, often using pressure rather than geopotential so that $\sigma = (p - p_a) / (p_b - p_a)$, where p is the pressure, $p_a = p_a(x, y, t)$ is the pressure applied at the top of the atmosphere (typically assumed to be zero), and $p_b = p_b(x, y, t)$ is the pressure at the bottom of the atmosphere.

2.14.1 Computing the horizontal pressure gradient

The horizontal pressure gradient is aligned perpendicular to the local gravitational direction, and it is generally among the dominant horizontal forces acting on a fluid element. Hence, its accurate representation in numerical models is crucial for the physical integrity of a simulation. Unfortunately, decomposition of the horizontal pressure gradient into two terms according to the transformation (2.142) can lead to numerical difficulties. For example, with a simple geopotential and a hydrostatic flow, equation (2.154) shows that the horizontal pressure gradient takes the form

$$\nabla_h p = \nabla_\sigma p + \rho \nabla_\sigma \Phi = \nabla_\sigma p + g \rho \nabla_\sigma z, \quad (2.157)$$

with this decomposition illustrated in Figure 2.10 for the case of terrain following vertical coordinates. Numerical difficulties occur when the two terms on the right hand side have comparable magnitude but distinct signs. We are thus confronted with computing the small difference between two large numbers, and that situation generally exposes a numerical simulation to nontrivial truncation errors. Unfortunately, these errors can corrupt the integrity of the computed pressure forces and in turn contribute to spurious flow. An overview of this issue for ocean models is given by [Haney \(1991\)](#), [Mellor et al. \(1998\)](#), [Griffies et al. \(2000\)](#), with advances offered by [Lin \(1997\)](#), [Shchepetkin and McWilliams \(2002\)](#), and [Adcroft et al. \(2008\)](#).

In the remainder of this section, we outline a finite volume method for computing the pressure force as proposed by [Lin \(1997\)](#) for atmosphere models and [Adcroft et al. \(2008\)](#) for ocean models. This approach starts from the middle expression in equation (2.156) for the pressure force; i.e., it formulates the pressure force as the area integral of the pressure contact force rather than the volume integral of the pressure gradient force. Throughout this discussion we consider the proto-typical model grid cell as depicted in Figure 2.11, and we make use of the discussion of pressure [form stress](#) in VOLUME 2.

¹See Section 4.4.4 of [Griffies \(2004\)](#) for a detailed derivation using arbitrary horizontal coordinates.

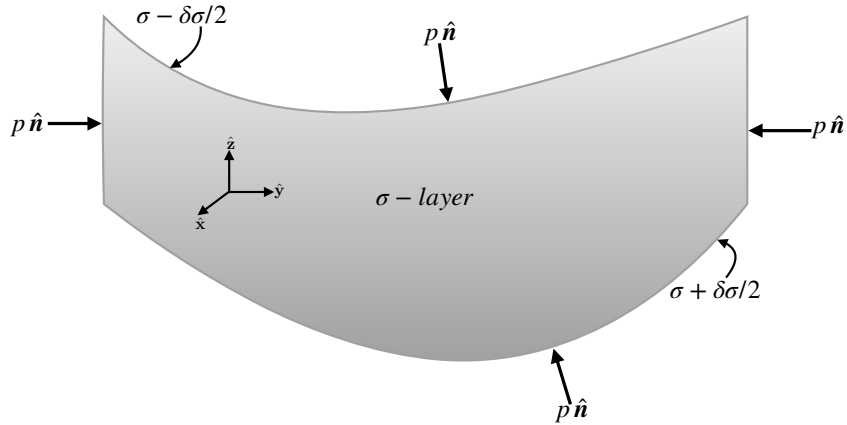


FIGURE 2.11: Schematic of pressure forces acting on the boundaries of a finite fluid region such as a discrete model grid cell. In generalized vertical coordinate models, the side faces are vertical, so that pressure acts only in the horizontal directions. The top and bottom faces are defined by surfaces of constant generalized vertical coordinates, $\sigma(x, y, z, t) = \text{constant}$, and we assume that these surfaces have an outward normal that has a nonzero projection into the vertical. As a result, we can write the depth of a point on the top and bottom surfaces as $z = \eta(x, y, \sigma, t)$. Because of the slope of the top and bottom surfaces, the surface normal vector has both a horizontal and vertical component. The net pressure force vector acting on the grid cell is given by the area integral of the pressure contact stress that acts on the grid cell boundary.

2.14.2 Integrated pressure contact stress on the cell faces

The inward normal on the grid cell vertical side boundaries points in the horizontal direction. For example, on the left side of Figure 2.11 the pressure force acts in the positive \hat{y} direction

$$\mathbf{F}_{\text{left}}^{\text{press}} = \hat{y} \int_{\text{left}} p \, dx \, dz \quad (2.158)$$

whereas pressure force on the right wall acts in the opposite direction

$$\mathbf{F}_{\text{right}}^{\text{press}} = -\hat{y} \int_{\text{right}} p \, dx \, dz. \quad (2.159)$$

Similar expressions appear for the front and back vertical boundaries acting in the $\pm \hat{x}$ directions.

Since the top and bottom boundaries of the grid cell are sloped, there is a pressure force acting on this surface directed in the horizontal and vertical directions. To unpack this force, write the vertical position of a point on the top interface as $z = \eta(x, y, t)$ so that the outward normal is given by

$$\hat{\mathbf{n}} = \frac{\nabla(z - \eta)}{|\nabla(z - \eta)|} = \frac{\hat{z} - \nabla\eta}{\sqrt{1 + |\nabla\eta|^2}}. \quad (2.160)$$

Following our discussion of dia-surface transport in Section 2.4.5, we know that the product of the normal direction and the area element can be written

$$\hat{\mathbf{n}} \, d\mathcal{S} = (\hat{z} - \nabla\eta) \, dA, \quad (2.161)$$

where $dA = dx \, dy$ is the horizontal projection of the area element (see Figure 2.3). Hence, the net pressure force acting on the top face is given by

$$\mathbf{F}_{\text{top}}^{\text{press}} = \int_{\text{top}} p (-\hat{z} + \nabla_{\text{h}} z) \, dx \, dy, \quad (2.162)$$

where we set $z = \eta$ in the second and third terms and recall that the horizontal slope vector for the top surface is given by

$$\nabla_{\text{h}} z = \hat{\mathbf{x}} (\partial z / \partial x)_{\sigma} + \hat{\mathbf{y}} (\partial z / \partial y)_{\sigma}, \quad (2.163)$$

where the σ subscript emphasizes that the horizontal derivative is taken with σ held constant. Notice that the pressure acts in the positive horizontal direction if the top surface slopes upward (surface shoaling) when directed in either of the two horizontal directions. Pressure acting on the bottom face has the same appearance yet with opposite signs

$$\mathbf{F}_{\text{bott}}^{\text{press}} = \int_{\text{bott}} p (\hat{\mathbf{z}} - \nabla_{\text{h}} z) \, dx \, dy. \quad (2.164)$$

The pressure acts in the positive horizontal direction if the bottom surface slopes downward (surface deepens) when directed in either of the two horizontal directions. As discussed in VOLUME 2, the horizontal pressure acting on a sloped surface is known as **form stress**. Here the sloped surface is defined by a constant generalized vertical coordinate.

2.14.3 Net vertical pressure force

Bringing the pieces together leads to the net vertical pressure force acting on the grid cell

$$\mathbf{F}_{\text{vertical}}^{\text{press}} = -\hat{\mathbf{z}} \left[\int_{\text{top}} p \, dx \, dy - \int_{\text{bott}} p \, dx \, dy \right]. \quad (2.165)$$

If the flow maintains a hydrostatic balance, then this vertical force is given by the weight of fluid within the cell

$$\mathbf{F}_{\text{vertical}}^{\text{press}} = \hat{\mathbf{z}} Mg, \quad (2.166)$$

where M is the mass of fluid in the grid cell. The net vertical hydrostatic pressure force acts vertically upward since hydrostatic pressure at the cell bottom is greater than at the cell top. This upward hydrostatic pressure force acting on the cell balances the downward weight of fluid in the cell.

2.14.4 Net horizontal pressure force

The net meridional pressure force is given by the forces acting on the sides as well as those acting on the sloped top and bottom boundaries. Taking the specific case of the $\hat{\mathbf{y}}$ pressure force yields

$$\begin{aligned} \hat{\mathbf{y}} \cdot \mathbf{F}^{\text{press}} &= \left[\int_{\text{left}} p \, dx \, dz - \int_{\text{right}} p \, dx \, dz \right] \\ &\quad + \left[\int_{\text{top}} p (\partial z / \partial y)_{\sigma} \, dx \, dy - \int_{\text{bott}} p (\partial z / \partial y)_{\sigma} \, dx \, dy \right]. \end{aligned} \quad (2.167)$$

We can write this expression in a more compact form by orienting the integration in a counter-clockwise manner around the cell boundaries, and making use of the identity $(\partial z / \partial y)_{\sigma} \, dy = dz$ on the top and bottom faces, so that

$$\hat{\mathbf{y}} \cdot \mathbf{F}^{\text{press}} = - \oint p \, dx \, dz. \quad (2.168)$$

For some purposes it is more convenient to work with the geopotential, $\Phi = g z$, than the pressure. In this case we can write the pressure force as

$$\hat{\mathbf{y}} \cdot \mathbf{F}^{\text{press}} = - \oint p \, dx \, dz = - \oint dx [d(pz) - z \, dp] = g^{-1} \oint \Phi \, dx \, dp, \quad (2.169)$$

where $\oint dx d(pz) = 0$. This form is useful with non-Boussinesq (compressible) flows, in which pressure is a natural vertical coordinate (e.g., see the caption to Figure 2.10). Notably, equation (2.169) holds whether the flow is hydrostatic or non-hydrostatic.

2.14.5 Comments

A numerical realization of the integrated contact pressure stress requires a representation of the pressure field along the boundaries of the grid cell. A variety of methods are available with differing accuracies. [Adcroft et al. \(2008\)](#) are notable in proposing an analytic form that allows for an exact integration along the cell faces in special cases, and a highly accurate numerical integration in other cases. In general, this method for computing pressure forces is highly suited to generalized vertical coordinate grid cells, which was the motivation offered by [Lin \(1997\)](#) in the context of terrain following atmospheric models.

2.15 Hydrostatic vorticity and potential vorticity

Generalized vertical coordinates are most commonly used to study flow that maintains the hydrostatic balance. We are thus motivated to develop the evolution equation for the vertical component of vorticity, $\tilde{\zeta}$, in a hydrostatic flow as written using generalized vertical coordinates. By extension, we derive the budget equation for the corresponding potential vorticity.

2.15.1 Basic manipulations

Recall the the vector-invariant velocity equation given by equation (2.155)

$$\left[\frac{\partial \mathbf{u}}{\partial t} \right]_\sigma + \dot{\sigma} \frac{\partial \mathbf{u}}{\partial \sigma} + \tilde{\zeta}_a \hat{\mathbf{z}} \times \mathbf{u} = -\nabla_\sigma (K + \Phi) - (1/\rho) \nabla_\sigma p + \mathbf{F}^h, \quad (2.170)$$

where $\tilde{\zeta}_a = \tilde{\zeta} + f$ is the absolute vorticity. Taking the curl of this equation and projecting onto the vertical direction leads to the vorticity equation

$$\frac{D\tilde{\zeta}_a}{Dt} = -\tilde{\zeta}_a \nabla_\sigma \cdot \mathbf{u} + \frac{\hat{\mathbf{z}} \cdot (\nabla_\sigma \rho \times \nabla_\sigma p)}{\rho^2} + \hat{\mathbf{z}} \cdot \left[\frac{\partial \mathbf{u}}{\partial \sigma} \times \nabla_\sigma \dot{\sigma} + \nabla_\sigma \times \mathbf{F}^h \right] \quad (2.171)$$

where we noted that the planetary vorticity, f , is independent of time and vertical position.

Making use of the mass conservation equation

Mass conservation in the form of equation (2.91)

$$\frac{1}{\rho} \frac{D(\rho)}{Dt} = -(\nabla_\sigma \cdot \mathbf{u} + \partial \dot{\sigma} / \partial \sigma), \quad (2.172)$$

renders

$$\rho \langle \frac{D}{Dt} \left[\frac{\tilde{\zeta}_a}{\rho \langle} \right] \rangle = \frac{\hat{z} \cdot (\nabla_{\text{h}} \rho \times \nabla_{\text{h}} p)}{\rho^2} + \tilde{\zeta}_a \frac{\partial \dot{\sigma}}{\partial \sigma} + \hat{z} \cdot \left[\frac{\partial \mathbf{u}}{\partial \sigma} \times \nabla_{\text{h}} \dot{\sigma} + \nabla_{\text{h}} \times \mathbf{F}^h \right]. \quad (2.173)$$

Massaging the $\dot{\sigma}$ terms

The terms containing $\dot{\sigma}$ can be written in the form

$$\tilde{\zeta}_a \partial_{\sigma} \dot{\sigma} + \hat{z} \cdot (\partial_{\sigma} \mathbf{u} \times \nabla_{\text{h}} \dot{\sigma}) = \tilde{\zeta}_a \partial_{\sigma} \dot{\sigma} + \hat{z} \cdot [-\nabla_{\text{h}} \times (\dot{\sigma} \partial_{\sigma} \mathbf{u}) + \dot{\sigma} \nabla_{\text{h}} \times \partial_{\sigma} \mathbf{u}] \quad (2.174a)$$

$$= \tilde{\zeta}_a \partial_{\sigma} \dot{\sigma} + \dot{\sigma} \partial_{\sigma} \tilde{\zeta}_a - \hat{z} \cdot [\nabla_{\text{h}} \times (\dot{\sigma} \partial_{\sigma} \mathbf{u})] \quad (2.174b)$$

$$= \partial_{\sigma} (\dot{\sigma} \tilde{\zeta}_a) - \hat{z} \cdot [\nabla_{\text{h}} \times (\dot{\sigma} \partial_{\sigma} \mathbf{u})]. \quad (2.174c)$$

2.15.2 Vorticity and potential vorticity equation

The above results allow us to write equation (2.173) in the form

$$\rho \langle \frac{DQ}{Dt} \rangle = \frac{\hat{z} \cdot (\nabla_{\text{h}} \rho \times \nabla_{\text{h}} p)}{\rho^2} + \partial_{\sigma} (\dot{\sigma} \tilde{\zeta}_a) + \nabla_{\text{h}} \cdot [\hat{z} \times \dot{\sigma} \partial_{\sigma} \mathbf{u} - \hat{z} \times \mathbf{F}^h], \quad (2.175)$$

where we introduced the potential vorticity defined according to the generalized vertical coordinates

$$Q = \frac{\tilde{\zeta}_a}{\rho \langle}. \quad (2.176)$$

The potential vorticity equation (2.175) has a generally nonzero baroclinicity

$$\frac{\hat{z} \cdot (\nabla_{\text{h}} \rho \times \nabla_{\text{h}} p)}{\rho^2}, \quad (2.177)$$

so that the potential vorticity (2.176) is generally not materially invariant even if $\dot{\sigma} = 0$ and $\mathbf{F}^h = 0$. Finally, note that it is sometimes convenient to make use of the potential vorticity (2.176) in the horizontal velocity equation (2.170) so that

$$\left[\frac{\partial \mathbf{u}}{\partial t} \right]_{\sigma} + \dot{\sigma} \frac{\partial \mathbf{u}}{\partial \sigma} + (\langle \rho Q \rangle \hat{z} \times \mathbf{u}) = -\nabla_{\text{h}} (K + \Phi) - (1/\rho) \nabla_{\text{h}} p + \mathbf{F}^h. \quad (2.178)$$

Pressure coordinates

The baroclinicity (2.177) vanishes when choosing $\sigma = p$, as noted when studying baroclinicity in VOLUME 3. However, pressure is not a useful scalar for defining potential vorticity since $\dot{\sigma} = \dot{p}$ does not generally vanish for a perfect fluid. Namely, a nonzero \dot{p} merely signals vertical motion, so that $\dot{p} \neq 0$ for both real and perfect fluids. Hence, even though the baroclinicity vanishes by choosing $\sigma = p$, the terms with $\dot{\sigma}$ do not.

Flux-form potential vorticity budget

Just like we did in Section 2.13.3 for the velocity equation, we can make use of the thickness equation (2.139a) to bring the material time derivative in equation (2.175) into the form

$$\rho \langle \frac{DQ}{Dt} \rangle = \rho \langle (\partial_t + \mathbf{u} \cdot \nabla_{\text{h}} + \dot{\sigma} \partial_{\sigma}) Q \rangle + Q [\partial_t (\rho \langle) + \nabla_{\text{h}} \cdot (\rho \langle \mathbf{u}) + \partial_{\sigma} (\rho \langle \dot{\sigma})] \quad (2.179a)$$

$$= \partial_t(\rho \langle Q \rangle) + \nabla_{\mathbf{h}} \cdot (\rho \langle \mathbf{u} Q \rangle) + \partial_{\sigma}(\rho \langle \dot{\sigma} Q \rangle). \quad (2.179b)$$

Since $\tilde{\zeta}_{\text{a}} = \langle \rho Q \rangle$, we see that the term

$$\partial_{\sigma}(\rho \langle \dot{\sigma} Q \rangle) = \partial_{\sigma}(\dot{\sigma} \tilde{\zeta}_{\text{a}}), \quad (2.180)$$

also appears on the right hand side of equation (2.175). Hence, it cancels from the flux form potential vorticity equation

$$\left[\frac{\partial(\rho \langle Q \rangle)}{\partial t} \right]_{\sigma} = \frac{\hat{\mathbf{z}} \cdot (\nabla_{\mathbf{h}} \rho \times \nabla_{\mathbf{h}} p)}{\rho^2} - \nabla_{\mathbf{h}} \cdot [\rho \langle \mathbf{u} Q + \hat{\mathbf{z}} \times \dot{\sigma} \partial_{\sigma} \mathbf{u} + \hat{\mathbf{z}} \times \mathbf{F}^{\text{h}} \rangle], \quad (2.181)$$

which is equivalent to the absolute vorticity equation

$$\left[\frac{\partial \tilde{\zeta}_{\text{a}}}{\partial t} \right]_{\sigma} = \frac{\hat{\mathbf{z}} \cdot (\nabla_{\mathbf{h}} \rho \times \nabla_{\mathbf{h}} p)}{\rho^2} - \nabla_{\mathbf{h}} \cdot [\mathbf{u} \tilde{\zeta}_{\text{a}} + \hat{\mathbf{z}} \times \dot{\sigma} \partial_{\sigma} \mathbf{u} + \hat{\mathbf{z}} \times \mathbf{F}^{\text{h}}]. \quad (2.182)$$

As a check, note that setting $\sigma = z$ so that $\langle \cdot \rangle = 1$ reduces the vorticity equation (2.182) to the vertical component of the vorticity equation

$$\rho \frac{D(\boldsymbol{\omega}_{\text{a}}/\rho)}{Dt} = (\boldsymbol{\omega}_{\text{a}} \cdot \nabla) \mathbf{v} + \mathbf{B} + \nabla \times \mathbf{F}. \quad (2.183)$$

2.15.3 Potential vorticity for the Boussinesq ocean

From VOLUME 3, the Boussinesq ocean vorticity budget has a vertical component to the absolute vorticity that is unaffected by baroclinicity. This property holds in the present context, as seen by returning to the vector-invariant velocity equation (2.170) and setting the factor $1/\rho$ multiplying the pressure gradient to $1/\rho_{\text{o}}$ as part of the Boussinesq ocean

$$(1/\rho) \nabla_{\mathbf{h}} p \longrightarrow (1/\rho_{\text{o}}) \nabla_{\mathbf{h}} p, \quad (2.184)$$

in which ρ_{o} is a constant. In this case the $\nabla_{\mathbf{h}} \times$ operation annihilates pressure and we are left with no vertical component to the baroclinicity. We are thus led to define the Boussinesq potential vorticity

$$Q = \frac{\tilde{\zeta}_{\text{a}}}{\langle \cdot \rangle} \quad (2.185)$$

which satisfies the material and flux-form evolution equations

$$\langle \frac{DQ}{Dt} \rangle = \partial_{\sigma}(\dot{\sigma} \langle Q \rangle) + \nabla_{\mathbf{h}} \cdot [\hat{\mathbf{z}} \times \dot{\sigma} \partial_{\sigma} \mathbf{u} - \hat{\mathbf{z}} \times \mathbf{F}^{\text{h}}] \quad (2.186)$$

$$\left[\frac{\partial(\langle Q \rangle)}{\partial t} \right]_{\sigma} = -\nabla_{\mathbf{h}} \cdot [\langle \mathbf{u} Q + \hat{\mathbf{z}} \times \dot{\sigma} \partial_{\sigma} \mathbf{u} + \hat{\mathbf{z}} \times \mathbf{F}^{\text{h}} \rangle]. \quad (2.187)$$

We again emphasize that $\dot{\sigma}$ is generally non-zero, even for a perfect fluid, so that potential vorticity as defined via σ is not generally a material constant for a perfect fluid. It is only when $\dot{\sigma} = 0$ for a perfect fluid (e.g., σ is buoyancy or specific entropy) that we recover the desirable perfect fluid properties of potential vorticity. We develop the theory for this case in Section 3.3.

2.15.4 Comments

We emphasize that the potential vorticity as given by either equations (2.176) or equation (2.185) are generally not materially invariant since they have a non-zero baroclinicity that remains even for a perfect fluid. The key point is that the vertical coordinate must itself be materially invariant, as per the case of a buoyancy coordinate in a perfect fluid that renders the Ertel potential vorticity. This point is easily lost in the details of generalized vertical coordinate numerical models (e.g., [Griffies et al. \(2020\)](#)). So although the numerical model might have a variable referred to as “potential vorticity”, it refers to the Ertel potential vorticity only when the layer specific thickness measures the buoyancy stratification. The special case of $\sigma = z$ offers a clear case in point, in which $\langle \cdot \rangle = 1$ so that Q reduces to the absolute vorticity.



2.16 Exercises

EXERCISE 2.1: PRACTICE WITH BOUSSINESQ TERRAIN FOLLOWING COORDINATES

In this exercise we derive some equations using the terrain following coordinate from Section 1.3.2

$$\sigma = \frac{z - \eta_s}{-\eta_b + \eta_s}, \quad (2.188)$$

with this coordinate suited to a Boussinesq ocean.

- Write the expression for the vertical grid cell increment, dz , in terms of $d\sigma$.
- Write the time tendency equation for dz .
- Compute the vertical integral, $\int_{\sigma(\eta_b)}^{\sigma(\eta_s)} d\sigma$.

EXERCISE 2.2: PRACTICE WITH BOUSSINESQ BOTTOM SLOPE COORDINATES

In this exercise we repeat Exercise 2.1 only here with the bottom slope coordinate from Section 1.3.4

$$\sigma = z - \mathbf{x} \cdot \nabla \eta_b. \quad (2.189)$$

These coordinates were used by [Peterson and Callies \(2022\)](#) in their study of turbulence along a sloping bottom.

- Write the expression for the vertical grid cell increment, dz , in terms of $d\sigma$.
- Write the time tendency equation for dz .
- Compute the vertical integral, $\int_{\sigma(\eta_b)}^{\sigma(\eta_s)} d\sigma$.

EXERCISE 2.3: PRACTICE WITH NON-BOUSSINESQ TERRAIN FOLLOWING COORDINATES

In this exercise we repeat Exercise 2.1, here using the pressure-based terrain following vertical coordinate,

$$\sigma = \frac{p - p_a}{p_b - p_a}, \quad (2.190)$$

for a fluid in approximate hydrostatic balance so that

$$\partial_z p = -\rho g. \quad (2.191)$$

In equation (2.190) we introduced the bottom pressure, $p_b(x, y, t)$, and the applied surface pressure, $p_a(x, y, t)$. For an atmosphere we might set $p_a = 0$ for the top of the atmosphere pressure.

- Write the expression for the density-weighted vertical grid cell increment, ρdz (also the mass per horizontal area), in terms of $d\sigma$.
- Write the time tendency equation for ρdz .
- Compute the vertical integral, $\int_{\sigma(\eta_b)}^{\sigma(\eta_s)} d\sigma$.
- Compute the vertical integral, $\int_{\eta_b}^{\eta_s} \rho dz$, thus determining the total mass per unit horizontal area for the fluid column.

EXERCISE 2.4: PRACTICE WITH NON-BOUSSINESQ RESCALED PRESSURE COORDINATES

In this exercise we repeat Exercise 2.3, here using the rescaled pressure vertical coordinate from Section 1.3.3,

$$\sigma = \frac{p_{bo} (p - p_a)}{p_b - p_a} \quad (2.192)$$

for a fluid in approximate hydrostatic balance so that

$$\partial_z p = -\rho g. \quad (2.193)$$

In equation (2.192), we introduced the bottom pressure, $p_b(x, y, t)$, the applied surface pressure, $p_a(x, y, t)$, and the bottom pressure for a resting fluid, p_{bo} .

- Write the expression for the density-weighted vertical grid cell increment, ρdz (also the mass per horizontal area), in terms of $d\sigma$.
- Write the time tendency equation for ρdz .
- Compute the vertical integral, $\int_{\sigma(\eta_b)}^{\sigma(\eta_s)} d\sigma$.
- Compute the vertical integral, $\int_{\eta_b}^{\eta_s} \rho dz$, thus determining the total mass per unit horizontal area for the fluid column.

EXERCISE 2.5: CHECKING THE VORTICITY EQUATION

Verify that for $2\Omega = f\hat{z}$ the choice $\sigma = z$ reduces the vorticity equation (2.182) to the vertical component of the vorticity equation (2.183).



Chapter 3

CONTINUOUS AND LAYERED ISOPYCNAL MODELS

Away from turbulent boundary layers, flows in stratified fluids are oriented according to buoyancy surfaces. For this reason, buoyancy in the ocean or specific entropy in the atmosphere play a key role in theoretical and numerical models of ocean and atmosphere circulation. In this chapter we study the hydrostatic Boussinesq ocean equations using buoyancy as the vertical coordinate, deriving their momentum equations as well as their vorticity and potential vorticity equations. The resulting primitive equations form the basis for *isopycnal* models of the ocean as well as isentropic models of the atmosphere.

We pay particular attention to the needs of vertically integrating the equations over discrete layers, as required to develop numerical layered isopycnal models. Since we are considering a perfect fluid, the vertically discrete layered isopycnal equations are identical to the stacked shallow water equations. We further an understanding of the stacked shallow water model by deriving, in some detail, the [thickness weighted averaging \(TWA\)](#) shallow water equations. The [TWA](#) equations provide a versatile mathematical and numerical framework for studying the physics of eddy and mean flow interactions.

READER'S GUIDE FOR THIS CHAPTER

Throughout this chapter we expose details for the practitioner interested in the mathematical physics of momentum, vorticity and potential vorticity as realized using buoyancy as a vertical coordinate. We assume a linear equation of state, thus allowing for buoyancy to provide a full expression of thermodynamics. The derivations require an understanding of the generalized vertical coordinate mathematics in Chapter 1 and geophysical fluid mechanics in Chapter 2. It is notable that the contravariant form of the horizontal velocity, \mathbf{u} , appears in both geopotential vertical coordinate and generalized vertical coordinate formulations, thus motivating its use throughout this chapter. In the second half of this chapter, we assume a working knowledge of the shallow water model from [VOLUME 3](#).

3.1	Loose threads	70
3.2	Layered isopycnal primitive equations	71
3.2.1	Montgomery potential and the pressure force	71
3.2.2	Material time derivative	73
3.2.3	Layer thickness and specific thickness	73
3.2.4	Summary of the isopycnal ocean equations	75
3.2.5	Thickness weighted velocity equation	75
3.2.6	Vector-invariant horizontal velocity equation	75
3.2.7	Connection to the stacked shallow water equations	76
3.2.8	Diapycnal transfer	76

3.2.9	Momentum transfer	77
3.2.10	Vanished isopycnal layers	77
3.3	Potential vorticity using isopycnal coordinates	77
3.3.1	The vorticity equation	78
3.3.2	Derivation of the potential vorticity equation	78
3.3.3	Potential vorticity with irreversible processes	79
3.3.4	Comments	81
3.4	Thickness weighted shallow water	81
3.4.1	Stacked shallow water versus continuous isopycnal	81
3.4.2	Concerning the gradient operator	82
3.4.3	The unaveraged thickness weighted equations	82
3.5	Thickness transport by the bolus velocity	83
3.5.1	Rectified effects	83
3.5.2	An undulating shallow water fluid layer	83
3.5.3	Stokes drift	84
3.5.4	Linearized thickness perturbations	85
3.5.5	Correlation between thickness and velocity	86
3.5.6	Is the bolus velocity needed for the mean-field equations?	86
3.6	A summary of averaging operators	86
3.6.1	Reynolds average	87
3.6.2	Ensemble average	87
3.6.3	The algebra of thickness weighted averages	88
3.6.4	Comments	89
3.7	TWA equations for thickness and tracer	89
3.7.1	TWA thickness equation	89
3.7.2	Tracer equation	90
3.7.3	Defining w^\sharp via continuity with \hat{u}	90
3.8	Horizontal momentum equation	91
3.8.1	Kinetic stress and Reynolds stress	91
3.8.2	Thickness and pressure gradient correlation	92
3.8.3	Unpacking the thickness and pressure gradient correlation	92
3.8.4	Zonal and meridional Eliassen-Palm fluxes: version I	96
3.8.5	Zonal and meridional Eliassen-Palm fluxes: version II	97
3.8.6	Interfacial stresses from geostrophic eddies	98
3.8.7	Comments	99
3.9	Vorticity and potential vorticity	99
3.9.1	Derivation	99
3.9.2	Concerning the mean field potential vorticity	100
3.9.3	Comments	100
3.10	Vorticity fluxes for non-divergent barotropic flow	101
3.11	Exercises	102

3.1 Loose threads

- Formulate the TWA energy equations as in [Loose et al. \(2022\)](#) or [Loose et al. \(2023\)](#).
- Formulate the thickness weighted tracer variance equations as in Appendix A of [Pudig et al. \(2026\)](#).

3.2 Layered isopycnal primitive equations

Rather than specializing the generalized vertical coordinate equations provided in Section 2.13, we find it pedagogical to start from the equations written using the geopotential vertical coordinate (VOLUME 2)

$$\frac{D\mathbf{u}}{Dt} + f \hat{z} \times \mathbf{u} = -\nabla_h \varphi + \mathbf{F}^h \quad \text{horizontal momentum} \quad (3.1a)$$

$$\frac{\partial \varphi}{\partial z} = b \quad \text{hydrostatic} \quad (3.1b)$$

$$\nabla_h \cdot \mathbf{u} + \frac{\partial w}{\partial z} = 0 \quad \text{continuity} \quad (3.1c)$$

$$\frac{Db}{Dt} = \dot{b} \quad \text{thermodynamics} \quad (3.1d)$$

$$\frac{DC}{Dt} = \dot{C} \quad \text{tracers,} \quad (3.1e)$$

In these equations, $\mathbf{v} = (\mathbf{u}, w)$ is the velocity field with \mathbf{u} its horizontal component, φ is the dynamic pressure, b is the Archimedean buoyancy, C is an arbitrary tracer concentration, \dot{b} and \dot{C} arise from processes leading to material time changes, and \mathbf{F}^h is an acceleration arising from friction and/or boundary stresses. A discrete realization of the isopycnal layer-integrated form of these equations is depicted in Figure 3.1, with the remainder of this section detailing the continuum formulation using isopycnal generalized vertical coordinates.

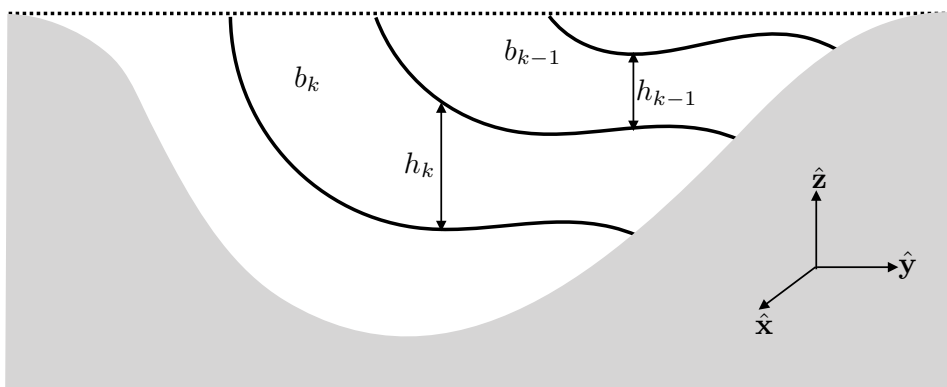


FIGURE 3.1: Schematic of an isopycnal model, formulated as stacked shallow water layers that generally allow for the transfer of matter and energy across the layer interfaces as well as across the ocean surface and ocean bottom. Discrete layer thicknesses are denoted h_k with corresponding layer buoyancy, b_k . The dark gray region is land.

3.2.1 Montgomery potential and the pressure force

We here consider the horizontal pressure force appearing in isopycnal models, in which we uncover the importance of the Montgomery potential.

Horizontal pressure gradient force

Throughout this chapter we make use of the horizontal derivatives on constant buoyancy surfaces (derived in Section 1.12), written here in the form

$$\nabla_{hb} = \hat{x} \left[\frac{\partial}{\partial x} \right]_b + \hat{y} \left[\frac{\partial}{\partial y} \right]_b. \quad (3.2)$$

Following the discussion in Section 2.13.2, the horizontal pressure gradient transforms as

$$\nabla_h \varphi = \nabla_{hb} \varphi - \frac{\partial \varphi}{\partial z} \nabla_{hb} z = \nabla_{hb} \varphi - b \nabla_{hb} z = \nabla_{hb} (\varphi - b z) = \nabla_{hb} M, \quad (3.3)$$

where

$$M = \varphi - b z \quad (3.4)$$

defines the [Montgomery potential](#). Furthermore, as shown in a few paragraphs below, the Montgomery potential satisfies the buoyancy coordinate form of the hydrostatic balance. Evidently, the Montgomery potential plays a role for isopycnal coordinates that is directly analogous to pressure in geopotential coordinates. Correspondingly, the Montgomery potential is the geostrophic streamfunction in buoyancy coordinates (see Section 3.2.4).

Concerning the horizontal pressure gradient force for numerical models

In deriving equation (3.3), a critical step concerns our ability to bring buoyancy inside the ∇_{hb} gradient operator, which follows from $\nabla_{hb} b = 0$. As a result, we can combine two terms into the single Montgomery potential. We contrast this key step with that found in the more general case considered in Section 2.14 and highlighted in Figure 2.10. For the general case, we cannot always combine the two terms, thus leading to difficulties with accurate numerical realizations of the horizontal pressure gradient. Evidently, the ability to make use of the Montgomery potential offers a distinct advantage for isopycnal coordinates over alternative approaches to studying stratified perfect fluid flows.

The property $\nabla_{hb} b = 0$ is available only under certain cases that utilize an idealized equation of state. In more realistic cases, the buoyancy determining the hydrostatic pressure (i.e., the *mass buoyancy*) is defined locally with the *in situ* density, whereas the generalized vertical coordinate must be defined globally. As a result, use of a realistic equation of state leads to two terms contributing to the pressure gradient in a manner similar to terrain-following models (Figure 2.10). [Sun et al. \(1999\)](#), [Hallberg \(2005\)](#), and [Adcroft et al. \(2008\)](#) discuss this issue in the context of numerical isopycnal ocean modeling. For the present chapter we ignore this detail and so assume a simplified equation of state so that $\nabla_{hb} b = 0$.

Hydrostatic balance

Supporting our use of the Montgomery potential as a pressure field, the hydrostatic balance takes the form

$$\frac{\partial M}{\partial b} = \frac{\partial \varphi}{\partial b} - b \frac{\partial z}{\partial b} - z = \frac{\partial \varphi}{\partial z} \frac{\partial z}{\partial b} - b \frac{\partial z}{\partial b} - z = -z, \quad (3.5)$$

where we made use of the hydrostatic balance $\partial \varphi / \partial z = b$ (equation (3.1b)). This result further supports considering the Montgomery potential as the buoyancy coordinate version of pressure.

3.2.2 Material time derivative

As seen in Section 2.5, there are two equivalent forms for the material time derivative

$$\frac{D}{Dt} = \left[\frac{\partial}{\partial t} \right]_z + \mathbf{u} \cdot \nabla_h + w \frac{\partial}{\partial z} \quad \text{geopotential form} \quad (3.6a)$$

$$= \left[\frac{\partial}{\partial t} \right]_b + \mathbf{u} \cdot \nabla_{hb} + w^{(b)} \frac{\partial}{\partial z} \quad \text{isopycnal form,} \quad (3.6b)$$

where

$$w^{(b)} = \frac{\partial z}{\partial b} \frac{Db}{Dt} \quad (3.7)$$

is the diapycnal velocity component that measures the rate that fluid crosses buoyancy surfaces (Section 2.4). Besides differences in the spatial operators, it is important to note that the time derivative operators in equations (3.6a) and (3.6b) are computed on constant geopotential and constant buoyancy surfaces, respectively. However, the horizontal velocity component is the *same* for both forms of the material time derivative

$$\mathbf{u} = \hat{\mathbf{x}} u + \hat{\mathbf{y}} v = (D/Dt) (\hat{\mathbf{x}} x + \hat{\mathbf{y}} y). \quad (3.8)$$

3.2.3 Layer thickness and specific thickness

The continuity equation, $\nabla_h \cdot \mathbf{u} + \partial_z w = 0$, is an expression of volume conservation. We already derived the generalized vertical coordinate version of this equation in Section 2.10.3, and thus quote the isopycnal layer thickness result here

$$\left[\frac{\partial h}{\partial t} \right]_b + \nabla_{hb} \cdot (h \mathbf{u}) + \Delta_b w^{(b)} = 0. \quad (3.9)$$

The field, h , measures the isopycnal layer thickness (with dimensions of length) and is given by the vertical integral over a layer

$$h = \int_{z(b-\delta b/2)}^{z(b+\delta b/2)} dz = \int_{b-\delta b/2}^{b+\delta b/2} \frac{\partial z}{\partial b} db = \int_{b-\delta b/2}^{b+\delta b/2} \langle db = \int_{b-\delta b/2}^{b+\delta b/2} N^{-2} db = \bar{b} db. \quad (3.10)$$

The specific thickness, $\langle \cdot \rangle$, is the thickness per buoyancy, and it equals to the inverse squared buoyancy frequency

$$\langle \cdot \rangle = \frac{\partial z}{\partial b} = N^{-2}, \quad (3.11)$$

with its layer averaged value

$$\bar{b} = h/\delta b. \quad (3.12)$$

Furthermore, the dia-surface transport velocity is given by

$$w^{(b)} = \langle \dot{b} \rangle. \quad (3.13)$$

Its difference across layer interfaces,

$$\Delta_b w^{(b)} = \int_{b-\delta b/2}^{b+\delta b/2} \frac{\partial w^{(b)}}{\partial b} db = w^{(b)}(b + \delta b/2) - w^{(b)}(b - \delta b/2) \quad (3.14)$$

measures the amount of fluid that diverges from the layer through cross-layer transport.

In the limit that $\delta b \rightarrow 0$, we find that the non-dimensional vertical difference operator can be written in one of the following equivalent manners

$$\lim_{\delta b \rightarrow 0} \Delta_b = \delta b \frac{\partial}{\partial b} = \delta b \frac{\partial z}{\partial b} \frac{\partial}{\partial z} = \delta z \frac{\partial}{\partial z} = h \frac{\partial}{\partial z}. \quad (3.15)$$

The relations are useful in moving between discrete and continuous formulations of the isopycnal equations.

Specific thickness equation

Inserting $h = \bar{\delta}b$ into the thickness equation (3.9) leads to

$$\left[\frac{\partial \bar{\delta}}{\partial t} \right]_b + \nabla_{hb} \cdot (\bar{\delta} \mathbf{u}) + \partial_b w^{(b)} = 0, \quad (3.16)$$

where we pulled the buoyancy increment, δb , outside of the time and horizontal derivative operators since δb is a fixed number for a chosen layer. We also used the identity (3.15) relating the difference operator to a differential operator

$$\delta b \partial_b = \Delta_b. \quad (3.17)$$

For a vertically continuous treatment, equation (3.16) can be written with $\langle \cdot \rangle$ rather than the discrete layer averaged value

$$\left[\frac{\partial \langle \delta \rangle}{\partial t} \right]_b + \nabla_{hb} \cdot (\langle \delta \mathbf{u} \rangle) + \partial_b w^{(b)} = 0. \quad (3.18)$$

It is generally more convenient to use the specific thickness when working with the vertically continuous equations, whereas the finite layer thickness, h , is more suitable for the layer integrated equations.

Perfect fluid limit

When $w^{(b)} \neq 0$, the three terms in the thickness equation (3.9) are coupled. Likewise, the three terms in the specific thickness equation (3.16) are coupled. We discussed this coupling in Section 2.6 as part of a broader study of the vertical velocity and the dia-surface velocity. When considering perfect fluids, we have $w^{(b)} = \langle \dot{b} \rangle = 0$ since buoyancy remains materially constant. In this case the layer thickness is altered only through horizontal rearrangements of volume within a layer according to the perfect fluid thickness equation

$$\left[\frac{\partial h}{\partial t} \right]_b + \nabla_{hb} \cdot (h \mathbf{u}) = 0. \quad (3.19)$$

As further discussed in Section 3.2.7, the perfect fluid limit brings the discrete isopycnal model into accord with the immiscible stacked shallow water models studied in VOLUME 3.

3.2.4 Summary of the isopycnal ocean equations

Bringing the pieces together leads to the isopycnal version of the hydrostatic Boussinesq equations

$$\left[\frac{\partial \mathbf{u}}{\partial t} \right]_b + (\mathbf{u} \cdot \nabla_{\text{hb}}) \mathbf{u} + (w^{(b)} \partial_z) \mathbf{u} + f \hat{\mathbf{z}} \times \mathbf{u} = -\nabla_{\text{hb}} M + \mathbf{F}^h \quad \text{momentum} \quad (3.20a)$$

$$\frac{\partial M}{\partial b} = -z \quad \text{hydrostatic} \quad (3.20b)$$

$$\left[\frac{\partial h}{\partial t} \right]_b + \nabla_{\text{hb}} \cdot (h \mathbf{u}) + \Delta_b w^{(b)} = 0 \quad \text{thickness} \quad (3.20c)$$

$$\left[\frac{\partial (h C)}{\partial t} \right]_b + \nabla_{\text{hb}} \cdot (h C \mathbf{u} + h \mathbf{J}^h) + \Delta_b (C w^{(b)} + J^{(b)}) = 0 \quad \text{tracer,} \quad (3.20d)$$

where the tracer equation includes possible subgrid scale flux contributions in addition to advective transport. Notice how the advective transport is two-dimensional in the perfect fluid limit where $\dot{b} = 0$, in which case layer-integrated scalar properties, such as volume and tracer content, are constant within buoyancy layers. Also note that geostrophic balance in the horizontal momentum equation (3.20a) gives

$$f \hat{\mathbf{z}} \times \mathbf{u}_g = -\nabla_{\text{hb}} M \implies f u_g = - \left[\frac{\partial M}{\partial y} \right]_b \quad \text{and} \quad f v_g = \left[\frac{\partial M}{\partial x} \right]_b. \quad (3.21)$$

Hence, the Montgomery potential is the streamfunction for geostrophic flow as represented using buoyancy coordinates.

3.2.5 Thickness weighted velocity equation

As in our discussion of the stacked shallow water model in VOLUME 3, we can write the velocity equation (3.20a) in its thickness weighted form, with this form suited to studying momentum balances and pressure form stresses. The manipulations are directly analogous to the shallow water case, whereby we multiply equation (3.20a) by the thickness, h , and multiply the thickness equation (3.20c) by the horizontal velocity, \mathbf{u} , and then summing to find

$$\left[\frac{\partial (h \mathbf{u})}{\partial t} \right]_b + \nabla_{\text{hb}} \cdot (h \mathbf{u} \otimes \mathbf{u}) + \Delta_b (w^{(b)} \mathbf{u}) + f \hat{\mathbf{z}} \times (h \mathbf{u}) = -h \nabla_{\text{hb}} M + h \mathbf{F}^h. \quad (3.22)$$

For the diapycnal transfer term, we made use of the operator identity

$$\lim_{\delta b \rightarrow 0} \Delta_b = h \partial_z \quad (3.23)$$

from equation (3.15).

3.2.6 Vector-invariant horizontal velocity equation

It is common for isopycnal models to make use of the vector-invariant form of the momentum equation derived in Section 2.13.4. Introducing the isopycnal version of the relative vorticity,

$$\hat{\mathbf{z}} \tilde{\zeta} \equiv \nabla_{\text{hb}} \times \mathbf{u} = \left[\frac{\partial v}{\partial x} \right]_b - \left[\frac{\partial u}{\partial y} \right]_b, \quad (3.24)$$

renders the vector-invariant horizontal velocity equation

$$\left[\frac{\partial \mathbf{u}}{\partial t} \right]_b + w^{(b)} \partial_z \mathbf{u} + \tilde{\zeta}_a \hat{z} \times \mathbf{u} = -\nabla_{hb} \mathcal{B} + \mathbf{F}^h, \quad (3.25)$$

where

$$\mathcal{B} = M + \mathbf{u} \cdot \mathbf{u} / 2 = \varphi - b z + \mathbf{u} \cdot \mathbf{u} / 2 \quad (3.26)$$

is the Bernoulli potential for a hydrostatic Boussinesq fluid, and

$$\tilde{\zeta}_a = \tilde{\zeta} + f \quad (3.27)$$

is the vertical component to the absolute vorticity using isopycnal coordinates. Note that we can further introduce the isopycnal potential vorticity (Section 3.3.2)

$$h Q = \tilde{\zeta}_a \quad (3.28)$$

to bring the horizontal velocity equation to the form

$$\left[\frac{\partial \mathbf{u}}{\partial t} \right]_b + w^{(b)} \partial_z \mathbf{u} + Q \hat{z} \times (h \mathbf{u}) = -\nabla_{hb} \mathcal{B} + \mathbf{F}^h. \quad (3.29)$$

This form is commonly used as the starting point for certain theoretical analyses, particularly when considering the perfect fluid limit in which $w^{(b)} = 0$.

3.2.7 Connection to the stacked shallow water equations

We can make use of the material time derivative operator (3.6b) to write the material form of the perfect fluid equations (3.20a)-(3.20c)

$$\frac{D \mathbf{u}}{Dt} + f \hat{z} \times \mathbf{u} = -\nabla_{hb} M \quad (3.30a)$$

$$\frac{\partial M}{\partial b} = -z \quad (3.30b)$$

$$\frac{D h}{Dt} + h \nabla_{hb} \cdot \mathbf{u} = 0. \quad (3.30c)$$

These isopycnal equations are isomorphic to those for a single layer of perfect shallow water fluid (VOLUME 3). This isomorphism allows us to derive the vorticity and potential vorticity equations in Section 3.3 by directly following the shallow water manipulations.

3.2.8 Diapycnal transfer

At ocean boundaries, the diapycnal term, $w^{(b)}$, accounts for the transfer of matter across the ocean boundaries via precipitation, evaporation, ice melt/form, and river runoff. Notably, this matter transfer also generally gives rise to a transfer of trace matter (tracers), heat (evaporation and precipitation carry a heat content), and momentum (precipitation generally has nonzero momentum). In the ocean interior, $w^{(b)}$ affects the transfer of volume, tracer, and momentum between layers as induced by irreversible processes such as mixing.

3.2.9 Momentum transfer

Pressure [form stress](#) mechanically couples isopycnal layers even in the absence of diapycnal matter transfer. We discussed the physics of form stress for the shallow water system in [VOLUME 3](#), and devoted a full chapter in [VOLUME 2](#) to this topic. Furthermore, there are a suite of unresolved processes giving rise to lateral and vertical stresses. Typical ocean model treatments incorporate a turbulent friction in the ocean interior, with lateral stresses acting within a layer and diapycnal stresses acting across isopycnal layer interfaces. A bottom drag is typically applied at the ocean bottom and a turbulent stress applied at the ocean surface. Details for the boundary stresses involve the physics of boundary layer turbulence, which is a topic outside of our scope.

3.2.10 Vanished isopycnal layers

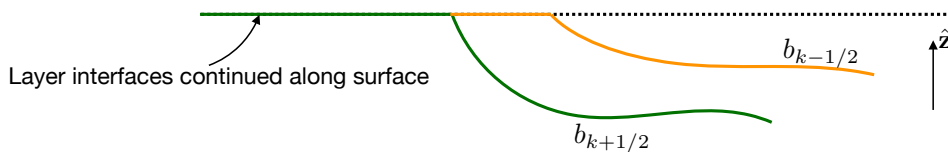


FIGURE 3.2: Schematic of isopycnal layer interfaces, $b_{k-1/2}$ and $b_{k+1/2}$, that intersect the surface boundary and are analytically continued along the boundary in zero thickness regions. This construct provides a conceptual and practical method for handling layers that intersect boundaries, and thus accounting for boundary transport of matter across layer interfaces. A similar construct is used in formulating available potential energy in the presence of boundaries in [VOLUME 2](#), and for processes leading to surface water mass transformation in Section 9.4.6.

Isopycnal layers have a transient existence at any particular horizontal position since a layer can incrop at the ocean bottom and outcrop at the ocean surface (see Figure 3.2). The seasonal cycle of warming and cooling is a canonical example of layer outcropping at the surface ocean. A formulation expedient to handle the creation and destruction of layers is to assume that all layers exist everywhere horizontally across the ocean domain, but to allow for zero layer thickness at a horizontal point where it does not exist. To admit this feature in a discrete model requires a careful realization of L'Hôpital's rule of differential calculus, thus ensuring the discrete model conserves properties in the presence of layers that can appear and disappear at any particular point in the domain.

3.3 Potential vorticity using isopycnal coordinates

In [VOLUME 3](#), we showed that the absolute vorticity in a Boussinesq and hydrostatic ocean with a simplified [equation of state](#), when projected into the direction normal to constant buoyancy surface, $\omega_a \cdot \nabla b$, is not affected by [baroclinicity](#); i.e., the projection annihilates the baroclinicity vector. From that property we conclude that $\omega_a \cdot \nabla b$ is the potential vorticity for the Boussinesq hydrostatic fluid.

For a Boussinesq hydrostatic fluid, isopycnal coordinates build in the above property of buoyancy surfaces. Indeed, as shown in Section 2.15.3, the vertical component to baroclinicity vanishes for any generalized vertical coordinate representation of a Boussinesq fluid. Hence, buoyancy coordinates are not special from this perspective. Instead, they are special since in the case of a perfect fluid, the buoyancy based potential vorticity is materially invariant. In

Section 2.15, we derived the potential vorticity equation for a hydrostatic fluid represented with generalized vertical coordinates. We could choose to specialize that result to the current case of isopycnal coordinates. We instead choose to step through the maths via a series of exercises, thus offering further experience performing manipulations with isopycnal coordinates and vorticity.

3.3.1 The vorticity equation

In Exercise 3.1 we perform the few steps needed to derive the isopycnal vorticity equation

$$\left[\frac{\partial \tilde{\zeta}_a}{\partial t} \right]_b + (\mathbf{u} \cdot \nabla_{hb}) \tilde{\zeta}_a = -\tilde{\zeta}_a \nabla_{hb} \cdot \mathbf{u} \quad (3.31)$$

where

$$\tilde{\zeta}_a = f + \hat{z} \cdot (\nabla_{hb} \times \mathbf{u}) = f + \tilde{\zeta} \quad (3.32)$$

is the absolute vorticity, written as the planetary vorticity plus the isopycnal relative vorticity. The left hand side of equation (3.31) is the material time derivative of absolute vorticity (see equation (3.6b)), so that we can write

$$\frac{D\tilde{\zeta}_a}{Dt} = -\tilde{\zeta}_a \nabla_{hb} \cdot \mathbf{u}. \quad (3.33)$$

As advertised above, there is no baroclinicity vector on the right hand side of this vorticity equation. Rather, the material time evolution of isopycnal absolute vorticity is only affected by the isopycnal convergence of the horizontal flow.

3.3.2 Derivation of the potential vorticity equation

In Exercise 3.2 we step through the few lines of maths to derive the potential vorticity equation

$$\frac{DQ}{Dt} = 0, \quad (3.34)$$

where the isopycnal potential vorticity is

$$Q = \frac{\tilde{\zeta}_a}{h} = \frac{f + \tilde{\zeta}}{h}. \quad (3.35)$$

Expanding the material time derivative into its components according to equation (3.6b), and making use of the perfect fluid form of the thickness equation leads to the flux-form potential vorticity equation

$$\left[\frac{\partial (h Q)}{\partial t} \right]_b + \nabla_{hb} \cdot (h Q \mathbf{u}) = 0. \quad (3.36)$$

When formulating the vertically continuous equations rather than finite thickness layered equations, it is more convenient to make use of the specific thickness, $\langle \rangle$, rather than the layer thickness, h (see Section 3.2.3). In this case we are motivated to define the potential vorticity as

$$Q = \frac{\tilde{\zeta}_a}{\langle \rangle} = \frac{f + \tilde{\zeta}}{\langle \rangle} = (f + \tilde{\zeta}) N^2. \quad (3.37)$$

The corresponding potential vorticity equation is identical to equation (3.36), only now with h replaced by $\langle \cdot \rangle$. Exercise 3.3 reveals that it is the potential vorticity (3.37) that appears when performing a coordinate transformation from the geopotential form, $Q = (\boldsymbol{\omega}^{\text{hy}} + f \hat{\mathbf{z}}) \cdot \nabla b$, into its isopycnal form.

3.3.3 Potential vorticity with irreversible processes

We now include friction and/or boundary stresses in the momentum equation and irreversible processes in the buoyancy equation (e.g., diffusion, heating). The manipulations are straightforward yet require a bit more work than for the perfect fluid case.

As summarized in Section 3.2.4, the equations of motion with irreversible buoyancy processes as well as friction, as written using isopycnal (or buoyancy) vertical coordinates, take the form

$$\left[\frac{\partial \mathbf{u}}{\partial t} \right]_b + (\mathbf{u} \cdot \nabla_{\text{hb}}) \mathbf{u} + \dot{b} \frac{\partial \mathbf{u}}{\partial b} + \mathbf{f} \times \mathbf{u} = -\nabla_{\text{hb}} M + \mathbf{F}^h \quad (3.38a)$$

$$\frac{\partial M}{\partial b} = -z \quad (3.38b)$$

$$\left[\frac{\partial \langle \cdot \rangle}{\partial t} \right]_b + \nabla_{\text{hb}} \cdot (\langle \mathbf{u} \rangle) = -\frac{\partial (\langle \dot{b} \rangle)}{\partial b} \quad (3.38c)$$

$$\frac{D b}{D t} = \dot{b}. \quad (3.38d)$$

Note that in this section choose to write the dia-surface transport operator in the form

$$w^{(b)} \partial_z = \dot{b} \partial_b. \quad (3.39)$$

We can make use of the material time derivative operator (3.6b) to write the material form of the equations

$$\frac{D \mathbf{u}}{D t} + \mathbf{f} \times \mathbf{u} = -\nabla_{\text{hb}} M + \mathbf{F}^h \quad (3.40a)$$

$$\frac{\partial M}{\partial b} = -z \quad (3.40b)$$

$$\frac{D \langle \cdot \rangle}{D t} + \langle \nabla_{\text{hb}} \cdot \mathbf{u} \rangle = -\langle \frac{\partial \dot{b}}{\partial b} \rangle \quad (3.40c)$$

$$\frac{D b}{D t} = \dot{b}. \quad (3.40d)$$

Curl of the velocity equation

Start taking the curl, $\nabla_{\text{hb}} \times$, of the velocity equation (3.38a), thus leading to the isopycnal vorticity equation

$$\left[\frac{\partial \tilde{\zeta}_a}{\partial t} \right]_b + (\mathbf{u} \cdot \nabla_{\text{hb}}) \tilde{\zeta}_a + \dot{b} \left[\frac{\partial \tilde{\zeta}_a}{\partial b} \right] = -\tilde{\zeta}_a \nabla_{\text{hb}} \cdot \mathbf{u} + \hat{\mathbf{z}} \cdot \left[\frac{\partial \mathbf{u}}{\partial b} \times \nabla_{\text{hb}} \dot{b} + \nabla_{\text{hb}} \times \mathbf{F}^h \right]. \quad (3.41)$$

The left hand side of equation (3.41) is the material time derivative of absolute vorticity (see equation (3.6b)), so that

$$\frac{D \tilde{\zeta}_a}{D t} = -\tilde{\zeta}_a \nabla_{\text{hb}} \cdot \mathbf{u} + \hat{\mathbf{z}} \cdot \left[\frac{\partial \mathbf{u}}{\partial b} \times \nabla_{\text{hb}} \dot{b} + \nabla_{\text{hb}} \times \mathbf{F}^h \right]. \quad (3.42)$$

Now make use of the thickness equation in the material form (3.40c) to eliminate the convergence, $-\nabla_{hb} \cdot \mathbf{u}$, on the right hand side, thus leading to

$$\frac{D\tilde{\zeta}_a}{Dt} - \frac{\tilde{\zeta}_a}{\langle \rangle} \left[\frac{D\langle \rangle}{Dt} - \langle \frac{\partial \dot{b}}{\partial b} \rangle \right] = \hat{\mathbf{z}} \cdot \left[\frac{\partial \mathbf{u}}{\partial b} \times \nabla_{hb} \dot{b} + \nabla_{hb} \times \mathbf{F}^h \right]. \quad (3.43)$$

Introducing the isopycnal potential vorticity

$$Q = \frac{\tilde{\zeta}_a}{\langle \rangle} = \frac{\tilde{\zeta} + f}{\langle \rangle} \quad (3.44)$$

leads to

$$\langle \frac{DQ}{Dt} \rangle = \zeta_a \frac{\partial \dot{b}}{\partial b} + \hat{\mathbf{z}} \cdot \left[\frac{\partial \mathbf{u}}{\partial b} \times \nabla_{hb} \dot{b} + \nabla_{hb} \times \mathbf{F}^h \right]. \quad (3.45)$$

Massaging the irreversible terms

The terms associated with material time changes to the buoyancy can be written

$$\zeta_a \frac{\partial \dot{b}}{\partial b} + \hat{\mathbf{z}} \cdot \left[\frac{\partial \mathbf{u}}{\partial b} \times \nabla_{hb} \dot{b} \right] = \zeta_a \frac{\partial \dot{b}}{\partial b} + \dot{b} \frac{\partial \tilde{\zeta}}{\partial b} - \hat{\mathbf{z}} \cdot \left[\nabla_{hb} \times \dot{b} \frac{\partial \mathbf{u}}{\partial b} \right] \quad (3.46a)$$

$$= \zeta_a \frac{\partial \dot{b}}{\partial b} + \dot{b} \frac{\partial \tilde{\zeta}_a}{\partial b} - \hat{\mathbf{z}} \cdot \left[\nabla_{hb} \times \dot{b} \frac{\partial \mathbf{u}}{\partial b} \right] \quad (3.46b)$$

$$= \frac{\partial(\zeta_a \dot{b})}{\partial b} - \hat{\mathbf{z}} \cdot \left[\nabla_{hb} \times \dot{b} \frac{\partial \mathbf{u}}{\partial b} \right] \quad (3.46c)$$

$$= \frac{\partial(\tilde{\zeta}_a \dot{b})}{\partial b} + \nabla_{hb} \cdot \left[\hat{\mathbf{z}} \times \dot{b} \frac{\partial \mathbf{u}}{\partial b} \right], \quad (3.46d)$$

where the second equality follows since the Coriolis parameter is independent of the buoyancy.

The potential vorticity equation

The potential vorticity equation takes the material form

$$\langle \left[\frac{DQ}{Dt} \right] \rangle = \frac{\partial(\tilde{\zeta}_a \dot{b})}{\partial b} + \nabla_{hb} \cdot \left[\hat{\mathbf{z}} \times \dot{b} \frac{\partial \mathbf{u}}{\partial b} - \hat{\mathbf{z}} \times \mathbf{F}^h \right]. \quad (3.47)$$

Expanding the material time derivative into its components (3.6b), and making use of the thickness equation (3.38c), leads to the flux-form equation

$$\left[\frac{\partial(\langle Q \rangle)}{\partial t} \right]_b + \nabla_{hb} \cdot (\langle Q \mathbf{u} \rangle) + \frac{\partial(\langle Q \dot{b} \rangle)}{\partial b} = \frac{\partial(\tilde{\zeta}_a \dot{b})}{\partial b} + \nabla_{hb} \cdot \left[\hat{\mathbf{z}} \times \dot{b} \frac{\partial \mathbf{u}}{\partial b} - \hat{\mathbf{z}} \times \mathbf{F}^h \right]. \quad (3.48)$$

Since $\langle Q \rangle = \tilde{\zeta}_a$, the ∂_b terms cancel, thus leaving the flux-form potential vorticity equation

$$\left[\frac{\partial(\langle Q \rangle)}{\partial t} \right]_b = -\nabla_{hb} \cdot \left[\langle Q \mathbf{u} - \hat{\mathbf{z}} \times \dot{b} \frac{\partial \mathbf{u}}{\partial b} + \hat{\mathbf{z}} \times \mathbf{F}^h \rangle \right]. \quad (3.49)$$

3.3.4 Comments

The flux-form potential vorticity equation (3.49) manifests the [ideal impermeability theorem](#) of [VOLUME 3](#), since the right hand side is the isopycnal convergence of a flux.

3.4 Thickness weighted shallow water

There are a variety of mathematical formalisms used to frame the study of how linear waves, nonlinear waves, eddies, and fully developed turbulence interact with a mean flow. A distinctly geophysical element enters these studies through the primary role of vertical stratification arising from gravitation, with stratification particularly important for large scales flows where motions are approximately hydrostatic. A further specialization to the ocean context arises since there are few regions where zonal averages apply, which contrasts to the atmospheric case. The [thickness weighted averaging \(TWA\)](#) method has emerged as an effective formalism for stratified flows, with particular use for studies of geostrophic eddies and their parameterization. In the remainder of this chapter, we develop the [TWA](#) equations for the perfect fluid stacked shallow water model. Our focus concerns the derivation of the thickness weighted averaged equations as well as their physical interpretation.

3.4.1 Stacked shallow water versus continuous isopycnal

The perfect fluid stacked shallow water model exposes key facets of stratified geophysical flows without requiring the full mathematical toolkit required for continuous generalized vertical coordinates. The core simplification arises by assuming that horizontal motion has no vertical dependence within each shallow water layer, which then means that vertical motion as well as the hydrostatic pressure are linear functions of vertical position within each layer. That is, the shallow water fluid moves as extensible vertical columns ([VOLUME 3](#)). It follows that horizontal pressure gradients do not need to be projected along the slope of the layer since they are vertically constant within a layer. In contrast, this projection is needed for a continuously stratified fluid described by generalized vertical coordinates, as illustrated in Figure 1.5. Hence, the shallow water equations for momentum, thickness, and tracers retain their use of Cartesian coordinates even though the layer interfaces undulate and are thus not generally horizontal. This mathematical feature of shallow water fluids aids in our pedagogical development of the TWA method.

[Young \(2012\)](#) offers an elegant application of thickness weighted averaging to the continuously stratified Boussinesq hydrostatic fluid, with his paper the culmination of many years of prior work. A natural step for our development is to work through [Young \(2012\)](#) since we have the full tensor toolkit needed for that purpose. However, we choose instead to specialize [Young \(2012\)](#) to the case of vertically discrete shallow water equations. In this manner, we minimize the required mathematical apparatus while exposing the key physical concepts. We also lay the mathematical physics foundation for the study of flow in stacked shallow water models (e.g., [Marques et al. \(2022\)](#), [Loose et al. \(2022\)](#), [Loose et al. \(2023\)](#), [Jansen et al. \(2024\)](#)). Digesting this presentation, and then coupling to the generalized vertical coordinate tensor analysis developed in this part of the book, prepares one for [Young \(2012\)](#) as well as the slightly more mathematical treatment of [Maddison and Marshall \(2013\)](#).

3.4.2 Concerning the gradient operator

When studying the shallow water equations, most fields are a continuous function of (x, y, t) and labeled with a discrete vertical index, k . As such, the gradient operator acting on one of these fields only has a horizontal component, so that we can equally write ∇ or ∇_h . However, the layer pressure, p_k , is a linear function of depth within the layer, in which case we must distinguish $\nabla_h p_k$ from ∇p_k . To help reduce confusion, particularly when in the midst of a detailed derivation, we write ∇_h with its extra subscript to emphasize that the gradient operator is horizontal. This extra notation is not needed in many cases, but it proves quite useful in those few places where it is needed.

3.4.3 The unaveraged thickness weighted equations

The thickness weighted averaging formalism starts from flux-form evolution equations rather than advective form equations. We thus focus on the thickness equation (3.50a), the thickness weighted tracer equation (3.50b), and the thickness weighted velocity equation (3.50c) (also called the momentum equation)

$$\frac{\partial h_k}{\partial t} + \nabla_h \cdot (h_k \mathbf{u}_k) = 0 \quad (3.50a)$$

$$\frac{\partial (h_k C)}{\partial t} + \nabla_h \cdot (h_k \mathbf{u}_k C) = 0 \quad (3.50b)$$

$$\frac{\partial (h_k \mathbf{u}_k)}{\partial t} + \nabla_h \cdot [h_k \mathbf{u}_k \otimes \mathbf{u}_k] + f \hat{\mathbf{z}} \times (h_k \mathbf{u}_k) = -(h_k / \rho_{\text{ref}}) \nabla_h p_k. \quad (3.50c)$$

The density, ρ_{ref} , appearing in the momentum equation (3.50c) is the Boussinesq reference density, often chosen as the density in the uppermost layer,

$$\rho_{\text{ref}} = \rho_1. \quad (3.51)$$

For the analysis of thickness weighted averaging, it proves useful to move seamlessly between the thickness weighted pressure gradient body force and its equivalent [contact force](#) version studied in [VOLUME 2](#). The contact force version of the momentum equation reveals the pressure form stresses acting on the upper and lower interfaces of a shallow water layer. It also brings stresses (kinetic stresses and pressure stresses) together into the divergence of a momentum flux. As such, this formulation follows that of Cauchy as discussed in [VOLUME 2](#). The eddy correlation portion of the momentum flux is known as the *Eliassen-Palm* flux.¹

When the dust settles, the [TWA](#) equations are isomorphic to the unaveraged thickness weighted equations (3.50a)-(3.50c), yet with the addition of momentum flux convergences to the right hand sides that arise from subgrid momentum eddy correlations. These eddy fluxes are connected to the potential vorticity fluxes, with the connection known as the *Taylor-Bretherton identity*. The isomorphism between unaveraged thickness and averaged thickness provides some motivation to favor the [TWA](#) approach. Namely, the properties of the unaveraged equations are directly reflected in the [TWA](#) equations. It also provides a suitable framework for parameterizing the subgrid correlations within the context of flux-form conservation laws. Even so, any formalism for an eddy and mean decomposition is subjective since the mean flow and eddying fluctuations are defined by the analyst rather than prescribed by the physics. Hence,

¹See [Bühler \(2014b\)](#) for a historical perspective on the Eliassen-Palm flux, which was introduced by [Eliassen and Palm \(1960\)](#) in their study of stationary mountain waves.

arguments concerning what is a preferable framework are subject to the needs of the analyst and yet they have no physically objective foundation.

3.5 Thickness transport by the bolus velocity

Prior to diving into the formalism of thickness weighted averaging, we study the eddy-induced volume transport (more precisely, thickness transport) realized by linear waves within a layer of shallow water fluid. This discussion provides a specific example of the thickness transport by the *bolus velocity*, with further discussion offered in Sections 3.7.1 and 6.5.9. Much of our intuition for bolus transport is based on the following relatively simple example of Stokes drift.²

Part of the motivation for TWA is that we do not need to compute the bolus velocity. Even so, understanding the basic physics of the bolus velocity renders useful insights into how eddies, even eddies as simple as linear waves, can provide a rectified transport of material and thermal properties.

3.5.1 Rectified effects

Rectification is the conversion of a fluctuating motion into motion in a particular direction. For example, the transformation of an alternating electrical current into a direct electrical current occurs through a rectifier. More generally, rectification arises from the breaking of a symmetry typically through a nonlinear mechanism. The primary example in fluid mechanics is Stokes drift. Stokes drift arises when linear waves have an amplitude that is a function of space, with this spatial dependence giving rise to net particle transport (the Stokes drift) in a preferred direction. Another example concerns the turbulent Stokes drift arising from nonlinear geostrophic waves and eddies in the ocean and atmosphere that lead to a net transport of buoyancy. The meridional transport of buoyancy by eddies in a channel provides the canonical geophysical example of eddy induced transport.

3.5.2 An undulating shallow water fluid layer

Figure 3.3 shows a layer of constant density shallow water fluid within a perfect fluid stacked shallow water model in a non-rotating reference frame. Since the layers are immiscible, the total volume of fluid within this layer remains constant. In its unperturbed state with flat layer interfaces, the meridional velocity in the fluid layer is zero and the thickness is a constant, h_0 . When perturbed, the thickness is written

$$h(y, t) = h_0 + h'(y, t), \quad (3.52)$$

where we assume the perturbation only depends on (y, t) for simplicity. The layer thickness changes in time according to the convergence of the advective transport of thickness as found by the thickness equation (3.50a)

$$\frac{\partial h}{\partial t} = -\nabla_h \cdot (h \mathbf{u}), \quad (3.53)$$

where the convergence is computed within the layer and we drop the k layer index for brevity. As seen by Figure 3.3, undulations of the layer thickness at a point arise from the convergence of thickness advected to that point. Further assuming that there is no zonal dependence ($\partial_x = 0$)

²This example is based Section 2 of [Lee et al. \(1997\)](#).

leads to the one-dimensional thickness equation

$$\frac{\partial h}{\partial t} = -\frac{\partial (h v)}{\partial y}. \quad (3.54)$$

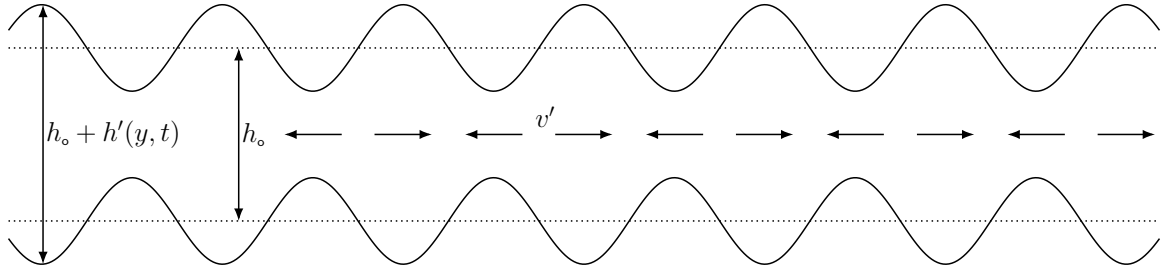


FIGURE 3.3: A single layer of constant density shallow water fluid, with resting thickness $h = h_o$ and instantaneous thickness $h = h_o + h'(y, t)$. Associated with the sinusoidal undulations in thickness are fluctuations in the meridional velocity, $v' = v_o \sin(k y - \omega t)$, depicted here by the alternating horizontal vectors within the layer. Since the velocity and thickness are in phase as per equation (3.65), the velocity fluctuates to the right ($v' > 0$) under a positive thickness anomaly ($h' > 0$) and to the left ($v' < 0$) with a negative anomaly ($h' < 0$). The nonzero correlation between h' and v' leads to a Stokes drift, with $v' \overline{h'}/\overline{h}$ referred to as the bolus velocity. The name *bolus velocity* (originating from [Rhines \(1982\)](#)) is motivated by the image of a bolus of matter that moves through a tube via periodic undulations, akin to the peristaltic contractions and expansions that move food through the digestive system.

3.5.3 Stokes drift

Consider a monochromatic wave perturbation in the meridional velocity that propagates in the meridional direction

$$v'(y, t) = v_o \sin(\kappa y - \omega t), \quad (3.55)$$

where κ is a constant wave number, $\omega > 0$ is a constant angular frequency, and v_o is the amplitude of the fluid particle velocity. This longitudinal wave is depicted in Figure 3.3. We now follow the general formalism developed in VOLUME 1 (see also Section 6.3.4) to derive an expression for the Stokes drift associated with this wave.

We are only concerned with the meridional component of the velocity, so the fluid particle trajectory equation is given by

$$\frac{dY}{dt} = v_o \sin(\kappa Y - \omega t), \quad (3.56)$$

where $Y = Y(Y_o, t)$ is the meridional trajectory with initial position, Y_o . We can write the difference between the velocity following a fluid particle (the Lagrangian velocity for the moving fluid particle) from the velocity at the initial particle point (the Eulerian velocity at the initial point of the trajectory)

$$\frac{dY}{dt} - v(y, t) = v_o^2 \kappa \cos(\kappa y - \omega t) \int_0^t \sin(\kappa y - \omega t') dt' \quad (3.57a)$$

$$= \frac{v_o^2 \kappa}{\omega} [\cos^2(\kappa y - \omega t) - \cos(\kappa y - \omega t) \cos(\kappa y)]. \quad (3.57b)$$

Time averaging over a single wave period,

$$T = 2\pi/\omega, \quad (3.58)$$

leads to the Stokes drift as per the general expression in VOLUME 2

$$V_{\text{stokes}} = \frac{v_o^2 \kappa}{2\omega}. \quad (3.59)$$

Introducing the phase speed for the monochromatic wave,

$$c = \omega/\kappa, \quad (3.60)$$

allows us to write the Stokes drift as

$$V_{\text{stokes}} = \frac{v_o^2}{2c}. \quad (3.61)$$

Notice how the Stokes drift becomes small when the phase speed is large. We expect this dependence since Stokes drift arises from fluid particles feeling the waves, so that for relatively fast waves the particles have little time for sampling the wave thus leading to a decrease in the Stokes drift. Correspondingly, there is only a small difference between the Eulerian and Lagrangian velocities with fast phase speeds, whereas the converse holds for slow phase speeds where Eulerian and Lagrangian velocities have a relatively large difference.³

3.5.4 Linearized thickness perturbations

The velocity and thickness are written in terms of their rest state plus a perturbation due to the wave

$$h = h_o + h' \quad \text{and} \quad v = v', \quad (3.62)$$

where the velocity vanishes when the wave is absent. The thickness equation (3.54) thus takes the form

$$\frac{\partial h'}{\partial t} + h_o \frac{\partial v'}{\partial y} + v' \frac{\partial h'}{\partial y} = 0. \quad (3.63)$$

Linearizing this equation, and using the wave perturbation (3.55), leads to

$$\frac{\partial h'}{\partial t} + h_o v_o \kappa \cos(\kappa y - \omega t) = 0. \quad (3.64)$$

Time integrating this equation, and making use of the velocity perturbation in the form of equation (3.55), renders the thickness perturbation

$$h' = h_o v' / c. \quad (3.65)$$

Hence, to leading order, the thickness perturbation is directly proportional to and in phase with the velocity perturbation. We depict this in-phase relation in Figure 3.3, whereby $v' > 0$ where $h' > 0$ (where the layer bulges) and $v' < 0$ where $h' < 0$ (where the layer thins).

³In the case of relatively slow phase speeds, we really should keep more terms in an asymptotic expansion than those carried here.

3.5.5 Correlation between thickness and velocity

Over a single wave period, $T = 2\pi/\omega$, the temporal correlation between the linear thickness perturbation and velocity perturbation is given by

$$\overline{h' v'} = \frac{1}{T} \int_0^T h' v' dt \quad (3.66a)$$

$$= \frac{h_o}{cT} \int_0^T v' v' dt \quad (3.66b)$$

$$= \frac{v_o^2 h_o}{cT} \int_0^T \sin^2(\kappa y - \omega t) dt \quad (3.66c)$$

$$= \frac{v_o^2 h_o}{2c} \quad (3.66d)$$

$$= h_o V_{\text{stokes}}, \quad (3.66e)$$

where we introduced the Stokes drift (3.61) to reach the final equality. A nonzero correlation, $\overline{h' v'} \neq 0$, means that the thickness has a nonzero tendency when averaged over a wave period.

The nonzero correlation in equation (3.66e) induces a thickness transport from the one-dimensional linear longitudinal waves. This transport arises from the Stokes drift induced by the waves; without Stokes drift there is no eddy thickness transport. This behavior exemplifies the case for more general waves and nonlinear eddies moving through fluid layers. For the general case, a nonzero bolus velocity (Section 3.7.1), as determined by velocity-thickness correlations, induces an eddy thickness transport. We see that for the one-dimensional linear longitudinal wave example, the bolus velocity is the Stokes velocity.

3.5.6 Is the bolus velocity needed for the mean-field equations?

The bolus transport is of fundamental importance for how we think about eddy induced Stokes transport from shallow water waves. More general fluctuations, such as those from turbulent geostrophic eddies, require a parameterization to determine the thickness transport. We consider such in VOLUME 2 when studying geostrophic eddies in a zonally reentrant channel. As we see in the remainder of the current chapter, the allure of the thickness weighted averaging formalism is that it dispenses with the need to parameterize the bolus velocity. Instead, the **TWA** equations absorb the bolus transport into the residual mean advection operator. Operationally, the **TWA** exposes the eddy correlation terms only in the momentum equation, leaving the **TWA** thickness and **TWA** tracer equations in a form directly parallel to the unaveraged equations.

3.6 A summary of averaging operators

There are many averaging operators used in fluid mechanics, such as the wave phase average from Section 3.5, which is useful when the flow is dominantly linear waves; a long time average (formally an infinitely long time average), which is commonly used for climate studies; a space average, which is appropriate when the spatial sampling is coarse; general space filters or kernels, which are commonly used in large eddy simulations; and ensemble averages, which are generally assumed in traditional studies of turbulence. In the following, we denote the averaging or mean operator by an overbar

$$\text{average}(\Phi) = \overline{\Phi}, \quad (3.67)$$

where Φ is any field such as velocity, thickness, or tracer concentration. Deviations (also called fluctuations) from the mean are denoted by a prime so that the full field is decomposed into a mean and eddy term according to

$$\Phi = \bar{\Phi} + \Phi'. \quad (3.68)$$

A fluctuation might be a linear wave feature moving relative to a static background flow, such as considered in Section 3.5. For nonlinear flows, a fluctuation can arise from coherent eddying flow features, such as vortices commonly generated from meandering jet-like flows (e.g., Gulf Stream rings or mid-latitude atmospheric storms spawned from the jet-stream). Furthermore, a fluctuation might represent the chaotic soup of whirls and eddies that comprise the background flow surrounding coherent vortices. In either of these cases, the nonlinear nature of the fluid mechanical equations means that any decomposition into eddy and mean leads to nonlinear eddy correlations, with such correlations the source of both the richness and complexity of geophysical fluid flows.

3.6.1 Reynolds average

A *Reynolds average* is an operator that annihilates its corresponding fluctuating quantity, which then means that the average of an average is the identity operator

$$\bar{\Phi}' = 0 \iff \bar{\bar{\Phi}} = \bar{\Phi}, \quad (3.69)$$

which in turn means that

$$\bar{\Phi} \bar{\Psi} = \overline{(\bar{\Phi} + \Phi')} \bar{\Psi} = \bar{\Phi} \bar{\Psi}. \quad (3.70)$$

Reynolds averages are commonly used when deriving mean field equations. Even so, the assumptions of Reynolds averaging operators are not satisfied by many operators in practice. Extra technical issues arise when averaging operators do not satisfy the properties of a Reynolds average, with these issues beyond our aims in the present chapter. Hence, in this chapter we retain the Reynolds average assumption (3.69) for the averaging operator.

3.6.2 Ensemble average

A further assumption we make is that the average operator commutes with space and time derivatives as well as integrals. This assumption does not strictly hold if the operator is a space and/or time average operator, at least not without a bit of work. However, this assumption holds for ensemble averages. An *ensemble mean* is computed over an infinite number of realizations of the fluid flow, with approximations to this average afforded by finite sized ensembles.

Ensemble averages are typically assumed in traditional fluid turbulence studies. However, they are not always very practical nor are they the obvious choice when targeting a framework for parameterization. Even so, we prefer ensemble averages for this chapter in order to dispense with concerns about commutation of the averaging operator with derivative and integral operators. We also make use of ensemble averaging for our discussion of tracer kinematics in Chapter 6.

3.6.3 The algebra of thickness weighted averages

The thickness weighted average of a field is defined as the ensemble average of the thickness weighted field, and then divided by the averaged thickness

$$\widehat{\Phi} \equiv \frac{\overline{h\Phi}}{\overline{h}} \iff \overline{h}\widehat{\Phi} = \overline{h\Phi}, \quad (3.71)$$

with widehats adorning a thickness weighted average. Deviations from the thickness weighted average are denoted with two primes so that the unaveraged field is decomposed into its average plus fluctuation

$$\Phi = \widehat{\Phi} + \Phi''. \quad (3.72)$$

Since the overline average from Section 3.6.1 satisfies the Reynolds averaging assumption, so too does the thickness weighted average

$$\Phi = \widehat{\Phi} + \Phi'' \implies \widehat{\Phi''} = \frac{\overline{h\Phi''}}{\overline{h}} = 0 \implies \widehat{\Phi} = \widehat{\Phi}. \quad (3.73)$$

We are thus able to derive the following related identities

$$\Phi\Psi = (\widehat{\Phi} + \Phi'') (\widehat{\Phi} + \Phi'') \implies \widehat{\Phi\Psi} = \widehat{\Phi}\widehat{\Psi} + \widehat{\Phi''}\widehat{\Psi''} \implies \overline{h\Phi\Psi} = \overline{h\Phi\Psi}. \quad (3.74)$$

We sometimes need to consider mixed averages and primes, such as for

$$\overline{h}\widehat{\Phi} = \overline{h\Phi} = \overline{h}\widehat{\Phi}, \quad (3.75)$$

in which case⁴

$$\overline{h\Phi''} = \overline{h}(\overline{\Phi} - \widehat{\Phi}) = \overline{h\Phi} - \overline{h'}\overline{\Phi'} \neq 0. \quad (3.76)$$

Hence, the ensemble average of a fluctuation, Φ'' (which is computed relative to the thickness weighted mean), is generally nonzero. Furthermore, we sometimes find it useful to write the ensemble mean correlation between thickness and a field according to

$$\overline{h}\widehat{\Phi'} = \overline{h\Phi'} = \overline{h'}\overline{\Phi'}, \quad (3.77)$$

with the second equality following since

$$\overline{h\Phi'} = \overline{h\overline{\Phi'}} = 0. \quad (3.78)$$

The identity (3.77) allows us to write equation (3.76) as

$$\overline{h\Phi''} = \overline{h}(\overline{\Phi} - \widehat{\Phi'}). \quad (3.79)$$

A similar identity holds according to the following manipulations

$$\overline{h'}\overline{\Phi'} = \overline{h\Phi'} = \overline{h(\Phi - \overline{\Phi})} = \overline{h\Phi} - \overline{h}\overline{\Phi} = \overline{h}(\widehat{\Phi} - \overline{\Phi}), \quad (3.80)$$

so that

$$\widehat{\Phi'} = \widehat{\Phi} - \overline{\Phi} = \frac{\overline{h'}\overline{\Phi'}}{\overline{h}}. \quad (3.81)$$

⁴Footnote #4 in [Young \(2012\)](#) is missing the $\overline{h\Phi}$ term appearing in equation (3.76).

Derivative operators *do not* commute with the thickness weighted average, so that, for example,

$$\partial_x \hat{u} \neq \widehat{\partial_x u}. \quad (3.82)$$

Hence, when deriving differential equations for thickness weighted fields, we first derive equations for the unaveraged thickness weighted quantities, and only thereafter do we apply the ensemble mean operator.

3.6.4 Comments

For the most part, we follow the notation of [Young \(2012\)](#). Nonetheless, we caution that notational clutter and distinct conventions can present a nontrivial barrier to reading the **TWA** literature. Indeed, for our purposes with the stacked shallow water model, there is one additional piece of notation concerning the discrete layer indices. Fortunately, much of the discrete layer notation can be streamlined by exposing just the half-integer indices for fields situated at layer interfaces, along with the layer density.

3.7 TWA equations for thickness and tracer

In this section we derive the **TWA** versions of the thickness equation (3.50a) and the tracer equation (3.50b). The derivations involve straightforward applications of the **TWA** averaging properties (3.73) and (3.74).

3.7.1 TWA thickness equation

Taking the ensemble average of the thickness equation (3.50a) renders

$$\partial_t \bar{h} + \nabla_h \cdot \bar{h} \bar{u} = 0, \quad (3.83)$$

where we dropped the layer index, k , to reduce notational clutter.⁵ Introducing the thickness weighted average according to equation (3.71) brings the thickness equation to the form

$$\partial_t \bar{h} + \nabla_h \cdot (\bar{h} \hat{u}) = 0. \quad (3.84)$$

Consequently, the mean layer thickness, \bar{h} , evolves at a point in space according to the convergence of the thickness flux, $-\nabla_h \cdot (\bar{h} \hat{u})$, with the flux determined by the thickness weighted velocity, \hat{u} .

We find it useful to introduce the material time derivative operator defined with the thickness weighted velocity

$$\frac{D^\#}{Dt} = \frac{\partial}{\partial t} + \hat{u} \cdot \nabla_h = \frac{\partial}{\partial t} + \hat{u} \partial_x + \hat{v} \partial_y, \quad (3.85)$$

so that the flux-form thickness equation (3.84) can be written in the material time derivative or advective form

$$\frac{D^\# \bar{h}}{Dt} = -\bar{h} \nabla_h \cdot \hat{u}. \quad (3.86)$$

⁵The thickness and tracer equations do not couple to other layers, and as such we can drop the layer index, $k = 1, N$, when analyzing these equations. The momentum equation, in contrast, is coupled through pressure form stresses acting at the layer interfaces.

The D^\sharp/Dt notation is based on that used by [Young \(2012\)](#). The alternative, \widehat{D}/Dt , is less suitable since $\overline{h(D/Dt)} \neq \overline{(D/Dt)h}$. In brief, an object adorned with a sharp symbol is consistent with thickness weighted averaging but is itself not the direct result of a thickness weighted average. In the following, we find it useful to also introduce the vertical velocity, w^\sharp , in equation (3.92), and the potential vorticity, Π^\sharp , in equation (3.143).

The isomorphism between the [TWA](#) thickness equation (3.84) with the unaveraged thickness equation (3.50a) illustrates a distinct advantage of using the thickness weighted velocity, $\widehat{\mathbf{u}}$. Even so, for some purposes it is useful to unpack the thickness weighted velocity into its two components

$$\widehat{\mathbf{u}} = \overline{\mathbf{u}} + \frac{\overline{h' \mathbf{u}'}}{\overline{h}} \equiv \overline{\mathbf{u}} + \mathbf{u}^{\text{bolus}}, \quad (3.87)$$

with the bolus velocity defined by

$$\mathbf{u}^{\text{bolus}} = \widehat{\mathbf{u}'} = \frac{\overline{h' \mathbf{u}'}}{\overline{h}}, \quad (3.88)$$

where we made use of the identity (3.77).

We discussed the bolus velocity in Section 3.5 and see it again in Section 6.5.9 when developing the ensemble mean tracer equation in isopycnal coordinates. However, as per our discussion in Section 3.5.6, we do not need to know the bolus velocity if we write the averaged tracer and momentum equations in terms of the thickness weighted velocity, $\widehat{\mathbf{u}}$.

3.7.2 Tracer equation

Taking the ensemble average of the tracer concentration equation (3.50b) for a shallow water fluid layer renders

$$\partial_t(\overline{hC}) + \nabla_h \cdot \overline{hC} \mathbf{u} = 0. \quad (3.89)$$

Making use of the thickness weighted averages from Section 3.6.3 allows us to write

$$\overline{hC} = \overline{h} \widehat{C} \quad \text{and} \quad \overline{hC} \mathbf{u} = \overline{h} (\widehat{C} \widehat{\mathbf{u}} + \widehat{C'' \mathbf{u}''}), \quad (3.90)$$

thus yielding the [TWA](#) tracer equation

$$\partial_t(\overline{h} \widehat{C}) + \nabla_h \cdot (\overline{h} \widehat{C} \widehat{\mathbf{u}}) = -\nabla_h \cdot (\overline{h} \widehat{C'' \mathbf{u}''}). \quad (3.91)$$

The right hand side is the convergence of the thickness weighted eddy tracer flux. As seen in Section 6.6, the isopycnal form of the tracer equation is identical to that given here for a shallow water layer. In that discussion we present methods commonly used to parameterize the eddy flux convergence.

3.7.3 Defining w^\sharp via continuity with $\widehat{\mathbf{u}}$

We generally have no need for the vertical velocity when working with the perfect fluid stacked shallow water model. Nonetheless, it is interesting to define a vertical velocity component, w^\sharp , satisfying the continuity equation

$$\nabla_h \cdot \widehat{\mathbf{u}} + \partial_z w^\sharp = 0. \quad (3.92)$$

As for the unaveraged vertical velocity component discussed in VOLUME 3, w^\sharp is a linear function of z within the ensemble mean shallow water layers. Note that w^\sharp is not a thickness weighted velocity. Rather, it is the vertical velocity that is compatible, through the continuity equation, with the thickness weighted horizontal velocity. A vertical velocity is needed for the continuously stratified Boussinesq fluid, and it is defined as done here for the shallow water.⁶

3.8 Horizontal momentum equation

Taking the ensemble mean of the horizontal momentum equation (3.50c) renders

$$\partial_t(\bar{h}\bar{\mathbf{u}}) + \nabla_h \cdot [\bar{h}\bar{\mathbf{u}} \otimes \bar{\mathbf{u}}] + f\hat{\mathbf{z}} \times (\bar{h}\bar{\mathbf{u}}) = -\bar{h}\nabla_h p/\rho_{\text{ref}}, \quad (3.93)$$

where we dropped the layer interface label, k , for brevity. Again, we make use of the thickness weighted averages from Section 3.6.3 to write

$$\bar{h}\bar{\mathbf{u}} = \bar{h}\hat{\mathbf{u}} \quad (3.94a)$$

$$\bar{h}\bar{\mathbf{u}} \otimes \bar{\mathbf{u}} = \bar{h}(\hat{\mathbf{u}} \otimes \hat{\mathbf{u}} + \widehat{\mathbf{u}'' \otimes \mathbf{u}''}), \quad (3.94b)$$

so that equation (3.93) becomes

$$\partial_t(\bar{h}\hat{\mathbf{u}}) + \nabla_h \cdot [\bar{h}\hat{\mathbf{u}} \otimes \hat{\mathbf{u}}] + f\hat{\mathbf{z}} \times (\bar{h}\hat{\mathbf{u}}) = -\nabla_h \cdot [\bar{h}\widehat{\mathbf{u}'' \otimes \mathbf{u}''}] - \bar{h}\nabla_h p/\rho_{\text{ref}}. \quad (3.95)$$

The first term on the right hand side is similar to the eddy tracer flux convergence appearing in the TWA tracer equation (3.91). In contrast, the thickness weighted pressure gradient is fundamentally distinct from anything appearing in the tracer equation. Much in the remainder of this section is devoted to developing a physical and mathematical understanding of $\bar{h}\nabla_h p$.

3.8.1 Kinetic stress and Reynolds stress

We now introduce the shallow water kinetic stress tensor

$$\mathbb{T}^{\text{sw kinetic}} = -\rho_{\text{ref}}\mathbf{u} \otimes \mathbf{u}. \quad (3.96)$$

The kinetic stress arises from motion of the fluid, with the divergence,

$$\nabla_h \cdot (h\mathbb{T}^{\text{sw kinetic}}) = -\rho_{\text{ref}}\nabla_h \cdot (\mathbf{u} \otimes \mathbf{u}), \quad (3.97)$$

contributing to changes in the momentum of a shallow water fluid column. Decomposing the velocity into the TWA velocity and fluctuation leads to the ensemble mean of the thickness weighted kinetic stress

$$\bar{h}\bar{\mathbb{T}}^{\text{sw kinetic}}(\mathbf{u}) = -\rho_{\text{ref}}\bar{h}\bar{\mathbf{u}} \otimes \bar{\mathbf{u}} \quad (3.98a)$$

$$= -\rho_{\text{ref}}\bar{h}[\hat{\mathbf{u}} \otimes \hat{\mathbf{u}} + \widehat{\mathbf{u}'' \otimes \mathbf{u}''}] \quad (3.98b)$$

$$= \bar{h}\bar{\mathbb{T}}^{\text{sw kinetic}}(\hat{\mathbf{u}}) + \bar{h}\bar{\mathbb{T}}^{\text{sw Reynolds}}, \quad (3.98c)$$

where the eddy correlation is known as the Reynolds stress tensor. The divergence of the thickness weighted Reynolds stress provides a rectified effect onto the mean flow.s

⁶See equation (73) in [Young \(2012\)](#).

3.8.2 Thickness and pressure gradient correlation

To expose the physics of the ensemble mean of the thickness weighted pressure gradient, $\overline{h \nabla_h p}$, we make use of the variety of identities that hold between layer and interface quantities, as well as between ensemble means and thickness weighted means. As a start, we write

$$\overline{h \nabla_h p} = \overline{h} \widehat{\nabla_h p} \quad \text{equation (3.71) defining the TWA} \quad (3.99a)$$

$$= \overline{h} \nabla_h \overline{p} + \overline{h'} \nabla_h \overline{p'} \quad \text{expanding the ensemble mean} \quad (3.99b)$$

$$= \overline{h} (\nabla_h \overline{p} + \widehat{\nabla_h p'}) \quad \text{equation (3.77).} \quad (3.99c)$$

The eddy term is the correlation between layer thickness fluctuations and horizontal pressure gradient fluctuations

$$\overline{h \widehat{\nabla_h p'}} = \overline{h'} \nabla_h \overline{p'}, \quad (3.100)$$

which can be written in terms of the eddy geostrophic velocity

$$\overline{h \widehat{\nabla_h p'}} = -\rho_{\text{ref}} f \hat{z} \times \overline{h' \mathbf{u}'_g} = -\rho_{\text{ref}} f \hat{z} \times \overline{h} \widehat{\mathbf{u}'_g}. \quad (3.101)$$

For the special case of geostrophic flows, the bolus velocity (3.88) equals to $\widehat{\mathbf{u}'_g}$ so that we write

$$\overline{h \widehat{\nabla_h p'}} = -\rho_{\text{ref}} f \hat{z} \times \overline{h} \mathbf{u}^{\text{bolus}}. \quad (3.102)$$

3.8.3 Unpacking the thickness and pressure gradient correlation

In this subsection we unpack the correlation between eddy thickness and eddy pressure gradient as given by

$$\overline{h_k \widehat{\nabla_h p'_k}} = \overline{h'_k \nabla_h \overline{p'_k}} \quad (3.103)$$

that appears in equation (3.100). Here we expose the layer index, k , since the thickness and pressure gradient correlation will be related to interface quantities (with indices $k \pm 1/2$) in the following. In words, the following manipulations proceed by writing the pressure force as a contact force rather than a body force, which exposes the eddy interfacial form stress acting at the upper and lower boundary of the layer, with the vertical divergence of this horizontal stress providing a vertical transfer of horizontal momentum between adjacent layers. In addition, we find a term arising from the horizontal gradient in the layer depth integrated pressure or, alternatively, the layer potential energy. Filling in the mathematical details requires the development given in VOLUME 2, in which we expose two equivalent expressions for the contact pressure force.

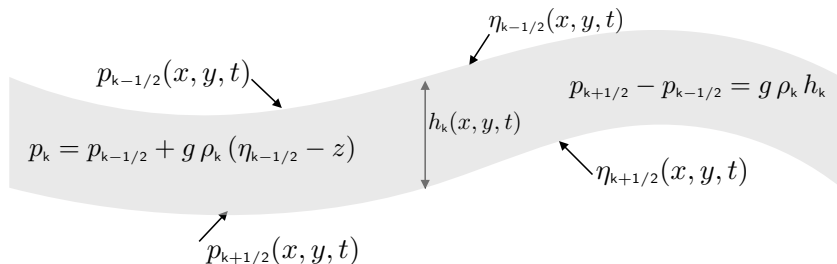


FIGURE 3.4: Schematic of the interface vertical positions, $\eta_{k+1/2}(x, y, t)$ and $\eta_{k-1/2}(x, y, t)$, the interface pressures, $p_{k+1/2}(x, y, t)$ and $p_{k-1/2}(x, y, t)$, and the layer pressure, $p_k(x, y, z, t)$, for a shallow water layer. Since $p_k(x, y, z, t)$ is a linear function of z within the layer, its horizontal gradient is independent of z within the layer.

As part of the following derivation we make use of relations for pressure within a layer and at an interface

$$p_k = p_{k-1/2} + g \rho_k (\eta_{k-1/2} - z) \quad (3.104a)$$

$$p_{k+1/2} - p_{k-1/2} = g \rho_k h_k = -g \rho_k (\eta_{k+1/2} - \eta_{k-1/2}) \quad (3.104b)$$

$$p_{1/2} = p_a, \quad (3.104c)$$

with p_a the applied (or atmospheric) pressure at the ocean surface. In addition, $z = \eta_{k+1/2}(x, y, t)$ is the vertical position of the lower interface, and $z = \eta_{k-1/2}(x, y, t)$ is the vertical position of the upper interface, with these fields illustrated in Figure 3.4. Since we are working with a shallow water fluid layer, the pressure at a position within the layer, $p_k(x, y, z, t)$, is a linear function of vertical position within the layer (equation (3.104a)) so that its horizontal gradient is independent of vertical position within the layer,

$$\nabla_h p_k = \nabla_h p_{k-1/2} + g \rho_k \nabla_h \eta_{k-1/2}. \quad (3.105)$$

Interfacial form stress plus gradient of layer depth integrated pressure

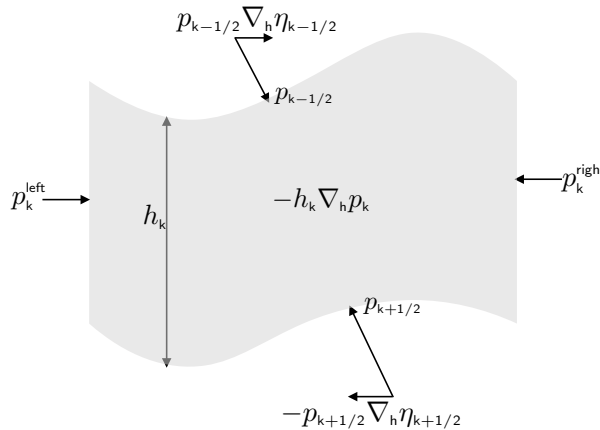


FIGURE 3.5: Illustrating the decomposition (3.106) for the thickness weighted pressure gradient acting within a shallow water layer. This volume integrated horizontal pressure body force can be decomposed into the area integrated pressure contact forces acting on the vertical sides, plus the area integrated pressure form stresses acting on the top and bottom interfaces. The pressure form stresses are drawn here as the horizontal components to the pressure contact stresses.

The first expression for thickness weighted pressure gradient is given by

$$-h_k \nabla_h p_k = -\nabla_h P_k + \mathbf{F}_k^{\text{form}}, \quad (3.106)$$

which is illustrated in Figure 3.5. In this equation we introduced the pressure that is vertically integrated over layer- k

$$P_k = \int_{\eta_{k+1/2}}^{\eta_{k-1/2}} p_k dz = h_k (g \rho_k h_k / 2 + p_{k-1/2}), \quad (3.107)$$

with its negative gradient,⁷

$$-\nabla_h P_k = -(h_k \nabla_h p_{k+1/2} + p_{k-1/2} \nabla_h h_k), \quad (3.108)$$

⁷See Exercise 3.5 for the derivation of equation (3.108).

leading to a horizontal acceleration due to imbalances in the area integrated pressure acting along the vertical sides of the shallow water region. The second stress in equation (3.106) is the pressure form stress acting on the upper and lower layer interfaces

$$\mathbf{F}_k^{\text{form}} = p_{k-1/2} \nabla_h \eta_{k-1/2} - p_{k+1/2} \nabla_h \eta_{k+1/2} \equiv \delta_k (p_{k-1/2} \nabla_h \eta_{k-1/2}), \quad (3.109)$$

where

$$\delta_k \Phi_{k-1/2} \equiv \Phi_{k-1/2} - \Phi_{k+1/2} = -(\Phi_{k+1/2} - \Phi_{k-1/2}) \quad (3.110)$$

is a discrete vertical difference operator acting on interface properties. The use of a backward difference operator is motivated since k increases down whereas \hat{z} points up. Additionally, we define the difference operator to only act on fields defined at the layer interface, with layer fields commuting with this operator so that, for example,

$$\delta_k (h_k \eta_{k-1/2}) = h_k \delta_k (\eta_{k-1/2}). \quad (3.111)$$

This convention helps produce a tidy form for the Eliassen-Palm flux in Sections 3.8.4 and 3.8.5.

Making use of the depth integrated pressure and form stress as given by equation (3.106) allows us to write the ensemble mean thickness weighted horizontal pressure gradient

$$-\overline{h_k \nabla_h p_k} = -\nabla_h \overline{P_k} + \delta_k [\overline{p_{k-1/2} \nabla_h \eta_{k-1/2}}]. \quad (3.112)$$

Evidently, the thickness weighted horizontal pressure gradient (left hand side) has been decomposed into a horizontal gradient of the layer depth integrated pressure (first right hand side term), plus the discrete vertical divergence of the form stresses that act on the top and bottom layer interfaces labelled by $k \pm 1/2$.

Following equation (3.107), we write the negative gradient of the ensemble mean layer integrated pressure

$$-\nabla_h \overline{P_k} = -\nabla_h [\overline{h_k} (\overline{p_{k-1/2}} + g \rho_k \overline{h_k}/2)] - \nabla_h [\overline{h'_k} (\overline{p'_{k-1/2}} + g \rho_k \overline{h'_k}/2)], \quad (3.113)$$

and the ensemble mean of the form stress vertical divergence

$$\overline{\mathbf{F}_k^{\text{form}}} = \delta_k [\overline{p_{k-1/2} \nabla_h \eta_{k-1/2}}] = \delta_k \left[\overline{p_{k-1/2} \nabla_h \eta_{k-1/2}} + \overline{p'_{k-1/2} \nabla_h \eta'_{k-1/2}} \right]. \quad (3.114)$$

We are thus led to the following decomposition of the eddy contribution to the thickness weighted pressure gradient

$$-\overline{h'_k \nabla_h p'_k} = -\nabla_h [\overline{h'_k} (\overline{p'_{k-1/2}} + g \rho_k \overline{h'_k}/2)] + \delta_k \left[\overline{p'_{k-1/2} \nabla_h \eta'_{k-1/2}} \right]. \quad (3.115)$$

The right hand side is much less mathematically compact than the left hand side. The payoff for such verbosity is that the right hand side provides an alternative physical interpretation for the thickness weighted pressure gradient, which we further advance in the following. For orientation, in Figure 3.6 we illustrate the deviations of the interface positions relative to the ensemble mean.

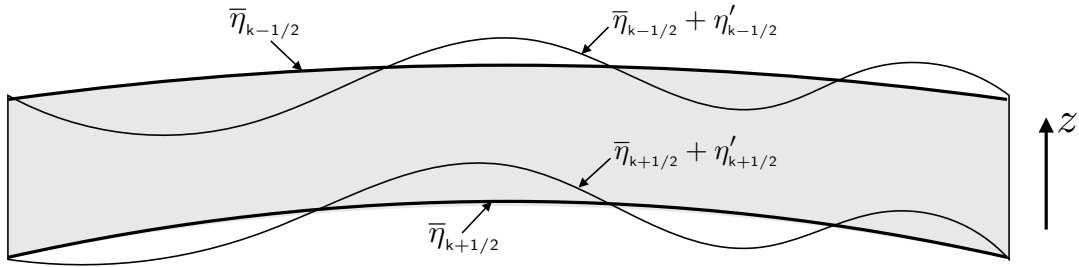


FIGURE 3.6: Schematic of the interface positions for a shallow water layer. The ensemble mean layer interfaces have vertical positions given by $z = \bar{\eta}_{k\pm 1/2}$, whereas the fluctuating interfaces are located at $z = \bar{\eta}_{k\pm 1/2} + \eta'_{k\pm 1/2}$. As depicted here, the ensemble mean interface positions are not generally horizontal.

Dual interfacial pressure form stress plus gradient of layer potential energy

An alternative formulation uses the dual form stress and potential energy, in which case we write the thickness weighted horizontal pressure gradient as

$$-h_k \nabla_h p_k = -\nabla_h \mathcal{P}_k + \mathbf{F}_k^{\text{dual}}. \quad (3.116)$$

In this equation we introduced the layer gravitational potential energy per area

$$\mathcal{P}_k = g \rho_k \int_{\eta_{k+1/2}}^{\eta_{k-1/2}} z \, dz = (g \rho_k/2) (\eta_{k-1/2}^2 - \eta_{k+1/2}^2) = (g \rho_k/2) \delta_k (\eta_{k-1/2}^2), \quad (3.117)$$

and the **dual form stress** from VOLUME 2.⁸

$$\mathbf{F}_k^{\text{dual}} = -\delta_k (\eta_{k-1/2} \nabla_h p_{k-1/2}) = \mathbf{F}_k^{\text{form}} - \nabla_h [\delta_k (\eta_{k-1/2} p_{k-1/2})]. \quad (3.118)$$

Since they differ by a gradient, the form stress and dual form stress have identical curls and so they contribute the same interfacial pressure torque as part of the layer vorticity evolution

$$-\nabla_h \times (h_k \nabla_h p_k) = \nabla_h \times \mathbf{F}_k^{\text{dual}} = \nabla_h \times \mathbf{F}_k^{\text{form}}. \quad (3.119)$$

However, for the momentum budget it is crucial to note that the form stress and dual form stress are distinct.

Making use of the potential energy and dual form stress as given by equation (3.116) allows us to write the ensemble mean thickness weighted pressure gradient as

$$-\bar{h}_k \nabla_h \bar{p}_k = -\nabla_h \bar{\mathcal{P}}_k - \delta_k [\overline{\eta_{k-1/2} \nabla_h p_{k-1/2}}], \quad (3.120)$$

where we decomposed the potential energy gradient as

$$-\nabla_h \bar{\mathcal{P}}_k = -(g \rho_k/2) \delta_k \left[\nabla_h (\overline{\eta_{k-1/2}})^2 + \nabla_h (\overline{\eta'_{k-1/2}})^2 \right], \quad (3.121)$$

and the vertical convergence of the dual form stress is

$$-\delta_k [\overline{\eta_{k-1/2} \nabla_h p_{k-1/2}}] = -\delta_k \left[\overline{\eta_{k-1/2} \nabla_h p_{k-1/2}} + \overline{\eta'_{k-1/2} \nabla_h p'_{k-1/2}} \right]. \quad (3.122)$$

⁸The form stress and dual form stress differ by a gradient, so that they are not equal. Indeed, the form stress is a force per area, whereas the dual form stress is not, even though it has the dimensions of a stress. It is unfortunate that the literature often ignores the difference between dual form stress and form stress.

We are thus led to decompose the thickness weighted pressure gradient correlation as

$$-\bar{h}' \nabla_h p'_k = -(g \rho_k / 2) \nabla_h [\delta_k (\bar{\eta}'_{k-1/2})^2] - \delta_k [\bar{\eta}'_{k-1/2} \nabla_h p'_{k-1/2}]. \quad (3.123)$$

Again, the first term on the right hand side arises from the eddy potential energy and the second term from the dual eddy form stress.

3.8.4 Zonal and meridional Eliassen-Palm fluxes: version I

Making use of the thickness and pressure gradient correlation in the form of equation (3.115) (the version with the form stress) leads to the thickness weighted momentum equation

$$\begin{aligned} \partial_t (\bar{h} \hat{\mathbf{u}}) + \nabla_h \cdot (\bar{h} \hat{\mathbf{u}} \otimes \hat{\mathbf{u}}) + f \hat{\mathbf{z}} \times \bar{h} \hat{\mathbf{u}} + \bar{h} \nabla_h \bar{p} / \rho_{\text{ref}} \\ = -\nabla_h \cdot (\bar{h} \hat{\mathbf{u}}'' \otimes \hat{\mathbf{u}}'') - \rho_{\text{ref}}^{-1} \nabla_h [\bar{h}'_k (p'_{k-1/2} + g \rho_k h'_k / 2)] + \rho_{\text{ref}}^{-1} \delta_k (\bar{p}' \nabla_h \eta')_{k-1/2}, \end{aligned} \quad (3.124)$$

where we only exposed the interface indices to reduce notational clutter, and where we introduced the shorthand for the eddy form stress at the $k - 1/2$ interface

$$(p' \nabla_h \eta')_{k-1/2} = p'_{k-1/2} \nabla_h \eta'_{k-1/2}. \quad (3.125)$$

The subgrid scale correlations on the right hand side of equation (3.124) can be organized into the divergence of two tensors

$$\begin{aligned} \nabla_h \cdot (\bar{h} \hat{\mathbf{u}}'' \otimes \hat{\mathbf{u}}'') + \rho_{\text{ref}}^{-1} \nabla_h [\bar{h}'_k (p'_{k-1/2} + g \rho_k h'_k / 2)] - (\bar{h} \rho_{\text{ref}})^{-1} \delta_k [\bar{h} (\bar{p}' \nabla_h \eta')_{k-1/2}] \\ = [\partial_x \quad \partial_y \quad (1/\bar{h}) \delta_k] \begin{bmatrix} \bar{h} \hat{\mathbf{u}}'' \hat{\mathbf{u}}'' & \bar{h} \hat{\mathbf{u}}'' \hat{\mathbf{v}}'' & 0 \\ \bar{h} \hat{\mathbf{u}}'' \hat{\mathbf{v}}'' & \bar{h} \hat{\mathbf{v}}'' \hat{\mathbf{v}}'' & 0 \\ 0 & 0 & 0 \end{bmatrix} \\ + \rho_{\text{ref}}^{-1} [\partial_x \quad \partial_y \quad (1/\bar{h}) \delta_k] \begin{bmatrix} \bar{h}'_k (p'_{k-1/2} + g \rho_k h'_k / 2) & 0 & 0 \\ 0 & \bar{h}'_k (p'_{k-1/2} + g \rho_k h'_k / 2) & 0 \\ -\bar{h} (\bar{p}' \partial_x \eta')_{k-1/2} & -\bar{h} (\bar{p}' \partial_y \eta')_{k-1/2} & 0 \end{bmatrix}, \end{aligned} \quad (3.126)$$

where we recall from equation (3.111) that the vertical difference operator, δ_k , only acts on layer interface fields so that \bar{h}_k commutes with δ_k . The first tensor in equation (3.126) arises from Reynolds stresses and the second tensor arises from eddy pressures, including the eddy form stress in the third row.

When combined, the columns of the tensors appearing in equation (3.126) are the thickness weighted shallow water *Eliassen-Palm fluxes* for the zonal (column 1) and meridional (column 2) momentum equation

$$\mathbf{E}^{(\text{uEP})} = \left[\bar{h} \hat{\mathbf{u}}'' \hat{\mathbf{u}}'' + \rho_{\text{ref}}^{-1} \bar{h}'_k (p'_{k-1/2} + g \rho_k h'_k / 2) \right] \hat{\mathbf{x}} + \bar{h} \hat{\mathbf{u}}'' \hat{\mathbf{v}}'' \hat{\mathbf{y}} - (\bar{h} / \rho_{\text{ref}}) \overline{(\bar{p}' \partial_x \eta')_{k-1/2}} \hat{\mathbf{z}} \quad (3.127a)$$

$$\mathbf{E}^{(\text{vEP})} = \bar{h} \hat{\mathbf{u}}'' \hat{\mathbf{v}}'' \hat{\mathbf{x}} + \left[\bar{h} \hat{\mathbf{v}}'' \hat{\mathbf{v}}'' + \rho_{\text{ref}}^{-1} \bar{h}'_k (p'_{k-1/2} + g \rho_k h'_k / 2) \right] \hat{\mathbf{y}} - (\bar{h} / \rho_{\text{ref}}) \overline{(\bar{p}' \partial_y \eta')_{k-1/2}} \hat{\mathbf{z}}. \quad (3.127b)$$

The thickness-weighted Eliassen-Palm flux has physical dimensions of thickness times velocity squared. We encounter the unaveraged version of the Eliassen-Palm flux when studying the shallow water momentum equation in VOLUME 3. [Maddison and Marshall \(2013\)](#) included the third column of zeros in equation (3.126) to emphasize that the Eliassen-Palm fluxes are the first and second columns to the *Eliassen-Palm flux tensor*. They illustrated the utility of this

perspective by considering gauge transformations that result in non-zero elements in the third column.

The Eliassen-Palm fluxes are second order in eddy amplitude; i.e., they are quadratic in eddy fluctuations. Furthermore, they bring together the Reynolds stress and eddy pressure terms, including the eddy form stress. The convergence of the Eliassen-Palm fluxes provides an eddy rectified acceleration to the thickness weighted velocity. To explicitly see this forcing, we write the components to the mean field momentum equation (3.124) as⁹

$$\partial_t(\bar{h}\hat{u}) + \nabla_h \cdot (\bar{h}\hat{u}\hat{u}) - f\bar{h}\hat{v} + \bar{h}\partial_x\bar{p}/\rho = -(\nabla_h + \hat{z}\bar{h}^{-1}\delta_k) \cdot \mathbf{E}^{(uEP)} \quad (3.128a)$$

$$\partial_t(\bar{h}\hat{v}) + \nabla_h \cdot (\bar{h}\hat{u}\hat{v}) + f\bar{h}\hat{u} + \bar{h}\partial_y\bar{p}/\rho = -(\nabla_h + \hat{z}\bar{h}^{-1}\delta_k) \cdot \mathbf{E}^{(vEP)}. \quad (3.128b)$$

Equations (3.128a) and (3.128b) are isomorphic to the unaveraged horizontal momentum equation (3.50c), yet with the addition of the convergence of the Eliassen-Palm flux on the right hand side that encapsulates rectified effects from eddies. They can be written using the material time derivative (3.85)

$$\frac{D^\sharp \hat{u}}{Dt} - f\hat{v} + \partial_x\bar{p}/\rho = -\bar{h}^{-1}(\nabla_h + \hat{z}\bar{h}^{-1}\delta_k) \cdot \mathbf{E}^{(uEP)} \quad (3.129a)$$

$$\frac{D^\sharp \hat{v}}{Dt} + f\hat{u} + \partial_y\bar{p}/\rho = -\bar{h}^{-1}(\nabla_h + \hat{z}\bar{h}^{-1}\delta_k) \cdot \mathbf{E}^{(vEP)}. \quad (3.129b)$$

We emphasize that these equations only make use of the thickness weighted velocity, \hat{u} , as do the averaged thickness equation (3.84) and averaged tracer equation (3.91). We advertised this point near the start of this chapter, noting that it facilitates the practical use of the **TWA** equations for numerical simulations. We further this correspondence in Section 3.9 by showing that the vorticity and potential vorticity equations also make use only of \hat{u} .

3.8.5 Zonal and meridional Eliassen-Palm fluxes: version II

We here follow the development in Section 3.8.4, only now making use of the thickness and pressure gradient correlation in the form of equation (3.123) (the version with the dual form stress). Our presentation is terse since there are few differences from Section 3.8.4. We start from the thickness weighted momentum equation

$$\begin{aligned} \partial_t(\bar{h}\hat{u}) + \nabla_h \cdot (\bar{h}\hat{u} \otimes \hat{u}) + f\hat{z} \times \bar{h}\hat{u} + \bar{h}\nabla_h\bar{p}/\rho_{ref} \\ = -\nabla_h \cdot (\widehat{\bar{h}\mathbf{u}'' \otimes \mathbf{u}''}) - (g\rho_k/2\rho_{ref})\nabla_h[\delta_k\overline{(\eta'_{k-1/2})^2}] - \delta_k\overline{[(\eta' \nabla_h p')_{k-1/2}]/\rho_{ref}}. \end{aligned} \quad (3.130)$$

The subgrid scale correlations on the right hand side can be organized into the divergence of two tensors

$$\begin{aligned} & \nabla_h \cdot (\widehat{\bar{h}\mathbf{u}'' \otimes \mathbf{u}''}) + (g\rho_k/2\rho_{ref})\nabla_h[\delta_k\overline{(\eta'_{k-1/2})^2}] + \delta_k\overline{[(\eta' \nabla_h p')_{k-1/2}]/\rho_{ref}} \\ &= \begin{bmatrix} \partial_x & \partial_y & \bar{h}^{-1}\delta_k \end{bmatrix} \begin{bmatrix} \widehat{\bar{h}\mathbf{u}'' \mathbf{u}''} & \widehat{\bar{h}\mathbf{u}'' \mathbf{v}''} & 0 \\ \widehat{\bar{h}\mathbf{u}'' \mathbf{v}''} & \widehat{\bar{h}\mathbf{v}'' \mathbf{v}''} & 0 \\ 0 & 0 & 0 \end{bmatrix} \end{aligned}$$

⁹Recall from equation (3.111) that the operator δ_k only acts on interface fields, so that $\bar{h}^{-1}\delta_k(\bar{h}) = \delta_k$. This convention allows us to combine the horizontal components to the Eliassen-Palm flux with the vertical component, as written in equations (3.132a) and (3.132b).

$$+ \begin{bmatrix} \partial_x & \partial_y & \bar{h}^{-1} \delta_k \end{bmatrix} \begin{bmatrix} (g \rho_k / 2 \rho_{ref}) [\delta_k \bar{h} \bar{h}^{-1} \delta_k] & 0 & 0 \\ 0 & (g \rho_k / 2 \rho_{ref}) [\delta_k \bar{h} \bar{h}^{-1} \delta_k] & 0 \\ (\bar{h} / \rho_{ref}) \bar{h} \bar{h}^{-1} \delta_k & (\bar{h} / \rho_{ref}) \bar{h} \bar{h}^{-1} \delta_k & 0 \end{bmatrix}. \quad (3.131)$$

The first tensor arises from Reynolds stresses and the second arises from eddy potential energy and dual eddy form stresses. When combined, the columns are the thickness weighted *Eliassen-Palm fluxes* for the zonal (column 1) and meridional (column 2), here making use of the dual form stress

$$\mathbf{E}_{dual}^{(uEP)} = \left[\bar{h} \widehat{u'' u''} + (g \rho_k / 2 \rho_{ref}) [\delta_k \bar{h} \bar{h}^{-1} \delta_k] \right] \hat{\mathbf{x}} + \bar{h} \widehat{u'' v''} \hat{\mathbf{y}} + \bar{h} \overline{(\eta' \partial_x p')_{k-1/2} / \rho_{ref}} \hat{\mathbf{z}} \quad (3.132a)$$

$$\mathbf{E}_{dual}^{(vEP)} = \bar{h} \widehat{u'' v''} \hat{\mathbf{x}} + \left[\bar{h} \widehat{v'' v''} + (g \rho_k / 2 \rho_{ref}) [\delta_k \bar{h} \bar{h}^{-1} \delta_k] \right] \hat{\mathbf{y}} + \bar{h} \overline{(\eta' \partial_y p')_{k-1/2} / \rho_{ref}} \hat{\mathbf{z}}. \quad (3.132b)$$

The convergence of the Eliassen-Palm fluxes provides an eddy rectified acceleration on the thickness weighted velocity

$$\partial_t (\bar{h} \hat{u}) + \nabla_h \cdot (\bar{h} \hat{\mathbf{u}} \hat{u}) - f \bar{h} \hat{v} + \bar{h} \partial_x \bar{p} / \rho = -(\nabla_h + \hat{\mathbf{z}} \bar{h}^{-1} \delta_k) \cdot \mathbf{E}_{dual}^{(uEP)} \quad (3.133a)$$

$$\partial_t (\bar{h} \hat{v}) + \nabla_h \cdot (\bar{h} \hat{\mathbf{u}} \hat{v}) + f \bar{h} \hat{u} + \bar{h} \partial_y \bar{p} / \rho = -(\nabla_h + \hat{\mathbf{z}} \bar{h}^{-1} \delta_k) \cdot \mathbf{E}_{dual}^{(vEP)}. \quad (3.133b)$$

3.8.6 Interfacial stresses from geostrophic eddies

In VOLUME 2 we study the rectified effects from geostrophic eddies in a zonally re-entrant channel for a continuously stratified fluid, where we show that the zonal mean of isopycnal eddy form stresses is equivalent to the meridional eddy flux of buoyancy. We consider similar questions within the context of the **TWA** shallow water fluid, here focusing on the interfacial transfer of momentum due to eddy dual form stresses as given by the vertical vectors

$$\rho_{ref} \left[\mathbf{E}_{dual}^{(uEP)} \right]_{interface} = \hat{\mathbf{z}} \bar{h} \overline{(\eta' \partial_x p')_{k-1/2}} \quad (3.134a)$$

$$\rho_{ref} \left[\mathbf{E}_{dual}^{(vEP)} \right]_{interface} = \hat{\mathbf{z}} \bar{h} \overline{(\eta' \partial_y p')_{k-1/2}}. \quad (3.134b)$$

Let us now write the interface pressure gradient fluctuation as

$$\nabla_h p_{k-1/2} = \nabla_h p_k - g \rho_k \nabla_h \eta_{k-1/2} \quad (3.135)$$

so that

$$\overline{(\eta' \nabla_h p')_{k-1/2}} = \overline{\eta'_{k-1/2} \nabla_h p'_k} + g \rho_k \overline{(\eta' \nabla_h \eta')_{k-1/2}}. \quad (3.136)$$

We now assume that the fluctuations are in **geostrophic balance**. Doing so allows us to introduce the layer geostrophic velocity corresponding to the gradient of the layer pressure fluctuations

$$\partial_x p'_k = \rho_{ref} f v'_k \quad \text{and} \quad \partial_y p'_k = -\rho_{ref} f u'_k. \quad (3.137)$$

The dual form stress portion of the Eliassen-Palm fluxes now takes the form

$$\rho_{ref} \left[\mathbf{E}_{dual}^{(uEP)} \right]_{interface} = \hat{\mathbf{z}} \bar{h} \left[f \rho_{ref} \overline{\eta'_{k-1/2} v'_k} + g \rho_k \overline{(\eta' \partial_x \eta')_{k-1/2}} \right] \quad (3.138a)$$

$$\rho_{ref} \left[\mathbf{E}_{dual}^{(vEP)} \right]_{interface} = \hat{\mathbf{z}} \bar{h} \left[-f \rho_{ref} \overline{\eta'_{k-1/2} u'_k} + g \rho_k \overline{(\eta' \partial_y \eta')_{k-1/2}} \right]. \quad (3.138b)$$

The $\overline{\eta'_{k-1/2} \mathbf{u}'_k}$ term is an eddy transport of the area between $z = \bar{\eta}_{k-1/2}$ and $z = \eta'_{k-1/2}$ (see Figure 3.6). We studied the same transport for the continuously stratified fluid in VOLUME 2. In that discussion, we found that the interface fluctuations, η' , can be related to the buoyancy fluctuations, b' , in which case $\overline{\eta'_{k-1/2} \mathbf{u}'_k}$ is proportional to the eddy buoyancy flux for the layer.

3.8.7 Comments

Greatbatch and Lamb (1990) and *Greatbatch* (1998) pursue a similar analysis for the purpose of framing the mesoscale eddy parameterization problem. They focus on the interfacial form stress contribution since, for geostrophic eddies, it dominates over the other terms in the Eliassen-Palm fluxes (3.132a) and (3.132b).

3.9 Vorticity and potential vorticity

We follow the procedure from our discussion of shallow water vorticity in VOLUME 3 to derive the vorticity and potential vorticity for the thickness weighted shallow water equations. In the process, we connect the eddy flux of potential vorticity to the Eliassen-Palm fluxes (3.127a) and (3.127b). Note that the same manipulations also hold for the dual Eliassen-Palm fluxes (3.132a) and (3.132b).

3.9.1 Derivation

We make use of the vector identities from our study of the shallow water equation in VOLUME 3 to bring the material evolution equations (3.129a) and (3.129b) into their equivalent vector invariant forms¹⁰

$$\partial_t \hat{\mathbf{u}} - (f + \hat{\zeta}) \hat{\mathbf{v}} = -\partial_x (\bar{p}/\rho + \hat{\mathbf{u}} \cdot \hat{\mathbf{u}}/2) - \bar{h}^{-1} (\nabla_h + \hat{\mathbf{z}} \bar{h}^{-1} \delta_k) \cdot \mathbf{E}^{(uEP)} \quad (3.139a)$$

$$\partial_t \hat{\mathbf{v}} + (f + \hat{\zeta}) \hat{\mathbf{u}} = -\partial_y (\bar{p}/\rho + \hat{\mathbf{u}} \cdot \hat{\mathbf{u}}/2) - \bar{h}^{-1} (\nabla_h + \hat{\mathbf{z}} \bar{h}^{-1} \delta_k) \cdot \mathbf{E}^{(vEP)}, \quad (3.139b)$$

where we introduced the relative vorticity of the thickness weighted horizontal velocity

$$\hat{\zeta} = \partial_x \hat{\mathbf{v}} - \partial_y \hat{\mathbf{u}}. \quad (3.140)$$

Taking ∂_x of the meridional equation (3.139b) and subtracting ∂_y of the zonal equation (3.139a) renders the evolution equation for absolute vorticity, $\hat{\zeta}_a = \hat{\zeta} + f$,

$$\frac{D^\# \hat{\zeta}_a}{Dt} + \hat{\zeta}_a \nabla_h \cdot \hat{\mathbf{u}} = \partial_y [\bar{h}^{-1} (\nabla_h + \hat{\mathbf{z}} \bar{h}^{-1} \delta_k) \cdot \mathbf{E}^{(uEP)}] - \partial_x [\bar{h}^{-1} (\nabla_h + \hat{\mathbf{z}} \bar{h}^{-1} \delta_k) \cdot \mathbf{E}^{(vEP)}]. \quad (3.141)$$

Making use of the thickness equation (3.86) to replace $\nabla_h \cdot \hat{\mathbf{u}}$ leads to the potential vorticity equation

$$\bar{h} \frac{D^\# \Pi^\#}{Dt} = -\nabla_h \cdot \mathbf{F}^\# \quad (3.142)$$

where

$$\Pi^\# = \frac{f + \partial_x \hat{\mathbf{v}} - \partial_y \hat{\mathbf{u}}}{\bar{h}} = \frac{f + \hat{\zeta}}{\bar{h}} \quad (3.143)$$

¹⁰In Section D.6 of *Griffies et al.* (2020), the authors state “In contrast to the flux-form momentum equation, the vector-invariant velocity equation does not admit a finite volume formulation.” That statement is incorrect, with equations (3.139a) and (3.139b) the finite volume vector-invariant velocity equation.

is the potential vorticity defined with the thickness weighted velocity and ensemble mean thickness. The corresponding eddy potential vorticity flux is a horizontal vector that is written in terms of the divergence of the Eliassen-Palm fluxes

$$\mathbf{F}^\sharp = \hat{\mathbf{x}} [\bar{h}^{-1} (\nabla_h + \hat{z} \bar{h}^{-1} \delta_k) \cdot \mathbf{E}^{(vEP)}] - \hat{\mathbf{y}} [\bar{h}^{-1} (\nabla_h + \hat{z} \bar{h}^{-1} \delta_k) \cdot \mathbf{E}^{(uEP)}] + \hat{z} \times \nabla_h \Upsilon, \quad (3.144)$$

where Υ is an arbitrary gauge function.¹¹ This equation connects the potential vorticity flux to the Eliassen-Palm fluxes and it is known as the *Taylor-Bretherton identity*. Remarkably, the potential vorticity flux also provides the eddy forcing to the thickness weighted velocity equation

$$\partial_t \hat{\mathbf{u}} + (f + \hat{\zeta}) \hat{z} \times \hat{\mathbf{u}} + \nabla_h (\bar{p}/\rho + \hat{\mathbf{u}} \cdot \hat{\mathbf{u}}/2) = -\hat{z} \times (\mathbf{F}^\sharp - \hat{z} \times \nabla_h \Upsilon), \quad (3.145)$$

which can also be written

$$\partial_t \hat{\mathbf{u}} + \hat{z} \times (\bar{h} \hat{\mathbf{u}} \Pi^\sharp + \mathbf{F}^\sharp - \hat{z} \times \nabla_h \Upsilon) + \nabla_h (\bar{p}/\rho + \hat{\mathbf{u}} \cdot \hat{\mathbf{u}}/2) = 0, \quad (3.146)$$

where $\bar{h} \hat{\mathbf{u}} \Pi^\sharp + \mathbf{F}^\sharp - \hat{z} \times \nabla_h \Upsilon$ is the net (mean plus eddy plus gauge) potential vorticity flux.

3.9.2 Concerning the mean field potential vorticity

We emphasize that the mean field potential vorticity arising from our development is Π^\sharp , which is defined by equation (3.143) using the thickness weighted velocity, $\hat{\mathbf{u}}$ for the relative vorticity. This potential vorticity is distinct from the thickness weighted average potential vorticity

$$\hat{\Pi} = \frac{\bar{\Pi} \bar{h}}{\bar{h}} = \frac{f + \bar{\zeta}}{\bar{h}} = \frac{f + \partial_x \bar{v} - \partial_y \bar{u}}{\bar{h}}, \quad (3.147)$$

which is the mean field potential vorticity considered by [Greatbatch \(1998\)](#) and [Peterson and Greatbatch \(2001\)](#). The two forms of potential vorticity differ by the potential vorticity of the bolus velocity

$$\Pi^\sharp - \hat{\Pi} = \frac{(f + \hat{\zeta}) - (f + \bar{\zeta})}{\bar{h}} = \frac{\hat{z} \cdot [\nabla_h \times (\hat{\mathbf{u}} - \bar{\mathbf{u}})]}{\bar{h}} = \frac{\hat{z} \cdot (\nabla_h \times \hat{\mathbf{u}'})}{\bar{h}} = \frac{\hat{z} \cdot (\nabla_h \times \mathbf{u}^{\text{bolus}})}{\bar{h}}, \quad (3.148)$$

where the penultimate equality made use of equation (3.81) for $\hat{\mathbf{u}'}$, and the final equality introduced the bolus velocity according to equation (3.88). Use of Π^\sharp allows us to develop a potential vorticity conservation statement solely in terms of $\hat{\mathbf{u}}$, whereas the use of $\hat{\Pi}$ by [Greatbatch \(1998\)](#) and [Peterson and Greatbatch \(2001\)](#) requires both $\bar{\mathbf{u}}$ and $\hat{\mathbf{u}}$.

3.9.3 Comments

As in [Young \(2012\)](#), and as advertised in Section 3.4, we have developed the full set of mechanical equations for the **TWA** shallow water solely in terms of the thickness weighted velocity, $\hat{\mathbf{u}}$. This development includes the thickness equation (3.84), the tracer equation (3.91), the velocity equation (3.95) and the potential vorticity equation (3.142). There is no need for the ensemble mean velocity, $\bar{\mathbf{u}}$, and thus no need to parameterize the bolus velocity.

¹¹Equation (129) in [Young \(2012\)](#) should have a gauge function on its right hand side, which follows from his footnote #3.

3.10 Vorticity fluxes for non-divergent barotropic flow

In our study of the horizontally non-divergent barotropic flow in VOLUME 3, we encountered the mechanics of a two dimensional fluid whose horizontal flow is non-divergent. As for the shallow water, the non-divergent flow moves as vertical columns. However, since the horizontal flow is non-divergent, each column is rigid so there is no stretching or squeezing of columns. Correspondingly, there are no form stresses acting on these columns since the top and bottom interfaces are flat. We here briefly specialize the shallow water vorticity analysis in this section to consider rigid columnar motion.

For rigid fluid columns, the thickness weighted average reduces to just the ensemble mean since all layer thicknesses are fixed constants. Correspondingly, there are no form stresses acting at the layer interfaces since the layer interfaces are horizontal. Hence, the Eliassen-Palm fluxes (3.127a) and (3.127b) reduce to just their Reynolds stress contributions

$$h^{-1} \mathbf{E}^{(uEP)} = \overline{u' u'} \hat{\mathbf{x}} + \overline{u' v'} \hat{\mathbf{y}} \quad (3.149a)$$

$$h^{-1} \mathbf{E}^{(vEP)} = \overline{u' v'} \hat{\mathbf{x}} + \overline{v' v'} \hat{\mathbf{y}}. \quad (3.149b)$$

The corresponding eddy potential vorticity flux (3.144), absent the gauge term, is

$$\mathbf{F}^\sharp = \hat{\mathbf{x}} \nabla_h \cdot [\overline{u' v'} \hat{\mathbf{x}} + \overline{v' v'} \hat{\mathbf{y}}] - \hat{\mathbf{y}} \nabla_h \cdot [\overline{u' u'} \hat{\mathbf{x}} + \overline{u' v'} \hat{\mathbf{y}}] \quad (3.150a)$$

$$= \hat{\mathbf{x}} [\partial_x (\overline{u' v'}) + \partial_y (\overline{v' v'})] - \hat{\mathbf{y}} [\partial_x (\overline{u' u'}) + \partial_y (\overline{u' v'})]. \quad (3.150b)$$

Does the eddy potential vorticity flux (3.150b) agree, to within a gauge function, with the eddy flux resulting from a direct decomposition into eddy and mean within a two dimensional non-divergent model? To address this question, note that from VOLUME 3 the advective flux of potential vorticity for the two dimensional non-divergent flow is given by

$$\mathbf{u} q = \mathbf{u} f + \nabla_h \cdot (\hat{\mathbf{z}} \times \mathcal{E}), \quad (3.151)$$

where \mathcal{E} is the trace-free anisotropic portion of the kinetic stress tensor

$$\mathcal{E} = \begin{bmatrix} -(u^2 - v^2)/2 & -uv \\ -uv & (u^2 - v^2)/2 \end{bmatrix}. \quad (3.152)$$

The mean of the potential vorticity flux is (3.151) is given by

$$\overline{\mathbf{u} q} = \overline{\mathbf{u} f} + \overline{\mathbf{u}' q'}, \quad (3.153)$$

where the flux computed from the mean fields is

$$\overline{\mathbf{u} q} = \overline{\mathbf{u}} (f + \bar{\zeta}), \quad (3.154)$$

whereas the eddy potential vorticity flux is

$$\overline{\mathbf{u}' q'} = \mathbf{F}^\sharp - \hat{\mathbf{z}} \times \nabla_h (\overline{\mathbf{u}' \cdot \mathbf{u}'})/2, \quad (3.155)$$

with the missing steps for this derivation provided in Exercise (3.6). Hence, $\overline{\mathbf{u}' q'}$ agrees with \mathbf{F}^\sharp in equation (3.150b) to within a gauge function given by the rotated gradient of the eddy

kinetic energy per mass, so that their divergences are equal

$$\nabla_h \cdot \mathbf{F}^\sharp = \nabla_h \cdot \overline{\mathbf{u}' q'}. \quad (3.156)$$

That is, when diagnosing contributions to the potential vorticity flux, the gauge term, $-\hat{\mathbf{z}} \times \nabla_h(\overline{\mathbf{u}' \cdot \mathbf{u}'})/2$, plays no role in forcing potential vorticity.



3.11 Exercises

EXERCISE 3.1: DERIVATION OF THE VORTICITY EQUATION

Derive the isopycnal version of the vorticity equation

$$\left[\frac{\partial \tilde{\zeta}_a}{\partial t} \right]_b + (\mathbf{u} \cdot \nabla_{hb}) \tilde{\zeta}_a = -\tilde{\zeta}_a \nabla_{hb} \cdot \mathbf{u}, \quad (3.157)$$

with this equation used in Section 3.3.1 for deriving the potential vorticity equation.

EXERCISE 3.2: DERIVATION OF THE POTENTIAL VORTICITY EQUATION

Derive the potential vorticity equation,

$$\frac{DQ}{Dt} = 0, \quad (3.158)$$

discussed in Section 3.3.2.

EXERCISE 3.3: COORDINATE TRANSFORMATION OF THE POTENTIAL VORTICITY

Show that a coordinate transformation from geopotential coordinates to isopycnal coordinates bring the potential vorticity, $Q = (\boldsymbol{\omega}^{hy} + f \hat{\mathbf{z}}) \cdot \nabla_h b$, into the isopycnal coordinate form of equation (3.37).

EXERCISE 3.4: POTENTIAL VORTICITY EQUATION WITH IRREVERSIBLE PROCESSES

In Section 3.3.3 we derived the potential vorticity equation in the presence of irreversible processes. We here consider an alternative derivation that is directly analogous to Exercise 3.3. Namely, start from the discussion in VOLUME 3 for the material evolution of potential vorticity in a hydrostatic and Boussinesq fluid

$$\frac{DQ}{Dt} = \nabla_h \cdot \left[(f \hat{\mathbf{z}} + \boldsymbol{\omega}_{hy}) \dot{b} + b \nabla_h \times \mathbf{F}^h \right], \quad (3.159)$$

where

$$Q = \boldsymbol{\omega}_a^{hy} \cdot \nabla_h b = \boldsymbol{\omega}^{hy} \cdot \nabla_h b + f \frac{\partial b}{\partial z} \quad \text{and} \quad \boldsymbol{\omega}_{hy} = -\hat{\mathbf{x}} \frac{\partial v}{\partial z} + \hat{\mathbf{y}} \frac{\partial u}{\partial z} + \hat{\mathbf{z}} \left[\frac{\partial v}{\partial x} - \frac{\partial u}{\partial y} \right]. \quad (3.160)$$

Perform a coordinate transformation from this geopotential form into its isopycnal form, thus confirming the potential vorticity equation (3.47) that we derived from the isopycnal version of the equations of motion. Hint: this exercise is a bit tedious but straightforward.

EXERCISE 3.5: DERIVING THE EXPRESSION FOR $\nabla_h P_k$

Fill in the details for the derivation of equation (3.108) for $\nabla_h P_k$. Hint: make use of the identities summarized in Figure 3.4.

EXERCISE 3.6: VORTICITY FLUXES FOR NON-DIVERGENT BAROTROPIC FLOW

Fill in the missing steps needed to derive equation (3.155) for $\overline{u'q'}$ in the two dimensional non-divergent barotropic flow.



Part II

Scalar fields

In this part of the book, we study the physics and maths of **passive tracers**, **conservative tracers**,¹² as well as density and **Archimedean buoyancy**. Tensorially, these fields are scalars and so they provide a number (e.g., temperature, humidity, mass density) throughout the continuum fluid. This study of **scalar mechanics** complements that of momentum, vorticity, and energy considered in other parts of this book, with each scalar offering information about the mechanics of fluid motion. Much of the material is relevant to both the atmosphere and ocean, though specialized topics are motivated from ocean applications.

Although the physics and maths of scalar fields are simpler than that describing momentum, vorticity, and energy, there is a remarkable richness to the study. We only touch upon a few of the many topics, aiming to provide a theoretical platform for further study by the interested reader. Here is a synopsis of the chapters in this part of the book.

- In Chapter 4 we focus on tracer diffusion in the absence of advection. There is a long and rich history of research into diffusive (or conductive) processes across science and engineering, with books such as *Crank (1956)* and *Carslaw and Jaeger (1959)* offering a wealth of theoretical results and mathematical methods.
- In Chapter 5 we consider advection along with diffusion in affecting the evolution of tracer concentration. Advection results through viewing fluid flow from within the Eulerian reference frame, rather than the Lagrangian material frame. When acting alone on a conservative tracer, advection affects a reversible stirring of tracer concentration that can increase tracer gradients. When diffusion is included along with advection, reversibility is lost and tracer gradients increase or decrease depending on the relative dominance of advection or diffusion.
- In Chapter 6 we introduce notions of wave-mean flow interactions that give rise to eddy-induced advection (or skew diffusion) as well as diffusion. This chapter, which mostly focuses on kinematic properties and is restricted to tracers, makes use of both geopotential coordinates as well as isopycnal coordinate equations from Chapter 3. Doing so provides examples of the dual roles these two vertical coordinate choices fill for describing turbulent geophysical flows.
- In Chapter 7 we study elements of tracer parameterizations used for coarse resolution models of the ocean circulation. We particularly focus on a variety of mathematical properties of the parameterizations, and unpack the physics embodied within the mathematics. This chapter exposes a handful of questions at the leading edge of research.
- In Chapter 8 we consider ocean density and the budget for global sea level. This study prompts us to dive into the niceties of the enthalpy (heat), salt, and mass budgets for the ocean. These budgets are central to climate science since the ocean is the dominant sink of the anthropogenically induced increase in planetary enthalpy, and with this increase affecting a global rise in sea level.
- In Chapter 9 we present fundamental elements of water mass transformation analysis, which offers a view on ocean circulation that complements those available from Eulerian and Lagrangian kinematics. Many of the methods of ocean water mass analysis are relevant to atmospheric analyses as well, though this chapter is written from an ocean

¹²Conservative tracers evolve only via the convergence of advective and diffusive fluxes within the fluid interior, along with boundary conditions. Conservative tracers have no interior sources or sinks, so the net content of a conservative tracer over any finite volume domain is affected only through transport across boundaries.

perspective. Furthermore, this chapter is arguably the toughest in this part of the book, with progress in understanding water mass transformation theory sometimes taking years to ponder the concepts and apply the methods.

MATHEMATICS AND KINEMATICS IN THIS PART

The mathematics in this part of the book rely mostly on the Cartesian tensor analysis and vector calculus from VOLUME 1, though with some exceptions such as the generalized Laplacian operator encountered with the diffusion equation. Additionally, we start this part with a chapter diving into the fundamentals of parabolic partial differential equations and Green's functions. This material again relies mostly on Cartesian vector calculus, though it does provide some heavy lifting particularly in the Green's function method. For water mass analysis, we make use of rudimentary ideas from generalized vertical coordinates studied earlier in Part I of this volume. In regards to fluid kinematics, we mostly stay within an Eulerian perspective, though at times we touch upon a bit of Lagrangian methods such as when introducing the generalized Lagrangian mean in the context of wave-mean flow interactions in Chapter 6.

Chapter 4

DIFFUSIVE PROCESSES

In this chapter we study the physics of [diffusion](#) with a focus on how diffusion affects properties of geophysical fluids. We start with a brief discussion of [molecular diffusion](#), which is the most basic form of diffusion affecting matter concentrations, temperature, momentum, and other properties. The [continuum approximation](#) proposes that a macroscopic description of fluid motion does not require direct information about the motion of individual molecules. Nonetheless, random molecular motion and properties of the constituent molecules impact on fluid properties through molecular diffusion. The presence of molecular diffusion signals a system that is not in [thermodynamic equilibrium](#), with diffusion affecting an irreversible exchange of properties between fluid elements.

[Brownian motion](#) refers to the transport of relatively large pieces of matter, such as dust and pollen, by the random effects from molecular impulses. Although not central to the property distributions in geophysical fluids, the description of Brownian motion introduces some generic physical and mathematical concepts that appear throughout the physics of diffusion and irreversible processes, thus prompting its study in this chapter. In particular, it presages the ideas of turbulent diffusion introduced by [Taylor \(1922\)](#). A successful mathematical physics description of Brownian motion originates from [Einstein \(1905a\)](#), whose statistical formulation planted the intellectual seeds for the study of stochastic physics.¹ His description offers a particle-level mechanism behind diffusive spreading of relatively large particles, whereas molecular diffusion is concerned with how matter, heat, and momentum diffuse through media. They both rely on molecular chaos, but are concerned with the transport of distinct material properties.

Turbulent flows provide a stirring of fluids that affect the macroscopic mixing rates found in geophysical fluids. Turbulent stirring acts to enhance the magnitude of property gradients, thus offering the means to increase the efficiency of molecular diffusion that acts to irreversibly mix. We only briefly discuss the notions of such turbulent diffusion by summarizing the ideas formulated by [Taylor \(1922\)](#).

¹The year 1905 was Einstein's *Annus mirabilis*. During that year, he published his Brownian motion paper ([Einstein, 1905a](#)), which provided direct evidence for the atomic nature of matter; his special relativity paper ([Einstein, 1905c](#)), which modified how we think about space and time; and his photoelectric effect paper ([Einstein, 1905b](#)), which provided evidence for the quantum nature of light.

CHAPTER GUIDE

This concepts detailed in this chapter are basic to how we consider diffusion at a fundamental as well as phenomenological level. Chapter 5 is a direct descendant of the current chapter, where we study the combined effects of advection plus diffusion. Exposure to basic properties of **parabolic partial differential equations** from VOLUME 1 can be useful for a grounding in the mathematics of diffusion.

4.1	Molecular diffusion	111
4.1.1	Kinetic theory and phenomenological laws	111
4.1.2	Comments and further study	111
4.2	Brownian motion	112
4.2.1	Einstein's formulation as a Markov process	112
4.2.2	The Chapman-Kolmogorov equation	113
4.2.3	Diffusion in the continuum limit	113
4.2.4	Moments of the particle density	114
4.2.5	Langevin equation	116
4.2.6	Dissipation time scale	117
4.2.7	Ensemble statistics from the Langevin equation	117
4.2.8	Further study	119
4.3	Turbulent diffusion	119
4.3.1	Introducing Taylor's Lagrangian description	119
4.3.2	Comments and further study	121
4.4	Phenomenological diffusion laws	121
4.4.1	Fick's law for matter diffusion	121
4.4.2	Fourier's law of conduction	123
4.4.3	Newtonian frictional stress and momentum diffusion	124
4.4.4	Comments	124
4.5	The scale selectivity of Laplacian diffusion	125
4.6	Gaussian concentration generated by a Dirac source	126
4.7	Mathematical interlude: tensor analysis tools	127
4.7.1	Concerning the upright versus slanted notation	127
4.7.2	Metric tensor allows us to measure distance	128
4.7.3	Raising and lowering tensor indices via the metric tensor	128
4.7.4	Divergence of a vector and the divergence theorem	129
4.7.5	Example tracer fluxes	130
4.7.6	Comments about the tensor tools	131
4.8	Further properties of tracer diffusion	131
4.8.1	Sample diffusion tensors	132
4.8.2	Diffusion of tracer concentration powers	132
4.8.3	Moments of tracer concentration	133
4.9	Connecting tracer dissipation to the diffusion operator	135
4.9.1	Fréchet derivative of the diffusion dissipation functional	135
4.9.2	Connection to the diffusion operator	137
4.9.3	Why we need to assume K^{mn} is independent of C	137
4.9.4	Relation to Hamilton's principle	137
4.10	Exercises	137

4.1 Molecular diffusion

Consider a fluid comprised of a single matter constituent, such as a lake of pure H_2O . As discussed in the kinematics of VOLUME 1, for a macroscopic description of this single-component fluid, a constant mass fluid element is identical to a constant mass material fluid parcel. Hence, there is no mixing of matter since there is just a single matter component. Now place a **passive tracer** (e.g., a dye tracer) into a corner of the lake so that the lake is comprised of two material components (H_2O and dye). Even in the absence of ambient macroscopic fluid motion, the random motion of water and dye molecules produces an exchange of matter constituents between fluid elements. Consequently, the dye spreads outward from its initial position; i.e., it diffuses into the surrounding water.

4.1.1 Kinetic theory and phenomenological laws

We introduced the notion of matter exchange between fluid elements when discussing the kinematics of tracers in VOLUME 1. In the present context, matter exchange occurs through the random motion of molecules acting in the presence of a matter concentration gradient. Even though the continuum approximation has removed all explicit concern for details of molecular motion, we confront the underlying molecular nature of matter since molecular motions have a measurable impact on macroscopic fluid properties. The transport of matter, heat, and momentum by random molecular motions is known as **molecular diffusion**. A statistical description of molecular diffusion is available for certain ideal-like gases using methods from kinetic theory largely developed in the 19th century. In that theory we are concerned with statistically describing the scattering of molecules off one another, and quantifying how such scattering affects a transport of matter, momentum, and heat.

A kinetic theory description of diffusive transport mathematically supports the phenomenological downgradient diffusive laws examined in Section 4.4, such as those for heat (Fourier's law of conduction), for matter (Fick's law of diffusion), and momentum (Newton's law of viscous friction), with these laws developed prior to kinetic theory. We extend the phenomenological laws to diffusion in liquids, though note that the associated kinetic theory is far less developed than for gases. We also note that for stratified fluids with multiple constituents, one encounters matter diffusion in the presence of a temperature gradient (Soret effect), and temperature diffusion in the presence of gradients of pressure and/or matter (Dufour effect).² However, geophysical fluids are nearly always dominated by turbulence, which renders a turbulent diffusion that swamps the effects from cross-diffusion. We thus ignore cross-diffusion in this chapter.

4.1.2 Comments and further study

Molecular diffusion as formulated by kinetic theory for ideal gases is examined in [Reif \(1965\)](#) and [Huang \(1987\)](#), as well as other statistical physics books. Molecular diffusion sets the ultimate dissipation scale and irreversibility of scalar variance. It is crucial microscopically as well as in boundary layers. Even so, it is too weak to explain large-scale mixing in the ocean and atmosphere without the aid of turbulent stirring to affect a downscale cascade of variance to the microscale.

²We study cross-diffusion in VOLUME 2 when examining energy and entropy flows in fluids.

4.2 Brownian motion

Brownian motion consists of the random walk motion of a macroscopically small but microscopically large particle (e.g., a pollen or dust particle) in a liquid. The motion of the Brownian particle arises from the incessant and random impacts on the particle by molecules from the surrounding liquid. A typical Brownian particle has size on the order of nanometers (10^{-9} m) to a few microns (10^{-6} m), which compares to the roughly 10^{-10} m for the mean free path of molecular motion. Smaller particles exhibit more vigorous motion, whereas larger particles have less motion due to their increased inertia. Evidently, size, and corresponding mass, is key since particles must be microscopically huge, so to experience significant molecular impulses, yet macroscopically tiny, so to exhibit motion from the molecular impulses.

4.2.1 Einstein's formulation as a Markov process

Einstein (1905a) advanced a theory of Brownian motion, making a key assumption that the motion arises from a series of discrete time random impulses. He assumed that the impulses are separated by a time increment, τ , that is tiny from the perspective of a macroscopic (human) observer but huge relative to the time scale of molecular motion. We return in Section 4.2.7 to provide an estimate for τ , with those results supporting the assumption that it is tiny macroscopically.

In this formulation, Einstein further assumed the impulses on the Brownian particle at times $\tau, 2\tau, 3\tau \dots$ are statistically uncorrelated. In today's language, we say that the impulses provide a white noise forcing, and that the resulting position of the particle manifests a **Markov processes**. A Markov process has a future depending on the present but independent of the past. In space, Brownian motion is generally two dimensional, as per the motion of a neutrally buoyant dust particle in a petri dish, or three-dimensional, as per a smoke/dust particle floating in a quiet room. For simplicity, and following Einstein, we here consider only a single space dimension. We can interpret the one-dimensional position as the projection of a two or three dimensional motion along the real line.

Consider N identical Brownian particles that do not interact with one another. During a time interval, τ , a particle moves a distance, ℓ , which is continuous (i.e., ℓ is not discretized). Let $p(\ell|\tau) \delta\ell$ be the probability that a particle moves a distance between ℓ and $\ell + \delta\ell$ during one of the τ intervals, thus measuring the probability of the particle transitioning to a new position. We write this transition probability density function as $p(\ell|\tau)$, with τ a parameter that reminds us of the discrete time interval between the impulsive movements of the Brownian particle. The transition probability density is normalized over the spatial range of the motion,

$$\int_{-\infty}^{\infty} p(\ell|\tau) d\ell = 1, \quad (4.1)$$

and the random walk displacements are assumed to be unbiased, in which case the probability density is symmetric

$$p(\ell|\tau) = p(-\ell|\tau). \quad (4.2)$$

In a liquid with N Brownian particles, and ignoring any interactions between the particles, the number of particles that moves a distance within the range $[\ell, \ell + \delta\ell]$ is written

$$\delta N = N p(\ell|\tau) \delta\ell. \quad (4.3)$$

We are interested in the case of many (effectively a continuum) of non-interacting Brownian particles that move through the fluid via the effects from molecular impulses. To connect to the notion of a tracer concentration, C (mass of tracer per mass of fluid element), we introduce the mass density, φ , of Brownian particles,

$$\varphi(x, t) = \rho(x, t) C(x, t), \quad (4.4)$$

with ρ the mass density of the fluid. Evidently, C is the mass concentration of Brownian particles, whereas φ is the mass density of Brownian particles. It follows that the total mass of Brownian particles is

$$M = \int_{-\infty}^{\infty} \rho C \, dx = \int_{-\infty}^{\infty} \varphi \, dx, \quad (4.5)$$

which we assume to be constant so that

$$\frac{dM}{dt} = \frac{d}{dt} \int_{-\infty}^{\infty} \varphi \, dx = \int_{-\infty}^{\infty} \frac{\partial \varphi}{\partial t} \, dx = 0. \quad (4.6)$$

4.2.2 The Chapman-Kolmogorov equation

Einstein introduced the following equation, now referred to as the one-step Chapman-Kolmogorov equation (also the discrete-time master equation), that determines the value of φ after a discrete time step

$$\varphi(x, t + \tau) = \int_{-\infty}^{\infty} p(\ell|\tau) \varphi(x - \ell, t) \, d\ell. \quad (4.7)$$

Reading this equation from right to left, we start with the particle density, $\varphi(x - \ell, t)$, at point $x - \ell$ and time t . Convoluting this density with the probability, $p(\ell|\tau) \, d\ell$, to transition a distance ℓ over a single time step, τ , we arrive at the density, $\varphi(x, t + \tau)$.

We can verify that the Chapman-Kolmogorov equation (4.7) is consistent with mass conservation by integrating over the full domain

$$\int_{-\infty}^{\infty} \varphi(x, t + \tau) \, dx = \int_{-\infty}^{\infty} \left[\int_{-\infty}^{\infty} p(\ell|\tau) \varphi(x - \ell, t) \, d\ell \right] \, dx. \quad (4.8)$$

The left hand side equals to the total mass, M , since the total mass remains constant in time as per equation (4.6). For the right hand side we swap the x and ℓ integrals to find³

$$\int_{-\infty}^{\infty} \left[\int_{-\infty}^{\infty} p(\ell|\tau) \varphi(x - \ell, t) \, d\ell \right] \, dx = \int_{-\infty}^{\infty} p(\ell|\tau) \left[\int_{-\infty}^{\infty} \varphi(x - \ell, t) \, dx \right] \, d\ell. \quad (4.9)$$

The x integral yields M , which then leaves the ℓ integral, which equals to unity due to the normalization condition (4.1).

4.2.3 Diffusion in the continuum limit

The Chapman-Kolmogorov equation (4.7) is an exact expression for the particle density at a new time step, $t + \tau$, given the density at time t and the probability for a displacement. For macroscopic purposes, we are most interested in the limit where the time step, τ , between impulses is small macroscopically, in which case we take a Taylor series on the left hand side of

³We assume $p(\ell|\tau)$ has a finite second moment and the particle density, $\varphi(x, t)$, decays fast enough at $x = \pm\infty$ that allows us to perform a Taylor expansion, swap integrals, and drop boundary terms.

the Chapman-Kolmogorov equation (4.7) to find

$$\varphi(x, t + \tau) \approx \varphi(x, t) + \tau \partial_t \varphi(x, t). \quad (4.10)$$

Likewise, if the probability for a displacement is assumed to be concentrated around zero, meaning that the individual displacements, ℓ , are macroscopically small, then we can expand the concentration inside the integral on the right hand side of the Chapman-Kolmogorov equation (4.7) to find

$$\int_{-\infty}^{\infty} p(\ell|\tau) \varphi(x - \ell, t) d\ell \approx \int_{-\infty}^{\infty} p(\ell|\tau) [\varphi(x, t) - \ell \partial_x \varphi(x, t) + \frac{1}{2} \ell^2 \partial_{xx} \varphi(x, t)] d\ell. \quad (4.11)$$

The integral is over the displacement, ℓ , so that the density, $\varphi(x, t)$ and its derivatives can be pulled outside of the integral. Making use of the normalization condition (4.1) and symmetry condition (4.2) leads to

$$\int_{-\infty}^{\infty} p(\ell|\tau) [\varphi(x, t) - \ell \partial_x \varphi(x, t) + \frac{1}{2} \ell^2 \partial_{xx} \varphi(x, t)] d\ell = \varphi(x, t) + \frac{1}{2} \partial_{xx} \varphi(x, t) \int_{-\infty}^{\infty} \ell^2 p(\ell) d\ell. \quad (4.12)$$

Bringing both sides together leads us to conclude that, in the macroscopic limit the particle density satisfies the diffusion equation

$$\partial_t \varphi = \kappa \partial_{xx} \varphi, \quad (4.13)$$

where we introduced the kinematic diffusivity

$$\kappa = \langle \ell^2 \rangle / (2 \tau) \quad \text{with} \quad \langle \ell^2 \rangle = \int_{-\infty}^{\infty} \ell^2 p(\ell|\tau) d\ell. \quad (4.14)$$

The diffusivity is seen to be directly proportional to the mean-square particle displacement, $\langle \ell^2 \rangle$, and inversely proportional to the time between impulses, τ .

4.2.4 Moments of the particle density

Introduce the Brownian particle density, φ , and define position moments with respect to the particle density

$$\bar{x^n} = M^{-1} \int_{-\infty}^{\infty} x^n \varphi(x, t) dx. \quad (4.15)$$

Moments based on the Brownian particle density are equivalent to moments computed from an ensemble of Brownian particles as considered in Section 4.2.5 as part of Langevin's formulation of Brownian motion. However, the Brownian moments (4.15) are distinct from moments defined with respect to the probability density, $p(\ell)$. So although the zeroth moment of both $p(\ell)$ and $\varphi(x, t)$ are unity

$$1 = \bar{x^0} = M^{-1} \int_{-\infty}^{\infty} \varphi(x, t) dx \quad \text{and} \quad 1 = \int_{-\infty}^{\infty} p(\ell|\tau) d\ell, \quad (4.16)$$

their higher moments are distinct, as seen in the following.

First moment of the particle density is static

The first moment of the transition probability vanishes since $p(\ell) = p(-\ell)$

$$\langle \ell \rangle = \int_{-\infty}^{\infty} \ell p(\ell|\tau) d\ell = 0. \quad (4.17)$$

In contrast, the first moment of the particle density, which we refer to as the particle center of mass, is generally nonzero,

$$\bar{x} = M^{-1} \int_{-\infty}^{\infty} x \varphi(x, t) dx. \quad (4.18)$$

However, we can show that this position is static for Brownian motion by multiplying the Chapman-Kolmogorov equation (4.7) by x and then integrating

$$\int_{-\infty}^{\infty} x \varphi(x, t + \tau) dx = \int_{-\infty}^{\infty} x \left[\int_{-\infty}^{\infty} p(\ell|\tau) \varphi(x - \ell, t) d\ell \right] dx. \quad (4.19)$$

For the right hand side we change variables to $y = x - \ell$ to find

$$\int_{-\infty}^{\infty} \left[\int_{-\infty}^{\infty} p(\ell|\tau) (y + \ell) \varphi(y, t) d\ell \right] dy = \int_{-\infty}^{\infty} \left[\int_{-\infty}^{\infty} p(\ell|\tau) y \varphi(y, t) d\ell \right] dy, \quad (4.20)$$

where we made use $\langle \ell \rangle = 0$. Making use of the normalization of $p(\ell)$ (so that $\langle \ell^0 \rangle = 1$), and then renaming y to x leads to

$$\int_{-\infty}^{\infty} x \varphi(x, t + \tau) dx = \int_{-\infty}^{\infty} x \varphi(x, t) dx, \quad (4.21)$$

which means that \bar{x} is independent of time

$$\frac{d\bar{x}}{dt} = 0. \quad (4.22)$$

We thus find that the Brownian process leaves the center of mass of the particle distribution unchanged. This result follows since there is an equal probability for a Brownian particle to be displaced in either direction, since $p(\ell|\tau) = p(-\ell|\tau)$. We can readily verify that for the diffusion equation description, we also find \bar{x} is static. To do so, multiply the diffusion equation (4.13) by x and integrate over the real line. Integration by parts, and assuming the particle density falls off sufficiently fast at $\pm\infty$, then leads to a time independent \bar{x} .

Second moment of the particle density evolves with unit power of time

Next consider the mean squared spread of the particle density

$$\bar{x^2} = M^{-1} \int_{-\infty}^{\infty} x^2 \varphi(x, t) dx. \quad (4.23)$$

We can determine its time evolution by multiplying the Chapman-Kolmogorov equation (4.7) by x^2 and integrating over space

$$\int_{-\infty}^{\infty} x^2 \varphi(x, t + \tau) dx = \int_{-\infty}^{\infty} x^2 \left[\int_{-\infty}^{\infty} p(\ell|\tau) \varphi(x - \ell, t) d\ell \right] dx. \quad (4.24)$$

Changing variables to $y = x - \ell$ and making use of normalization and symmetry of $p(\ell)$ leads to

$$\int_{-\infty}^{\infty} x^2 \varphi(x, t + \tau) dx = M \langle \ell^2 \rangle + \int_{-\infty}^{\infty} y^2 \varphi(y, t) dy, \quad (4.25)$$

which then renders

$$\int_{-\infty}^{\infty} x^2 [\varphi(x, t + \tau) - \varphi(x, t)] dx = M \langle \ell^2 \rangle = 2 \tau \kappa M, \quad (4.26)$$

where the final equality introduced the Brownian diffusivity (4.14). Taking the continuous time limit with small τ leads to

$$\frac{d\bar{x}^2}{dt} = 2 \kappa = \langle \ell^2 \rangle / \tau. \quad (4.27)$$

Evidently, the mean-squared spread of a cloud of Brownian particles grows as the first power of time. It is notable that there are processes that display fractional time dependencies, with such processes referred to as **anomalous diffusion**.

4.2.5 Langevin equation

[Langevin \(1908\)](#)⁴ provided an alternative formulation of Brownian motion, with his approach initiating the study of stochastic differential equations. In his formulation, Langevin assumed the Brownian particle experiences two forces. The first force arises from the Stokes' drag acting on a spherical body moving through a viscous fluid and with velocity, V

$$F_{\text{drag}} = -\alpha V \quad \text{with} \quad \alpha = 6 \pi \mu R. \quad (4.28)$$

In this equation, R is the radius of the Brownian particle, and μ is the molecular dynamic viscosity of the liquid (dimensions of $M L^{-1} T$). The drag parameter, α , has dimensions of $M T^{-1}$. The second force, \mathcal{N} , is a white noise force that arises from the random and uncorrelated impulses imparted by the liquid molecules. The resulting **Langevin equation** for the position of the Brownian particle is given by

$$m \ddot{X} = -\alpha \dot{X} + \mathcal{N}. \quad (4.29)$$

Note that since we are here focused on particle trajectories, we use the capital, X , to denote the position in space of a Brownian particle, and write

$$V = \dot{X} \quad (4.30)$$

for its velocity. It is notable that Langevin's equation is identical to the response function equation studied in VOLUME 1, only here we have introduced a random forcing via the noise term, \mathcal{N} .

⁴For an English translation, see [Lemons and Gythiel \(1997\)](#).

4.2.6 Dissipation time scale

We derive the evolution equation for kinetic energy of the Brownian particle by multiplying the Langevin equation (4.29) by $V = \dot{X}$

$$m \frac{dV^2}{dt} = -\alpha V^2 + V \mathcal{N}. \quad (4.31)$$

As expected, the viscous term acts to dissipate the ensemble averaged kinetic energy, whereas the noise acts to increase or decrease the kinetic energy. We now estimate the dissipation time scale,

$$\tau_d = m/\alpha, \quad (4.32)$$

which we assume corresponds to the time interval, τ , between the discrete impulses assumed by Einstein in Section 4.2.1. To do so requires details of the Brownian particle, which we assume to be spherical and with density, ρ_p , so that

$$\tau_d = \frac{\frac{4}{3} \pi R^3 \rho_p}{6 \pi \mu R} = \frac{2 \rho_p R^2}{9 \mu} = \frac{2 \rho_p R^2}{9 \rho \nu}, \quad (4.33)$$

where the final equality introduced the kinematic viscosity, ν , through

$$\mu = \rho \nu. \quad (4.34)$$

For the Brownian particle density and size, assume a pollen particle and make use of its hydrated density (i.e., density of a saturated particle)

$$\rho_p = 1.1 \rho_{\text{water}} \quad \text{and} \quad L_{\text{brownian}} = 10^{-5} \text{ m}. \quad (4.35)$$

Note that the approximate size of a water molecule is

$$L_{\text{water}} = 10^{-10} \text{ m}, \quad (4.36)$$

so that the pollen particle is indeed far larger than water molecules, even though it is tiny macroscopically. The kinematic molecular viscosity of water at room temperature is around $10^{-6} \text{ m}^2 \text{ s}^{-1}$, and its density is $\rho = 10^3 \text{ kg m}^{-3}$. Taking the radius of the pollen equal to L_{brownian} , we have

$$\tau_d = \frac{2 \rho_p L_{\text{brownian}}^2}{9 \rho_{\text{water}} \nu} \approx 2.4 \times 10^{-5} \text{ s}. \quad (4.37)$$

This is a tiny time interval from a macroscopic perspective, which supports the use of Einstein's continuum limit of the Chapman-Kolmogorov equation in Section 4.2.3.

4.2.7 Ensemble statistics from the Langevin equation

The trajectory, $X(t)$, for a single Brownian particle is stochastic (i.e., random), with such randomness induced by the white noise forcing, \mathcal{N} , appearing in the Langevin equation (4.29). We are thus interested in developing the statistics arising from an ensemble of many Brownian particles. As noted in Section 4.2.4, statistics based on an ensemble of Brownian particles is the same, in the continuum limit, as when examining statistics based on the particle density function, $\varphi(x, t)$. Hence, we use the overline here for the ensemble statistics developed from the Langevin equation.

Evolution of the ensemble mean kinetic energy

The evolution equation for the ensemble mean kinetic energy of the Brownian particle is found by taking the ensemble average of the kinetic energy equation (4.31)

$$m \frac{d\overline{V^2}}{dt} = -\alpha \overline{V^2} + \overline{V \mathcal{N}}. \quad (4.38)$$

Note that we assumed the ensemble average commutes with the time derivative. As expected, the viscous term acts to dissipate the ensemble averaged kinetic energy, whereas correlations between the velocity and the noise acts to increase or decrease the kinetic energy.

Evolution of ensemble mean squared spread

Rather than kinetic energy, consider now an expression for the ensemble mean squared spread, $\overline{X^2}$, whose evolution equation is derived by multiplying the Langevin equation (4.29) by X and rearranging

$$m \frac{d}{dt} \left[\frac{dX^2}{dt} + \alpha X^2 \right] = 2m \dot{X}^2 + 2X \mathcal{N}. \quad (4.39)$$

We now take an ensemble average and make two key assumptions. First, assume that the Brownian particle is in thermal equilibrium with the surrounding liquid. This assumption allows us to use the equipartition theorem from classical statistical mechanics to equate the ensemble average kinetic energy to the thermal energy⁵

$$\frac{1}{2} \overline{m \dot{X}^2} = \frac{1}{2} k_B T, \quad (4.40)$$

where T is the absolute temperature (in Kelvin) of the liquid, and k_B is Boltzmann's constant. The second assumption sets to zero the correlation between the particle position and the noise forcing

$$\overline{X \mathcal{N}} = 0. \quad (4.41)$$

This assumption means that the noise and Brownian particle positions are statistically independent and so do not somehow conspire to produce a nonzero correlation.

The above two assumptions in equation (4.39) yield the evolution equation for the ensemble mean squared distance

$$m \frac{d}{dt} \left[\frac{d\overline{X^2}}{dt} + \alpha \overline{X^2} \right] = 2k_B T. \quad (4.42)$$

We solve this differential equation by first deriving the homogeneous solution (with zero on the right hand side), which is given by

$$e^{-t/\tau_d} \overline{X^2(0)}, \quad (4.43)$$

where $\overline{X^2(0)}$ is the mean squared spread at the initial time. Adding in the particular solution leads to

$$\overline{X^2}(t) = e^{-\alpha t/\tau_d} \overline{X^2(0)} + (2k_B T/\alpha) t. \quad (4.44)$$

Since τ_d is quite tiny macroscopically, we can ignore the decaying exponential term in

⁵The equipartition theorem (4.40) was also made by [Einstein \(1905a\)](#) in his formulation, which connects the diffusivity of the Brownian particle motion, κ , to the fluid viscosity. We see this connection in the following approach as well.

equation (4.44), so that the mean squared spread evolves approximately as

$$\overline{X^2} \approx (2 k_B T / \alpha) t \implies \frac{d\overline{X^2}}{dt} \approx 2 k_B T / \alpha. \quad (4.45)$$

Recalling our approach following Einstein earlier in this section, in particular equation (4.27), we identify the diffusivity acting to spread the Brownian particle distribution

$$\kappa = \frac{2 k_B T}{\alpha} = \frac{k_B T}{3\pi\rho\nu R} = \frac{R^g T}{3\pi\rho\nu R A^v}, \quad (4.46)$$

where the final equality introduced the universal gas constant, R^g , and Avogadro's number, A^v ,

$$R^g = 8.314 \text{ kg m}^2 \text{ s}^{-2} \text{ mole}^{-1} \text{ K}^{-1} \quad \text{and} \quad A^v = 6.0222 \times 10^{23} \text{ mole}^{-1}. \quad (4.47)$$

This same result was also derived by [Einstein \(1905a\)](#), and it was used by [Perrin \(1909\)](#) to estimate Avogadro's number using macroscopically measurable properties.

4.2.8 Further study

A summary of Brownian motion as formulated by [Einstein \(1905a\)](#) and [Langevin \(1908\)](#) can be found in Section 1.2 of [Gardiner \(1985\)](#). Section 3 of [Young \(1999\)](#) also discusses Einstein's approach, and then introduces anomalous diffusion, such as occurs with interrupted random walk processes. The concepts and methods promoted by [Einstein \(1905a\)](#) and [Langevin \(1908\)](#) formed the seeds for the study of stochastic processes during the 20th century, with [Gardiner \(1985\)](#) providing a lucid presentation. We return to the evolution of the tracer moments in Exercise 5.3 as part of our study of the advection-diffusion equation.

4.3 Turbulent diffusion

Turbulent flow is the norm for geophysical fluids, with turbulence greatly enhancing the efficiency of property mixing relative to the case without flow.⁶ Namely, the stirring of fluid properties by turbulent flows acts to stretch and fold contours/surfaces of constant properties, thus increasing property gradients and so increasing the action of molecular diffusion. We refer to this turbulent enhanced mixing as [turbulent diffusion](#).

Turbulent diffusion is not concerned with molecular properties of the fluid. Rather, the properties of turbulent diffusion (e.g., its efficiency) depend on the nature of the turbulent motion of fluid elements. Hence, each type of turbulent motion gives rise to a distinct form of turbulent diffusion. For example, turbulent diffusion associated with a turbulent field of breaking internal gravity waves is distinct from turbulent diffusion from geostrophic eddies. In this way, turbulent diffusion sits within the realm of continuum mechanics, whereas molecular diffusion is a subject for kinetic theory. Furthermore, turbulent diffusion concerns fluid motions that are continuous in time, which contrasts to the discrete time impulses assumed by Einstein in his formulation of Brownian motion in Section 4.2.

4.3.1 Introducing Taylor's Lagrangian description

[Taylor \(1922\)](#) described the statistical properties of turbulent flows by focusing on an ensemble

⁶Turbulent flow is characterized by a quasi-random fluid motion that acts to transport fluid elements and their properties.

of fluid particles and thus deriving statistics for the ensemble. The mathematical apparatus is very similar to that encountered in the trajectory analysis of Brownian particles in Section 4.2, with the analogy allowing us to infer that turbulent transport has a diffusive quality at its core. Indeed, the many stochastic theories of turbulent diffusion make use of the Langevin equation originally formulated for Brownian motion.⁷

Following our study of fluid kinematics in VOLUME 1, recall that the Cartesian position and velocity of a typical fluid particle is written

$$\frac{d\mathbf{X}(t)}{dt} = \mathbf{V}(t) \implies \mathbf{X}(t) = \mathbf{X}(t_0) + \int_{t_0}^t \mathbf{V}(t') dt', \quad (4.48)$$

where t_0 is some arbitrary initial time. Now take the ensemble mean and, just as for the Brownian motion analysis, assume the time derivative commutes with the ensemble mean to yield

$$\overline{\mathbf{X}(t)} = \overline{\mathbf{X}(0)} + \int_{t_0}^t \overline{\mathbf{V}(t')} dt'. \quad (4.49)$$

Assuming the velocity field has stationary and unbiased statistics, and there is no drift velocity, then we are led to conclude that the ensemble mean position remains unchanged from its initial position

$$\overline{\mathbf{X}(t)} = \overline{\mathbf{X}(0)}. \quad (4.50)$$

For simplicity, and without loss of generality, we set

$$\overline{\mathbf{X}(0)} = 0. \quad (4.51)$$

Now multiply the trajectory equation (4.48) by $\mathbf{X}(t)$ to render an equation for the evolution of the squared position

$$\frac{d\mathbf{X}(t)^2}{dt} = \mathbf{V}(t) \cdot \mathbf{X}(t) = \mathbf{V}(t) \cdot \int_{t_0}^t \mathbf{V}(t') dt' = \int_{t_0}^t \mathbf{V}(t) \cdot \mathbf{V}(t') dt', \quad (4.52)$$

where the second equality follows from the trajectory equation (4.48). Taking the ensemble mean yields

$$\frac{1}{2} \frac{d\overline{\mathbf{X}(t)^2}}{dt} = \int_{t_0}^t \overline{\mathbf{V}(t) \cdot \mathbf{V}(t')} dt' \equiv \int_{t_0}^t C(t, t') dt', \quad (4.53)$$

where we introduced the correlation function between the velocity of fluid particles⁸

$$C(t, t') = \overline{\mathbf{V}(t) \cdot \mathbf{V}(t')}. \quad (4.54)$$

Equation (4.53) describes the ensemble mean dispersion of a fluid particle trajectories relative to a center of mass position which, as noted above, we assume to vanish, $\overline{\mathbf{X}(0)} = 0$. More specifically, it says that the time derivative of the ensemble mean of the squared fluid particle trajectory equals to the time integral of the time correlation between the fluid particle's velocity.

Assuming the correlation (4.54) is localized in time, so that it has a finite limit as $t \rightarrow \infty$,

⁷See [McComb \(1990\)](#) for an in-depth study of stochastic theories of turbulence.

⁸The correlation, $C(t, t')$, in equation (4.54) is a one-point correlation, since it is computed between the velocity of a single fluid particle and so it is computed at a single point in space. Multiple point correlations are also of interest in fluid turbulence theories, with Section 13.3 of [Vallis \(2017\)](#) providing an introduction to two-point or two-particle correlations.

yields

$$\frac{d\overline{\mathbf{X}(t)^2}}{dt} = 2 \int_{t_0}^{\infty} C(t, t') dt' \equiv 2 D, \quad (4.55)$$

where we introduced the Lagrangian diffusivity,

$$D \equiv \int_{t_0}^{\infty} C(t, t') dt'. \quad (4.56)$$

We thus find that the mean-squared spread of the ensemble trajectories grows as

$$\overline{\mathbf{X}(t)^2} = 2 D t, \quad (4.57)$$

which is identical to the diffusive behavior of a Brownian particle found in Section 4.2. It is this connection that prompts us to conclude that the spread of fluid particle trajectories by turbulent flows is directly akin to a Brownian/diffusive process.

4.3.2 Comments and further study

The conceptual and technical advances from [Taylor \(1922\)](#) remain part of the null hypothesis for how turbulent flow affects mixing in geophysical fluids. However, there is a nontrivial level of work required to make use of these insights for practical parameterizations, with that work remaining at the forefront of research in ocean and atmospheric physics. We do not pursue this analysis in this book, deferring to the various chapters in [McComb \(1990\)](#) and [Vallis \(2017\)](#) (for example) for in-depth analyses of turbulent diffusion. Even so, we do pursue a phenomenological perspective on parameterized turbulent mixing in the remainder of this chapter as well as in Chapter 7.

An introduction to turbulent diffusion can be found in [Young \(1999\)](#). More detailed treatments are given in [Csanady \(1973\)](#), who focuses on turbulent diffusion in the environment (e.g., for the study of pollution dispersal), and in Chapter 13 of [Vallis \(2017\)](#), who focuses on geophysical flows. Further elements can be found in Section 1.5 of [Kundu et al. \(2016\)](#).

4.4 Phenomenological diffusion laws

In this section we summarize a suite of phenomenological laws that result in a diffusion equation. These laws were formulated prior to the ideas from kinetic theory, Brownian motion, and turbulent diffusion. They remain a very useful null hypothesis for turbulent diffusive transport in geophysical fluids, with the diffusivities set according to their turbulent eddy values rather than molecular values.

4.4.1 Fick's law for matter diffusion

Consider a fluid with a non-uniform tracer concentration such as that drawn for a one-dimensional case in Figure 4.1. Random motion, due either to molecular motion or turbulent fluctuations, transfers tracer across an arbitrary point, line, or plane. Random motion preferentially moves tracer from regions of high concentration to regions of low concentration, thus smoothing gradients.

To a good approximation, the mass flux (mass per time per cross-sectional area) of a material tracer is linearly proportional to the concentration gradient, and thus can be written

in the form

$$\mathbf{J} = -\kappa_c \rho \nabla C. \quad (4.58)$$

In this equation, we introduced the positive proportionality factor, $\kappa_c > 0$, known as the kinematic diffusivity, whereas the product $\kappa_c \rho$ is known as the dynamic diffusivity:

$$\kappa_c \quad \text{kinematic diffusivity with SI units } \text{m s}^{-2} \quad (4.59)$$

$$\rho \kappa_c \quad \text{dynamic diffusivity with SI units } \text{kg m}^{-2} \text{ s}^{-2}. \quad (4.60)$$

The kinematic diffusivity has dimensions of squared length per time and it sets the efficiency of diffusion when acting within a fluid with a tracer gradients. The diffusive flux (4.58) is known as [Fick's law of diffusion](#), and it is commonly used in geophysical fluid mechanics to represent the mixing of matter through diffusion. The minus sign in the diffusive flux arises since the flux is directed down the concentration gradient. When considering molecular diffusion, we distinguish diffusivities according to their respective tracers since they generally differ. In contrast, turbulent diffusivities are commonly assumed to be independent of tracer since they are determined by the flow, in which case we write the generic, κ .

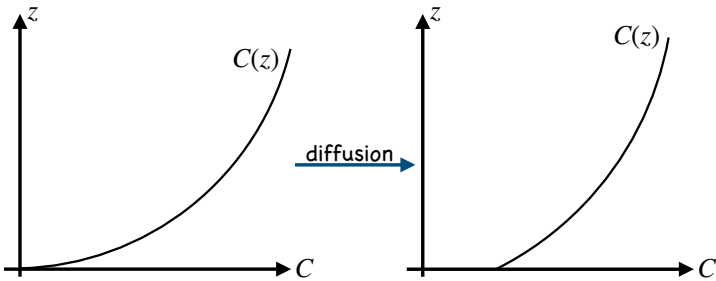


FIGURE 4.1: A graph illustrating a material tracer concentration, C as a function of the space coordinate z , with the left panel showing the concentration at an earlier time than the right panel. Across any arbitrary point, matter is transported through random motions, with this transport generally reducing the magnitude of the concentration gradient. This reduction of concentration gradient is a direct result of the downgradient (i.e., down the concentration gradient) orientation of the diffusive transport. For example, where the concentration is relatively high, random motion mixes this high concentration with adjacent lower concentration, thus acting to lower the concentration in the originally high concentration region and raise the concentration in the originally low concentration region. In this particular example, $\partial C / \partial z > 0$, so that random fluid motions (either molecular or turbulent) lead to a diffusive flux directed in the $-\hat{z}$ direction; i.e., downward. This downward flux brings high concentration fluid into the lower regions and low concentration fluid into higher regions. The concentration is vertically uniform if allowed to equilibrate under the action of diffusion.

The kinematic diffusivity has physical dimensions equal to the product of a length and a speed. For molecular diffusion, the kinematic diffusivity is proportional to the mean free path, L_{mfp} and the root-mean-square molecular speed, v_{rms} , both of which are described in the chapter in [VOLUME 1](#) describing kinetic theory and the continuum approximation. Both L_{mfp} and v_{rms} are functions of the molecules comprising the matter. For air, the mean free path is roughly 2×10^{-7} m and the root-mean-square speed is 500 m s⁻¹, so that $L_{\text{mfp}} v_{\text{rms}} \approx 10^{-4}$ m² s⁻¹. The precise value for the molecular diffusivity depends on the molecular properties of the matter diffusing through the fluid; e.g., molecular size and speed.

For turbulent diffusion, Prandtl suggested that the characteristic length and velocity scales are determined by properties of the turbulent flow, not by the molecular properties of the fluid or the tracer.⁹ The turbulent length scale (also called the [mixing length](#)) is generally much

⁹ [Prandtl \(1925\)](#) is the original paper, with an English translation given by [Prandtl \(1949\)](#) and further historical context given by [Bradshaw \(1974\)](#).

larger than the molecular mean free path, whereas the [turbulent velocity scale](#) is much smaller than molecular speeds. Determination of turbulent length and velocity scales is subject to large uncertainties given the multiple regimes of turbulence exhibited by geophysical flows. As a result, tracer transport by turbulent flows remains an active topic of research.

In regions where the diffusive flux converges, there is a net transport of matter that leads to the reduction of the tracer concentration gradient as determined by the convergence of the diffusive flux

$$\rho \frac{DC}{Dt} = -\nabla \cdot \mathbf{J} = \nabla \cdot (\kappa_c \rho \nabla C). \quad (4.61)$$

That is, the concentration increases in regions where the diffusive flux, \mathbf{J} , converges, and decreases where the flux diverges. Expanding the divergence operator leads to

$$\rho \frac{DC}{Dt} = \nabla(\kappa_c \rho) \cdot \nabla C + \kappa_c \rho \nabla^2 C. \quad (4.62)$$

The first term is nonzero in regions where the [dynamic diffusivity](#), $\kappa_c \rho$, spatially varies. This term vanishes for molecular diffusion, in which case the diffusivity is a spatial constant. However, for turbulent diffusion this term can be quite important given the potential for strong flow dependence to the diffusivity. Indeed, there are cases in which this spatial dependence can enhance tracer gradients, overcoming the effects from the curvature term. We consider an example in [Exercise 4.6](#) known as the [Phillip's layering instability](#).

The second term in the diffusion equation (4.62) is proportional to the Laplacian of the tracer concentration, which provides a measure of the curvature in the tracer field. Hence, this term vanishes when the tracer concentration is a constant or a linear function of space, whereas it is nonzero for tracers having less trivial spatial structure. As discussed in [Section 4.5](#), this term provides a scale selectivity to the diffusion operator, thus resulting in a preferential dampening of small scale features relative to large scale features.

4.4.2 Fourier's law of conduction

In the same way that matter concentration gradients lead to diffusion by random motions, temperature gradients lead to diffusion of heat. The corresponding phenomenological relation is known as [Fourier's law of conduction](#), with the diffusive (or conductive) flux given by

$$\mathbf{J} = -\kappa_T \rho \nabla T, \quad (4.63)$$

where $\kappa_T > 0$ is the kinematic thermal diffusivity. As for the matter diffusivity, the molecular thermal diffusivity can be expressed in terms of fundamental properties of the fluid, and it is different from the diffusivity for matter concentration diffusion. In general, molecular processes diffuse matter concentrations slower than temperature, so that the molecular matter diffusivity is smaller than the molecular thermal diffusivity. The reason for the difference is that the diffusion of material concentration requires the movement of matter (molecules), whereas thermal diffusion occurs through the exchange of thermal energy between molecules, and that exchange does not require the motion of matter. For turbulent transport, however, the turbulent thermal diffusivity is roughly the same as the turbulent matter diffusivity. The reason is that the turbulent diffusion of both matter and heat are mediated by the same turbulent fluctuations of fluid elements.

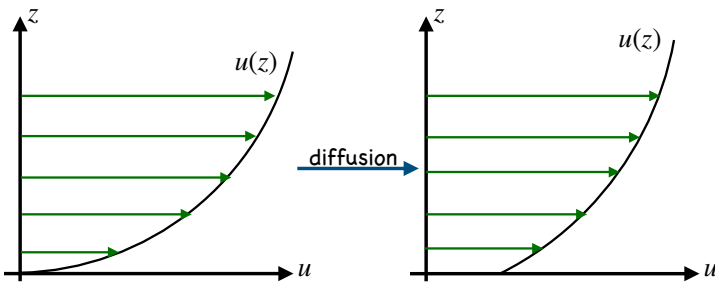


FIGURE 4.2: A graph illustrating the zonal velocity, u , as a function of the space coordinate z , with the left panel showing the velocity at an earlier time than the right panel. Across any arbitrary point, transport of momentum through random motions generally reduces the magnitude of the velocity gradient; i.e., the diffusive transport leads to a viscous stress that acts to reduce the velocity shear.

4.4.3 Newtonian frictional stress and momentum diffusion

In the same way that gradients in matter concentration and temperature lead to diffusion by random molecular and turbulent motions, the momentum of fluid elements is exchanged through diffusion in the presence of viscosity. The corresponding phenomenological relation is known as [Newton's law of viscous friction](#). As momentum is a vector, a general treatment of momentum transport through irreversible viscous processes involves a second order stress tensor and a fourth order viscosity tensor. For the specific case shown in Figure 4.2, with shear (i.e., nonzero velocity gradient) in a single direction, Newtonian frictional stress takes the form

$$\tau = \rho \mu \partial_z u, \quad (4.64)$$

where $\mu > 0$ is the kinematic viscosity. Note the absence of a minus sign, in contrast to diffusive fluxes of scalars. The sign difference arises since it is the divergence of the [stress tensor](#) that leads to contact forces on the fluid, whereas it is the convergence of [diffusive fluxes](#) that leads to diffusion of matter and heat. We consider these general properties of the stress tensor in [VOLUME 2](#).

For geophysical fluid mechanics, we are most generally interested in the molecular viscosity of water and air. Quite generally, the dynamic viscosity of water ($\rho \mu$) is about 10^2 times larger than that for air. But since the density of water is about 10^3 times larger than air, the kinematic viscosity of air is roughly 10 times greater than that of water.

The molecular kinematic viscosity can be expressed in terms of fundamental properties of the fluid, and it is different from the molecular matter diffusivity and molecular thermal diffusivity. For some turbulent processes, the turbulent viscosity, μ , is proportional to the turbulent diffusivity, κ , of scalar fields (e.g., temperature, salinity, humidity). In general, the non-dimensional ratio of the viscosity to the diffusivity is known as the [Prandtl number](#)

$$\text{Pr} = \mu/\kappa. \quad (4.65)$$

Theories for the turbulent Prandtl number are largely empirical, with first principles arguments elusive.

4.4.4 Comments

As noted on page 4 of [Csanady \(1973\)](#), results from both kinetic theory of gases and Brownian motion suggest that the distance over which a typical mixing “event” occurs is small relative to the macroscopic scales of motion of concern for continuum mechanics. Consequently, we

are justified in using the diffusive flux expression (4.58) arising from Fick's law of diffusion as considered in Section 4.4.1.

4.5 The scale selectivity of Laplacian diffusion

Let us focus on the Laplacian term appearing in the tracer equation (4.62) to establish some properties characteristic of Laplacian diffusion. Start by considering a tracer concentration whose spatial structure is given by two Fourier modes,

$$C(\mathbf{x}) = C_{\mathbf{p}} \sin(\mathbf{p} \cdot \mathbf{x}) + C_{\mathbf{q}} \sin(\mathbf{q} \cdot \mathbf{x}), \quad (4.66)$$

where \mathbf{p} and \mathbf{q} are specified wavevectors and $C_{\mathbf{p}}, C_{\mathbf{q}}$ are their corresponding amplitudes. In this case the Laplacian of the tracer is given by

$$\nabla^2 C = -[|\mathbf{p}|^2 C_{\mathbf{p}} \sin(\mathbf{p} \cdot \mathbf{x}) + |\mathbf{q}|^2 C_{\mathbf{q}} \sin(\mathbf{q} \cdot \mathbf{x})]. \quad (4.67)$$

Consequently, the Laplacian diffusion operator acts preferentially on waves of smaller wavelength (and larger wavenumber). For example, assume $|\mathbf{p}| \ll |\mathbf{q}|$, in which case the \mathbf{q} -mode is more rapidly damped towards zero than the \mathbf{p} -mode.¹⁰ For this reason we say that Laplacian diffusion is **scale selective**. Note that zero is the wave averaged concentration for each Fourier mode. We thus see that diffusion acts to dampen each mode towards its average. Scale selectivity results geometrically from a property of the Laplacian operator as a measure of curvature. Tracer features with large curvature have a larger magnitude for their Laplacian, and as such they are damped more rapidly than tracer features with relatively small curvature.

As a second means to understand properties of Laplacian diffusion, consider a Taylor series for the tracer concentration computed relative to an arbitrarily chosen origin,

$$C(\mathbf{x}) = C(0) + x^m \partial_m C|_{\mathbf{x}=0} + (1/2) x^m x^n \partial_n \partial_m C|_{\mathbf{x}=0} + \dots \quad (4.68)$$

Now compute the average of this tracer concentration over a cube centered at the origin with sides L and volume L^3 , and furthermore make use of the identities

$$\int_{-L/2}^{L/2} \int_{-L/2}^{L/2} \int_{-L/2}^{L/2} x^m dx dy dz = 0 \quad \forall m \quad (4.69a)$$

$$\int_{-L/2}^{L/2} \int_{-L/2}^{L/2} \int_{-L/2}^{L/2} x^m x^n dx dy dz = \delta^{mn} (L^5/12). \quad (4.69b)$$

We thus find that the volume averaged tracer concentration, $\langle C \rangle$, deviates from the concentration at the origin by a term proportional to the Laplacian of the concentration evaluated at the origin

$$\langle C \rangle - C(0) = (L^2/24) \nabla^2 C|_{\mathbf{x}=0} \implies \partial_t C|_{\mathbf{x}=0} = -(24 \kappa_c \rho / L^2) [C(0) - \langle C \rangle], \quad (4.70)$$

where we made use of the Laplacian portion of the diffusion equation (4.62) for the second expression. We can perform this calculation for any point taken as the origin. So this result says that Laplacian diffusion generally provides a tendency to damp the tracer concentration at a point towards the average tracer concentration in the region surrounding that point. For

¹⁰In VOLUME 5, we study this process of scale selectivity in the context of Fourier analysis.

example, consider the case where the averaged tracer concentration has no time dependence, as occurs in a region with zero boundary fluxes of tracer. If we are at a point in the region where the concentration is less than the average concentration, $C < \langle C \rangle$, then diffusion provides a positive tendency to increase C towards $\langle C \rangle$, and vice versa if $C > \langle C \rangle$. These results offer another expression of what we found in studying Laplacian diffusion on Fourier modes. In that case, the Laplacian operator, as revealed through equation (4.67), damps each mode towards its average, which is zero.

4.6 Gaussian concentration generated by a Dirac source

Consider a one-dimensional tracer concentration in an unbounded domain whose initial ($t = 0$) value vanishes everywhere except at the origin, where it is given by a **Dirac delta**

$$C(x, t = 0) = Q \delta(x), \quad (4.71)$$

where $\delta(x)$ is the Dirac delta. The Dirac delta has dimensions of inverse length, so that the constant, Q , has dimensions of $[C] L$. Integrating over any region containing the origin reveals that Q is the domain integrated tracer concentration at the initial time,

$$\int_{-\infty}^{\infty} C(x, t = 0) dx = Q. \quad (4.72)$$

We are ensured that this integral holds for all time if the domain has no boundary fluxes of tracer nor any interior tracer sources.

Assume now that the tracer concentration evolves according to the one-dimensional (one space dimension) diffusion equation with a constant diffusivity, $\kappa > 0$, and in a fluid with a constant density. In the absence of spatial boundaries (i.e., diffusion occurs on the real line, \mathbb{R}^1), the concentration is proportional to the causal free space Green's function given by the Gaussian

$$C(x, t) = \frac{Q}{(4 \pi \kappa t)^{1/2}} e^{-x^2/(4 \kappa t)}, \quad (4.73)$$

which indeed satisfies (for any time, t)

$$Q = \int_{-\infty}^{\infty} C(x, t) dx, \quad (4.74)$$

as required by tracer conservation (4.72) for the infinite domain. We illustrate the Gaussian tracer concentration (4.73) in Figure 4.3. The variance of the tracer distribution is given by

$$Q^{-1} \int_{-\infty}^{\infty} C x^2 dx = 2 \kappa t, \quad (4.75)$$

so that the standard deviation grows according to $\sqrt{2 \kappa t}$. As seen in earlier sections, this square root time dependence is characteristic of diffusive processes, which is distinct from the time dependence of ballistic processes, which have a power of t behavior.¹¹

¹¹The simplest ballistic process arises for particles moving with a constant velocity, v , so that the position is $x(t) = v t$.

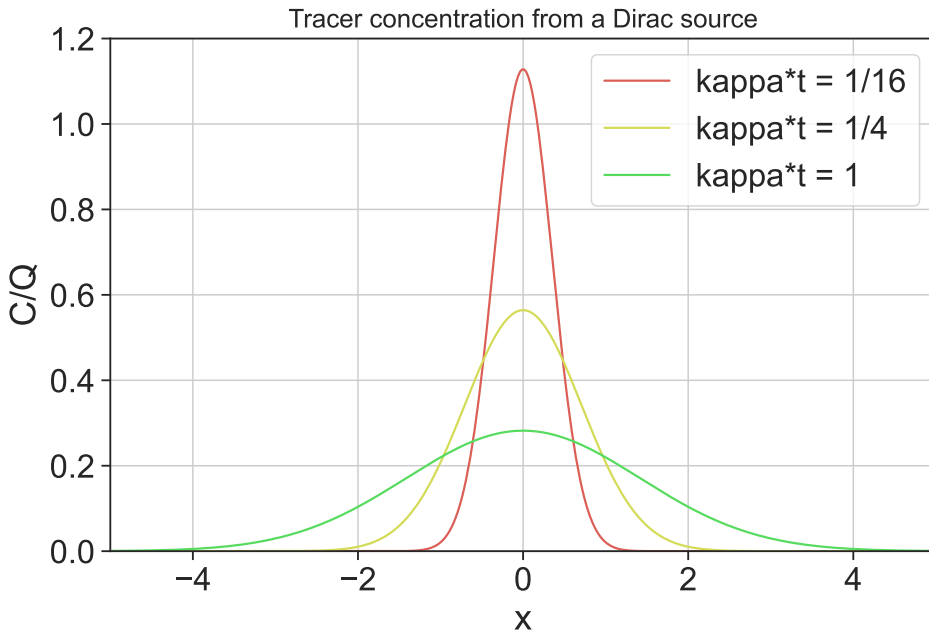


FIGURE 4.3: Illustrating the tracer concentration resulting from a Dirac source at the origin, as given by the Gaussian Green's function (4.73) for three values of κt . According to equation (4.75), the standard deviation is given by $\sqrt{2\kappa t}$, with the standard deviation measuring the spread of the distribution.

4.7 Mathematical interlude: tensor analysis tools

As derived in VOLUME 1, the equation for a conservative tracer¹² takes on the form

$$\rho \frac{DC}{Dt} = -\nabla \cdot \mathbf{J}, \quad (4.76)$$

where C is the tracer concentration scalar, and \mathbf{J} is a tracer flux vector that embodies molecular diffusion as well as subgrid scale advection and subgrid scale diffusion (Chapter 7). Advective transport from the resolved flow, \mathbf{v} , appears when transforming to an Eulerian or laboratory reference frame, in which case the tracer equation takes on the equivalent forms

$$\rho \frac{DC}{Dt} = -\nabla \cdot \mathbf{J} \iff \partial_t(\rho C) + \nabla \cdot (\mathbf{v} \rho C + \mathbf{J}) = 0, \quad (4.77)$$

with $\mathbf{v} \rho C$ the advective flux. In this chapter we assume \mathbf{J} arises just from diffusion, and we furthermore ignore any flow (i.e., $\mathbf{v} = 0$) so that advection is absent.

4.7.1 Concerning the upright versus slanted notation

The two forms of the tracer in equation (4.77) are written as a tensor equation, prompting the upright C , \mathbf{v} , \mathbf{J} , and ∇ , which follows the notation convention from the tensor analysis in VOLUME 1. Hence, these equations are valid in any coordinate system. When represented in a particular coordinate system, such as Cartesian, then we write the slanted C , \mathbf{v} , \mathbf{J} , and ∇ , which are particular coordinate representations of C , \mathbf{v} , \mathbf{J} , and ∇ .

The upright versus slanted notation is fundamental conceptually, since it is important to

¹²Conservative tracers evolve without sources or sinks, and so their material time evolution is only affected by the convergence of a flux.

appreciate that tensors are geometric objects that are not subject to the whims of a particular coordinate choice. Correspondingly, physically robust differential and integral equations are coordinate invariant. Even so, the upright-slanted notation can be softly adhered to without much cause for concern, so long as we are careful to write the coordinate equations using rules of tensor analysis. In that case, the coordinate equations are unaltered in form when changing coordinates; i.e., they are tensor equations. Developing a practical and conceptual understanding of what careful means in this context requires the tensor analysis material presented in VOLUME 1. In the remainder of this section, we summarize salient points from those chapters that are of particular use in the study of tracer diffusion.

4.7.2 Metric tensor allows us to measure distance

The **metric** tensor, g , is a symmetric and positive-definite (i.e., all eigenvalues are positive) second order tensor that is used to measure the distance between points in space. The **Kronecker delta** is the Cartesian coordinate representation of the metric tensor for Euclidean space. In this case, $g_{mn} = \delta_{mn}$, where δ_{mn} is unity when $m = n$ and zero otherwise. In this book, we are only concerned with fluid motion through a background Euclidean space. Even so, we find many occasions to use non-Cartesian coordinates and/or to consider flow constrained to non-Euclidean surfaces that are embedded in Euclidean space (e.g., a spherical planet or an isopycnal surface). Example non-Cartesian coordinates of use for geophysical fluids include the spherical coordinates and cylindrical-polar coordinates detailed in VOLUME 1, the **generalized vertical coordinate** in the present volume, and the Lagrangian or material coordinates of VOLUME 1. For these cases, and others, a coordinate representation of the metric tensor is distinct from the Kronecker delta.

We often have need to work with the inverse metric tensor, g^{-1} , which we know exists since the metric is a symmetric and positive-definite tensor. To reduce notational clutter, we write g^{mn} for the coordinate representation of the inverse metric, rather than the more clumsy $(g^{-1})^{mn}$. By definition of the inverse metric, we have the following identity holding for any coordinate choice

$$\delta^m{}_n = g^{mp} g_{pn}, \quad (4.78)$$

where $\delta^m{}_n$ is an expression of the identity tensor, which is coordinate invariant, meaning that it has the same numerical values for all coordinates. Notably, for Cartesian tensors, where $g_{mn} = \delta_{mn}$, the identity (4.78) reduces to the identity

$$\delta^m{}_n = \delta^{mp} \delta_{pn}. \quad (4.79)$$

Since $\delta^{mn} = \delta_{mn}$ (inverse of the Kronecker delta is the same), equation (4.79) means that numerically we have

$$\delta^{mn} = \delta_{mn} = \delta^m{}_n. \quad (4.80)$$

Identities (4.79) and (4.80) are indicative of the relative simplicity of Cartesian tensor analysis, in which there is no distinction between index placement so that there is no quantitative need to keep track of upstairs versus downstairs indices. Yet there is a distinction for general tensors, and so we must be careful to use the metric tensor to raise and lower indices, as now discussed.

4.7.3 Raising and lowering tensor indices via the metric tensor

Besides measuring distance between points in space, the metric tensor provides the operational means to raise and lower indices that appear on the representations of tensors. For example,

consider the second order diffusion tensor, \mathbf{K} , with a particular coordinate representation $K^m{}_n$. The $K^m{}_n$ representation is sometimes referred to as the (1, 1) **natural representation**, and it is related to its totally contravariant (2, 0) **sharp representation**, K^{mn} , through contraction with the metric tensor,¹³

$$K^m{}_n = \mathfrak{g}_{pn} K^{mp}. \quad (4.81)$$

It follows that to relate the **flat representation** (the (0, 2) representation) to the **sharp representation** requires two contractions with the metric tensor,

$$K_{mn} = \mathfrak{g}_{mq} \mathfrak{g}_{pn} K^{qp}. \quad (4.82)$$

Since the metric is symmetric, $\mathfrak{g}_{mn} = \mathfrak{g}_{nm}$, there is no need to be concerned with the ordering of its indices.

4.7.4 Divergence of a vector and the divergence theorem

As seen from the tracer equation (4.77), the convergence of the tracer flux drives the time evolution of conservative tracers. It is thus important to know how the divergence is expressed as a tensor equation. In the general tensor analysis chapter in VOLUME 1, we derived the following coordinate invariant expression for the divergence of a vector

$$\nabla \cdot \mathbf{J} = \nabla_m J^m = \frac{1}{\sqrt{\det(\mathfrak{g}_{mn})}} \partial_m [\sqrt{\det(\mathfrak{g}_{mn})} J^m], \quad (4.83)$$

where ∇_m are components to the **covariant derivative**. Equation (4.85) is a convenient result since it only requires partial derivatives in the chosen coordinate system, with all the coordinate dependent properties summarized by the square root of the metric determinant, $\sqrt{\det(\mathfrak{g}_{mn})}$. Since $\sqrt{\det(\mathfrak{g}_{mn})}$ appears in many places within this chapter, we find it useful to introduce the shorthand

$$\} \equiv \sqrt{\det(\mathfrak{g}_{mn})}, \quad (4.84)$$

in which the covariant divergence (4.85) is written in the more tidy manner

$$\nabla \cdot \mathbf{J} = \}^{-1} \partial_m (\} J^m). \quad (4.85)$$

For Cartesian coordinates, $\} = \sqrt{\det(\mathfrak{g}_{mn})} = 1$, in which case the divergence in equation (4.85) reduces to its familiar Cartesian form. Yet other coordinates have a nonzero $\}$, which accounts for the squeezing and expansion of the coordinate surfaces that affect the divergence. We display the divergence in spherical coordinates and cylindrical-polar coordinates in VOLUME 1, and for **generalized vertical coordinate** in Sections 1.14 and 1.15.

The $1/\}$ factor appearing in the covariant divergence (4.85) is convenient since it cancels the same factor appearing in the coordinate representation of the volume element. As seen in the general tensor analysis chapter in VOLUME 1, this cancellation greatly simplifies the

¹³In the tensor algebra chapter of VOLUME 1, we introduced the **musical nomenclature** sometimes used for the representations of second order tensors. The **natural representation** of a second order tensor occurs with one tensor index upstairs and the other downstairs. The natural representation is sometimes denoted by (1, 1), to indicate the number of indices up and down. The **sharp representation**, or (2, 0) representation, is when the tensor is represented with both indices upstairs. Finally, the **flat representation** or (0, 2) representation is where both indices are downstairs.

divergence theorem, which takes on the form

$$\int_{\mathcal{R}} \nabla \cdot \mathbf{J} dV = \int_{\mathcal{R}} \nabla_m J^m dV = \int_{\mathcal{R}} \partial_m (\} J^m) d^3\xi = \oint_{\partial\mathcal{R}} J^m \hat{n}_m d\mathcal{S}, \quad (4.86)$$

where $\hat{\mathbf{n}}$ is the outward normal, and $d^3\xi = d\xi^1 d\xi^2 d\xi^3$ is the coordinate volume element.

4.7.5 Example tracer fluxes

We here briefly consider example tracer fluxes that are studied later in this chapter or in Chapter 5. We start from their form written in Cartesian coordinates and then transform to general coordinates.

Advection tracer flux

The advective tracer flux, as represented using Cartesian coordinates (denoted by ξ^m), is written as

$$J^m = \rho v^m C, \quad (4.87)$$

where ρ , C , and v^m are functions that represent the density, tracer concentration, and velocity using Cartesian coordinates as independent variables. To transform the advective tracer flux to another set of coordinates, $\xi^{\bar{m}}$, requires the transformation matrix, $\Lambda^{\bar{m}}_m$ (see VOLUME 1), where

$$J^{\bar{m}} = \bar{\rho} \bar{C} \Lambda^{\bar{m}}_m v^m = \bar{\rho} \bar{C} v^{\bar{m}}. \quad (4.88)$$

In this equation we wrote $\bar{\rho}$, \bar{C} , and $v^{\bar{m}}$ for the functions representing the density, tracer concentration, and velocity with $\xi^{\bar{m}}$ as the independent variables. Furthermore, the transformation matrix, $\Lambda^{\bar{m}}_m$, is built from the partial derivatives of the two sets of coordinates

$$\Lambda^{\bar{m}}_m = \partial \xi^{\bar{m}} / \partial \xi^m. \quad (4.89)$$

For nomenclature brevity in the following, we do not write $\bar{\rho}$ and \bar{C} for the scalar fields, thus relying on the functional dependence implicit in the coordinate choice.

Isotropic diffusive tracer flux and the Laplace-Beltrami operator

The isotropic diffusive tracer flux has the following representation using Cartesian coordinates

$$J^m = -\rho \kappa \delta^{mn} \partial_n C, \quad (4.90)$$

with $\kappa > 0$ the diffusivity scalar. We generalize the isotropic diffusive flux to arbitrary coordinates, $\xi^{\bar{m}}$, by introducing the inverse metric tensor represented using the $\xi^{\bar{m}}$ coordinates¹⁴

$$J^{\bar{m}} = -\rho \kappa \bar{g}^{\bar{m}\bar{n}} \partial_{\bar{n}} C. \quad (4.91)$$

Making use of equation (4.85) leads to the flux convergence

$$-\nabla \cdot \mathbf{J} = \}^{-1} \partial_{\bar{m}} (\rho \kappa \} \bar{g}^{\bar{m}\bar{n}} \partial_{\bar{n}} C). \quad (4.92)$$

¹⁴The covariant derivative acting on a scalar field is just the partial derivative. So we could just as well have written $J^{\bar{m}} = -\rho \bar{g}^{\bar{m}\bar{n}} \nabla_{\bar{n}} C$ for equation (4.91).

If the product, $\rho \kappa$, is a constant in space then the resulting flux convergence exposes the **Laplace-Beltrami operator** acting on the tracer concentration

$$-\nabla \cdot \mathbf{J} = \rho \kappa \underbrace{\{\}^{-1} \partial_{\bar{m}} (\{\} g^{\bar{m}\bar{n}} \partial_{\bar{n}} C)}_{\text{Laplace-Beltrami acting on } C} \equiv \rho \kappa \bar{\nabla}^2 C. \quad (4.93)$$

Diffusive tracer flux with an anisotropic diffusion tensor

With a general diffusion tensor (whose form is discussed more in later sections), the Cartesian expression for the diffusive flux is given by

$$J^m = -\rho K^{mn} \partial_n C. \quad (4.94)$$

The tracer flux has a corresponding expression using arbitrary coordinates

$$J^{\bar{m}} = -\rho K^{\bar{m}\bar{n}} \partial_{\bar{n}} C, \quad (4.95)$$

which is identical in form to the Cartesian expression (4.94). We make use of the transformation matrix and its inverse to write

$$\partial_{\bar{n}} = \partial_n \Lambda^n_{\bar{n}} \quad \text{and} \quad K^{\bar{m}\bar{n}} = \Lambda^{\bar{m}}_m \Lambda^{\bar{n}}_n K^{mn}. \quad (4.96)$$

Note that we actually only need to perform a single transformation since the contraction between the diffusion tensor and the derivative of the tracer concentration is coordinate invariant

$$J^{\bar{m}} = -\rho K^{\bar{m}\bar{n}} \partial_{\bar{n}} C = -\rho K^{\bar{m}n} \partial_n C = -\rho \Lambda^{\bar{m}}_m K^{mn} \partial_n C = \Lambda^{\bar{m}}_m J^m. \quad (4.97)$$

4.7.6 Comments about the tensor tools

Most of this chapter is unconcerned with the niceties of general tensor analysis. Part of the reason is that Cartesian coordinates are sufficient to exemplify the key maths and physics ideas. Even so, we are mindful to use rudimentary tensor notation, thus allowing for the equations derived with Cartesian coordinates to be valid tensor equations that hold for all coordinates. Given the growing suite of coordinates used in geophysical fluid studies, this extra bit of formalism has a nontrivial payoff.

4.8 Further properties of tracer diffusion

We examined a variety of mathematical properties of the diffusion equation in VOLUME 1, as part of our study of **parabolic partial differential equations**. We also examined the diffusion equation as part of our analysis of the **Green's function** method of solutions for **passive tracers**. Here, we explore further mathematical properties of diffusion. In particular, we here allow for distinct behavior of the diffusive fluxes in the different directions. Such distinctions are relevant especially for the turbulent diffusivity arising in stratified fluids, where turbulent mixing across stratification surfaces is suppressed relative to turbulent mixing parallel to these surfaces¹⁵ For this purpose we make use of the second order positive definite and symmetric **diffusion tensor**,

¹⁵We pursue this idea far more thoroughly in Chapter 7 when describing closures for the tracer equation in the presence of turbulence.

$\mathbf{K} = \mathbf{K}^T$, with the resulting downgradient diffusive tracer flux given by

$$J^m = -\rho K^{mn} \partial_n C. \quad (4.98)$$

4.8.1 Sample diffusion tensors

For the case of molecular diffusion considered in equation (4.58), the diffusion tensor is generally assumed to be isotropic. Written in Cartesian coordinates, the isotropic diffusion tensor takes the form

$$K^{mn} = \kappa \delta^{mn}, \quad (4.99)$$

whereas with general coordinates it is

$$K^{\overline{mn}} = \kappa g^{\overline{mn}}. \quad (4.100)$$

It is notable that the natural or $(1, 1)$ form for the molecular diffusion tensor is numerically identical across coordinates, in that

$$K^m{}_p = \kappa \delta^m{}_p \quad \text{and} \quad K^{\overline{m}}{}_{\overline{p}} = \kappa g_{\overline{np}} g^{\overline{mn}} = \kappa \delta^{\overline{m}}{}_{\overline{p}}, \quad (4.101)$$

where we made use of the identity (4.78) satisfied by the metric and its inverse.

To parameterize flows that are turbulent and larger than the microscale (e.g., ocean mesoscale turbulence), it is common to rotate the diffusive fluxes to be along surfaces of constant scalar field, $\gamma(\mathbf{x}, t)$, in which case the diffusion tensor is

$$K^{mn} = \kappa (\delta^{mn} - \hat{\gamma}^m \hat{\gamma}^n), \quad (4.102)$$

where

$$\hat{\gamma}_n = \frac{\partial_n \gamma}{|\nabla \gamma|} \quad (4.103)$$

is the surface normal direction. The general coordinate representation of this anisotropic diffusion tensor is

$$K^{\overline{mn}} = \kappa (g^{\overline{mn}} - \hat{\gamma}^{\overline{m}} \hat{\gamma}^{\overline{n}}). \quad (4.104)$$

One choice for the orientation direction is to set $\hat{\gamma} = \hat{z}$, in which case the diffusion tensor orients the tracer fluxes along surfaces of constant geopotential to thus realize [horizontal diffusion](#). Another choice, motivated from the physics of ocean mesoscale eddy transport, sets γ equal to a measure of the local buoyancy. In this case we have the [neutral diffusion](#) process studied in Section 7.4.

4.8.2 Diffusion of tracer concentration powers

In Exercise 4.3, we assume that the tracer concentration satisfies the tracer equation

$$\rho \frac{DC}{Dt} = -\nabla \cdot \mathbf{J}, \quad (4.105)$$

for a diffusive flux, \mathbf{J} , and then show that for any $\Gamma \geq 1$ that

$$\rho \frac{DC^\Gamma}{Dt} = -\nabla \cdot \mathbf{J}(C^\Gamma) + \Gamma(\Gamma - 1) C^{\Gamma-2} \mathbf{J} \cdot \nabla C. \quad (4.106)$$

The first term in equation (4.106) is the convergence of the diffusive flux defined in terms of C^Γ . This term acts to diffuse C^Γ just like diffusion acts on C . The second term in equation (4.106) is negative since the diffusion tensor is symmetric and positive-definite so that

$$\mathbf{J} \cdot \nabla C = -\rho K^{mn} \partial_m C \partial_n C < 0. \quad (4.107)$$

That is, the diffusive flux, by construction, is oriented down the tracer concentration gradient. Consequently, the second term in equation (4.106) always acts to reduce the magnitude of C^Γ towards zero.

4.8.3 Moments of tracer concentration

Next we consider the evolution of domain integrated tracer concentration and its powers. To focus on impacts just from diffusion, we assume the boundaries are insulating (i.e., zero normal boundary flux) so that $\mathbf{J} \cdot \hat{\mathbf{n}} = 0$ with $\hat{\mathbf{n}}$ the outward normal at the boundary. We also assume the total fluid mass in the domain remains fixed

$$M = \int \rho dV \quad \text{with} \quad \frac{dM}{dt} = 0. \quad (4.108)$$

We can thus treat the domain as material given that there is no exchange of mass or tracer across the boundaries. These assumptions allow us to focus just on the effects from tracer diffusion.

Domain average tracer concentration

The domain averaged tracer concentration is defined by

$$\bar{C} = \frac{\int C \rho dV}{M}, \quad (4.109)$$

and it follows that its time derivative vanishes since

$$M \frac{d\bar{C}}{dt} = \frac{d}{dt} \int C \rho dV = \int \frac{DC}{Dt} \rho dV = - \int \nabla \cdot \mathbf{J} \rho dV = - \oint \mathbf{J} \cdot \hat{\mathbf{n}} dS = 0, \quad (4.110)$$

where $\mathbf{J} \cdot \hat{\mathbf{n}} = 0$ since we are assuming an insulating boundary. Also note that we brought the time derivative inside the integral as a material derivative since the region is itself material, thus allowing us to make use of [Reynolds transport theorem](#) from [VOLUME 1](#). The result (4.110) follows since there is no change in the total mass of fluid nor is there any exchange of tracer across the boundaries. Hence, the domain averaged tracer concentration remains fixed in time.

Tracer variance within the domain

The variance of the tracer concentration is defined by

$$\text{var}(C) \equiv \frac{\int (C - \bar{C})^2 \rho dV}{M} = \bar{C^2} - \bar{C}^2 \geq 0. \quad (4.111)$$

The tracer variance measures the deviation of the tracer concentration relative to the domain averaged concentration. Since the domain average remains fixed in time, the time change of

the variance is given by

$$\frac{d[\text{var}(C)]}{dt} = \frac{d\bar{C}^2}{dt}. \quad (4.112)$$

Thus, it is common to refer to \bar{C}^2 as the tracer variance, although strictly speaking only time derivatives of \bar{C}^2 and $\text{var}(C)$ are equal as per equation (4.112). Performing the time derivative, and again noting that the domain is material so that we can use Reynolds transport theorem, renders

$$M \frac{d\bar{C}^2}{dt} = \frac{d}{dt} \int C^2 \rho dV = 2 \int C \frac{DC}{Dt} \rho dV = -2 \int C \nabla \cdot \mathbf{J} dV = 2 \int \nabla C \cdot \mathbf{J} dV. \quad (4.113)$$

The final equality again made use of the insulating boundary condition, $\mathbf{J} \cdot \hat{\mathbf{n}} = 0$. The time change in the tracer variance is thus determined by the integral of the projection of the tracer flux onto the tracer gradient. We already saw from equation (4.107) that diffusive fluxes are oriented down the tracer gradient. Consequently, diffusion of the tracer concentration results in a reduction in tracer variance

$$\frac{d[\text{var}(C)]}{dt} = \frac{d\bar{C}^2}{dt} \leq 0. \quad (4.114)$$

This result further supports our common experience where diffusion removes differences (i.e., gradients) within the tracer field.

Turbulent stirring enhances the efficiency of mixing from molecular diffusion

Let us expose the diffusion tensor in equation (4.113) to have

$$M \frac{d[\text{var}(C)]}{dt} = -2 \int \nabla C \cdot \mathbf{K} \cdot \nabla C dV, \quad (4.115)$$

which takes on the particularly simple form for molecular diffusion

$$M \frac{d[\text{var}(C)]}{dt} = -2 \kappa \int |\nabla C|^2 dV, \quad (4.116)$$

These expressions highlight a key point that we return to in Chapter 5 as part of our study of advection plus diffusion. In that chapter, we show that advection has no direct impact on tracer variance or any other tracer moments. However, and crucially, advection affects changes to the tracer gradient. Indeed, turbulent flows generally increase the magnitude of the gradient via a stirring process that stretches and folds tracer contours and surfaces. Consequently, as seen from equation (4.116), turbulent stirring increases the impacts from molecular diffusion by enhancing the magnitude of tracer gradients that diffusion can act upon. This mechanism is the fundamental reason that mixing in turbulent flows is far more efficient than mixing in quiescent flows.

Diffusion of arbitrary tracer moments

Proceeding as before, and dropping boundary contributions since the domain is material and insulating, the identity (4.106) shows that the time derivative of an arbitrary tracer moment is given by

$$\frac{d\bar{C}^\Gamma}{dt} = \Gamma(\Gamma - 1) \int C^{\Gamma-2} \nabla C \cdot \mathbf{J} dV \leq 0. \quad (4.117)$$

For $\Gamma = 0$ we have an expression of mass conservation for the domain, whereas $\Gamma = 1$ is an expression of tracer conservation. The case of $\Gamma = 2$ yields the tracer variance result (4.114). The result for higher powers also holds. Hence, we conclude that the downgradient orientation of diffusive tracer fluxes acts to dissipate all powers of tracer concentration when integrated globally; i.e., all tracer moments are dissipated by diffusion.

4.9 Connecting tracer dissipation to the diffusion operator

We here take an excursion into linear operator theory. In particular, we make a connection between the diffusion operator with natural boundary conditions (defined below) and the functional derivative of the global tracer dissipation functional. This connection holds so long as the diffusion operator is **self-adjoint** and linear, as it is when diffusing passive tracers and with natural boundary conditions. The connection between a linear self-adjoint operator and a functional is developed in such books as *Courant and Hilbert* (1953, 1962). In the simplest case, the Laplacian of the tracer, $\nabla^2 C$, is equal to the functional derivative,

$$\nabla^2 C = \frac{\delta \mathcal{F}}{\delta C}, \quad (4.118)$$

where¹⁶

$$\mathcal{F} \equiv -\frac{1}{2} \int |\nabla C|^2 \rho d^3x \quad (4.119)$$

is the associated functional. In the following, we prove this result for a general diffusion tensor acting on an arbitrary tracer concentration, C , with the proof holding so long as the diffusion tensor is not a function of the tracer concentration. Besides offering an interesting theoretical tidbit, this result provides a suitable framework for developing numerical methods for discretizing the diffusion operator, with examples provided by *Griffies et al.* (1998) and Chapter 16 of *Griffies* (2004).

4.9.1 Fréchet derivative of the diffusion dissipation functional

Define the **diffusion dissipation functional**

$$\mathcal{F} = \int \mathcal{L} d^3x, \quad (4.120)$$

where the integrand is the negative semi-definite quadratic form

$$2\mathcal{L} = \mathbf{J} \cdot \nabla C = -\rho K^{mn} \partial_m C \partial_n C \leq 0. \quad (4.121)$$

The goal is to relate the diffusion operator, given by the convergence of the diffusion flux, $-\nabla \cdot \mathbf{J}$, to the functional derivative of \mathcal{F} , with the derivative taken with respect to the tracer concentration, C . We compute the functional derivative using variational calculus technology from VOLUME 1, as well as in Chapters 10 11 in relation to Hamilton's variational principle.

For that purpose, consider a functional variation to the tracer concentration, δC , and insert

¹⁶In this section we write the integration volume element as $d^3x = dV$. Motivation for this notation will become apparent at the point of equation (4.127).

it into the dissipation functional

$$\delta\mathcal{F} = \int \left[\delta C \frac{\delta\mathcal{L}}{\delta C} + \delta(\partial_m C) \frac{\delta\mathcal{L}}{\delta(\partial_m C)} \right] d^3x. \quad (4.122)$$

As discussed in Chapter 10, functional variations are perturbations to the form of the function, in which case

$$C \rightarrow C + \delta C \quad \text{with} \quad |\delta C| \ll |C|. \quad (4.123)$$

Notably, δC is itself a function of space and time, $\delta C(\mathbf{x}, t)$, but it is assumed to have much smaller magnitude than the concentration, $C(\mathbf{x}, t)$. Additionally, the functional variation, δC , has no affect on the space-time points so that the variational operator, δ , commutes with space and time derivatives and integrals. Integration by parts on the second term in equation (4.122) leads to

$$\delta\mathcal{F} = \int \left[\delta C \frac{\delta\mathcal{L}}{\delta C} + \partial_m \left(\delta C \frac{\delta\mathcal{L}}{\delta(\partial_m C)} \right) - \delta C \partial_m \left(\frac{\delta\mathcal{L}}{\delta(\partial_m C)} \right) \right] d^3x. \quad (4.124)$$

The middle term is a total derivative that integrates to a boundary contribution and the associated [natural boundary condition](#)

$$\hat{\mathbf{n}} \cdot \frac{\delta\mathcal{L}}{\delta \nabla C} = \hat{\mathbf{n}} \cdot \mathbf{J} = \text{boundary flux}, \quad (4.125)$$

with $\hat{\mathbf{n}}$ the boundary outward normal. This natural boundary condition is the [Neumann boundary condition](#).

To focus on the connection between the diffusion operator and the diffusion dissipation functional, we ignore boundary fluxes so that the functional variation is given by

$$\delta\mathcal{F} = \int \delta C \left[\frac{\delta\mathcal{L}}{\delta C} - \partial_m \left(\frac{\delta\mathcal{L}}{\delta(\partial_m C)} \right) \right] d^3x. \quad (4.126)$$

Consequently, the [functional derivative](#) (also known as the Fréchet derivative) is given by

$$(d^3y)^{-1} \frac{\delta\mathcal{F}}{\delta C(\mathbf{y})} = \frac{\delta\mathcal{L}}{\delta C} - \partial_m \left[\frac{\delta\mathcal{L}}{\delta(\partial_m C)} \right], \quad (4.127)$$

where d^3y is the volume element at the field point, \mathbf{y} . To reach the last step required the identity

$$\frac{\delta C(\mathbf{x})}{\delta C(\mathbf{y})} = d^3y \delta(\mathbf{x} - \mathbf{y}), \quad (4.128)$$

where $\delta(\mathbf{x} - \mathbf{y})$ is the [Dirac delta](#)¹⁷ satisfying

$$\int \delta(\mathbf{x} - \mathbf{y}) d^3y = 1, \quad (4.129)$$

so long as the integration domain includes the singular point $\mathbf{x} = \mathbf{y}$. Note that the Dirac delta has dimensions of inverse volume, which necessitates the appearance of the volume factor, d^3y , on the right hand side of equation (4.128).¹⁸

¹⁷Note the unfortunate, though nearly universal, double meaning for the δ symbol: one referring to the variation operator and one referring to the Dirac delta.

¹⁸Many treatments of functional derivatives in mathematics texts ignore the volume factor, d^3y , in equation (4.128). Yet for physical applications it is necessary to maintain dimensional consistency, with the volume factor required for that reason. The volume factor also appears when using functional methods to derive numerical

4.9.2 Connection to the diffusion operator

Reintroducing the specific form of the diffusion integrand $2\mathcal{L} = -\rho K^{mn} \partial_m C \partial_n C$ leads to

$$\frac{\delta \mathcal{F}}{\delta C(\mathbf{y})} = -\partial_m \left[\frac{\delta \mathcal{L}}{\delta(\partial_m C)} \right] d^3y = \partial_m(\rho K^{mn} \partial_n C) d^3y. \quad (4.130)$$

The second equality identifies the diffusion operator, thus revealing the connection between the dissipation functional, the diffusion fluxes, and the diffusion operator

$$\frac{\delta \mathcal{F}}{\delta C(\mathbf{y})} = -(\nabla \cdot \mathbf{J}) d^3y. \quad (4.131)$$

4.9.3 Why we need to assume K^{mn} is independent of C

There are many geophysical applications in which the diffusion tensor is a function of the tracer concentration, in which case the diffusion equation is no longer a linear differential equation. For example, the neutral diffusion of Section 7.4 makes use of a diffusion tensor that is a function of temperature and salinity gradients. In this case the functional derivative in terms of temperature or salinity appearing in equation (4.130) becomes

$$2 \frac{\delta \mathcal{L}}{\delta(\partial_m C)} = -2\rho K^{mn} \partial_n C - \rho \partial_m C \partial_n C \frac{\delta K^{mn}}{\delta(\partial_m C)}. \quad (4.132)$$

The specific form of the term $\delta K^{mn}/\delta(\partial_m C)$ depends on details of the diffusion tensor. Hence, the general results derived above for the linear diffusion equation no longer hold for this nonlinear diffusion equation. We have more to say about nonlinear advection-diffusion in Section 5.7.

4.9.4 Relation to Hamilton's principle

We make use of functional derivatives when using Hamilton's principle for non-dissipative continuous systems in Part III of this volume. For those systems, the Euler-Lagrange equation equations of motion result from setting the functional derivative of the action to zero, which is the mathematical statement of Hamilton's principle. In contrast, we here showed that the functional derivative of the tracer dissipation equals to the diffusion operator. In fact, the construction in this section suggests that linear self-adjoint operators, such as generalized Laplacian operators, can generally be expressed as the functional derivative of its corresponding functional. Chapters 16 and 19 of [Griffies \(2004\)](#) provide further examples, with applications to numerical methods. Further mathematical details can be found in such books as [Courant and Hilbert \(1953, 1962\)](#).



4.10 Exercises

EXERCISE 4.1: VERTICAL DIFFUSION OF TEMPERATURE IN THE OCEAN ([Vallis, 2017](#))

There is a natural time scale associated with diffusive transport. This time scale can be found

discretizations, with examples provided by [Griffies et al. \(1998\)](#), [Griffies and Hallberg \(2000\)](#), and [Griffies \(2004\)](#).

from scaling the diffusion equation, which reveals that it takes the form

$$\tau_{\text{diffusion}} = \Delta^2 / \kappa, \quad (4.133)$$

where Δ is the length scale and κ is the kinematic diffusivity (dimensions of squared length per time). We now make use of this time scale to consider the diffusion of temperature in the ocean, with diffusion due solely to molecular processes.

Using the observed value of molecular diffusivity of temperature in water (look it up), estimate the time for a temperature anomaly to mix from the top of the ocean to the bottom, assuming vertical diffusion through the molecular diffusivity is the only means for mixing. This time scale follows from the one-dimensional diffusion equation and is determined by the diffusivity and the depth of the ocean. Comment on whether you think the real ocean has reached equilibrium after the last ice age (which ended about 12Kyr ago).

EXERCISE 4.2: SOLUTION TO ONE-DIMENSIONAL DIFFUSION EQUATION

Consider a one-dimensional diffusion equation

$$\partial_t C = \kappa \partial_{zz} C, \quad (4.134)$$

where C is a tracer concentration (e.g., temperature or salinity), κ is a constant kinematic diffusivity, and z is the vertical coordinate. Assume the domain has fixed boundaries at $z = 0$ and $z = H$.

- (a) Assume there is a zero flux of tracer at the two boundaries. Mathematically express this no-flux boundary condition.
- (b) Assume that the initial tracer concentration is confined to an area near the center of the domain. Use dimensional analysis to estimate the time scale for the concentration to homogenize throughout the domain.
- (c) Consider the initial-boundary value problem

$$\partial_t C = \kappa \partial_{zz} C, \quad (4.135a)$$

$$\text{no-flux boundary condition from part (b)} \quad (4.135b)$$

$$C(z, t = 0) = C_0 \cos(kz), \quad (4.135c)$$

where C_0 is a constant. What values for the wave-number, k , satisfy the no-flux boundary condition?

- (d) Solve the diffusion equation analytically for the given initial condition. Hint: consult your favorite partial differential equation book to learn how to solve this linear 1+1 dimensional diffusion equation.
- (e) Explain how the analytical answer you obtained is consistent with the dimensional analysis answer from part (b).

EXERCISE 4.3: DIFFUSION OF TRACER CONCENTRATION POWERS

Derive equation (4.106) for the diffusion of tracer concentration powers.

EXERCISE 4.4: LOCALLY DISSIPATIVE PROPERTIES OF DIFFUSION

This exercise explores the dissipative property of diffusion when acting on a tracer extrema.

- (a) ONE-DIMENSIONAL DIFFUSION

Consider the diffusion equation in one spatial dimension, and assume a Boussinesq ocean

in which case the density factors are all constant and so can be dropped

$$\partial_t C = \partial_z (\kappa \partial_z C) = \partial_z \kappa \partial_z C + \kappa \partial_{zz} C, \quad (4.136)$$

where $\kappa(z, t)$ is an **eddy diffusivity** (also *turbulent diffusivity*). The eddy diffusivity is assumed to be a function of (z, t) , with the spatial dependence determined by the flow. Show that a tracer extrema, C^* , evolves under diffusion according to

$$\partial_t C^* = \kappa \partial_{zz} C^*. \quad (4.137)$$

So what does diffusion do to a local maxima (e.g., a local hot region) in the tracer field? What about a minima (e.g., a local cold region)? To answer this question, discuss the mathematical equation satisfied by the tracer extrema.

(b) THREE-DIMENSIONAL DIFFUSION

Generalize the above one dimensional result to three dimensions, whereby the diffusivity κ becomes a symmetric positive-definite diffusion *tensor*, in which case

$$\partial_t C = \partial_m (K^{mn} \partial_n C). \quad (4.138)$$

Now consider an extrema in the tracer field, which is defined by

$$\partial_n C^* = 0 \quad \forall n = 1, 2, 3. \quad (4.139)$$

Prove that three dimensional diffusion acts to *dissipate* an extrema. Hint: recall some linear algebra properties of a symmetric positive-definite matrix. In particular, note that a symmetric positive-definite matrix has positive eigenvalues.

EXERCISE 4.5: DIFFUSION INCREASES INFORMATION ENTROPY OF A TRACER

Diffusion is an irreversible process. Here we illustrate this property by considering the **information entropy** associated with a non-negative tracer concentration¹⁹

$$\mathcal{S}_C \equiv - \int (C \ln C) \rho \, dV, \quad (4.140)$$

where $C \in [0, 1]$ is the non-dimensional material concentration of a tracer. Show that

$$\frac{d\mathcal{S}_C}{dt} \geq 0 \quad (4.141)$$

over a material region with $C > 0$ and with downgradient diffusion, $\mathbf{J} \cdot \nabla C < 0$. Consequently, diffusion always increases the information entropy. Hint: follow the discussion of tracer moments in Section 4.8.3. This result is related to the **H-theorem** proven by [Boltzmann \(1966\)](#) for the kinetic theory of gases.

EXERCISE 4.6: PHILLIPS LAYERING INSTABILITY

This exercise is based on the discussion in Section 12.2 of [Smyth and Carpenter \(2019\)](#), in which we consider an oceanographically relevant example of a turbulent diffusivity that is a function of vertical buoyancy stratification. Under certain circumstances, the flow dependent diffusivity can enhance, rather than reduce, vertical gradients in the buoyancy, with the associated **Phillip's layering instability** leading to layering. We here only work through the basic mathematical

¹⁹Information entropy is used in statistical physics as a measure of the order/disorder of a probability distribution. We here apply these notions to measure the information entropy of a tracer concentration.

formulation, leaving the interested reader to consult [Smyth and Carpenter \(2019\)](#) for more details.

Consider a buoyancy field that is a function of vertical position and time, $b(z, t)$, and let the squared buoyancy frequency be given by the vertical derivative of the buoyancy

$$N^2 = \partial_z b. \quad (4.142)$$

If buoyancy is affected only by vertical diffusion, then its evolution equation is the one-dimensional vertical diffusion equation

$$\partial_t b = \partial_z (\kappa N^2), \quad (4.143)$$

where $\kappa > 0$ is the vertical diffusivity for buoyancy. Correspondingly, a vertical derivative of the buoyancy equation leads to the evolution equation for the squared buoyancy frequency

$$\partial_t N^2 = \partial_{zz} (\kappa N^2). \quad (4.144)$$

Assume the diffusivity has the following functional dependence

$$\kappa = \kappa(N^2), \quad (4.145)$$

so that it is a function of the squared buoyancy frequency. A physically relevant choice has the diffusivity get smaller as the stratification increases, so that

$$\frac{d\kappa}{dN^2} < 0. \quad (4.146)$$

Now consider the case of a squared buoyancy frequency that is a small deviation relative to a constant background value

$$N^2(z, t) = N_0^2 + \epsilon N_1^2(z, t), \quad (4.147)$$

where ϵ is a small non-dimensional number. Derive the condition whereby, to first order in ϵ , we have N_1^2 growing in the presence of downgradient diffusion rather than decaying. That is, what is the condition satisfied by $d\kappa/dN^2$, N_0^2 , and κ that renders an unstable diffusion equation, whereby $\kappa > 0$ leads to an increase in N^2 rather than a decrease?



Chapter 5

TRACER ADVECTION AND DIFFUSION

In this chapter we study tracer advection and diffusion, building on the study of tracer diffusion in Chapter 4 and the mathematics of [parabolic partial differential equations](#) in [VOLUME 1](#). We focus on the particular case of [conservative tracers](#), which are tracers whose evolution is only affected by advection and diffusion within the fluid interior, along with either a [Neumann boundary condition](#) or a [Dirichlet boundary condition](#). The adjective “conservative” refers to the property that such tracers evolve only through the convergence of a tracer flux vector, and so the net tracer content is altered only through transport across boundaries. That is, conservative tracers have no interior sources or sinks, thus making their budgets simpler than other tracers, such as chemical and biogeochemical tracers, that are also affected by sources and sinks.

Example geophysical tracers that are nearly conservative include salinity in the ocean and humidity in the atmosphere. Both of these tracers are [material tracers](#), which measure the ratio of the mass of a matter substance within a fluid element to the mass of the fluid element. Hence, we treat material tracers as non-dimensional scalar fields whose concentrations range from zero to unity. In [VOLUME 1](#) we derived their mass budget equation (also referred to as a [continuity equation](#)) when studying the kinematics of material tracers. [Conservative Temperature](#), Θ , as defined [VOLUME 2](#), is a nearly conservative thermodynamical tracer that provides a measure of the [potential enthalpy](#) in a fluid element.¹ [Conservative Temperature](#) is typically measured in K in the atmosphere and $^{\circ}\text{C}$ in the ocean. Finally, there are many applications of conceptual [passive tracers](#), with such tracers assumed to have zero impact on the flow. Passive tracers are versatile theoretical tools allowing us to probe aspects of the flow, including pathways and time scales ([Haine et al., 2025](#)). It is notable that passive tracers afford a Green’s function solution, which proves quite useful in both theory and applications.

CHAPTER GUIDE

This chapter follows directly from our study of the maths of tracer diffusion in [VOLUME 1](#), as well as the physics of diffusive processes in Chapter 4. Results for the [Boussinesq ocean](#) from [VOLUME 2](#) are found merely by setting the density factor, ρ , to the Boussinesq reference density, ρ_0 , where it appears in the budget equations of this chapter. We generally assume Cartesian coordinates in this chapter. Even so, the equations are written in a tensorially consistent manner to allow for extension to arbitrary coordinates.

¹By convention, [Conservative Temperature](#) uses capital letters for its name.

5.1	Introduction to advection and diffusion	143
5.1.1	Eckart's conceptual description of stirring and mixing	143
5.1.2	A kinematic model	144
5.1.3	Further study	145
5.2	Perfect fluid tracer advection	146
5.2.1	The advection equation	146
5.2.2	Eulerian time tendencies from advection	147
5.2.3	Impermeability property of tracer isosurfaces	147
5.3	Worked example: hyperbolic flow	147
5.3.1	Solution via the fluid particle trajectories	148
5.3.2	Further study	149
5.4	Mathematical properties of tracer advection	149
5.4.1	Material constancy of C^F	149
5.4.2	Evolution of squared tracer gradient	149
5.4.3	Eddy-induced and residual mean	150
5.4.4	Advection tracer fluxes and skew tracer fluxes	151
5.4.5	Skew diffusion	152
5.4.6	A comment about skew fluxes and Lagrangian kinematics	153
5.4.7	Further reading	153
5.5	Advection and skewson	153
5.5.1	Choosing a gauge	153
5.5.2	Vertical gauge	154
5.5.3	Boundary conditions	155
5.6	Finite volume budgets with eddy velocities	156
5.6.1	Advection flux formulation	157
5.6.2	Skew flux formulation	158
5.6.3	Domain with a tracer boundary	158
5.6.4	Budget for a region with interior sides	161
5.6.5	Budget for a perfect fluid in a region with interior sides	163
5.7	Active tracers and dia-surface flow	165
5.7.1	Adiabatic flow	166
5.7.2	Diabatic processes generating dia- Θ transport	166
5.8	Tracer homogenization inside closed tracer contours	167
5.8.1	Proof of the theorem	167
5.8.2	Comments	169
5.8.3	Further study	170
5.9	Green's function method for passive tracers	170
5.9.1	Concerning time dependent domain boundaries	170
5.9.2	Passive tracer boundary conditions	171
5.9.3	Advection-diffusion initial-boundary value problem	172
5.9.4	The Green's function problem	173
5.9.5	Adjoint Green's function problem	173
5.9.6	Reciprocity condition	174
5.9.7	Composition property	177
5.9.8	Integral expression for the tracer concentration	178
5.9.9	Properties of the Green's function solution	180
5.9.10	Boundary propagator	181
5.9.11	Comments	183
5.10	Exercises	183

5.1 Introduction to advection and diffusion

In this chapter we consider the equation describing the evolution of a [conservative tracer](#)

$$\rho \frac{DC}{Dt} = -\nabla \cdot \mathbf{J} \iff \partial_t(\rho C) + \nabla \cdot (\mathbf{v} \rho C + \mathbf{J}) = 0, \quad (5.1)$$

where the flow is nonzero, $\mathbf{v} \neq 0$, so that advection contributes to tracer evolution in addition to subgrid scale fluxes, such as [diffusion](#), captured by the tracer flux \mathbf{J} . For the first part of this chapter, we focus on the effects from advection alone, in which $\mathbf{J} = 0$ thus reducing equation (5.1) to [advection equation](#)

$$\rho \frac{DC}{Dt} = \partial_t(\rho C) + \nabla \cdot (\mathbf{v} \rho C) = 0. \quad (5.2)$$

In this case, convergences of the advective tracer flux render a reversible [stirring](#) that stretches fluid elements. This stirring, particularly in the presence of turbulent flows, can increase the magnitude of tracer concentration gradients (see Section 5.4.2), and it does so while maintaining, for each fluid element, a fixed mass for all matter constituents and fixed specific entropy.²

When [diffusion](#) is enabled, as seen in Chapter 4, the fluid experiences an irreversible exchange that causes [mixing](#) of properties between fluid elements. Correspondingly, diffusion reduces the magnitude of property gradients between fluid elements. When acting together, advection is no longer a pure stirring and diffusion is no longer a pure mixing. Indeed, in the steady state, advection and diffusion exactly balance. [Eckart \(1948\)](#) articulated what has become the standard conceptual paradigm for stirring and mixing in geophysical fluids, with elements of that paradigm reflected in this chapter.

5.1.1 Eckart's conceptual description of stirring and mixing

[Eckart \(1948\)](#) provided a conceptual description of transport in fluids that describes the combined roles of advection plus molecular diffusion in affecting the mixing of fluid properties. Quoting from his introduction, he proposes the following three phases.

It is useful to consider a trivial experiment by way of introduction: the mixing of coffee and cream. Three more or less distinct stages can be observed.

1. The initial stage, in which rather large volumes of cream and coffee are distinctly visible; there are sharp gradients at the interfaces between the volumes, but elsewhere the gradient is practically zero. Averaged over the entire volume, the gradient is small. If motion of the liquid is avoided, this state persists for a considerable time.
2. The intermediate stage, after motion has been induced by stirring the liquids; the masses of cream and coffee are distorted, with a rapid increase in the extent of the interfacial regions having high concentration gradients. The average value of the gradient is correspondingly increased.
3. The final stage, in which the gradients disappear, apparently quite suddenly and spontaneously, with the liquid becoming homogeneous.

It is a reasonable working hypothesis to assume that these three stages (or at least

²Recall from our study of thermodynamics in VOLUME 2 that specific entropy remains materially constant on fluid elements in the absence of mixing or [diabatic](#) sources.

the second and third) also occur in the ocean and atmosphere when concentration or temperature differences arise.

5.1.2 A kinematic model

Consider the following kinematic advection-diffusion model to illustrate Eckart's three stages of stirring and mixing

$$\partial_t C + u \partial_x C = \kappa (\partial_{xx} + \partial_{yy}) C, \quad (5.3)$$

with tracer concentration, $C = C(x, y, t)$, and the domain a zonally periodic channels with free-slip walls at the northern boundaries. The prescribed zonal and non-divergent flow is static and a quadratic function of meridional position

$$u(y) = u_\circ (y/L)^2, \quad (5.4)$$

with u_\circ an arbitrary velocity scale, and $y \in [0, L]$ the meridional domain. We non-dimensionalize the advection-diffusion equation (5.3) using the following non-dimensional variables

$$(\bar{x}, \bar{y}) = (x, y)/L \quad \text{and} \quad \bar{t} = (u_\circ/L) t, \quad (5.5)$$

which renders

$$\partial_{\bar{t}} C + \bar{y}^2 \partial_{\bar{x}} C = \text{Pe}^{-1} (\partial_{\bar{xx}} + \partial_{\bar{yy}}) C, \quad (5.6)$$

where we introduced the **Peclet number**,

$$\text{Pe} = u_\circ L / \kappa. \quad (5.7)$$

The Peclet number is sole non-dimensional number for this system and it measures the strength of the advection versus the diffusion. Note that we chose to non-dimensionalize time according to an advective time scale, L/u_\circ , which is the natural time scale for this system.

Figure 5.1 illustrates numerical solutions for two cases, one without diffusion and one with diffusion. As time moves ahead, the meridional sheared zonal flow causes flow next to the northern boundary to wrap around the periodic channel, whereas flow near the southern boundary is quiescent. Such differential flow acts to progressively increase the magnitude of the tracer gradient. Absent diffusion, this tracer gradient magnitude grows unbounded. In contrast, and as described by [Eckart \(1948\)](#), once the tracer gradient magnitudes are sufficiently large, diffusion damps the tracer gradients toward zero magnitude, which is precisely what we see in Figure 5.1 for the case with diffusion.

To be a bit more quantitative requires us to anticipate results derived later in this chapter. In Section 5.4.1 we show that advection leaves all powers of the tracer concentration unchanged, so that advection leaves the domain integrated tracer variance unchanged.⁴ In contrast, from Section 4.8.2 we showed that diffusion always reduces the magnitude of tracer powers, which means that it decreases the tracer variance. The key role for advection appears when characterizing the evolution of $|\nabla C|^2$, in which equation (5.32) shows that

$$\frac{1}{2} \frac{D|\nabla C|^2}{Dt} = -\nabla C \cdot \mathbf{S} \cdot \nabla C. \quad (5.8)$$

⁴Numerical discretization errors in Figure 5.1 cause a slight decrease in the tracer variance, but the decrease is negligible for our purposes.

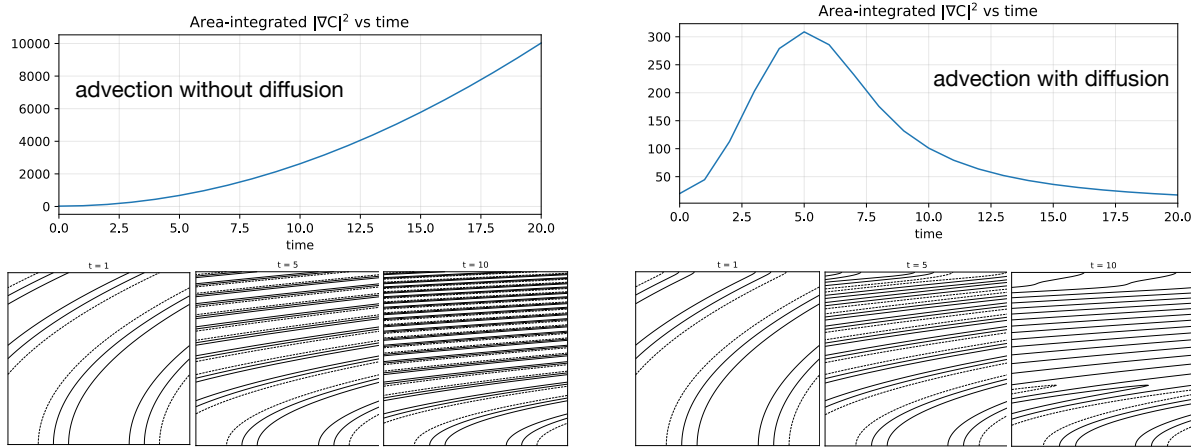


FIGURE 5.1: Illustrating Eckart’s stirring and mixing mechanism for a non-dimensional meridionally sheared zonal flow, $\bar{u} = \bar{y}^2$, in a zonally periodic and square channel with solid walls at the north and southern boundaries. The tracer satisfies homogeneous Neumann boundary conditions at the walls, so that the area integrated tracer concentration remains constant in time. The initial tracer profile is given by $C(x, y, 0) = \cos(2\pi x/L)$, in which the tracer contours are aligned parallel to the y -axis.³ The left panels show three snapshots of the tracer field ($t = 1, 5, 10$) for the case of advection without diffusion. Here, the area integrated tracer variance remains unchanged, and yet the squared tracer gradient grows monotonically as the tracer contours get progressively wrapped around the periodic channel so to introduce increasingly fine scale gradients. The right panel shows the case with a diffusivity, measured by $\text{Pe}^{-1} = 10^{-4}$, in which case $\int |\nabla C|^2 dA$ peaks around non-dimensional time 5 (the non-dimensional time step is $1/10$), and then drops thereafter. Evidently, once the tracer gradient reaches large enough magnitude, the mixing from Laplacian diffusion can efficiently act to mix the concentration. Note that the contours on each panel extend over the range ± 1 so that they are all directly comparable. However, the vertical range for the top panel is different, with the case on the right with diffusion having a much smaller vertical range than the left pure advection case.

For the prescribed zonal flow in Figure 5.1, we have the tracer gradient source term given by

$$-\nabla C \cdot \mathbf{S} \cdot \nabla C = -2\bar{y}\partial_{\bar{x}}C\partial_{\bar{y}}C. \quad (5.9)$$

The non-dimensional meridional position is positive, $\bar{y} > 0$, for this domain, and it weights properties in the north more than in the south. Evidently, a sufficient condition for growth of the squared tracer gradient is that the slope of a tracer contour line in the \bar{x} - \bar{y} plane is positive

$$\text{slope} = \left[\frac{\partial \bar{y}}{\partial \bar{x}} \right]_C = -\frac{\partial_{\bar{x}}C}{\partial_{\bar{y}}C}. \quad (5.10)$$

This slope is indeed positive throughout the simulation with pure advection. However, in the presence of diffusion, the source becomes negative around time 5 (see Figure 5.1), which then acts to reduce the tracer gradients. Apparently, the diffusion, primarily that acting in the far north, wipes out tracer gradients sufficiently to change the sign of the source.

5.1.3 Further study

Eckart’s conceptual description of stirring and mixing pervades our understanding of mixing within geophysical fluids, where turbulence is ubiquitous. [Young \(1999\)](#), [Müller and Garrett \(2002\)](#), and [Garrett \(2006\)](#) provide updated discussions drawing mostly on ocean examples though with relevance to all geophysical fluids.

The kinematic model in Figure 5.1 is inspired by a similar model considered by [Young \(1999\)](#), who used a circular domain rather than a zonally periodic channel. We chose the zonally

periodic channel in order to avoid the polar coordinate singularity arising at the center of the circle. Such coordinate singularities are a pesky feature of any numerical discretization, particularly for the Laplacian operator that takes on the polar coordinate form (see VOLUME 1)

$$\nabla^2 C = r^{-2} \partial_{\varphi\varphi} C + r^{-1} \partial_r (r \partial_r C). \quad (5.11)$$

5.2 Perfect fluid tracer advection

A **perfect fluid** is comprised of material fluid elements whose matter content and thermodynamic properties remain fixed. From the discussion of **molecular diffusion** in Chapter 4, we know that a perfect fluid can at most consist of a single matter constituent and uniform thermodynamic properties. The reason is that in the presence of multiple constituents with non-uniform concentrations, molecular motions irreversibly exchange matter and thermodynamic properties (e.g., temperature, specific entropy) among fluid elements. This exchange, or **mixing**, breaks the assumption of a perfect fluid. Nonetheless, we find many occasions to ignore molecular diffusion when focusing on macroscopic motions of the continuum fluid. Such is the case when considering the advection equation in the absence of mixing.

5.2.1 The advection equation

In the absence of mixing or other irreversible processes, the matter content of a fluid element remains fixed as the element moves within the fluid environment. Since the total mass of the element is also constant, then the tracer concentration remains constant and thus satisfies the reversible (source-free) **advection equation**

$$\frac{DC}{Dt} = (\partial_t + \mathbf{v} \cdot \nabla) C = 0. \quad (5.12)$$

The first equality relates the material time derivative to the Eulerian time derivative plus advective transport, with \mathbf{v} the **barycentric velocity** of a fluid element. We can convert the material form of the advection equation (5.12) into a **flux-form conservation law** or **tracer continuity equation** by combining with the mass continuity equation

$$\partial_t \rho + \nabla \cdot (\rho \mathbf{v}) = 0, \quad (5.13)$$

which yields

$$\partial_t (\rho C) + \nabla \cdot (\rho C \mathbf{v}) = 0. \quad (5.14)$$

The material form of the advection equation states that tracer concentration is a **material invariant** in the absence of sources or mixing. Hence, a general solution to the advection equation is

$$C(\mathbf{x}, t) = C[\mathbf{X}(0)], \quad (5.15)$$

where $\mathbf{X}(0)$ is the initial position of a fluid element that is at the position \mathbf{x} at time t . If we know the trajectories for all fluid elements and their initial tracer concentration, then we know the tracer concentration for all space and time. For those cases where trajectories are unknown (which is the normal case), it is useful to make use of the Eulerian form of the advection equation to deduce the evolution of tracer concentration.

5.2.2 Eulerian time tendencies from advection

At a point in the fluid, the advection equation (5.12) leads to the Eulerian time tendency for tracer concentration

$$\partial_t C = -\mathbf{v} \cdot \nabla C. \quad (5.16)$$

Geometrically, the tendency arises from the projection of the fluid velocity onto the normal to surfaces of constant tracer concentration (isosurfaces). The concentration remains fixed in time (steady) at points where the velocity is parallel to tracer surfaces.

From the flux-form advection equation (5.14), the density-weighted tracer concentration (the tracer mass per volume) has an Eulerian time tendency given by the convergence of the advective flux

$$\partial_t (\rho C) = -\nabla \cdot (\rho C \mathbf{v}). \quad (5.17)$$

The tendency vanishes at a point if there is no convergence of tracer mass towards the point.

5.2.3 Impermeability property of tracer isosurfaces

We offer a geometric interpretation of the advection equation

$$(\partial_t + \mathbf{v} \cdot \nabla) C = 0, \quad (5.18)$$

following the discussion of dia-surface transport in Section 2.4. For this purpose, introduce the unit normal on a tracer isosurface

$$\hat{\mathbf{n}} = \frac{\nabla C}{|\nabla C|} \quad (5.19)$$

and the normal projection for the velocity of a point on that surface

$$\mathbf{v}^{(c)} \cdot \hat{\mathbf{n}} = -\frac{\partial_t C}{|\nabla C|}. \quad (5.20)$$

The advection equation (5.18) thus can be written as an impermeability condition for a tracer isosurface

$$\rho (\mathbf{v} - \mathbf{v}^{(c)}) \cdot \hat{\mathbf{n}} = 0 \quad \text{on } C \text{ isosurfaces.} \quad (5.21)$$

We encountered this condition in VOLUME 1 when studying the kinematics of a moving material surface. Hence, in the absence of mixing, tracer isosurfaces are indeed material surfaces since they allow no fluid elements, moving with the fluid velocity \mathbf{v} , to cross them. This is an important kinematic result that is extended in Section 5.6.5 to include effects from an eddy induced velocity.

5.3 Worked example: hyperbolic flow

Consider the following two-dimensional flow in a constant density fluid

$$\mathbf{u} = \hat{\mathbf{z}} \times \nabla \psi \quad \text{with} \quad \psi = -\alpha x y \implies \mathbf{u} = \alpha (\hat{\mathbf{x}} x - \hat{\mathbf{y}} y), \quad (5.22)$$

where α is a constant with dimensions of inverse time. This horizontally non-divergent hyperbolic flow stretches tracer contours along the x -axis and compresses along the y -axis. We depict this flow in Figure 5.2, which we studied as part of fluid kinematics in VOLUME 1. This flow is simple enough to allow for an exact solution to the fluid particle trajectories, which then

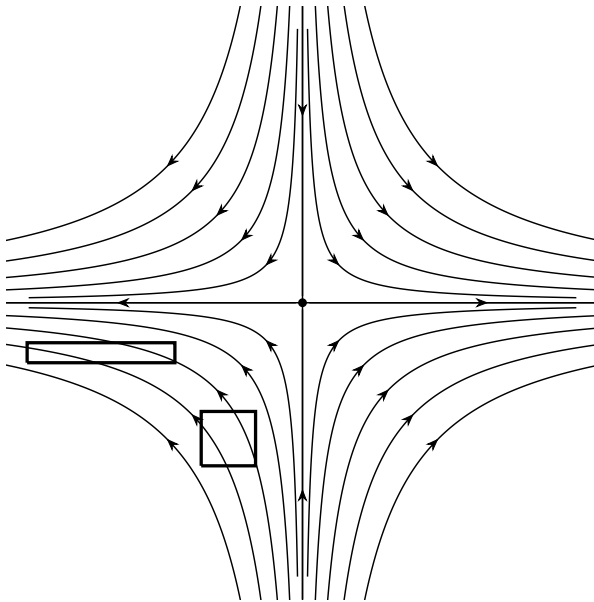


FIGURE 5.2: An ensemble of hyperbolic fluid particle trajectories defined from the horizontally non-divergent velocity field, $\mathbf{u} = \alpha(\hat{\mathbf{x}}x - \hat{\mathbf{y}}y)$ and streamfunction, $\psi = -\alpha xy$. The flow stretches along the x direction and compresses along the y direction, as depicted by the material square region evolving to a rectangular region.

means we can provide an exact solution to the tracer advection equation

$$(\partial_t + \alpha x \partial_x - \alpha y \partial_y)C = 0. \quad (5.23)$$

5.3.1 Solution via the fluid particle trajectories

A fluid particle trajectory, $\mathbf{X}(t)$, is found through time integrating

$$\frac{dX}{dt} = \alpha X \implies X(t) = X(0) e^{\alpha t} \quad (5.24a)$$

$$\frac{dY}{dt} = -\alpha Y \implies Y(t) = Y(0) e^{-\alpha t}, \quad (5.24b)$$

where $\hat{\mathbf{x}}X(0) + \hat{\mathbf{y}}Y(0)$ is the initial position for the fluid particle. Knowing the fluid particle trajectory allows us to determine the tracer concentration at any time, t , given the initial concentration, $C(x, y, 0)$. We do so by noting that at time t , the trajectory that passes through the point (x, y) started at at time $t = 0$ at the point

$$\hat{\mathbf{x}}X(0) + \hat{\mathbf{y}}Y(0) = \hat{\mathbf{x}}x e^{-\alpha t} + \hat{\mathbf{y}}y e^{\alpha t}. \quad (5.25)$$

Consequently, the concentration is

$$C(x, y, t) = C(x e^{-\alpha t}, y e^{\alpha t}, 0). \quad (5.26)$$

Referring to Figure 5.2, we know the concentration in the rectangular box region at time t , if we know the concentration in the square box at some earlier time.

5.3.2 Further study

This example is taken from Section 4.3 of [Young \(1999\)](#). Furthermore, we provide details for the Lagrangian coordinate representation in VOLUME 1, including an expression for the diffusion operator in Lagrangian coordinates.

5.4 Mathematical properties of tracer advection

We now explore various mathematical properties of the advection equation. For that purpose, recall the mass continuity equation (5.13) and flux-form tracer advection equation (5.17)

$$\partial_t \rho + \nabla \cdot (\rho \mathbf{v}) = 0 \quad (5.27a)$$

$$\partial_t (\rho C) + \nabla \cdot (\rho C \mathbf{v}) = 0. \quad (5.27b)$$

These equations manifest compatibility whereby the tracer equation (5.27b) reduces to the mass continuity equation (5.27a) if the tracer concentration is spatially uniform.

5.4.1 Material constancy of C^Γ

C^Γ , for any constant Γ , is materially constant due to the material constancy of C . We show this property mathematically by noting that the chain rule holds for a material time derivative, so that

$$\frac{DC^\Gamma}{Dt} = \Gamma C^{\Gamma-1} \frac{DC}{Dt} = 0. \quad (5.28)$$

Likewise, making use of the Eulerian form yields

$$\partial_t C^\Gamma + \mathbf{v} \cdot \nabla C^\Gamma = \Gamma C^{\Gamma-1} [\partial_t C + \mathbf{v} \cdot \nabla C] = 0. \quad (5.29)$$

We conclude that advection, in the absence of diffusion, serves to reversibly transport the tracer concentration without altering any of its powers. Correspondingly, all tracer moments are untouched by advection.

5.4.2 Evolution of squared tracer gradient

As noted at the start of Section 5.1, some flows can enhance the magnitude of the tracer concentration gradient, $|\nabla C|^2 = \partial_m C \delta^{mn} \partial_n C$. To mathematically manifest that process, consider the following equation for the evolution of the squared tracer gradient under the effects of advection

$$(1/2) \partial_t (\partial_m C \delta^{mn} \partial_n C) = \partial_m C \delta^{mn} \partial_n \partial_t C \quad (5.30a)$$

$$= -\partial_m C \delta^{mn} \partial_n (v^k \partial_k C) \quad (5.30b)$$

$$= -\partial_m C \delta^{mn} (v^k \partial_k \partial_n C + \partial_n v^k \partial_k C) \quad (5.30c)$$

$$= -(1/2) v^k \partial_k (\partial_m C \delta^{mn} \partial_n C) - \partial_m C \delta^{mn} G^k_n \partial_k C \quad (5.30d)$$

$$= -(1/2) (\mathbf{v} \cdot \nabla) |\nabla C|^2 - \partial_m C \delta^{mn} S^k_n \partial_k C \quad (5.30e)$$

$$= -(1/2) (\mathbf{v} \cdot \nabla) |\nabla C|^2 - \nabla C \cdot \mathbf{S} \cdot \nabla C. \quad (5.30f)$$

The second equality made use of the advection equation, $\partial_t C = -v^k \partial_k C$, and then we introduced the velocity gradient tensor, \mathbf{G} , from our study of flow kinematics in VOLUME 1, as well as its

symmetric component, the strain rate tensor, \mathbf{S} ,

$$G^m{}_n = \partial_n v^m \quad \text{and} \quad S^m{}_n = (G^m{}_n + G_n{}^m)/2. \quad (5.31)$$

We are thus led to the material evolution equation

$$\frac{1}{2} \frac{D|\nabla C|^2}{Dt} = -\nabla C \cdot \mathbf{S} \cdot \nabla C. \quad (5.32)$$

The strain rate tensor is symmetric and yet it is not positive-definite. Hence, we can have either growth or decay of the squared tracer gradient depending on details of the velocity gradient and tracer gradient.

Much of the stirring by turbulent geophysical fluid flows occurs on quasi-horizontal surfaces. Following [Okubo \(1970\)](#); [Weiss \(1991\)](#); [Lapeyre et al. \(1999\)](#); [Balwada et al. \(2021\)](#), we find it useful to examine the evolution of $|\nabla C|^2$ in a two-dimensional flow. In this case it is relatively straightforward to diagonalize the strain rate tensor.⁵ The two-dimensional rate of strain tensor has the following eigenvalues

$$\lambda = (\Delta \pm \sigma)/2 \quad \text{with} \quad \Delta = \nabla \cdot \mathbf{u} \quad \text{and} \quad \sigma^2 = (\partial_x v + \partial_y u)^2 + (\partial_x u - \partial_y v)^2, \quad (5.33)$$

with Δ the horizontal divergence and σ the magnitude of the strain rate. By rotating to directions defined by the eigenvectors, we simplify the source in the evolution equation (5.32) to read

$$\frac{D|\nabla C|^2}{Dt} = -(\partial_{\bar{x}} C)^2 (\Delta + \sigma) - (\partial_{\bar{y}} C)^2 (\Delta - \sigma) = -\Delta |\nabla C|^2 - \sigma [(\partial_{\bar{x}} C)^2 - (\partial_{\bar{y}} C)^2], \quad (5.34)$$

where \bar{x} and \bar{y} are the orthogonal coordinates aligned with the directions defined by the eigenvectors. Evidently, any horizontal flow convergence, $\Delta < 0$, leads to $|\nabla C|^2$ growth, whereas the strain magnitude, $\sigma \geq 0$, leads to growth or decay depending on the relative magnitude of the tracer gradient along the eigendirections.

5.4.3 Eddy-induced and residual mean

The mass density time tendency

$$\partial_t \rho = -\nabla \cdot (\mathbf{v} \rho) \quad (5.35)$$

remains unchanged if the advective mass flux, $\rho \mathbf{v}$ (dimensions of mass per time per area), is modified by the addition of a total curl

$$\rho \mathbf{v} \rightarrow \rho \mathbf{v}^\dagger = \rho \mathbf{v} + \nabla \times (\rho \Psi^*). \quad (5.36)$$

The arbitrariness manifest in equation (5.36) is known as a [gauge symmetry](#). The additional mass flux, $\nabla \times (\rho \Psi^*)$, leads to no accumulation of mass at a point since it has zero divergence. In the case of a Boussinesq ocean with ρ set to a constant ρ_0 , the divergent-free velocity $\nabla \times \Psi^*$ leads to zero accumulation of volume at a point.

The non-divergent mass flux

$$\rho \mathbf{v}^* \equiv \nabla \times (\rho \Psi^*) \quad (5.37)$$

often arises when we decompose the mass flux into a mean and non-divergent eddy fluctuations.

⁵The strain rate tensor is symmetric so it has real and orthogonal eigenvectors. The three dimensional case is algebraically more tedious than the two dimensional case considered here.

In that context, we use the following terminology:

$$\mathbf{v} = \text{Eulerian mean velocity} \quad (5.38a)$$

$$\rho \mathbf{v} = \text{Eulerian mean mass flux} \quad (5.38b)$$

$$\mathbf{v}^* = \text{eddy-induced velocity} \quad (5.38c)$$

$$\rho \Psi^* = \text{eddy-induced mass streamfunction} \quad (5.38d)$$

$$\rho \mathbf{v}^* = \nabla \times (\rho \Psi^*) = \text{eddy-induced mass flux} \quad (5.38e)$$

$$\mathbf{v}^\dagger = \mathbf{v} + \mathbf{v}^* = \text{residual mean velocity} \quad (5.38f)$$

$$\rho \mathbf{v}^\dagger = \rho (\mathbf{v} + \mathbf{v}^*) = \text{residual mean mass flux.} \quad (5.38g)$$

The name “residual mean” is motivated since the **residual mean velocity**, $\mathbf{v}^\dagger = \mathbf{v} + \mathbf{v}^*$, is often smaller than either term individually. That is, the eddy contribution often compensates for the mean, with sum of the mean and eddy representing a residual. We study particular forms of the parameterized eddy induced velocity in Chapter 7.

5.4.4 Advection tracer fluxes and skew tracer fluxes

Following from the previous discussion, we consider the advection equation with the advective tracer transport determined by the residual mean velocity

$$\partial_t (\rho C) + \nabla \cdot (\rho C \mathbf{v}^\dagger) = 0. \quad (5.39)$$

Given the form (5.37) for the eddy mass flux $\rho \mathbf{v}^*$, we can write the **advective tracer flux** as

$$\rho C \mathbf{v}^\dagger = C (\rho \mathbf{v} + \rho \mathbf{v}^*) \quad (5.40a)$$

$$= C \rho \mathbf{v} + C \nabla \times (\rho \Psi^*) \quad (5.40b)$$

$$= C \rho \mathbf{v} + \nabla \times (C \rho \Psi^*) - \nabla C \times \rho \Psi^*. \quad (5.40c)$$

It is the convergence of the tracer flux that determines the time tendency, in which the total curl plays no role

$$-\nabla \cdot (\rho C \mathbf{v}^\dagger) = -\nabla \cdot (\rho C \mathbf{v} + \rho C \mathbf{v}^*) \quad (5.41a)$$

$$= -\nabla \cdot (\rho C \mathbf{v} - \nabla C \times \rho \Psi^*). \quad (5.41b)$$

That is, the convergence of the advective tracer flux equals to the convergence of the **skew tracer flux**

$$\underbrace{-\nabla \cdot (\rho C \mathbf{v}^*)}_{\text{advective flux convergence}} = \underbrace{-\nabla \cdot (-\nabla C \times \rho \Psi^*)}_{\text{skew flux convergence}} \quad (5.42)$$

since the advective flux and skew flux differ by a rotational flux,

$$\mathbf{J}^{\text{adv}} = \mathbf{J}^{\text{skew}} + \mathbf{J}^{\text{rot}}, \quad (5.43)$$

where

$$\mathbf{J}^{\text{adv}} = C \rho \mathbf{v}^* \quad \text{and} \quad \mathbf{J}^{\text{skew}} = -\nabla C \times \rho \Psi^* \quad \text{and} \quad \mathbf{J}^{\text{rot}} = \nabla \times (\rho C \Psi^*). \quad (5.44)$$

Notably, the skew tracer flux is neither upgradient nor downgradient. Rather, it is oriented parallel to isosurfaces of tracer concentration (see Figure 5.3)

$$\nabla C \cdot \mathbf{J}^{\text{skew}} = \nabla C \cdot (-\nabla C \times \rho \Psi^*) = 0. \quad (5.45)$$

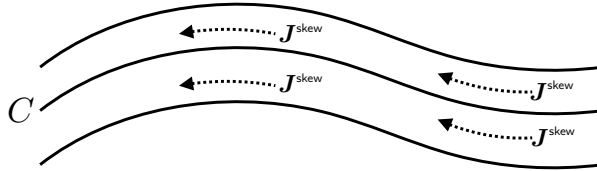


FIGURE 5.3: Skew tracer flux (dotted lines with arrows) for a tracer concentration, C , are oriented parallel to lines of constant tracer concentration (tracer isolines are the solid lines). Even though the skew fluxes are aligned with tracer contours, skew fluxes generally affect a time change to the tracer concentration through their convergence.

5.4.5 Skew diffusion

Introducing tensor labels brings the skew tracer flux into the form

$$(\mathbf{J}^{\text{skew}})^m = -(\nabla C \times \rho \Psi^*)^m \quad (5.46a)$$

$$= -\epsilon^{mnp} \partial_n C \rho \Psi_p^* \quad (5.46b)$$

$$\equiv -\rho A^{mn} \partial_n C, \quad (5.46c)$$

where we defined the anti-symmetric skew diffusion tensor

$$A^{mn} \equiv \epsilon^{mnp} \Psi_p^* \Rightarrow \mathbf{A} = \begin{bmatrix} 0 & \Psi_3^* & -\Psi_2^* \\ -\Psi_3^* & 0 & \Psi_1^* \\ \Psi_2^* & -\Psi_1^* & 0 \end{bmatrix}. \quad (5.47)$$

Evidently, tracer advection by a non-divergent mass flux is equivalent to skew-diffusion through the action of an anti-symmetric tensor.

Skew and advective fluxes possess the following dual properties.

- **DERIVATIVE OPERATOR:** The skew flux is proportional to the vector streamfunction and the gradient of the tracer, whereas the advective flux is related to the curl of the streamfunction and the value of the tracer concentration. In effect, the fluxes swap their placement of the derivative operator. Correspondingly, the advective flux vanishes if the velocity vanishes, whereas the skew flux vanishes if the tracer gradient vanishes (just as for a diffusive flux).
- **FLUX ORIENTATION:** The orientation of the advective flux is determined by the velocity field, which is oriented according to trajectories of fluid particles. This orientation is the same regardless of the tracer. In contrast, a skew tracer flux is directed along lines of constant tracer; i.e., it is neither upgradient nor downgradient. Hence, orientation of the skew flux is directly tied to the tracer field, with each tracer yielding a generally distinct flux orientation. The distinct orientations of the advective and skew fluxes can cause confusion. We explore features of these geometric distinctions in Section 6.4 in studying eddy induced tracer fluxes.

- MATERIAL FLUX: Fluid elements carry a particular amount of trace matter so that an advective flux of a material tracer measures the passage of matter across an area per unit time (dimensions of mass per area per time). In contrast, a skew flux is not interpreted as the passage of matter across an area per time. This distinction is particularly important when deriving boundary conditions discussed in Section 5.5.3.

In Section 5.5 we pursue the above points to further reveal the dual relation between advective fluxes and skew fluxes.

5.4.6 A comment about skew fluxes and Lagrangian kinematics

The advective tracer flux and skew tracer flux are very distinct vectors and we further explore the distinction in Sections 5.5 and 6.4. As detailed in each of those sections, it is a matter of convenience how one chooses to mathematically formulate the Eulerian tracer equation since the advective flux and skew flux lead to the same tracer evolution. Furthermore, the choice to formulate the tracer equation in terms of a skew flux in no way eliminates the Lagrangian fluid particle perspective. That is, we still conceive of fluid particles as moving through the fluid transporting tracer as part of this motion, regardless of how we choose to mathematically describe the consequences of that transport.

5.4.7 Further reading

The uses of residual-mean transport are many and varied in the ocean and atmospheric literature. [Vallis \(2017\)](#) offers a thorough and pedagogical treatment. Skew diffusion is treated in [Moffatt \(1983\)](#), in which he raises the connection to rotating and/or magnetic fluids. [Middleton and Loder \(1989\)](#) applied these ideas to ocean gravity waves, tides, and Rossby waves. [Griffies \(1998\)](#) applied these ideas to the methods used for parameterizing tracer transport from ocean mesoscale eddies.

5.5 Advection and skewson

We introduced skew diffusion in Section 5.4.5 and will again encounter it in Chapters 6 and 7. Following the terminology of Section 9.2 of [Griffies \(2004\)](#), we refer to **skewson** as any process that leads to tracer transport via skew fluxes, with skew diffusion a particular example. There are occasions where it is conceptually and operationally more convenient to use advective fluxes, such as when considering the transport of tracers by the flow field explicitly resolved by a numerical simulation. In contrast, skew fluxes are sometimes more convenient for certain subgrid scale eddy parameterizations, such as the one discussed in Section 7.1. We here consider facets of advection and skewson for those interested in diving deeper into the mathematical physics.

5.5.1 Choosing a gauge

Consider an arbitrary divergent-free mass transport

$$\nabla \cdot (\rho \mathbf{v}^*) = 0, \quad (5.48)$$

where the divergent-free constraint is satisfied by introducing a vector streamfunction

$$\rho \mathbf{v}^* = \nabla \times (\rho \Psi^*). \quad (5.49)$$

The streamfunction is arbitrary up to a gauge transformation

$$\rho \Psi' = \rho \Psi^* + \nabla(\rho \Lambda), \quad (5.50)$$

where Λ is a gauge function.

Changes to the skew flux under a gauge transformation

Although the velocity is invariant up to an arbitrary gauge function, the skew flux, $\mathbf{J}^{\text{skew}} = -\nabla C \times \rho \Psi^*$, changes. Nonetheless, the divergence of the skew flux is invariant, as we see by noting that

$$\nabla C \times [\rho \Psi^* + \nabla(\rho \Lambda)] = \nabla C \times (\rho \Psi^*) + \nabla \times [C \nabla(\rho \Lambda)]. \quad (5.51)$$

and since $\nabla \cdot \nabla \times [C \nabla(\rho \Lambda)] = 0$, the flux divergence, $\nabla \cdot \mathbf{J}^{\text{skew}}$, remains unchanged.

Coulomb gauge

We have some freedom in specifying the gauge function. One choice is to set $\Lambda = 0$. However, there are occasions in which it is useful to set the gauge function in a manner to cancel unwanted terms. The Coulomb gauge is commonly used in electrodynamics (e.g., [Jackson \(1975\)](#); [Griffiths \(1981\)](#)), which is defined by setting

$$\nabla \cdot (\rho \Psi^*) = 0. \quad (5.52)$$

Making use of the vector calculus identity (see VOLUME 1 for a proof)

$$\nabla \times (\nabla \times \mathbf{F}) = -\nabla^2 \mathbf{F} + \nabla(\nabla \cdot \mathbf{F}), \quad (5.53)$$

leads to Poisson's equation for the vector potential

$$\nabla^2(\rho \Psi^*) = -\nabla \times (\rho \mathbf{v}^*). \quad (5.54)$$

In the absence of boundaries, this equation has a Coulomb-Ampere solution comprised of the convolution of the source with the free-space Green's function⁶

$$\rho(\mathbf{x}, t) \Psi^*(\mathbf{x}, t) = \int \frac{\nabla \times [\rho(\mathbf{x}', t) \mathbf{v}^*(\mathbf{x}', t)]}{4 \pi |\mathbf{x} - \mathbf{x}'|} dV', \quad (5.55)$$

where dV' is the volume element for integration over the test points, \mathbf{x}' . We know of no geophysical fluid application making use of the Coulomb gauge, perhaps because it can be difficult to determine an expression for $\rho \Psi^*$ in the presence of boundaries.

5.5.2 Vertical gauge

As introduced in VOLUME 1 as part of the kinematics in non-divergent flows, a gauge commonly used for eddy parameterizations (Section 7.1) sets to zero one of the three components of the vector streamfunction. This gauge choice is available since there are only two independent functional degrees of freedom available from a divergence-free vector. A common choice is the

⁶See the chapter in VOLUME 1 that discusses elliptic partial differential equation and their corresponding Green's function solutions.

vertical gauge in which

$$\Psi_3^* = 0. \quad (5.56)$$

To further specify the vertical gauge we invert the relations

$$\rho u^* = -\partial_z(\rho\Psi_2^*) \quad \text{and} \quad \rho v^* = \partial_z(\rho\Psi_1^*) \quad \text{and} \quad \rho w^* = \partial_x(\rho\Psi_2^*) - \partial_y(\rho\Psi_1^*), \quad (5.57)$$

to render the vector streamfunction

$$\rho \Psi^* = \hat{z} \times \int_{-H}^z \rho \mathbf{u}^* dz' = \hat{z} \times \underline{\mathbf{U}}^{(\rho)} \quad (5.58)$$

where

$$\underline{\mathbf{U}}^{(\rho)}(z) = \int_{\eta_b}^z \rho \mathbf{u}^* dz' \quad (5.59)$$

is the horizontal mass transport associated with \mathbf{u}^* passing between the bottom and a vertical position, $z \geq \eta_b$. The anti-symmetric stirring tensor for the vertical gauge is given by

$$\rho A^{mn} = \begin{pmatrix} 0 & 0 & \underline{U}^{(\rho)} \\ 0 & 0 & \underline{V}^{(\rho)} \\ -\underline{U}^{(\rho)} & -\underline{V}^{(\rho)} & 0 \end{pmatrix}, \quad (5.60)$$

and the corresponding skew, rotational, and advective fluxes are

$$\mathbf{J}^{\text{skew}} = -\underline{\mathbf{U}}^{(\rho)} \partial_z C + \hat{z} \underline{\mathbf{U}}^{(\rho)} \cdot \nabla_h C \quad (5.61a)$$

$$\mathbf{J}^{\text{rot}} = \partial_z(C \underline{\mathbf{U}}^{(\rho)}) - \hat{z} \nabla_h \cdot (C \underline{\mathbf{U}}^{(\rho)}) \quad (5.61b)$$

$$\mathbf{J}^{\text{adv}} = C(\partial_z \underline{\mathbf{U}}^{(\rho)}) - \hat{z} C \nabla_h \cdot \underline{\mathbf{U}}^{(\rho)}. \quad (5.61c)$$

Note that the identity $\mathbf{J}^{\text{adv}} = \mathbf{J}^{\text{skew}} + \mathbf{J}^{\text{rot}}$ is manifest in these expressions. The horizontal components to the skew flux vanish when the tracer is uniform in the vertical, and the vertical skew flux vanishes with a horizontally uniform tracer field. These properties manifest the skewed nature of the fluxes.

5.5.3 Boundary conditions

We assume that all external domain boundaries are material in regards to the eddy-induced velocity, \mathbf{v}^* . Furthermore, even for moving domain boundaries, we assume that the suite of kinematic boundary conditions is based on the **barycentric velocity**, \mathbf{v} , introduced in VOLUME 1. Consequently, \mathbf{v}^* satisfies the no-normal flow condition even on moving boundaries

$$\hat{\mathbf{n}} \cdot \mathbf{v}^* = 0 \quad \text{external domain boundaries.} \quad (5.62)$$

As we discuss in Section 5.6.1, this boundary condition is required for the eddy-induced velocity to have zero impact on the total mass of an arbitrary tracer within the fluid domain.

Correspondingly, the advective tracer flux also satisfies a no-normal boundary condition on all external boundaries

$$\hat{\mathbf{n}} \cdot \mathbf{J}^{\text{adv}} = \hat{\mathbf{n}} \cdot \mathbf{v}^* \rho C = 0. \quad (5.63)$$

The corresponding boundary condition for the skew flux is found by inserting the relation (5.43)

into the advective flux boundary condition (5.63) to render

$$\hat{\mathbf{n}} \cdot \mathbf{J}^{\text{adv}} = \hat{\mathbf{n}} \cdot [\mathbf{J}^{\text{skew}} + \mathbf{J}^{\text{rot}}] = 0. \quad (5.64)$$

Hence, the skew flux generally has a non-zero normal component at the solid boundaries as determined by the rotational flux

$$\hat{\mathbf{n}} \cdot \mathbf{J}^{\text{skew}} = -\hat{\mathbf{n}} \cdot \mathbf{J}^{\text{rot}}. \quad (5.65)$$

Even so, there might be occasions in which $\hat{\mathbf{n}} \cdot \mathbf{J}^{\text{skew}} = 0$, which is ensured so long as

$$(-\nabla C \times \rho \Psi^*) \cdot \hat{\mathbf{n}} = -(\rho \Psi^* \times \hat{\mathbf{n}}) \cdot \nabla C = 0. \quad (5.66)$$

A sufficient condition is to have $\Psi^* \times \hat{\mathbf{n}} = 0$, in which case the vector streamfunction is parallel to the boundary normal. An alternative sufficient condition is to have the streamfunction vanish at the boundary. Further details for boundary conditions depend on physical properties of the velocity \mathbf{v}^* . We discuss one example in Section 7.1 as prescribed by the [Gent et al. \(1995\)](#) mesoscale eddy parameterization.

5.6 Finite volume budgets with eddy velocities

In this section we examine how an [eddy-induced velocity](#) modifies the budgets for fluid mass and tracer mass in finite domains. We start by writing the local/differential mass and tracer budgets in the form

$$\partial_t \rho + \nabla \cdot (\rho \mathbf{v}^\dagger) = 0 \quad (5.67a)$$

$$\partial_t (\rho C) + \nabla \cdot (\rho \mathbf{v}^\dagger C + \mathbf{J}^{\text{diff}}) = 0, \quad (5.67b)$$

where (see Section 5.5)

$$\mathbf{v}^\dagger = \mathbf{v} + \mathbf{v}^* \quad \text{and} \quad \nabla \cdot (\rho \mathbf{v}^*) = 0, \quad (5.68)$$

and where \mathbf{J}^{diff} is a subgrid scale flux encompassing all processes, such as diffusion and boundary conditions, that are not represented by an eddy-induced advection. Given that $\nabla \cdot (\rho \mathbf{v}^*) = 0$ in the fluid interior and $\mathbf{v}^* \cdot \hat{\mathbf{n}} = 0$ along all boundaries (including moving boundaries), the mass budget (5.67a) can be written in the equivalent manners

$$\partial_t \rho + \nabla \cdot (\rho \mathbf{v}^\dagger) = \partial_t \rho + \nabla \cdot (\rho \mathbf{v}) = 0. \quad (5.69)$$

That is, the eddy-induced velocity does not lead to any local or global sources of fluid mass. This property is central to the budget analysis in this section.

As shown in the following, the finite volume budgets for fluid mass and tracer mass also make use of the residual mean velocity, \mathbf{v}^\dagger . That result is not surprising, since the finite volume budgets are consistent with the differential budgets (5.67a) and (5.67b). Nonetheless, it is useful to expose the details as they appear in many budget analysis applications, such as the water mass and tracer mass analysis of Chapter 9. We furthermore explore how the budgets for tracer mass appear when formulated using advective fluxes versus skew fluxes. As we show, the finite volume budgets are consistent across the variety of formulations only if the eddy velocity and eddy vector streamfunction satisfy boundary conditions detailed in Section 5.5.3.

5.6.1 Advection flux formulation

Making use of the tracer equation (5.67b) in the **Leibniz-Reynolds transport theorem** (see VOLUME 1) renders the finite volume tracer mass budget for an arbitrary domain, \mathcal{R}

$$\frac{d}{dt} \left[\int_{\mathcal{R}} \rho C dV \right] = - \oint_{\partial\mathcal{R}} \left[\rho C (\mathbf{v}^\dagger - \mathbf{v}^{(b)}) + \mathbf{J}^{\text{diff}} \right] \cdot \hat{\mathbf{n}} dS, \quad (5.70)$$

where $\mathbf{v}^{(b)}$ is the velocity of a point on the domain boundary. Appearance of the residual mean velocity, \mathbf{v}^\dagger , in the finite volume budget (5.70) follows from its appearance in the local tracer budget (5.67b). We thus see that the eddy-induced velocity impacts on the tracer mass budget for an arbitrary domain. However, its impacts disappear when integrating over a closed or periodic fluid domain so long as

$$\mathbf{v}^* \cdot \hat{\mathbf{n}} = 0 \quad \text{on all boundaries.} \quad (5.71)$$

We already encountered this boundary condition in Section 5.5.3. It holds on all boundaries, including those such as the ocean free surface that are time dependent and/or permeable. It is required if we assume the eddy-induced velocity does not modify the mass of any tracer in the full fluid domain. That assumption is generally made for eddy-induced velocities such as those associated with mesoscale and submesoscale eddies in the ocean (see Section 7.3).

Setting the tracer concentration to a constant in equation (5.70) leads to the fluid mass budget

$$\frac{d}{dt} \left[\int_{\mathcal{R}} \rho dV \right] = - \oint_{\partial\mathcal{R}} \rho (\mathbf{v}^\dagger - \mathbf{v}^{(b)}) \cdot \hat{\mathbf{n}} dS, \quad (5.72)$$

where we set the diffusive tracer flux, \mathbf{J}^{diff} , to zero since there is no diffusion of fluid mass between fluid elements.⁷ As for the differential expression (5.67a), the mass budget for any domain is not changed by the eddy-induced velocity since

$$\nabla \cdot (\rho \mathbf{v}^*) = 0 \implies \oint_{\partial\mathcal{R}} \rho \mathbf{v}^* \cdot \hat{\mathbf{n}} dS = 0, \quad (5.73)$$

so that the mass budget is given by

$$\frac{d}{dt} \left[\int_{\mathcal{R}} \rho dV \right] = - \oint_{\partial\mathcal{R}} \left[\rho (\mathbf{v}^\dagger - \mathbf{v}^{(b)}) \right] \cdot \hat{\mathbf{n}} dS = - \oint_{\partial\mathcal{R}} [\rho (\mathbf{v} - \mathbf{v}^{(b)})] \cdot \hat{\mathbf{n}} dS \quad (5.74)$$

Hence, the eddy velocity contribution to the mass budget for any finite region vanishes, which is expected since it provides no local nor finite volume mass source to the fluid. Furthermore, one may choose to diagnose the right hand side of the mass budget in either the residual mean or Eulerian mean form. The choice is based on convenience, such as whether one has easier access to the residual mean velocity or the Eulerian mean velocity. Although the patterns of the fluxes across any particular boundary differs if $\mathbf{v}^* \neq 0$, the accumulation of mass within the region is identical for the two formulations.

⁷We emphasized this property when discussing the **barycentric velocity** as part of material tracer conservation in VOLUME 1.

5.6.2 Skew flux formulation

Now consider the perspective afforded by the skew flux formulation from Section 5.5. Here we decompose the advective tracer flux according to

$$C \rho \mathbf{v}^\dagger = C \rho \mathbf{v} - \nabla C \times \rho \Psi^* + \nabla \times (C \rho \Psi^*) = C \rho \mathbf{v} + \mathbf{J}^{\text{skew}} + \mathbf{J}^{\text{rot}}, \quad (5.75)$$

where we introduced the skew tracer flux and rotational flux arising from the eddy-induced streamfunction

$$\mathbf{J}^{\text{skew}} = -\nabla C \times (\rho \Psi^*) \quad \text{and} \quad \mathbf{J}^{\text{rot}} = \nabla \times (\rho C \Psi^*). \quad (5.76)$$

The flux-form tracer equation is thus given by

$$\partial_t(\rho C) + \nabla \cdot [\rho C \mathbf{v} + \mathbf{J}^{\text{skew}} + \mathbf{J}^{\text{diff}}] = 0, \quad (5.77)$$

where $\nabla \cdot \mathbf{J}^{\text{rot}} = 0$ and so \mathbf{J}^{rot} does not affect the tracer budget. The corresponding finite volume tracer mass budget is

$$\frac{d}{dt} \left[\int_{\mathcal{R}} \rho C \, dV \right] = - \oint_{\partial \mathcal{R}} [\rho C (\mathbf{v} - \mathbf{v}^{(b)}) - \nabla C \times (\rho \Psi^*) + \mathbf{J}^{\text{diff}}] \cdot \hat{\mathbf{n}} \, d\mathcal{S}. \quad (5.78)$$

In this form, the contribution from the eddy induced transport is included inside the skew tracer flux rather than in the residual mean advective tracer flux. Setting C to a constant reveals the mass budget as in the second form of equation (5.74).

5.6.3 Domain with a tracer boundary

We now apply the previous general budget discussion to a specific domain that anticipates the more complete budget analysis provided in Section 9.9 as part of our study of water mass analysis. Here, as in Figure 5.4, we consider the fluid mass and tracer mass within an ocean region with at least one of its bounds determined by an isosurface of constant tracer concentration.

Advective formulation

The tracer mass budget written using the advective formulation (5.70) is given by

$$\frac{d}{dt} \left[\int_{\mathcal{R}} \rho C \, dV \right] = \int_{\partial \Omega_{\text{surf}}(\tilde{C})} Q_m C \, dA - \tilde{C} \int_{C=\tilde{C}} \rho (\mathbf{v}^\dagger - \mathbf{v}^{(b)}) \cdot \hat{\mathbf{n}} \, d\mathcal{S} - \oint_{\partial \mathcal{R}} \mathbf{J}^{\text{diff}} \cdot \hat{\mathbf{n}} \, d\mathcal{S}. \quad (5.79)$$

For the first right hand side term we made use of the surface kinematic boundary condition from our discussion of mass budgets in VOLUME 1, with $Q_m \, dA$ the mass per time crossing the surface interface and where dA is the horizontal projection of the interface area element, $d\mathcal{S}$. We also made use of the exterior boundary condition (5.71) for the eddy-induced velocity. For the second term, we pulled the tracer concentration outside of the boundary integral over the $C = \tilde{C}$ interface, since the concentration is fixed at \tilde{C} on this interface.

The mass budget for this region, also formulated using advective fluxes, is given by

$$\frac{d}{dt} \left[\int_{\mathcal{R}} \rho \, dV \right] = \int_{\partial \Omega_{\text{surf}}(\tilde{C})} Q_m \, dA - \int_{C=\tilde{C}} \rho (\mathbf{v}^\dagger - \mathbf{v}^{(b)}) \cdot \hat{\mathbf{n}} \, d\mathcal{S}. \quad (5.80)$$

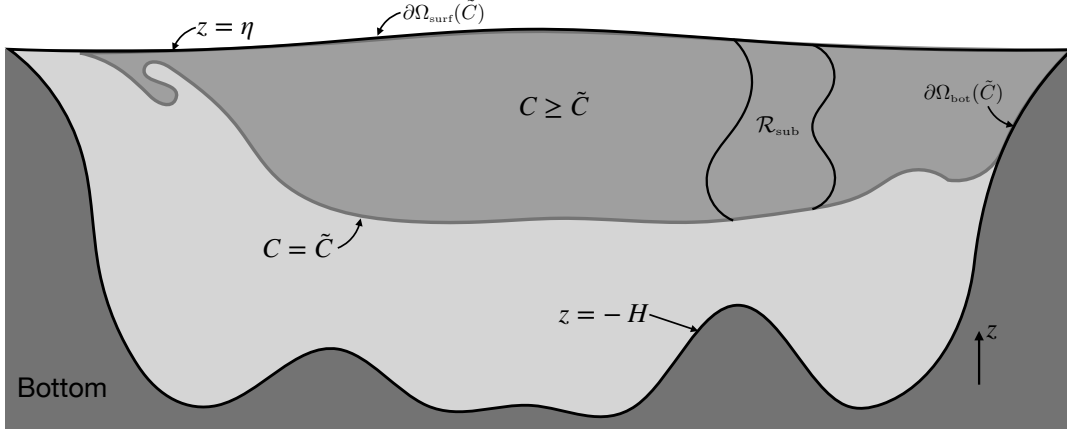


FIGURE 5.4: An ocean region with one of its boundaries set by a surface of constant tracer, $C = \tilde{C}$. Note that the region need not be monotonically stratified in the tracer concentration, nor does it need to be simply connected. The region is bounded at the top by $\partial\Omega_{\text{surf}}(\tilde{C})$, with the geometry of this surface depending on \tilde{C} . The bottom boundary is set by the tracer surface, $C = \tilde{C}$, as well as the solid-earth bottom, $\partial\Omega_{\text{bot}}(\tilde{C})$. The region can generally be multiply connected. A subregion, \mathcal{R}_{sub} , is also considered where its sides extend from the free surface to the tracer isosurface, and they are assumed to be fully within the fluid domain. We develop the tracer and fluid mass budgets for region \mathcal{R}_{sub} in Section 5.6.4, whereas the budget in the full region $C \geq \tilde{C}$ is considered in Section 5.6.3.

Combining this budget with the tracer mass budget allows us to write

$$\frac{d}{dt} [M_C - \tilde{C} M] = \int_{\partial\Omega_{\text{surf}}(\tilde{C})} Q_m (C - \tilde{C}) dA - \oint_{\partial\mathcal{R}} \mathbf{J}^{\text{diff}} \cdot \hat{\mathbf{n}} d\mathcal{S}, \quad (5.81)$$

where we introduced the shorthand for the tracer mass and fluid mass in the region

$$M_C = \int_{\mathcal{R}} C \rho dV \quad \text{and} \quad M = \int_{\mathcal{R}} \rho dV. \quad (5.82)$$

In Section 9.9.2 we motivate the name *internal tracer mass* for the quantity $M_C - \tilde{C} M$.

Skew flux formulation

The tracer mass budget formulated using skew tracer fluxes is generally given by equation (5.78). It takes on the following specific form for the domain in Figure 5.4

$$\begin{aligned} \frac{d}{dt} \left[\int_{\mathcal{R}} \rho C dV \right] = & \int_{\partial\Omega_{\text{surf}}(\tilde{C})} Q_m C dA - \tilde{C} \int_{C=\tilde{C}} \rho (\mathbf{v} - \mathbf{v}^{(b)}) \cdot \hat{\mathbf{n}} d\mathcal{S} \\ & - \oint_{\partial\mathcal{R}} [-\nabla C \times (\rho \Psi^*) + \mathbf{J}^{\text{diff}}] \cdot \hat{\mathbf{n}} d\mathcal{S}, \end{aligned} \quad (5.83)$$

and the corresponding budget for the fluid mass is

$$\frac{d}{dt} \left[\int_{\mathcal{R}} \rho dV \right] = \int_{\partial\Omega_{\text{surf}}(\tilde{C})} Q_m dA - \int_{C=\tilde{C}} \rho (\mathbf{v} - \mathbf{v}^{(b)}) \cdot \hat{\mathbf{n}} d\mathcal{S}. \quad (5.84)$$

As for the advective formulation, we combine the fluid mass budget equation (5.84) with the tracer mass equation (5.83) to render a budget equation for the internal mass content

$$\frac{d}{dt} \left[M_C - \tilde{C} M \right] = \int_{\partial\Omega_{\text{surf}}(\tilde{C})} Q_m (C - \tilde{C}) dA - \oint_{\partial\mathcal{R}} \mathbf{J}^{\text{diff}} \cdot \hat{\mathbf{n}} d\mathcal{S}, \quad (5.85)$$

which is identical to the advective formulation given by equation (5.81).

Proving the budgets based on the two formulations are equivalent

The two tracer budgets, (5.79) and (5.83), must be the same since they measure changes to the tracer mass within the same region. Likewise, the two mass budgets, (5.80) and (5.84), must be the same, as are the two internal tracer mass budgets (5.81) and (5.85). We here expose the manipulations required to verify these equalities.

To prove the $C = \tilde{C}$ terms in the tracer budget equations (5.79) and (5.83) are the same, consider the identity (5.73) applied to the region under consideration

$$0 = \oint_{\partial\mathcal{R}} \rho \mathbf{v}^* \cdot \hat{\mathbf{n}} d\mathcal{S} = \int_{\partial\Omega_{\text{surf}}(\tilde{C})} \rho \mathbf{v}^* \cdot \hat{\mathbf{n}} d\mathcal{S} + \int_{\partial\Omega_{\text{bot}}(\tilde{C})} \rho \mathbf{v}^* \cdot \hat{\mathbf{n}} d\mathcal{S} + \int_{C=\tilde{C}} \rho \mathbf{v}^* \cdot \hat{\mathbf{n}} d\mathcal{S}. \quad (5.86)$$

The surface and bottom boundary terms vanish due to the external boundary condition (5.71); namely, $\mathbf{v}^* \cdot \hat{\mathbf{n}} = 0$ for each point along an external fluid boundary. We are thus led to conclude that

$$\int_{C=\tilde{C}} \rho \mathbf{v}^* \cdot \hat{\mathbf{n}} d\mathcal{S} = 0. \quad (5.87)$$

This boundary integral means that there is no net accumulation of mass in the region due to action of the eddy velocity. Notably, we generally have $\mathbf{v}^* \cdot \hat{\mathbf{n}} \neq 0$ at any particular point on the $C = \tilde{C}$ surface, yet its integral over the $C = \tilde{C}$ interface vanishes. Given the boundary integral (5.87) we are led to conclude

$$\int_{C=\tilde{C}} \rho (\mathbf{v}^\dagger - \mathbf{v}^{(b)}) \cdot \hat{\mathbf{n}} d\mathcal{S} = \int_{C=\tilde{C}} \rho (\mathbf{v} - \mathbf{v}^{(b)}) \cdot \hat{\mathbf{n}} d\mathcal{S}. \quad (5.88)$$

This identity proves that the two mass budgets (5.80) and (5.84) are indeed measuring changes to the same fluid mass, even though one computes the domain boundary fluxes based on the residual mean velocity, \mathbf{v}^\dagger , whereas the other uses the Eulerian mean, \mathbf{v} .

Next we need to show that the skew flux term vanishes when integrated around the domain boundary. For the $C = \tilde{C}$ boundary we have

$$\int_{C=\tilde{C}} [\nabla C \times (\rho \Psi^*)] \cdot \hat{\mathbf{n}} d\mathcal{S} = 0, \quad (5.89)$$

which follows since $\hat{\mathbf{n}}$ is parallel to ∇C along this boundary. For the external boundaries, equality of the tracer mass budgets (5.79) and (5.83) is satisfied for an arbitrary tracer concentration if one of the boundary conditions discussed in Section (5.5.3) is maintained; i.e., if Ψ^* vanishes on an external boundary or if it is parallel to the boundary normal direction ($\hat{\mathbf{n}} \times \Psi^* = 0$). Maintenance of either of these two boundary conditions allows us to conclude that the two budgets (5.79) and (5.83) are indeed identical.

5.6.4 Budget for a region with interior sides

Consider the subregion, \mathcal{R}_{sub} , shown in Figure 5.4. This region is bounded above by the free surface and below by the tracer isosurface, $C = \tilde{C}$, just like the region \mathcal{R} encountered in Section 5.6.3. Additionally, region \mathcal{R}_{sub} is bounded along its sides by surfaces assumed to be within the fluid interior. For much of this discussion we allow the sides to have an arbitrary shape and to move. Towards the end of this section we specialize to the case of static sides, such as relevant for a vertical section through the fluid and/or a numerical model grid cell.

Fluid mass budget

The fluid mass budget for the region, \mathcal{R}_{sub} , can be formulated using either the residual mean velocity or the Eulerian mean velocity

$$\frac{d}{dt} \left[\int_{\mathcal{R}_{\text{sub}}} \rho dV \right] = \int_{\partial\Omega_{\text{surf}}(\tilde{C})} Q_m dA - \int_{C=\tilde{C}} \rho (\mathbf{v}^\dagger - \mathbf{v}^{(b)}) \cdot \hat{\mathbf{n}} dS - \int_{\text{sides}} \rho (\mathbf{v}^\dagger - \mathbf{v}^{(b)}) \cdot \hat{\mathbf{n}} dS \quad (5.90a)$$

$$\frac{d}{dt} \left[\int_{\mathcal{R}_{\text{sub}}} \rho dV \right] = \int_{\partial\Omega_{\text{surf}}(\tilde{C})} Q_m dA - \int_{C=\tilde{C}} \rho (\mathbf{v} - \mathbf{v}^{(b)}) \cdot \hat{\mathbf{n}} dS - \int_{\text{sides}} \rho (\mathbf{v} - \mathbf{v}^{(b)}) \cdot \hat{\mathbf{n}} dS. \quad (5.90b)$$

The two budgets are identical since the eddy velocity satisfies $\oint \rho \mathbf{v}^* \cdot \hat{\mathbf{n}} dS = 0$ for any domain, as well as $\mathbf{v}^* \cdot \hat{\mathbf{n}} = 0$ along any external domain boundary. Hence, as already noted in Section 5.6.1, the eddy velocity contribution to the right hand side of equation (5.90a) vanishes; it provides no net mass source to any region. We next show the same equality holds for the tracer mass budgets, with that equality requiring a bit more effort.

Tracer mass budget

The advective flux formulation of the tracer mass budget is given by

$$\begin{aligned} \frac{d}{dt} \left[\int_{\mathcal{R}_{\text{sub}}} \rho C dV \right] &= \int_{\partial\Omega_{\text{surf}}(\tilde{C})} Q_m C dA - \tilde{C} \int_{C=\tilde{C}} \rho (\mathbf{v}^\dagger - \mathbf{v}^{(b)}) \cdot \hat{\mathbf{n}} dS \\ &\quad - \oint_{\partial\mathcal{R}_{\text{sub}}} \mathbf{J}^{\text{diff}} \cdot \hat{\mathbf{n}} dS - \int_{\text{sides}} C \rho (\mathbf{v}^\dagger - \mathbf{v}^{(b)}) \cdot \hat{\mathbf{n}} dS, \end{aligned} \quad (5.91)$$

and the corresponding skew flux formulation is

$$\begin{aligned} \frac{d}{dt} \left[\int_{\mathcal{R}_{\text{sub}}} \rho C dV \right] &= \int_{\partial\Omega_{\text{surf}}(\tilde{C})} Q_m C dA - \tilde{C} \int_{C=\tilde{C}} \rho (\mathbf{v} - \mathbf{v}^{(b)}) \cdot \hat{\mathbf{n}} dS \\ &\quad - \oint_{\partial\mathcal{R}_{\text{sub}}} \mathbf{J}^{\text{diff}} \cdot \hat{\mathbf{n}} dS - \int_{\text{sides}} C \rho (\mathbf{v} - \mathbf{v}^{(b)}) \cdot \hat{\mathbf{n}} dS - \int_{\text{sides}} [-\nabla C \times (\rho \Psi^*)] \cdot \hat{\mathbf{n}} dS. \end{aligned} \quad (5.92)$$

As for the discussion in Section 5.6.3, we introduce the internal tracer mass and make use of the fluid mass budgets (5.90a) and (5.90b) to write the advective form of the internal mass budget

$$\begin{aligned} \frac{d}{dt} \left[M_C - \tilde{C} M \right] &= \int_{\partial\Omega_{\text{surf}}(\tilde{C})} Q_m (C - \tilde{C}) dA - \oint_{\partial\mathcal{R}} \mathbf{J}^{\text{diff}} \cdot \hat{\mathbf{n}} dS \\ &\quad - \int_{\text{sides}} (C - \tilde{C}) \rho (\mathbf{v}^\dagger - \mathbf{v}^{(b)}) \cdot \hat{\mathbf{n}} dS, \end{aligned} \quad (5.93)$$

and the corresponding skew flux form of the same budget

$$\begin{aligned} \frac{d}{dt} [M_C - \tilde{C} M] &= \int_{\partial\Omega_{\text{surf}}(\tilde{C})} Q_m (C - \tilde{C}) dA - \oint_{\partial\mathcal{R}} \mathbf{J}^{\text{diff}} \cdot \hat{\mathbf{n}} d\mathcal{S} \\ &\quad - \int_{\text{sides}} (C - \tilde{C}) \rho (\mathbf{v} - \mathbf{v}^{(b)}) \cdot \hat{\mathbf{n}} d\mathcal{S} - \int_{\text{sides}} [-\nabla C \times (\rho \Psi^*)] \cdot \hat{\mathbf{n}} d\mathcal{S}. \end{aligned} \quad (5.94)$$

We now examine the right hand side of the budgets (5.93) and (5.94) to show they are indeed measuring the same tracer mass budget. For that purpose, consider the skew flux integral in equation (5.94) and note that the integrand vanishes on both the top of the domain, at $z = \eta$, and bottom at $C = \tilde{C}$, thus allowing us to write

$$-\int_{\text{sides}} [-\nabla C \times (\rho \Psi^*)] \cdot \hat{\mathbf{n}} d\mathcal{S} = -\oint_{\partial\mathcal{R}_{\text{sub}}} [-\nabla C \times (\rho \Psi^*)] \cdot \hat{\mathbf{n}} d\mathcal{S}, \quad (5.95)$$

where the right hand side is an integral around the full domain boundaries. Now reintroduce the eddy induced velocity and rotational flux to have

$$-\oint_{\partial\mathcal{R}_{\text{sub}}} [-\nabla C \times (\rho \Psi^*)] \cdot \hat{\mathbf{n}} d\mathcal{S} = -\oint_{\partial\mathcal{R}_{\text{sub}}} [C \rho \mathbf{v}^* - \nabla \times (C \rho \Psi^*)] \cdot \hat{\mathbf{n}} d\mathcal{S}. \quad (5.96)$$

The rotational flux has zero divergence, so that Gauss's divergence theorem means that the rotational flux vanishes when integrated along the domain boundaries

$$\oint_{\partial\mathcal{R}_{\text{sub}}} \nabla \times (C \rho \Psi^*) \cdot \hat{\mathbf{n}} d\mathcal{S} = 0. \quad (5.97)$$

The eddy advection term in equation (5.96) vanishes on the top boundary at $z = \eta$ due to the boundary condition $\mathbf{v}^* \cdot \hat{\mathbf{n}} = 0$, thus yielding

$$\oint_{\partial\mathcal{R}_{\text{sub}}} C \rho \mathbf{v}^* \cdot \hat{\mathbf{n}} d\mathcal{S} = \int_{\text{sides}} C \rho \mathbf{v}^* \cdot \hat{\mathbf{n}} d\mathcal{S} + \int_{C=\tilde{C}} C \rho \mathbf{v}^* \cdot \hat{\mathbf{n}} d\mathcal{S} \quad (5.98a)$$

$$= \int_{\text{sides}} C \rho \mathbf{v}^* \cdot \hat{\mathbf{n}} d\mathcal{S} + \tilde{C} \int_{C=\tilde{C}} \rho \mathbf{v}^* \cdot \hat{\mathbf{n}} d\mathcal{S}. \quad (5.98b)$$

Again make use of the property $\nabla \cdot (\rho \mathbf{v}^*) = 0$ and $\hat{\mathbf{n}} \cdot \mathbf{v}^* = 0$ at $z = \eta$ to write

$$0 = \oint_{\partial\mathcal{R}_{\text{sub}}} \rho \mathbf{v}^* \cdot \hat{\mathbf{n}} d\mathcal{S} = \oint_{\text{sides}} \rho \mathbf{v}^* \cdot \hat{\mathbf{n}} d\mathcal{S} + \oint_{C=\tilde{C}} \rho \mathbf{v}^* \cdot \hat{\mathbf{n}} d\mathcal{S}. \quad (5.99)$$

We are thus led to

$$-\int_{\text{sides}} [-\nabla C \times (\rho \Psi^*)] \cdot \hat{\mathbf{n}} d\mathcal{S} = -\oint_{\partial\mathcal{R}_{\text{sub}}} C \rho \mathbf{v}^* \cdot \hat{\mathbf{n}} d\mathcal{S} \quad (5.100a)$$

$$= -\int_{\text{sides}} (C - \tilde{C}) \rho \mathbf{v}^* \cdot \hat{\mathbf{n}} d\mathcal{S}. \quad (5.100b)$$

Making use of this result in the skew flux formulated budget equation (5.94) brings it to the advective flux form found in equation (5.93).

We are thus led to conclude that the right hand side to equation (5.94) does indeed equal to the right hand side of equation (5.93). So although the formulation of the boundary flux contributions is rather distinct between the advective flux and skew flux formulations, the

resulting tracer mass budget is the same. The choice for how to formulate the budget is thus a matter of convenience.

5.6.5 Budget for a perfect fluid in a region with interior sides

Although contained within the formalism developed in Section 5.6.4, it is revealing to specialize those budgets to the case of zero mixing, in which $\mathbf{J}^{\text{diff}} = 0$, and there is zero boundary mass flux, $Q_m = 0$. In this case the fluid is reversibly stirred. Examining the finite region budgets for this perfect fluid allows us to further reveal the complementary treatments available from advection versus skewson.

Summary of the differential stirring formalism

As explored in this chapter, an Eulerian description of tracer stirring can arise from either advection or skewson. In the presence of an eddy induced velocity we consider two representations of tracer stirring, with the first being advection by the residual mean velocity, \mathbf{v}^\dagger

$$\rho \frac{D^\dagger C}{Dt} = \partial_t(\rho C) + \nabla \cdot (\rho \mathbf{v}^\dagger C) = 0. \quad (5.101)$$

This formulation makes it clear that surfaces of constant C are material as defined by the residual mean velocity rather than by the Eulerian mean, \mathbf{v} . That is, tracer isosurfaces satisfy the residual mean impermeability condition

$$\rho (\mathbf{v}^\dagger - \mathbf{v}^{(b)}) \cdot \hat{\mathbf{n}} = 0 \quad \text{on } C \text{ isosurfaces}, \quad (5.102)$$

with

$$\hat{\mathbf{n}} = \frac{\nabla C}{|\nabla C|} \quad \text{and} \quad \mathbf{v}^{(b)} \cdot \hat{\mathbf{n}} = -\frac{\partial_t C}{|\nabla C|}. \quad (5.103)$$

The impermeability condition (5.102) offers a geometric interpretation of the tracer equation (5.101) following from the discussion of dia-surface transport in Section 2.4. Correspondingly, Lagrangian fluid particles moving with the residual mean velocity do not cross tracer isosurfaces even if those isosurfaces move. Furthermore, we observe that the eddy induced velocity has a nonzero projection across tracer isosurfaces

$$(\mathbf{v}^\dagger - \mathbf{v}^{(b)}) \cdot \hat{\mathbf{n}} = 0 \implies (\mathbf{v} - \mathbf{v}^{(b)}) \cdot \hat{\mathbf{n}} = -\mathbf{v}^* \cdot \hat{\mathbf{n}} \quad \text{on } C \text{ isosurfaces}. \quad (5.104)$$

This property of the eddy induced velocity was emphasized by [McDougall and McIntosh \(2001\)](#). It reveals that in the absence of mixing, eddy motion crossing tracer isosurfaces is exactly balanced by Eulerian motion plus surface motion, thus leaving a net zero residual mean transfer of matter across the surface. Equation (5.104) is a key kinematic property used for interpreting features of the finite volume budgets detailed below.

Our second means to represent tracer stirring makes use of advection by the Eulerian mean velocity plus skewson by the eddy induced streamfunction

$$\rho \frac{DC}{Dt} + \nabla \cdot [-\nabla C \times (\rho \Psi^*)] = \partial_t(\rho C) + \nabla \cdot [\rho \mathbf{v} C - \nabla C \times (\rho \Psi^*)] = 0. \quad (5.105)$$

In terms of the eddy streamfunction, $\rho \Psi^*$, the impermeability condition (5.102) takes on the form

$$[\rho \mathbf{v} + \nabla \times (\rho \Psi^*) - \rho \mathbf{v}^{(b)}] \cdot \hat{\mathbf{n}} = 0 \quad \text{on } C \text{ isosurfaces}. \quad (5.106)$$

Budgets via residual mean advection

The mass budget formulated in terms of residual mean advection, and the corresponding residual mean advective flux formulation of the tracer mass budget, are given by

$$\frac{d}{dt} \left[\int_{\mathcal{R}_{\text{sub}}} \rho dV \right] = - \int_{C=\tilde{C}} \rho (\mathbf{v}^\dagger - \mathbf{v}^{(b)}) \cdot \hat{\mathbf{n}} d\mathcal{S} - \int_{\text{sides}} \rho (\mathbf{v}^\dagger - \mathbf{v}^{(b)}) \cdot \hat{\mathbf{n}} d\mathcal{S} \quad (5.107\text{a})$$

$$\frac{d}{dt} \left[\int_{\mathcal{R}_{\text{sub}}} \rho C dV \right] = - \tilde{C} \int_{C=\tilde{C}} \rho (\mathbf{v}^\dagger - \mathbf{v}^{(b)}) \cdot \hat{\mathbf{n}} d\mathcal{S} - \int_{\text{sides}} C \rho (\mathbf{v}^\dagger - \mathbf{v}^{(b)}) \cdot \hat{\mathbf{n}} d\mathcal{S}. \quad (5.107\text{b})$$

The residual mean impermeability condition (5.102) for the $C = \tilde{C}$ surface renders a simplification to the fluid mass and tracer mass budgets

$$\frac{d}{dt} \left[\int_{\mathcal{R}_{\text{sub}}} \rho dV \right] = - \int_{\text{sides}} \rho (\mathbf{v}^\dagger - \mathbf{v}^{(b)}) \cdot \hat{\mathbf{n}} d\mathcal{S} \quad (5.108\text{a})$$

$$\frac{d}{dt} \left[\int_{\mathcal{R}_{\text{sub}}} \rho C dV \right] = - \int_{\text{sides}} C \rho (\mathbf{v}^\dagger - \mathbf{v}^{(b)}) \cdot \hat{\mathbf{n}} d\mathcal{S}. \quad (5.108\text{b})$$

Hence, in the residual mean formulation, the only fluxes that affect changes to the mass budgets are those that cross the side faces of the region.

Budgets via Eulerian mean advection plus eddy skewson

The mass budget formulated in terms of Eulerian mean advection, and the corresponding tracer mass budget using eddy skewson, are given by

$$\frac{d}{dt} \left[\int_{\mathcal{R}_{\text{sub}}} \rho dV \right] = - \int_{C=\tilde{C}} \rho (\mathbf{v} - \mathbf{v}^{(b)}) \cdot \hat{\mathbf{n}} d\mathcal{S} - \int_{\text{sides}} \rho (\mathbf{v} - \mathbf{v}^{(b)}) \cdot \hat{\mathbf{n}} d\mathcal{S} \quad (5.109\text{a})$$

$$\begin{aligned} \frac{d}{dt} \left[\int_{\mathcal{R}_{\text{sub}}} \rho C dV \right] = & - \tilde{C} \int_{C=\tilde{C}} \rho (\mathbf{v} - \mathbf{v}^{(b)}) \cdot \hat{\mathbf{n}} d\mathcal{S} - \int_{\text{sides}} C \rho (\mathbf{v} - \mathbf{v}^{(b)}) \cdot \hat{\mathbf{n}} d\mathcal{S} \\ & - \int_{\text{sides}} [-\nabla C \times (\rho \Psi^*)] \cdot \hat{\mathbf{n}} d\mathcal{S}. \end{aligned} \quad (5.109\text{b})$$

We already saw in Section 5.6.4 how to bring the right hand side terms into the form realized by the residual mean advective approach. So there is no question concerning the equivalence of the advective and skew flux formulations for the tracer mass budget. Nonetheless, what is here clearly emphasized is that the skew flux approach requires us to account for Eulerian advective transport across the $C = \tilde{C}$ isosurface, whereas for the advective flux approach the only flux in equation (5.108b) is that crossing the region side boundaries. Even so, as stated earlier, an Eulerian mean transport of tracer across the $C = \tilde{C}$ isosurface *does not* correspond to material transport across this surface. The reason is that material transport is determined by the residual mean velocity, \mathbf{v}^\dagger , as per the residual mean impermeability conditions (5.104) and (5.106). So even though there is a contribution to the skew flux formulated budget from Eulerian transport across the $C = \tilde{C}$ material surface, there remains zero net material crossing that surface.

Zero Eulerian mean advection and static side walls

One further specialization serves to clearly emphasize the complementary nature of the advective and skew flux approaches. Here, we assume the sides of the region are static and the Eulerian

mean velocity vanishes. With a zero Eulerian velocity, the residual mean impermeability condition (5.104) means that on the $C = \tilde{C}$ isosurface, the normal component of the eddy-induced velocity is balanced by the boundary velocity as per the impermeability condition (5.110):

$$(\mathbf{v}^* - \mathbf{v}^{(b)}) \cdot \hat{\mathbf{n}} = 0 \quad \text{on } C \text{ isosurfaces and with } \mathbf{v} = 0. \quad (5.110)$$

When formulated using the residual mean advection, the fluid mass budget (5.108a) and tracer mass budget (5.108b) reduce in this case to

$$\frac{d}{dt} \left[\int_{\mathcal{R}_{\text{sub}}} \rho dV \right] = - \int_{\text{sides}} \rho \mathbf{v}^* \cdot \hat{\mathbf{n}} d\mathcal{S} \quad (5.111a)$$

$$\frac{d}{dt} \left[\int_{\mathcal{R}_{\text{sub}}} \rho C dV \right] = - \int_{\text{sides}} C \rho \mathbf{v}^* \cdot \hat{\mathbf{n}} d\mathcal{S}, \quad (5.111b)$$

so that these budgets are only affected by eddy advection across the side boundaries. The corresponding mass budget written in terms of Eulerian mean advection (5.109a), and tracer mass budget written in terms of skew fluxes (5.109b), are given by

$$\frac{d}{dt} \left[\int_{\mathcal{R}_{\text{sub}}} \rho dV \right] = + \int_{C=\tilde{C}} \rho \mathbf{v}^{(b)} \cdot \hat{\mathbf{n}} d\mathcal{S} \quad (5.112a)$$

$$\frac{d}{dt} \left[\int_{\mathcal{R}_{\text{sub}}} \rho C dV \right] = + \tilde{C} \int_{C=\tilde{C}} \rho \mathbf{v}^{(b)} \cdot \hat{\mathbf{n}} d\mathcal{S} - \int_{\text{sides}} [-\nabla C \times (\rho \Psi^*)] \cdot \hat{\mathbf{n}} d\mathcal{S}. \quad (5.112b)$$

For the mass budget, (5.112a), there are no contributions to the side walls since they are static and the Eulerian velocity is assumed to vanish. The only contribution comes from the eddy term acting on the $C = \tilde{C}$ isosurface where $\mathbf{v}^{(b)} \cdot \hat{\mathbf{n}} = \mathbf{v}^* \cdot \hat{\mathbf{n}}$. For the tracer mass budget (5.112b), we also have the eddy contribution on the $C = \tilde{C}$ isosurface, plus skew fluxes that penetrate the side walls.

The right hand sides to the fluid mass budgets (5.111a) and (5.112a), and tracer mass budgets (5.111b) and (5.112b), are remarkably distinct. Even so, they both measure the same budgets. Furthermore, in both cases the $C = \tilde{C}$ boundary is a material boundary as defined by the residual mean velocity.

5.7 Active tracers and dia-surface flow

An **active tracer** impacts the fluid flow through its impacts on buoyancy, which in turn affects pressure and velocity. Hence, the advection-diffusion equation for active tracers is nonlinear since the velocity field is dependent on active tracers. We here write the advection-diffusion equation in terms of the residual mean velocity using **Conservative Temperature** as an example active tracer

$$\rho \frac{D^\dagger \Theta}{Dt} = \rho (\partial_t + \mathbf{v}^\dagger \cdot \nabla) \Theta = -\nabla \cdot \mathbf{J}^{\text{diff}}(\Theta). \quad (5.113)$$

Further nonlinearities arise when the subgrid scale diffusion tensor is itself a function of the buoyancy, as discussed at the end of Section 4.9, and/or when the parameterized eddy-induced velocity is a function of the buoyancy, as discussed in Section 7.3.

5.7.1 Adiabatic flow

Conservative Temperature is materially invariant (as defined by the residual mean velocity) in an adiabatic flow

$$\frac{D^\dagger \Theta}{Dt} = (\partial_t + \mathbf{v}^\dagger \cdot \nabla) \Theta = 0. \quad (5.114)$$

Furthermore, following the mass kinematics in VOLUME 1, the adiabatic residual mean flow field does not penetrate surfaces of constant Conservative Temperature (Θ -isosurfaces are impermeable) since

$$\mathbf{v}^\dagger \cdot \nabla \Theta = -\partial_t \Theta. \quad (5.115)$$

In this case we say that residual mean advection reversibly stirs the Conservative Temperature field. This property of the residual mean velocity was also considered in the discussion of pure stirring in Section 5.6.4.

5.7.2 Diabatic processes generating dia- Θ transport

Conservative Temperature is not materially invariant in the presence of diabatic processes such as mixing. Correspondingly, the residual mean velocity picks up a dia-surface transport velocity, w^{dia} , that crosses the moving Conservative Temperature surface, thus making Θ surfaces permeable to fluid flow. In turn, advective transport in the presence of mixing is not reversible. Following the kinematics from Section 2.4, we have the expression (2.26) for w^{dia} written as

$$w^{\text{dia}} \equiv \hat{\mathbf{n}} \cdot (\mathbf{v}^\dagger - \mathbf{v}^{(\Theta)}) = \frac{1}{|\nabla \Theta|} \frac{D^\dagger \Theta}{Dt} \quad (5.116)$$

where

$$\hat{\mathbf{n}} = \frac{\nabla \Theta}{|\nabla \Theta|} \quad \text{and} \quad \mathbf{v}^{(\Theta)} \cdot \nabla \Theta = -\partial_t \Theta. \quad (5.117)$$

Rearrangement of equation (5.116) renders the kinematic identity

$$\frac{D^\dagger \Theta}{Dt} = \partial_t \Theta + \mathbf{v}^\dagger \cdot \nabla \Theta = w^{\text{dia}} |\nabla \Theta|. \quad (5.118)$$

With nonzero w^{dia} , we no longer have residual mean advection preserving properties along fluid element trajectories. There can be many physical processes contributing to a nonzero w^{dia} , most notably mixing as in the following examples.

Diffusion with no fluid motion

Diffusion is the canonical example of a diabatic process, with molecular diffusion leading to

$$\rho \frac{D^\dagger \Theta}{Dt} = \nabla \cdot (\kappa \rho \nabla \Theta), \quad (5.119)$$

with $\kappa > 0$ the scalar kinematic diffusivity and the product, $\kappa \rho$, the dynamic diffusivity. Following the definition (5.116), we see that diffusion drives the following diabatic transport velocity

$$\rho w^{\text{dia}} = \frac{\nabla \cdot (\kappa \rho \nabla \Theta)}{|\nabla \Theta|}. \quad (5.120)$$

Consider a horizontally homogeneous Conservative Temperature field. If buoyancy is alone determined by Θ , then there is no fluid motion since buoyancy surfaces are flat (and we assume

the eddy-induced motion is also zero). Yet in the presence of vertical diffusion and vertical stratification there is a diabatic transport since

$$\rho w^{\text{dia}} = \frac{\partial_z(\kappa \rho \partial_z \Theta)}{|\partial_z \Theta|} \neq 0. \quad (5.121)$$

In the absence of fluid flow, the dia-surface transport is determined solely by movement of the Θ surfaces. Correspondingly, Θ evolution is determined only by vertical diffusion since with $\mathbf{v}^\dagger = 0$ we have

$$\partial_t \Theta = \rho^{-1} \partial_z(\kappa \rho \partial_z \Theta) = w^{\text{dia}} |\partial_z \Theta|. \quad (5.122)$$

Steady state advective-diabatic balance

A steady state Conservative Temperature field in the presence of diabatic processes is realized when there is an exact balance between advective transport and dia-surface transport enabled by diffusion

$$\rho \mathbf{v}^\dagger \cdot \nabla \Theta = \rho w^{\text{dia}} |\nabla \Theta| = \nabla \cdot (\kappa \rho \nabla \Theta). \quad (5.123)$$

That is, maintaining static Θ -surfaces ($\partial_t \Theta = 0$) requires the residual mean advective transport to cross Θ surfaces (left hand side) by an amount that exactly balances diabatic processes such as diffusion (right hand side).

5.8 Tracer homogenization inside closed tracer contours

In this section we prove a theorem involving the steady advective-diffusive balance that holds within regions on a surface that are bounded by tracer contours. For this purpose, consider the equation for a conservative tracer

$$\partial_t(\rho C) + \nabla \cdot (\rho \mathbf{v} C) = -\nabla \cdot \mathbf{J} \quad (5.124)$$

where

$$\mathbf{J} = -\rho \mathbf{K} \cdot \nabla C \quad (5.125)$$

is a downgradient diffusive flux with \mathbf{K} a symmetric positive-definite diffusion tensor. In the steady state, the divergence of the advective tracer flux balances the convergence of the diffusive flux

$$\nabla \cdot (\rho \mathbf{v} C) = -\nabla \cdot \mathbf{J}. \quad (5.126)$$

We use this identity to prove that the tracer concentration is homogeneous (i.e., a spatially constant) within a region bounded by a contour of constant C , such as shown in Figure 5.5. Evidently, in the steady state, diffusion removes all tracer variations within closed tracer contours; i.e., there are no tracer extrema within a closed tracer contour.

5.8.1 Proof of the theorem

The following proof follows that given in Section 3.2 of [Rhines and Young \(1982\)](#) and Section 13.5 of [Vallis \(2017\)](#), both given for flow in a Boussinesq ocean. We slightly extend their proof by working with a non-Boussinesq fluid. The proof is based on a *reductio ad absurdum* argument, whereby we first assume the tracer is not homogeneous within a closed tracer contour, and then show that this assumption leads to an inconsistency and so is wrong. Notably, if the tracer

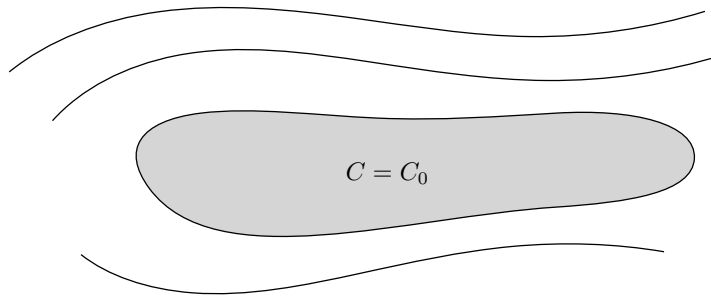


FIGURE 5.5: In a steady flow, the tracer concentration within a region bounded by a constant tracer contour is uniform. Diffusion provides the mechanism for homogenizing the tracer. Evidently, diffusion expels all variations in tracer concentration from the region. In this figure, the concentration within the closed region has constant value, $C = C_0$. Note that the region need not be horizontal. For example, it could be an undulating constant buoyancy surface, or it could be the surface of a sphere. The only condition is that the region is bounded by a closed tracer contour.

concentration is not homogeneous within a closed tracer contour, then there is necessarily an extrema within that contour.

To start the proof, integrate the left hand side of the steady state advection-diffusion equation (5.126) over an arbitrary simply connected surface (not necessarily a horizontal surface) and make use of the divergence theorem

$$\int_S \nabla \cdot (\rho \mathbf{v} C) dS = \oint_{\partial S} \rho \mathbf{v} C \cdot \hat{\mathbf{n}} dl, \quad (5.127)$$

where $\hat{\mathbf{n}}$ is the outward normal along the area's boundary, ∂S , and dl is the line element on the boundary. Now assume the surface is bounded by a constant tracer contour whose value is $C = C_0$. We can thus remove the tracer concentration from the contour integral to have

$$\oint_{\partial S} \rho \mathbf{v} C \cdot \hat{\mathbf{n}} dl = C_0 \oint_{\partial S} \rho \mathbf{v} \cdot \hat{\mathbf{n}} dl = C_0 \int_S \nabla \cdot (\rho \mathbf{v}) dS. \quad (5.128)$$

The second equality follows from the divergence theorem, only now observe that the tracer concentration is outside of the area integral. For a steady state flow, mass continuity means that density at a point is time independent, so that the density-weighted velocity has zero divergence

$$\nabla \cdot (\rho \mathbf{v}) = 0. \quad (5.129)$$

Consequently, when integrated over a closed tracer contour we have the identity

$$\int_S \nabla \cdot (\rho \mathbf{v} C) dS = C_0 \int_S \nabla \cdot (\rho \mathbf{v}) dS = 0 \quad \text{with } S \text{ enclosed by a closed } C \text{ contour.} \quad (5.130)$$

Returning to the steady state advection-diffusion equation (5.126), the identity (5.130) then implies the analogous result for the diffusive flux

$$\int_S \nabla \cdot \mathbf{J} dS = 0 \quad \text{with } S \text{ enclosed by a closed } C \text{ contour.} \quad (5.131)$$

We now provide two arguments to show that the identity (5.131) holds only if the tracer is homogeneous inside the closed contour; i.e., there are no extrema within a closed contour.

Argument 1: Appealing to a nonzero diffusive flux in the presence of an extrema

Consider the right hand side of the steady state advection-diffusion equation (5.126) and integrate it over a closed region

$$-\int_{\mathcal{S}} \nabla \cdot \mathbf{J} d\mathcal{S} = -\oint_{\partial\mathcal{S}} \mathbf{J} \cdot \hat{\mathbf{n}} dl = \oint_{\partial\mathcal{S}} (\mathbf{K} \cdot \nabla C) \cdot \hat{\mathbf{n}} \rho dl. \quad (5.132)$$

If the contour surrounds an extremum of the tracer concentration, then a downgradient diffusive flux is nonzero and has a nonzero projection in the outward normal direction. For example, consider a circular tracer contour surrounding a circular maximum, and assume isotropic diffusion. In this case the diffusive flux is radial so that it has a nonzero projection onto the outward normal. So when there is an extrema within the closed contour, the surface integral (5.132) is nonzero. But a nonzero integral of the diffusive flux around the contour contradicts equation (5.131). The inconsistency arose from assuming the existence of a tracer extrema. Dispensing with this assumption means that the tracer concentration is homogeneous inside the closed tracer contour.

Argument 2: Considering the outward normal

Let us again presume that the tracer is not homogeneous within the domain. In this case $\nabla C \neq 0$ so that we can introduce the normal direction along the tracer contour,

$$\hat{\mathbf{n}} = \frac{\nabla C}{|\nabla C|}, \quad (5.133)$$

which is directed orthogonal to a constant tracer contour. Using this expression for the normal direction within the tracer flux integral leads to

$$-\int_{\mathcal{S}} \nabla \cdot \mathbf{J} d\mathcal{S} = \oint_{\partial\mathcal{S}} \nabla C \cdot \mathbf{K} \cdot \nabla C \frac{\rho dl}{|\nabla C|}. \quad (5.134)$$

The diffusion tensor is a symmetric positive-definite second order tensor, so that the quadratic form in the integral is non-negative

$$\nabla C \cdot \mathbf{K} \cdot \nabla C = K^{mn} \partial_m C \partial_n C \geq 0. \quad (5.135)$$

Furthermore, the line element, dl , is positive, and so are ρ and $|\nabla C|$. Consequently, the integral around a closed tracer contour, where the normal to that contour is given by equation (5.133), is positive

$$-\int_{\mathcal{S}} \nabla \cdot \mathbf{J} d\mathcal{S} = \int_{\partial\mathcal{S}} \partial_m C K^{mn} \partial_n C dl > 0 \quad \text{if } \hat{\mathbf{n}} = \nabla C / |\nabla C|. \quad (5.136)$$

Again, we reach a conclusion that contradicts the zero result (5.131). The zero result (5.131) is based only on the steady state assumption, whereas the inequality (5.136) is a direct result of assuming the tracer is inhomogeneous. Dropping the tracer inhomogeneity assumption is the only way to recover consistency.

5.8.2 Comments

Both of the above arguments lead us to conclude that the steady state tracer concentration is homogeneous within a closed tracer contour. Given enough time to reach a steady state,

diffusion, even arbitrarily weak diffusion, expels all steady state tracer gradients from within regions bounded by closed tracer contours.

We presented the arguments based on integration over a surface bounded by a tracer contour. The result can be extended to integration over volumes in three dimensions, in which case steady state tracers are found to be homogeneous within closed volumes bounded by a surface of constant tracer concentration. However, such bubble-like tracer bounded regions are not common for large-scale geophysical flows. In contrast, closed tracer contours are commonly found in quasi-two dimensional flows, including flows on isopycnals. So the theorem is more readily applied to two dimensional (or quasi two dimensional) flows. We offer another proof of the tracer homogenization result in Section 9.9.1 as part of our study of tracer mass analysis.

We assumed that the tracer equation include just a symmetric diffusion tensor, \mathbf{K} , in defining the subgrid flux (5.125). However, the theorem also holds if there is an additional anti-symmetric tensor, \mathbf{A} , added to \mathbf{K} . The reason is that an anti-symmetric tensor vanishes from the quadratic form (5.135)

$$\nabla C \cdot \mathbf{A} \cdot \nabla C = A^{mn} \partial_m C \partial_n C = 0. \quad (5.137)$$

That is, the tracer skew flux, $\mathbf{J}^{\text{skew}} = -\mathbf{A} \cdot \nabla C$, does not cross tracer isolines: $\nabla C \cdot \mathbf{J} = 0$, which we already found when studying skew fluxes in Section 5.5.

5.8.3 Further study

A prominent application of this theorem appears when the tracer, C , is a dynamically active tracer, such as vorticity or quasi-geostrophic potential vorticity (VOLUME 3). The case of vorticity was discussed by [Batchelor \(1956\)](#), with [Rhines and Young \(1982\)](#) extending that work to the case of quasi-geostrophic potential vorticity. For the quasi-geostrophic case, contours of constant potential vorticity are known as geostrophic contours, and [Rhines and Young \(1982\)](#) used the homogenization theorem to develop a theory of ocean circulation in wind-driven gyre regions. They did so by considering potential vorticity homogenization by the mesoscale eddies that are active in regions of closed geostrophic contours, such as in mid-latitude ocean gyres.

5.9 Green's function method for passive tracers

A [passive tracer](#) has no impact on the fluid density nor the diffusion tensor, which means it has no impact the fluid flow. Consequently, a passive tracer provides a theoretical tool to probe the effects from advective and diffusive transport without affecting the flow. Furthermore, the advection-diffusion equation for a passive tracer is a linear partial differential equation, and as such it affords a [Green's function](#) solution. With some qualifications identified below, we here extend the Green's function method studied for the diffusion equation in VOLUME 1. There are many parallels to that discussion, so it is a very good idea to have VOLUME 1 accessible. Although our formulation is largely based on ocean applications, the Green's function method for the advection-diffusion equation is also applicable to the atmosphere.

5.9.1 Concerning time dependent domain boundaries

The ocean free surface is time dependent, so that the ocean domain, \mathcal{R} , is itself time dependent. Mathematically, this time dependence means that time and space integrations do not commute.

In particular, space integration is generally written in the form

$$\int_{\mathcal{R}} dV = \iint \left[\int_{\eta_b}^{\eta} dz \right] dx dy, \quad (5.138)$$

where $z = \eta_b(x, y)$ is the static bottom and $z = \eta(x, y, t)$ is the time dependent free surface. We must, in turn, first compute the space integration over the full domain and then do the time integration when deriving the **reciprocity condition** satisfied by the Green's function, as well as the integral expression for the tracer concentration in terms of the Green's function.

The free surface undulations make the vertical extent of the domain time dependent. Additionally, in an ocean with sloping sidewalls, the horizontal domain boundaries are time dependent due to the motion of the ocean up and down the sloping sides. However, allowing for a fluctuating horizontal domain extent does not introduce any fundamentally new kinematics to the analysis. The reason is that when integrating to the lateral domain boundaries, all terms vanish since the water depth vanishes at the edge of the sloping beaches. We saw this kinematic result in VOLUME 2 when integrating the angular momentum budget in a channel with sloping sidewalls.

To slightly ease the analysis in this section, we assume the horizontal extent of the domain to be static. We do so by imagining a few meter high vertical seawall placed around the ocean domain edges, and by assuming a minimum depth so that there is nonzero water everywhere in the domain. These assumptions are common in ocean modeling, except in models allowing for wetting and drying of land/ocean cells. So in conclusion, we limit our analysis to time dependence of the vertical extent of the domain, with the horizontal extent static. Such limitation can be removed without much difficulty, but doing so adds nothing new fundamentally.

5.9.2 Passive tracer boundary conditions

In this section, we are concerned with the evolution of a smooth passive tracer concentration, C , which is the dimensionless number between zero and unity. Boundary conditions play a key role in the evolution. We here discuss the boundary conditions placed on the passive tracer along the ocean bottom, at $z = \eta_b(x, y)$, and the ocean free surface, at $z = \eta(x, y, t)$.

Ocean bottom

At the static and solid-earth bottom to the ocean, we consider a no-flux condition for the diffusive flux

$$\mathbf{J} \cdot \hat{\mathbf{n}} = -\rho \mathbf{K} \cdot \nabla C \cdot \hat{\mathbf{n}} = 0 \quad \text{at } z = \eta_b. \quad (5.139)$$

The no-flux condition, along with the kinematic no-normal flow condition, $\mathbf{v} \cdot \hat{\mathbf{n}} = 0$, means that there is zero flux of the passive tracer through the bottom. This assumption can be readily modified if interested in probing the role of processes next to the ocean bottom that carry boundary data into the interior. However, most applications are concerned with surface boundary data, thus motivating us to consider homogeneous Neumann bottom boundary conditions.

Ocean free surface

At the ocean free surface we use results from our study of mass kinematics in VOLUME 1, in which we developed the boundary conditions for mass flux \mathcal{Q}_m (mass per time per area) across

a permeable free surface, as well as our study of tracer mass kinematics also in VOLUME 1, where we developed the analogous boundary conditions for tracers. In particular, we make use of the following expression for the net mass flux of tracer crossing the free surface, \mathcal{Q}_c , written as the sum of an advective flux plus a non-advective flux

$$\mathcal{Q}_c = C \mathcal{Q}_m - \mathbf{J} \cdot \hat{\mathbf{n}} = \underbrace{C \mathcal{Q}_m}_{\text{advective}} + \underbrace{\rho \mathbf{K} \cdot \nabla C \cdot \hat{\mathbf{n}}}_{\text{diffusive}} \quad \text{for } \mathbf{x} \in \partial \mathcal{R}_{\text{surf}}, \quad (5.140)$$

where C is the concentration at the free surface, $z = \eta(x, y, t)$, and we assumed the non-advective flux is given by a diffusive flux. We consider the following prescribed boundary conditions.

- **ROBIN CONDITIONS:** Prescribing the boundary tracer mass flux, \mathcal{Q}_c , leads to a [Robin boundary condition](#), also called a mixed boundary condition

$$\mathcal{Q}_c = \text{prescribed} = C \mathcal{Q}_m + \rho \mathbf{K} \cdot \nabla C \cdot \hat{\mathbf{n}} \quad \text{for } \mathbf{x} \in \partial \mathcal{R}_{\text{surf}}. \quad (5.141)$$

This boundary condition is relevant for enthalpy and salt, with full discussion given in [Section 8.5](#). However, the Robin condition is rarely used for passive tracers along the ocean surface and so it is not further considered in this section.

- **NEUMANN CONDITIONS:** Prescribing the diffusive flux leads to the [Neumann boundary condition](#)

$$\rho \mathbf{K} \cdot \nabla C \cdot \hat{\mathbf{n}} = \text{prescribed} \equiv \Sigma(\mathbf{x}, t) \quad \text{for } \mathbf{x} \in \partial \mathcal{R}_{\text{surf}}. \quad (5.142)$$

This surface ocean boundary condition is also rarely used for passive tracers, though we do examine it within the following.

- **DIRICHLET CONDITIONS:** Prescribing the value of the tracer concentration at the boundary leads to the [Dirichlet boundary condition](#)

$$C = \text{prescribed} \equiv \sigma(\mathbf{x}, t) \quad \text{for } \mathbf{x} \in \partial \mathcal{R}_{\text{surf}}. \quad (5.143)$$

The Dirichlet boundary condition is the most commonly used condition for passive tracers. Hence it is our focus in this section. Note that both the Neumann and Dirichlet conditions generally involve a net transport of tracer, $\mathcal{Q}_c \neq 0$, across the ocean boundary.

As shown in [Section 5.9.6](#), the Neumann boundary condition in the presence of a surface mass flux is problematic due to the associated non-closed reciprocity relation satisfied by the Green's function and its adjoint. The absence of a suitable reciprocity relation makes it difficult to use the Green's function method. In contrast, the Dirichlet condition allows for a reciprocity corresponding to that found for the diffusion equation in VOLUME 1. Hence, the advection-diffusion Green's function, with a Dirichlet condition, is suitable even in the presence of a surface mass flux.⁸

5.9.3 Advection-diffusion initial-boundary value problem

We study the initial-boundary value problem for a smooth passive tracer concentration, C , which is the dimensionless ratio of the tracer mass to seawater mass. The tracer is affected by advection and diffusion on a spatial domain, \mathcal{R} , in the presence of a tracer source, $\rho \Lambda$ (with

⁸See page 2450 of [Larson \(1999\)](#) for a similar point.

dimensions of tracer mass per volume per time), with initial data available for the density and tracer concentration at time $t = t_{\text{init}}$. The initial-boundary value problem in the presence of Neumann or Dirichlet boundary conditions is given by

$$\partial_t(\rho C) + \nabla \cdot (\rho \mathbf{v}^\dagger C - \rho \mathbf{K} \cdot \nabla C) = \rho \Lambda \quad \mathbf{x} \in \mathcal{R}, t \geq t_{\text{init}} \quad (5.144a)$$

$$\rho C = \rho I \quad \mathbf{x} \in \mathcal{R}, t = t_{\text{init}} \quad (5.144b)$$

$$\hat{\mathbf{n}} \cdot \rho \mathbf{K} \cdot \nabla C = \rho \Sigma \quad \text{or} \quad \rho C = \rho \sigma \quad \mathbf{x} \in \partial \mathcal{R}, t \geq t_{\text{init}}. \quad (5.144c)$$

The prescribed initial condition data for the tracer concentration at time $t = t_{\text{init}}$ is given by $I(\mathbf{x})$, and the initial fluid density is also prescribed at this time, $\rho(\mathbf{x}, t_{\text{init}})$. We consider two options for the boundary condition at $\mathbf{x} \in \partial \mathcal{R}$: (i) the Neumann boundary condition with a prescribed flux, $\hat{\mathbf{n}} \cdot \rho \mathbf{K} \cdot \nabla C = \rho \Sigma$, or the (ii) Dirichlet boundary condition with a prescribed value, $\rho C = \rho \sigma$. Furthermore, we assume the flow field, $\mathbf{v}(\mathbf{x}, t)$, the eddy-induced velocity, $\mathbf{v}^*(\mathbf{x}, t)$, the seawater density, $\rho(\mathbf{x}, t)$, and the diffusion tensor, $\mathbf{K}(\mathbf{x}, t)$, are known functions of space-time that are determined by solving for the dynamics, kinematics, thermodynamics, and material tracers. Finally, we assume the tracer concentration source, $\Lambda(\mathbf{x}, t)$, does not itself depend on the tracer concentration, C , thus ensuring linearity of the partial differential equation (5.144a).

5.9.4 The Green's function problem

The Green's function corresponding to the passive tracer advection-diffusion equations (5.144a)-(5.144c) satisfies the following causal boundary value problem

$$\partial_t[\rho G(\mathbf{x}, t | \mathbf{x}_o, t_o)] + \nabla_{\mathbf{x}} \cdot [\rho \mathbf{v}^\dagger G(\mathbf{x}, t | \mathbf{x}_o, t_o) - \rho \mathbf{K} \cdot \nabla_{\mathbf{x}} G(\mathbf{x}, t | \mathbf{x}_o, t_o)] = \delta(\mathbf{x} - \mathbf{x}_o) \delta(t - t_o) \quad (5.145a)$$

$$G(\mathbf{x}, t < t_o | \mathbf{x}_o, t_o) = 0 \quad (5.145b)$$

$$\hat{\mathbf{n}}_{\mathbf{x}} \cdot \mathbf{K} \cdot \nabla_{\mathbf{x}} G(\mathbf{x} \in \partial \mathcal{R}, t | \mathbf{x}_o, t_o) = 0 \quad \text{or} \quad G(\mathbf{x} \in \partial \mathcal{R}, t | \mathbf{x}_o, t_o) = 0. \quad (5.145c)$$

The space-time point, (\mathbf{x}_o, t_o) , is where the Dirac delta source is located, which is within the spatial domain, \mathcal{R} , and it fires at a time after the initial time

$$\mathbf{x}_o \in \mathcal{R} \quad \text{and} \quad t_o \geq t_{\text{init}}. \quad (5.146)$$

The Green's function satisfies homogeneous boundary conditions that correspond to the boundary conditions satisfied by the passive tracer concentration in equation (5.144c). That is, if the passive tracer satisfies a Dirichlet boundary condition, then the Green's function satisfies a homogeneous Dirichlet condition, and likewise for Neumann boundary conditions. Finally, since the Dirac delta source, $\delta(\mathbf{x} - \mathbf{x}_o) \delta(t - t_o)$, has dimensions of inverse volume times inverse time, the Green's function has dimensions of inverse mass. We physically interpret the Green's function as the tracer concentration resulting from an impulsive tracer concentration source, divided by the mass of tracer injected by the source.

5.9.5 Adjoint Green's function problem

The adjoint Green's function, G^\ddagger , satisfies the adjoint problem⁹

$$-\partial_t[\rho G^\ddagger(\mathbf{x}, t | \mathbf{x}_o, t_o)] + \nabla_{\mathbf{x}} \cdot [-\rho \mathbf{v}^\dagger G^\ddagger(\mathbf{x}, t | \mathbf{x}_o, t_o) - \rho \mathbf{K} \cdot \nabla_{\mathbf{x}} G^\ddagger(\mathbf{x}, t | \mathbf{x}_o, t_o)] = \delta(\mathbf{x} - \mathbf{x}_o) \delta(t - t_o) \quad (5.147a)$$

⁹We use the double dagger for the adjoint Green's function, G^\ddagger , to distinguish it from the single dagger used for the residual velocity, \mathbf{v}^\dagger .

$$G^\dagger(\mathbf{x}, t > t_o | \mathbf{x}_o, t_o) = 0 \quad (5.147b)$$

$$\hat{n}_x \cdot \mathbf{K} \cdot \nabla_x G^\dagger(\mathbf{x} \in \partial\mathcal{R}, t | \mathbf{x}_o, t_o) = 0 \text{ or } G^\dagger(\mathbf{x} \in \partial\mathcal{R}, t | \mathbf{x}_o, t_o) = 0. \quad (5.147c)$$

Note the sign change on both the time derivative, as for the diffusion equation in VOLUME 1, as well as the advection term. The sign change on advection is expected since with time running backwards, so too does the velocity. Hence, the adjoint advection-diffusion equation is a backwards in time advection-diffusion equation.

5.9.6 Reciprocity condition

We here derive the reciprocity condition satisfied by the Green's function, G , and its adjoint, G^\dagger . The derivation follows that in VOLUME 1 for the diffusion equation. A new feature here arises from the advection operator, and another arises from allowing the domain boundary to be time dependent as occurs at the ocean free surface. We will see that reciprocity for Neumann boundary conditions (5.145c) and (5.147c) does not “close” when there is mass transport across the ocean free surface (see equation (5.165) below). In contrast, reciprocity closes with Dirichlet boundary conditions, taking the same form as for the diffusion equation from VOLUME 1. We have more to say on this distinct behavior after its derivation.

Notation and setup

Consider the Green's function partial differential equation (5.145a) with a Dirac delta source, $\delta(\mathbf{x} - \mathbf{x}_1) \delta(t - t_1)$, along with the adjoint Green's function equation (5.147a) with a Dirac delta source, $\delta(\mathbf{x} - \mathbf{x}_2) \delta(t - t_2)$, where both sources are within the spatial domain and both occur later than the initial time:

$$\mathbf{x}_1, \mathbf{x}_2 \in \mathcal{R} \quad \text{and} \quad t_{\text{init}} < t_1, t_2. \quad (5.148)$$

We follow the approach for the diffusion equation in VOLUME 1 by introducing the arbitrarily large time, T , such that

$$-T < t_1, t_2 < T. \quad (5.149)$$

As for the diffusion equation, causality conditions ensure that T drops out from the final expression. Additionally, to help ease notational clutter, we make use of the following shorthand where convenient

$$G(\mathbf{x}, t | \mathbf{x}_1, t_1) = G(1) \quad \text{and} \quad G^\dagger(\mathbf{x}, t | \mathbf{x}_2, t_2) = G^\dagger(2). \quad (5.150)$$

Cross-multiplication

Multiply the Green's function equation (5.145a) by $G^\dagger(2)$ and the adjoint equation (5.147a) by $G(1)$ to find

$$G^\dagger(2) (\partial_t [\rho G(1)] + \nabla_{\mathbf{x}} \cdot [\rho \mathbf{v}^\dagger G(1) - \rho \mathbf{K} \cdot \nabla_x G(1)]) = G^\dagger(2) \delta(\mathbf{x} - \mathbf{x}_1) \delta(t - t_1) \quad (5.151a)$$

$$G(1) (-\partial_t [\rho G^\dagger(2)] + \nabla_{\mathbf{x}} \cdot [-\rho \mathbf{v}^\dagger G^\dagger(2) - \rho \mathbf{K} \cdot \nabla_x G^\dagger(2)]) = G(1) \delta(\mathbf{x} - \mathbf{x}_2) \delta(t - t_2). \quad (5.151b)$$

In the following, we work from the left hand side of equation (5.151a) and bring the differential operators from $G(1)$ onto $G^\dagger(2)$. The result of this movement will be equation (5.151b) plus some extra terms whose form depends on the causality condition and boundary conditions. Integration over space and time will then render the reciprocity relation.

Self-adjointness of the generalized Laplacian operator

The generalized Laplacian operator term on the left hand side of equation (5.151a) can be written

$$\begin{aligned} & -G^\ddagger(2) \nabla_{\mathbf{x}} \cdot [\rho \mathbf{K} \cdot \nabla_{\mathbf{x}} G(1)] \\ & = \nabla_{\mathbf{x}} \cdot [-G^\ddagger(2) \rho \mathbf{K} \cdot \nabla_{\mathbf{x}} G(1) + G(1) \rho \mathbf{K} \cdot \nabla_{\mathbf{x}} G^\ddagger(2)] - G(1) \nabla_{\mathbf{x}} \cdot [\rho \mathbf{K} \cdot \nabla_{\mathbf{x}} G^\ddagger(2)]. \end{aligned} \quad (5.152)$$

A spatial integration of this equation over the region \mathcal{R} , and use of the homogeneous boundary conditions in equations (5.144c) or (5.147c), eliminates the divergence term to reveal

$$\begin{aligned} & \int_{\mathcal{R}} G^\ddagger(\mathbf{x}, t | \mathbf{x}_2, t_2) \nabla_{\mathbf{x}} \cdot [\rho \mathbf{K} \cdot \nabla_{\mathbf{x}} G(\mathbf{x}, t | \mathbf{x}_1, t_1)] dV \\ & = \int_{\mathcal{R}} G(\mathbf{x}, t | \mathbf{x}_1, t_1) \nabla_{\mathbf{x}} \cdot [\rho \mathbf{K} \cdot \nabla_{\mathbf{x}} G^\ddagger(\mathbf{x}, t | \mathbf{x}_2, t_2)] dV. \end{aligned} \quad (5.153)$$

This equality proves that the generalized Laplacian operator with a symmetric diffusion tensor is self-adjoint, which is a result encountered in our study of the diffusion equation in VOLUME 1. This result holds for either Neumann or Dirichlet boundary conditions.

Time derivative plus advection

Next write the time derivative and advection portion of equation (5.151a) as

$$\begin{aligned} & G^\ddagger(2) \left(\partial_t [\rho G(1)] + \nabla_{\mathbf{x}} \cdot [\rho \mathbf{v}^\dagger G(1)] \right) \\ & = \partial_t [G^\ddagger(2) \rho G(1)] + \nabla_{\mathbf{x}} \cdot [G^\ddagger(2) \rho \mathbf{v}^\dagger G(1)] - G(1) \rho \left[\partial_t G^\ddagger(2) + \mathbf{v}^\dagger \cdot \nabla_{\mathbf{x}} G^\ddagger(2) \right] \\ & = \partial_t [G^\ddagger(2) \rho G(1)] + \nabla_{\mathbf{x}} \cdot [G^\ddagger(2) \rho \mathbf{v}^\dagger G(1)] - G(1) \left(\partial_t (\rho G^\ddagger(2)) + \nabla \cdot [\rho \mathbf{v}^\dagger G^\ddagger(2)] \right), \end{aligned} \quad (5.154)$$

where we used mass continuity (5.67a) for the final equality. Rearrangement thus leads to

$$\begin{aligned} & G^\ddagger(2) \left(\partial_t [\rho G(1)] + \nabla_{\mathbf{x}} \cdot [\rho \mathbf{v}^\dagger G(1)] \right) - G(1) \left(-\partial_t [\rho G^\ddagger(2)] - \nabla \cdot [\rho \mathbf{v}^\dagger G^\ddagger(2)] \right) \\ & = \partial_t [G^\ddagger(2) \rho G(1)] + \nabla_{\mathbf{x}} \cdot [G^\ddagger(2) \rho \mathbf{v}^\dagger G(1)]. \end{aligned} \quad (5.155)$$

Space integration

Now integrate equations (5.151a) and (5.151b) over the spatial domain, \mathcal{R} , subtract these two equations, and make use of the results (5.153) and (5.155) to reveal

$$\begin{aligned} & G^\ddagger(\mathbf{x}_1, t | \mathbf{x}_2, t_2) \delta(t - t_1) - G(\mathbf{x}_2, t | \mathbf{x}_1, t_1) \delta(t - t_2) \\ & = \int_{\mathcal{R}} \left[\partial_t [G^\ddagger(2) \rho G(1)] + \nabla_{\mathbf{x}} \cdot [G^\ddagger(2) \rho \mathbf{v}^\dagger G(1)] \right] dV. \end{aligned} \quad (5.156)$$

The divergence term on the right hand side takes the form

$$\int_{\mathcal{R}} \nabla_{\mathbf{x}} \cdot [G^\ddagger(2) \rho \mathbf{v}^\dagger G(1)] dV = \oint_{\partial\mathcal{R}} G^\ddagger(2) G(1) \rho \mathbf{v}^\dagger \cdot \hat{\mathbf{n}}_{\mathbf{x}} d\mathcal{S} \quad \text{divergence thm} \quad (5.157a)$$

$$= \oint_{\partial\mathcal{R}} G^\ddagger(2) G(1) \rho \mathbf{v} \cdot \hat{\mathbf{n}}_{\mathbf{x}} d\mathcal{S} \quad \hat{\mathbf{n}} \cdot \mathbf{v}^* = 0 \quad (5.157b)$$

$$= \int_{z=\eta} G^\ddagger(2) G(1) \rho \mathbf{v} \cdot \hat{\mathbf{n}}_x d\mathcal{S} \quad \mathbf{v} \cdot \hat{\mathbf{n}} = 0 \text{ at } z = \eta_b \quad (5.157c)$$

$$= \int_{z=\eta} G^\ddagger(2) G(1) \rho \mathbf{v} \cdot \nabla(z - \eta) dA \quad \text{area relation} \quad (5.157d)$$

$$= \int_{z=\eta} G^\ddagger(2) G(1) \rho (w - \mathbf{u} \cdot \nabla \eta) dA. \quad (5.157e)$$

Equation (5.157d) made use of the area relation from the kinematics in VOLUME 1 that relates the surface area element, $d\mathcal{S}$, on the free surface, to its horizontal projection, dA ,

$$\hat{\mathbf{n}}_x d\mathcal{S} = \nabla(z - \eta) dA. \quad (5.158)$$

The time derivative term in equation (5.156) takes the form

$$\int_{\mathcal{R}} \partial_t [G^\ddagger(2) G(1) \rho] dV = \frac{\partial}{\partial t} \left[\int_{\mathcal{R}} G^\ddagger(2) G(1) \rho dV \right] - \int_{z=\eta} [G^\ddagger(2) G(1) \rho \partial_t \eta] dA, \quad (5.159)$$

where we made use of Leibniz's rule to bring the time derivative across the integral sign and made note of the time dependent free surface, $z = \eta(x, y, t)$. Combining equations (5.159) and (5.157e) leads to

$$G^\ddagger(\mathbf{x}_1, t | \mathbf{x}_2, t_2) \delta(t - t_1) - G(\mathbf{x}_2, t | \mathbf{x}_1, t_1) \delta(t - t_2) \quad (5.160a)$$

$$= \frac{\partial}{\partial t} \left[\int_{\mathcal{R}} G^\ddagger(2) G(1) \rho dV \right] + \int_{z=\eta} G^\ddagger(2) G(1) [\rho (w - \mathbf{u} \cdot \nabla \eta - \partial_t \eta)] dA \quad (5.160b)$$

$$= \frac{\partial}{\partial t} \left[\int_{\mathcal{R}} G^\ddagger(2) G(1) \rho dV \right] - \int_{z=\eta} G^\ddagger(2) G(1) Q_m dA, \quad (5.160c)$$

where the final equality follows from the surface ocean kinematic boundary condition from VOLUME 1,

$$(\partial_t + \mathbf{u} \cdot \nabla_h) \eta = w + Q_m / \rho, \quad (5.161)$$

with Q_m the mass per time per horizontal area crossing the ocean free surface.

Time integration

We are now ready to time integrate equation (5.160c), with the left hand side leading to

$$\begin{aligned} \int_{-T}^T \left[G^\ddagger(\mathbf{x}_1, t | \mathbf{x}_2, t_2) \delta(t - t_1) - G(\mathbf{x}_2, t | \mathbf{x}_1, t_1) \delta(t - t_2) \right] dt \\ = G^\ddagger(\mathbf{x}_1, t_1 | \mathbf{x}_2, t_2) - G(\mathbf{x}_2, t_2 | \mathbf{x}_1, t_1), \end{aligned} \quad (5.162)$$

which used the sifting property of the Dirac delta. There are two terms that appear when time integrating the time derivative on the right hand side of equation (5.160c), with each term vanishing due to the causality conditions (5.145b) and (5.147b)

$$\int_{\mathcal{R}} G^\ddagger(\mathbf{x}, t = T | \mathbf{x}_2, t_2) G(\mathbf{x}, t = T | \mathbf{x}_1, t_1) \rho dV = 0 \iff G^\ddagger(\mathbf{x}, t = T | \mathbf{x}_2, t_2) = 0 \quad (5.163)$$

$$\int_{\mathcal{R}} G^\ddagger(\mathbf{x}, t = t_{\text{init}} | \mathbf{x}_2, t_2) G(\mathbf{x}, t = t_{\text{init}} | \mathbf{x}_1, t_1) \rho dV = 0 \iff G(\mathbf{x}, t = t_{\text{init}} | \mathbf{x}_1, t_1) = 0. \quad (5.164)$$

We are thus left with

$$G^\dagger(\mathbf{x}_1, t_1 | \mathbf{x}_2, t_2) - G(\mathbf{x}_2, t_2 | \mathbf{x}_1, t_1) = - \int_{t_{\text{init}}}^{t_1} \left[\int_{z=\eta} \mathcal{G}^\dagger(\mathbf{x}, t | \mathbf{x}_2, t_2) G(\mathbf{x}_1, t_1 | \mathbf{x}, t) Q_m \, dA \right] dt, \quad (5.165)$$

which we refer to as a *non-closed reciprocity relation* between G and G^\dagger . Note that the time limits on the integral follow from causality on the Green's function and its adjoint.

Closed form reciprocity in special cases

There are two cases in which the relation (5.165) leads to a closed reciprocity relation:

- Zero mass flux across the ocean free surface: $Q_m = 0$.
- Homogeneous Dirichlet boundary conditions at the ocean free surface, in which case $\mathcal{G}^\dagger(\mathbf{x} \in \partial\mathcal{R}, t | \mathbf{x}_o, t_o) = G(\mathbf{x} \in \partial\mathcal{R}, t | \mathbf{x}_o, t_o) = 0$.

In either case we are led to

$$\mathcal{G}^\dagger(\mathbf{x}_1, t_1 | \mathbf{x}_2, t_2) = G(\mathbf{x}_2, t_2 | \mathbf{x}_1, t_1), \quad (5.166)$$

which is the same reciprocity condition satisfied for the diffusion equation Green's functions in VOLUME 1.

The more nuanced reciprocity for the advection-diffusion equation arises from the advective mass flux at the ocean free surface boundary. The mass flux couples the ocean with its surrounding media (e.g., the atmosphere, rivers, or cryosphere), even when using homogeneous Neumann conditions. In so doing, we are not afforded a generally closed reciprocity relation. The Dirichlet boundary condition closes the surface boundary by eliminating the direct role of the surface mass flux. Most applications of Green's function methods for passive ocean tracers make use of Dirichlet boundary conditions, in which case we are afforded a closed reciprocity relation even with a free surface open to mass transport.

5.9.7 Composition property

We here follow the analysis of the diffusion equation Green's function in VOLUME 1 to derive the composition property of the Green's function for the advection-diffusion equation. For this purpose, return to the cross-multiplication equations (5.151a) and (5.151b) used to derive reciprocity, here written as

$$G^\dagger(2) \left(\partial_t [\rho G(1)] + \nabla_{\mathbf{x}} \cdot [\rho \mathbf{v}^\dagger G(1) - \rho \mathbf{K} \cdot \nabla_{\mathbf{x}} G(1)] \right) = G^\dagger(2) \delta(\mathbf{x} - \mathbf{x}_1) \delta(t - t_1) \quad (5.167a)$$

$$G(1) \left(\partial_t [\rho G^\dagger(2)] + \nabla_{\mathbf{x}} \cdot [\rho \mathbf{v}^\dagger G^\dagger(2) + \rho \mathbf{K} \cdot \nabla_{\mathbf{x}} G^\dagger(2)] \right) = -G(1) \delta(\mathbf{x} - \mathbf{x}_2) \delta(t - t_2). \quad (5.167b)$$

Adding these two equations and use of mass continuity (5.67a) brings the left hand side to

$$\begin{aligned} \text{LHS} &= \partial_t [\rho G(1) G^\dagger(2)] \\ &\quad + \nabla_{\mathbf{x}} \cdot [\rho \mathbf{v}^\dagger G(1) G^\dagger(2) + \rho G(1) \mathbf{K} \cdot \nabla_{\mathbf{x}} G^\dagger(2) - \rho G^\dagger(2) \mathbf{K} \cdot \nabla_{\mathbf{x}} G(1)]. \end{aligned} \quad (5.168)$$

For the time derivative term we use Leibniz's rule to write

$$\int_{\mathcal{R}} \partial_t [\rho G(1) G^\dagger(2)] dV = \frac{d}{dt} \int_{\mathcal{R}} \rho G(1) G^\dagger(2) dV - \int_{z=\eta} \rho G(1) G^\dagger(2) \partial_t \eta dA. \quad (5.169a)$$

For the advection term we follow the manipulations used for equation (5.157e) to derive

$$\int_{\mathcal{R}} \nabla_{\mathbf{x}} \cdot [\rho \mathbf{v}^\dagger G(1) G^\dagger(2)] dV = \int_{z=\eta} \rho G(1) G^\dagger(2) \mathbf{v}^\dagger \cdot \hat{\mathbf{n}} d\mathcal{S} \quad (5.170a)$$

$$= \int_{z=\eta} \rho G(1) G^\dagger(2) (w - \mathbf{u} \cdot \nabla \eta) dA \quad (5.170b)$$

$$= \int_{z=\eta} G(1) G^\dagger(2) (\rho \partial_t \eta - Q_m) dA. \quad (5.170c)$$

Bringing the pieces together we find that the $\partial_t \eta$ term is eliminated, so that

$$\begin{aligned} \frac{d}{dt} \int_{\mathcal{R}} \rho(\mathbf{x}, t) G(\mathbf{x}, t | \mathbf{x}_1, t_1) G^\dagger(\mathbf{x}, t | \mathbf{x}_2, t_2) dV &= G^\dagger(\mathbf{x}_1, t | \mathbf{x}_2, t_2) \delta(t - t_1) \\ &\quad - G(\mathbf{x}_2, t | \mathbf{x}_1, t_1) \delta(t - t_2) - \int_{z=\eta} G(\mathbf{x}, t | \mathbf{x}_1, t_1) G^\dagger(\mathbf{x}, t | \mathbf{x}_2, t_2) Q_m(\mathbf{x}, t) dA. \end{aligned} \quad (5.171)$$

As for the derivation of reciprocity in Section 5.9.6, we here assume either $Q_m = 0$ or a homogeneous Dirichlet boundary condition so that

$$\begin{aligned} \frac{d}{dt} \int_{\mathcal{R}} \rho(\mathbf{x}, t) G(\mathbf{x}, t | \mathbf{x}_1, t_1) G^\dagger(\mathbf{x}, t | \mathbf{x}_2, t_2) dV &= G^\dagger(\mathbf{x}_1, t | \mathbf{x}_2, t_2) \delta(t - t_1) \\ &\quad - G(\mathbf{x}_2, t | \mathbf{x}_1, t_1) \delta(t - t_2). \end{aligned} \quad (5.172)$$

Equation (5.172) is identical to that satisfied by the diffusion equation Green's function, as found in VOLUME 1. As for the diffusion case, time integration of equation (5.172) requires care about how the time limits are placed relative to the two Dirac sources. However, all of these details are identical to the diffusion case from VOLUME 1, so we can simply take those results to write the composition property for the advection-diffusion Green's function

$$G(\mathbf{x}_2, t_2 | \mathbf{x}_1, t_1) = \int_{\mathcal{R}} \rho(\mathbf{x}, \tau) G(\mathbf{x}_2, t_2 | \mathbf{x}, \tau) G(\mathbf{x}, \tau | \mathbf{x}_1, t_1) dV \quad \text{if } t_1 < \tau < t_2. \quad (5.173)$$

The left hand side of this equation is the response from a Dirac source that is advected-diffused from (\mathbf{x}_1, t_1) and measured at the space-time point (\mathbf{x}_2, t_2) . The right hand side is the composition of a Green's function feeling the source at (\mathbf{x}_1, t_1) but now sampled at an intermediate space-time position, (\mathbf{x}, τ) , and then further advective-diffused to (\mathbf{x}_2, t_2) , with integration over all possible intermediate positions \mathbf{x} . The intermediate sampling can occur at an arbitrary intermediate time τ , so long as $t_1 < \tau < t_2$. The composition property (5.173) allows us to conceive of a long-time interval Green's function as the composition of an arbitrary number of shorter time interval Green's functions.

5.9.8 Integral expression for the tracer concentration

We are now ready to express the passive tracer concentration, C , as a suite of integrals involving the Green's function and the known boundary and initial conditions as well as the known source

function. The process for deriving this expression is identical to that used in Section 5.9.6 for reciprocity, with the following steps offered for completeness.

Derivation setup

The initial-boundary value problem for the passive tracer is given by

$$\partial_t(\rho C) + \nabla \cdot (\rho \mathbf{v}^\dagger C - \rho \mathbf{K} \cdot \nabla C) = \rho \Lambda \quad \mathbf{x} \in \mathcal{R}, t \geq t_{\text{init}} \quad (5.174a)$$

$$\rho C = \rho I \quad \mathbf{x} \in \mathcal{R}, t = t_{\text{init}} \quad (5.174b)$$

$$\rho C = \rho \sigma \quad \mathbf{x} \in \partial \mathcal{R}, t \geq t_{\text{init}} \quad (5.174c)$$

where we only consider the Dirichlet boundary condition to ensure a closed reciprocity relation in the presence of surface mass fluxes (Section 5.9.6). The corresponding adjoint Green's function satisfies

$$-\partial_t[\rho G^\ddagger(\mathbf{x}, t | \mathbf{x}_o, t_o)] + \nabla_{\mathbf{x}} \cdot [-\rho \mathbf{v}^\dagger G^\ddagger(\mathbf{x}, t | \mathbf{x}_o, t_o) - \rho \mathbf{K} \cdot \nabla_{\mathbf{x}} G^\ddagger(\mathbf{x}, t | \mathbf{x}_o, t_o)] = \delta(\mathbf{x} - \mathbf{x}_o) \delta(t - t_o) \quad (5.175a)$$

$$G^\ddagger(\mathbf{x}, t > t_o | \mathbf{x}_o, t_o) = 0 \quad (5.175b)$$

$$G^\ddagger(\mathbf{x} \in \partial \mathcal{R}, t | \mathbf{x}_o, t_o) = 0, \quad (5.175c)$$

with the reciprocity condition (5.166) holding since we chose Dirichlet boundary conditions. Multiplying the adjoint Green's function equation (5.175a) by $C(\mathbf{x}, t)$ and performing manipulations just like those for reciprocity leads to

$$\begin{aligned} -\partial_t(\rho C G^\ddagger) + \nabla_{\mathbf{x}} \cdot \left[G^\ddagger \rho \mathbf{K} \cdot \nabla C - C \rho \mathbf{K}(\mathbf{x}, t) \cdot \nabla_{\mathbf{x}} G^\ddagger - C \rho \mathbf{v}^\dagger G^\ddagger \right] + G^\ddagger \rho \Lambda \\ = C(\mathbf{x}, t) \delta(\mathbf{x} - \mathbf{x}_o) \delta(t - t_o). \end{aligned} \quad (5.176)$$

With the homogeneous Dirichlet conditions satisfied by G^\ddagger on the spatial boundaries, a space and time integration over (\mathbf{x}, t) leads to

$$\begin{aligned} C(\mathbf{x}_o, t_o) &= \int_{\mathcal{R}} G^\ddagger(\mathbf{x}, t_{\text{init}} | \mathbf{x}_o, t_o) \rho(\mathbf{x}, t_{\text{init}}) I(\mathbf{x}) dV \\ &\quad + \int_{t_{\text{init}}}^{t_o} \left[\int_{\mathcal{R}} G^\ddagger(\mathbf{x}, t | \mathbf{x}_o, t_o) \rho(\mathbf{x}, t) \Lambda(\mathbf{x}, t) dV \right] dt \\ &\quad - \int_{t_{\text{init}}}^{t_o} \left[\oint_{\partial \mathcal{R}} \sigma(\mathbf{x}, t) \rho(\mathbf{x}, t) \mathbf{K}(\mathbf{x}, t) \cdot \nabla_{\mathbf{x}} G^\ddagger(\mathbf{x}, t | \mathbf{x}_o, t_o) \cdot \hat{\mathbf{n}}_{\mathbf{x}} d\mathcal{S} \right] dt. \end{aligned} \quad (5.177)$$

Use of the reciprocity relation (5.166) allows us to write this equation in terms of the Green's function rather than the adjoint Green's function

$$\begin{aligned} C(\mathbf{x}_o, t_o) &= \int_{\mathcal{R}} G(\mathbf{x}_o, t_o | \mathbf{x}, t_{\text{init}}) \rho(\mathbf{x}, t_{\text{init}}) I(\mathbf{x}) dV \\ &\quad + \int_{t_{\text{init}}}^{t_o} \left[\int_{\mathcal{R}} G(\mathbf{x}_o, t_o | \mathbf{x}, t) \rho(\mathbf{x}, t) \Lambda(\mathbf{x}, t) dV \right] dt \\ &\quad - \int_{t_{\text{init}}}^{t_o} \left[\oint_{\partial \mathcal{R}} \sigma(\mathbf{x}, t) \rho(\mathbf{x}, t) \mathbf{K}(\mathbf{x}, t) \cdot \nabla_{\mathbf{x}} G(\mathbf{x}_o, t_o | \mathbf{x}, t) \cdot \hat{\mathbf{n}}_{\mathbf{x}} d\mathcal{S} \right] dt. \end{aligned} \quad (5.178)$$

Finally, swapping labels $(\mathbf{x}_o, t_o) \leftrightarrow (\mathbf{x}, t)$ renders

$$\begin{aligned}
 C(\mathbf{x}, t) = & \int_{\mathcal{R}} G(\mathbf{x}, t | \mathbf{x}_o, t_{\text{init}}) \rho(\mathbf{x}_o, t_{\text{init}}) I(\mathbf{x}_o) dV_0 \\
 & + \int_{t_{\text{init}}}^t \left[\int_{\mathcal{R}} G(\mathbf{x}, t | \mathbf{x}_o, t_o) \rho(\mathbf{x}_o, t_o) \Lambda(\mathbf{x}_o, t_o) dV_0 \right] dt_o \\
 & - \int_{t_{\text{init}}}^t \left[\oint_{\partial\mathcal{R}} \sigma(\mathbf{x}_o, t_o) \rho(\mathbf{x}_o, t_o) \mathbf{K}(\mathbf{x}_o, t_o) \cdot \nabla_{\mathbf{x}_o} G(\mathbf{x}, t | \mathbf{x}_o, t_o) \cdot \hat{\mathbf{n}}_{\mathbf{x}_o} d\mathcal{S}_0 \right] dt_o. \quad (5.179)
 \end{aligned}$$

This solution manifests causality since the tracer concentration at time t is a function only of processes occurring from t_{init} up to time t .

5.9.9 Properties of the Green's function solution

The integral solution (5.179) is of the same form as that for the diffusion equation in VOLUME 1. We here summarize properties of the solution, which largely follow those for the diffusion equation.

The role of advection and diffusion at boundaries

Explicit contributions from the advective flux are absent from the solution (5.179). Namely, there are no advective flux contributions at the surface boundary. Such contributions are missing due to the homogeneous Dirichlet boundary conditions imposed on the Green's function. For the ocean bottom, material and rigid no-flux conditions mean that $\mathbf{v} \cdot \hat{\mathbf{n}} = 0$ at the bottom. The presence of advection arises only through its effect on the Green's function, which is affected by both advection and diffusion.

Furthermore, notice how in the absence of diffusion (i.e., $\mathbf{K} = 0$) the Dirichlet boundary data is unable to penetrate into the ocean interior since the surface boundary integral vanishes from equation (5.179). In effect, the surface boundary becomes a material surface when there is no diffusion. That is, diffusive mixing is needed for boundary data to move into the interior. This role for diffusion again appears in our study of the surface flux condition for salt and freshwater in Section 8.5 (see also [Nurser and Griffies \(2019\)](#)).

Initial conditions

When sampling the tracer concentration at the initial time, $t \downarrow t_{\text{init}}$, causality means that all the time integrals vanish from the solution (5.179), thus leaving

$$\lim_{t \downarrow t_{\text{init}}} C(\mathbf{x}, t) = \lim_{t \downarrow t_{\text{init}}} \int_{\mathcal{R}} G(\mathbf{x}, t | \mathbf{x}_o, t_{\text{init}}) \rho(\mathbf{x}_o, t_{\text{init}}) I(\mathbf{x}_o) dV_0. \quad (5.180)$$

Self-consistency implies that the Green's function satisfies

$$\lim_{t \downarrow t_{\text{init}}} G(\mathbf{x}, t | \mathbf{x}_o, t_{\text{init}}) \rho(\mathbf{x}_o, t_{\text{init}}) = \delta(\mathbf{x} - \mathbf{x}_o) \quad \text{with } \mathbf{x}, \mathbf{x}_o \in \mathcal{R}, \quad (5.181)$$

so that

$$\lim_{t \downarrow t_{\text{init}}} \int_{\mathcal{R}} \rho(\mathbf{x}, t_{\text{init}}) G(\mathbf{x}, t | \mathbf{x}_o, t_{\text{init}}) I(\mathbf{x}_o) dV_0 = \int_{\mathcal{R}} \delta(\mathbf{x} - \mathbf{x}_o) I(\mathbf{x}_o) dV_0 = I(\mathbf{x}). \quad (5.182)$$

Dirichlet boundary conditions

Evaluating the Dirichlet solution (5.179) on a spatial boundary, $\mathbf{x} \in \partial\mathcal{R}$, eliminates both the volume integrals given that the Green's function satisfies homogeneous Dirichlet boundary conditions. The tracer concentration (5.179) thus takes the form

$$C(\mathbf{x}, t) = - \int_{t_{\text{init}}}^t \left[\oint_{\partial\mathcal{R}} \sigma(\mathbf{x}_o, t_o) \rho(\mathbf{x}_o, t_o) \mathbf{K}(\mathbf{x}_o, t_o) \cdot \nabla_{\mathbf{x}_o} G(\mathbf{x}, t | \mathbf{x}_o, t_o) \cdot \hat{\mathbf{n}}_{\mathbf{x}_o} d\mathcal{S}_0 \right] dt_o \quad \text{with } \mathbf{x} \in \partial\mathcal{R}. \quad (5.183)$$

Self-consistency with the Dirichlet boundary condition (5.144c) implies that the Green's function, when both spatial points are evaluated on the boundary, satisfies

$$\rho(\mathbf{x}_o, t_o) \mathbf{K}(\mathbf{x}_o, t_o) \cdot \nabla_{\mathbf{x}_o} G(\mathbf{x}, t | \mathbf{x}_o, t_o) \cdot \hat{\mathbf{n}}_{\mathbf{x}_o} = -\delta(t - t_o) \delta^{(2)}(\mathbf{x} - \mathbf{x}_o) \quad \text{with } \mathbf{x}, \mathbf{x}_o \in \partial\mathcal{R}, \quad (5.184)$$

so that

$$C(\mathbf{x}, t) = \int_{t_{\text{init}}}^t \left[\oint_{\partial\mathcal{R}} \sigma(\mathbf{x}_o, t_o) \delta(t - t_o) \delta^{(2)}(\mathbf{x} - \mathbf{x}_o) d\mathcal{S}_0 \right] dt_o = \sigma(\mathbf{x}, t) \quad \text{with } \mathbf{x} \in \partial\mathcal{R}. \quad (5.185)$$

5.9.10 Boundary propagator

Defining the boundary propagator

As for the diffusion equation in VOLUME 1, we here introduce the **boundary propagator** for the advection-diffusion equation with Dirichlet boundary conditions. For this purpose, consider the special case of a passive tracer with zero interior source and with zero initial condition, thus satisfying the initial-boundary value problem

$$\partial_t(\rho C) + \nabla \cdot (\rho \mathbf{v}^\dagger C - \rho \mathbf{K} \cdot \nabla C) = 0 \quad \mathbf{x} \in \mathcal{R}, t \geq t_{\text{init}} \quad (5.186a)$$

$$\rho C = 0 \quad \mathbf{x} \in \mathcal{R}, t = t_{\text{init}} \quad (5.186b)$$

$$\rho C = \rho \sigma \quad \mathbf{x} \in \partial\mathcal{R}, t \geq t_{\text{init}}, \quad (5.186c)$$

which leads to the simplification of the Green's function solution (5.179)

$$C(\mathbf{x}, t) = - \int_{t_{\text{init}}}^t \left[\oint_{\partial\mathcal{R}} \sigma(\mathbf{x}_o, t_o) \rho(\mathbf{x}_o, t_o) \mathbf{K}(\mathbf{x}_o, t_o) \cdot \nabla_{\mathbf{x}_o} G(\mathbf{x}, t | \mathbf{x}_o, t_o) \cdot \hat{\mathbf{n}}_{\mathbf{x}_o} d\mathcal{S}_0 \right] dt_o. \quad (5.187)$$

The tracer concentration at a point in space-time is determined by the history of the advection and diffusion that transfers boundary information to this point. To manifest this cause-effect relation, it is useful to define the boundary propagator just as for the diffusion equation

$$G^{\text{bp}}(\mathbf{x}, t | \mathbf{x}_o, t_o) \equiv -\rho(\mathbf{x}_o, t_o) \mathbf{K}(\mathbf{x}_o, t_o) \cdot \nabla_{\mathbf{x}_o} G(\mathbf{x}, t | \mathbf{x}_o, t_o) \cdot \hat{\mathbf{n}}_{\mathbf{x}_o} \quad \text{with } \mathbf{x}_o \in \partial\mathcal{R}, \quad (5.188)$$

with G^{bp} having dimensions $\text{L}^{-2} \text{T}^{-1}$. The boundary propagator thus brings the tracer concentration (5.187) into the rather tidy form

$$C(\mathbf{x}, t) = \int_{t_{\text{init}}}^t \left[\oint_{\partial\mathcal{R}} \sigma(\mathbf{x}_o, t_o) G^{\text{bp}}(\mathbf{x}, t | \mathbf{x}_o, t_o) d\mathcal{S}_0 \right] dt_o. \quad (5.189)$$

Inhomogeneous Dirichlet at the surface and homogeneous Neumann at the bottom

In applications of passive tracers to study ocean circulation, it is common to apply inhomogeneous Dirichlet boundary conditions just at the ocean surface, and homogeneous Neumann boundary conditions (no-flux) at the ocean bottom

$$\partial_t(\rho C) + \nabla \cdot (\rho \mathbf{v}^\dagger C - \rho \mathbf{K} \cdot \nabla C) = 0 \quad \mathbf{x} \in \mathcal{R}, t \geq t_{\text{init}} \quad (5.190a)$$

$$C = 0 \quad \mathbf{x} \in \mathcal{R}, t = t_{\text{init}} \quad (5.190b)$$

$$\rho C = \rho \sigma \quad \mathbf{x} \in \partial \mathcal{R}_{\text{surf}}, t \geq t_{\text{init}} \quad (5.190c)$$

$$\hat{\mathbf{n}}_{\mathbf{x}} \cdot \mathbf{K} \cdot \nabla_{\mathbf{x}} C = 0 \quad \mathbf{x} \in \partial \mathcal{R}_{\text{bot}}, t \geq t_{\text{init}}. \quad (5.190d)$$

Note that since $\hat{\mathbf{n}} \cdot \mathbf{v} = 0$ at the solid earth ocean bottom, kinematics imposes no advective flux through the bottom, $\hat{\mathbf{n}} \cdot \mathbf{v} C = 0$. Since the bottom boundary conditions are homogeneous, the solution (5.187) also holds for the initial-boundary value problem (5.190a)-(5.190d). The key distinction, however, is that the Green's function now satisfies the following boundary value problem

$$\partial_t[\rho G(\mathbf{x}, t | \mathbf{x}_o, t_o)] + \nabla_{\mathbf{x}} \cdot [\rho \mathbf{v}^\dagger G(\mathbf{x}, t | \mathbf{x}_o, t_o) - \rho \mathbf{K} \cdot \nabla_{\mathbf{x}} G(\mathbf{x}, t | \mathbf{x}_o, t_o)] = \delta(\mathbf{x} - \mathbf{x}_o) \delta(t - t_o) \quad (5.191a)$$

$$G(\mathbf{x}, t < t_o | \mathbf{x}_o, t_o) = 0 \quad (5.191b)$$

$$G(\mathbf{x}, t | \mathbf{x}_o, t_o) = 0 \quad \mathbf{x} \in \partial \mathcal{R}_{\text{surf}} \quad (5.191c)$$

$$\hat{\mathbf{n}}_{\mathbf{x}} \cdot \mathbf{K} \cdot \nabla_{\mathbf{x}} G(\mathbf{x}, t | \mathbf{x}_o, t_o) = 0 \quad \mathbf{x} \in \partial \mathcal{R}_{\text{bot}}. \quad (5.191d)$$

Boundary value problem for the boundary propagator

Following the more detailed presentation in VOLUME 1 for the diffusion equation, we are led to the following boundary value problem satisfied by the boundary propagator

$$\partial_t[\rho G^{\text{bp}}(\mathbf{x}, t | \mathbf{x}_o, t_o)] + \nabla_{\mathbf{x}} \cdot [\rho \mathbf{v}^\dagger G^{\text{bp}}(\mathbf{x}, t | \mathbf{x}_o, t_o) - \rho \mathbf{K} \cdot \nabla_{\mathbf{x}} G^{\text{bp}}(\mathbf{x}, t | \mathbf{x}_o, t_o)] = 0, \quad \mathbf{x} \in \mathcal{R} \quad (5.192a)$$

$$G^{\text{bp}}(\mathbf{x}, t | \mathbf{x}_o, t_o) = 0, \quad \mathbf{x} \notin \partial \mathcal{R}, t \leq t_o \quad (5.192b)$$

$$G^{\text{bp}}(\mathbf{x}, t | \mathbf{x}_o, t_o) = \delta(t - t_o) \delta^{(2)}(\mathbf{x} - \mathbf{x}_o), \quad \mathbf{x}, \mathbf{x}_o \in \partial \mathcal{R}. \quad (5.192c)$$

The boundary propagator acts as the mediator between boundary data, σ , and interior points, with the transfer of information realized through both advection and diffusion. A focus on the boundary propagator rather than the Green's function allows us to reduce the dimensionality of the problem by placing source points only on the boundary rather than both the boundary and throughout the interior. Also recall our discussion in VOLUME 1, where we argued that the boundary propagator can be considered the **impulse response function** for spatially distributed sources. Here, the mediation of the Dirac delta boundary sources is performed by advection plus diffusion, whereas in VOLUME 1 we only considered linear damping and diffusion.

Normalization of the boundary propagator

As seen in Chapter 4, diffusion acts to smooth all structure in the tracer field. Hence, if the boundary data is a uniform constant, $\sigma = \sigma_{\text{const}}$, then given sufficient time the tracer concentration will equal to this constant, $C = \sigma_{\text{const}}$. This steady state result is independent of details for the velocity field and the diffusivity tensor, with details of advection and the diffusivity acting only to modify the transient behavior during equilibration. Assuming we wait long enough, or equivalently that the initial condition occurs infinitely far in the past, then the

tracer concentration solution (5.189) leads to the normalization of the boundary propagator

$$\lim_{t_{\text{init}} \rightarrow -\infty} \int_{t_{\text{init}}}^t \left[\oint_{\partial\mathcal{R}} G^{\text{bp}}(\mathbf{x}, t | \mathbf{x}_o, t_o) d\mathcal{S}_0 \right] dt_o = 1 \quad \text{for } \mathbf{x} \in \mathcal{R}. \quad (5.193)$$

This normalization holds for all field points, \mathbf{x} , within the region. Even though this condition was derived by assuming the special case of constant boundary data, it holds in general since the Green's function, and by extension the boundary propagator, are independent of the boundary data prescribed for the tracer concentration.

5.9.11 Comments

A careful reading of this section is best considered along with the analogous, yet more detailed, treatment of the diffusion equation Green's function in VOLUME 1. Furthermore, these two presentations offer technical introductions to the review paper from [Haine et al. \(2025\)](#), who synthesize the variety of Green's function methods for studying age and ventilation time scales in geophysical flows, with particular focus on the ocean. The Green's function method is technically challenging in realistic numerical models due to the extra space-time dimensions needed to hold the Green's function, $G(\mathbf{x}, t | \mathbf{x}_o, t_o)$, in computer memory. As a result, realistic applications typically make approximations to reduce the dimensionality, such as by assuming steady state or by focusing on boundary propagators. Hence, there has yet to be a calculation of the full Green's function for a realistic ocean, with that calculation awaiting bigger computers and/or novel methods to side-step the nontrivial memory requirements. [Haine et al. \(2025\)](#) provide further discussion of numerical considerations.



5.10 Exercises

EXERCISE 5.1: ONE-DIMENSIONAL ADVECTION

Consider the advection equation in one space dimension without boundaries

$$(\partial_t + u \partial_x) C = 0 \quad (5.194a)$$

$$C(x, z, t = 0) = C_o \cos(k x) \quad (5.194b)$$

$$u(z, t) = \alpha z \cos(\omega t). \quad (5.194c)$$

The specified zonal velocity is non-divergent, oscillatory in time, and vertically sheared

$$\partial_z u = \alpha \cos(\omega t), \quad (5.195)$$

with ω the angular frequency of the temporal oscillations. What is the tracer concentration at times $t > 0$? Hint: make use of the exact solution given by equation (5.15).

EXERCISE 5.2: SKEW FLUX FOR OCEAN MESOSCALE EDDIES

Consider a Boussinesq ocean description of a middle-latitude mesoscale ocean eddy respecting geostrophic balance on an f-plane. In this case, the horizontal eddy-induced velocity at the ocean surface is non-divergent

$$\mathbf{u}^* = \nabla \times \hat{\mathbf{z}} \psi. \quad (5.196)$$

In this equation, the geostrophic streamfunction is given by

$$\psi = -\hat{\mathbf{z}} g \eta / f, \quad (5.197)$$

with f the Coriolis parameter, g the gravitational acceleration, and η the sea level undulation associated with the eddy. Since the fluid is incompressible, the mass transport equals to the volume transport times a constant reference density, ρ_0 .

- (a) Determine the skew diffusion tensor (5.47).
- (b) Determine the skew tracer flux (5.61a).

EXERCISE 5.3: EVOLUTION OF TRACER CENTER OF MASS IN A STATIC MATERIAL DOMAIN

The exercise introduces us to how the tracer center of mass evolves within a Boussinesq ocean. We define the tracer center of mass as

$$\langle \mathbf{x} \rangle^C = \frac{\int \mathbf{x} C \, dV}{\int C \, dV}, \quad (5.198)$$

with C the tracer concentration, \mathbf{x} the coordinate of a point in the fluid, and integration is over the full fluid domain. For example, with a spherically symmetric tracer cloud, the center of mass position is at the sphere's center. The center of mass position is not necessarily where the largest tracer concentration sits, in the same way that the center of mass of a massive object is not necessarily where the object is most dense. For example, a hollow spherical shell has its center of mass at the center of the sphere, even though there is no mass there.

For this exercise, assume the fluid is within a domain whose static boundaries are either material (no normal component to the boundary flux) or periodic. Hence, the total fluid volume and total tracer content remain constant

$$\mathcal{V} = \int dV \quad \text{and} \quad \mathcal{C} = \int C \, dV. \quad (5.199)$$

Furthermore, assume the region boundaries are static, so that the time derivative commutes with the spatial integral

$$\frac{d}{dt} \int \varphi \, dV = \int \partial_t \varphi \, dV, \quad (5.200)$$

which follows since the region boundaries are assumed to be static. Equivalently, since the region under consideration is material (no matter crosses the boundaries), we can make use of [Reynolds transport theorem](#) from [VOLUME 1](#) to write

$$\frac{d}{dt} \int \varphi \, dV = \int \frac{D\varphi}{Dt} \, dV. \quad (5.201)$$

Finally, note that we considered the case of tracer concentration moments in [Section 4.2.4](#) when studying the diffusion equation.

- (a) Consider a tracer concentration whose tendency at a point in space is affected only by advection

$$\frac{DC}{Dt} = 0 \implies \partial_t C + \nabla \cdot (\mathbf{v} C) = 0, \quad (5.202)$$

with \mathbf{v} a non-divergent velocity, $\nabla \cdot \mathbf{v} = 0$. Show that the tracer center of mass position evolves according to the tracer center of mass velocity

$$\frac{d\langle \mathbf{x} \rangle^C}{dt} = \langle \mathbf{v} \rangle^C, \quad (5.203)$$

where the tracer center of mass velocity is given by

$$\langle \mathbf{v} \rangle^C = \frac{\int \mathbf{v} C \, dV}{\int C \, dV} = \frac{1}{C} \int \mathbf{v} C \, dV. \quad (5.204)$$

- (b) Consider a tracer concentration whose tendency at a point in space affected only by diffusion

$$\partial_t C = \nabla \cdot (K \cdot \nabla C), \quad (5.205)$$

where $K = K(\mathbf{x}, t) > 0$ is a kinematic diffusivity (physical dimensions of squared length per time), and which is assumed to vanish at the domain boundaries. Show that the tracer center of mass drifts up the diffusivity gradient

$$\frac{d\langle \mathbf{x} \rangle^C}{dt} = \langle \nabla K \rangle^C. \quad (5.206)$$

Hint: use the product rule and drop boundary terms.

- (c) Consider an initial tracer concentration that is a function only of latitude,

$$C(x, y, z, t = 0) = C_o(y), \quad (5.207)$$

and assume a smooth spherical domain. Assume the diffusivity, K , is a turbulent diffusivity proportional to the eddy kinetic energy of the flow, so that large diffusivity occurs in regions with large eddy activity; i.e., there is a lot of turbulent mixing where turbulence is active. Introduce an stirring from the eddies that breaks the zonal symmetry. Qualitatively discuss the process whereby this turbulent diffusive mixing causes the tracer center of mass to drift towards the turbulent region.

- (d) Generalize the result from part (b) to the case of the diffusion equation

$$\partial_t C = \nabla \cdot (\mathbf{K} \cdot \nabla C) = \partial_p (K^{pq} \partial_q C), \quad (5.208)$$

where \mathbf{K} is a second order symmetric diffusion tensor.

EXERCISE 5.4: EVOLUTION OF TRACER CENTER OF MASS IN MOVING REGION

Consider a finite region of fluid with fixed mass that is moving with the fluid velocity field, $\mathcal{R}(\mathbf{v})$. The fluid is assumed to have a tracer whose concentration is affected by an irreversible process so that

$$\frac{DC}{Dt} = \dot{C} \neq 0. \quad (5.209)$$

For example, \dot{C} may represent a diffusive process, in which case the tracer content within the region changes due to diffusion of tracer across the region boundary.

Determine the evolution equation for the tracer center of mass position

$$\langle \mathbf{x} \rangle^C = \frac{\int_{\mathcal{R}(\mathbf{v})} \mathbf{x} C \rho \, dV}{\int_{\mathcal{R}(\mathbf{v})} C \rho \, dV}. \quad (5.210)$$

Hint: the region under consideration is moving with the fluid and has constant mass. Although the region boundaries are not material, we can make use of Reynold's transport

theorem from VOLUME 1 since the region has a constant mass. Consequently, we can set

$$\frac{d}{dt} \int_{\mathcal{R}(\mathbf{v})} \psi \rho dV = \int_{\mathcal{R}(\mathbf{v})} \frac{D\psi}{Dt} \rho dV. \quad (5.211)$$

EXERCISE 5.5: STEADY TWO DIMENSIONAL ADVECTION-DIFFUSION

Consider the steady state advection-diffusion equation for a scalar field, Q , in a two dimensional non-divergent flow

$$\nabla \cdot (\mathbf{u} Q) = \nabla \cdot (\mathbf{K} \cdot \nabla Q) \quad \text{with} \quad \mathbf{u} = \hat{\mathbf{z}} \times \nabla \psi, \quad (5.212)$$

and \mathbf{K} a diffusion tensor. Show that when evaluated along a contour of constant Q we can write

$$-(\hat{\mathbf{n}} \cdot \nabla Q) (\hat{\mathbf{t}} \cdot \nabla \psi) = \nabla \cdot (\mathbf{K} \cdot \nabla Q) \quad (5.213)$$

where $\hat{\mathbf{t}}$ is the unit tangent along the contour and $\hat{\mathbf{n}}$ is a unit vector pointing to the left of the tangent. Assuming $\hat{\mathbf{n}} \cdot \nabla Q \neq 0$, this equation takes on the form

$$\hat{\mathbf{t}} \cdot \nabla \psi = -\frac{\nabla \cdot (\mathbf{K} \cdot \nabla Q)}{(\hat{\mathbf{n}} \cdot \nabla Q)}, \quad (5.214)$$

which provides a means to integrate the streamfunction, ψ , along contours of constant Q .

If Q is the quasi-geostrophic potential vorticity (see VOLUME 3), then contours of constant Q are known as *geostrophic contours*. Within this context, [Rhines and Holland \(1979\)](#) made use of the identity (5.214) in their study of ocean circulation in the presence of eddy diffusion of potential vorticity.

Hint: write the advection operator as a Jacobian and make use of the Jacobian exercise in the vector calculus chapter in VOLUME 1.

EXERCISE 5.6: DISTRIBUTION OF ONE TRACER WITH RESPECT TO ANOTHER

Consider two tracers, ψ and B , that satisfy the advection-diffusion equation with the same diffusion tensor

$$\rho \frac{D\psi}{Dt} = \nabla \cdot (\rho \mathbf{K} \cdot \nabla \psi) \quad (5.215a)$$

$$\rho \frac{DB}{Dt} = \nabla \cdot (\rho \mathbf{K} \cdot \nabla B). \quad (5.215b)$$

Having access to two tracers allows us to diagnose certain properties of the flow, both in geographical/depth space as well as in the space defined by the tracers. We here study how the tracer B is distributed within layers defined by ψ , and how that distribution evolves in time. These considerations are partly motivated by the work of [Ruan and Ferrari \(2021\)](#), who assumed B to be buoyancy (with a linear equation of state). Whereas [Ruan and Ferrari \(2021\)](#) assumed a Boussinesq ocean with a constant scalar diffusivity, here we generalize to the non-Boussinesq case with a flow-dependent diffusion tensor, \mathbf{K} , which is a symmetric and positive-definite second order tensor.

- (a) Derive the following identity

$$\rho \frac{D(\psi B^\Gamma)}{Dt} = \nabla \cdot (B^\Gamma \rho \mathbf{K} \cdot \nabla \psi - \psi \rho \mathbf{K} \cdot \nabla B^\Gamma) + \Gamma \psi \nabla B^{\Gamma-1} \cdot \rho \mathbf{K} \cdot \nabla B + 2 \Gamma \psi B^{\Gamma-1} \rho \dot{B}, \quad (5.216)$$

where B^Γ is B raised to the integer power Γ , and where we made use of the shorthand

$$\dot{B} = \frac{DB}{Dt}. \quad (5.217)$$

Show all relevant steps in the derivation of equation (5.216). Hint: as an optional warm-up, derive the special case with $\Gamma = 1$

$$\rho \frac{D(\psi B)}{Dt} = \nabla \cdot (B \rho \mathbf{K} \cdot \nabla \psi - \psi \rho \mathbf{K} \cdot \nabla B) + 2 \psi \rho \dot{B} \quad (5.218)$$

and then the case with $\Gamma = 2$

$$\rho \frac{D(\psi B^2)}{Dt} = \nabla \cdot (B^2 \rho \mathbf{K} \cdot \nabla \psi - \psi \rho \mathbf{K} \cdot \nabla B^2) + 2 \psi \nabla B \cdot \rho \mathbf{K} \cdot \nabla B + 4 \psi B \rho \dot{B}. \quad (5.219)$$

(b) Introduce the ψ -weighted mean of an arbitrary field, $\bar{\Gamma}$, according to

$$\bar{\Gamma} \equiv \frac{\int_{\mathcal{R}} \Gamma \psi \rho dV}{\int_{\mathcal{R}} \psi \rho dV}. \quad (5.220)$$

Furthermore, assume all boundaries to the domain are material, which means that the domain matter content is fixed in time

$$\frac{d}{dt} \int_{\mathcal{R}} \rho dV = 0 \quad \text{and} \quad \frac{d}{dt} \int_{\mathcal{R}} \psi \rho dV = 0 \quad \text{and} \quad \frac{d}{dt} \int_{\mathcal{R}} B \rho dV = 0. \quad (5.221)$$

Make use of equation (5.218) to derive the following identity

$$\frac{d\bar{B}}{dt} = 2 \bar{\dot{B}}, \quad (5.222)$$

and offer some discussion.

EXERCISE 5.7: EVOLUTION OF TRACER MOMENTS

In Section 4.8.3 we studied how tracer diffusion affects tracer moments. Here we consider the combined effects of advection and diffusion. We assume the boundaries are insulating (i.e., zero normal boundary flux of tracer) so that $\mathbf{J} \cdot \hat{\mathbf{n}} = 0$ with $\hat{\mathbf{n}}$ the outward normal at the boundary. We also assume there is no matter crossing the boundary, so that $(\mathbf{v} - \mathbf{v}^{(b)}) \cdot \hat{\mathbf{n}} = 0$, where $\mathbf{v}^{(b)}$ is the velocity of a point stuck to the boundary. Correspondingly, the total fluid mass in the domain remains fixed

$$M = \int \rho dV \quad \text{with} \quad \frac{dM}{dt} = 0, \quad (5.223)$$

so that the domain is material since we assume no exchange of mass or tracer across the boundaries. These assumptions allow us to focus on the effects from tracer diffusion and advection within the domain interior.

(a) DOMAIN AVERAGED TRACER CONCENTRATION: The domain averaged tracer concentration is defined by

$$\bar{C} = \frac{\int_{\mathcal{R}} C \rho dV}{M}. \quad (5.224)$$

Show that its time derivative vanishes.

(b) TRACER VARIANCE WITHIN THE DOMAIN: The variance of the tracer concentration is

defined by

$$\text{var}(C) \equiv \frac{\int_{\mathcal{R}} (C - \bar{C})^2 \rho dV}{M} = \bar{C^2} - \bar{C}^2 \geq 0. \quad (5.225)$$

The tracer variance measures the deviation of the tracer concentration relative to the domain averaged concentration. Since the domain average tracer concentration remains fixed in time, the time change of the variance is given by

$$\frac{d[\text{var}(C)]}{dt} = \frac{d\bar{C^2}}{dt}. \quad (5.226)$$

Thus, it is common to refer to $\bar{C^2}$ as the tracer variance, though strictly speaking only time derivatives of $\bar{C^2}$ and $\text{var}(C)$ are equal as per equation (5.226). Show that

$$\frac{d[\text{var}(C)]}{dt} = \frac{d\bar{C^2}}{dt} \leq 0, \quad (5.227)$$

with this inequality determined solely by diffusion, whereas advection has no impact on the variance.

(c) DIFFUSION OF ARBITRARY TRACER MOMENTS: Prove that

$$\frac{d\bar{C^\Gamma}}{dt} = \Gamma(\Gamma - 1) \int C^{\Gamma-2} \nabla C \cdot \mathbf{J} dV \leq 0. \quad (5.228)$$

For $\Gamma = 0$ we have an expression of mass conservation for the domain, whereas $\Gamma = 1$ is an expression of tracer conservation. The case of $\Gamma = 2$ yields the tracer variance result (5.227).

Hint: This exercise reveals that tracer moments evolve solely through the effects of diffusion, whereas advection does not touch the tracer moments. The goal of this exercise is to emphasize these results by working through the details, which are largely identical to those presented in Section 4.8.3 when studying diffusion alone.



Chapter 6

EDDY-MEAN INTERACTION FOR SCALARS

Geophysical fluid flows have multiple scales in both space and time. In the analysis of these flows, it is useful to seek a description that decomposes fluid properties into a mean component and a departure from the mean, with the departure referred to as an [eddy](#). [Rectification](#) occurs if oscillatory or turbulent eddying motions produce a mean flow through nonlinear terms in the governing equations. The mean field can be defined in many fashions with subjective choices based on particulars of the flow and the analysis goals. In turn, the chosen definition for the mean affects what we refer to as an eddy. Quite generally, eddy fluctuations take the form of transient linear waves, nonlinear and/or breaking waves, coherent structures, and/or a chaotic/turbulent soup of eddying features. In this chapter we develop a kinematic framework motivated by the analysis of scalar transport induced by small amplitude wave-like eddying features. This framework can also be used for turbulent processes and their parameterizations, though we do not pursue that application here.

We consider two related kinematic methods to decompose the flow into a mean and eddy. The first is the [generalized Lagrangian mean \(GLM\)](#), which is a hybrid Eulerian/Lagrangian method that introduces an Eulerian disturbance field to measure the position of a fluid particle relative to its mean position ([Andrews and McIntyre, 1978a,b](#); [Bühler, 2014a](#); [Gilbert and Vanneste, 2025](#)). We access a small portion of the GLM framework, focusing on the needs for describing the kinematics of eddy scalar fluxes following from [Middleton and Loder \(1989\)](#). A more thorough treatment that considers the momentum and vorticity equations is outside the scope for this chapter. The second kinematic method makes use of the [isopycnal](#) vertical coordinate, which is Eulerian in the horizontal yet Lagrangian in the vertical. Isopycnal coordinates are frequently used to describe how ocean mesoscale eddies affect stratification and tracer transport in stably stratified flows, with a thorough treatment of these coordinates presented in Part I of this volume.

We emphasize our limited exploration of GLM, with a far more thorough presentation given in the primary literature and follow on work cited in the previous paragraph. Indeed, we could have avoided GLM altogether in this chapter given that we limit attention to small amplitude disturbances. However, the conceptual framework offered by the GLM is very useful to be exposed to since it is extensive within the literature, even for small amplitude disturbances. Furthermore, as we propose, it provides a fruitful intellectual introduction to isopycnal averaging methods, which form a central framework for parameterizing ocean mesoscale eddies. So even if one remains skeptical of the utility of GLM for their particular studies, its conceptual and technical features remain pervasive in geophysical fluid mechanics.

CHAPTER GUIDE

This chapter relies on an understanding of the maths and physics of the advection-diffusion equation explored in Chapter 5. We focus on non-divergent flows with kinematics presented in VOLUME 1 as applicable to the Boussinesq ocean studied in VOLUME 2. Generalizations to non-Boussinesq flows are straightforward, with examples provided by [Griffies and Greatbatch \(2012\)](#). The kinematics of isopycnal fluid layers in a perfect fluid (Sections 6.5 and 6.6) are posed using the isopycnal vertical coordinates detailed in Chapter 3, which also develops the shallow water thickness weighted averaged equations. Our presentation of the isopycnal eddy-mean flow decomposition follows the methods developed by [McDougall and McIntosh \(2001\)](#) and summarized in Chapter 9 of [Griffies \(2004\)](#). A directly related approach is considered in Chapter 3 for the stacked shallow water equations, in which we develop the thickness weighted tracer, momentum, and vorticity budgets (see also [Young \(2012\)](#) and [Jansen et al. \(2024\)](#)).

Throughout this chapter we assume Cartesian tensors in the horizontal directions, which is sufficient for the isopycnal averaging in Sections 6.5 and 6.6. However, to extend the full [GFM](#) theory to arbitrary horizontal coordinates requires more general mathematical tools, such as those reviewed by [Gilbert and Vanneste \(2025\)](#).

6.1	Loose threads	191
6.2	Methods for decomposing the flow	191
6.2.1	Eulerian and Lagrangian means	191
6.2.2	Operators used to compute means	191
6.2.3	Reynolds property	192
6.3	Generalized Lagrangian mean for scalar fields	193
6.3.1	Motivation from the advection equation	193
6.3.2	Length scales and the small parameter	195
6.3.3	Decomposing the particle trajectory	195
6.3.4	GLM and the Stokes mean	196
6.3.5	Stokes drift	198
6.3.6	An example wave	198
6.3.7	GLM with a materially constant scalar	200
6.3.8	Further study	201
6.4	Eddy tracer fluxes and particle displacements	201
6.4.1	Particle displacements and eddy tracer fluxes	202
6.4.2	Decomposing into symmetric and skew symmetric fluxes	202
6.4.3	The symmetric tracer flux	203
6.4.4	Skew, advective, and rotational tracer fluxes	203
6.4.5	What does a point measurement yield?	204
6.4.6	Further study	205
6.5	Volume transport in an isopycnal ensemble	205
6.5.1	Specifying the vertical position	206
6.5.2	Modified mean density	206
6.5.3	Isopycnal mean and modified mean	207
6.5.4	Transformed residual mean (TRM)	208
6.5.5	Depth integrated TRM transport	209
6.5.6	Quasi-Stokes transport	210
6.5.7	Three-component TRM velocity	210
6.5.8	Volume conservation and the thickness equation	211

6.5.9	Ensemble mean thickness equation	212
6.5.10	Ensemble mean kinematics in geopotential coordinates	213
6.5.11	Approximate ϱ -ensemble kinematics in geopotential coordinates	213
6.5.12	Further study	215
6.6	Isopycnal mean tracer equation	215
6.6.1	Thickness weighted average	215
6.6.2	Isopycnal mean thickness weighted tracer equation	216
6.6.3	Subgrid scale tracer transport tensor	216
6.6.4	Summary of the tracer parameterization problem	217
6.6.5	Comments	218
6.7	Exercises	218

6.1 Loose threads

- Formulate the thickness weighted tracer variance equations as in Appendix A of *Pudig et al. (2026)*.

6.2 Methods for decomposing the flow

There are many methods used to decompose flow into mean and eddy components. There is no unique or objective choice, with each offering pros and cons. Furthermore, there is dependence on the coordinate choice used to represent the fields. So although physics is independent of coordinates, it is an unfortunate fact that computing a mean results in a flow decomposition that inherits particulars of the subjectively chosen coordinate representation.

6.2.1 Eulerian and Lagrangian means

At any point in space and time, we can decompose a field into its **Eulerian mean**, $\bar{\chi}(\mathbf{x}, t)$, and departures from the mean that are referred to as the eddy fluctuation, $\chi'(\mathbf{x}, t)$:

$$\chi(\mathbf{x}, t) = \bar{\chi}(\mathbf{x}, t) + \chi'(\mathbf{x}, t). \quad (6.1)$$

This choice is the default when working with Eulerian coordinates. It also accords with common laboratory or field methods that provide point measurements. The complement approach arises when representing fields using Lagrangian coordinates, in which we decompose a field into its **Lagrangian mean** and the departure from the mean. This choice is convenient if having knowledge of fluid particle trajectories, such as in simulations or field platforms (e.g., floats or balloons) that move with the fluid. Finally, there are hybrid approaches that we encounter in this chapter that are motivated by the generalized Lagrangian mean.

6.2.2 Operators used to compute means

We here summarize a variety of mean operators, whether realized using Eulerian coordinates, Lagrangian coordinates, or hybrids, with the following list non-exhaustive.

Time mean

If the mean operator is based on a long time average, then the mean fields are either time independent or they vary over a far longer time scale than the unaveraged fields. This is a

common operator when interest is focused on the long term mean fluid properties, such as in climate science where 30 years is often considered the minimum time average for developing climate statistics.

Phase average

Rather than a time mean, we may choose to average over the phase (or period) of a wave. A **phase average** is particularly relevant when the fluctuating field involves quasi-linear waves. Hence, we make extensive use of phase averaging when studying waves in **VOLUME 5**.

Zonal mean

The **zonal mean** refers to a spatial averaging operation computed by a line integral of a field over the longitudinal extent of the domain, and then dividing by the zonal length of the domain. The zonal mean is particularly relevant for regions that are zonally periodic, such as the atmosphere as well as the ocean in the latitudes around the Drake Passage. The resulting zonal mean field is independent of longitude.

Coarse graining

Coarse graining refers to the process of spatial averaging over specific scales through use of a filtering operator. Coarse graining originates from renormalization methods in theoretical physics and engineering, and it provides a useful method to control the length scales over which the flow is decomposed. *Buzzicotti et al. (2023)* reviewed the method and its use with global ocean models.

Ensemble mean

An **ensemble mean** is computed through generating an ensemble of flow realizations that differ in a controlled manner, such as through the initial conditions, and then averaging over the many (formally infinite) realizations. This method is theoretically quite convenient since space and time operators commute with the ensemble mean operator, which is not a property shared by the other operators listed above. It is for this reason we make use of the ensemble mean in this chapter in order to avoid a variety of technical details that arise with the other operators.

6.2.3 Reynolds property

If a mean operator satisfies the following properties then it is said to provide a **Reynolds decomposition**

$$\bar{\chi}' = 0 \quad \text{and} \quad \bar{\bar{\chi}} = \bar{\chi} \quad \text{and} \quad \bar{c\bar{\chi}} = c\bar{\chi}. \quad (6.2)$$

The first equation says that the mean of an eddy fluctuation vanishes. The second says that the mean of a mean returns the mean. The final equality says that a constant, c , commutes with the mean operator. Notably, some or all of these properties are not satisfied by certain operators used for eddy-mean decompositions. However, in the following we assume they are satisfied by our mean operator.

A Reynolds average acting on a linear equation means that both the mean and eddy quantity satisfy the linear equation. In particular, consider the non-divergence condition for a Boussinesq ocean flow, $\nabla \cdot \mathbf{v} = 0$. Taking the mean of this equation renders

$$\nabla \cdot \mathbf{v} = 0 \implies \nabla \cdot \bar{\mathbf{v}} = 0, \quad (6.3)$$

so that the mean velocity is non-divergent. Since both the unaveraged velocity and the mean velocity are non-divergent, it follows that the eddy velocity is also non-divergent

$$\nabla \cdot (\bar{\mathbf{v}} + \mathbf{v}') = \nabla \cdot \mathbf{v}' = 0. \quad (6.4)$$

6.3 Generalized Lagrangian mean for scalar fields

We here consider basic elements of **generalized Lagrangian mean (GLM)** theory. GLM is a hybrid between Lagrangian and Eulerian descriptions of fluid motions, so that it might be more appropriate to refer to it as the “hybrid Lagrangian-Eulerian mean theory”. The GLM and the Eulerian mean for a fluid property are generally distinct, with their difference referred to as the **Stokes mean**

$$\text{generalized Lagrangian mean} = \text{Eulerian mean} + \text{Stokes mean}. \quad (6.5)$$

This name is motivated from the **Stokes drift** encountered in our study of fluid kinematics in VOLUME 1, with Stokes drift referring to the difference between the Lagrangian mean velocity and Eulerian mean velocity. Note that the literature sometimes refers to the Stokes mean as the “Stokes correction”. We avoid that terminology in order to avoid the spurious notion that one type of mean operator is more correct than the other. Instead, a mean operator is subjectively chosen based on its suitability to a particular question.

6.3.1 Motivation from the advection equation

For much of this chapter we are concerned with a materially constant scalar field

$$\frac{D\chi}{Dt} = (\partial_t + \mathbf{v} \cdot \nabla)\chi = 0, \quad (6.6)$$

and the description of χ when it, and the non-divergent velocity, are decomposed into a mean and eddy. The scalar field, χ , remains constant when following trajectories of fluid particles. As described in the kinematics chapters in VOLUME 2, each fluid particle trajectory forms an integral curve of the velocity field. Furthermore, the congruence of such integral curves forms the **motion field**, $\boldsymbol{\varphi}(\mathbf{a}, T)$. The motion field generates a nonlinear time dependent and invertible **flow map** that continuously and smoothly reshapes the fluid continuum. We write the motion field as a function of the material space coordinate, \mathbf{a} , and the material time coordinate, T .¹

Eulerian mean

An Eulerian mean operator considered in Section 6.2 leads to the following mean version of the advection equation (6.6), here written both in the advective form and the flux form

$$\partial_t \bar{\chi} + \bar{\mathbf{v}} \cdot \nabla \bar{\chi} = -\bar{\mathbf{v}}' \cdot \nabla \bar{\chi}' \quad \text{advective form} \quad (6.7a)$$

$$\partial_t \bar{\chi} + \nabla \cdot (\bar{\mathbf{v}} \bar{\chi}) = -\nabla \cdot (\bar{\mathbf{v}}' \bar{\chi}'). \quad \text{flux form.} \quad (6.7b)$$

¹Throughout this book, we are considering all speeds (particles and waves) to be far slower than light speed. Hence, the material time coordinate equals to the Eulerian time, $T = t$. However, we use a distinct symbol to indicate what spatial coordinates are held fixed when taking the Eulerian time derivative, ∂_t , versus the Lagrangian time derivative, ∂_T .

The equations are equivalent since both the Eulerian mean velocity and the eddy velocity are non-divergent, as shown in Section 6.2.3 for a Reynolds decomposition. Evidently, the Eulerian mean, $\bar{\chi}$, is not materially constant when following trajectories defined by the Eulerian mean velocity, $\bar{\mathbf{v}}$. The reason is that flow following such trajectories encounters a source term, $-\bar{\mathbf{v}} \cdot \nabla \chi'$, due to correlations between the velocity and tracer. Hence, the $\bar{\chi}$ evolution equation is mathematically distinct from that of χ . Furthermore, when given information only about the mean fields, then we must develop a closure for the unresolved correlation. This point touches on the largely unsolved *turbulence closure* problem pervasive in fluid mechanics.

Lagrangian mean

An alternative approach makes use of the Lagrangian reference frame, where we sample the fluid property along a fluid particle trajectory²

$$\chi^L(\mathbf{a}, T) = \text{property } \chi \text{ following the fluid particle trajectory, } \mathbf{X}(\mathbf{a}, T). \quad (6.8)$$

In Lagrangian coordinates, the material constancy equation (6.6) becomes

$$\partial_T \chi^L(\mathbf{a}, T) = 0. \quad (6.9)$$

Consider a mean operator computed as an average over a region of material space. For example, if \mathbf{a} is the initial fluid particle position, then a mean coordinate, $\bar{\mathbf{a}}$, and corresponding mean field, $\bar{\chi}^L$, render a coarse-graining over the initial positions. Since each member of the Lagrangian mean satisfies equation (6.9), so too does the Lagrangian mean

$$\partial_T \bar{\chi}^L(\bar{\mathbf{a}}, T) = 0. \quad (6.10)$$

Notably, this equation retains the simplicity of the unaveraged version.

The elegance of the Lagrangian mean equation (6.10) hides a major limitation when applied to fluid flow. Namely, the flow map can become quite complex for turbulent flows, and even for laminar flow (e.g., chaotic advection). Such complexity makes a fully Lagrangian approach technically impractical. We thus seek something in between the Eulerian and Lagrangian approach, which leads to the generalized Lagrangian mean.

Generalized Lagrangian mean

The *generalized Lagrangian mean* (GLM) melds elements of the Eulerian and the Lagrangian approaches. It does so by retaining the Eulerian space and time coordinates, plus by adding an additional field, $\xi(\mathbf{x}, t)$, that measures the position of a fluid particle relative to its mean position. Adding a new dynamical field is clearly a double-edged sword. On the positive side it provides the means to obtain Lagrangian information when using Eulerian kinematics. On the negative side we must concern ourselves with determining this new field and its evolution.

For the tracer equation, the net effect of the GLM approach is the mean scalar field that remains constant following trajectories that form integral curves of the GLM velocity

$$\partial_t \bar{\chi}^{(\text{GLM})} + \bar{\mathbf{v}}^{(\text{GLM})} \cdot \nabla \bar{\chi}^{(\text{GLM})} = 0. \quad (6.11)$$

²We here use the notation $\mathbf{X}(\mathbf{a}, T)$ for a fluid particle, whereas we could alternatively make use of the motion field, $\boldsymbol{\varphi}(\mathbf{a}, T)$, introduced just following equation (6.6) and studied in VOLUME 1. The motion field and the particle trajectory are the same when fixing a particular particle label, \mathbf{a} . We choose the particle trajectory notion as it is somewhat more familiar.

We do not derive the GLM equation (6.11).³ Even so, we motivate the GLM average from the analysis of small amplitude eddying motions, making use of this analysis as a framework for describing scalar transport.⁴

6.3.2 Length scales and the small parameter

We consider two length scales associated with an eddy. One length characterizes the size of the eddy whose length scale we write as λ . If the eddy is a monochromatic wave, then λ is its wave length. The second length scale characterizes the size of particle displacements relative to the mean position of the particle, $|\xi|$. In the following, we assume the particle displacements are small relative to λ

$$|\xi| \ll \lambda \quad \text{small amplitude waves.} \quad (6.12)$$

We thus introduce the small non-dimensional ratio of length scales for the following analysis

$$\alpha = |\xi|/\lambda \ll 1. \quad (6.13)$$

6.3.3 Decomposing the particle trajectory

From the discussion of fluid particle trajectories given in VOLUME 1, we know that the trajectory of a fluid particle is determined by integrating the relation between the particle trajectory and the particle velocity

$$\left[\frac{\partial \mathbf{X}(\mathbf{a}, T)}{\partial T} \right]_{\mathbf{a}} = \mathbf{v}[\mathbf{X}(\mathbf{a}, T)] \implies \mathbf{X}(\mathbf{a}, T) = \mathbf{X}(\mathbf{a}, 0) + \int_0^T \mathbf{v}[\mathbf{X}(\mathbf{a}, T')] dT'. \quad (6.14)$$

As expressed here, a trajectory describes the position of an individual fluid particle relative to a chosen origin. The congruence of all trajectories forms the integral curves of the velocity field, thus providing a Lagrangian description of the flow. The material coordinate, \mathbf{a} , distinguishes the continuum of fluid particles, thus making the trajectory a field in material space-time.

The GLM develops a hybrid Eulerian-Lagrangian method and it is motivated by linear or quasi-linear disturbances. Keeping this motivation in mind, we consider each point in space, \mathbf{x} , to be the mean position of a unique fluid particle. This identification acts to couple the Eulerian and Lagrangian kinematic descriptions. To realize this coupling, we introduce an Eulerian field, $\xi(\mathbf{x}, t)$, which measures the position of all fluid particles relative to their respective mean positions.⁵ That is, at each point, \mathbf{x} , the disturbance field, $\xi(\mathbf{x}, t)$, measures the displacement of the particular fluid particle whose mean position is \mathbf{x} . At another point in space, \mathbf{y} , the same disturbance field measures the displacement of a distinct fluid particle whose mean position is \mathbf{y} .

As basic assumption of the method is that $\xi(\mathbf{x}, t)$ provides a one-to-one invertible map⁶ from the Eulerian mean spatial position of a fluid particle, \mathbf{x} , to the actual particle position, $\mathbf{x} + \xi(\mathbf{x}, t)$. We illustrate this decomposition in Figure 6.1. By definition, the Eulerian mean of

³See section 10.2.2 of [Bühler \(2014a\)](#).

⁴It is useful to note that even if the Eulerian velocity is non-divergent, as for a Boussinesq ocean, the GLM velocity is divergent.

⁵We introduce a one-dimensional disturbance field when taking a Lagrangian perspective to derive the equations for acoustic waves in VOLUME 5. The GLM disturbance field, $\xi(\mathbf{x}, t)$, provides a three-dimensional generalization of that approach.

⁶Section 10.2.1 of [Bühler \(2014a\)](#) refers to $\xi(\mathbf{x}, t)$ as the lifting map.

the disturbance field vanishes

$$\overline{\xi(\mathbf{x}, t)} = 0, \quad (6.15)$$

which follows by considering each point in space to be the ensemble mean position of a unique fluid particle. Note that the Eulerian mean operator can be any of the operators (or others) satisfying the Reynold's decomposition property discussed in Section 6.2. Even so, we generally consider it to be an ensemble mean, both for conceptual and technical reasons. Finally, for flows that become quite nonlinear, the mapping loses its one-to-one invertible property, in which case the method breaks down.

Specification of $\xi(\mathbf{x}, t)$ for large amplitude disturbances (i.e., nonlinear waves) requires the full machinery of GLM, which is beyond our scope. Instead, to expose the rudiments we assume small amplitude disturbances, for which the particle displacement amplitude is much smaller than the wavelength of the disturbance as given by the inequality (6.13). In this case the disturbance field is constructed by time integration of the eddy velocity field

$$\left[\frac{\partial \xi(\mathbf{x}, t)}{\partial t} \right]_{\mathbf{x}} = \mathbf{v}'(\mathbf{x}, t) \implies \xi(\mathbf{x}, t) = \int_0^t \mathbf{v}'(\mathbf{x}, t') dt', \quad (6.16)$$

where we assume, for convenience, that $\xi(\mathbf{x}, t = 0) = 0$. It follows that if the eddy velocity is non-divergent then so is the disturbance field

$$\nabla \cdot \mathbf{v}' = 0 \implies \nabla \cdot \xi = 0. \quad (6.17)$$

The definition (6.16) for the disturbance field is directly analogous to the particle trajectory position, $\mathbf{X}(\mathbf{a}, T)$, given by equation (6.14). However, there are important distinctions. Namely, the disturbance, $\xi(\mathbf{x}, t)$, is an Eulerian space-time field that measures the position of all fluid particles relative to their respective mean positions, with each Eulerian position, \mathbf{x} , corresponding to the mean position for a distinct fluid particle. In contrast, the particle position, $\mathbf{X}(\mathbf{a}, T)$, is a Lagrangian space-time field that is attached to each fluid particle and measures the position of particles relative to a chosen origin.

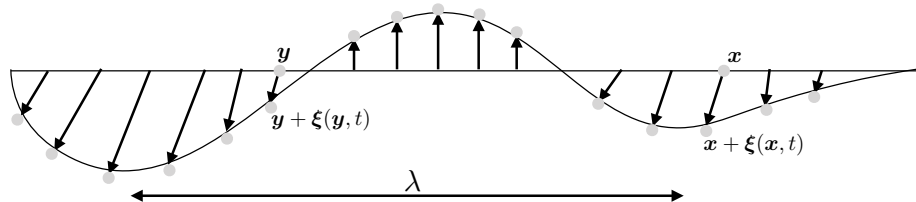


FIGURE 6.1: Illustrating the displacement of fluid particles in a wave disturbance. Each of the particle positions can be written, $\mathbf{x}^{(\xi)}(\mathbf{x}, t) = \mathbf{x} + \xi(\mathbf{x}, t)$, with the disturbance field, $\xi(\mathbf{x}, t)$, having a zero Eulerian mean, $\overline{\xi} = 0$. We here illustrate this role for the disturbance field for two particular fluid particles, one with mean position \mathbf{x} and the other with mean position \mathbf{y} . Small amplitude disturbances satisfy $|\xi| \ll \lambda$, where λ is the wavelength.

6.3.4 GLM and the Stokes mean

Generalized Lagrangian mean of a fluid property

The mean of a fluid property, χ , is a function of how the property is sampled when computing the mean. For example, the mean sampled on a fluctuating fluid particle differs from the mean

sampled at the particle's mean position. Mathematically, this distinction implies that

$$\underbrace{\bar{\chi}(\mathbf{x} + \boldsymbol{\xi}(\mathbf{x}, t))}_{\text{GLM}} \neq \underbrace{\bar{\chi}(\mathbf{x}, t)}_{\text{Eulerian}}, \quad (6.18)$$

where it is common to make use of the shorthand

$$\mathbf{x}^{(\xi)}(\mathbf{x}, t) \equiv \mathbf{x} + \boldsymbol{\xi}(\mathbf{x}, t) \quad (6.19)$$

for the position of the fluid particle. The mean operation,

$$\bar{\chi}^{(\text{GLM})}(\mathbf{x}, t) \equiv \bar{\chi}(\mathbf{x} + \boldsymbol{\xi}(\mathbf{x}, t), t) = \bar{\chi}(\mathbf{x}^{(\xi)}, t), \quad (6.20)$$

defines the generalized Lagrangian mean for the fluid property, χ . That is, the generalized Lagrangian mean is computed by evaluating the property, χ , at the position of a fluid particle, $\mathbf{x}^{(\xi)}(\mathbf{x}, t) = \mathbf{x} + \boldsymbol{\xi}(\mathbf{x}, t)$, and then performing an Eulerian mean operation relative to the position, \mathbf{x} . In this manner we see how \mathbf{x} is both an arbitrary Eulerian field point and the mean position of a unique fluid particle,

$$\bar{\mathbf{x}}^{(\xi)} = \bar{\mathbf{x}} + \bar{\boldsymbol{\xi}}(\mathbf{x}, t) = \mathbf{x}. \quad (6.21)$$

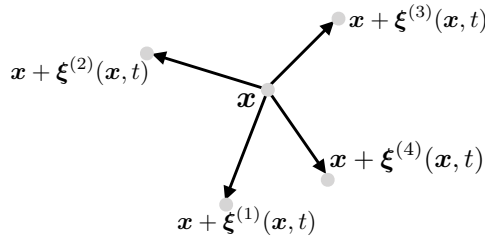


FIGURE 6.2: This figure depicts how we sample the fluid to compute the generalized Lagrangian mean of a fluid property. The central point, \mathbf{x} , is an arbitrary point in the fluid that is also the mean position of a unique fluid particle. We here interpret the Eulerian mean operation as an ensemble mean. We sample the fluid at the position of a fluid particle, and then do so again for another realization of the flow, and then again, thus building up an ensemble of flow samples, here depicting four. The ensemble mean of this sampling provides the generalized Lagrangian mean at the mean particle position, \mathbf{x} .

Since the Eulerian mean in equation (6.20) is computed with the particle disturbance as the argument to χ , it produces a Lagrangian mean. That is, the disturbance field renders a Lagrangian mean without tracking fluid particle trajectories. Instead, we only need to keep track of the particle position relative to its mean position. The approach and works so long as the disturbance field provides a one-to-one mapping between the mean particle position of all fluid particles and their instantaneous positions.

Recall from Section 6.2 that the traditional Eulerian mean is determined by evaluating χ at a fixed Eulerian point in space

$$\bar{\chi}^{(\text{E})}(\mathbf{x}, t) \equiv \bar{\chi}(\mathbf{x}, t). \quad (6.22)$$

There is no consideration of instantaneous particle positions for this mean operation. Note that we typically drop the (E) superscript on the Eulerian mean to reduce clutter.

Stokes mean

Following our discussion at the start of Section 6.3, we define the Stokes mean for a fluid property as the difference between the GLM and Eulerian mean

$$\bar{\chi}^{(s)}(\mathbf{x}, t) \equiv \bar{\chi}^{(GLM)}(\mathbf{x}, t) - \bar{\chi}(\mathbf{x}, t). \quad (6.23)$$

The Stokes mean arises from spatial structure in $\chi(\mathbf{x}, t)$, which in turn leads to differences in its mean depending on whether it is sampled on a fluid particle, $\mathbf{x}^{(\xi)}(\mathbf{x}, t)$, or sampled at the mean position of the fluid particle, \mathbf{x} .

We mathematically expose the origin of the Stokes mean by performing a Taylor series expansion around the mean particle position

$$\chi(\mathbf{x} + \boldsymbol{\xi}, t) = \chi(\mathbf{x}, t) + \boldsymbol{\xi} \cdot \nabla \chi(\mathbf{x}, t) + \frac{1}{2} \boldsymbol{\xi}^m \boldsymbol{\xi}^n \partial_m \partial_n \chi(\mathbf{x}, t) + \mathcal{O}(\alpha^3). \quad (6.24)$$

The non-dimensional ratio, $\alpha = |\boldsymbol{\xi}|/\lambda \ll 1$, was introduced in equation (6.13). It measures the ratio of the amplitude of particle displacements to the wavelength, λ , of fluctuations in the field χ (see Figure 6.1). Taking the mean of equation (6.24) then leads to an expression for the Stokes mean

$$\bar{\chi}^{(s)}(\mathbf{x}, t) = \bar{\chi}^{(GLM)}(\mathbf{x}, t) - \bar{\chi}(\mathbf{x}, t) \quad (6.25a)$$

$$= \overline{\boldsymbol{\xi} \cdot \nabla \chi} + \frac{1}{2} \overline{\boldsymbol{\xi}^m \boldsymbol{\xi}^n \partial_m \partial_n \chi} + \mathcal{O}(\alpha^3). \quad (6.25b)$$

$$= \overline{\boldsymbol{\xi} \cdot \nabla \chi'} + \frac{1}{2} \overline{\boldsymbol{\xi}^m \boldsymbol{\xi}^n} \partial_m \partial_n \bar{\chi} + \mathcal{O}(\alpha^3), \quad (6.25c)$$

where we introduced the Eulerian fluctuation,

$$\chi'(\mathbf{x}, t) = \chi(\mathbf{x}, t) - \bar{\chi}(\mathbf{x}, t), \quad (6.26)$$

and all terms on the right hand side of equation (6.25c) are evaluated at (\mathbf{x}, t) . Observe that the Stokes mean (6.25c) is nonzero only starting at $\mathcal{O}(\alpha^2)$.

6.3.5 Stokes drift

When χ represents the velocity field, we refer to the Stokes mean as the **Stokes drift**, in which

$$\mathbf{v}^{(s)} = \overline{(\boldsymbol{\xi} \cdot \nabla) \partial_t \boldsymbol{\xi}} + \frac{1}{2} \overline{\boldsymbol{\xi}^m \boldsymbol{\xi}^n} \partial_m \partial_n \bar{\mathbf{v}} + \mathcal{O}(\alpha^3), \quad (6.27)$$

where we set $\mathbf{v}' = \partial_t \boldsymbol{\xi}$ according to equation (6.16). Furthermore, the traditional case of Stokes drift occurs when the Eulerian mean field has a zero shear, so that⁷

$$\mathbf{v}^{(s)} = \overline{(\boldsymbol{\xi} \cdot \nabla) \partial_t \boldsymbol{\xi}} + \mathcal{O}(\alpha^3) \quad \text{if } \partial_n \bar{\mathbf{v}} = 0. \quad (6.28)$$

6.3.6 An example wave

Consider a small amplitude wave with zero Eulerian mean, $\bar{\mathbf{v}} = 0$, along with the wave fields

$$\boldsymbol{\xi} = -\omega^{-1} \mathbf{U}(\mathbf{x}) \sin(\mathbf{k} \cdot \mathbf{x} - \omega t) \quad (6.29a)$$

$$\mathbf{v}' = \partial_t \boldsymbol{\xi} = \mathbf{U}(\mathbf{x}) \cos(\mathbf{k} \cdot \mathbf{x} - \omega t) \quad (6.29b)$$

⁷We derive the Stokes' drift equation (6.28) using traditional Lagrangian methods when studying surface gravity waves in VOLUME 5.

$$\nabla v'^p = \nabla U^p \cos(\mathbf{k} \cdot \mathbf{x} - \omega t) - \mathbf{k} U^p \sin(\mathbf{k} \cdot \mathbf{x} - \omega t) \quad (6.29c)$$

$$\nabla \cdot \mathbf{v}' = (\nabla \cdot \mathbf{U}) \cos(\mathbf{k} \cdot \mathbf{x} - \omega t) - \mathbf{k} \cdot \mathbf{U} \sin(\mathbf{k} \cdot \mathbf{x} - \omega t), \quad (6.29d)$$

where \mathbf{U} is the velocity amplitude that is generally a function of space, \mathbf{k} is the wavevector, and $2\pi/\omega$ is the wave period. The wave renders an oscillatory motion to fluid particles, with the disturbance field specifying the instantaneous position of fluid particles whose mean position is \mathbf{x} . The disturbance field and velocity field both have a zero mean when time integrated over a wave period

$$\frac{1}{2\pi/\omega} \int_0^{2\pi/\omega} \boldsymbol{\xi}(\mathbf{x}, t) dt = 0 \quad \text{and} \quad \frac{1}{2\pi/\omega} \int_0^{2\pi/\omega} \mathbf{v}'(\mathbf{x}, t) dt = 0. \quad (6.30)$$

To maintain a non-divergent eddy velocity at arbitrary times requires

$$\nabla \cdot \mathbf{v}' = 0 \implies \nabla \cdot \mathbf{U} = \mathbf{U} \cdot \mathbf{k} = 0. \quad (6.31)$$

As studied in VOLUME 5, $\mathbf{U} \cdot \mathbf{k} = 0$ means that the wave is transverse, so that particle displacements arising from the wave are orthogonal to the wavevector.

Stokes drift

Specializing to the wave velocity field (6.29b), substituting into the Stokes drift expression (6.28), and making use of an average over a wave period yields

$$\overline{(\boldsymbol{\xi} \cdot \nabla) v'^p} = \frac{U^p \mathbf{U} \cdot \mathbf{k}}{2\omega} \quad \text{and} \quad \bar{v} = 0. \quad (6.32)$$

Hence, to $\mathcal{O}(\alpha^3)$, the Stokes drift velocity associated with the GLM is given by

$$\mathbf{v}^{(s)} = \frac{\mathbf{U}(\mathbf{U} \cdot \mathbf{k})}{2\omega} + \mathcal{O}(\alpha^3). \quad (6.33)$$

The Stokes drift vanishes at this order of accuracy for transverse waves since $\mathbf{U} \cdot \mathbf{k} = 0$.

As a check on the formalism, consider a one-dimensional longitudinal wave, in which the Stokes drift is given by

$$\bar{v}^{(s)} = \frac{U^2}{2c} + \mathcal{O}(\alpha^3), \quad (6.34)$$

where $c = \omega/k$ is the wave speed. This result agrees with that derived using Lagrangian trajectories in VOLUME 1. It is notable that the GLM displacement field offers a somewhat more streamlined method for computing Stokes drift.

Stokes mean for an arbitrary field

The Stokes mean for an arbitrary field is given by

$$\bar{\chi}^{(s)}(\mathbf{x}, t) = -\omega^{-1} \mathbf{U} \cdot \overline{\nabla \chi' \sin(\mathbf{k} \cdot \mathbf{x} - \omega t)} + \mathcal{O}(\alpha^3) \quad (6.35a)$$

$$= -\omega^{-1} \overline{\nabla \cdot (\mathbf{U} \chi') \sin(\mathbf{k} \cdot \mathbf{x} - \omega t)} + \mathcal{O}(\alpha^3), \quad (6.35b)$$

where the second equality made use of the non-divergent nature of the wave field (6.31). We also assumed the Eulerian mean for this field vanishes, $\bar{\chi} = 0$. To third order in wave amplitude, the Stokes mean is determined by the projection of the gradient of the Eulerian fluctuation,

$\nabla\chi'$, onto the wave amplitude, \mathbf{U} . For example, consider a transverse wave such as that shown in Figure 6.1. Even though the Stokes drift vanishes to order $\mathcal{O}(\alpha^3)$, the Stokes mean, $\bar{\chi}^{(s)}(\mathbf{x}, t)$, can be nonzero.

6.3.7 GLM with a materially constant scalar

Consider a materially constant scalar field, such as a tracer concentration in the absence of mixing and sources

$$\frac{DC}{Dt} = 0. \quad (6.36)$$

This equation means that fluid particles retain their value of C . We here derive some expressions that are fundamental to the kinematics studied in the remaining sections of this chapter, with Figure 6.3 providing a key schematic.

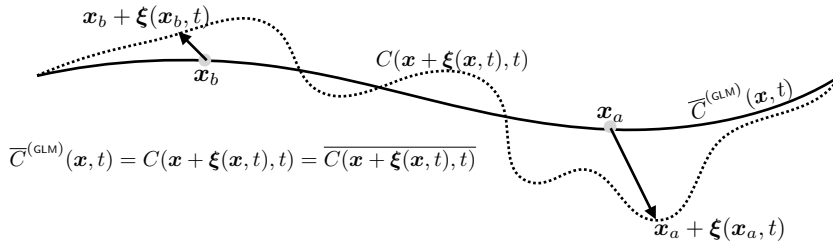


FIGURE 6.3: This figure depicts the GLM tracer concentration, $\bar{C}^{(\text{GLM})}(\mathbf{x}, t)$, along with one particular realization of the unaveraged tracer concentration, $C(\mathbf{x} + \boldsymbol{\xi}, t)$, that is part of building the GLM. That is, $\bar{C}^{(\text{GLM})}(\mathbf{x}, t) = C(\mathbf{x} + \boldsymbol{\xi}, t)$. For example, C could be the Conservative Temperature, Θ , with interest in the 12°C isotherm, in which case $\bar{\Theta}^{(\text{GLM})}(\mathbf{x}, t) = \Theta(\mathbf{x} + \boldsymbol{\xi}, t) = 12^\circ\text{C}$. We highlight two fluid particles labelled by a and b . The mean positions for these particles are \mathbf{x}_a and \mathbf{x}_b , and the positions for the single ensemble member are $\mathbf{x}_a + \boldsymbol{\xi}(\mathbf{x}_a, t)$ and $\mathbf{x}_b + \boldsymbol{\xi}(\mathbf{x}_b, t)$.

The GLM and its individual realizations

Since C is a materially invariant tracer concentration, the generalized Lagrangian mean of C equals to the value of C when sampled on fluid particles

$$\bar{C}(\mathbf{x} + \boldsymbol{\xi}, t) = \bar{C}^{(\text{GLM})}(\mathbf{x}, t) = C(\mathbf{x} + \boldsymbol{\xi}, t). \quad (6.37)$$

This identity contains in a lot of kinematic information that is basic to the GLM as well as the isopycnal averaging considered in Sections 6.5 and 6.6. Equation (6.37) says that when evaluated at the mean fluid particle position, \mathbf{x} , the GLM tracer concentration, $\bar{C}^{(\text{GLM})}(\mathbf{x}, t)$, equals to the concentration evaluated on a fluid particle, $C(\mathbf{x} + \boldsymbol{\xi}, t)$. Hence, the GLM averaging operator has no effect on $C(\mathbf{x} + \boldsymbol{\xi}, t)$, simply because the averaging operator follows fluid particles with constant C . Hence, the GLM for C equals the value of C on each member of the ensemble.

Relating the particle disturbance field to Eulerian properties of C

There is a frequently used small amplitude consequence of the identity (6.37) involving the Eulerian fluctuation

$$C'(\mathbf{x}, t) = C(\mathbf{x}, t) - \bar{C}(\mathbf{x}, t) \quad (6.38)$$

and the Eulerian mean

$$C^{(\mathbb{E})}(\mathbf{x}, t) = \overline{C}(\mathbf{x}, t). \quad (6.39)$$

To derive the identity, recall the Taylor series expansion (6.24), truncated here to first order accuracy

$$C(\mathbf{x} + \boldsymbol{\xi}, t) = C(\mathbf{x}, t) + \boldsymbol{\xi} \cdot \nabla \overline{C}(\mathbf{x}, t) + \mathcal{O}(\alpha^2). \quad (6.40)$$

An Eulerian mean of both sides to this equation renders

$$\overline{C}(\mathbf{x} + \boldsymbol{\xi}, t) = \overline{C}(\mathbf{x}, t) + \mathcal{O}(\alpha^2), \quad (6.41)$$

which follows since $\overline{\xi^p} = 0$ for each component of the displacement field. The identity (6.41) says that the GLM tracer concentration equals to the Eulerian mean tracer concentration to order $\mathcal{O}(\alpha^2)$. This result is consistent with the Stokes mean appearing only at order $\mathcal{O}(\alpha^2)$, as revealed by equation (6.25c). From equation (6.37) we know that $C(\mathbf{x} + \boldsymbol{\xi}, t) = \overline{C}(\mathbf{x} + \boldsymbol{\xi}, t)$. As a result, subtracting equations (6.40) and (6.41) yields⁸

$$C'(\mathbf{x}, t) = -\boldsymbol{\xi} \cdot \nabla \overline{C}(\mathbf{x}, t) + \mathcal{O}(\alpha^2). \quad (6.42)$$

Evidently, the Eulerian eddy tracer concentration is first order in the particle disturbance. More precisely, the eddy tracer concentration equals to minus the disturbance field as projected onto the gradient of the Eulerian mean tracer concentration. Hence, the magnitude of the eddy tracer concentration is maximized for fluid particle disturbances aligned with the gradient of the Eulerian mean tracer concentration, and the eddy concentration vanishes when particle disturbances align with surfaces of constant Eulerian mean tracer. Equation (6.42) forms the starting point for our study in Section 6.4 of the kinematics of eddy tracer fluxes.

6.3.8 Further study

GLM was introduced in the seminal papers by [Andrews and McIntyre \(1978a,b\)](#). These papers offer a wealth of intellectual rewards after much study. GLM is also detailed in the monograph on waves and mean flows by [Böhler \(2014a\)](#). [Gilbert and Vanneste \(2025\)](#) provide an elegant and powerful mathematical framework for GLM that allows for its use on arbitrary manifolds.

6.4 Eddy tracer fluxes and particle displacements

As introduced in Section 6.3.1, consider the Eulerian eddy-mean decomposition for a materially constant tracer in a non-divergent flow ($\nabla \cdot \mathbf{v} = 0$). The advection equation for this tracer is given by

$$\partial_t C + \nabla \cdot (\mathbf{v} C) = 0, \quad (6.43)$$

and its Eulerian mean is

$$\partial_t \overline{C} + \nabla \cdot (\overline{\mathbf{v}} \overline{C}) = -\nabla \cdot (\overline{\mathbf{v}' C'}). \quad (6.44)$$

The eddy advective flux, $\mathbf{v}' C'$, is the product of the eddy velocity and eddy tracer concentration. Its Eulerian mean provides a measure of the statistical correlation between \mathbf{v}' and C' , which is commonly referred to as the Eulerian mean eddy tracer flux, $\overline{\mathbf{v}' C'}$. Equation (6.44) says that the convergence of the Eulerian mean eddy flux provides a source to the advection equation

⁸The minus sign in equation (6.42) is crucial and yet can be easily missed in a cursory analysis.

satisfied by the Eulerian mean tracer concentration, with advection by the Eulerian mean velocity, $\bar{\mathbf{v}}$.

In this section we make use of the particle disturbance field of Section 6.3 to help interpret the kinematics of eddy tracer fluxes induced by small amplitude waves. As we show, the particle disturbance field affords a useful conceptual tool to frame the kinematics of eddy tracer fluxes. The kinematic expressions are accurate only for small amplitude disturbances. Even so, they provide a useful conceptual framework for interpreting eddy fluxes from large amplitude turbulent stirring.

6.4.1 Particle displacements and eddy tracer fluxes

Following Section 6.3, we introduce a particle disturbance vector corresponding to small amplitude eddy fluctuations

$$\partial_t \boldsymbol{\xi}(\mathbf{x}, t) = \mathbf{v}'(\mathbf{x}, t) + \mathcal{O}(\alpha^2) \quad (6.45a)$$

$$\overline{\boldsymbol{\xi}(\mathbf{x}, t)} = 0. \quad (6.45b)$$

The disturbance vector, $\boldsymbol{\xi}(\mathbf{x}, t)$, is an Eulerian space-time field that is defined at each spatial point. It allows us to consider each spatial point, \mathbf{x} , as the Eulerian mean position of fluid particles whose position is $\mathbf{x} + \boldsymbol{\xi}(\mathbf{x}, t)$; that is,

$$\overline{\mathbf{x} + \boldsymbol{\xi}(\mathbf{x}, t)} = \bar{\mathbf{x}} = \mathbf{x}. \quad (6.46)$$

Following the results from Section 6.3.7, to leading order we can write the Eulerian fluctuation in terms of the particle displacement (equation (6.42))

$$C'(\mathbf{x}, t) = -\boldsymbol{\xi} \cdot \nabla \bar{C}(\mathbf{x}, t) + \mathcal{O}(\alpha^2). \quad (6.47)$$

Notice that if the particle displacement is oriented along a mean tracer iso-surface, then $\boldsymbol{\xi} \cdot \nabla \bar{C}(\mathbf{x}, t) = 0$ and there is no tracer fluctuation, $C' = 0$, to order $\mathcal{O}(\alpha^2)$. More general eddying motions lead to a nonzero tracer fluctuation with the eddy tracer flux taking on the form

$$\mathbf{v}' C' = -\partial_t \boldsymbol{\xi} (\boldsymbol{\xi} \cdot \nabla) \bar{C} + \mathcal{O}(\alpha^3). \quad (6.48)$$

6.4.2 Decomposing into symmetric and skew symmetric fluxes

From equation (6.48), the m 'th component of the eddy tracer flux is given by

$$v'^m C' = -[(\partial_t \xi^m) \xi^n] \partial_n \bar{C}. \quad (6.49)$$

To explore the kinematic properties of this tracer flux, decompose the second order tensor, $(\partial_t \xi^m) \xi^n$, into its symmetric and anti-symmetric components⁹

$$2(\partial_t \xi^m) \xi^n = [(\partial_t \xi^m) \xi^n + (\partial_t \xi^n) \xi^m] + [(\partial_t \xi^m) \xi^n - (\partial_t \xi^n) \xi^m] \quad (6.50a)$$

$$= \partial_t (\xi^m \xi^n) + [(\partial_t \xi^m) \xi^n - (\partial_t \xi^n) \xi^m]. \quad (6.50b)$$

⁹This decomposition is ubiquitous in matrix and tensor algebra, given that the symmetric and anti-symmetric components have distinct kinematic properties.

Introducing the symmetric and anti-symmetric correlation tensors

$$2K^{mn} \equiv \overline{\partial_t(\xi^m \xi^n)} \quad (6.51a)$$

$$2A^{mn} \equiv \overline{(\partial_t \xi^m) \xi^n} - \overline{(\partial_t \xi^n) \xi^m} \quad (6.51b)$$

allows us to write the mean eddy tracer flux

$$\overline{v'^m C'} = -(K^{mn} + A^{mn}) \partial_n \overline{C} \quad (6.52)$$

and the mean field tracer equation (6.44)

$$\partial_t \overline{C} + \nabla \cdot (\overline{\mathbf{v}} \overline{C}) = \partial_m [(K^{mn} + A^{mn}) \partial_n \overline{C}] = \nabla \cdot [(\mathbf{K} + \mathbf{A}) \cdot \nabla \overline{C}]. \quad (6.53)$$

The right hand side of this equation equals to the convergence of the symmetric and skew-symmetric tracer fluxes

$$\nabla \cdot [(\mathbf{K} + \mathbf{A}) \cdot \nabla \overline{C}] = -\nabla \cdot (\mathbf{F}^{\text{sym}} + \mathbf{F}^{\text{skew}}), \quad (6.54)$$

where

$$\mathbf{F}^{\text{sym}} = -\mathbf{K} \cdot \nabla \overline{C} \quad (6.55a)$$

$$\mathbf{F}^{\text{skew}} = -\mathbf{A} \cdot \nabla \overline{C} \quad (6.55b)$$

$$\overline{\mathbf{v}' C'} = \mathbf{F}^{\text{sym}} + \mathbf{F}^{\text{skew}} = -(\mathbf{K} + \mathbf{A}) \cdot \nabla \overline{C}. \quad (6.55c)$$

6.4.3 The symmetric tracer flux

In terms of particle displacements, the symmetric flux (6.55a) is given by

$$(F^{\text{sym}})^m = -K^{mn} \partial_n \overline{C} = -\frac{1}{2} \overline{\partial_t(\xi^m \xi^n)} \partial_n \overline{C}. \quad (6.56)$$

The symmetric tensor, \mathbf{K} , vanishes when the average is over the period of a periodic wave, in which the particle displacements undergo reversible periodic excursions (see Exercise 6.5). For waves that decay in amplitude over the averaging period, particle displacements decrease in magnitude so that $K^{mn} < 0$. In this case, the symmetric flux is oriented up the gradient of the Eulerian mean tracer field. In contrast, particle displacements increase in magnitude for waves that grow over the averaging period, in which case the flux is downgradient, just as for diffusion. Furthermore, growing nonlinear waves generally break and then develop into turbulence, with turbulence leading to further particle separation and tracer mixing. We thus find it sensible to parameterize turbulent motions via downgradient diffusion, with much of Chapter 7 focused on diffusive parameterizations of lateral mixing.

6.4.4 Skew, advective, and rotational tracer fluxes

Following our discussion in Section 5.5, we write the m 'th component to the skew flux

$$(F^{\text{skew}})^m = -A^{mn} \partial_n \overline{C} = -\epsilon^{mnp} \Psi_p \partial_n \overline{C} = -(\nabla \overline{C} \times \Psi)^m, \quad (6.57)$$

where we introduced the vector streamfunction (dimensions squared length per time)¹⁰

$$\Psi = \frac{1}{2} \partial_t \xi \times \xi = \frac{1}{2} \mathbf{v}' \times \xi. \quad (6.58)$$

As defined, the vector streamfunction is minus one half the angular momentum per mass of a fluid particle undergoing eddying motion, with the angular momentum computed relative to the mean particle position. The vector streamfunction is nonzero only if the eddy has a preferred sense of rotation (i.e., a nonzero mean angular momentum), in which case the wave field is said to be **polarized**. That is, polarization results if the eddy velocity, \mathbf{v}' , is correlated to a fluid particle displacement, ξ , in an orthogonal direction, thus giving rise to a nonzero angular momentum.

The skew flux can be written

$$\mathbf{F}^{\text{skew}} = -\nabla \bar{C} \times \Psi \quad (6.59a)$$

$$= (\nabla \times \Psi) \bar{C} - \nabla \times (\bar{C} \Psi) \quad (6.59b)$$

$$= \mathbf{U}^A \bar{C} - \nabla \times (\bar{C} \Psi) \quad (6.59c)$$

$$= \mathbf{F}^{\text{adv}} - \mathbf{F}^{\text{rot}}, \quad (6.59d)$$

so that the skew flux equals to an advective flux minus a rotational flux. We here introduced the non-divergent velocity,

$$\mathbf{U}^A = \nabla \times \Psi, \quad (6.60)$$

and the non-divergent rotational flux,

$$\mathbf{F}^{\text{rot}} = \nabla \times (\bar{C} \Psi). \quad (6.61)$$

Since $\nabla \cdot \mathbf{F}^{\text{rot}} = 0$, we see that the divergence of the skew flux equals to the divergence of the advective flux

$$\nabla \cdot \mathbf{F}^{\text{skew}} = \nabla \cdot (\mathbf{F}^{\text{adv}} - \mathbf{F}^{\text{rot}}) = \nabla \cdot \mathbf{F}^{\text{adv}}. \quad (6.62)$$

Consequently, the rotational flux, \mathbf{F}^{rot} , has no impact on evolution of the mean tracer concentration.

6.4.5 What does a point measurement yield?

From equation (6.55c), we see that a point measurement of the correlation, $\bar{\mathbf{v}' C'}$, provides an estimate of the symmetric tracer flux plus the skew tracer flux

$$\bar{\mathbf{v}' C'} = \mathbf{F}^{\text{sym}} + \mathbf{F}^{\text{skew}} = -(\mathbf{K} + \mathbf{A}) \cdot \nabla \bar{C}. \quad (6.63)$$

Furthermore, for a periodic wave field, where the symmetric tensor vanishes, the correlation, $\bar{\mathbf{v}' C'}$, provides a direct estimate of the skew flux, $-\nabla \bar{C} \times \Psi$. This particular result might seem puzzling on first encounter, since one could imagine $\bar{\mathbf{v}' C'}$ instead provides an estimate for the advective flux, $\mathbf{U}^A \bar{C}$. But that presumption is wrong, as indicated by the decomposition (6.63). We emphasize this point by summarizing the various relations

$$\bar{\mathbf{v}' C'} = \mathbf{F}^{\text{sym}} + \mathbf{F}^{\text{skew}} \quad (6.64a)$$

¹⁰ Middleton and Loder (1989) and Garrett (2006) introduce a skew-diffusivity, \mathbf{D} , which is opposite in sign to the vector streamfunction: $\Psi = -\mathbf{D}$.

$$= -\mathbf{K} \cdot \nabla \bar{C} - \nabla \bar{C} \times \Psi \quad (6.64b)$$

$$= -\mathbf{K} \cdot \nabla \bar{C} - \nabla \times (\bar{C} \Psi) + \bar{C} \nabla \times \Psi \quad (6.64c)$$

$$= -\mathbf{K} \cdot \nabla \bar{C} - \nabla \times (\bar{C} \Psi) + \bar{C} \mathbf{U}^A \quad (6.64d)$$

$$= \mathbf{F}^{\text{sym}} - \mathbf{F}^{\text{rot}} + \mathbf{F}^{\text{adv}}. \quad (6.64e)$$

The rotational flux is generally nontrivial for polarized waves or turbulent eddies. As a result, the rotational flux provides a sizable contribution to any measurement of $\bar{v}' \bar{C}'$ either from a field measurement or numerical simulation. For some purposes it can be more convenient to work directly with the skew flux rather than the advective flux.

6.4.6 Further study

Much of this section follows [Plumb \(1979\)](#), [Middleton and Loder \(1989\)](#), and [Garrett \(2006\)](#), each of whom considered elements of tracer dispersion by waves and nonlinear eddies. [Middleton and Loder \(1989\)](#) work through a few oceanographically motivated examples that offer further understanding of skew fluxes. Additional treatments can be found in the review article of [Moffatt \(1983\)](#), who considers flow in a rotating reference frame as well as magneto-hydrodynamic flows.

Exercises 6.2 through 6.6 help build further insights into the kinematics introduced in this section.

6.5 Volume transport in an isopycnal ensemble

In this section we study the kinematics of stirring by a turbulent flow in a perfect stratified Boussinesq fluid. We move beyond the finite amplitude motions considered in the previous sections, and yet make use of the generalized Lagrangian mean kinematics to conceptually frame the formulation. As [fluid parcels](#) are stirred by turbulent and non-divergent flows, they preserve their volume while changing their shape and stretching into finer scale features. This process accords with the conceptual picture of [Eckart \(1948\)](#) discussed in Section 5.1. The turbulent motion in ocean mesoscale/baroclinic eddies, as well as nonlinear baroclinic waves in the atmosphere, offer geophysical examples of flows that lead to such stirring. We are not directly concerned with mixing in this section, instead focusing on the kinematics of eddy stirring in a stratified Boussinesq ocean.¹¹

With a focus on stirring, we assume that each fluid particle preserves its potential density, ϱ (equivalently its specific entropy). This property motivates us to take an isopycnal coordinate approach in formulating the kinematics. Here, we track the vertical motion of potential density layer interfaces during the motion, whereas we are not concerned with following the lateral position of a fluid particle within a layer. We examine the kinematics of a ϱ -ensemble of eddying flows, whereby we focus on an ensemble of flows along an arbitrary isopycnal surface labelled by ϱ . We interpret this isopycnal approach as a vertical GLM, in which we focus on the vertical particle displacement rather than the three dimensional displacement of Section 6.3.¹²

We are concerned with the kinematics of parcel rearrangement in this section, with eddy correlations appearing between the specific thickness of an isopycnal fluid layer and the flow

¹¹Although focusing on the perfect Boussinesq fluid, keep in mind that the fluid is forced to support an active and stationary turbulent flow. For example, the flow in a mechanically (wind driven) isopycnal model offers a numerical realization of this flow.

¹²We emphasize that the fluid particles move in three directions within the ϱ -ensemble. However, the isopycnal kinematic approach focuses just on the vertical particle displacement.

velocity within that layer. We extend the analysis to tracers in Section 6.6. We offer many details since the kinematics of isopycnal ensembles appears throughout the study of wave-mean flow interactions in geophysical fluid mechanics, with particular importance to the study of ocean mesoscale eddy transport and its parameterization. Sections 6.5.1 through 6.5.4 introduce the main ingredients of the method, whereas the following sections develop expressions for the transport of volume. Mastery of this material is not simple.

6.5.1 Specifying the vertical position

When studying the [generalized Lagrangian mean](#) in Section 6.3, we interpret each point in space, \mathbf{x} , as the mean position of a unique fluid particle. This interpretation acts to couple the Eulerian and Lagrangian kinematic descriptions. For purposes in this section we only track the vertical position as defined by the position of an isopycnal surface. As such, we identify each vertical position in space, z , with the mean vertical position of an isopycnal whose particular value is ϱ :

$$z = \bar{\eta}^{(\varrho)}(x, y, t) = \text{mean vertical position of isopycnal } \varrho \text{ at } (x, y, t). \quad (6.65)$$

The overline in this equation signals an ensemble mean operation as computed over the ϱ -ensemble of isopycnal surfaces with potential density, ϱ . Notably, isopycnals are generally not horizontal nor are they static (remember, the flows are forced). Hence, the mean vertical position of the ϱ -ensemble is a function of horizontal position and time.¹³

We write

$$z = \eta(x, y, \varrho, t) \quad (6.66)$$

for the vertical position of an isopycnal labeled by ϱ as located at a horizontal point, (x, y) , and time, t . We decompose this vertical position into its ensemble mean position, $\bar{\eta}^{(\varrho)}(x, y, t)$, and a vertical displacement, $\xi(x, y, \varrho, t)$, relative to the mean we introduce the vertical displacement field, $\xi(x, y, \varrho, t)$, thus writing

$$\eta(x, y, \varrho, t) = \bar{\eta}^{(\varrho)}(x, y, t) + \xi(x, y, \varrho, t) = \text{vertical position of isopycnal } \varrho. \quad (6.67)$$

Just like the vertical position, $\eta(x, y, \varrho, t)$, we see that the vertical displacement is a function of the chosen isopycnal, ϱ , as well as the horizontal position and time. As for the GLM displacement vector, $\xi(\mathbf{x}, t)$, the isopycnal vertical displacement has a zero ϱ -ensemble mean

$$\overline{\xi(x, y, \varrho, t)}^{(\varrho)} = 0 \implies \overline{\eta(x, y, \varrho, t)}^{(\varrho)} = \bar{\eta}^{(\varrho)}(x, y, t). \quad (6.68)$$

Hence, the vertical displacement field, $\xi(x, y, \varrho, t)$, serves to couple Eulerian kinematics to the quasi-Lagrangian kinematics of isopycnals.

6.5.2 Modified mean density

Figure 6.4 provides a schematic to illustrate the mean vertical position of the ϱ -ensemble of isopycnals, and the corresponding displacement field that locates the vertical position of a particular member of the ϱ -ensemble. This figure also motivates us to define a new density

¹³We slightly abuse notation by writing ϱ for a specific value of the density held by each ϱ -ensemble member (e.g., $\varrho = 1030 \text{ kg m}^{-3}$). We also write $\varrho(x, y, z, t)$ for a particular ensemble member whose value at each point in space and time is $\varrho(x, y, z, t) = \varrho$. A more careful notation involves extra adornments to each symbol and can become rather tedious and difficult to parse. We thus rely on understanding the meaning based on the context.

field, $\tilde{\varrho}$, which equals to ϱ when evaluated at the ϱ -ensemble mean vertical position. Following [McDougall and McIntosh \(2001\)](#), we refer to $\tilde{\varrho}$ as the [modified mean](#) potential density, and it is written mathematically as¹⁴

$$\tilde{\varrho}(x, y, \bar{\eta}^{(\varrho)}(x, y, t), t) = \overline{\varrho(x, y, \eta(x, y, \varrho, t), t)}^{(\varrho)} = \varrho(x, y, \eta(x, y, \varrho, t), t) = \varrho. \quad (6.69)$$

The final equality follows since each space-time functions in this equation takes on the same value of potential density (e.g., $\varrho = 1030 \text{ kg m}^{-3}$) when evaluated at their respective space-time points. The second equality follows since each member of the ϱ -ensemble has the same potential density, so that $\varrho(x, y, \eta(x, y, \varrho, t), t)$ is invisible to the ϱ -ensemble mean operator.

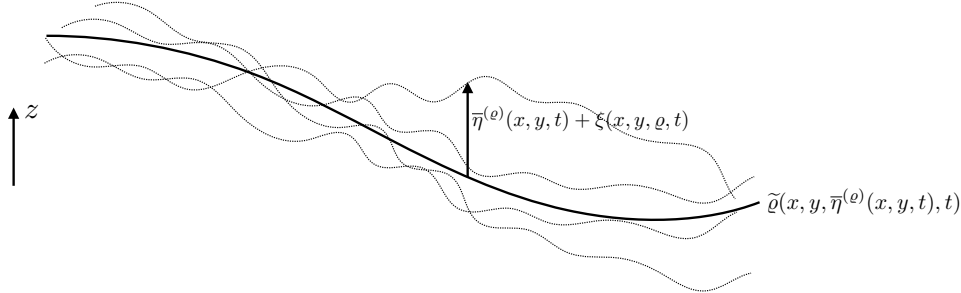


FIGURE 6.4: We here depict a few elements of the ϱ -ensemble (dotted lines; in principle there are an infinity of elements in the ϱ -ensemble) as well as the ensemble mean position of these isopycnals (dark line). The ensemble mean has a vertical position $z = \bar{\eta}^{(\varrho)}(x, y, t)$, whereas the vertical position of each ensemble member is $z = \eta(x, y, \varrho, t) = \bar{\eta}^{(\varrho)}(x, y, t) + \xi(x, y, \varrho, t)$, with a distinct displacement field, ξ , for each ensemble member. Each potential density surface within the ϱ -ensemble has the same numerical value, $\varrho(x, y, z, t) = \varrho$ (e.g., $\varrho = 1030 \text{ kg m}^{-3}$). We define the modified mean density, $\tilde{\varrho}$, as the space-time field that equals to ϱ when evaluated at the mean vertical position: $\tilde{\varrho}(x, y, \bar{\eta}^{(\varrho)}(x, y, t), t) = \varrho$.

6.5.3 Isopycnal mean and modified mean

Each member of the ϱ -ensemble has the same potential density, ϱ . However, each member generally has distinct values for other fluid properties. Consider a physical scalar property, χ , such as the temperature. It has a value at an Eulerian space point, $\chi(x, y, z, t)$, and a generally distinct value on a ϱ isopycnal, $\chi(x, y, z = \eta(x, y, \varrho, t), t)$. We may also represent this property using isopycnal coordinates, in which case we write the ϱ -ensemble mean for this property as¹⁵

$$\bar{\chi}^{(\varrho)}(x, y, \varrho, t) \equiv \varrho\text{-ensemble mean}. \quad (6.70)$$

This isopycnal mean is operationally computed just like an Eulerian mean, only now the field is represented using isopycnal coordinates, and it is sampled at the position of each member of the ϱ -ensemble that has fixed (x, y, ϱ, t) .

Following from our definition of the modified mean density, $\tilde{\varrho}$, we define the [modified mean](#) scalar field¹⁶

$$\tilde{\chi}(x, y, \bar{\eta}^{(\varrho)}(x, y, t), t) \equiv \overline{\chi(x, y, \eta(x, y, \varrho, t), t)}^{(\varrho)} = \overline{\chi(x, y, \bar{\eta}^{(\varrho)}(x, y, t) + \xi(x, y, \varrho, t), t)}^{(\varrho)}. \quad (6.71)$$

¹⁴Following our connection to the GLM, we consider $\tilde{\varrho}$ as the vertical GLM density.

¹⁵The physical scalar property, χ , can be represented as a function of z or as a function of ϱ . These two coordinate representations require distinct mathematical functions. We could introduce distinct function names to distinguish these functions. But we choose not to in order to reduce notation. Rather, we let the distinct dependent variables signal the use of a distinct mathematical function.

¹⁶We again interpret the modified mean scalar as a vertical GLM field.

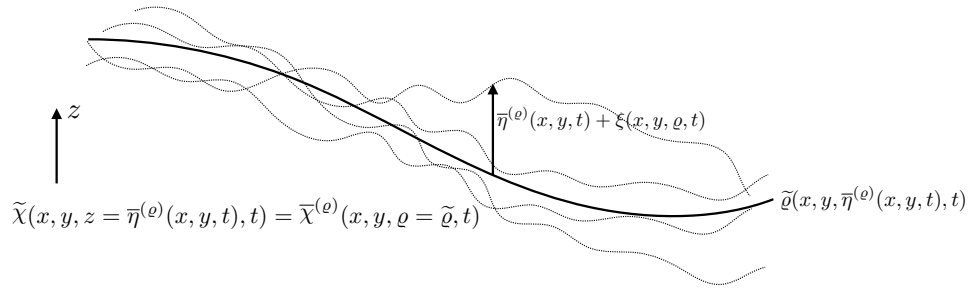


FIGURE 6.5: This figure depicts the duality relation $\tilde{\chi}(x, y, z = \bar{\eta}^{(\varrho)}(x, y, t), t) = \bar{\chi}^{(\varrho)}(x, y, \varrho = \tilde{\varrho}, t)$ between the modified mean scalar property, $\tilde{\chi}$, and the ϱ -ensemble mean of that property. It expresses the objective nature of the ϱ -ensemble mean of the property, with distinct mathematical functional forms depending on whether it is represented using either (x, y, z, t) Eulerian coordinates or isopycnal coordinates, (x, y, ϱ, t) . This duality is basic to the ϱ -ensemble kinematics.

The modified mean field is a function of space and time, with the vertical position given by the ϱ -ensemble mean vertical position, $z = \bar{\eta}^{(\varrho)}(x, y, t)$. By construction, the modified mean, when evaluated at $\bar{\eta}^{(\varrho)}(x, y, t)$, equals to the ϱ -ensemble mean evaluated using the modified mean density

$$\tilde{\chi}(x, y, z = \bar{\eta}^{(\varrho)}(x, y, t), t) = \bar{\chi}^{(\varrho)}(x, y, \varrho = \tilde{\varrho}, t). \quad (6.72)$$

Evidently, as a space-time function, $\tilde{\chi}(x, y, \bar{\eta}^{(\varrho)}(x, y, t), t)$ is numerically equal to the ϱ -ensemble mean of χ . This identity results from the objective nature of the isopycnal averaged property, χ , with that average represented either via (x, y, z) Eulerian coordinates or (x, y, ϱ) isopycnal coordinates. We illustrate this identity in Figure 6.5, and make use of it in the following.

6.5.4 Transformed residual mean (TRM)

When working with isopycnal layers, it is very useful to employ specific thickness weighting to account for the net amount of material within a layer, or to measure the net transport in the layer.¹⁷ For this purpose we introduce the **specific thickness** from Section 2.3 as given by¹⁸

$$\langle = \partial z / \partial \varrho = 1 / (\partial \varrho / \partial z), \quad (6.73)$$

and thus make use of thickness weighted fields, $\langle \chi$, and the corresponding thickness weighted isopycnal ensemble mean

$$\widehat{\chi} = \frac{\langle \chi^{(\varrho)} \rangle}{\langle \rangle^{(\varrho)}}. \quad (6.74)$$

Following from the duality relation (6.72) we introduce

$$\chi^\#(x, y, \bar{\eta}^{(\varrho)}, t) \equiv \widehat{\chi}(x, y, \tilde{\varrho}, t), \quad (6.75)$$

¹⁷We pursue a vertical discrete version of this **thickness weighted averaging (TWA)** approach for the stacked shallow water model in Chapter 3.

¹⁸As discussed in Section 1.10.2, specific thickness is the Jacobian of transformation between geopotential coordinates, (x, y, z, t) , and isopycnal coordinates, (x, y, ϱ, t) . For stably stratified ideal fluids, \langle is one-signed, hence making the coordinate transformation well defined. It is also related to the buoyancy frequency through $N^2 = -(g/\rho_0) (\partial \varrho / \partial z) = -g/(\rho_0 \langle \rangle)$.

where $\bar{\chi}^\#$ is the **transformed residual mean (TRM)** evaluated at the isopycnal ensemble mean vertical position.¹⁹ This is yet another important identity that is used in the following.

6.5.5 Depth integrated TRM transport

The horizontal TRM velocity is a particularly key field

$$\hat{\mathbf{u}}(x, y, \tilde{\varrho}, t) = \bar{\mathbf{u}}^\#(x, y, \bar{\eta}^{(\varrho)}, t), \quad (6.76)$$

where we make use of a somewhat more abbreviated notation for the functional dependencies. Following the discussion of the vertical gauge in Section 5.5.1 (see in particular equation (5.59)), we are led to define the depth integrated TRM transport as in Figure 6.6

$$\bar{\mathbf{U}}^\#(x, y, \bar{\eta}^{(\varrho)}, t) = \int_{\eta_b}^{\bar{\eta}^{(\varrho)}} \bar{\mathbf{u}}^\#(x, y, z, t) dz = \int_{\varrho(x, y, \eta_b, t)}^{\tilde{\varrho}(x, y, \bar{\eta}^{(\varrho)}, t)} \hat{\mathbf{u}}(x, y, \gamma, t) \bar{\zeta}^{(\gamma)}(x, y, t) d\gamma, \quad (6.77)$$

with the second equality following from a change of coordinates from geopotential to isopycnal, and with $z = \eta_b(x, y)$ the vertical position of the ocean bottom topography.

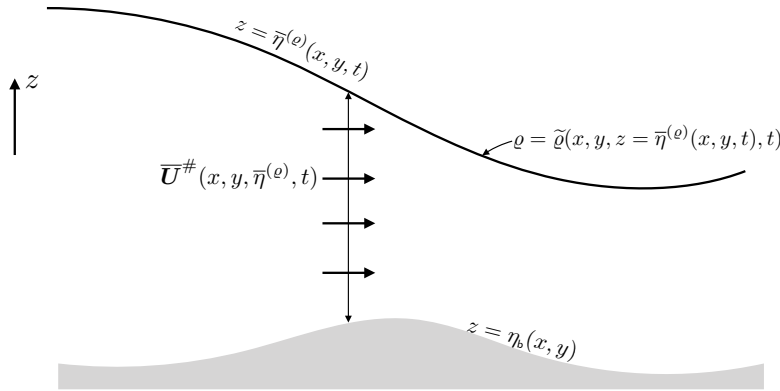


FIGURE 6.6: Depicting the horizontal TRM transport as computed from the ocean bottom at $z = \eta_b(x, y)$, and the vertical position $z = \bar{\eta}^{(\varrho)}(x, y, t)$.

We can go further with equation (6.77) by writing (and suppressing some functional dependencies for brevity)

$$\bar{\mathbf{U}}^\#(x, y, \bar{\eta}^{(\varrho)}, t) = \int_{\varrho(\eta_b)}^{\tilde{\varrho}(\bar{\eta}^{(\varrho)})} \hat{\mathbf{u}}(\gamma) \bar{\zeta}^{(\gamma)} d\gamma \quad \text{from equation (6.77)} \quad (6.78a)$$

$$= \int_{\varrho(\eta_b)}^{\tilde{\varrho}(\bar{\eta}^{(\varrho)})} \bar{\mathbf{u}} \bar{\zeta}^{(\gamma)} d\gamma \quad \text{from equation (6.74)} \quad (6.78b)$$

$$= \int_{\varrho(\eta_b)}^{\varrho(\bar{\eta}^{(\varrho)} + \xi)} \bar{\mathbf{u}} \bar{\zeta}^{(\gamma)} d\gamma \quad \text{from equation (6.69).} \quad (6.78c)$$

The final equality makes it clear that the TRM transport, $\bar{\mathbf{U}}^\#$, is the ensemble mean volume transport for fluid denser than $\varrho(\bar{\eta}^{(\varrho)} + \xi) = \tilde{\varrho}(\bar{\eta}^{(\varrho)})$. This transport can also be written using

¹⁹ McDougall and McIntosh (2001) pioneered the use of TRM. Since their averaging operator was based on a time mean, they referred to it as the temporal residual mean.

geopotential coordinates

$$\overline{\mathbf{U}}^\#(x, y, \bar{\eta}^{(\varrho)}, t) = \overline{\int_{\eta_b}^{\bar{\eta}^{(\varrho)} + \xi} \mathbf{u} dz}. \quad (6.79)$$

The transport from each ensemble member is determined by integrating from the ocean bottom to the vertical position, $\bar{\eta}^{(\varrho)} + \xi$, and then the TRM transport is determined by computing the ensemble mean for this transport.

6.5.6 Quasi-Stokes transport

The TRM transport (6.79) can be decomposed into an Eulerian mean plus an eddy correlation

$$\overline{\mathbf{U}}^\#(\bar{\eta}^{(\varrho)}) \equiv \overline{\mathbf{U}}(\bar{\eta}^{(\varrho)}) + \overline{\mathbf{U}}^{\text{qs}}(\bar{\eta}^{(\varrho)}), \quad (6.80)$$

where we exposed just the vertical dependency to these functions. The first term,

$$\overline{\mathbf{U}}(\bar{\eta}^{(\varrho)}) = \overline{\int_{\eta_b}^{\bar{\eta}^{(\varrho)}} \mathbf{u} dz}, \quad (6.81)$$

is the ensemble mean transport between the ocean bottom and the ensemble mean vertical position, $\bar{\eta}^{(\varrho)}$. We interpret this transport as an Eulerian mean since the depth ranges are fixed. In contrast, the quasi-Stokes transport

$$\overline{\mathbf{U}}^{\text{qs}}(\bar{\eta}^{(\varrho)}) \equiv \overline{\int_{\bar{\eta}^{(\varrho)}}^{\bar{\eta}^{(\varrho)} + \xi} \mathbf{u} dz} \quad (6.82)$$

measures the ensemble mean transport between the vertical position of the ϱ -ensemble mean, $z = \bar{\eta}^{(\varrho)}$, and that of each ensemble member, $z = \bar{\eta}^{(\varrho)} + \xi(\varrho)$. We refer to transport as “quasi-Stokes” given that it is the difference between an isopycnal (i.e., quasi-Lagrangian) mean and an Eulerian mean (see Section 6.3)

$$\overline{\mathbf{U}}^{\text{qs}} = \overline{\mathbf{U}}^\# - \overline{\mathbf{U}}. \quad (6.83)$$

As for the traditional Stokes drift discussed in Section 6.3.6, the quasi-Stokes transport arises from a correlation between the velocity and the undulation of the isopycnal interface.

6.5.7 Three-component TRM velocity

Following from the vertical gauge expression (5.58), we introduce the TRM vector streamfunction

$$\overline{\Psi}^\# = \overline{\mathbf{U}}^\# \times \hat{\mathbf{z}}, \quad (6.84)$$

and the corresponding three-dimensional non-divergent TRM velocity

$$\overline{\mathbf{v}}^\# = \nabla \times \overline{\Psi}^\#. \quad (6.85)$$

The vertical component,

$$\overline{w}^\# = \hat{\mathbf{z}} \cdot (\nabla \times \overline{\Psi}^\#), \quad (6.86)$$

has no corresponding component in an isopycnal description, which only requires the horizontal thickness weighted transport, $\hat{\mathbf{u}}$. However, the TRM vector streamfunction only requires the

horizontal TRM transport, $\bar{\mathbf{U}}^\#$, so the two descriptions make use of the same number of degrees of freedom.

6.5.8 Volume conservation and the thickness equation

Consider two perspectives on volume conservation: one based on isopycnal coordinates and the other based on geopotential coordinates.

Isopycnal coordinates

In isopycnal vertical coordinates, the volume of a fluid element is written

$$\delta V = \delta x \delta y \delta z = \delta x \delta y \langle \varrho \rangle, \quad (6.87)$$

where we introduced the specific thickness, $\langle \cdot \rangle$, from equation (6.73). Geometrically, the product

$$\delta z = |\langle \varrho \rangle| \quad (6.88)$$

represents the vertical thickness between two infinitesimally close potential density interfaces, ϱ and $\varrho + \delta\varrho$ (see Figure 6.7). Material conservation of both volume and potential density implies conservation of the product of specific thickness and horizontal area, $\delta x \delta y \langle \cdot \rangle$, which leads to the thickness equation (Section 3.2.3)

$$\partial_t \langle \cdot \rangle + \nabla_{\mathbf{h}} \cdot (\langle \mathbf{u} \rangle) = 0, \quad (6.89)$$

with \mathbf{u} the horizontal velocity field, the time derivative is computed with ϱ held fixed, and

$$\nabla_{\mathbf{h}} = \nabla_{\mathbf{h}} + \mathbf{S} \partial_z \quad (6.90)$$

is the horizontal derivative operator with ϱ held fixed, and

$$\mathbf{S} = \nabla_{\mathbf{h}} z \quad (6.91)$$

is the horizontal slope of the potential density surface. This equation is the continuous isopycnal version of the thickness equation appearing in vertically discrete shallow water layers.

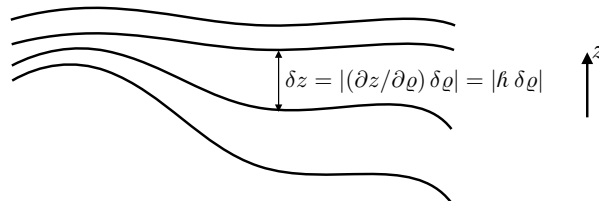


FIGURE 6.7: Illustrating the thickness between surfaces of constant generalized vertical coordinates, $\delta z = (\partial z / \partial \sigma) \delta \sigma$. In regions with larger magnitude for the specific thickness, $\partial z / \partial \sigma$, or equivalently smaller vertical stratification of the σ surfaces, $\partial \sigma / \partial z$, the layers are thicker so that isolines of constant σ are further apart. The converse holds where $\partial z / \partial \sigma$ is small (equivalently $\partial \sigma / \partial z$ is large).

Geopotential coordinates

An Eulerian z -coordinate description of volume stirring within isopycnal layers is rendered via a combination of volume conservation, $\nabla \cdot \mathbf{v} = 0$, and material conservation of potential density, $D\varrho/Dt = 0$. When written as skewson rather than advection, the natural gauge is the vertical gauge introduced in Section 5.5.1, since this gauge only requires the same horizontal velocity field, \mathbf{u} , used with the isopycnal coordinate description. This gauge has an associated potential density skew flux, $\mathbf{F}^{\text{skew}} = -\nabla\varrho \times \Psi$, which leads to the evolution

$$\partial_t \varrho = \nabla \cdot (\nabla\varrho \times \Psi), \quad (6.92)$$

where all derivatives are here taken with fixed Eulerian (geopotential) coordinates, (x, y, z) , and the ∇ operator is three-dimensional.

6.5.9 Ensemble mean thickness equation

Consider an ensemble of stably stratified (so that the layer specific thickness, $\langle \cdot \rangle$, is single-signed and nonvanishing) perfect Boussinesq fluid parcels with the same infinitesimal volume, $\delta V = \delta x \delta y \delta z = \delta x \delta y \langle \delta\varrho \rangle$, and same potential density, ϱ . Lacking any other marker, such as a tracer concentration, the ensemble members are distinguished from one another by values of their horizontal area, $\delta A = \delta x \delta y$, and their specific thickness, $\langle \cdot \rangle$, that is, their geometric attributes. The ensemble members are assumed to be stirred by different stochastic realizations of the fluid flow. Since each flow realization alters the geometric properties of the parcels, a mean field description focuses on the mean of these geometric properties.

In isopycnal coordinates, (x, y, ϱ, t) , the thickness equation (6.89) is satisfied by each ensemble member

$$\partial_t \langle \cdot \rangle + \nabla_{\mathbf{v}} \cdot (\langle \cdot \rangle \mathbf{u}) = 0. \quad (6.93)$$

The ensemble mean computed over these fluid parcels, each with potential density ϱ , satisfies

$$\partial_t \bar{\langle}^{(\varrho)} + \nabla_{\mathbf{v}} \cdot \left(\bar{\langle}^{(\varrho)} \bar{\mathbf{u}}^{(\varrho)} + \bar{\langle} \mathbf{u}'^{(\varrho)} \right) = 0, \quad (6.94)$$

where primed variables represent deviations from the isopycnal mean. It follows that the mean specific thickness, $\bar{\langle}^{(\varrho)}$, of parcels with potential density, ϱ , satisfies the conservation equation

$$\partial_t \bar{\langle}^{(\varrho)} + \nabla_{\mathbf{v}} \cdot (\bar{\langle}^{(\varrho)} \hat{\mathbf{u}}) = 0. \quad (6.95)$$

In this equation we introduced the thickness weighted isopycnal ensemble mean horizontal velocity

$$\hat{\mathbf{u}} = \frac{\bar{\langle}^{(\varrho)} \bar{\mathbf{u}}^{(\varrho)}}{\bar{\langle}^{(\varrho)}} = \bar{\mathbf{u}}^{(\varrho)} + \frac{\bar{\langle} \mathbf{u}'^{(\varrho)}}{\bar{\langle}^{(\varrho)}} \equiv \bar{\mathbf{u}}^{(\varrho)} + \mathbf{u}^{\text{bolus}}, \quad (6.96)$$

along with the isopycnal ensemble mean horizontal velocity, $\bar{\mathbf{u}}^{(\varrho)}$, and the horizontal **bolus velocity**, $\mathbf{u}^{\text{bolus}}$, originally introduced by [Rhines \(1982\)](#). The bolus velocity for an isopycnal layer corresponds to the transport

$$\bar{\langle}^{(\varrho)} \mathbf{u}^{\text{bolus}} = \bar{\langle}^{(\varrho)} (\hat{\mathbf{u}} - \bar{\mathbf{u}}^{(\varrho)}) = \bar{\langle} \mathbf{u}'^{(\varrho)}, \quad (6.97)$$

which arises from the along-isopycnal correlations between specific thickness and horizontal velocity.

Quite conveniently, the mean conservation equation (6.95) takes the *same* mathematical form as the conservation equation (6.93) satisfied by each ensemble member. The key difference is that the isopycnal ensemble mean thickness, $\bar{\eta}^{(\varrho)}$, is stirred by the thickness weighted isopycnal ensemble mean horizontal velocity, $\hat{\mathbf{u}}$, whereas the thickness of each ensemble member is stirred by a randomly different realization of the horizontal velocity, \mathbf{u} . The simplicity of the mean field description (6.95) is afforded by use of the Lagrangian vertical coordinate, ϱ .

6.5.10 Ensemble mean kinematics in geopotential coordinates

Now consider a geopotential coordinate description of the isopycnal ensemble. For this purpose, we interpret a vertical position, z , as the ensemble mean vertical position, $\bar{\eta}^{(\varrho)}$. Consequently, mean fields defined at the fixed vertical position correspond to either modified mean fields when not thickness weighted (equation (6.71)), or TRM fields when thickness weighted (equation (6.75)).

Evolution of modified mean density

Following the skewson formulation from Section 5.5, at the ensemble mean vertical position, $z = \bar{\eta}^{(\varrho)}(x, y, t)$, the streamfunction, $\bar{\Psi}^\#$, defines an effective skew flux of the modified mean potential density given by

$$\bar{\mathbf{F}}^\# = -\nabla \bar{\varrho} \times \bar{\Psi}^\#. \quad (6.98)$$

Using the identity $\bar{\Psi}^\# = \bar{\mathbf{U}}^\# \times \hat{\mathbf{z}}$ (equation (6.84)) we can write this skew flux as

$$\bar{\mathbf{F}}^\# = -\bar{\mathbf{U}}^\# \partial_z \bar{\varrho} + \hat{\mathbf{z}} \bar{\mathbf{U}}^\# \cdot \nabla_h \bar{\varrho} \quad (6.99a)$$

$$= -(\bar{\mathbf{U}}^\# + \hat{\mathbf{z}} \mathbf{S} \cdot \bar{\mathbf{U}}^\#) \partial_z \bar{\varrho}, \quad (6.99b)$$

where

$$\mathbf{S} = -\frac{\nabla_h \bar{\varrho}}{\partial_z \bar{\varrho}} \quad (6.100)$$

is the slope of the modified mean density originally introduced via equation (6.91), and $\nabla_h = (\partial_x, \partial_y, 0)$ is the horizontal gradient operator taken with constant vertical position. The convergence of the effective skew flux leads to a stirring of the modified mean density $\bar{\varrho}$ at the mean vertical position, $z = \bar{\eta}^{(\varrho)}$,

$$\partial_t \bar{\varrho} = \nabla \cdot (\nabla \bar{\varrho} \times \bar{\Psi}^\#). \quad (6.101)$$

This equation represents a geopotential coordinate specification of the evolution of the modified mean density due to stirring by the mean eddies. It corresponds directly to the evolution equation (6.92) satisfied at vertical position, z , by a single member of the ϱ -ensemble.

6.5.11 Approximate ϱ -ensemble kinematics in geopotential coordinates

Equation (6.101) represents an exact z -coordinate description of the stirring of modified mean potential density. However, when working in geopotential coordinates, all that is available is Eulerian information. Hence, the isopycnal information used to realize this exact description can only be approximated.

Approximating the quasi-Stokes transport

We require an approximation of the quasi-Stokes transport, \bar{U}^{qs} , defined by equation (6.82). We addressed a similar estimation in Section 6.3.4 when discussing the Stokes mean. Here, we expand the TRM transport in a Taylor series about the vertical position, $z = \bar{\eta}^{(\varrho)}$

$$\bar{U}^{\#}(z) = \overline{\int_{\eta_b}^{z+\xi} \mathbf{u}(s) \, ds} \quad (6.102a)$$

$$= \bar{U}(z) + \overline{\mathbf{u} \xi}^{(z)} + \frac{1}{2} \overline{\partial_z \mathbf{u} \xi \xi}^{(z)} + \mathcal{O}(\alpha^3), \quad (6.102b)$$

where neglected terms are third order in deviation quantities. All ensemble means are taken at fixed vertical position (hence the z label on the overline), which accords with taking a Taylor series about the ensemble mean vertical position, $z = \bar{\eta}^{(\varrho)}$.

The ensemble means in equation (6.102b) are interpreted as follows. The first term is the Eulerian mean horizontal transport passing beneath the ensemble mean vertical position, $z = \bar{\eta}^{(\varrho)}$. The second term, $\overline{\mathbf{u} \xi}$, is the horizontal velocity evaluated at the ensemble mean vertical position and multiplied by the deviation, ξ , of the potential density surface from its mean vertical position, all averaged at fixed vertical position. An Eulerian split of the horizontal velocity, \mathbf{u} , into its Eulerian mean, $\bar{\mathbf{u}}^{(z)}$, and deviation, \mathbf{u}' , leads to the correlation

$$\overline{\mathbf{u} \xi}^{(z)} = \overline{\mathbf{u}' \xi}^{(z)}. \quad (6.103)$$

For the second order term, similar considerations lead to

$$\overline{\partial_z \mathbf{u} \xi \xi}^{(z)} \approx \partial_z \overline{\mathbf{u}^{(z)} \xi \xi}^{(z)}, \quad (6.104)$$

where neglected terms are third order and higher. Combining these relations leads to the second order accurate expression

$$\bar{U}^{\#} \approx \bar{U} + \overline{\mathbf{u}' \xi}^{(z)} + \frac{1}{2} \overline{\xi \xi}^{(z)} \partial_z \overline{\mathbf{u}^{(z)}}. \quad (6.105)$$

The disturbance field

Following the discussion in Section 6.3.7, we here determine the disturbance field, ξ , in terms of fields at constant vertical position. For this purpose, use the identity (6.69) to give

$$\tilde{\varrho}(z) = \varrho(z + \xi) \quad (6.106a)$$

$$= \varrho(z) + \partial_z \varrho(z) \xi + \frac{1}{2} \partial_{zz} \varrho(z) \xi^2 + \mathcal{O}(\alpha^3). \quad (6.106b)$$

Subtracting the Eulerian mean of equation (6.106b) from the unaveraged equation (6.106b), and noting that $\tilde{\varrho}$ is already a mean field, leads to the second order accurate expression for the deviation

$$\xi = -\varrho'(z) / \partial_z \bar{\varrho}^{(z)} + \mathcal{O}(\alpha^2), \quad (6.107)$$

where

$$\varrho(z) = \bar{\varrho}^{(z)} + \varrho'(z). \quad (6.108)$$

To within the same order, the deviation can be written

$$\xi = -\varrho'(z) / \partial_z \tilde{\varrho}(z) + \mathcal{O}(\alpha^2). \quad (6.109)$$

Approximate quasi-Stokes transport

Substituting the deviation (6.109) into the approximate expression (6.102b) for the TRM transport yields an approximate expression for the quasi-Stokes transport

$$\bar{U}^{\text{qs}} = -\frac{\bar{u}' \bar{\varrho}'^{(z)}}{\partial_z \bar{\varrho}} + \frac{\bar{\phi}'^{(z)} \partial_z \bar{u}'^{(z)}}{(\partial_z \bar{\varrho})^2} + \mathcal{O}(\alpha^3), \quad (6.110)$$

where

$$\bar{\phi}'^{(z)} = \frac{1}{2} \bar{\varrho}' \bar{\varrho}'^{(z)} \quad (6.111)$$

is the mean potential density variance. [McDougall and McIntosh \(2001\)](#) noted that the [Gent et al. \(1995\)](#) scheme offers a parameterization of the two correlations on the right hand side of equation (6.110). We have more to say regarding this parameterization in Section 7.1.

Substituting the deviation (6.109) into the approximate expression (6.106b) yields, to within terms of third order, the relation

$$\bar{\varrho} = \bar{\varrho}^{(z)} - \partial_z \left[\frac{\bar{\phi}'^{(z)}}{\partial_z \bar{\varrho}^{(z)}} \right] + \mathcal{O}(\alpha^3). \quad (6.112)$$

As for the Stokes transport, the modified mean density and Eulerian mean density, when evaluated at the same vertical position, differ by terms that are second order in eddy amplitude.

6.5.12 Further study

This section is largely based on presentations given by [DeSzeke and Bennett \(1993\)](#), [McIntosh and McDougall \(1996\)](#), [Kushner and Held \(1999\)](#), and [McDougall and McIntosh \(2001\)](#) as summarized in Section 9.3 of [Griffies \(2004\)](#). Many other papers have applied this formalism to a variety of analyses, with examples including [Nurser and Lee \(2004a\)](#), [Nurser and Lee \(2004b\)](#), [Young \(2012\)](#), [Wolfe \(2014\)](#), and [Jansen et al. \(2024\)](#). [Young \(2012\)](#) offers a particularly general and rewarding presentation making use of basic notions from tensor analysis.

6.6 Isopycnal mean tracer equation

We now include a tracer field to the perfect Boussinesq fluid and determine a mean field description for the tracer. The transport of tracer by eddies has both a reversible stirring component and an irreversible mixing component. The stirring arises from both the thickness correlation to velocity as well as the velocity correlated with tracer.

6.6.1 Thickness weighted average²⁰

In equation (6.96) we introduced a specific thickness weighted average (or mean) operator, which is quite useful when considering the mean tracer equation. In general, for any field, χ , associated with a potential density layer, ϱ , we define the decomposition into thickness weighted

²⁰We also consider thickness weighted averaging for the stacked shallow water equations in Chapter 3. Many identities hold for both the continuously stratified fluid and the stacked shallow water.

average and deviation

$$\chi(\varrho) = \widehat{\chi}(\varrho) + \chi''(\varrho) \quad (6.113a)$$

$$= \frac{\overline{\chi}^{(\varrho)}}{\overline{\zeta}^{(\varrho)}} + \chi''. \quad (6.113b)$$

It follows by definition that the thickness weighted average of χ'' vanishes,

$$\overline{\chi''}^{(\varrho)} = 0. \quad (6.114)$$

6.6.2 Isopycnal mean thickness weighted tracer equation

When attaching a tracer, C , to fluid elements, each member of a ϱ -ensemble satisfies the isopycnal tracer equation

$$\partial_t C + \mathbf{u} \cdot \nabla_{\mathbf{h}} C = 0. \quad (6.115)$$

Combining the tracer and thickness equations leads to the thickness weighted tracer equation

$$\partial_t (\langle C \rangle) + \nabla_{\mathbf{h}} \cdot (\langle \mathbf{u} C \rangle) = 0. \quad (6.116)$$

Hence, in isopycnal coordinates and in the absence of irreversible processes, the evolution of thickness weighted tracer occurs via the isopycnally oriented convergence of the two-dimensional thickness weighted horizontal advective flux, $\langle \mathbf{u} C \rangle$.

To address the problem of describing the ensemble mean tracer equation in isopycnal coordinates, decompose the tracer and velocity field into their thickness weighted average and deviation

$$\partial_t [\langle (\widehat{C} + C'') \rangle] + \nabla_{\mathbf{h}} \cdot [\langle (\widehat{\mathbf{u}} + \mathbf{u}'') (\widehat{C} + C'') \rangle] = 0. \quad (6.117)$$

Taking a mean over the ϱ -ensemble, and using equation (6.114), yield the ensemble mean thickness weighted tracer equation

$$\partial_t (\overline{h}^{(\varrho)} \widehat{C}) + \nabla_{\mathbf{h}} \cdot (\overline{h}^{(\varrho)} \widehat{C} \widehat{\mathbf{u}}) = -\nabla_{\mathbf{h}} \cdot (\overline{h} C'' \mathbf{u}''^{(\varrho)}). \quad (6.118)$$

Now introduce the correlation,

$$\overline{\langle C'' \mathbf{u}'' \rangle}^{(\varrho)} = \overline{\zeta}^{(\varrho)} \widehat{\langle C'' \mathbf{u}'' \rangle}, \quad (6.119)$$

(see equation (6.113b)), and recall that the mean thickness $\overline{\zeta}^{(\varrho)}$ satisfies the mean thickness equation (6.95). These two points lead to the evolution equation for the mean thickness weighted tracer concentration

$$(\partial_t + \widehat{\mathbf{u}} \cdot \nabla_{\mathbf{h}}) \widehat{C} = -\frac{1}{\overline{\zeta}^{(\varrho)}} \nabla_{\mathbf{h}} \cdot (\overline{\zeta}^{(\varrho)} \widehat{\langle C'' \mathbf{u}'' \rangle}), \quad (6.120)$$

which can also be written in the flux form

$$\partial_t (\overline{\zeta}^{(\varrho)} \widehat{C}) + \nabla_{\mathbf{h}} \cdot (\overline{\zeta}^{(\varrho)} \widehat{\mathbf{u}} \widehat{C}) = -\nabla_{\mathbf{h}} \cdot (\overline{\zeta}^{(\varrho)} \widehat{\langle C'' \mathbf{u}'' \rangle}). \quad (6.121)$$

6.6.3 Subgrid scale tracer transport tensor

The correlation between tracer and velocity found on the right-hand side of the mean thickness weighted tracer equation (6.120) is typically written in terms of a subgrid scale tracer transport

tensor

$$\widehat{C'' \mathbf{u}''} = -\mathbb{J} \cdot \nabla_{\mathbf{h}} \widehat{C}. \quad (6.122)$$

This definition leads to the evolution equation

$$(\partial_t + \widehat{\mathbf{u}} \cdot \nabla_{\mathbf{h}}) \widehat{C} = \frac{1}{\bar{h}^{(\varrho)}} \nabla_{\mathbf{h}} \cdot (\bar{h}^{(\varrho)} \mathbb{J} \cdot \nabla_{\mathbf{h}} \widehat{C}), \quad (6.123)$$

which can also be written in the flux form

$$\partial_t (\bar{\zeta}^{(\varrho)} \widehat{C}) + \nabla_{\mathbf{h}} \cdot (\bar{\zeta}^{(\varrho)} \widehat{\mathbf{u}} \widehat{C}) = \nabla_{\mathbf{h}} \cdot (\bar{h}^{(\varrho)} \mathbb{J} \cdot \nabla_{\mathbf{h}} \widehat{C}). \quad (6.124)$$

The subgrid scale operator on the right hand side has the same general form as the diffusion operator written in isopycnal coordinates as derived in Section 1.15. However, in addition to symmetric diffusion processes, this operator includes skewed fluxes that lead to skew diffusion as discussed in Section 6.4.2. Whereas the diffusive aspect is commonly parameterized as dianeutral diffusion and neutral diffusion (Section 7.1), there is no parameterization for the skewed correlations for use in ocean models. We comment further on this situation in Section 7.3.8.

6.6.4 Summary of the tracer parameterization problem

Traditionally, the isopycnal parameterization problem for the evolution of the mean thickness weighted tracer requires a parameterization of the bolus velocity $\mathbf{u}^{\text{bolus}}$, which is related to the thickness weighted horizontal velocity via

$$\widehat{\mathbf{u}}(\varrho) = \frac{\langle \mathbf{u} \rangle^{(\varrho)}}{\bar{\zeta}^{(\varrho)}} = \bar{\mathbf{u}}^{(\varrho)} + \frac{\langle' \mathbf{u}' \rangle^{(\varrho)}}{\bar{h}^{(\varrho)}} = \bar{\mathbf{u}}^{(\varrho)} + \mathbf{u}^{\text{bolus}}. \quad (6.125)$$

In addition to the bolus velocity, it is necessary to parameterize the subgrid scale tracer transport tensor

$$\widehat{C'' \mathbf{u}''} = -\mathbb{J} \cdot \nabla_{\mathbf{h}} \widehat{C}, \quad (6.126)$$

which generally has symmetric (diffusive) and antisymmetric (stirring) components (Section 6.4).

For a geopotential coordinate description, equation (6.75) is used to relate thickness weighted mean fields, defined as a function of ϱ , and TRM fields, defined as a function of the mean vertical position of ϱ , to write for the tracer field

$$\widehat{C}(x, y, \bar{\varrho}, t) = \bar{C}^{\#}(x, y, \bar{\eta}^{(\varrho)}, t). \quad (6.127)$$

Equation (6.127), and the developed formalism, leads to the mean field tracer equation in geopotential coordinates

$$\partial_t \bar{C}^{\#} = \nabla \cdot (\nabla \bar{C}^{\#} \times \bar{\Psi}^{\#}) + R(\bar{C}^{\#}), \quad (6.128)$$

where $R(\bar{C}^{\#})$ is the geopotential coordinate form of the mixing/stirring operator on the right-hand side of equation (6.123). Details for the transformation of the mixing/stirring operator from isopycnal to geopotential coordinates are provided in Section 1.15.

6.6.5 Comments

Much in this section follows from [Smith \(1999\)](#), [McDougall and McIntosh \(2001\)](#), [Young \(2012\)](#), and [Jansen et al. \(2024\)](#), each of which focused on the hydrostatic primitive equations assuming a vertically stable buoyancy stratification. The paper by [Young \(2012\)](#) is the first to formulate the ensemble mean primitive equations (continuity, tracer, momentum, vorticity, and energy equations) in a form where only the thickness weighted (residual mean) velocity appears. Hence, the formulation of [Young \(2012\)](#) eliminates the need to parameterize the [bolus velocity](#) or the [quasi-Stokes transport](#) since neither appear as separately identified terms. The paper by [Jansen et al. \(2024\)](#) further pursues the ideas from [Young \(2012\)](#) within the context of [generalized vertical coordinate](#) ocean models, and they identify some inconsistencies in how certain ocean models are implementing the eddy parameterizations. The topic of formulating the equations of motion remains an active topic of research for purposes of facilitating subgrid scale closure.



6.7 Exercises

EXERCISE 6.1: STOKES DRIFT AND PSEUDOMOMENTUM

Consider a small amplitude disturbance field, $\xi(\mathbf{x}, t)$ with an Eulerian mean velocity having zero shear, $\partial_m \bar{v} = 0$, so that the Stokes drift is given by equation (6.28)

$$\mathbf{v}^{(S)} = \overline{(\xi \cdot \nabla) \partial_t \xi} + \mathcal{O}(\alpha^3) = \overline{(\xi \cdot \nabla) \mathbf{v}'} + \mathcal{O}(\alpha^3) \quad \text{if } \partial_n \bar{v} = 0. \quad (6.129)$$

Show that the Stokes drift can be written as

$$\mathbf{p} = \mathbf{v}^{(S)} + \overline{\xi \times \omega'} - \frac{1}{2} \nabla \overline{\partial_t (\xi \cdot \xi)} + \mathcal{O}(\alpha^3), \quad (6.130)$$

where (using Cartesian tensors)

$$p_i = -\overline{(\partial_i \xi^j) \delta_{jk} v'^k} = -\overline{(\partial_i \xi^j) \delta_{jk} \partial_t \xi^k} \quad (6.131)$$

is known as the pseudomomentum of the disturbance.

EXERCISE 6.2: AREA INTEGRATED TRACER FLUX

Following the GLM formalism in Section 6.4, consider the mean of the tracer flux as integrated over a static area

$$\mathcal{T} = \overline{\int_S \mathbf{v} C \cdot \hat{\mathbf{n}} \, d\mathcal{S}}. \quad (6.132)$$

Extract the rotational term and use Stokes' theorem to write it as a contour integral around the boundary of the domain.

EXERCISE 6.3: CONNECTING GLM AND STOKES DRIFT

Consider a pure wave field in which $\bar{v} = 0$. Connect the GLM transport to the symmetric and anti-symmetric transport tensors defined in Section 6.3.

EXERCISE 6.4: MASSAGING THE MEAN FIELD TRACER EQUATION

Massage the mean field tracer equation (6.53) to bring it into a variety of flux-form expressions. Connect these expressions to the Stokes drift from Exercise 6.60.

EXERCISE 6.5: LINEAR ROTATING WAVE

We illustrate some of the analysis of Section 6.4 by considering a particle displacement vector comprised of periodic and polarized motion in the horizontal plane

$$\xi(\mathbf{x}, t) = \Gamma [\hat{\mathbf{x}} \cos(\omega t) + \hat{\mathbf{y}} \sin(\omega t)] \quad (6.133a)$$

$$\partial_t \xi(\mathbf{x}, t) = \omega \Gamma [-\hat{\mathbf{x}} \sin(\omega t) + \hat{\mathbf{y}} \cos(\omega t)], \quad (6.133b)$$

where $\Gamma > 0$ a time-independent amplitude and $2\pi/\omega > 0$ is the period. Compute the rotational flux, skew flux, and advective flux for a tracer. Is there any evolution of the GLM tracer concentration?

EXERCISE 6.6: SKEW FLUXES IN A SHALLOW WATER GRAVITY WAVE

In VOLUME 5 we study shallow water gravity waves. Here we compute tracer transport properties of these waves using the technology from Section 6.4, assuming the waves have small amplitude. For this purpose, consider the following x - z traveling gravity waves with fluid particle velocity given by

$$\mathbf{v}' = U [\hat{\mathbf{x}} \cos(kx - \omega t) + \hat{\mathbf{z}} (z - \eta_b) |k| \sin(kx - \omega t)], \quad (6.134)$$

where $\mathbf{k} = k \hat{\mathbf{x}}$ is the zonal wave vector, $\omega > 0$ is the angular frequency (period = $2\pi/\omega > 0$), $z = \eta_b$ is the flat bottom, and U is the constant wave amplitude (dimensions of length per time). Compute the particle trajectories, assuming small amplitude waves. Show that the particle trajectories have a zero phase average, which means they serve as a suitable particle displacement vector for computation of wave properties and tracer transport as per Section 6.4. Compute those properties and discuss.

EXERCISE 6.7: MEAN TRACER TRANSPORT BENEATH A DENSITY SURFACE

Making use of the formalism from Section 6.6, consider the mean horizontal tracer transport occurring beneath a particular potential density surface, $\varrho = \tilde{\varrho}$, which is here given by the TRM tracer concentration

$$\overline{\mathbf{C}}^\#(\bar{\eta}^{(\varrho)}) = \overline{\int_{\eta_b}^{\bar{\eta}^{(\varrho)} + \xi} \mathbf{C} \mathbf{u} dz}. \quad (6.135)$$

Connect this transport to the mean fields defined in Section 6.6.



PARAMETERIZED OCEAN TRACER TRANSPORT

As discussed in Section 5.1, and following the conceptual picture of [Eckart \(1948\)](#), turbulent geophysical fluid flows affect a transfer of tracer variance to the small scales, as signaled by an increase in the magnitude of tracer gradients. This [downscale cascade](#) is facilitated by reversible stirring from balanced and unbalanced fluctuations (e.g., mesoscale eddies, submesoscale eddies, breaking gravity and lee waves, turbulent boundary layer processes). The cascade to progressively smaller scales eventually reaches the [Batchelor scale](#) (order millimetres; e.g., Section 11.5.1 of [Vallis \(2017\)](#)). At this scale, tracer gradients are sufficiently large in magnitude that molecular diffusion can readily act to dissipate tracer variance through irreversible diffusive mixing. Tracer transport at scales larger than the Batchelor scale is dominated by nearly reversible stirring, whereas transport at and below the Batchelor scale is dominated by irreversible mixing from molecular diffusion. This phenomenology provides a constraint on the form of the tracer equation to be used for coarse grained numerical models, where the model grid scale is generally much larger than the Batchelor scale.

In this chapter, we study certain of the mathematical and physical properties of parameterized advective and diffusive tracer transport. Such parameterizations aim to encapsulate key aspects of physical processes too small to observe and/or to simulate. This [subgrid scale](#) parameterization problem is far broader and deeper than available from a single chapter. We focus mostly on subgrid scale tracer advection and diffusion operators arising from ocean mesoscale eddy motions, yet even this limited focus involves far more than can be covered here. In particular, we do not discuss theories for how the eddy diffusivities are computed, which generally require studies of the momentum, energy, and vorticity budgets that are not considered here. Furthermore, we only consider parameterizations of the subgrid scale tracer flux, whose convergence provides a subgrid tendency for the coarse-grained tracer equation. Focusing on fluxes supports locality and conservation for the coarse-grained tracer equation, with these properties also shared by the uncoarsened tracer equation.

CHAPTER GUIDE

We studied the physics of tracer diffusion in Chapter 4 and then advection-diffusion in Chapter 5. We also studied the kinematics of tracer transport in Chapter 6. The present chapter relies on that material, with a focus on the maths and physics of advective-diffusive parameterizations of tracer transport. We also make use of neutral directions as detailed in VOLUME 2. Mathematically, we rely on Cartesian tensor analysis from VOLUME 1.

The notation in this chapter is somewhat tedious, which arises from the many variants of tracer fluxes considered. Furthermore, there are many unanswered research questions about the suitability of certain parameterizations for ocean circulation models, particularly the anisotropic neutral diffusion discussed in Section 7.5 and the anisotropic Gent-McWilliams stirring in Section 7.6.

7.1	Summarizing tracer transport parameterizations	223
7.1.1	A synopsis of ocean mixing processes	223
7.1.2	A rough comparison	224
7.1.3	Diffusive parameterization of fine scale mixing	224
7.1.4	Advective-diffusive parameterization of eddy-induced transport	225
7.1.5	Mathematical elements of eddy-induced stirring	225
7.1.6	Dianeutral unit vector and the neutral slope	226
7.2	Expressions of small scale diffusion	227
7.2.1	Isotropic diffusion	227
7.2.2	Vertical diffusion	228
7.2.3	Dianeutral diffusion	228
7.3	Gent-McWilliams eddy-induced advection	228
7.3.1	Details of the parameterization	229
7.3.2	Effects on buoyancy	230
7.3.3	Local dissipation of available potential energy	231
7.3.4	Connection to form stress	233
7.3.5	Connection to isopycnal thickness diffusion	234
7.3.6	Connection to Gent-McWilliams parameterization	236
7.3.7	A parameterization based on a boundary value problem	237
7.3.8	Comments	238
7.4	Neutral diffusion	238
7.4.1	Motivation for neutral diffusion	238
7.4.2	Redi neutral diffusion	239
7.4.3	Small slope neutral diffusion	240
7.4.4	Neutral tangent plane neutral diffusion	241
7.4.5	Neutrality condition	242
7.4.6	Symmetry condition	242
7.4.7	GM skewson plus small slope neutral diffusion	242
7.4.8	Generalized vertical coordinates	243
7.5	Anisotropic neutral diffusion	245
7.5.1	Orthonormal triad of basis vectors	245
7.5.2	Anisotropic neutral diffusion tensor	246
7.5.3	Properties of the anisotropic neutral diffusive fluxes	247
7.5.4	Small slope anisotropic neutral diffusion	247
7.6	Anisotropic Gent-McWilliams stirring	249

7.6.1	Streamfunction and anti-symmetric tensor	249
7.6.2	Anisotropic Gent-McWilliams skew tracer flux	249
7.6.3	Anisotropic GM skewson plus small slope neutral diffusion	250
7.6.4	A parameterization based on a boundary value problem	250
7.7	Exercises	251

7.1 Summarizing tracer transport parameterizations

In this section we offer an outline of tracer transport parameterizations, starting from the small scales and moving to the mesoscale. We mostly focus on ocean applications, though similar arguments hold for the atmosphere as well.

7.1.1 A synopsis of ocean mixing processes

As reviewed in Chapters 4 and 5, irreversible mixing in the ocean takes place at the millimeter scale through the action of chaotic molecular motions that act to dissipate property gradients. This mixing is generally represented by downgradient molecular diffusion. The molecular diffusivity of matter (e.g., salt) in seawater is roughly $10^{-9} \text{ m}^2 \text{ s}^{-1}$, whereas the molecular thermal diffusivity is roughly 100 times larger (it is easier to diffuse enthalpy (heat) than matter, [Gill, 1982](#)). Reversible stirring by turbulent eddies greatly increases the magnitude of property gradients upon which molecular diffusion acts ([Eckart, 1948](#); [Nakamura, 2001](#); [Müller and Garrett, 2002](#)), thereby increasing the total amount of irreversible mixing. Motivated by the transport afforded by molecular diffusion and Brownian motion as studied in Chapter 4, and following the pioneering work on turbulent diffusion by [Taylor \(1922\)](#), it is common to parameterize mixing induced by turbulent eddy stirring as a diffusive closure with an eddy diffusivity that is far larger than molecular values. Furthermore, the eddy diffusivities are generally the same for all tracers since eddies generally act the same regardless the tracer. Double diffusive processes are the notable counter-example to this equivalence ([Schmitt, 1994](#)).

Mixing induced by eddies of length scale $\mathcal{O}(\text{centimeters} - \text{meters})$ is associated with fine scale mixing processes such as gravitational instability, shear instability and breaking internal gravity waves ([MacKinnon et al., 2013](#)), as well as a suite of boundary layer processes ([Mellor and Yamada, 1982](#); [Large et al., 1994](#); [Kantha and Clayson, 2000](#); [Thorpe, 2005](#)). This mixing is commonly parameterized by a flow dependent isotropic eddy diffusivity. The magnitude of the eddy diffusivity is typically $\mathcal{O}(10^{-3} - 10^{-2} \text{ m}^2 \text{ s}^{-1})$ in boundary layers, and $\mathcal{O}(10^{-5} \text{ m}^2 \text{ s}^{-1})$ in the relatively quiescent ocean interior ([Polzin et al., 1997](#); [Whalen et al., 2012](#); [Waterhouse et al., 2014](#)).

Ocean mesoscale eddies, with size $\mathcal{O}(10 - 100) \text{ km}$ and Rossby numbers much less than unity, preferentially stir tracers along neutral directions ([McDougall, 1987a,b](#); [McDougall et al., 2014](#)). The mesoscale eddy stirring in turn induces a mixing that is parameterized by downgradient diffusion along neutral directions (Section 7.4). When feeling the geometric constraints of the surface boundary, mesoscale stirring leads to horizontal oriented mixing across outcropped density surfaces ([Treguier et al., 1997](#); [Ferrari et al., 2008](#); [Danabasoglu et al., 2008](#)). This mixing is parameterized by downgradient horizontal diffusion. The neutral and horizontal eddy diffusivities associated with mesoscale processes are typically $\mathcal{O}(10^2 - 10^3 \text{ m}^2 \text{ s}^{-1})$ in the ocean interior and can rise to $\mathcal{O}(10^4 \text{ m}^2 \text{ s}^{-1})$ in the ocean surface layer ([Abernathay et al., 2013](#); [Klocker and Abernathay, 2014](#); [Cole et al., 2015](#)).

7.1.2 A rough comparison

What process is more important for setting tracer distributions: neutral diffusion induced by mesoscale eddies or small scale isotropic diffusion induced by breaking gravity waves? Since the neutral diffusivity arises from mesoscale eddy stirring, it is many orders of magnitude larger than the isotropic diffusivity arising from fine scale mixing. However, these two eddy diffusivities act on very different tracer gradients, in which case the net effects on tracer distributions can be more comparable.

To help understand the issue, consider a scaling with a constant neutral diffusivity and a constant isotropic diffusivity. Furthermore, assume Cartesian orientation of the diffusion operators (i.e., zero neutral slope) and assume the isotropic diffusion is dominated by vertical diffusion (see Section 7.2). We are thus comparing the following two diffusion processes

$$\text{horizontal diffusion} = \kappa_{\text{horz}} \nabla_h^2 C \quad \text{and} \quad \text{vertical diffusion} = \kappa_{\text{vert}} \partial_{zz} C. \quad (7.1)$$

Now introduce a vertical length scale, H , and horizontal scale, L , over which the tracer concentration changes by the same amount δC . Doing so leads to the scaled diffusion operators

$$\text{horizontal diffusion} \sim (\kappa_{\text{horz}}/L^2) \delta C \quad \text{and} \quad \text{vertical diffusion} \sim (\kappa_{\text{vert}}/H^2) \delta C. \quad (7.2)$$

These operators have the same scale when

$$\kappa_{\text{vert}} = (H/L)^2 \kappa_{\text{horz}}. \quad (7.3)$$

Choosing $L = 10^5$ m and $H = 10^1$ m leads to

$$\kappa_{\text{vert}} = 10^{-8} \kappa_{\text{horz}}. \quad (7.4)$$

Furthermore, if $\kappa_{\text{horz}} = 10^3$ m² s⁻¹, then the two operators provide a similar contribution to tracer evolution if $\kappa_{\text{vert}} = 10^{-5}$ m² s⁻¹. This is a rather small diffusivity that is generally thought to be on the order of that afforded by the background of breaking gravity waves in the ocean interior (MacKinnon *et al.*, 2013). This scaling is crude since the length scales are dependent on details of the flow regime, as are the eddy diffusivities. Even so, it suggests that the two diffusive processes can indeed contribute to tracer distributions by a similar amount.

7.1.3 Diffusive parameterization of fine scale mixing

Ignoring the cross-diffusion processes introduced in our discussion of ocean energetics in VOLUME 2 (see also IOC *et al.* (2010), Section 2.5 of Olbers *et al.* (2012), and Graham and McDougall (2013)), the molecular diffusion of Θ and S lead to the material evolution equations

$$\rho \frac{D\Theta}{Dt} = \nabla \cdot (\rho \kappa_\Theta \nabla \Theta) \quad (7.5a)$$

$$\rho \frac{DS}{Dt} = \nabla \cdot (\rho \kappa_S \nabla S), \quad (7.5b)$$

where $\kappa_\Theta \approx 100 \kappa_S > 0$ are the molecular kinematic diffusivities for Conservative Temperature, Θ , and salinity, S , respectively.

For a measured or simulated scale, Δ , that is larger than the scale where gravity waves break and dissipate kinetic energy (i.e., tens to hundreds of metres), we commonly assume a diffusive parameterization for the associated irreversible tracer mixing (e.g., MacKinnon *et al.*, 2013).

Diffusion is also used to parameterize mixing from other small scale processes, such as turbulent boundary layer processes, double-diffusion, and breaking leewaves. As discussed in Section 4 of [McDougall et al. \(2014\)](#), small scale mixing generally takes place in an isotropic manner. Its parameterization thus appears just as for isotropic molecular diffusion given by equations (7.5a) and (7.5b), yet with a far larger eddy diffusivity $\kappa_{\text{fine}} \gg \kappa_{\Theta}, \kappa_S$ that is a function of the flow

$$\rho \frac{D\Theta}{Dt} = \nabla \cdot (\rho \kappa_{\text{fine}} \nabla \Theta) \quad (7.6a)$$

$$\rho \frac{DS}{Dt} = \nabla \cdot (\rho \kappa_{\text{fine}} \nabla S). \quad (7.6b)$$

The same eddy diffusivity is used for both Θ and S . This assumption follows the general approach for turbulent transport parameterizations (e.g, [Vallis, 2017](#)), whereby eddies are assumed to act in the same manner on any conserved scalar tracer.

7.1.4 Advection-diffusive parameterization of eddy-induced transport

Stirring from turbulent scales smaller than the grid scale is commonly parameterized by an **eddy-induced velocity**, \mathbf{v}^* . For ocean mesoscale eddies, such parameterized stirring generally follows a variant of [Gent and McWilliams \(1990\)](#) and [Gent et al. \(1995\)](#), with this stirring quite important for setting large-scale ocean tracer distributions. In addition, mixing is promoted by the direct cascade from stirring. This mixing is parameterized by **neutral diffusion**, which is distinct from that used for the small scale mixing discussed in Section 7.1.3.

Consider a second order subgrid scale eddy transport tensor, \mathbf{E} , meant to parameterize both subgrid scale eddy stirring and eddy mixing. With this tensor, the evolution of salinity and Conservative Temperature takes the form

$$\rho \frac{DS}{Dt} = \nabla \cdot (\rho \mathbf{E} \cdot \nabla S) \quad (7.7a)$$

$$\rho \frac{D\Theta}{Dt} = \nabla \cdot (\rho \mathbf{E} \cdot \nabla \Theta). \quad (7.7b)$$

As for the fine scale diffusion equations (7.6a) and (7.6b), we here use the same transport tensor for both S and Θ as eddies are assumed to act in the same manner on any conserved scalar tracer. As presented in Chapter 5, we decompose the second order transport tensor into the sum of its symmetric and anti-symmetric components

$$\mathbf{E} = \mathbf{K} + \mathbf{A}. \quad (7.8)$$

When the symmetric tensor, \mathbf{K} , is positive-definite, it gives rise to downgradient diffusion, whereas the **anti-symmetric tensor** (also skew-symmetric tensor), \mathbf{A} , gives rise to **skew diffusion** or eddy-induced advection affected by an **eddy-induced velocity**.

7.1.5 Mathematical elements of eddy-induced stirring

As detailed in Sections 5.2, 5.4, and 6.4, the anti-symmetric tensor contributes to the parameterized transport according to

$$\nabla \cdot (\rho \mathbf{A} \cdot \nabla S) = \partial_m (\rho A^{mn} \partial_n S) \quad (7.9a)$$

$$= \partial_m (\rho A^{mn}) \partial_n S + \rho A^{mn} \partial_m \partial_n S \quad (7.9b)$$

$$= -\rho v^{*n} \partial_n S, \quad (7.9c)$$

where A^{mn} are the components to the anti-symmetric transport tensor, \mathbf{A} . Additionally, we noted that

$$\rho A^{mn} \partial_m \partial_n S = 0 \quad (7.10)$$

since A^{mn} is anti-symmetric on the indices m, n whereas $\partial_m \partial_n S$ is symmetric. Finally, we introduced a density-weighted eddy-induced velocity

$$\rho v^{*n} = -\partial_m (\rho A^{mn}) \iff \rho \mathbf{v}^* = -\nabla \cdot (\rho \mathbf{A}). \quad (7.11)$$

Importantly, $\rho \mathbf{v}^*$ has a zero divergence, again due to anti-symmetry of A^{mn}

$$\nabla \cdot (\rho \mathbf{v}^*) = \partial_n (\rho v^{*n}) = -\partial_n \partial_m (\rho A^{mn}) = 0. \quad (7.12)$$

A zero-divergence for $\rho \mathbf{v}^*$ means that it contributes no mass sources or sinks to the fluid.¹

Transport from the parameterized anti-symmetric tensor thus provides a means to stir tracers with the eddy-induced velocity arising from unresolved eddy stirring. The mathematical form of the parameterized stirring can be either through skew-diffusion or through advection (see Section 5.4). Choosing to make use of the advection form allows us to combine the contribution from the anti-symmetric transport tensor with the resolved advection operator, thus resulting in a material transport equation making use of the residual mean velocity

$$\rho \frac{D^\dagger S}{Dt} = \nabla \cdot (\rho \mathbf{K} \cdot \nabla S) \quad (7.13a)$$

$$\rho \frac{D^\dagger \Theta}{Dt} = \nabla \cdot (\rho \mathbf{K} \cdot \nabla \Theta), \quad (7.13b)$$

where the residual mean material time derivative is given by

$$\frac{D^\dagger}{Dt} = \frac{\partial}{\partial t} + \mathbf{v}^\dagger \cdot \nabla \quad (7.14)$$

and the residual mean velocity is

$$\mathbf{v}^\dagger = \mathbf{v} + \mathbf{v}^*. \quad (7.15)$$

7.1.6 Dianeutral unit vector and the neutral slope

When considering closures for subgrid tracer mixing and stirring arising from ocean mesoscale motions, we orient the parameterized tracer fluxes according to locally defined buoyancy, as that reflects the physics of mesoscale motions.² We thus work with locally referenced Archimedean buoyancy to determine neutral directions. In particular, at each point in the fluid we orient stirring and mixing through unit directions that point in the dianeutral direction

$$\hat{\gamma} = \frac{-\alpha \nabla \Theta + \beta \nabla S}{|-\alpha \nabla \Theta + \beta \nabla S|} \quad \text{and} \quad \hat{\gamma} = \hat{\mathbf{x}} \hat{\gamma}_x + \hat{\mathbf{y}} \hat{\gamma}_y + \hat{\mathbf{z}} \hat{\gamma}_z \quad \text{and} \quad \hat{\gamma} \cdot \hat{\gamma} = 1, \quad (7.16)$$

¹For a Boussinesq ocean, the density factor is replaced by the constant reference density, ρ , so that $\nabla \cdot \mathbf{v}^* = 0$ in the Boussinesq ocean. See section 7 of [Griffies and Greatbatch \(2012\)](#) for more details of the Boussinesq and non-Boussinesq forms for the parameterized eddy-induced transport.

²We offer further discussion of this point at the start of Section 7.4.

with $\hat{\gamma}$ pointing perpendicular to the neutral tangent plane in a direction towards larger density.³ Furthermore, when the fluid is stably stratified in the vertical, which is common for the mesoscale and larger, then the squared **buoyancy frequency** is positive

$$N^2 = -g(-\alpha \partial_z \Theta + \beta \partial_z S) > 0. \quad (7.17)$$

We can thus introduce the slope of the neutral tangent plane relative to the (x, y) horizontal plane⁴

$$\mathbf{S} = - \begin{bmatrix} -\alpha \nabla_h \Theta + \beta \nabla_h S \\ -\alpha \partial_z \Theta + \beta \partial_z S \end{bmatrix} = \frac{g(-\alpha \nabla_h \Theta + \beta \nabla_h S)}{N^2} = \hat{\mathbf{x}} S_x + \hat{\mathbf{y}} S_y. \quad (7.18)$$

For such stably stratified fluids, the dianeutral direction can be written in terms of the neutral slope

$$\hat{\gamma} = \frac{\mathbf{S} - \hat{\mathbf{z}}}{(1 + \mathbf{S}^2)^{1/2}}. \quad (7.19)$$

In this form we see that the dianeutral direction is vertically downward when the slopes vanish (i.e., horizontal neutral directions), which accords with this direction generally pointing toward increasing density.

7.2 Expressions of small scale diffusion

We here follow Section 4 from [McDougall et al. \(2014\)](#) to highlight distinctions between isotropic diffusion, **dianeutral diffusion**,⁵ and vertical diffusion. Although commonly considered interchangeable in the literature as parameterizations of small scale mixing, there are conceptual distinctions that we identify here. Note that the distinctions between these three diffusions are quantitatively small when neutral slopes are modest and when $\kappa_{\text{ntr}} \gg \kappa_{\text{fine}}$.

7.2.1 Isotropic diffusion

As discussed in Section 7.1.3, we generally parameterize fine scale mixing processes via an isotropic diffusion process using a diffusivity $\kappa_{\text{fine}} > 0$, diffusion tensor

$$\mathbf{K}^{\text{iso}} = \kappa_{\text{fine}} \begin{bmatrix} 1 & 0 & 0 \\ 0 & 1 & 0 \\ 0 & 0 & 1 \end{bmatrix}, \quad (7.20)$$

and corresponding diffusion flux

$$\mathbf{J}^{\text{iso}} = -\rho \mathbf{K}^{\text{iso}} \cdot \nabla C. \quad (7.21)$$

As illustrated in Figure 7.1, under the effects from isotropic diffusion, a region of tracer is diffused the same in all three directions so that, for example, a spherical tracer distribution remains spherical.

³Equation (4) in [McDougall et al. \(2014\)](#) makes use of the opposite convention so that their dianeutral direction points towards decreasing density. We instead follow the water mass transformation convention as in equation (9.38), so that $\hat{\gamma}$ points in the direction of increasing density.

⁴Be careful to not confuse S , for salinity, with the slope components, S_x and S_y .

⁵Dianeutral diffusion is commonly also referred to as diapycnal diffusion, with diapycnal diffusion referring to diffusion across constant potential density surfaces. We distinguish dianeutral from diapycnal in this chapter since neutral directions are defined by locally referenced potential density, and as such neutral directions generally differ from isopycnals. Further discussion is provided in VOLUME 2 as well as [McDougall \(1987a\)](#) and [McDougall et al. \(2014\)](#).

7.2.2 Vertical diffusion

Because vertical density gradients are generally much larger than lateral gradients, it is common to approximate the small scale isotropic diffusion tensor with a vertical diffusion tensor

$$\mathbf{K}^{\text{vert}} = \kappa_{\text{fine}} \begin{bmatrix} 0 & 0 & 0 \\ 0 & 0 & 0 \\ 0 & 0 & 1 \end{bmatrix}, \quad (7.22)$$

with a corresponding vertical diffusive flux

$$\mathbf{J}^{\text{vert}} = -\rho \kappa_{\text{fine}} (\nabla C \cdot \hat{\mathbf{z}}) \hat{\mathbf{z}} = -\rho \mathbf{K}^{\text{vert}} \cdot \nabla C = -\rho \kappa_{\text{fine}} \partial_z C \hat{\mathbf{z}}. \quad (7.23)$$

In this manner, vertical mixing of a tracer patch occurs only in the vertical direction (see Figure 7.1).

7.2.3 Dianeutral diffusion

Dianeutral diffusion orients tracer fluxes according to the dianeutral direction (7.16)

$$\mathbf{J}^{\text{dia}} = -\rho \kappa_{\text{fine}} (\nabla C \cdot \hat{\boldsymbol{\gamma}}) \hat{\boldsymbol{\gamma}} = -\rho \mathbf{K}^{\text{dia}} \cdot \nabla C, \quad (7.24)$$

where the dianeutral diffusion tensor is given by

$$\mathbf{K}^{\text{dia}} = \kappa_{\text{fine}} \begin{bmatrix} \hat{\gamma}_x^2 & \hat{\gamma}_x \hat{\gamma}_y & \hat{\gamma}_x \hat{\gamma}_z \\ \hat{\gamma}_x \hat{\gamma}_y & \hat{\gamma}_y^2 & \hat{\gamma}_y \hat{\gamma}_z \\ \hat{\gamma}_x \hat{\gamma}_z & \hat{\gamma}_y \hat{\gamma}_z & \hat{\gamma}_z^2 \end{bmatrix}. \quad (7.25)$$

Assuming a vertically stable stratification, we can make use of the relation (7.19) to write $\hat{\boldsymbol{\gamma}}$ in terms of the slope, \mathbf{S} , thus rendering

$$(\nabla C \cdot \hat{\boldsymbol{\gamma}}) \hat{\boldsymbol{\gamma}} = \frac{(\mathbf{S} - \hat{\mathbf{z}}) \cdot \nabla C}{1 + \mathbf{S}^2} (\mathbf{S} - \hat{\mathbf{z}}) = \frac{1}{1 + \mathbf{S}^2} \begin{bmatrix} S_x^2 & S_x S_y & -S_x \\ S_x S_y & S_y^2 & -S_y \\ -S_x & -S_y & 1 \end{bmatrix} \begin{bmatrix} \partial_x C \\ \partial_y C \\ \partial_z C \end{bmatrix}, \quad (7.26)$$

so that the dianeutral diffusion tensor now takes on the form

$$\mathbf{K}^{\text{dia}} = \frac{\kappa_{\text{fine}}}{1 + \mathbf{S}^2} \begin{bmatrix} S_x^2 & S_x S_y & -S_x \\ S_x S_y & S_y^2 & -S_y \\ -S_x & -S_y & 1 \end{bmatrix}. \quad (7.27)$$

As illustrated in Figure 7.1, dianeutral diffusion elongates a tracer patch in the direction normal to the neutral tangent plane.

7.3 Gent-McWilliams eddy-induced advection

As mentioned in Section 6.6.3, there are two processes that contribute to eddy-induced advection/stirring. One involves the correlations between eddy fluctuations in the velocity and tracer fields. In Section 6.4, we considered the kinematics of correlations induced by small amplitude eddying motions, where we found that the eddy-induced motion of fluid particles leads to both a symmetric (mixing) and anti-symmetric (stirring) dispersion of tracer concentrations. There

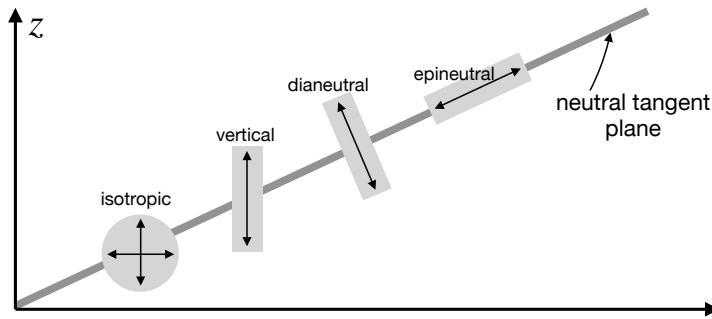


FIGURE 7.1: Illustrating the effects from various forms of diffusion on an initially spherical tracer patch. When diffused with an isotropic diffusion tensor (equation (7.20)), a spherical patch remains spherical. When diffused with a vertical diffusion tensor (equation (7.22)), a tracer patch elongates in the vertical direction. When diffused with a dianeutral diffusion tensor (equation (7.27)), a tracer patch elongates in the direction normal to the slanted neutral tangent plane. Finally, when diffused with a neutral diffusion tensor, such as the Redi tensor (7.72) or the small slope tensor (7.73), a tracer patch elongates along the neutral tangent plane; i.e., in the epineutral direction. This figure is adapted from Figure 4 of [McDougall et al. \(2014\)](#).

is currently no method proposed for parameterizing this form of eddy-induced stirring when it arises from subgrid scale processes, thus leaving unanswered its importance to large-scale tracer distributions.

The second process leading to eddy-induced stirring arises from correlations between fluctuations in isopycnal layer thickness and horizontal velocity. As detailed in Section 6.5, this second effect leads to a movement of volume between isopycnal layers, or equivalently we can conceive of it as the quasi-Stokes transport of volume arising from transient eddy motion. This eddy-induced volume transport affects an eddy-induced tracer transport within isopycnal layers. Transient mesoscale eddies are the canonical dynamical process leading to this form of transport. For simulations that do not resolve transient mesoscale eddies, we commonly parameterize the subgrid scale stirring through variants of the [Gent et al. \(1995\)](#) scheme. Mathematical elements of this scheme are detailed in this section.

Most presentations of the [Gent et al. \(1995\)](#) scheme assume a Boussinesq ocean, with Section 7 of [Griffies and Greatbatch \(2012\)](#) an exception. We here present the non-Boussinesq form, though in places make the Boussinesq approximation since doing so simplifies the presentation without losing anything fundamental.⁶

7.3.1 Details of the parameterization

[Gent et al. \(1995\)](#) parameterize the three-dimensional non-divergent eddy-induced mass flux (recall Section 5.4.3) according to

$$\rho \mathbf{v}^* = \nabla \times (\rho \Psi^*) \quad \text{with} \quad \Psi^* = \hat{z} \times \kappa_{gm} \mathbf{S}, \quad (7.28)$$

where \mathbf{S} is the neutral slope given by equation (7.18), and $\kappa_{gm} > 0$ is a kinematic eddy diffusivity with dimensions of velocity times a length. As defined, the eddy-induced mass flux is determined by the neutral slope, with larger slopes, and thus more baroclinicity, leading to larger flux magnitudes.⁷

⁶For the Boussinesq ocean, the *in situ* density factor found throughout this section is set to the constant Boussinesq reference density, ρ_0 . We study the Boussinesq ocean in VOLUME 2.

⁷Recalling our discussion of volume transport by eddying motion in Section 6.5, we can interpret the Gent-McWilliams parameterization (7.28) as a parameterization of the quasi-Stokes transport.

Performing the curl on the streamfunction leads to the horizontal and vertical components to the eddy-induced mass flux

$$\rho \mathbf{u}^* = -\partial_z (\kappa_{\text{gm}} \rho \mathbf{S}) \quad \text{and} \quad \rho w^* = \nabla_h \cdot (\kappa_{\text{gm}} \rho \mathbf{S}), \quad (7.29)$$

along with the skew diffusive tensor

$$\mathbf{A}^{\text{gm}} = \kappa_{\text{gm}} \begin{bmatrix} 0 & 0 & -S_x \\ 0 & 0 & -S_y \\ S_x & S_y & 0 \end{bmatrix}. \quad (7.30)$$

Following the discussion in Section 5.4.4, we identify the advective tracer flux, skew tracer flux, and rotational tracer flux

$$\mathbf{J}^{\text{adv}} = \mathbf{J}^{\text{skew}} + \mathbf{J}^{\text{rot}} \quad (7.31)$$

where

$$\mathbf{J}^{\text{adv}} = C \rho \mathbf{v}^* = C \rho [-\partial_z (\kappa_{\text{gm}} \rho \mathbf{S}) + \hat{z} \nabla_h \cdot (\kappa_{\text{gm}} \rho \mathbf{S})] \quad (7.32a)$$

$$\mathbf{J}^{\text{skew}} = -\nabla C \times \rho \Psi^* = \rho \kappa_{\text{gm}} [\mathbf{S} \partial_z C - \hat{z} (\mathbf{S} \cdot \nabla C)] \quad (7.32b)$$

$$\mathbf{J}^{\text{rot}} = \nabla \times (\rho C \Psi^*). \quad (7.32c)$$

7.3.2 Effects on buoyancy

To help understand the physics of the Gent-McWilliams parameterization (7.28), we here focus on how it affects buoyancy in a perfect Boussinesq ocean with a linear equation of state. Using potential density, ϱ , as a measure of buoyancy, we find the parameterized skew flux of potential density is given by

$$\rho_o^{-1} \mathbf{J}^{\text{skew}} = -\kappa_{\text{gm}} [\nabla_h \varrho - \hat{z} \mathbf{S}^2 \partial_z \varrho] = -\kappa_{\text{gm}} [\nabla_h \varrho + \hat{z} (\rho_o/g) (\mathbf{S} N)^2], \quad (7.33)$$

with the squared neutral slope and squared buoyancy frequency written

$$\mathbf{S}^2 = \mathbf{S} \cdot \mathbf{S} \quad \text{and} \quad N^2 = -\frac{g}{\rho_o} \frac{\partial \varrho}{\partial z}. \quad (7.34)$$

The parameterization yields a horizontal downgradient diffusive flux of potential density along with a vertical upgradient diffusive flux. Geostrophic turbulence is characterized by large Richardson numbers, so that the vertical stratification is stable ($N^2 > 0$). As a result, the vertical component to the potential density skew flux is vertically downward, which corresponds to a vertically upward buoyancy skew flux. We illustrate this orientation of the skew flux components in Figure 7.2.

As we see in Section 7.3.3, this orientation of the skew flux ensures that the parameterization reduces available potential energy. Additionally, [Gent et al. \(1995\)](#) prescribe a diffusivity that vanishes at the ocean surface and ocean bottom. [McIntosh and McDougall \(1996\)](#) and [McDougall and McIntosh \(2001\)](#) present more discussion of the boundary conditions, which can be understood by considering the exact form of the quasi-Stokes transport defined by equation (6.82). Furthermore, we consider a boundary value problem approach in Section 7.3.7 that also pays particular attention to the boundary conditions.

Figure 7.3 brings elements of the parameterization together by illustrating the [Gent-McWilliams effect](#) for a meridional potential density front in the southern hemisphere. The

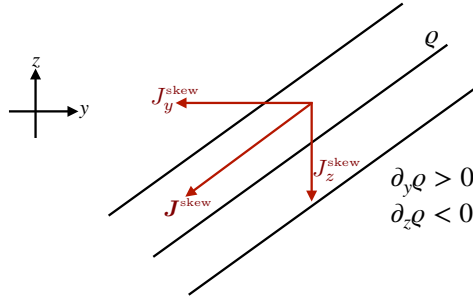


FIGURE 7.2: Orientation of the skew flux of potential density, ϱ , arising from the [Gent et al. \(1995\)](#) parameterization and as described by [Griffies \(1998\)](#). The sloped black lines are constant ϱ isosurfaces (isopycnals). The horizontal skew flux of potential density is downgradient (directed from high density to low density), whereas the vertical skew flux component is upgradient (directed from low density to high density). The net effect is a skew flux that is oriented parallel to isopycnals.

thermal wind flow is eastward, as in the Antarctic Circumpolar Current, whereas a parameterized [secondary circulation](#) acts to weaken the front, with the secondary circulation proportional to the strength of the front as measured by the isopycnal slope. That is, the Gent-McWilliams parameterization assumes that the mean effects from geostrophic eddies, whose kinetic energy is supported by the potential energy in the front, lead to a weakening of the potential density slope so that the front relaxes toward the horizontal. It is notable that on the scale of the resolved flow, the secondary circulation is [ageostrophic](#), with the geostrophic flow having a zero component in the cross-front direction.

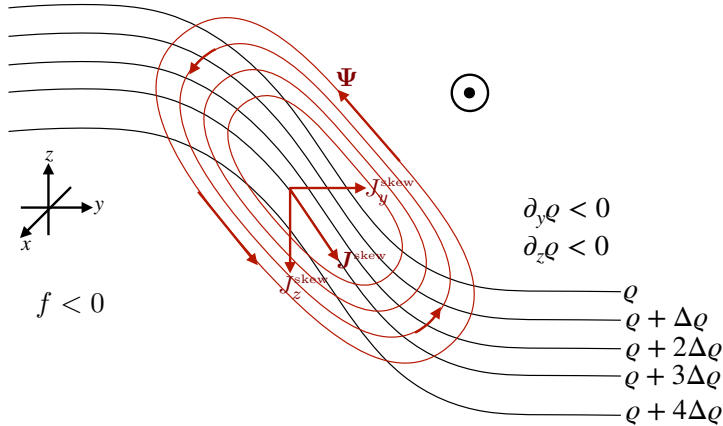


FIGURE 7.3: The [Gent-McWilliams effect](#) for a meridional potential density front in the Southern Hemisphere, where dense water rises to the south so that $\partial_y \varrho < 0$. The mean geostrophic thermal wind flow is eastward (out of the page), such as for the Antarctic Circumpolar Current. With a gravitationally stable stratification, whereby $\partial_z \varrho < 0$ so that $N^2 > 0$, the Gent-McWilliams streamfunction given by equation (7.28) leads to a counter-clockwise [secondary circulation](#) (red isolines), which is ageostrophic. The dual perspective offered by the Gent-McWilliams skew flux for potential density, given by equation (7.33), reveals a northward (downgradient) meridional skew flux component along with a downward (upgradient) vertical component (red vectors). The result from either the streamfunction perspective or the skew flux perspective is a potential density tendency that relaxes the front towards the horizontal so to reduce the isopycnal slope.

7.3.3 Local dissipation of available potential energy

Now consider effects from the [Gent et al. \(1995\)](#) scheme on available potential energy, continuing to assume a Boussinesq ocean with a linear equation of state. Note that the parameterization, as an advective stirring process, preserves the quantity of fluid within density layers; i.e., there

is no dianeutral transport.⁸ Hence, the change in potential energy is identical to the change in available potential energy. Results from this discussion support the intuition from Figure 7.3 that the scheme relaxes geostrophic fronts and thus reduces potential energy.

Skew flux approach

Let us approach the parameterization problem from the perspective of satisfying two general properties: (I) the subgrid scale operator stirs while maintaining the same amount of fluid within isopycnal layers, (II) the subgrid operator locally dissipates potential energy through a rearrangement of the potential density surfaces, with the potential energy dissipation vanishing when there is zero baroclinicity. That is, the scheme dissipates available potential energy. What is the form of the stirring operator implied by these two assumptions?

Stirring of potential density can be realized via the convergence of a skew flux oriented parallel to potential density surfaces

$$\rho_0^{-1} \mathbf{J}^{\text{skew}} = -\nabla \varrho \times \boldsymbol{\Psi}^*, \quad (7.35)$$

where at this point we have yet to specify $\boldsymbol{\Psi}^*$. To see what the local dissipation of available potential energy imposes, consider the gravitational potential energy

$$P = g \int \varrho z \, dV, \quad (7.36)$$

where, again, we assume the *in situ* density equals to the potential density as per a linear equation of state. Assuming all boundaries are material and static allows us to focus on the time tendency of potential energy associated with the unknown flux

$$\frac{dP}{dt} = g \int z \frac{\partial \varrho}{\partial t} \, dV = -\frac{g}{\rho_0} \int (z \nabla \cdot \mathbf{J}^{\text{skew}}) \, dV = -\frac{g}{\rho_0} \int (z \partial_z J^z) \, dV = \frac{g}{\rho_0} \int J^z \, dV, \quad (7.37)$$

where J^z is the vertical flux component. We drop boundary effects by assuming the subgrid scale flux vanishes on all boundaries. To provide a local available potential energy sink requires

$$J^z \leq 0, \quad (7.38)$$

where zero occurs when the isopycnals are flat. It is sufficient to construct the vertical flux component using only the potential density field itself. For a stably stratified fluid in which $\partial_z \varrho < 0$, the following form provides a local available potential energy sink

$$\rho_0^{-1} J^z = \kappa_{\text{gm}} \mathbf{S}^2 \partial_z \varrho = -(\kappa_{\text{gm}} \rho_0 / g) (\mathbf{S} \mathbf{N})^2 \leq 0. \quad (7.39)$$

The corresponding horizontal flux is given by a downgradient diffusive flux

$$\mathbf{J}^h = -\rho_0 \kappa_{\text{gm}} \nabla_h \varrho. \quad (7.40)$$

We have thus recovered the skew flux (7.33) as proposed by [Gent et al. \(1995\)](#). Note that [Aiki et al. \(2004\)](#) proceed in a similar manner yet do not assume locality of the available potential

⁸In the ocean physics literature, such transport is often referred to as “adiabatic.” That terminology is appropriate if the density surfaces are parallel to Conservative Temperature surfaces, in which case there is no transfer of temperature as part of the stirring process. However, potential density surfaces are not parallel to temperature surfaces when the ocean has salinity, in which case we can mix temperature (and thus no longer remain adiabatic) even while maintaining a constant amount of fluid within density layers.

energy sink, thus deriving a more general subgrid scale operator.

Advective flux approach

The impacts on potential energy should be the same when representing the parameterization as an advective flux. To verify this result, return to equation (7.37) and make use of the vertical component of the advective flux rather than the skew flux

$$\frac{dP}{dt} = -g \int z \mathbf{v}^* \cdot \nabla \varrho dV \quad (7.41a)$$

$$= g \int \varrho w^* dV \quad (7.41b)$$

$$= g \int \varrho \nabla_h \cdot (\kappa_{gm} \mathbf{S}) dV \quad (7.41c)$$

$$= g \int \nabla_h \cdot (\varrho \kappa_{gm} \mathbf{S}) dV - g \int \nabla_h \varrho \cdot \kappa_{gm} \mathbf{S} dV \quad (7.41d)$$

$$= -\rho_o \int \kappa_{gm} (\mathbf{S} \cdot \mathbf{N})^2 dV, \quad (7.41e)$$

which is the same result as for the skew flux. Note that to reach this result we dropped the boundary contribution, which follows since the closure assumes $\kappa_{gm} = 0$ on boundaries.

7.3.4 Connection to form stress

We now connect the [Gent et al. \(1995\)](#) closure, normally implemented in the tracer equation, to vertical transfer of momentum through form stress. For this purpose, we recall the general discussion of form stress in VOLUME 2, where we identify form stress as the horizontal pressure force acting on a sloped surface, with our present concern being form stresses acting on isopycnal surfaces.⁹ For this purpose, assume the fluid is in Boussinesq frictional planetary geostrophic balance¹⁰, whereby the horizontal momentum equation is given by

$$\rho_o f (\hat{\mathbf{z}} \times \mathbf{u}) = -\nabla_h p + \partial_z \boldsymbol{\tau}, \quad (7.42)$$

with $\boldsymbol{\tau}$ a horizontal subgrid scale stress vector. The Coriolis acceleration balances the acceleration from horizontal pressure gradients plus a vertical transfer of horizontal stress. The horizontal stress term is generally quite small in the ocean interior, where the flow is in geostrophic balance, whereas it is large at the ocean boundaries where it arises from turbulent boundary layer processes (e.g., turbulent wind stress and bottom stresses).

To make the connection between [Gent et al. \(1995\)](#) and the vertical transfer of horizontal form stress, add $\rho_o f (\hat{\mathbf{z}} \times \mathbf{u}^*)$ to both sides of equation (7.42) to obtain

$$\rho_o f (\hat{\mathbf{z}} \times \mathbf{u}^\dagger) = -\nabla_h p + \partial_z \boldsymbol{\tau} + \rho_o f (\hat{\mathbf{z}} \times \mathbf{u}^*), \quad (7.43)$$

where $\mathbf{u}^\dagger = \mathbf{u} + \mathbf{u}^*$ is the horizontal residual mean velocity. This equation says that the Coriolis acceleration from the horizontal residual mean velocity balances pressure gradients,

⁹ [Young \(2012\)](#) provides a general method for making the connection between [Gent et al. \(1995\)](#) and form stress for a continuously stratified fluid. [Loose et al. \(2023\)](#) and [Jansen et al. \(2024\)](#) provide further theoretical and numerical analysis of this approach. For our more schematic purposes, we follow the treatment in [Greatbatch and Lamb \(1990\)](#), [Gent et al. \(1995\)](#) (their Section 4), [Ferreira and Marshall \(2006\)](#) (their Section 2), and [Zhao and Vallis \(2008\)](#) (their Section 2.2).

¹⁰We discuss planetary geostrophic vorticity balances in VOLUME 3.

the vertical divergence of the horizontal frictional stresses, plus the Coriolis acceleration from the eddy-induced velocity. We further unpack the eddy Coriolis acceleration by noting that the planetary geostrophic velocity satisfies the thermal wind relation in the ocean interior, whereby

$$f \partial_z \mathbf{u} = -(g/\rho_0) \hat{\mathbf{z}} \times \nabla \rho = -\hat{\mathbf{z}} \times N^2 \mathbf{S}. \quad (7.44)$$

We can thus write the Coriolis acceleration from the eddy-induced velocity as

$$f (\hat{\mathbf{z}} \times \mathbf{u}^*) = -f [\hat{\mathbf{z}} \times \partial_z (\kappa_{\text{gm}} \mathbf{S})] \quad (7.45a)$$

$$= -\partial_z [\hat{\mathbf{z}} \times (f \kappa_{\text{gm}} \mathbf{S})] \quad (7.45b)$$

$$= \frac{\partial}{\partial z} \left[\frac{\kappa_{\text{gm}} f^2}{N^2} \frac{\partial \mathbf{u}}{\partial z} \right] \quad (7.45c)$$

$$= \partial_z (\nu_e \partial_z \mathbf{u}), \quad (7.45d)$$

where the final equality introduced an eddy-induced vertical viscosity

$$\nu_e \equiv \kappa_{\text{gm}} (f^2/N^2). \quad (7.46)$$

Making use of this result in the planetary geostrophic equation (7.43) thus leads to

$$\rho_0 f (\hat{\mathbf{z}} \times \mathbf{u}^\dagger) = -\nabla_h p + \partial_z (\boldsymbol{\tau} + \boldsymbol{\tau}_e), \quad (7.47)$$

where

$$\rho_0^{-1} \boldsymbol{\tau}_e = \nu_e \partial_z \mathbf{u} \quad (7.48)$$

defines a horizontal stress vector arising from the thermal wind shears and due to the mesoscale eddies. Equation (7.47) says that the Coriolis acceleration from the horizontal residual mean velocity is in balance with the horizontal pressure gradient plus the vertical transfer of horizontal shears arising from both friction/wind/bottom drag plus a contribution from parameterized mesoscale eddies.

We conclude that the [Gent et al. \(1995\)](#) parameterization appears in the planetary geostrophic residual mean momentum equation as a vertical transport of horizontal stress whose magnitude is set by a viscosity, $\nu_e = \kappa_{\text{gm}} (f/N)^2$. Notably, this vertical eddy transfer occurs in the absence of irreversible mixing. We thus interpret it as a parameterization of the vertical transfer of pressure form stress via mesoscale eddies that act between isopycnal layers. That is, the [Gent et al. \(1995\)](#) scheme offers a means to parameterize vertical transfer of horizontal form stress arising from undulating mesoscale eddies in the ocean interior. This interpretation is more thoroughly considered in our study of geostrophy in VOLUME 2 (see also [Greatbatch and Lamb \(1990\)](#) and [Loose et al. \(2023\)](#)).

7.3.5 Connection to isopycnal thickness diffusion

Recall the ensemble mean thickness equation (6.95) for a Boussinesq ocean as derived in Section 6.5.9

$$\partial_t \langle \cdot \rangle + \nabla_h \cdot (\langle \hat{\mathbf{u}} \rangle) = 0, \quad (7.49)$$

where

$$\hat{\mathbf{u}} = \mathbf{u} + \mathbf{u}^{\text{bulus}} \quad (7.50)$$

is the thickness weighted transport velocity affecting evolution of the ensemble mean thickness $\langle \cdot \rangle$. Note that for brevity we here drop the nomenclature $(\cdot)^{(\varrho)}$ used in Section 6.5.9.

Isopycnal correlations of horizontal velocity and layer thickness define the bolus velocity via

$$\langle \mathbf{u}^{\text{bolus}} \rangle = \overline{\langle' \mathbf{u}' \rangle^{(\varrho)}} \quad (7.51)$$

Now consider a downgradient diffusive closure for this correlation

$$\langle \mathbf{u}^{\text{bolus}} \rangle = \overline{\langle' \mathbf{u}' \rangle^{(\varrho)}} = -\mathbf{K}^{\text{thick}} \cdot \nabla_{\mathbf{h}} h, \quad (7.52)$$

with $\mathbf{K}^{\text{thick}}$ a symmetric and positive-definite 2×2 diffusion tensor. The mean thickness equation thus takes the form of an advection-diffusion equation in isopycnal coordinates

$$\partial_t \langle \cdot \rangle + \nabla_{\mathbf{h}} \cdot (\langle \mathbf{u} \rangle) = \nabla_{\mathbf{h}} \cdot (\mathbf{K}^{\text{thick}} \cdot \nabla_{\mathbf{h}} \langle \cdot \rangle). \quad (7.53)$$

We note one special property of the closure (7.52) revealed when considering discrete shallow water layers and assuming the thickness diffusion tensor is depth independent. Vertically summing the eddy transport from the ocean bottom up to a particular layer yields

$$\sum_{n=k_b}^{n=k} \overline{\langle' \mathbf{u}'_n \rangle^{(\varrho)}} = - \sum_{n=k_b}^{n=k} \mathbf{K}^{\text{thick}} \cdot \nabla_{\mathbf{h}} h_n = -\mathbf{K}^{\text{thick}} \cdot \sum_{n=k_b}^{n=k} \nabla_{\mathbf{h}} h_n = -\mathbf{K}^{\text{thick}} \cdot \nabla_{\mathbf{h}} \eta_{k-1/2}, \quad (7.54)$$

where $\eta_{k-1/2}$ is the upper interface of layer k (see Figure 7.4), and where k_b is the index for the layer at the ocean bottom. In this case we see that the eddy transport below an isopycnal interface is directly proportional to the slope of that interface.

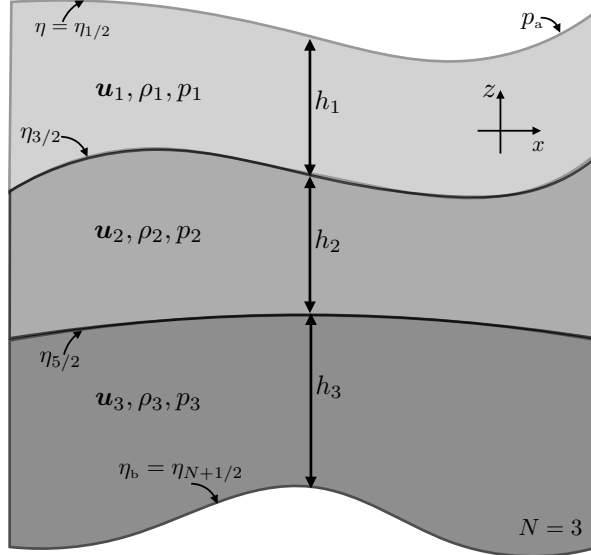


FIGURE 7.4: Three dynamically active layers of stacked shallow water fluid ($N = 3$). In particular, $\eta_{1/2}$ is the free surface, $\eta_{1/2} = \eta$, whereas $\eta_{N+1/2} = \eta_b$ is the bottom interface. Hence, the total thickness of a column is $h_1 + h_2 + h_3 = \eta_{1/2} - \eta_b$. The “atmosphere” above the layers is assumed to apply a pressure, p_a , to the upper surface. The reduced gravity defined between each layer is given by $g_{k+1/2}^r = g(\rho_{k+1} - \rho_k)/\rho_{\text{ref}}$. We take the reference density as $\rho_{\text{ref}} = \rho_1$, which results in a tidy set of layer equations. This figure is more thoroughly discussed in our study of shallow wave models in VOLUME 3.

7.3.6 Connection to Gent-McWilliams parameterization

To make a direct connection between the thickness diffusion closure (7.52) and the [Gent et al. \(1995\)](#) closure discussed in Section 7.3.1, note that the specific thickness is the inverse of the vertical derivative of the potential density

$$\langle = (\partial_z \varrho)^{-1}. \quad (7.55)$$

Correspondingly, using the relation between the horizontal derivative operators, $\nabla_{\mathbf{v}} = \nabla_{\mathbf{h}} + \mathbf{S} \partial_z$, gives

$$\langle^{-1} \nabla_{\mathbf{v}} \langle = -\langle \nabla_{\mathbf{v}} (1/\langle) \quad \text{product rule identity} \quad (7.56a)$$

$$= -(\partial_z \varrho)^{-1} (\nabla_{\mathbf{h}} + \mathbf{S} \partial_z) \partial_z \varrho \quad \langle = \partial z / \partial \varrho \text{ and } \nabla_{\mathbf{v}} = \nabla_{\mathbf{h}} + \mathbf{S} \partial_z \quad (7.56b)$$

$$= -\frac{\partial_z (\nabla_{\mathbf{h}} \varrho)}{\partial_z \varrho} + \frac{\partial_{zz} \varrho \nabla_{\mathbf{h}} \varrho}{(\partial_z \varrho)^2} \quad \text{rearrangement} \quad (7.56c)$$

$$= -\partial_z [\nabla_{\mathbf{h}} \varrho / (\partial_z \varrho)] \quad \text{product rule identity} \quad (7.56d)$$

$$= \partial_z \mathbf{S} \quad \text{isopycnal slope } \mathbf{S} = -\nabla_{\mathbf{h}} \varrho / (\partial_z \varrho). \quad (7.56e)$$

Consequently, the bolus velocity takes the form

$$\mathbf{u}^{\text{bolus}} = -\langle^{-1} \mathbf{K}^{\text{thick}} \cdot \nabla_{\mathbf{v}} \langle = -\mathbf{K}^{\text{thick}} \cdot \partial_z \mathbf{S}. \quad (7.57)$$

The special case of depth independent diffusivity

For the special case of $\mathbf{K}^{\text{thick}}$ that is independent of depth and proportional to the 2×2 identity matrix, we recover the identity

$$\mathbf{u}^{\text{bolus}} = -\partial_z (\kappa_{\text{gm}} \mathbf{S}) = \mathbf{u}^*, \quad (7.58)$$

where the horizontal component of the [Gent et al. \(1995\)](#) velocity, \mathbf{u}^* , was identified from equation (7.29). Again, this identity holds only for the special case of a vertically independent diffusivity tensor proportional to the identity.

Further caveats

The relevance of a depth-independent diffusivity has been questioned by many authors, such as [Killworth \(1997\)](#), [Treguier et al. \(1997\)](#), [Smith and Vallis \(2002\)](#), [Smith and Marshall \(2009\)](#), and [Abernathy et al. \(2013\)](#). We conclude from these studies that a depth independent diffusivity is not the best choice for the [Gent et al. \(1995\)](#) parameterization, in which case where one places the vertical derivative is crucial.

The relation between thickness diffusion with the [Gent et al. \(1995\)](#) parameterization further breaks down near boundaries. The reason is that the eddy diffusivity vanishes next to boundaries and thus has a depth-dependence. Additionally, as noted by [Holloway \(1997\)](#) and [Griffies et al. \(2000\)](#), thickness diffusion next to solid earth boundaries leads to an increase in potential energy, with isopycnals creeping up the topographic slope. Such unphysical behavior motivates isopycnal modelers instead to use *interfacial height* diffusion to dissipate noise in the thickness field.

7.3.7 A parameterization based on a boundary value problem

There have been variants of the [Gent et al. \(1995\)](#) scheme proposed in the literature, such as those of [Aiki et al. \(2004\)](#) and [Ferrari et al. \(2010\)](#). As for the [Gent et al. \(1995\)](#) scheme, these alternatives dissipate available potential energy without mixing between isopycnal classes. We here briefly discuss the scheme of [Ferrari et al. \(2010\)](#), which is used by a variety of ocean climate models largely since it contains a natural means to numerically regularize the eddy-induced streamfunction in regions of weak vertical stratification. These considerations are relevant especially in ocean climate models, where weak or zero vertical stratification is inevitable and it is necessary to carefully handle such regimes.

For the [Ferrari et al. \(2010\)](#) scheme we write the parameterized eddy streamfunction as

$$\Psi^* = \hat{z} \times \Upsilon \implies \mathbf{u}^* = -\partial_z \Upsilon \quad \text{and} \quad w^* = \nabla_h \cdot \Upsilon, \quad (7.59)$$

with Υ determined by solving the following vertical boundary value problem at each horizontal position¹¹

$$(c^2 \partial_{zz} - N^2) \Upsilon = -N^2 \Upsilon^{\text{gm}} \quad \text{and} \quad \Upsilon(\eta_b) = \Upsilon(\eta) = 0, \quad (7.60)$$

where (see equation (7.28))

$$\Upsilon^{\text{gm}} = \kappa_{\text{gm}} \mathbf{S} \quad \text{and} \quad N^2 \mathbf{S} = (g/\rho_o) \nabla_h \varrho. \quad (7.61)$$

We recover the [Gent et al. \(1995\)](#) scheme when setting the squared speed to zero, $c^2 = 0$, in which case $\Upsilon = \Upsilon^{\text{gm}}$. For $c^2 > 0$, the second order differential operator ensures that Υ smoothly and continuously transitions through regions where the vertical stratification is weak (N^2 is small), and hence where $|\mathbf{S}|$ is large. In contrast, the standard regularization approaches, with $c^2 = 0$, are somewhat more *ad hoc* (e.g., see Chapter 15 of [Griffies \(2004\)](#)) or very tedious (e.g., [Ferrari et al. \(2008\)](#)).

Following the discussion in Section 7.3.3, we deduce the impacts on potential energy (assuming a linear equation of state) via equation (7.37), where we make use of the vertical component of the potential density skew flux

$$\frac{1}{g} \frac{dP}{dt} = \frac{1}{\rho_o} \int J^z dV = - \int \hat{z} \cdot (\nabla \varrho \times \Psi^*) dV = - \int \nabla_h \varrho \cdot \Upsilon dV = - \frac{\rho_o}{g} \int N^2 \mathbf{S} \cdot \Upsilon dV. \quad (7.62)$$

The governing differential equation (7.60) leads to

$$\Upsilon \cdot (c^2 \partial_{zz} - N^2) \Upsilon = -(g/\rho_o) \kappa_{\text{gm}} \Upsilon \cdot \nabla_h \varrho, \quad (7.63)$$

which rearranges to

$$(g/\rho_o) \kappa_{\text{gm}} \Upsilon \cdot \nabla_h \varrho = -c^2 \partial_z (\Upsilon \cdot \partial_z \Upsilon) + c^2 (\partial_z \Upsilon \cdot \partial_z \Upsilon) + N^2 \Upsilon \cdot \Upsilon. \quad (7.64)$$

Integrating over a vertical column and making use of the homogeneous Dirichlet boundary conditions from equation (7.60) leads to

$$\frac{g}{\rho_o} \int \kappa_{\text{gm}} \Upsilon \cdot \nabla_h \varrho dz = \int (c^2 \partial_z \Upsilon \cdot \partial_z \Upsilon + N^2 \Upsilon \cdot \Upsilon) dz \geq 0. \quad (7.65)$$

This inequality means that the potential energy of a vertical column is dissipated. However,

¹¹Note that [Ferrari et al. \(2010\)](#) used the opposite sign convention on Υ from that used here.

locally at any point in the column the potential energy might increase due to the sign-indefinite term, $-c^2 \partial_z (\mathbf{Y} \cdot \partial_z \mathbf{Y})$. Notably, there is no *a priori* reason that mesoscale eddies dissipate potential energy locally at every point in space. Furthermore, numerical experiments documented in [Ferrari et al. \(2010\)](#) suggest that local potential energy dissipation is not necessary for a numerically stable operator. We conclude that this approach offers a suitable method for ocean climate simulations.

7.3.8 Comments

As noted in Section 6.6.3, there is presently no parameterization of subgrid scale stirring along neutral directions arising from the correlations between tracer and velocity fluctuations. Rather, the only parameterized subgrid scale stirring is associated with quasi-Stokes transport, with [Gent et al. \(1995\)](#) providing the canonical approach as summarized in this section. To parameterize the skew fluxes arising from tracer-velocity correlations requires one to study the polarization of the eddies giving rise to these skew fluxes, as per the discussion in Section 6.4.2 and [Middleton and Loder \(1989\)](#).

7.4 Neutral diffusion

Neutral diffusion, also referred to as epineutral diffusion, parameterizes the lateral mixing induced by mesoscale eddy stirring. The parameterization assumes that the neutral diffusive flux of a tracer is oriented along neutral directions, which are oriented on a neutral tangent plane. Consequently, the neutral diffusive tracer flux, \mathbf{J} , for an arbitrary tracer, C , is perpendicular to the dianeutral direction

$$\mathbf{J} \cdot \hat{\gamma} = 0 \implies \mathbf{J} \cdot (-\alpha \nabla \Theta + \beta \nabla S) = 0, \quad (7.66)$$

where $\hat{\gamma}$ is defined by equation (7.16).

7.4.1 Motivation for neutral diffusion

Pioneering numerical models of the ocean general circulation, such as [Cox and Bryan \(1984\)](#), were formulated with the tracer mixing tensor oriented according to the horizontal and vertical directions, which corresponded to the orientation of the discrete grid cells. These simulations exhibited problems near strong density fronts, such as those found in western boundary currents. In such regions, the horizontally oriented tracer diffusion spuriously fluxed temperature and salinity across isopycnals, thus degrading the strength of the front and leading to, among other problems, unphysically weak meridional heat transport ([Böning et al., 1995](#)). In earlier work based on tracer measurements, [Montgomery \(1938\)](#), [Veronis \(1975\)](#), and [Rooth \(1982\)](#) suggested that ocean properties are preferentially homogenized along local potential density surfaces rather than geopotential surfaces. Such measurements motivated [Solomon \(1971\)](#) and [Redi \(1982\)](#) to propose rotating the tracer mixing tensor according to isopycnal directions, which were later generalized to neutral directions.

We offer further indirect evidence that mesoscale eddy induced diffusion is preferentially aligned along neutral directions. For that purpose, consider a diffusive flux that is not aligned with neutral directions. In this case, diffusive mixing can cause tracer distributions to cross neutral directions, thus adding to the mixing that is already parameterized from small scale mixing processes from Section 7.2. As discussed in Section 14.1.5 of [Griffies \(2004\)](#) as well as

Section 1 of [McDougall et al. \(2014\)](#), the extra mixing induced by this non-neutral orientation of the mesoscale induced diffusive fluxes is proportional to the squared slope between the proposed new direction and the neutral tangent plane. Estimates based on field measurements for interior ocean mixing constrain the magnitude of the miss-alignment to be less than 10^{-4} . This number is very small, indeed it is zero within error bars of field measurements. Although the measurements are sparse, they do support the use of mesoscale eddy induced diffusive fluxes that are oriented according to neutral directions. We thus make use of this constraint in designing the diffusion tensor in the remainder of this section.¹²

7.4.2 Redi neutral diffusion

One diffusive flux satisfying the property (7.66) is given by

$$\mathbf{J}^{\text{redi}} = -\rho \kappa_{\text{ntr}} [\nabla C - \hat{\gamma} (\hat{\gamma} \cdot \nabla C)], \quad (7.67)$$

where $\kappa_{\text{ntr}} > 0$ is the eddy neutral diffusivity (dimensions of squared length per time). In Figure 7.5 we illustrate the diffusive flux arising for a particular configuration of the neutral directions and the tracer concentration.

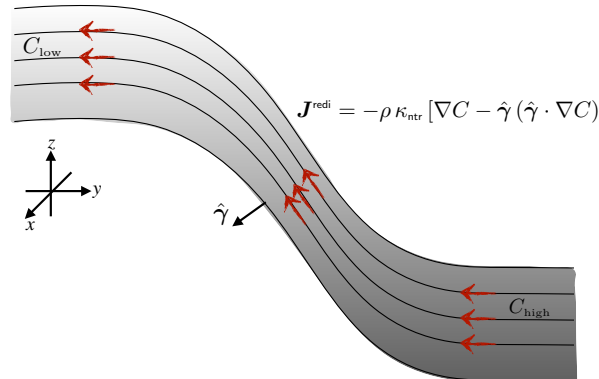


FIGURE 7.5: Schematic of the Redi neutral diffusion flux, $\mathbf{J}^{\text{redi}} = -\rho \kappa_{\text{ntr}} [\nabla C - \hat{\gamma} (\hat{\gamma} \cdot \nabla C)]$, from equation (7.67). The sloping lines represent surfaces whose local tangent define the neutral tangent plane with neutral directions, and with the dianeutral direction, $\hat{\gamma}$, perpendicular to the neutral directions. The tracer flux is aligned parallel to these surfaces. We here depict the case with higher tracer concentration on the right side so that the downgradient neutral diffusive flux is to the left and upward.

We confirm that \mathbf{J}^{redi} is oriented down the tracer gradient by noting that

$$\mathbf{J}^{\text{redi}} \cdot \nabla C = -\rho \kappa_{\text{ntr}} [|\nabla C|^2 - (\hat{\gamma} \cdot \nabla C)^2] \leq 0. \quad (7.68)$$

We can write the neutral diffusive flux (7.67) in the downgradient flux-gradient relation

$$\mathbf{J}^{\text{redi}} = -\rho \mathbf{K}^{\text{redi}} \cdot \nabla C, \quad (7.69)$$

¹²There have been attempts to provide a first principles argument for aligning the subgrid diffusive tracer operators along neutral directions. [McDougall et al. \(2014\)](#) provide a summary of such arguments. Currently, the strongest argument in support of neutral diffusion remains empirical.

with the neutral diffusion tensor, \mathbf{K}^{redi} , given by

$$\mathbf{K}^{\text{redi}} = \kappa_{\text{ntr}} \begin{bmatrix} 1 - \hat{\gamma}_x^2 & -\hat{\gamma}_x \hat{\gamma}_y & -\hat{\gamma}_x \hat{\gamma}_z \\ -\hat{\gamma}_x \hat{\gamma}_y & 1 - \hat{\gamma}_y^2 & -\hat{\gamma}_y \hat{\gamma}_z \\ -\hat{\gamma}_x \hat{\gamma}_z & -\hat{\gamma}_y \hat{\gamma}_z & 1 - \hat{\gamma}_z^2 \end{bmatrix} \implies (K^{\text{redi}})^{mn} = \kappa_{\text{ntr}} (\delta^{mn} - \hat{\gamma}^m \hat{\gamma}^n). \quad (7.70)$$

The corresponding neutral diffusion operator is given by the three-dimensional flux convergence

$$\mathcal{R}^{\text{redi}} = -\nabla \cdot \mathbf{J}^{\text{redi}} = \nabla \cdot (\rho \mathbf{K}^{\text{redi}} \cdot \nabla C). \quad (7.71)$$

When the neutral tangent planes are stably stratified in the vertical, so that their slopes are bounded, then the diffusion tensor takes the following form originally suggested by *Redi* (1982), which is written in terms of the neutral slope

$$\mathbf{K}^{\text{redi}} = \frac{\kappa_{\text{ntr}}}{1 + \mathbf{S}^2} \begin{bmatrix} 1 + S_y^2 & -S_x S_y & S_x \\ -S_x S_y & 1 + S_x^2 & S_y \\ S_x & S_y & \mathbf{S}^2 \end{bmatrix}. \quad (7.72)$$

7.4.3 Small slope neutral diffusion

Another form of the neutral diffusion flux is based on assuming a small magnitude for the slope of the neutral tangent plane relative to the horizontal, which is the case for mesoscale fronts and eddies. With this approximation, the small slope neutral diffusion tensor takes the form

$$\mathbf{K}^{\text{small}} = \kappa_{\text{ntr}} \begin{bmatrix} 1 & 0 & S_x \\ 0 & 1 & S_y \\ S_x & S_y & \mathbf{S}^2 \end{bmatrix}. \quad (7.73)$$

The corresponding small slope neutral diffusive flux is

$$\mathbf{J}^{\text{small}} = -\rho \kappa_{\text{ntr}} [\nabla_{\text{h}} + \hat{\mathbf{z}} (\mathbf{S} \cdot \nabla_{\text{h}})] C \quad (7.74)$$

where

$$\nabla_{\text{h}} = \nabla_{\text{h}} + \mathbf{S} \partial_z \quad (7.75)$$

is the horizontal derivative operator computed on the neutral tangent plane (see equation (1.85)). To show that $\mathbf{J}^{\text{small}} \cdot \hat{\gamma} = 0$, we make use of the identity (7.19) so that

$$\mathbf{J}^{\text{small}} \cdot \hat{\gamma} = \frac{\mathbf{J}^{\text{small}} \cdot \mathbf{S} - \mathbf{J}^{\text{small}} \cdot \mathbf{S}}{(1 + \mathbf{S}^2)^{1/2}} = 0. \quad (7.76)$$

Furthermore, we confirm that $\mathbf{J}^{\text{small}}$ is oriented down the tracer gradient by noting that

$$\mathbf{J}^{\text{small}} \cdot \nabla C = -\rho \kappa_{\text{ntr}} [\nabla_{\text{h}} C \cdot \nabla_{\text{h}} C + (\mathbf{S} \cdot \nabla_{\text{h}} C) \partial_z C] \quad (7.77a)$$

$$= -\rho \kappa_{\text{ntr}} [|\nabla_{\text{h}} C|^2 + 2 (\mathbf{S} \cdot \nabla_{\text{h}} C) \partial_z C + |\mathbf{S} \partial_z C|^2] \quad (7.77b)$$

$$= -\rho \kappa_{\text{ntr}} |\nabla_{\text{h}} C + \mathbf{S} \partial_z C|^2 \quad (7.77c)$$

$$= -\rho \kappa_{\text{ntr}} |\nabla_{\text{h}} C|^2 \quad (7.77d)$$

$$\leq 0. \quad (7.77e)$$

The small slope approximation was proposed by *Cox* (1987). However, his form for the

small slope neutral diffusion flux was incorrect as it did not satisfy $\mathbf{J}^{\text{small}} \cdot \hat{\gamma} = 0$. The corrected form given by equation (7.74) was first written by [Gent and McWilliams \(1990\)](#). The resulting small slope neutral diffusion operator is commonly used in ocean climate models ([Griffies et al., 1998](#); [Lemarié et al., 2012](#)), which results from computing the three-dimensional convergence

$$\mathcal{R}^{\text{small}} = -\nabla \cdot \mathbf{J}^{\text{small}} = \nabla_h \cdot (\rho \kappa_{\text{ntr}} \nabla_{h\gamma} C) + \partial_z (\rho \kappa_{\text{ntr}} \mathbf{S} \cdot \nabla_{h\gamma} C). \quad (7.78)$$

In Exercise 7.5 we compute the flux from the [Cox \(1987\)](#) tensor and show why it is physically wrong.

7.4.4 Neutral tangent plane neutral diffusion

A third method to compute neutral diffusion is motivated by the form of isopycnal diffusion in isopycnal layered models (e.g., see Chapter 3). Rather than isopycnal layers, we work with layers determined locally by neutral tangent planes. The neutral tangent frame makes use of projected non-orthogonal generalized vertical coordinates detailed in Chapter 1.

Following the derivations given in Section 1.15, the neutral diffusive flux in the neutral tangent frame is given by the horizontal flux

$$\mathbf{J}^{\text{ntp}} = -\rho \kappa_{\text{ntr}} \nabla_{h\gamma} C. \quad (7.79)$$

This flux is oriented down the tracer gradient as oriented along neutral directions

$$\mathbf{J}^{\text{ntp}} \cdot \nabla_{h\gamma} C = -\rho \kappa_{\text{ntr}} |\nabla_{h\gamma} C|^2, \quad (7.80)$$

which is the same as equation (7.77d) for the small slope fluxes. However, as a purely horizontal flux, \mathbf{J}^{ntp} is not oriented along neutral directions

$$\mathbf{J}^{\text{ntp}} \cdot \hat{\gamma} \neq 0. \quad (7.81)$$

Nevertheless, rather than computing the neutral diffusion operator as a horizontal convergence of this flux, the neutral tangent plane diffusion operator is computed by taking the convergence of \mathbf{J}^{ntp} along the neutral tangent plane as per equation (1.107)

$$\mathcal{R}^{\text{ntp}} = -\frac{1}{h^\gamma} [\nabla_{h\gamma} \cdot (h^\gamma \mathbf{J}^{\text{ntp}})] = \frac{1}{h^\gamma} [\nabla_{h\gamma} \cdot (h^\gamma \rho \kappa_{\text{ntr}} \nabla_{h\gamma} C)], \quad (7.82)$$

where

$$h^\gamma = \frac{\partial z}{\partial \gamma} d\gamma = - \left[\frac{g}{\rho_0 N^2} \right] d\gamma \quad (7.83)$$

measures the thickness of a layer defined by two neutral tangent planes (see equation (1.104)).

As detailed in Section 1.15, \mathcal{R}^{ntp} is identical to the small slope neutral diffusion operator (7.78)

$$\mathcal{R}^{\text{ntp}} = \mathcal{R}^{\text{small}}. \quad (7.84)$$

In principle, it is a matter of convenience which form of the operator one uses. However, there are certain issues to consider when implementing these operators in a numerical model. Notably, a discrete realization of \mathcal{R}^{ntp} allows for a diagonal downgradient implementation of neutral diffusion, just as isopycnal diffusion in an isopycnal ocean model. In contrast, a discrete realization of either $\mathcal{R}^{\text{redi}}$ or $\mathcal{R}^{\text{small}}$ cannot guarantee downgradient fluxes due to the off-diagonal nature of its neutral diffusive flux components ([Griffies et al. \(1998\)](#), [Beckers et al. \(1998\)](#),

[Gnanadesikan \(1999\)](#), [Beckers et al. \(2000\)](#) [Lemarié et al. \(2012\)](#), [Shao et al. \(2020\)](#)). As a result, discrete realizations of $\mathcal{R}^{\text{redi}}$ or $\mathcal{R}^{\text{small}}$ can produce extrema, which are distinctly not properties of diffusion in the continuum (see Exercise 4.4). Hence, even though the continuum identity holds $\mathcal{R}^{\text{ntp}} = \mathcal{R}^{\text{small}}$, there are important differences that arise upon realizing these operators on a discrete lattice. [Shao et al. \(2020\)](#) provide further discussion of these points as part of their numerical realization of neutral diffusion.

7.4.5 Neutrality condition

Given the expression (7.16) for the dianeutral unit vector, $\hat{\gamma}$, it is straightforward to show that the neutral diffusive flux for Conservative Temperature and salinity satisfy the constraints

$$\nabla\Theta \cdot [-\alpha \mathbf{J}(\Theta) + \beta \mathbf{J}(S)] = 0 \quad \text{and} \quad \nabla S \cdot [-\alpha \mathbf{J}(\Theta) + \beta \mathbf{J}(S)] = 0. \quad (7.85)$$

These constraints are generally satisfied if the diffusive fluxes satisfy the balance

$$\alpha \mathbf{J}(\Theta) = \beta \mathbf{J}(S) \implies \mathbf{K} \cdot \hat{\gamma} = 0. \quad (7.86)$$

We refer to this balance as the [neutrality condition](#). It reflects the vanishing of the neutral diffusive flux of locally referenced potential density. It is maintained by the diffusive flux (7.67) of [Redi \(1982\)](#), the small slope flux (7.74) of [Gent and McWilliams \(1990\)](#), and the neutral tangent frame neutral diffusive flux (7.79). However, it is not maintained by the small slope fluxes from [Cox \(1987\)](#). Furthermore, [Griffies et al. \(1998\)](#) argued for the importance of maintaining this balance to avoid a nonlinear instability plaguing certain numerical realizations of neutral diffusion such as that from [Cox \(1987\)](#).

7.4.6 Symmetry condition

Since the neutral diffusion tensor is symmetric (as are all diffusion tensors), we have

$$\mathbf{J}(\Theta) \cdot \nabla S = -\kappa_{\text{ntr}} \rho K^{mn} \partial_n \Theta \partial_m S \quad (7.87a)$$

$$= -\kappa_{\text{ntr}} \rho K^{nm} \partial_n S \partial_m \Theta \quad (7.87b)$$

$$= -\kappa_{\text{ntr}} \rho K^{nm} \partial_n S \partial_m \Theta \quad (7.87c)$$

$$= \mathbf{J}(S) \cdot \nabla \Theta. \quad (7.87d)$$

This symmetry condition holds for any of the diffusion tensors introduced in this chapter. It is particularly useful in our discussion of cabbeling and thermobaricity in Section 8.3.

7.4.7 GM skewusion plus small slope neutral diffusion

A parameterization of mesoscale eddy stirring and mixing often appears in geopotential coordinate ocean models in the form of GM skewusion (Section 7.3.1) and small slope neutral diffusion (Section 7.4.3). The combined tracer flux takes the form

$$\rho^{-1} \mathbf{J} = -\kappa_{\text{ntr}} \nabla_h C - (\kappa_{\text{ntr}} - \kappa_{\text{gm}}) \mathbf{S} \partial_z C - \hat{\mathbf{z}} [(\kappa_{\text{ntr}} + \kappa_{\text{gm}}) \mathbf{S} \cdot \nabla_h C + \kappa_{\text{ntr}} \mathbf{S}^2 \partial_z C], \quad (7.88)$$

which can be written in terms of a subgrid scale transport tensor

$$\rho^{-1} \begin{bmatrix} J^x \\ J^y \\ J^z \end{bmatrix} = - \begin{bmatrix} \kappa_{\text{ntr}} & 0 & (\kappa_{\text{ntr}} - \kappa_{\text{gm}}) S_x \\ 0 & \kappa_{\text{ntr}} & (\kappa_{\text{ntr}} - \kappa_{\text{gm}}) S_y \\ (\kappa_{\text{ntr}} + \kappa_{\text{gm}}) S_x & (\kappa_{\text{ntr}} + \kappa_{\text{gm}}) S_y & \kappa_{\text{ntr}} S^2 \end{bmatrix} \begin{bmatrix} \partial_x C \\ \partial_y C \\ \partial_z C \end{bmatrix}. \quad (7.89)$$

In the 1990s and throughout much of the 2000s, it was common to assume that $\kappa_{\text{ntr}} = \kappa_{\text{gm}}$, in which case the combined mixing tensor is

$$\mathbf{K}^{\text{small}} + \mathbf{A}^{\text{gm}} = \kappa_{\text{ntr}} \begin{bmatrix} 1 & 0 & 0 \\ 0 & 1 & 0 \\ 2 S_x & 2 S_y & S^2 \end{bmatrix} \quad \text{if } \kappa_{\text{ntr}} = \kappa_{\text{gm}}, \quad (7.90)$$

so that the subgrid scale flux simplifies to

$$\rho^{-1} \mathbf{J} = -\kappa_{\text{ntr}} \nabla_h C - \hat{\mathbf{z}} \kappa_{\text{ntr}} (2 \mathbf{S} \cdot \nabla_h C + \mathbf{S}^2 \partial_z C) \quad \text{if } \kappa_{\text{ntr}} = \kappa_{\text{gm}}. \quad (7.91)$$

Notably, the 2×2 horizontal mixing tensor is diagonal. Hence, the horizontal tracer flux is the same as that which arises from downgradient horizontal tracer diffusion. The simplicity of the horizontal flux component was alluring to modelers. It was furthermore argued by [Dukowicz and Smith \(1997\)](#) to be a fundamental property of mesoscale turbulence. However, as emphasized through the works of [Treguier et al. \(1997\)](#), [Ferrari et al. \(2008\)](#), [Danabasoglu et al. \(2008\)](#), and [Ferrari et al. \(2010\)](#), the boundary conditions for neutral diffusion and GM skewness are distinct, thus breaking their symmetry. Furthermore, studies such as [Smith and Marshall \(2009\)](#) and [Abernathy et al. \(2013\)](#) clearly point to the distinct vertical structure for the two diffusivities. Such distinctions are expected since the skew diffusivity and neutral diffusivity parameterize physically distinct processes: one parameterizes the quasi-Stokes transport, associated with velocity and layer thickness correlations, whereas the other parameterizes downgradient diffusion along neutral directions, associated with velocity and tracer correlations.

7.4.8 Generalized vertical coordinates

Thus far we have considered neutral diffusion as realized in geopotential coordinates or using neutral tangent plane coordinates. Here, we detail the steps needed to realize neutral diffusion using [generalized vertical coordinates](#) from Part I of this volume. This formulation is relevant for the now common use of generalized vertical coordinates for ocean modeling as reviewed by [Griffies et al. \(2020\)](#).

Start by recalling the expression (1.106) for a general diffusion operator written in terms of the generalized vertical coordinate, $\sigma = \sigma(x, y, z, t)$

$$\mathcal{R} = -\frac{1}{h^\sigma} [\nabla_h \cdot (h^\sigma \mathbf{J}^h) + \delta_\sigma(z_\sigma \nabla \sigma \cdot \mathbf{J})], \quad (7.92)$$

where $\delta_\sigma \equiv d\sigma / \partial \sigma$ is the dimensionless derivative operator, and the thickness of a σ -layer is

$$h^\sigma = dz = z_\sigma d\sigma = \frac{\partial z}{\partial \sigma} d\sigma. \quad (7.93)$$

Now assume the flux, \mathbf{J} , is given by equation (7.74) for small slope neutral diffusion. Trans-

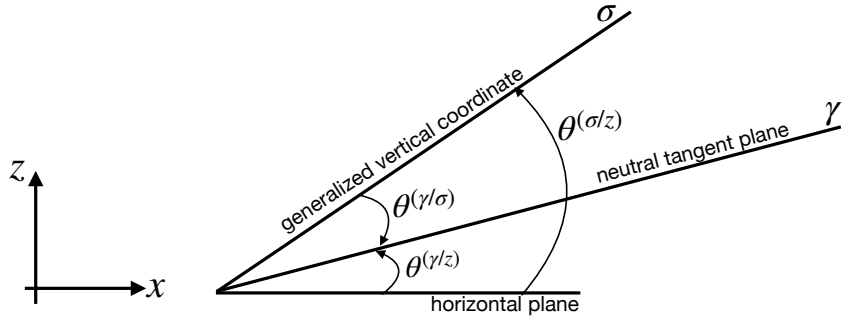


FIGURE 7.6: Slopes of a neutral tangent plane (denoted by γ) relative to both the horizontal plane, $\tan \theta^{(\gamma/z)}$, and relative to a generalized vertical coordinate isoline, $\tan \theta^{(\gamma/\sigma)}$, where σ is a generalized vertical coordinate. We assume positive angles as measure counter-clockwise relative to the horizontal and relative to the σ -isoline, respectively. Hence, for this example, $\theta^{(\gamma/z)} > 0$ yet $\theta^{(\gamma/\sigma)} < 0$. When extending to the two horizontal directions, the slopes generally satisfy $\mathbf{S}^{(\sigma/z)} = \mathbf{S}^{(\gamma/z)} - \mathbf{S}^{(\gamma/\sigma)}$, where $|\mathbf{S}^{(\gamma/z)}| = |\tan \theta^{(\gamma/z)}|$ and $|\mathbf{S}^{(\gamma/\sigma)}| = |\tan \theta^{(\gamma/\sigma)}|$. Note that this relation between slope vectors also holds for arbitrary orientations of the σ isolines and neutral tangent planes.

forming to generalized vertical coordinates leads to the horizontal flux component

$$\mathbf{J}^{h\text{small}} = -\rho \kappa_{\text{ntr}} \nabla_{\text{h}} C \quad (7.94\text{a})$$

$$= -\rho \kappa_{\text{ntr}} [\nabla_{\text{h}} + (\nabla_{\text{h}} z) \partial_z] C \quad (7.94\text{b})$$

$$= -\rho \kappa_{\text{ntr}} [\nabla_{\text{h}} + (-\nabla_{\text{h}} z + \nabla_{\text{h}} z) \partial_z] C \quad (7.94\text{c})$$

$$= -\rho \kappa_{\text{ntr}} [\nabla_{\text{h}} + (-\mathbf{S}^{(\sigma/z)} + \mathbf{S}^{(\gamma/z)}) \partial_z] C \quad (7.94\text{d})$$

$$= -\rho \kappa_{\text{ntr}} (\nabla_{\text{h}} + \mathbf{S}^{(\gamma/\sigma)} \partial_z) C, \quad (7.94\text{e})$$

where the neutral slopes as shown in Figure 7.6 satisfy the identity

$$\mathbf{S}^{(\sigma/z)} = \mathbf{S}^{(\gamma/z)} - \mathbf{S}^{(\gamma/\sigma)}. \quad (7.95)$$

Furthermore, we made use of the identity (1.85) relating the partial derivative operators

$$\nabla_{\text{h}} = \nabla_{\text{h}} + (\nabla_{\text{h}} z) \partial_z \quad \text{and} \quad \nabla_{\text{h}} = \nabla_{\text{h}} - (\nabla_{\text{h}} z) \partial_z. \quad (7.96)$$

The horizontal flux (7.94e) has the same form as when written using geopotential coordinates, only now with the derivative operator ∇_{h} and the slope $\mathbf{S}^{(\gamma/\sigma)}$. Correspondingly, the vertical flux component

$$\mathbf{J}^{z\text{small}} = \mathbf{J}^{h\text{small}} \cdot \mathbf{S}^{(\gamma/z)} \quad (7.97)$$

takes the form

$$z_{\sigma} \nabla_{\sigma} \cdot \mathbf{J}^{\text{small}} = -\mathbf{S}^{(\sigma/z)} \cdot \mathbf{J}^{h\text{small}} + \mathbf{J}^{z\text{small}} = \mathbf{J}^{h\text{small}} \cdot \mathbf{S}^{(\gamma/\sigma)}, \quad (7.98)$$

which in turn yields the diffusion operator (7.92)

$$\mathcal{R} = -\frac{1}{h^{\sigma}} \left[\nabla_{\text{h}} \cdot (h^{\sigma} \mathbf{J}^{h\text{small}}) + \delta_{\sigma} (\mathbf{J}^{h\text{small}} \cdot \mathbf{S}^{(\gamma/\sigma)}) \right]. \quad (7.99)$$

In the special case when σ is parallel to the neutral direction so that $\mathbf{S}^{(\gamma/\sigma)} = 0$, the diffusion operator (7.99) reduces to the neutral tangent plane version given by equation (7.82).

7.5 Anisotropic neutral diffusion

The neutral diffusion discussed in Section 7.4 is based on isotropic diffusion in the neutral tangent plane. That assumption has been questioned by *Smith and Gent* (2004), *Le Sommer et al.* (2011), and *Fox-Kemper et al.* (2013). We here develop some of the formalism appropriate for studying anisotropic neutral diffusion. It is notable, however, that anisotropic neutral diffusion has been rarely tested in realistic models.

7.5.1 Orthonormal triad of basis vectors

We make use of the following orthonormal unit vectors¹³ as depicted in Figure 7.7

$$\hat{\mathbf{e}}_{\bar{1}} = \frac{\hat{\mathbf{d}} \times \hat{\gamma}}{|\hat{\mathbf{d}} \times \hat{\gamma}|} \quad (7.100a)$$

$$\hat{\mathbf{e}}_{\bar{2}} = \frac{\hat{\gamma} \times (\hat{\mathbf{d}} \times \hat{\gamma})}{|\hat{\mathbf{d}} \times \hat{\gamma}|} = \frac{\hat{\mathbf{d}} - (\hat{\gamma} \cdot \hat{\mathbf{d}}) \hat{\gamma}}{|\hat{\mathbf{d}} \times \hat{\gamma}|} \quad (7.100b)$$

$$\hat{\mathbf{e}}_{\bar{3}} = \hat{\gamma} \quad (7.100c)$$

where

$$\hat{\mathbf{d}} = \hat{\mathbf{x}} \hat{d}_x + \hat{\mathbf{y}} \hat{d}_y + \hat{\mathbf{z}} \hat{d}_z \quad (7.101)$$

is an arbitrary unit vector that is not parallel to $\hat{\gamma}$. The three unit vectors $(\hat{\mathbf{e}}_{\bar{1}}, \hat{\mathbf{e}}_{\bar{2}}, \hat{\mathbf{e}}_{\bar{3}})$ form an orthonormal triad at each point in the fluid so that

$$\hat{\mathbf{e}}_{\bar{1}} = \hat{\mathbf{e}}_{\bar{2}} \times \hat{\mathbf{e}}_{\bar{3}} \quad \text{and} \quad \hat{\mathbf{e}}_{\bar{2}} = \hat{\mathbf{e}}_{\bar{3}} \times \hat{\mathbf{e}}_{\bar{1}} \quad \text{and} \quad \hat{\mathbf{e}}_{\bar{3}} = \hat{\mathbf{e}}_{\bar{1}} \times \hat{\mathbf{e}}_{\bar{2}}. \quad (7.102)$$

These vectors are oriented by the arbitrary direction, $\hat{\mathbf{d}}$, and the dianeutral direction, $\hat{\gamma}$. We verify that $\hat{\mathbf{e}}_{\bar{2}}$ has unit magnitude by noting that

$$|\hat{\mathbf{d}} \times \hat{\gamma}|^2 = |\hat{\gamma} \times (\hat{\mathbf{d}} \times \hat{\gamma})|^2 = 1 - (\hat{\mathbf{d}} \cdot \hat{\gamma})^2. \quad (7.103)$$

It is also useful to verify that $\hat{\mathbf{e}}_{\bar{3}} = \hat{\mathbf{e}}_{\bar{1}} \times \hat{\mathbf{e}}_{\bar{2}}$ through the following vector identity (see VOLUME 1)

$$(\hat{\mathbf{d}} \times \hat{\gamma}) \times [\hat{\gamma} \times (\hat{\mathbf{d}} \times \hat{\gamma})] = \hat{\gamma} |\hat{\mathbf{d}} \times \hat{\gamma}|^2. \quad (7.104)$$

The unit vectors $\hat{\mathbf{e}}_{\bar{1}}$ and $\hat{\mathbf{e}}_{\bar{2}}$ are both within the neutral tangent plane since they are both orthogonal to $\hat{\gamma}$.

The unit vector $\hat{\mathbf{e}}_{\bar{1}}$ is orthogonal to $\hat{\mathbf{d}}$ whereas $\hat{\mathbf{e}}_{\bar{2}}$ is parallel to $\hat{\mathbf{d}}$ if $\hat{\mathbf{d}} \cdot \hat{\gamma} = 0$. For example, *Smith and Gent* (2004) proposed setting $\hat{\mathbf{d}}$ to be a horizontal vector set according to the local horizontal flow direction, in which case

$$\hat{\mathbf{d}} = \frac{u \hat{\mathbf{x}} + v \hat{\mathbf{y}}}{(u^2 + v^2)^{1/2}}. \quad (7.105)$$

With $\hat{\gamma}$ nearly vertical for much of the ocean interior, then $\hat{\mathbf{e}}_{\bar{2}}$ becomes nearly aligned with $\hat{\mathbf{d}}$. For these reasons we refer to $\hat{\mathbf{e}}_{\bar{1}}$ as the across- $\hat{\mathbf{d}}$ direction and $\hat{\mathbf{e}}_{\bar{2}}$ as the along- $\hat{\mathbf{d}}$ direction.

¹³The basis vectors (7.100a)-(7.100c) are more suitable for present purposes than the analogous basis vectors defined by equations (14.4)-(14.6) in *Griffies* (2004). In particular, the basis (7.100a)-(7.100c) has a sensible limit when the neutral slopes are horizontal, in which $\hat{\gamma} = -\hat{\mathbf{z}}$.

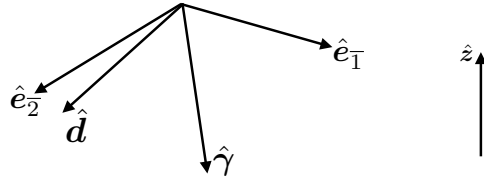


FIGURE 7.7: Depicting the orthonormal triad of basis vectors given by equations (7.100a)-(7.100c). Our convention is such that $\hat{\gamma}$ typically points downward toward increasing density. The unit vector \hat{d} is arbitrary so long as it is not parallel to the dianeutral unit vector, $\hat{\gamma}$. It is horizontal when making use of the [Smith and Gent \(2004\)](#) proposal whereby $\hat{d} = \mathbf{u}/|\mathbf{u}|$, with $\mathbf{u} = \hat{x} u + \hat{y} v$ the horizontal velocity vector. Since $\hat{e}_{\bar{1}}$ is orthogonal to \hat{d} , we refer to $\hat{e}_{\bar{1}}$ as the cross- \hat{d} basis vector. Likewise, since $\hat{e}_{\bar{2}}$ is nearly parallel to \hat{d} , especially when \hat{d} is close to horizontal and $\hat{\gamma}$ is close to vertical (e.g., Section 7.5.4), then $\hat{e}_{\bar{2}}$ is referred to as the along- \hat{d} basis vector.

7.5.2 Anisotropic neutral diffusion tensor

We consider anisotropy according to the unit vectors $\hat{e}_{\bar{1}}$ and $\hat{e}_{\bar{2}}$. Hence, the diffusion tensor as represented using the locally orthogonal triad $(\hat{e}_{\bar{1}}, \hat{e}_{\bar{2}}, \hat{e}_{\bar{3}})$ is given by

$$\overline{\mathbf{K}^{\text{aniso}}} = \begin{bmatrix} \kappa_{\text{cross}} & 0 & 0 \\ 0 & \kappa_{\text{along}} & 0 \\ 0 & 0 & 0 \end{bmatrix}, \quad (7.106)$$

where $\kappa_{\text{cross}} > 0$ and $\kappa_{\text{along}} > 0$ are the generally distinct neutral diffusivities. This tensor takes on the component form

$$(\mathbf{K}^{\text{aniso}})^{\bar{m}\bar{n}} = \kappa_{\text{cross}} \hat{e}_{\bar{1}}^{\bar{m}} \hat{e}_{\bar{1}}^{\bar{n}} + \kappa_{\text{along}} \hat{e}_{\bar{2}}^{\bar{m}} \hat{e}_{\bar{2}}^{\bar{n}} \quad (7.107a)$$

$$= \kappa_{\text{cross}} (\delta^{\bar{m}\bar{n}} - \hat{e}_{\bar{2}}^{\bar{m}} \hat{e}_{\bar{2}}^{\bar{n}} - \hat{e}_{\bar{3}}^{\bar{m}} \hat{e}_{\bar{3}}^{\bar{n}}) + \kappa_{\text{along}} (\delta^{\bar{m}\bar{n}} - \hat{e}_{\bar{1}}^{\bar{m}} \hat{e}_{\bar{1}}^{\bar{n}} - \hat{e}_{\bar{3}}^{\bar{m}} \hat{e}_{\bar{3}}^{\bar{n}}), \quad (7.107b)$$

where the second expression made use of the following decomposition of the unit tensor in terms of the orthonormal basis vectors

$$\delta^{\bar{m}\bar{n}} = \hat{e}_{\bar{1}}^{\bar{m}} \hat{e}_{\bar{1}}^{\bar{n}} + \hat{e}_{\bar{2}}^{\bar{m}} \hat{e}_{\bar{2}}^{\bar{n}} + \hat{e}_{\bar{3}}^{\bar{m}} \hat{e}_{\bar{3}}^{\bar{n}}. \quad (7.108)$$

Note that $(\mathbf{K}^{\text{aniso}})^{\bar{m}\bar{n}}$ is invariant under $\hat{d} \rightarrow -\hat{d}$. Likewise, it is invariant under a change in the sign of $\hat{\gamma}$. Furthermore, we recover the isotropic Redi diffusion tensor (7.70) by setting $\kappa_{\text{cross}} = \kappa_{\text{along}} = \kappa_{\text{ntr}}$, in which case

$$(K^{\text{aniso}})^{\bar{m}\bar{n}} = 2 \kappa_{\text{ntr}} (\delta^{\bar{m}\bar{n}} - \hat{e}_{\bar{3}}^{\bar{m}} \hat{e}_{\bar{3}}^{\bar{n}}) - \kappa_{\text{ntr}} (\hat{e}_{\bar{1}}^{\bar{m}} \hat{e}_{\bar{1}}^{\bar{n}} + \hat{e}_{\bar{2}}^{\bar{m}} \hat{e}_{\bar{2}}^{\bar{n}}) \quad (7.109a)$$

$$= \kappa_{\text{ntr}} (\delta^{\bar{m}\bar{n}} - \hat{e}_{\bar{3}}^{\bar{m}} \hat{e}_{\bar{3}}^{\bar{n}}) \quad (7.109b)$$

$$= (K^{\text{redi}})^{\bar{m}\bar{n}} \quad (7.109c)$$

To render a geopotential-Cartesian representation of the anisotropic diffusion tensor, we can make use of the transformation methods for Cartesian tensors developed in VOLUME 1. We do so by transforming from the locally orthogonal neutral plane coordinate system, defined by the orthonormal triad (7.100a)-(7.100c), to the geopotential-Cartesian coordinate system, defined by the Cartesian triad

$$\hat{e}_1 = \hat{x} \quad \text{and} \quad \hat{e}_2 = \hat{y} \quad \text{and} \quad \hat{e}_3 = \hat{z}. \quad (7.110)$$

Since we are working with Cartesian tensors, this transformation is a local rotation matrix, \mathcal{R} ,

so that¹⁴

$$(K^{\text{aniso}})^{mn} = \mathcal{R}^m_{\bar{m}} \mathcal{R}^n_{\bar{n}} (K^{\text{aniso}})^{\bar{m}\bar{n}} \implies \mathbf{K}^{\text{aniso}} = \mathcal{R} \bar{\mathbf{K}}^{\text{aniso}} \mathcal{R}^T, \quad (7.111)$$

where the second equality made use of matrix notation with \mathcal{R}^T the transpose, and where the elements to the rotation matrix are given by the direction cosines

$$\mathcal{R} = \begin{bmatrix} \hat{\mathbf{e}}^1 \cdot \hat{\mathbf{e}}_{\bar{1}} & \hat{\mathbf{e}}^1 \cdot \hat{\mathbf{e}}_{\bar{2}} & \hat{\mathbf{e}}^1 \cdot \hat{\mathbf{e}}_{\bar{3}} \\ \hat{\mathbf{e}}^2 \cdot \hat{\mathbf{e}}_{\bar{1}} & \hat{\mathbf{e}}^2 \cdot \hat{\mathbf{e}}_{\bar{2}} & \hat{\mathbf{e}}^2 \cdot \hat{\mathbf{e}}_{\bar{3}} \\ \hat{\mathbf{e}}^3 \cdot \hat{\mathbf{e}}_{\bar{1}} & \hat{\mathbf{e}}^3 \cdot \hat{\mathbf{e}}_{\bar{2}} & \hat{\mathbf{e}}^3 \cdot \hat{\mathbf{e}}_{\bar{3}} \end{bmatrix} = \begin{bmatrix} \hat{\mathbf{x}} \cdot \hat{\mathbf{e}}_{\bar{1}} & \hat{\mathbf{x}} \cdot \hat{\mathbf{e}}_{\bar{2}} & \hat{\mathbf{x}} \cdot \hat{\mathbf{e}}_{\bar{3}} \\ \hat{\mathbf{y}} \cdot \hat{\mathbf{e}}_{\bar{1}} & \hat{\mathbf{y}} \cdot \hat{\mathbf{e}}_{\bar{2}} & \hat{\mathbf{y}} \cdot \hat{\mathbf{e}}_{\bar{3}} \\ \hat{\mathbf{z}} \cdot \hat{\mathbf{e}}_{\bar{1}} & \hat{\mathbf{z}} \cdot \hat{\mathbf{e}}_{\bar{2}} & \hat{\mathbf{z}} \cdot \hat{\mathbf{e}}_{\bar{3}} \end{bmatrix}. \quad (7.112)$$

The machinery outlined here for the transformation is straightforward but tedious (i.e., two matrix multiplies). A more streamlined approach, also used for determining the Cartesian components to the Redi tensor (7.72), is to simply express $(\hat{\mathbf{e}}_{\bar{1}}, \hat{\mathbf{e}}_{\bar{2}}, \hat{\mathbf{e}}_{\bar{3}})$ using geopotential-Cartesian coordinates and then plug directly into equation (7.107b).

7.5.3 Properties of the anisotropic neutral diffusive fluxes

We here verify some standard properties for the anisotropic neutral diffusive flux for tracers

$$\mathbf{J}^{\text{aniso}} = -\rho \mathbf{K}^{\text{aniso}} \cdot \nabla C. \quad (7.113)$$

Downgradient orientation within the neutral tangent plane

By construction, the flux is downgradient along the two orthogonal directions, $\hat{\mathbf{e}}_{\bar{1}}$ and $\hat{\mathbf{e}}_{\bar{2}}$,

$$\mathbf{J}^{\text{aniso}} = -\rho \kappa_{\text{cross}} \hat{\mathbf{e}}_{\bar{1}} (\hat{\mathbf{e}}_{\bar{1}} \cdot \nabla C) - \rho \kappa_{\text{along}} \hat{\mathbf{e}}_{\bar{2}} (\hat{\mathbf{e}}_{\bar{2}} \cdot \nabla C). \quad (7.114)$$

Furthermore, the flux is within the neutral tangent plane

$$\mathbf{J}^{\text{aniso}} \cdot \hat{\gamma} = 0 \quad (7.115)$$

due to orthogonality between the basis vectors

$$\hat{\mathbf{e}}_{\bar{1}} \cdot \hat{\gamma} = \hat{\mathbf{e}}_{\bar{2}} \cdot \hat{\gamma} = 0. \quad (7.116)$$

Neutrality condition

The neutrality condition (7.86) follows since

$$(-\alpha \nabla \Theta + \beta \nabla S) \cdot \hat{\mathbf{e}}_{\bar{1}} = (-\alpha \nabla \Theta + \beta \nabla S) \cdot \hat{\mathbf{e}}_{\bar{2}} = 0, \quad (7.117)$$

so that

$$\alpha \mathbf{J}^{\text{aniso}}(\Theta) = \beta \mathbf{J}^{\text{aniso}}(S). \quad (7.118)$$

7.5.4 Small slope anisotropic neutral diffusion

We now consider the special case in which the orientation direction, $\hat{\mathbf{d}}$, is strictly horizontal and normalized so that

$$\hat{\mathbf{d}} \cdot \hat{\mathbf{d}} = \hat{d}_x^2 + \hat{d}_y^2 = 1. \quad (7.119)$$

¹⁴Since we are dealing with Cartesian tensors there is no distinction between raised or lowered tensor indices in equation (7.111). Even so, we choose to follow the convention of general tensors in VOLUME 1 to help organize elements of the tensor and to facilitate use of the Einstein summation convention.

Additionally, we assume the neutral slope is small so that the neutral directions are nearly horizontal. In this case the basis vectors (7.100a)-(7.100c) take on the following form valid to $\mathcal{O}(|\mathbf{S}|)$

$$\hat{\mathbf{e}}_1^{\text{small}} = \hat{\mathbf{d}} \times (\mathbf{S} - \hat{\mathbf{z}}) \quad (7.120\text{a})$$

$$\hat{\mathbf{e}}_2^{\text{small}} = \hat{\mathbf{d}} + \hat{\mathbf{z}} (\hat{\mathbf{d}} \cdot \mathbf{S}) \quad (7.120\text{b})$$

$$\hat{\mathbf{e}}_3^{\text{small}} = \mathbf{S} - \hat{\mathbf{z}}. \quad (7.120\text{c})$$

Note that $\hat{\mathbf{e}}_3^{\text{small}}$ is orthogonal to $\hat{\mathbf{e}}_1^{\text{small}}$ and $\hat{\mathbf{e}}_2^{\text{small}}$, however $\hat{\mathbf{e}}_1^{\text{small}} \cdot \hat{\mathbf{e}}_2^{\text{small}}$ is $\mathcal{O}(\mathbf{S} \cdot \mathbf{S})$. Likewise, each of these vectors is normalized only to $\mathcal{O}(\mathbf{S} \cdot \mathbf{S})$.

Making use of the small slope basis vectors in the anisotropic diffusion tensor (7.107a), and expressing them in geopotential-Cartesian coordinates leads to the small slope anisotropic neutral diffusion tensor¹⁵

$$\mathbf{K}^{\text{smallaniso}} = \kappa_{\text{cross}} \begin{bmatrix} 1 & 0 & S_x \\ 0 & 1 & S_y \\ S_x & S_y & \mathbf{S} \cdot \mathbf{S} \end{bmatrix} + \Delta \kappa_{\text{ntr}} \begin{bmatrix} \hat{d}_x^2 & \hat{d}_x \hat{d}_y & (\hat{\mathbf{d}} \cdot \mathbf{S}) \hat{d}_x \\ \hat{d}_x \hat{d}_y & \hat{d}_y^2 & (\hat{\mathbf{d}} \cdot \mathbf{S}) \hat{d}_y \\ (\hat{\mathbf{d}} \cdot \mathbf{S}) \hat{d}_x & (\hat{\mathbf{d}} \cdot \mathbf{S}) \hat{d}_y & (\hat{\mathbf{d}} \cdot \mathbf{S})^2 \end{bmatrix}, \quad (7.121)$$

where

$$\Delta \kappa_{\text{ntr}} = \kappa_{\text{along}} - \kappa_{\text{cross}}. \quad (7.122)$$

As for the unapproximated anisotropic neutral diffusion tensor (7.107a), its small slope version, $\overline{\mathbf{K}^{\text{smallaniso}}}$, is invariant if we swap the direction $\hat{\mathbf{d}} \rightarrow -\hat{\mathbf{d}}$. Furthermore, in the form (7.121) we trivially see that $\mathbf{K}^{\text{smallaniso}} = \mathbf{K}^{\text{small}}$ (equation (7.73)) in the isotropic limit where $\kappa_{\text{cross}} = \kappa_{\text{along}} = \kappa_{\text{ntr}}$.

The anisotropic small slope neutral diffusive flux is given by

$$\mathbf{J}^{h\text{smallaniso}} = -\rho \mathbf{K}^{\text{smallaniso}} \cdot \nabla C, \quad (7.123)$$

with horizontal and vertical components

$$\mathbf{J}^{h\text{smallaniso}} = -\rho \kappa_{\text{cross}} \nabla_{\text{h}} C - \rho \Delta \kappa_{\text{ntr}} \hat{\mathbf{d}} (\hat{\mathbf{d}} \cdot \nabla_{\text{h}}) C \quad (7.124\text{a})$$

$$J^{z\text{smallaniso}} = \mathbf{S} \cdot \mathbf{J}^{h\text{smallaniso}}, \quad (7.124\text{b})$$

where $\nabla_{\text{h}} = \nabla_{\text{h}} + \mathbf{S} \partial_z$ is the horizontal operator as per equation (7.75). By making use of the expression (7.19), $\hat{\gamma} = (\mathbf{S} - \hat{\mathbf{z}})(1 + \mathbf{S}^2)^{-1/2}$, we readily find that

$$\mathbf{J}^{h\text{smallaniso}} \cdot \hat{\gamma} = 0. \quad (7.125)$$

Similarly, we can verify that the neutrality condition (Section 7.4.5) is maintained

$$\mathbf{K}^{\text{smallaniso}} \cdot \hat{\gamma} = 0 \implies \alpha \mathbf{J}^{h\text{smallaniso}}(\Theta) = \beta \mathbf{J}^{h\text{smallaniso}}(S). \quad (7.126)$$

Finally, as per the discussion in Section 7.4.4, we can evaluate the small slope anisotropic neutral diffusion operator by following the non-orthogonal neutral tangent approach rather than the three-dimensional Cartesian approach. It is the non-orthogonal neutral tangent approach that is appropriate for vertical Lagrangian ocean models such as detailed in [Griffies et al. \(2020\)](#) and [Shao et al. \(2020\)](#).

¹⁵Equation (7.121) agrees with equations (10) and (14) from [Smith and Gent \(2004\)](#).

7.6 Anisotropic Gent-McWilliams stirring

In addition to proposing the use of a small slope anisotropic neutral diffusion tensor (equation (7.121)), [Smith and Gent \(2004\)](#) proposed a complementary anisotropic version of the Gent-McWilliams stirring. We here detail the parameterization, again assuming the orientation direction, $\hat{\mathbf{d}}$, is horizontal

$$\hat{\mathbf{d}} = \hat{\mathbf{x}} \hat{d}_x + \hat{\mathbf{y}} \hat{d}_y, \quad (7.127)$$

just as assumed when discussing the anisotropic small slope neutral diffusion operator in Section 7.5.4.

7.6.1 Streamfunction and anti-symmetric tensor

The parameterized eddy-induced streamfunction is generalized from that in equation (7.28) to read

$$\Psi^* = \hat{\mathbf{z}} \times \kappa_{\text{gmcross}} \mathbf{S} + \hat{\mathbf{z}} \times (\kappa_{\text{gmcross}} - \kappa_{\text{gmalong}}) (\hat{\mathbf{d}} \cdot \mathbf{S}) \hat{\mathbf{d}}, \quad (7.128)$$

and the corresponding anti-symmetric stirring tensor is

$$A^{\text{gmaniso}} = \kappa_{\text{gmcross}} \begin{bmatrix} 0 & 0 & -S_x \\ 0 & 0 & -S_y \\ S_x & S_y & 0 \end{bmatrix} + \Delta \kappa_{\text{gm}} (\hat{\mathbf{d}} \cdot \mathbf{S}) \begin{bmatrix} 0 & 0 & -\hat{d}_x \\ 0 & 0 & -\hat{d}_y \\ \hat{d}_x & \hat{d}_y & 0 \end{bmatrix}, \quad (7.129)$$

where

$$\Delta \kappa_{\text{gm}} = \kappa_{\text{gmalong}} - \kappa_{\text{gmcross}}. \quad (7.130)$$

As for the small slope anisotropic neutral diffusion tensor (7.121), we write the skew tensor A^{gmaniso} in equation (7.129) in a form that manifestly reduces to the isotropic Gent-McWilliams stirring tensor A^{gm} when $\kappa_{\text{gmalong}} = \kappa_{\text{gmcross}} = \kappa_{\text{gm}}$.

7.6.2 Anisotropic Gent-McWilliams skew tracer flux

The anisotropic Gent-McWilliams skew tracer flux is

$$\mathbf{J}_{\text{gm-aniso}} = -\rho A^{\text{gmaniso}} \cdot \nabla C \quad (7.131a)$$

$$= \rho \kappa_{\text{gmcross}} [\mathbf{S} \partial_z C - \hat{\mathbf{z}} (\mathbf{S} \cdot \nabla_h C)] + \rho \Delta \kappa_{\text{gm}} (\hat{\mathbf{d}} \cdot \mathbf{S}) [\hat{\mathbf{d}} \partial_z C - \hat{\mathbf{z}} (\hat{\mathbf{d}} \cdot \nabla_h C)]. \quad (7.131b)$$

When acting on locally referenced potential density, $C = \gamma$, the flux reduces to

$$\mathbf{J}_{\text{gm-aniso}} = \rho \kappa_{\text{gmcross}} [-\nabla_h \gamma + \hat{\mathbf{z}} \mathbf{S}^2 \partial_z \gamma] + \rho \Delta \kappa_{\text{gm}} (\mathbf{d} \cdot \mathbf{S}) [\hat{\mathbf{d}} + \hat{\mathbf{z}} (\hat{\mathbf{d}} \cdot \mathbf{S})] \partial_z \gamma. \quad (7.132)$$

As discussed in Section 7.3.3, a negative vertical component to the potential density skew flux ensures that the available potential energy is dissipated,

$$\hat{\mathbf{z}} \cdot \mathbf{J}_{\text{gm-aniso}} = \rho [\kappa_{\text{gmcross}} \mathbf{S}^2 + \Delta \kappa_{\text{gm}} (\mathbf{d} \cdot \mathbf{S})^2] \partial_z \gamma < 0 \implies \text{APE dissipated.} \quad (7.133)$$

Stably stratified water means that $\partial_z \gamma < 0$, in which case $\hat{\mathbf{z}} \cdot \mathbf{J}_{\text{gm-aniso}} < 0$ since

$$\kappa_{\text{gmcross}} \mathbf{S}^2 + \Delta \kappa_{\text{gm}} (\mathbf{d} \cdot \mathbf{S})^2 = \kappa_{\text{gmcross}} [\mathbf{S}^2 - (\hat{\mathbf{d}} \cdot \mathbf{S})^2] + \kappa_{\text{gmalong}} (\hat{\mathbf{d}} \cdot \mathbf{S})^2 > 0. \quad (7.134)$$

7.6.3 Anisotropic GM skewion plus small slope neutral diffusion

As noted in Section 7.4.7, there are strong reasons to keep the Gent-McWilliams skew flux parameterization distinct from the neutral diffusion parameterization. The central practical reason for the distinction concerns their different treatment of boundary conditions and generally distinct diffusivities. Even so, we here briefly comment on the special case where we ignore these distinctions and set the skew flux diffusivities equal to the neutral diffusivities

$$\kappa_{\text{gmcross}} = \kappa_{\text{cross}} \quad \text{and} \quad \kappa_{\text{gmalong}} = \kappa_{\text{along}}. \quad (7.135)$$

This is the approach assumed by *Smith and Gent (2004)*. With the small slope approximation to neutral diffusion, we find the combined anisotropic mixing tensor becomes

$$\begin{aligned} \mathbf{K}^{\text{smallaniso}} + \mathbf{A}^{\text{gmaniso}} = \\ \kappa_{\text{cross}} \begin{bmatrix} 1 & 0 & 0 \\ 0 & 1 & 0 \\ 2S_x & 2S_y & \mathbf{S} \cdot \mathbf{S} \end{bmatrix} + \Delta\kappa \begin{bmatrix} \hat{d}_x^2 & \hat{d}_x \hat{d}_y & 0 \\ \hat{d}_x \hat{d}_y & \hat{d}_y^2 & 0 \\ 2(\hat{\mathbf{d}} \cdot \mathbf{S}) \hat{d}_x & 2(\hat{\mathbf{d}} \cdot \mathbf{S}) \hat{d}_y & (\hat{\mathbf{d}} \cdot \mathbf{S})^2 \end{bmatrix}. \end{aligned} \quad (7.136)$$

The vanishing right hand column terms simplifies the horizontal tracer fluxes computed from this tensor. Even so, this formulation is inconsistent with the theories that support a distinct treatment of the skew flux and neutral flux.

7.6.4 A parameterization based on a boundary value problem

We now follow the approach from Section 7.3.7 to develop a boundary value problem version of the anisotropic Gent-McWilliams stirring. For this purpose consider the vertical boundary value problem

$$(c^2 \partial_{zz} - N^2) \boldsymbol{\Upsilon} = -N^2 \boldsymbol{\Upsilon}^{\text{gmaniso}} \quad \text{and} \quad \boldsymbol{\Upsilon}(\eta_b) = \boldsymbol{\Upsilon}(\eta) = 0, \quad (7.137)$$

where (see equation (7.128))

$$\boldsymbol{\Upsilon}^{\text{gmaniso}} = \kappa_{\text{gmcross}} \mathbf{S} + \hat{\mathbf{z}} \times \Delta\kappa_{\text{gm}} (\hat{\mathbf{d}} \cdot \mathbf{S}) \hat{\mathbf{d}}. \quad (7.138)$$

As in Section 7.3.7, we deduce the impacts on potential energy (assuming a linear equation of state) via the vertical component of the potential density skew flux,

$$\frac{1}{g} \frac{dP}{dt} = \frac{1}{\rho_0} \int J^z dV = - \int \nabla_h \varrho \cdot \boldsymbol{\Upsilon} dV. \quad (7.139)$$

The governing differential equation (7.137) leads to

$$\boldsymbol{\Upsilon} \cdot (c^2 \partial_{zz} - N^2) \boldsymbol{\Upsilon} = -N^2 \boldsymbol{\Upsilon} \cdot \boldsymbol{\Upsilon}^{\text{gmaniso}} \quad (7.140)$$

which rearranges to

$$N^2 \boldsymbol{\Upsilon} \cdot \boldsymbol{\Upsilon}^{\text{gmaniso}} = -c^2 \partial_z (\boldsymbol{\Upsilon} \cdot \partial_z \boldsymbol{\Upsilon}) + c^2 \partial_z \boldsymbol{\Upsilon} \cdot \partial_z \boldsymbol{\Upsilon} + N^2 \boldsymbol{\Upsilon} \cdot \boldsymbol{\Upsilon}. \quad (7.141)$$

Integrating over a vertical column and making use of the homogeneous Dirichlet boundary conditions in equation (7.137) leads to

$$\frac{g}{\rho_0} \int \mathbf{\Upsilon} \cdot \nabla_h \varrho dz = - \int N^2 \Delta \kappa_{\text{gm}} (\hat{\mathbf{d}} \cdot \mathbf{S}) (\hat{\mathbf{d}} \cdot \mathbf{\Upsilon}) dz + \int [c^2 \partial_z \mathbf{\Upsilon} \cdot \partial_z \mathbf{\Upsilon} + N^2 \mathbf{\Upsilon} \cdot \mathbf{\Upsilon}] dz, \quad (7.142)$$

which can be rearranged into the equivalent form

$$\begin{aligned} & \frac{g}{\rho_0} \int \mathbf{\Upsilon} \cdot \nabla_h \varrho dz \\ &= \underbrace{\int [c^2 \partial_z \mathbf{\Upsilon} \cdot \partial_z \mathbf{\Upsilon} + N^2 (\mathbf{\Upsilon} \cdot \mathbf{\Upsilon} - (\hat{\mathbf{d}} \cdot \mathbf{\Upsilon})^2)] dz}_{\text{positive semi-definite}} + \underbrace{\int N^2 (\hat{\mathbf{d}} \cdot \mathbf{\Upsilon}) \hat{\mathbf{d}} \cdot (\mathbf{\Upsilon} - \mathbf{S} \Delta \kappa_{\text{gm}}) dz}_{\text{sign indefinite}}. \end{aligned} \quad (7.143)$$

The first term on the right hand side is positive semi-indefinite whereas the second term is sign indefinite. If the second term is positive, or smaller in magnitude than the first term, then the parameterization provides a column integrated sink of potential energy. Otherwise, potential energy for the column can increase. There are no existing numerical implementations of this scheme to determine its suitability for realistic ocean climate simulations.



7.7 Exercises

EXERCISE 7.1: SQUARED BUOYANCY AND THE OCEAN MODEL EQUATIONS

In this exercise we develop some properties of the squared buoyancy for the hydrostatic Boussinesq equations from VOLUME 2, written here in the form

$$\frac{D\mathbf{v}}{Dt} + 2\boldsymbol{\Omega} \times \mathbf{v} = -\nabla \varphi + b \hat{\mathbf{z}} + \mathbf{F} \quad \text{velocity equation} \quad (7.144a)$$

$$\nabla \cdot \mathbf{v} = 0 \quad \text{continuity equation} \quad (7.144b)$$

$$\frac{Db}{Dt} = \dot{b} \quad \text{buoyancy equation} \quad (7.144c)$$

$$b = -\frac{g \rho'}{\rho_0} = -\frac{g (\rho - \rho_0)}{\rho_0} \quad \text{buoyancy defined} \quad (7.144d)$$

$$\varphi = \frac{p'}{\rho_0} = \frac{p - p_0(z)}{\rho_0} \quad \text{dynamic pressure defined} \quad (7.144e)$$

$$\rho = \rho_0 (1 - \alpha \Theta + \beta S) \quad \text{linear equation of state} \quad (7.144f)$$

$$\frac{dp_0}{dz} = -\rho_0 g \quad \text{background hydrostatic pressure.} \quad (7.144g)$$

Furthermore, we make use of a buoyancy flux in the form

$$\mathbf{F}^b = -\kappa \partial_z b \hat{\mathbf{z}} + \mathbf{v}^* b. \quad (7.145)$$

The first term is a downgradient vertical diffusive flux with the vertical **eddy diffusivity**, $\kappa > 0$, a function of the flow state so that

$$\kappa = \kappa(\mathbf{x}, t). \quad (7.146)$$

The second term is an advective flux, where the advective velocity, $\mathbf{v}^* = (\mathbf{u}^*, w^*)$, is assumed to be non-divergent

$$\nabla \cdot \mathbf{v}^* = \nabla_h \cdot \mathbf{u}^* + \partial_z w^* = 0. \quad (7.147)$$

The velocity, \mathbf{v}^* , is the [eddy-induced velocity](#), such as that discussed in Section 7.3 from [Gent et al. \(1995\)](#).

- (a) Write the flux-form budget describing the evolution of b^2 , the squared buoyancy. Write the budget equation using the residual mean velocity, $\mathbf{v}^\dagger = \mathbf{v} + \mathbf{v}^*$. Hint: start from the buoyancy equation written in the form

$$Db/Dt = -\nabla \cdot \mathbf{F}^b. \quad (7.148)$$

- (b) Discuss the impacts from vertical diffusion on the b^2 budget.

EXERCISE 7.2: PARAMETERIZED EDDY VELOCITY AND THE OCEAN MODEL EQUATIONS

In this exercise we develop some implications of assuming a specific form for the parameterized eddy velocity for the hydrostatic Boussinesq equations from Exercise 7.1. Namely, we consider the specific form for the parameterized eddy-induced velocity proposed by [Gent et al. \(1995\)](#)

$$\mathbf{u}^* = -\partial_z(B \mathbf{S}) \quad (7.149a)$$

$$w^* = \nabla_h \cdot (B \mathbf{S}) \quad (7.149b)$$

$$\mathbf{S} = -\frac{\nabla_h b}{N^2} \quad (7.149c)$$

$$\mathbf{v}^* \cdot \hat{\mathbf{n}} = 0 \quad \text{at all ocean boundaries.} \quad (7.149d)$$

In this expression, $B > 0$ is an eddy diffusivity. To ensure $\mathbf{v}^* \cdot \hat{\mathbf{n}} = 0$ at all domain boundaries requires that $B = 0$ along these boundaries. The horizontal vector, $\mathbf{S} = (S_x, S_y, 0)$, measures the slope of the buoyancy surfaces relative to the horizontal. We assume the ocean is stably stratified in the vertical, so that $\partial b / \partial z = N^2 > 0$.

- (a) Determine the vector streamfunction, Ψ^* , such that

$$\mathbf{v}^* = \nabla \times \Psi^*. \quad (7.150)$$

Choose the gauge with $\hat{\mathbf{z}} \cdot \Psi^* = 0$.

- (b) Show that

$$\int_{-H}^{\eta} \mathbf{u}^* \, dz = 0, \quad (7.151)$$

so that the parameterized horizontal flow has a zero depth integral.

- (c) At any chosen meridional position, y , the meridional buoyancy transport from advection (resolved plus parameterized) is computed by

$$\mathcal{B}^{(y)}(y, t) = \int_{x_1}^{x_2} dx \int_{-H}^{\eta} b (v + v^*) \, dz. \quad (7.152)$$

The zonal and vertical integrals are over the full zonal and vertical extent of the ocean domain. Show that the effects from v^* are to reduce the meridional gradients of buoyancy. That is, if buoyancy decreases poleward, then v^* will flux buoyancy poleward to reduce the gradient.

- (d) How does the introduction of \mathbf{v}^* to the buoyancy equation (7.144c) affect the global

integrated gravitational potential energy? Discuss.

- (e) How does the introduction of v^* to the buoyancy equation (7.144c) affect the global integrated available potential energy? Discuss.

EXERCISE 7.3: MERIDIONAL OVERTURNING WITH [Gent et al. \(1995\)](#)

It is often of interest to compute the mass transport across a portion of the ocean. In particular, meridional-depth or meridional-potential density streamfunctions allow one to visualize and quantify the zonally integrated transport occurring in a closed basin or over the full globe. The quasi-Stokes transport provides a transport in addition to that from the resolved scale Eulerian mean transport, and the parameterization of [Gent et al. \(1995\)](#) leads to a straightforward computation of the quasi-Stokes contribution. For this purpose, write the net meridional mass transport of fluid across a basin and passing beneath a particular depth in the form (the minus sign is conventional)

$$\mathcal{T}(y, z, t) = - \int dx \int_{-H}^z \rho(v + v^*) dz. \quad (7.153)$$

Make use of the expression for the [Gent et al. \(1995\)](#) parameterized v^* and simplify this expression. Discuss its scaling for the Southern Ocean.

EXERCISE 7.4: BIHARMONIC HORIZONTAL MIXING

A [biharmonic operator](#) is commonly employed for dissipation in numerical models due to its enhanced scale selectivity. However, biharmonic operators have some unphysical properties, such as those encountered in this exercise focused on the biharmonic mixing oriented in the horizontal direction, with the flux given by

$$\mathbf{F}^{\text{bih}} = \sqrt{B} \nabla_h L, \quad (7.154)$$

where

$$L = \nabla_h \cdot (\sqrt{B} \nabla_h C) \quad (7.155)$$

is the horizontal Laplacian operator acting on the tracer and $B > 0$ is a biharmonic mixing coefficient with units $\text{L}^4 \text{T}^{-1}$. The convergence of the biharmonic flux \mathbf{F}^{bih} yields the horizontal biharmonic mixing operator

$$R^{\text{bih}} = -\nabla \cdot \mathbf{F}^{\text{bih}}. \quad (7.156)$$

Examine the biharmonic operator's effects on tracer variance by computing the time tendency of the squared tracer concentration over the full domain, ignoring all boundary contributions. Discuss the result.

EXERCISE 7.5: [Cox \(1987\)](#) SMALL SLOPE DIFFUSION

As noted in Section 7.4.3, the neutral diffusion tensor proposed by [Cox \(1987\)](#) did not satisfy the neutrality condition of Section 7.4.5, with this incorrect tensor given by

$$\mathbf{K}^{\text{cox}} = \kappa_{\text{ntr}} \begin{bmatrix} 1 & S_x S_y & S_x \\ S_x S_y & 1 & S_y \\ S_x & S_y & S^2 \end{bmatrix}. \quad (7.157)$$

We here illustrate the basic problem with this tensor by considering the special case of neutral directions aligned with Conservative Temperature surfaces, such as occurs in an ocean with constant salinity. Show that the diffusive flux

$$\mathbf{J}^{\text{cox}}(\Theta) = -\mathbf{K}^{\text{cox}} \cdot \nabla \Theta \neq 0, \quad (7.158)$$

so that there is a non-zero flux of Conservative Temperature. Instead, a proper neutral diffusion flux leads to an identically zero flux, such as for fluxes defined by \mathbf{K}^{redi} (Section 7.4.2), $\mathbf{K}^{\text{small}}$ (Section 7.4.3), and the neutral tangent plane method from Section 7.4.4.

EXERCISE 7.6: *Roberts and Marshall (1998)* BIHARMONIC OPERATOR

Assuming a Boussinesq ocean, consider the *Roberts and Marshall (1998)* divergence-free velocity

$$\mathbf{v}^* = \nabla \times \mathbf{\Upsilon} = \partial_z [\nabla_h^2 (B \mathbf{S})] - \hat{z} \nabla_h \cdot \nabla_h^2 (B \mathbf{S}), \quad (7.159)$$

with the vector streamfunction given by

$$\mathbf{\Upsilon} = -\hat{z} \times \nabla_h^2 (B \mathbf{S}) \quad (7.160)$$

and with $B > 0$ a biharmonic mixing coefficient. The corresponding skew tracer flux is given by

$$\mathbf{F} = -\partial_z C \nabla_h^2 (B \mathbf{S}) + \hat{z} \nabla_h C \cdot \nabla_h^2 (B \mathbf{S}). \quad (7.161)$$

Dropping the horizontal Laplacian ∇_h^2 and setting $B \rightarrow -\kappa$ recovers the Laplacian scheme of *Gent et al. (1995)* as discussed in Section 7.3. *Roberts and Marshall (1998)* proposed this operator as a means to dissipate grid scale variance in the density field, yet to do so without compromising the volume of fluid within isopycnal layers. Derive an expression for the effects of this biharmonic operator on the potential energy, assuming a linear equation of state and ignoring boundary terms. Discuss the result.



Chapter 8

OCEAN DENSITY AND SEA LEVEL

As discussed in VOLUME 2, **Conservative Temperature**, Θ , is the preferred means to measure the transport of enthalpy in the ocean, and **salinity**, S , measures the concentration of dissolved salt matter. These two scalar fields are referred to as **active tracers** since they both impact density and in turn affect pressure and ocean currents. In this chapter we study how the evolution of Θ and S affects seawater density as well as buoyancy. As part of this study, we examine how to compute air-sea buoyancy fluxes and to compute budgets for global mean sea level.

Θ and S are **conservative tracers** so that the net changes in potential enthalpy and salt over the global ocean domain arise from net imbalances in their boundary fluxes. Likewise, ocean mass is a conserved field, with global mass changes arising from imbalances in boundary mass fluxes such as those occurring from increases in land ice melt. However, ocean volume, and hence ocean density and buoyancy, are not conserved fields. Consequently, ocean volume can change even if there is no net volume transferred to the ocean. These points have direct impact on how global mean sea level is affected by ocean processes such as mixing and heating, with the rudiments presented in this chapter.

CHAPTER GUIDE

Our study of thermo-hydrodynamics in VOLUME 2 motivates the use of **Conservative Temperature**, Θ , as a measure of ocean enthalpy transfer, rather than *in situ* temperature or **potential temperature**. We also make use of the ideas of parameterized turbulent mixing discussed in Chapters 4 and 7 when formulating the budget equations for Θ and S . We use Cartesian tensors to reduce the mathematical overhead. Also note that we use subscripts on specific volume, ν , and density, ρ , for partial derivatives with respect to Θ and S . This is the only chapter in this book that makes use of subscript notation for partial derivatives, and we only use it for thermodynamic derivatives.

8.1	Loose threads	256
8.2	Material evolution of <i>in situ</i> density	256
8.2.1	Material changes to pressure	257
8.2.2	Material changes to Θ and S	257
8.2.3	General expression for density changes	258
8.2.4	Unpacking the subgrid contributions	258
8.2.5	Synthesis of the density equation	260
8.3	Cabbeling and thermobaricity	261
8.3.1	Basic manipulations	262
8.3.2	Cabbeling	263

8.3.3	Thermobaricity	263
8.3.4	Comments	264
8.3.5	Further study	264
8.4	Salt and freshwater continuity equations	264
8.4.1	Salt and freshwater	264
8.4.2	Continuity equations	265
8.5	Surface boundary conditions for S and Θ	266
8.5.1	Salt and freshwater	266
8.5.2	The non-advective salt flux boundary condition	267
8.5.3	Conservative Temperature boundary condition	269
8.5.4	Comments and further reading	269
8.6	Surface boundary fluxes of buoyancy	269
8.6.1	Surface boundary fluxes of enthalpy and salt	270
8.6.2	Evolution from surface boundary fluxes	270
8.6.3	Buoyancy tendency from surface fluxes	271
8.6.4	Comments	273
8.7	Global mean sea level	273
8.7.1	Definitions and assumptions	273
8.7.2	Budget for global mean sea level	274
8.7.3	Changes due to mass input	275
8.7.4	Steric changes due to changes in density	275
8.7.5	Enthalpy flux imbalances implied by thermosteric sea level	276
8.7.6	Barystatic versus steric effects from near future land ice melt	277
8.7.7	Further study	280
8.8	Exercises	280

8.1 Loose threads

- More on patterns of sea level and the problems with global mean of local steric not equaling global mean.

8.2 Material evolution of *in situ* density

Changes to the *in situ* density of seawater affects pressure forces in the ocean as well as the volume occupied by the ocean fluid (i.e., sea level). In this section we provide a mathematical framework for studying processes that affect density changes.

As discussed in VOLUME 2, we write the seawater equation of state for density as a function of **salinity**, S , and **Conservative Temperature**, Θ , where Conservative Temperature is the **potential enthalpy** divided by a constant heat capacity ([McDougall \(2003\)](#); [IOC et al. \(2010\)](#)). We thus make use of the empirical equation of state for the seawater density using the functional form

$$\rho = \rho(S, \Theta, p), \quad (8.1)$$

where S is the salinity rather than the salt concentration ($S = 1000 \text{ S}$).

In this section we formulate the material time evolution of density as weighted by the specific volume¹

$$\nu = \rho^{-1}, \quad (8.2)$$

¹In other chapters we write the specific volume as $\nu_s = 1/\rho$ to distinguish it from ν that is used for kinematic viscosity. However, in this chapter we write $\nu = 1/\rho$ to enable a shorthand for partial derivatives as defined by equation (8.8). We have no use kinematic viscosity in this chapter.

so that, using the chain rule, we have

$$\frac{D \ln \rho}{Dt} = \frac{\partial \ln \rho}{\partial \Theta} \frac{D\Theta}{Dt} + \frac{\partial \ln \rho}{\partial S} \frac{DS}{Dt} + \frac{\partial \ln \rho}{\partial p} \frac{Dp}{Dt} \quad (8.3a)$$

$$= -\alpha \frac{D\Theta}{Dt} + \beta \frac{DS}{Dt} + \frac{\dot{p}}{\rho c_s^2}. \quad (8.3b)$$

In this equation we introduced the [thermal expansion coefficient](#), the [haline contraction coefficient](#), the squared speed of sound, and the vertical pseudo-velocity in pressure

$$\alpha = - \left[\frac{\partial \ln \rho}{\partial \Theta} \right]_{p,S} \quad \beta = \left[\frac{\partial \ln \rho}{\partial S} \right]_{p,\Theta} \quad c_s^2 = \left[\frac{\partial p}{\partial \rho} \right]_{S,\Theta} \quad \dot{p} = \frac{Dp}{Dt}. \quad (8.4)$$

For the remainder of this section we unpack the processes contributing to the density material time evolution appearing in equation (8.3b).

8.2.1 Material changes to pressure

To garner some exposure to the physics of \dot{p} as it appears in equation (8.3b), consider the case of a hydrostatic fluid, where the volume per time per horizontal area of fluid crossing a surface of constant hydrostatic pressure is given by (see Section 2.4.6)

$$w^{(p)} = \frac{\partial z}{\partial p} \frac{Dp}{Dt} = -(\rho g)^{-1} \dot{p}. \quad (8.5)$$

The transport measured by $w^{(p)}$ is the pressure-coordinate analog of the vertical velocity component, $w = Dz/Dt$, that arises in a geopotential coordinate representation of the vertical. That is, fluid moving into regions of increasing hydrostatic pressure ($\dot{p} > 0$) represents downward movement of fluid, with $w^{(p)} < 0$ in this case. Conversely, motion into decreasing hydrostatic pressure represents upward motion, with $w^{(p)} > 0$. This vertical movement generally occurs in the presence of waves, currents, and mixing; i.e., both reversible and irreversible processes give rise to vertical motion.

8.2.2 Material changes to Θ and S

We next assume the material evolution of, S , and Conservative Temperature, Θ , are affected by the convergence of a subgrid scale flux

$$\rho \frac{D\Theta}{Dt} = -\nabla \cdot \mathbf{J}^{(\Theta)} \quad (8.6a)$$

$$\rho \frac{DS}{Dt} = -\nabla \cdot \mathbf{J}^{(S)}. \quad (8.6b)$$

The Conservative Temperature equation (8.6a) was derived in [VOLUME 2](#), whereas the salinity equation (8.6b) follows from our study of material tracers in [VOLUME 1](#).²

²For stratified fluids with multiple constituents, one encounters the effects of matter diffusion in the presence of a temperature gradient ([Soret effect](#)), and temperature diffusion in the presence of gradients of pressure and/or matter ([Dufour effect](#)). We introduced these cross-diffusion processes in [VOLUME 2](#) when studying energy and entropy flows in fluids. However, geophysical fluids are nearly always dominated by turbulence, which renders a turbulent diffusion that swamps the effects from cross-diffusion. We thus ignore cross-diffusion in this chapter. We also ignore remineralization processes that can contribute to a source term in the salinity equation (8.6b). Cross-diffusion and remineralization sources are discussed in [IOC et al. \(2010\)](#).

8.2.3 General expression for density changes

The expressions (8.6a) and (8.6b) for material changes in Θ and S then lead to

$$-\alpha \frac{D\Theta}{Dt} + \beta \frac{DS}{Dt} = \nu_\Theta \nabla \cdot \mathbf{J}^{(\Theta)} + \nu_S \nabla \cdot \mathbf{J}^{(S)} \quad (8.7a)$$

$$= \nabla \cdot [\nu_\Theta \mathbf{J}^{(\Theta)} + \nu_S \mathbf{J}^{(S)}] - [\mathbf{J}^{(\Theta)} \cdot \nabla \nu_\Theta + \mathbf{J}^{(S)} \cdot \nabla \nu_S] \quad (8.7b)$$

where again $\nu = \rho^{-1}$ is the specific volume and its thermodynamic partial derivatives are written using the shorthand

$$\nu_\Theta = \frac{\partial \nu}{\partial \Theta} = \frac{\alpha}{\rho} \quad \text{and} \quad \nu_S = \frac{\partial \nu}{\partial S} = -\frac{\beta}{\rho}. \quad (8.8)$$

Bringing the above results together leads to the density equation

$$\frac{D \ln \rho}{Dt} - \frac{\dot{p}}{\rho c_s^2} = \nabla \cdot [\nu_\Theta \mathbf{J}^{(\Theta)} + \nu_S \mathbf{J}^{(S)}] - [\mathbf{J}^{(\Theta)} \cdot \nabla \nu_\Theta + \mathbf{J}^{(S)} \cdot \nabla \nu_S], \quad (8.9)$$

which has the equivalent form

$$\frac{D \rho}{Dt} - \frac{\dot{p}}{c_s^2} = \nabla \cdot [\alpha \mathbf{J}^{(\Theta)} - \beta \mathbf{J}^{(S)}] - [\mathbf{J}^{(\Theta)} \cdot \nabla \alpha - \mathbf{J}^{(S)} \cdot \nabla \beta]. \quad (8.10)$$

We brought the source term from motion across pressure surfaces (Section 8.2.1) onto the left hand side, since this term appears in the absence of subgrid processes. The first term on the right hand side represents the divergence of a buoyancy flux due to subgrid scale fluxes of Conservative Temperature and salinity. In turn, density increases in regions where the buoyancy flux diverges (e.g., reducing Θ and increasing S). These fluxes arise from a variety of mixing processes, some of which are surveyed in Section 7.1.1. The second term on the right hand side of equations (8.9) and (8.10) relates to local properties of the density surface. We study this source term in Section 8.3 assuming the flux arises from **neutral diffusion**. Further effects arise from an unresolved **eddy-induced velocity**, whose stirring contributes to the **residual mean velocity** as discussed in Section 7.1.4.

8.2.4 Unpacking the subgrid contributions

Recall from Section 7.1 that the **subgrid scale** tracer fluxes are generally written in terms of a second order eddy transport tensor, \mathbf{E} , so that

$$\mathbf{J}^{(\Theta)} = -\rho \mathbf{E} \cdot \nabla \Theta \quad \text{and} \quad \mathbf{J}^{(S)} = -\rho \mathbf{E} \cdot \nabla S. \quad (8.11)$$

Furthermore, \mathbf{E} is typically decomposed as in equation (7.8) into a symmetric downgradient diffusion tensor, \mathbf{K} , and an anti-symmetric skew diffusion (or stirring) tensor, \mathbf{A} ,

$$\mathbf{E} = \mathbf{K} + \mathbf{A}. \quad (8.12)$$

We decompose the contributions to density according to these subgrid tensors using the following manipulations

$$\frac{D \rho}{Dt} - \frac{\dot{p}}{c_s^2} = \alpha \nabla \cdot \mathbf{J}^{(\Theta)} - \beta \nabla \cdot \mathbf{J}^{(S)} \quad (8.13a)$$

$$= -\alpha \nabla \cdot (\rho \mathbf{E} \cdot \nabla \Theta) + \beta \nabla \cdot (\rho \mathbf{E} \cdot \nabla S). \quad (8.13b)$$

Expanding the Θ term leads to

$$\alpha \nabla \cdot \mathbf{J}^{(\Theta)} = -\alpha \nabla \cdot (\rho \mathbf{E} \cdot \nabla \Theta) \quad (8.14a)$$

$$= -\alpha \nabla \cdot (\rho \mathbf{A} \cdot \nabla \Theta) - \alpha \nabla \cdot (\rho \mathbf{K} \cdot \nabla \Theta) \quad (8.14b)$$

$$= -\alpha \nabla \cdot (\rho \mathbf{A}) \cdot \nabla \Theta - \alpha \nabla \cdot (\rho \mathbf{K} \cdot \nabla \Theta), \quad (8.14c)$$

$$= \alpha \mathbf{v}^* \cdot \nabla \Theta - \alpha \nabla \cdot (\rho \mathbf{K} \cdot \nabla \Theta). \quad (8.14d)$$

To reach this result we made use of the identities

$$-\nabla \cdot (\rho \mathbf{A} \cdot \nabla \Theta) = -\partial_m (\rho A^{mn} \partial_n \Theta) \quad \text{expose tensor indices} \quad (8.15a)$$

$$= -\partial_m (\rho A^{mn}) \partial_n \Theta - \rho A^{mn} \partial_m \partial_n \Theta \quad \text{product rule} \quad (8.15b)$$

$$= -\partial_m (\rho A^{mn}) \partial_n \Theta \quad A^{mn} \partial_m \partial_n \Theta = 0 \quad (8.15c)$$

$$= \rho \mathbf{v}^* \cdot \nabla \Theta \quad \partial_m (\rho A^{mn}) = -\rho v^{*n}. \quad (8.15d)$$

In the final equality we introduced the density weighted eddy-induced velocity, $\rho \mathbf{v}^*$, defined by equation (7.11). The same manipulations for the salinity term lead to

$$\frac{D\rho}{Dt} - \frac{\dot{p}}{c_s^2} + \rho \mathbf{v}^* \cdot (-\alpha \nabla \Theta + \beta \nabla S) = -\alpha \nabla \cdot (\rho \mathbf{K} \cdot \nabla \Theta) + \beta \nabla \cdot (\rho \mathbf{K} \cdot \nabla S). \quad (8.16)$$

We can write this expression in terms of the residual mean material time operator

$$\frac{D^\dagger}{Dt} = \partial_t + \mathbf{v}^\dagger \cdot \nabla = \frac{D}{Dt} + \mathbf{v}^* \cdot \nabla \quad (8.17)$$

through adding and subtracting $c_s^{-2} \mathbf{v}^* \cdot \nabla p$

$$\rho \mathbf{v}^* \cdot (-\alpha \nabla \Theta + \beta \nabla S) = \mathbf{v}^* \cdot (-\rho \alpha \nabla \Theta + \rho \beta \nabla S + c_s^{-2} \nabla p) - c_s^{-2} \mathbf{v}^* \cdot \nabla p = \mathbf{v}^* \cdot (\nabla \rho - c_s^{-2} \nabla p), \quad (8.18)$$

which then leads to

$$\frac{D\rho}{Dt} - \frac{\dot{p}}{c_s^2} + \rho \mathbf{v}^* \cdot (-\alpha \nabla \Theta + \beta \nabla S) = \frac{D^\dagger \rho}{Dt} - \frac{1}{c_s^2} \frac{D^\dagger p}{Dt}, \quad (8.19)$$

so that

$$\frac{D^\dagger \rho}{Dt} - \frac{1}{c_s^2} \frac{D^\dagger p}{Dt} = -\alpha \nabla \cdot (\rho \mathbf{K} \cdot \nabla \Theta) + \beta \nabla \cdot (\rho \mathbf{K} \cdot \nabla S). \quad (8.20)$$

Transport from the symmetric tensor, \mathbf{K} , corresponds to diffusion so long as the tensor is positive definite. The diffusion operator in the residual mean evolution equation (8.20) can be written

$$\begin{aligned} & -\alpha \nabla \cdot (\rho \mathbf{K} \cdot \nabla \Theta) + \beta \nabla \cdot (\rho \mathbf{K} \cdot \nabla S) \\ &= \nabla \cdot [\rho \mathbf{K} \cdot (-\alpha \nabla \Theta + \beta \nabla S)] + \rho \nabla \alpha \cdot \mathbf{K} \cdot \nabla \Theta - \rho \nabla \beta \cdot \mathbf{K} \cdot \nabla S, \end{aligned} \quad (8.21)$$

so that the *in situ* density evolves according to

$$\frac{D^\dagger \rho}{Dt} - \frac{1}{c_s^2} \frac{D^\dagger p}{Dt} = - \underbrace{\nabla \cdot [\rho \mathbf{K} \cdot (\alpha \nabla \Theta - \beta \nabla S)]}_{\text{conservative processes}} + \underbrace{\rho \nabla \alpha \cdot \mathbf{K} \cdot \nabla \Theta - \rho \nabla \beta \cdot \mathbf{K} \cdot \nabla S}_{\text{sources from nonlinear EOS processes}}. \quad (8.22)$$

We now discuss the physical processes associated with the right hand side terms.

- LINEAR EQUATION OF STATE: A linear equation of state has $\nabla \alpha = \nabla \beta = 0$, with density independent of pressure. As a result, the evolution equation (8.22) takes the form

$$\frac{D^\dagger \rho}{Dt} = - \nabla \cdot [\rho \mathbf{K} \cdot (\alpha \nabla \Theta - \beta \nabla S)]. \quad (8.23)$$

Consequently, under the residual mean advective transport with a linear equation of state, density remains materially constant in the absence of any diffusion.

- NONLINEAR EQUATION OF STATE: A nonlinear equation of state is characterized by spatially dependent thermal expansion and haline contraction coefficients. Mixing of Θ and S in the presence of a nonlinear equation of state generally gives rise to material evolution of *in situ* density through *cabbeling* and *thermobaricity* (McDougall, 1987b). We offer a mathematical summary of these processes in Section 8.3.

- NEUTRAL DIFFUSION:

Neutral diffusion from Section 7.4 maintains a density-compensated diffusive flux of Θ and S so that

$$\mathbf{K}^{\text{neutral}} \cdot (\alpha \nabla \Theta - \beta \nabla S) = 0. \quad (8.24)$$

Hence, neutral diffusion leaves *in situ* density changed only via the nonlinear equation of state processes.

- ISOTROPIC SMALL SCALE DIFFUSION:

As discussed in Section 7.1.3, it is common to parameterize fine scale mixing processes using an isotropic diffusivity so that the diffusion tensor is given by

$$\mathbf{K}^{\text{iso}} = \kappa \mathbb{I}, \quad (8.25)$$

where \mathbb{I} is the unit tensor and $\kappa > 0$ is the isotropic eddy diffusivity.

8.2.5 Synthesis of the density equation

In summary, the material time evolution equation for *in situ* density in the presence of subgrid scale processes takes the form

$$\frac{D\rho}{Dt} = \underbrace{\frac{1}{c_s^2} \frac{Dp}{Dt}}_{\text{compressibility}} - \underbrace{\mathbf{v}^* \cdot (-\alpha \nabla \Theta + \beta \nabla S)}_{\text{eddy-induced advection}} - \underbrace{\nabla \cdot [\rho \kappa (-\alpha \nabla \Theta + \beta \nabla S)]}_{\text{small scale diffusive mixing}} + \underbrace{\rho \nabla \alpha \cdot \mathbf{K} \cdot \nabla \Theta - \rho \nabla \beta \cdot \mathbf{K} \cdot \nabla S}_{\text{nonlinear EOS processes from eddy mixing}}. \quad (8.26)$$

We thus have the following physical processes contributing to the evolution of *in situ* density.

- ADIABATIC COMPRESSION: Material changes to pressure in the presence of a finite sound speed lead to changes in the seawater density.
- SMALL SCALE MIXING: Small scale mixing is parameterized by an isotropic diffusivity, $\kappa > 0$. This kinematic diffusivity is the same for all tracers, with the exception of [double diffusive processes](#) whereby material tracers (e.g., salinity, nutrients) have a diffusivity distinct from temperature ([Schmitt, 1994](#)). Given the dominance of vertical stratification over the horizontal, it is common to approximate the isotropic diffusion operator with a vertical diffusion operator (but see Section 4 of [McDougall *et al.* \(2014\)](#) for caveats).
- EDDY-INDUCED VELOCITY: As studied in Chapter 7, subgrid scale correlations between eddy velocity and eddy isopycnal layer thickness lead to an [eddy-induced velocity](#) which, when combined with the resolved flow velocity, leads to the residual mean material time derivative, D^\dagger/Dt acting on the tracer fields. Equivalently, eddy-induced advective transport can be realized via [skew diffusion](#).
- EDDY-INDUCED DIFFUSION: As studied in Chapter 7, subgrid scale correlations between eddy velocity and eddy tracer concentration lead to a direct cascade of Θ and S variance to the small scales. Mixing arising from this cascade is parameterized by [neutral diffusion](#), whereby the diffusive fluxes of Θ and S are density compensated according to the constraint [\(8.24\)](#).
- NONLINEAR EOS PROCESSES: Mixing of Θ and S in the presence of a nonlinear equation of state means that *in situ* density evolves due to [cabbeling](#) and [thermobaricity](#) (Section 8.3). The dominant contributions to these processes arise from eddy induced mixing (i.e., neutral diffusion) ([McDougall, 1987b](#)), though small scale mixing also contributes.

8.3 Cabbeling and thermobaricity

We now return to the density equation (8.10)

$$\frac{D \ln \rho}{Dt} - \frac{\dot{p}}{\rho c_s^2} = \nabla \cdot [\nu_\Theta \mathbf{J}^{(\Theta)} + \nu_S \mathbf{J}^{(S)}] - (\mathbf{J}^{(\Theta)} \cdot \nabla \nu_\Theta + \mathbf{J}^{(S)} \cdot \nabla \nu_S), \quad (8.27)$$

and focus on Θ and S fluxes arising just from the neutral diffusion process described in Section 7.4. The neutrality condition (7.86) is a fundamental property of neutral diffusion, and it takes the following form in terms of specific volume

$$\nu_\Theta \mathbf{J}^{(\Theta)} + \nu_S \mathbf{J}^{(S)} = 0. \quad (8.28)$$

Consequently, neutral diffusion affects density evolution only through the nonlinear equation of state source term

$$\left[\frac{D \ln \rho}{Dt} \right]_{\text{ntrldiff}} = -\mathbf{J}^{(\Theta)} \cdot \nabla \nu_\Theta - \mathbf{J}^{(S)} \cdot \nabla \nu_S. \quad (8.29)$$

In the remainder of this section we manipulate the source term with the goal to identify the variety of physical processes associated with neutral diffusion in the presence of a nonlinear equation of state.

8.3.1 Basic manipulations

As a first step, eliminate the salt flux by using the neutrality condition (8.28)

$$\mathbf{J}^{(\Theta)} \cdot \nabla \nu_\Theta + \mathbf{J}^{(S)} \cdot \nabla \nu_S = \mathbf{J}^{(\Theta)} \cdot [\nu_S \nabla \nu_\Theta - \nu_\Theta \nabla \nu_S] / \nu_S. \quad (8.30)$$

Next, expand the gradients of the specific volume to write

$$\nabla \nu_\Theta = \nu_{\Theta\Theta} \nabla \Theta + \nu_{\Theta S} \nabla S + \nu_{\Theta p} \nabla p \quad \text{and} \quad \nabla \nu_S = \nu_{S S} \nabla S + \nu_{\Theta S} \nabla \Theta + \nu_{S p} \nabla p, \quad (8.31)$$

so that

$$\begin{aligned} \nu_S \nabla \nu_\Theta - \nu_\Theta \nabla \nu_S &= \nabla \Theta (\nu_S \nu_{\Theta\Theta} - \nu_\Theta \nu_{\Theta S}) \\ &\quad + \nabla S (\nu_S \nu_{\Theta S} - \nu_\Theta \nu_{S S}) + \nabla p (\nu_S \nu_{\Theta p} - \nu_\Theta \nu_{S p}). \end{aligned} \quad (8.32)$$

We again make use of the neutrality condition (8.28), as well as the symmetry condition (7.87d) to write

$$\mathbf{J}^{(\Theta)} \cdot \nabla S (\nu_S \nu_{\Theta S} - \nu_\Theta \nu_{S S}) = -\mathbf{J}^{(\Theta)} \cdot \nabla \Theta \left[\nu_\Theta \nu_{\Theta S} - \nu_{S S} \frac{(\nu_\Theta)^2}{\nu_S} \right]. \quad (8.33)$$

Bringing these results together leads to

$$\begin{aligned} \mathbf{J}^{(\Theta)} \cdot \nabla \nu_\Theta + \mathbf{J}^{(S)} \cdot \nabla \nu_S &= \mathbf{J}^{(\Theta)} \cdot \nabla p (\nu_{\Theta p} - \nu_{p S} \nu_\Theta / \nu_S) \\ &\quad + \mathbf{J}^{(\Theta)} \cdot \nabla \Theta [\nu_{\Theta\Theta} - 2 \nu_{\Theta S} \nu_\Theta / \nu_S + \nu_{S S} (\nu_\Theta / \nu_S)^2], \end{aligned} \quad (8.34)$$

which can be written in terms of density partial derivatives as

$$\begin{aligned} \mathbf{J}^{(\Theta)} \cdot \nabla \nu_\Theta + \mathbf{J}^{(S)} \cdot \nabla \nu_S &= -\rho^{-2} \mathbf{J}^{(\Theta)} \cdot \nabla p (\rho_{\Theta p} - \rho_{p S} \rho_\Theta / \rho_S) \\ &\quad - \rho^{-2} \mathbf{J}^{(\Theta)} \cdot \nabla \Theta [\rho_{\Theta\Theta} - 2 \rho_{\Theta S} \rho_\Theta / \rho_S + \rho_{S S} (\rho_\Theta / \rho_S)^2]. \end{aligned} \quad (8.35)$$

Following Exercise 8.1, we write the bracket terms appearing in equation (8.35) in forms consistent with those written by [McDougall \(1987b\)](#). We do so by introducing the **thermobaricity** parameter (dimensions of inverse temperature times inverse pressure)

$$\mathcal{T} = \beta \partial_p \left[\frac{\alpha}{\beta} \right], \quad (8.36)$$

and the **cabbeling** parameter (dimensions of squared inverse temperature)

$$\mathcal{C} = \frac{\partial \alpha}{\partial \Theta} + 2 \frac{\alpha}{\beta} \frac{\partial \alpha}{\partial S} - \left(\frac{\alpha}{\beta} \right)^2 \frac{\partial \beta}{\partial S}, \quad (8.37)$$

which then leads to the tidy result

$$\mathbf{J}^{(\Theta)} \cdot \nabla \nu_\Theta + \mathbf{J}^{(S)} \cdot \nabla \nu_S = \rho^{-1} \mathbf{J}^{(\Theta)} \cdot (\mathcal{T} \nabla p + \mathcal{C} \nabla \Theta). \quad (8.38)$$

Finally, we are thus led to the material time evolution of *in situ* density due to neutral diffusion

$$\left[\frac{D \rho}{D t} \right]_{\text{ntrldiff}} = -\mathbf{J}^{(\Theta)} \cdot (\mathcal{T} \nabla p + \mathcal{C} \nabla \Theta). \quad (8.39)$$

We next discuss the terms in this equation.

8.3.2 Cabbeling

The intrinsic geometry of density surfaces in Conservative Temperature and salinity space render the following inequality for the cabbeling parameter

$$\mathcal{C} = \frac{\partial \alpha}{\partial \Theta} + 2 \frac{\alpha}{\beta} \frac{\partial \alpha}{\partial S} - \left[\frac{\alpha}{\beta} \right]^2 \frac{\partial \beta}{\partial S} \geq 0. \quad (8.40)$$

With this inequality in mind, now consider the mixing of two adjacent elements of seawater. Let the fluid elements separately have distinct Conservative Temperature and/or salinity, but equal **locally referenced potential density**. For a linear equation of state, whereby density is a linear function of Θ and S , the resulting mixed fluid element has the same density as the unmixed separate elements. However, for a nonlinear equation of state, the mixed element generally has a different density. Furthermore, the effects from downgradient diffusion of Θ , coupled to the sign-definite nature of the cabbeling coefficient, render a mixed fluid element with a greater density than the unmixed elements. This densification upon mixing is a physical process known as **cabbeling** (McDougall, 1987b).

As noted above, the sign definite nature of cabbeling (i.e., cabbeling always results in denser fluid elements after mixing) is a direct result of the intrinsic geometry of density surfaces in Conservative Temperature and salinity space, combined with the downgradient orientation of the neutral diffusive flux of Θ . As a result, the cabbeling source satisfies

$$\text{cabbeling} \equiv -\mathcal{C} \mathbf{J}^{(\Theta)} \cdot \nabla \Theta \geq 0, \quad (8.41)$$

thus providing a mathematical expression for the cabbeling source (with dimensions of density per time). An increase in the density within a column of seawater results in the reduction of the sea level due to compression of the water column.

8.3.3 Thermobaricity

The thermobaricity parameter

$$\mathcal{T} = \beta \partial_p(\alpha/\beta) \quad (8.42)$$

is nonzero due to pressure dependence of the ratio of the thermal expansion coefficient to the haline contraction coefficient. As both thermal and haline effects are present, the parameter \mathcal{T} is more precisely split into two terms

$$\mathcal{T} = \frac{\partial \alpha}{\partial p} - \frac{\alpha}{\beta} \frac{\partial \beta}{\partial p} = -\frac{\rho_{\Theta p}}{\rho} + \frac{\rho_{\Theta}}{\rho_S} \frac{\rho_{pS}}{\rho}. \quad (8.43)$$

Thermobaricity is the common name for this two-term expression, since pressure variations in the thermal expansion coefficient dominate those of the haline contraction coefficient; i.e., halobaricity is subdominant to thermobaricity. The thermal expansion coefficient generally increases as pressure increases, thus making the thermobaric parameter positive.

Since the neutral gradient of Θ need not be oriented in a special manner relative to the neutral gradient of pressure, there is no sign-definite nature to the thermobaricity source term (with units of density per time)

$$\text{thermobaricity} \equiv -\mathcal{T} \mathbf{J}^{(\Theta)} \cdot \nabla p \quad (8.44)$$

appearing in equation (8.38). Thus, thermobaricity can either increase or decrease density,

depending on details of the density and fluxes. However, as noted by [McDougall and You \(1990\)](#), thermobaricity typically increases density in much of the World Ocean.

8.3.4 Comments

Cabbeling and thermobaricity lead to watermass transformation and associated dianeutral transport of seawater. However, these processes are distinct from other mixing processes such as breaking gravity waves (Section 7.1). Namely, cabbeling and thermobaricity arise from the transport of Θ and S by mesoscale eddies along neutral directions, which in turn is parameterized via neutral diffusion of these two active tracers. Transient mesoscale eddies impart a downscale cascade of tracer variance that is ultimately halted by irreversible molecular mixing. This mixing is the ultimate cause for cabbeling and thermobaricity, with the overall strength of the cabbeling and thermobaricity determined by the strength of the mesoscale stirring.

8.3.5 Further study

[Griffies and Greatbatch \(2012\)](#) discuss the impacts on global mean sea level from thermobaricity and cabbeling as diagnosed from an ocean model. Given that cabbeling always densifies and thermobaricity is also dominated by densification, these processes lead to a general reduction in global mean sea level. [Klocker and McDougall \(2010\)](#), [Groeskamp et al. \(2016\)](#), and [Groeskamp et al. \(2019\)](#) diagnose cabbeling and thermobaricity from observational based measurements, with [Groeskamp et al. \(2019\)](#) also offering a more robust numerical method for performing that diagnostic calculation. [McDougall \(2025\)](#) provides a review of various thermodynamic concepts used in ocean physics, including a discussion of cabbeling and thermobaricity.

8.4 Salt and freshwater continuity equations

We specialize the kinematics of material tracers given in VOLUME 1 to here focus on seawater, which we treat as a two component fluid comprised of salt and freshwater. We extend this discussion in Section 8.6 by studying the role of surface boundary transports of salt, enthalpy, and water, and how they affect ocean buoyancy.

8.4.1 Salt and freshwater

Seawater is comprised of two material tracers: freshwater plus a suite of dissolved trace “salts”. The ratio of salts is roughly constant over the World Ocean. We are thus able to make use of a single effective mass concentration known as the *salt concentration*³

$$S = \frac{\text{mass of salt}}{\text{mass of seawater}} = \frac{\text{mass of salt}}{\text{mass of freshwater} + \text{mass of salt}} \quad (8.45)$$

to specify the amount of salt within an element of seawater. In practice oceanographers choose to work with the *salinity*,⁴

$$S = 1000 S, \quad (8.46)$$

³We use the salt concentration, S , in this section to avoid 1/1000 factors needed if working with salinity, $S = 1000 S$.

⁴More precisely, the *salinity*, S , as defined by equation (8.46) is the *Absolute Salinity*. Absolute Salinity is distinct from the *practical salinity* determined by conductivity measurements. [IOC et al. \(2010\)](#) provides a full accounting of the theory and practice of ocean salinity.

which converts from typical salt concentrations of $S = 0.035$ to a salinity of $S = 35$. The complement to salt concentration is the freshwater concentration or mass fraction for an element of seawater

$$F = \frac{\text{mass of freshwater}}{\text{mass of seawater}} = \frac{\text{mass of freshwater}}{\text{mass of freshwater} + \text{mass of salt}} = 1 - S. \quad (8.47)$$

Other trace matter occurs at very low concentrations so as to make seawater, in effect, a two-component fluid consisting of freshwater plus dissolved salt.⁵ We here derive the mass budget for salt and freshwater as well as the associated kinematic boundary conditions.

8.4.2 Continuity equations

Following our discussion of the material tracer equation in VOLUME 1, we write the mass continuity equations for an element of seawater as

$$\partial_t \rho + \nabla \cdot (\rho \mathbf{v}) = 0 \quad \text{seawater} \quad (8.48)$$

$$\partial_t (\rho S) + \nabla \cdot (\rho \mathbf{v} S + \mathbf{J}^{(S)}) = 0 \quad \text{salt} \quad (8.49)$$

$$\partial_t (\rho F) + \nabla \cdot (\rho \mathbf{v} F + \mathbf{J}^{(F)}) = 0 \quad \text{freshwater.} \quad (8.50)$$

Equation (8.48) is the mass continuity equation for seawater and equation (8.49) is the mass continuity equation for salt. The freshwater continuity equation (8.50) is derived by subtracting the salt equation (8.49) from the seawater equation (8.48). Hence, only two of the three continuity equations (8.48)-(8.50) are independent.

We make use of the [barycentric velocity](#) in the above conservation laws, where the barycentric velocity for the ocean is given by

$$\mathbf{v} = S \mathbf{v}^{(S)} + F \mathbf{v}^{(F)}. \quad (8.51)$$

The velocities $\mathbf{v}^{(S)}$ and $\mathbf{v}^{(F)}$ are, respectively, the molecular center of mass velocities for salt and freshwater within a fluid element, in which case

$$\partial_t S + \mathbf{v}^{(S)} \cdot \nabla S = 0 \quad \text{and} \quad \partial_t F + \mathbf{v}^{(F)} \cdot \nabla F = 0. \quad (8.52)$$

Furthermore, the fluxes $\mathbf{J}^{(S)}$ and $\mathbf{J}^{(F)}$ arise from the difference of the salt and freshwater velocities from the barycentric velocity

$$\mathbf{J}^{(S)} = \rho S (\mathbf{v}^{(S)} - \mathbf{v}) \quad \text{and} \quad \mathbf{J}^{(F)} = \rho F (\mathbf{v}^{(F)} - \mathbf{v}). \quad (8.53)$$

As seen in Chapter 7, these fluxes are commonly parameterized using a subgrid tensor as per

$$\mathbf{J}^{(S)} = -\rho \mathbf{E} \cdot \nabla S \quad \text{and} \quad \mathbf{J}^{(F)} = -\rho \mathbf{E} \cdot \nabla F, \quad (8.54)$$

where \mathbf{E} is the subgrid scale (eddy) transport tensor for salt in seawater, which includes both diffusive and skew diffusive elements. We use the same eddy tensor for salt and freshwater since the eddy mixing of one is balanced by the other

$$\mathbf{J}^{(S)} = -\rho \mathbf{E} \cdot \nabla S = \rho \mathbf{E} \cdot \nabla F = -\mathbf{J}^{(F)}. \quad (8.55)$$

⁵See [IOC et al. \(2010\)](#) for more discussion of the variations of salt concentration ratios over the ocean, as well as the impacts from biogeochemical tracers.

The advective flux of seawater is comprised of a salt flux plus a freshwater flux

$$\rho \mathbf{v} = \rho S \mathbf{v}^{(S)} + \rho F \mathbf{v}^{(F)}. \quad (8.56)$$

Conversely, the salt flux and freshwater flux can be represented as a non-advective flux plus an advective flux, where advection is defined by the barycentric velocity

$$\rho S \mathbf{v}^{(S)} = \rho S (\mathbf{v}^{(S)} - \mathbf{v}) + \rho S \mathbf{v} = \mathbf{J}^{(S)} + \rho S \mathbf{v} \quad (8.57a)$$

$$\rho F \mathbf{v}^{(F)} = \rho F (\mathbf{v}^{(F)} - \mathbf{v}) + \rho F \mathbf{v} = \mathbf{J}^{(F)} + \rho F \mathbf{v}. \quad (8.57b)$$

The non-advective fluxes, $\mathbf{J}^{(S)}$ and $\mathbf{J}^{(F)}$, lead to an exchange of mass with zero net movement of mass. In contrast, the advective flux moves mass according to the barycentric velocity. Furthermore, the center of mass velocities, $\mathbf{v}^{(S)}$ and $\mathbf{v}^{(F)}$, offer a conceptual framework of use to formulate the kinematic boundary conditions. Even so, they offer no new information beyond that contained in the fluxes $\mathbf{J}^{(S)}$ and $\mathbf{J}^{(F)}$.

8.5 Surface boundary conditions for S and Θ

In this section we summarize the surface boundary conditions holding for the salinity and Conservative Temperature equations. This treatment complements that given in VOLUME 2 when studying boundary conditions for material tracers.

8.5.1 Salt and freshwater

In deriving the surface [kinematic boundary condition](#) in VOLUME 2, we made use of the [barycentric velocity](#), \mathbf{v} , for an element of seawater. We can garner further kinematic insights into the two-component ocean system by decomposing the boundary mass flux into contributions from salt and freshwater

$$\mathcal{Q}_m = \mathcal{Q}_S + \mathcal{Q}_F, \quad (8.58)$$

and by introducing the center of mass velocities for salt and freshwater according to

$$-\mathcal{Q}_m = \rho (\mathbf{v} - \mathbf{v}^{(\eta)}) \cdot \hat{\mathbf{n}} \quad (8.59a)$$

$$= \rho [S \mathbf{v}^{(S)} + F \mathbf{v}^{(F)} - \mathbf{v}^{(\eta)}] \cdot \hat{\mathbf{n}} \quad (8.59b)$$

$$= \rho [S (\mathbf{v}^{(S)} - \mathbf{v}^{(\eta)}) + F \mathbf{v}^{(F)} - \mathbf{v}^{(\eta)}] \cdot \hat{\mathbf{n}} \quad (8.59c)$$

$$= S \rho (\mathbf{v}^{(S)} - \mathbf{v}^{(\eta)}) \cdot \hat{\mathbf{n}} + (1 - S) \rho (\mathbf{v}^{(F)} - \mathbf{v}^{(\eta)}) \cdot \hat{\mathbf{n}} \quad (8.59d)$$

$$= S \rho (\mathbf{v}^{(S)} - \mathbf{v}^{(\eta)}) \cdot \hat{\mathbf{n}} + F \rho (\mathbf{v}^{(F)} - \mathbf{v}^{(\eta)}) \cdot \hat{\mathbf{n}} \quad (8.59e)$$

$$\equiv -(\mathcal{Q}_S + \mathcal{Q}_F), \quad (8.59f)$$

where we wrote

$$S \rho (\mathbf{v}^{(S)} - \mathbf{v}^{(\eta)}) \cdot \hat{\mathbf{n}} = -\mathcal{Q}_S \quad (8.60a)$$

$$F \rho (\mathbf{v}^{(F)} - \mathbf{v}^{(\eta)}) \cdot \hat{\mathbf{n}} = -\mathcal{Q}_F. \quad (8.60b)$$

In these equations, we introduced the velocity, $\mathbf{v}^{(\eta)}$, of a point fixed to the free surface. We only need the projection of this velocity in the outward normal direction, which is written (see

the kinematics from VOLUME 2)

$$\mathbf{v}^{(\eta)} \cdot \hat{\mathbf{n}} = \frac{\partial \eta / \partial t}{|\nabla(z - \eta)|} = \frac{\partial \eta / \partial t}{\sqrt{1 + |\nabla \eta|^2}} \implies \mathbf{v}^{(\eta)} \cdot \hat{\mathbf{n}} d\mathcal{S} = \partial_t \eta dA, \quad (8.61)$$

where $d\mathcal{S}$ is the area element on the free surface and dA is its horizontal projection. Note that in many regions, there is zero flux of salt across the ocean surface, in which case the ocean surface acts as a material surface in terms of the salt velocity

$$\rho (\mathbf{v}^{(S)} - \mathbf{v}^{(\eta)}) \cdot \hat{\mathbf{n}} = 0 \quad \text{zero surface salt flux.} \quad (8.62)$$

The key exception to this boundary condition concerns sea ice, whereby salt is exchanged between liquid seawater and sea ice upon the melting or freezing of ice.

For most applications, it is preferable to make use of equation (8.57a) to eliminate the salt velocity $\mathbf{v}^{(S)}$ in favor of the non-advection flux $\mathbf{J}^{(S)} = \rho S (\mathbf{v}^{(S)} - \mathbf{v})$, in which case the kinematic boundary condition (8.60a) takes the form

$$-\mathcal{Q}_S = S \rho (\mathbf{v}^{(S)} - \mathbf{v}^{(\eta)}) \cdot \hat{\mathbf{n}} = S \rho (\mathbf{v}^{(S)} - \mathbf{v} + \mathbf{v} - \mathbf{v}^{(\eta)}) \cdot \hat{\mathbf{n}} = \mathbf{J}^{(S)} \cdot \hat{\mathbf{n}} - S \mathcal{Q}_m. \quad (8.63)$$

Turning this equation around leads to the expression for the non-advection flux

$$\mathbf{J}^{(S)} \cdot \hat{\mathbf{n}} = S \mathcal{Q}_m - \mathcal{Q}_S = S \mathcal{Q}_F - F \mathcal{Q}_S, \quad (8.64)$$

which relates the mass transport crossing the ocean surface at $z = \eta$ (right hand side) to the non-advection salt transport on the ocean side of the surface boundary (left hand side). A form of this equation is also given in VOLUME 2 as part of the study of tracer kinematics.

To support intuition and to check signs, consider the case with $\mathcal{Q}_S = 0$ so that $\mathbf{J}^{(S)} \cdot \hat{\mathbf{n}} = S \mathcal{Q}_F$. Equation (8.64) then means there is an upward non-advection flux of salt ($\mathbf{J}^{(S)} \cdot \hat{\mathbf{n}} > 0$) on the ocean side of the $z = \eta$ boundary in the presence of an input of freshwater through the ocean surface ($S \mathcal{Q}_F > 0$). For the converse, let $\mathcal{Q}_F = 0$ so that $\mathbf{J}^{(S)} \cdot \hat{\mathbf{n}} = -F \mathcal{Q}_S$. Now, there is a downward non-advection flux of salt ($\mathbf{J}^{(S)} \cdot \hat{\mathbf{n}} < 0$) on the ocean side of the $z = \eta$ boundary in the presence of salt input through the ocean surface ($F \mathcal{Q}_S > 0$).

8.5.2 The non-advection salt flux boundary condition

The above properties of boundary mass transfer result from the kinematic property of a fluid element whose mass is constant, and so the transfer of freshwater across the boundary of a fluid element is compensated by an opposite transfer of salt. The ocean boundary interface acts as a boundary for the fluid elements adjacent to the surface. Hence, to move mass across the $z = \eta$ interface requires mass to be replenished to the surface fluid elements.

Diffusive closure for the non-advection flux

Consider an ocean without any mixing, such as for a perfect fluid. In this case, mass arriving to the ocean surface from $\mathcal{Q}_m > 0$ cannot be incorporated into the ambient ocean fluid, but instead will form a separate unmixed surface lens. When mass is exchanged across the ocean surface, mixing is required to incorporate the mass into the ambient ocean fluid. To determine the level of mixing, assume that $\mathbf{J}^{(S)}$ takes the form of a diffusive flux (8.54) so that the boundary

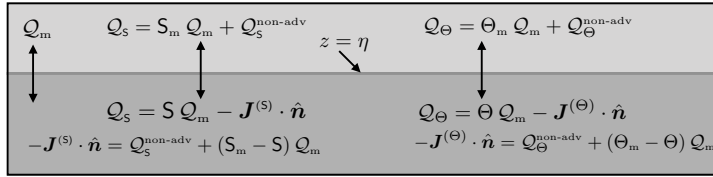


FIGURE 8.1: A schematic of an infinitesimal region of the ocean surface boundary at $z = \eta(x, y, t)$, with $z < \eta$ the liquid ocean. $\mathcal{Q}_m \, d\mathcal{S} = Q_m \, dA$ is the mass transport (mass per time) that crosses the $z = \eta$ interface. We depict the case for salt concentration, S , and Conservative Temperature, Θ , and the expressions for their net boundary fluxes. These boundary conditions are derived in Section 8.5.2 for salinity and Section 8.5.3 for Conservative Temperature.

condition (8.64) becomes

$$\mathbf{J}^{(S)} \cdot \hat{\mathbf{n}} = -\rho [\mathbf{K} \cdot \nabla S] \cdot \hat{\mathbf{n}} = S \mathcal{Q}_m - \mathcal{Q}_s = S \mathcal{Q}_F - F \mathcal{Q}_s, \quad (8.65)$$

where \mathbf{K} is the symmetric diffusion tensor.⁶ This equation sets the level of diffusion on the ocean side of the surface boundary that is needed to generate the non-advectional transport. The diffusive mixing of salt and freshwater mediate the transfer of mass across the ocean surface so to incorporate that mass into the ambient ocean fluid. For example, freshwater added to the ocean ($\mathcal{Q}_F > 0$) diffuses downward as salt diffuses upward toward the surface.

Salt dissolved within the mass transport

In the case when salt is transported across the ocean boundary, as occurs with sea ice melting and formation, it does so largely dissolved in the water that is transported. There can also be a non-advectional transport, such as via parameterized turbulent fluxes, so that the net salt flux is given by

$$\mathcal{Q}_s = S_m \mathcal{Q}_m + \mathcal{Q}_s^{\text{non-adv}}. \quad (8.66)$$

If there are more sources of this transfer then a relation such as this holds for each process. We are thus led to the net salt flux

$$\mathcal{Q}_s = -[\rho S (\mathbf{v} - \mathbf{v}^{(\eta)}) + \mathbf{J}^{(S)}] \cdot \hat{\mathbf{n}} = S \mathcal{Q}_m - \mathbf{J}^{(S)} \cdot \hat{\mathbf{n}} = S_m \mathcal{Q}_m + \mathcal{Q}_s^{\text{non-adv}}. \quad (8.67)$$

which leads to the non-advectional salt flux on the ocean side of the boundary

$$-\mathbf{J}^{(S)} \cdot \hat{\mathbf{n}} = \mathcal{Q}_s^{\text{non-adv}} + (S_m - S) \mathcal{Q}_m. \quad (8.68)$$

Figure 8.1 provides a schematic summary of the salt flux boundary condition. Furthermore, note that this boundary condition is consistent with that derived in VOLUME 1 for a general tracer.

Treatment in observational analyses and numerical models

In ocean climate modeling applications, the salt mass flux, \mathcal{Q}_s , typically does not affect the kinematic boundary conditions. This approximation is reasonable given that the dominant contributor to the mass flux, \mathcal{Q}_m , is the freshwater. Even so, there remains a net salt transported across the ocean surface in the presence of sea ice melt and formation. The above boundary conditions, in particular equations (8.67) and (8.68), remain unchanged. Furthermore, it is

⁶As seen in Chapter 7, parameterized skew fluxes satisfy a no-flux condition at boundaries.

necessary to specify the $z = \eta$ boundary concentration. For salt, this concentration is typically set equal to that within the ocean model surface grid cell. This choice is also common for observation-based studies.

8.5.3 Conservative Temperature boundary condition

Conservative Temperature, potential temperature, potential vorticity, and passive tracers each satisfy the tracer equation (8.49), with distinct tracer flux vectors, \mathbf{J} . However, they are not material tracers and so the kinematic constraints holding for salt and freshwater do not hold for these non-material tracers. We study the thermodynamic properties of Conservative Temperature in VOLUME 2, and the processes affecting its boundary fluxes in Section 8.6. Here we begin our treatment of this tracer by deriving its surface boundary condition, largely following our treatment of salinity in Section 8.5.2.

The net surface boundary flux of Conservative Temperature is written

$$\mathcal{Q}_\Theta = \Theta_m \mathcal{Q}_m + \mathcal{Q}_\Theta^{\text{non-adv}} = -[\rho \Theta (\mathbf{v} - \mathbf{v}^{(\eta)}) + \mathbf{J}^{(\Theta)}] \cdot \hat{\mathbf{n}} = \Theta \mathcal{Q}_m - \mathbf{J}^{(\Theta)} \cdot \hat{\mathbf{n}}. \quad (8.69)$$

In this equation, $\mathcal{Q}_\Theta^{\text{non-adv}}$ arises from the non-advective enthalpy fluxes outside the ocean domain that impact on the upper ocean interface, such as from radiant and turbulent fluxes, whereas Θ_m is the Conservative Temperature of the boundary mass flux. Rearrangement leads to the non-advective flux on the ocean side of the upper ocean boundary

$$-\mathbf{J}^{(\Theta)} \cdot \hat{\mathbf{n}} = \mathcal{Q}_\Theta^{\text{non-adv}} + (\Theta_m - \Theta) \mathcal{Q}_m, \quad (8.70)$$

where $\Theta = \Theta(z = \eta)$ is the Conservative Temperature at the surface interface. A common assumption made for models and observational studies is to set $\Theta_m - \Theta(z = \eta) = 0$, in which case

$$-\mathbf{J}^{(\Theta)} \cdot \hat{\mathbf{n}} = \mathcal{Q}_\Theta^{\text{non-adv}} \quad \text{if} \quad \Theta_m = \Theta(z = \eta). \quad (8.71)$$

Figure 8.1 provides a schematic summary of the Θ flux boundary condition.

8.5.4 Comments and further reading

We make use of many results from this section when discussing surface ocean buoyancy fluxes in Section 8.6 and water mass transformation in Section 9.6. Furthermore, [Nurser and Griffies \(2019\)](#) offer further discussion of the kinematic boundary condition for salt and freshwater, with that paper motivated by questions related to water mass transformation considered in Section 9.6.

8.6 Surface boundary fluxes of buoyancy

As studied in VOLUME 2, **buoyancy** measures the gravitational acceleration of a fluid element relative to that of the fluid environment surrounding the element. Changes in buoyancy arise through changes in density associated with temperature and salinity changes, with buoyancy changes computed relative to a fixed pressure level. In this section we derive the equation describing changes in ocean buoyancy due to enthalpy (commonly referred to as “heat”), salt, and water fluxes crossing the ocean surface boundary. For this purpose, we expose certain of the issues associated with coupling numerical models of the ocean, atmosphere, and land. A detailed treatment of boundary layer physics is well outside of our scope. We thus take

a phenomenological perspective, developing budget equations but not diving into details of the turbulent exchange of matter and enthalpy across the ocean surface boundary. Similar considerations hold for the ocean bottom boundary, which is insulating and material except in regions of geothermal fluxes.

8.6.1 Surface boundary fluxes of enthalpy and salt

Broadly, the surface boundary fluxes are associated with the following physical processes.

- Turbulent processes transfer enthalpy through latent and sensible heating.
- Longwave radiation cools the upper ocean, with this radiation affected by the upper ocean skin temperature.
- Penetrative shortwave radiation is absorbed in seawater and so increases buoyancy in regions where the thermal expansion coefficient is positive.⁷
- All of the above transports arise from [non-advection fluxes](#) in that they are not associated with a net mass transport across the ocean surface. In contrast, advective processes transfer enthalpy and salt across the ocean surface through the transfer of mass.
- Salt is transferred between the liquid ocean and sea ice when sea ice melts and forms. This transfer is proportional to the boundary flux of water and the difference in salinity between the liquid ocean and solid sea ice. There can be additional turbulent salt fluxes as well, but there is typically a negligible transfer of salt associated with precipitation, evaporation, and river runoff.

8.6.2 Evolution from surface boundary fluxes

We now develop finite volume budget equations for potential enthalpy (via Conservative Temperature, Θ), salt, and seawater mass for a grid cell region next to the ocean surface (see Figure 8.2), with a focus on contributions due to surface boundary fluxes. For that purpose, introduce the following quantities for a grid cell,

$$M = \int_{\text{cell}} \rho \, dV = \langle \rho \rangle V \quad V = \int_{\text{cell}} dV = A \bar{h} \quad A = \int_{\text{cell}} dA \quad (8.72\text{a})$$

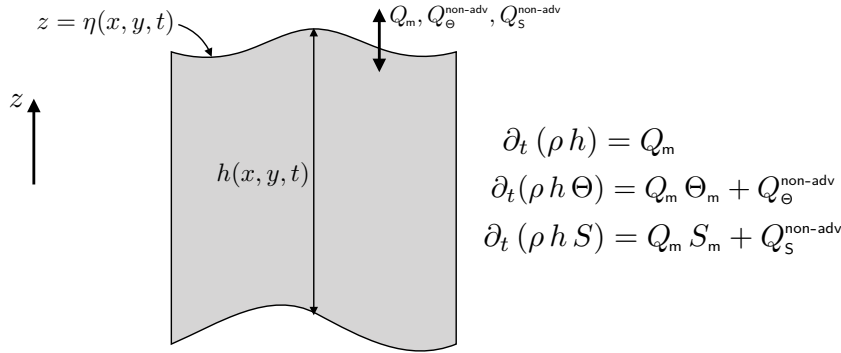
$$\bar{h} A = \int_{\text{cell}} \left[\int_{\text{cell}} dz \right] dA \quad \langle C \rangle M = \int_{\text{cell}} C \rho \, dV, \quad (8.72\text{b})$$

so that $\langle \rho \rangle$ is the cell averaged density, $\langle C \rangle$ is the cell averaged tracer concentration, \bar{h} is the cell area averaged thickness, V is the cell volume, and A is the cell horizontal area. These definitions allow us to write

$$\frac{d}{dt} \left[\int_{\text{cell}} \rho C \, dV \right] = \frac{d}{dt} [\langle C \rangle M] = A \frac{d}{dt} [\bar{h} \langle C \rangle \langle \rho \rangle], \quad (8.73)$$

where the horizontal area of a cell is assumed to be constant in time and the cell is bounded by vertical side walls. The surface boundary fluxes have similar grid cell area averages.

⁷The Baltic Sea is an outlier in the World Ocean, whose fresh and cold waters often realize a negative thermal expansion so that shortwave radiation can increase density rather than reduce it.



$$\begin{aligned}\partial_t(\rho h) &= Q_m \\ \partial_t(\rho h \Theta) &= Q_m \Theta_m + Q_\Theta \\ \partial_t(\rho h S) &= Q_m S_m + Q_S^{\text{non-adv}}\end{aligned}$$

FIGURE 8.2: Schematic of a finite volume region next to the ocean surface used to develop the budget equations for mass, enthalpy, and salt. To derive the surface boundary condition for buoyancy, it is sufficient to ignore all fluxes crossing interior surfaces, focusing instead on those fluxes crossing the ocean free surface at $z = \eta(x, y, t)$.

Focusing just on contributions from surface boundary transport leads to the budget equations

$$\partial_t(\rho h \Theta) = Q_m \Theta_m + Q_\Theta^{\text{non-adv}} \quad (8.74a)$$

$$\partial_t(\rho h S) = Q_m S_m + Q_S^{\text{non-adv}} \quad (8.74b)$$

$$\partial_t(\rho h) = Q_m, \quad (8.74c)$$

where we wrote a partial time derivative since we are holding the horizontal position fixed. Furthermore, we reduced notational clutter by dropping the angle brackets for volume average and the horizontal overline for area average. For a three-dimensional budget, the right hand side to these equations is combined with fluxes crossing interior cell boundaries, which are ignored here since we are focused just on surface fluxes. Finally, we wrote the fluxes as

$$Q_m A = Q_m \mathcal{S} \quad \text{and} \quad Q_\Theta^{\text{non-adv}} A = Q_\Theta^{\text{non-adv}} \mathcal{S} \quad \text{and} \quad Q_S^{\text{non-adv}} A = Q_S^{\text{non-adv}} \mathcal{S}, \quad (8.75)$$

where \mathcal{S} is the area on the free surface and A is the corresponding horizontal area of the grid cell.⁸

8.6.3 Buoyancy tendency from surface fluxes

For many purposes, it is of interest to quantify the impacts on ocean buoyancy arising from surface boundary fluxes. For that purpose, we here develop the budget for buoyancy in a surface model grid cell region, focusing on surface flux contributions.

Buoyancy has a local time tendency given by

$$-\frac{\rho_0}{g} \frac{\partial b}{\partial t} = \rho_\Theta \frac{\partial \Theta}{\partial t} + \rho_S \frac{\partial S}{\partial t}, \quad (8.76)$$

where we introduced the shorthand

$$\rho_\Theta = \left[\frac{\partial \rho}{\partial \Theta} \right]_{S,p} \quad \text{and} \quad \rho_S = \left[\frac{\partial \rho}{\partial S} \right]_{\Theta,p} \quad (8.77)$$

⁸The surface area, \mathcal{S} , along the $z = \eta$ boundary is not generally horizontal and it is not generally constant in time. Yet its horizontal projection, A , is time independent since we fix the horizontal positions for the vertical cell walls.

for the partial derivatives of density with respect to Conservative Temperature and salinity, respectively, each with pressure held constant. We wish to form an evolution equation for buoyancy at the ocean surface grid cell just due to the effects of surface forcing. For this purpose, multiply the temperature equation (8.74a) by ρ_Θ and add to the salinity equation (8.74b) multiplied by ρ_S

$$\rho_\Theta \left[\frac{\partial(\rho h \Theta)}{\partial t} \right] + \rho_S \left[\frac{\partial(\rho h S)}{\partial t} \right] = Q_m (\rho_\Theta \Theta_m + \rho_S S_m) + \rho_\Theta Q_\Theta^{\text{non-adv}} + \rho_S Q_S^{\text{non-adv}}. \quad (8.78)$$

Now use the mass budget (8.74c) and introduce the buoyancy tendency according to equation (8.76) to render an expression for the time tendency of the surface ocean buoyancy⁹

$$-(\rho/g) \rho h \left[\frac{\partial b}{\partial t} \right]^{\text{surf}} = Q_m [\rho_\Theta (\Theta_m - \Theta) + \rho_S (S_m - S)] + \rho_\Theta Q_\Theta^{\text{non-adv}} + \rho_S Q_S^{\text{non-adv}}. \quad (8.79)$$

Introducing the thermal expansion and saline contraction coefficients

$$\alpha = -\frac{1}{\rho} \left[\frac{\partial \rho}{\partial \Theta} \right]_{S,p} \quad \text{and} \quad \beta = \frac{1}{\rho} \left[\frac{\partial \rho}{\partial S} \right]_{\Theta,p} \quad (8.80)$$

yields

$$\left[\frac{\partial b}{\partial t} \right]^{\text{surf}} = \frac{g}{\rho_\Theta h} \left(Q_m [\alpha (\Theta_m - \Theta) - \beta (S_m - S)] + \alpha Q_\Theta^{\text{non-adv}} - \beta Q_S^{\text{non-adv}} \right) \quad (8.81a)$$

$$= \frac{g}{\rho_\Theta h} \left(\alpha [Q_m (\Theta_m - \Theta) + Q_\Theta^{\text{non-adv}}] - \beta [Q_m (S_m - S) + Q_S^{\text{non-adv}}] \right). \quad (8.81b)$$

In regions where the thermal expansion coefficient is positive ($\alpha > 0$), adding a boundary mass ($Q_m > 0$) that has $\Theta_m > \Theta$ increases the buoyancy of the surface ocean; i.e., adding relatively warm water increases surface ocean buoyancy. Likewise, where the haline contraction coefficient is positive ($\beta > 0$), adding boundary mass with $S_m < S$ increases buoyancy of the surface ocean; i.e., adding relatively freshwater increases surface ocean buoyancy. The same behavior holds for the turbulent fluxes, where $Q_\Theta^{\text{non-adv}} > 0$ (adding turbulent thermal energy to the ocean) increases surface ocean buoyancy whereas $Q_S^{\text{non-adv}} > 0$ (adding salt to the ocean) decreases buoyancy.

Following from our study of Green's functions for Neumann boundary conditions in VOLUME 1, we consider the limit as the thickness, h , becomes vanishingly small, in which case we introduce a **Dirac delta**

$$\left[\frac{\partial b}{\partial t} \right]^{\text{surf}} = \frac{g \delta(z - \eta)}{\rho_\Theta} \left(Q_m [\alpha (\Theta_m - \Theta) - \beta (S_m - S)] + \alpha Q_\Theta^{\text{non-adv}} - \beta Q_S^{\text{non-adv}} \right) \quad (8.82a)$$

$$= \frac{g \delta(z - \eta)}{\rho_\Theta} \left(\alpha [Q_m (\Theta_m - \Theta) + Q_\Theta^{\text{non-adv}}] - \beta [Q_m (S_m - S) + Q_S^{\text{non-adv}}] \right). \quad (8.82b)$$

This **Dirac delta** sheet form for the boundary fluxes is quite useful when organizing physical processes according to whether they arise from the ocean interior versus ocean boundary. It proves particularly useful for water mass transformation analysis in Section 9.7.

⁹We provide the few missing details in Exercise 8.2.

8.6.4 Comments

The buoyancy flux expression (8.81b) is of use for boundary layer parameterizations, such as the KPP scheme of [Large et al. \(1994\)](#) and [Van Roekel et al. \(2018\)](#). It is furthermore used in our study of water mass transformations in Chapter 9.

8.7 Global mean sea level

In this section we consider some basic features of global mean sea level by making use of the mass budget of liquid seawater. This analysis highlights the distinction between the mass budget and the volume (sea level) budget. In particular, mass is an extensive property and so it satisfies a conservation budget, with the total ocean mass affected only through boundary fluxes. In contrast, volume, just like buoyancy, has interior sources and sinks so that the ocean volume can change even if there are no boundary fluxes of volume.

8.7.1 Definitions and assumptions

The liquid seawater mass is given by the integral

$$M = \int_{\mathcal{R}} \rho dV, \quad (8.83)$$

with our interest in a global integral over the full liquid ocean domain, \mathcal{R} . Since mass is an extensive quantity, it has a time tendency due to boundary transport, here written as

$$\frac{dM}{dt} = A \overline{Q_m}, \quad (8.84)$$

where A is the ocean surface area,

$$\overline{Q_m} = \frac{1}{A} \int Q_m dA, \quad (8.85)$$

is the area averaged surface mass flux, and we ignore any mass entering through the ocean bottom. The global volume of liquid seawater

$$V = \int_{\mathcal{R}} dV = \frac{M}{\langle \rho \rangle} \quad (8.86)$$

changes due to mass changes and changes to the global mean density,

$$\langle \rho \rangle = \frac{\int_{\mathcal{R}} \rho dV}{\int_{\mathcal{R}} dV} = \frac{M}{V}. \quad (8.87)$$

Throughout this section we assume the surface area is constant in time, thus neglecting the relatively small changes associated with volume changes along sloping beaches. We also assume a temporally constant area averaged ocean bottom depth, \overline{H} . These two assumptions result in a time tendency in ocean volume that arises just from time tendencies in the global mean sea level, $\overline{\eta}$. Since around the year 2000, measurements estimate that global area mean sea level has increased at a rate of

$$\left[\frac{d\overline{\eta}}{dt} \right]_{\text{observed}} \approx 3 \text{ mm yr}^{-1}. \quad (8.88)$$

To attach further numbers to the analysis in this section we make use of the following phenomenological numbers and make a few assumptions to facilitate calculations.

- global seawater volume $V \approx 1.3 \times 10^{18} \text{ m}^3$
- global ocean surface area $A \approx 3.6 \times 10^{14} \text{ m}^2$
- global ocean mean density $\langle \rho \rangle \approx 1035 \text{ kg m}^{-3}$
- specific heat capacity for seawater $c_p \approx 3992 \text{ J kg}^{-1}\text{K}^{-1}$
- Ignore mass fluxes transported through the sea floor, which are small relative to surface mass fluxes.
- Ignore salinity and pressure effects on density, so that changes in global mean density arise just from changes in global mean Conservative Temperature.
- Assume a constant thermal expansion coefficient

$$\alpha = -\frac{1}{\rho} \left[\frac{\partial \rho}{\partial \Theta} \right]_{S,p} \approx 2 \times 10^{-4} \text{ K}^{-1}. \quad (8.89)$$

This is not a great approximation, since the thermal expansion coefficient ranges over the ocean by a factor of 10. Nonetheless, for this section it is sufficient for computing estimates that support conceptual understanding that is not outside the bounds of error bars in measurements for global boundary enthalpy and mass fluxes.

8.7.2 Budget for global mean sea level

Expression (8.86) for ocean volume leads to its time derivative

$$\frac{dV}{dt} = \frac{1}{\langle \rho \rangle} \frac{dM}{dt} - \frac{M}{\langle \rho \rangle^2} \frac{d\langle \rho \rangle}{dt} \quad (8.90a)$$

$$= \frac{A \overline{Q_m}}{\langle \rho \rangle} - \frac{V}{\langle \rho \rangle} \frac{d\langle \rho \rangle}{dt}, \quad (8.90b)$$

where we used equation (8.84) to express mass changes in terms of the surface mass flux. Additionally, the ocean volume is connected to sea level via

$$V = \int dA \int_{-H}^{\eta} dz = A (\overline{H} + \bar{\eta}), \quad (8.91)$$

so that time changes in ocean volume arise from time changes in the global mean sea level

$$\frac{dV}{dt} = A \frac{d\bar{\eta}}{dt}. \quad (8.92)$$

Combining the two volume equations (8.90b) and (8.92) yields the budget equation for global mean sea level

$$\frac{d\bar{\eta}}{dt} = \frac{\overline{Q_m}}{\langle \rho \rangle} - \frac{V}{A \langle \rho \rangle} \frac{d\langle \rho \rangle}{dt}. \quad (8.93)$$

The first term arises from changes in ocean mass (increasing total mass increases sea level) whereas the second term arises from changes in global mean seawater density (increasing the mean density decreases sea level).

8.7.3 Changes due to mass input

To ground these formula in phenomenology, assume that a surface mass flux gives one-half of the observed sea level rise

$$\frac{1}{2} \left[\frac{d\bar{\eta}}{dt} \right]_{\text{observed}} = \frac{\bar{Q}_m}{\langle \rho \rangle}, \quad (8.94)$$

with the other half due to changes in mean density. With $\langle \rho \rangle = 1035 \text{ kg m}^{-3}$ and $d\bar{\eta}/dt \approx 3 \text{ mm yr}^{-1}$, we need an area averaged mass flux across the ocean surface

$$\bar{Q}_m \approx 5 \times 10^{-8} \text{ kg m}^{-2} \text{ s}^{-1}. \quad (8.95)$$

Integrated over the global ocean area, this flux leads to a mass transport of

$$\mathcal{T} = A \bar{Q}_m \approx 1.8 \times 10^7 \text{ kg s}^{-1} \approx 0.015 \times \mathcal{T}^{\text{river}}. \quad (8.96)$$

That is, global mean sea level rises at a rate of 1.5 mm yr^{-1} if there is a net additional mass added to the ocean equal to roughly 1.5% of the net river water entering the ocean, $\mathcal{T}^{\text{river}}$. This additional net mass is largely coming from the melting of land-ice in the form of mountain glaciers and ice sheets.

8.7.4 Steric changes due to changes in density

Steric effects generally refer to properties of a substance associated with the space occupied by atoms and molecules. In the sea level context, steric effects refer to changes in sea level associated with density changes, with changes in density associated with changes in the volume occupied by seawater molecules.

Changes in global mean sea level arising from changes in the global mean density are called global **steric sea level changes**. From the sea level budget equation (8.93) we know that steric changes are written mathematically as

$$\left[\frac{d\bar{\eta}}{dt} \right]_{\text{steric}} \equiv -\frac{V}{A \langle \rho \rangle} \frac{d\langle \rho \rangle}{dt}. \quad (8.97)$$

In Section 8.7.6 we show that global mean density has a time tendency arising primarily from the time tendency in global mean Conservative Temperature. If we assume the ocean thermal expansion is constant, then

$$\frac{1}{\langle \rho \rangle} \frac{d\langle \rho \rangle}{dt} = -\alpha \frac{d\langle \Theta \rangle}{dt}, \quad (8.98)$$

so that steric sea level changes are primarily driven by **thermosteric** effects

$$\left[\frac{d\bar{\eta}}{dt} \right]_{\text{thermosteric}} \equiv \frac{\alpha V}{A} \frac{d\langle \Theta \rangle}{dt}, \quad (8.99)$$

with increasing water temperature, in the presence of $\alpha > 0$, leading to higher sea levels. With $\alpha \approx 2 \times 10^{-4} \text{ K}^{-1}$ and $d\bar{\eta}/dt \approx 1.5 \text{ mm yr}^{-1}$, we have

$$\frac{d\langle \Theta \rangle}{dt} \approx 0.2 \text{ K century}^{-1}. \quad (8.100)$$

That is, a global thermosteric sea level rise of 1.5 mm yr^{-1} corresponds to a rate of increase in the global volume mean ocean temperature of roughly $0.2 \text{ K century}^{-1}$.

8.7.5 Enthalpy flux imbalances implied by thermosteric sea level

The global budget for potential enthalpy is given by

$$\frac{d}{dt} \int_{\mathcal{R}} c_p \rho \Theta dV = \int_{\partial \mathcal{R}} Q_H dA, \quad (8.101)$$

where Q_H is the boundary flux of enthalpy. Introducing the area and volume mean quantities leads to

$$c_p \frac{d(V\langle \rho \Theta \rangle)}{dt} = A \overline{Q_H}, \quad (8.102)$$

with the expanded left hand side rendering

$$\frac{V}{A} \frac{d\langle \rho \Theta \rangle}{dt} + \langle \rho \Theta \rangle \frac{d\bar{\eta}}{dt} = \overline{Q_H}/c_p. \quad (8.103)$$

Rearrangement then leads to an expression for the global mean sea level tendency

$$\frac{d\bar{\eta}}{dt} = \frac{1}{\langle \rho \Theta \rangle} \left[\overline{Q_H} - \frac{V}{A} \frac{d\langle \rho \Theta \rangle}{dt} \right], \quad (8.104)$$

which is directly analogous to the sea level equation (8.93) based on the mass budget. A positive tendency in global mean sea level implies a positive right hand side to equation (8.104).

In Exercise 8.6 we show that any conservative tracer, C , leads to a corresponding kinematic sea level equation just like equation (8.104). These sea level equations arise kinematically through defining the volume mean according to

$$V\langle \rho \rangle = \int_{\mathcal{R}} \rho dV \quad \text{and} \quad V\langle \rho C \rangle = \int_{\mathcal{R}} \rho C dV. \quad (8.105)$$

These definitions then lead to diagnostic connections between changes in conservative scalar properties (seawater mass, tracer mass) and sea level changes.

Rather than focus on the sea level tendency, return to equation (8.102) and estimate $V/A \approx \overline{H}$, thus dropping the contribution from $d\bar{\eta}/dt$, and further estimate a Boussinesq ocean so that

$$\frac{d\langle \rho \Theta \rangle}{dt} \approx \rho_o \frac{d\langle \Theta \rangle}{dt}, \quad (8.106)$$

in which case

$$\overline{Q_H} \approx \rho_o c_p \overline{H} \frac{d\langle \Theta \rangle}{dt}. \quad (8.107)$$

Inserting the global mean temperature tendency of $0.2 \text{ K century}^{-1}$ from equation (8.100), as estimated from the sea level tendency, then affords an estimate of the global area mean heat flux crossing the ocean boundary¹⁰

$$\overline{Q_H} \approx 1 \text{ W m}^{-2}. \quad (8.108)$$

That is, a surface ocean enthalpy flux of roughly 1 W m^{-2} (ocean area normalized) gives rise to a global mean thermosteric sea level rise of roughly 1.5 mm yr^{-1} .

An enthalpy flux of 1 W m^{-2} is small compared to, say, that crossing the surface of a typical light bulb. However, 1 W m^{-2} is comparable to that accumulating within the earth system due

¹⁰The global area mean geothermal heat flux is roughly 0.094 W m^{-2} ([Huw Davies, 2013](#)), so that most of the thermosteric sea level rise comes from surface fluxes.

to increases in greenhouse gases ([Otto et al., 2013](#)). That is, 1 W m^{-2} averaged over the global ocean, or 0.7 W m^{-2} averaged over the surface area of the planet,¹¹ is roughly the net heating associated with anthropogenic climate change. This increase in surface heating represents a nontrivial increase in the earth's energy budget that is leading to the observed climate changes and sea level rise.¹²

8.7.6 Barystatic versus steric effects from near future land ice melt

In this subsection we consider a thought experiment to expose some questions about how global mean sea level changes when melted land ice is added to the ocean. Our concern is mostly with near future sea level rise due to melting land ice, with assumptions made based on that application.¹³

Freshwater melt and sea level changes

When freshwater enters the ocean, such as from melting glaciers or continental ice sheets, it adds to the ocean mass and in turn increases global mean sea level. This change is referred to as [barystatic sealevel](#) change according to the sea level terminology reviewed by [Gregory et al. \(2019\)](#). Although ocean salinity, temperature, and pressure changes upon changing the freshwater content, the net effect on global mean sea level is almost entirely barystatic. We here focus on questions related to the changes in salinity, showing how the global halosteric effect is negligible relative to the barystatic effect. But in general, we can understand why the global steric effect (due to changes in salinity, temperature, and pressure) is so tiny by recognizing that freshwater entering the ocean sees its properties change whilst the ambient seawater is itself changed. In particular, the added freshwater has its salinity increase while the ambient seawater is freshened. These compensating effects have corresponding compensating sea level changes, thus bringing the global steric effect to near zero.¹⁴

We here summarize a two-bucket thought experiment from Appendix B of [Gregory et al. \(2019\)](#) (see also the appendix to [Lowe and Gregory \(2006\)](#)), which focuses on the questions related to salinity. In this experiment, one bucket initially holds freshwater and the other initially holds seawater, with the Conservative Temperature and pressure assumed to be identical for the two buckets, with this assumption not suited to paleoclimate questions such as those considered by [Gebbie \(2020\)](#). Even so, the analysis provides a framing of how to study steric effects associated with changes in ocean mass, with [Gebbie \(2020\)](#) pursuing these questions in far more detail.

Formulating the change in volume

Referring to Figure 8.3, consider two buckets that initially contain water with mass M_n , volume V_n , density $\rho_n = M_n/V_n$, and salinity S_n , where $n = 1, 2$ labels the two buckets. Now fully mix

¹¹The ocean covers roughly 70% of the earth surface. This factor is commonly forgotten when quoting heat flux numbers, so it is important to note whether the number refers to global area normalized or ocean area normalized.

¹²In Exercise 8.3 we compare the net power input to the ocean from anthropogenic effects to the power associated with atomic bombs.

¹³See [Gebbie \(2020\)](#) for applications to paleoclimate studies, where the amount of melt is far larger than that assumed in this subsection. In particular, we here ignore pressure effects, whereas pressure changes are central to the paleoclimate study of [Gebbie \(2020\)](#).

¹⁴As noted in the appendices to [Lowe and Gregory \(2006\)](#) and [Gregory et al. \(2019\)](#), these compensating effects are often mistakenly ignored.

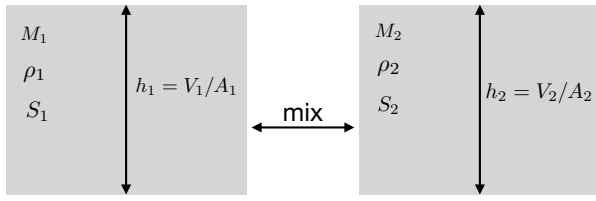


FIGURE 8.3: Schematic of the two-bucket thought experiment from [Gregory et al. \(2019\)](#), used to illustrate the tiny effects on global mean sea level from the global halosteric effect. We consider two homogeneous regions of seawater with mass M_n , volume V_n , density $\rho_n = M_n/V_n$, and salinity S_n (or salt concentration $S_n = S_n/1000$), where $n = 1, 2$ labels the two buckets. The water in the two buckets initially has different salinity, but they are then mixed fully, with the total mass and total salt both conserved during the mixing experiment. We ignore heat of mixing and pressure effects, which is a good approximation for buckets that correspond to upper ocean regions where melt enters, but it is not appropriate for paleoclimate questions such as considered by [Gebbie \(2020\)](#). After mixing, mass M_1 of the homogenized water is put back into the first bucket and M_2 is put into the second bucket. The question is how much has the volume (and hence the vertical thickness) changed upon mixing?

the water in the two buckets. In so doing, the mass, M , of seawater remains constant, as does the total mass of salt

$$M = M_1 + M_2 \quad \text{and} \quad M S = M_1 S_1 + M_2 S_2, \quad (8.109)$$

where S is the salt concentration of the homogenized fluid so that $M S$ is the total mass of salt in the combined system. After mixing, we return a mass, M_1 , of the homogenized water back in the first bucket, and a mass, M_2 , into the second bucket. Our goal is to compute the change in seawater volume

$$\delta V = \delta V_1 + \delta V_2. \quad (8.110)$$

In determining this volume change, we ignore pressure changes as well as changes in enthalpy associated with the heat of mixing since we are focused here on volume changes arising from salinity changes. Both approximations are quite accurate when considering one of the buckets to be a surface ocean model grid cell and the other to be a bucket from melted land ice. However, when considering longer term paleoclimate questions, these assumptions must be removed as done by [Gebbie \(2020\)](#).

Since the mass of each bucket remains the same before and after homogenization, then the density of seawater in each bucket changes only due to the volume changes

$$\delta \rho_n = \delta(M_n/V_n) = -(M_n/V_n^2) \delta V_n \implies \delta \rho_n / \rho_n = -\delta V_n / V_n. \quad (8.111)$$

That is, the relative change in density equals to minus the relative change in volume. Now the density changes arise just from salinity changes, in which

$$\delta \rho_n / \rho_n = \beta_n \delta S_n, \quad (8.112)$$

where β_n is the haline contraction coefficient that measures changes in density when fixing pressure and Conservative Temperature. We are thus led to the volume change

$$\delta V = -(V_1 \delta \rho_1 / \rho_1 + V_2 \delta \rho_2 / \rho_2) = -(V_1 \beta_1 \delta S_1 + V_2 \beta_2 \delta S_2). \quad (8.113)$$

We can simplify this expression by making use of salt conservation in equation (8.109), thus

constraining salinity changes according to

$$M_1 \delta S_1 + M_2 \delta S_2 = 0 \implies \delta S_2 = -(M_1/M_2) \delta S_1, \quad (8.114)$$

in which case the volume change takes on the form

$$\delta V = -V_1 \delta S_1 (\beta_1 - \beta_2 \rho_1/\rho_2). \quad (8.115)$$

The haline contraction coefficient changes only by a few percent globally (see [Roquet et al. \(2015\)](#) or Figure 1 in [Griffies et al. \(2014\)](#)), in which case we set $\beta_1 = \beta_2 = \beta$. Furthermore, to connect to sea level changes we assume the horizontal cross-sectional area of the two buckets is the same, so that the water column thickness differs between the two buckets by the amount

$$\delta h = -h_1 \beta \delta S_1 (1 - \rho_1/\rho_2). \quad (8.116)$$

Numbers for the ocean

We can compute the relative change in thickness using equation (8.116) and plugging in some numbers. Namely, we assume the first bucket is initially filled with freshwater ($S_1 = 0$) whereas the second bucket is initially filled with ambient seawater, with salinity $S_2 = 1000$ S₂ = 35 ppt a representative value. Homogenization of the two buckets then raises salinity in the first bucket and lowers it for the second. Assume the first bucket has its salinity raised to by $\delta S_1 = S/2$, let the density ratio be $\rho_1/\rho_2 = 1000/1028$, and haline contraction coefficient¹⁵ be $\beta = 0.8 \times 10^{-3}$. These values then yield a thickness change¹⁶

$$\delta h/h_1 = -3.8 \times 10^{-4}. \quad (8.117)$$

Hence, for every meter of fresh water added to the ocean surface, the halosteric effect contributes a 0.38 mm contraction of the water thickness. That is, the total volume of homogenized water equals to the sum of the volume initially in the two separate buckets to within better than 0.04%. We conclude that the volume change is almost entirely barystatic, so that the global halosteric effect is entirely negligible when considering global sea level changes. Furthermore, it is notable that the global halosteric changes are negative, so that we expect the salinity changes to reduce sea level relative to the case in its absence. As noted by [Gebbie \(2020\)](#), the global halosteric contraction becomes somewhat larger when accounting for the addition of pressure effects as needed for paleoclimate studies.

It is important to emphasize that this bucket thought experiment only concerns global sea level. Regional halosteric effects can be important for studies of sea level patterns, and as such they are the topic of many studies such as [Griffies et al. \(2014\)](#).

What about global thermosteric sea level changes from melt?

The above derivation for the global halosteric changes can be directly transferred to the case of mixing two buckets whose water has different Conservative Temperatures but identical pressure and salinity. Conservation of salt is here replaced by conservation of potential enthalpy, so that

¹⁵We measure the haline contraction coefficient, $\beta = 0.8 \times 10^{-3}$, as $\beta = \rho^{-1} \partial \rho / \partial S = 10^{-3} \rho^{-1} \partial \rho / \partial S$. The product $\beta \delta S_1$ is invariant to whether we use salinity or salt concentration.

¹⁶Depending on the sample size, $\delta S_1 = S/2$ is far larger than ocean salinity changes affected by mixing meltwater with ambient seawater in the upper ocean. So the value for $\delta h/h_1$ in equation (8.117) is likely an upper bound for what one might expect in an oceanographic setting.

the relative thickness change is given by

$$\delta h/h_1 = \alpha \delta \Theta_1 (1 - \rho_1/\rho_2), \quad (8.118)$$

where α is the thermal expansion coefficient. Taking $\alpha \approx 2 \times 10^{-4} \text{ K}^{-1}$, we find that δh from thermal effects are on the same order as those from haline effects given by equation (8.116). That is, the contributions to the column thickness are dominated by the barystatic (mass) effects.

However, there is a key distinction between how the ocean is forced by thermal and haline effects. Namely, ocean thermal properties are affected by boundary radiant and turbulent enthalpy fluxes that are not necessarily associated with boundary mass fluxes. These boundary heat fluxes were studied in Section 8.7.5, where we identified the key role for ocean warming on global thermosteric sea level changes. Such changes are certainly not negligible. Indeed, they compare to the observed global barystatic sealevel changes.

Comments

We conclude from this subsection that melting land ice, as conceived for near future climate change, alters global mean sea level almost exclusively through barystatic effects. Barystatic sea level is transferred very quickly around the World Ocean via barotropic waves. [Lorbacher et al. \(2012\)](#) present model simulations that emphasize the important distinctions between barotropic wave signals of barystatic sea level changes, versus the baroclinic signals associated with steric changes. Global steric effects from meltwater are negligible for near future climate change, though [Gebbie \(2020\)](#) noted its relative increased importance for paleoclimate studies, in which thermosteric, halosteric, and barosteric (due to pressure changes), are sizable. Furthermore, even for modern climate change, once meltwater enters the ocean, it contributes to local steric effects through impacts on temperature and salinity. These local steric effects are transported via advection and diffusion throughout the ocean, thus affecting sea level in the far field away from the melt source, yet doing so on the much longer baroclinic time scales whereas barystatic effects are transmitted on barotropic time scales.

8.7.7 Further study

The discussion of steric and thermosteric sea level changes are further explored in [Griffies and Greatbatch \(2012\)](#) and [Griffies et al. \(2014\)](#).



8.8 Exercises

EXERCISE 8.1: A TIDY FORM FOR CABBELING AND THERMOBARICITY

Introduce the [thermobaricity](#) parameter from equation (8.36) and the [cabbeling](#) parameter from equation (8.37) to write the bracket terms appearing in equation (8.35) in forms consistent with those written by [McDougall \(1987b\)](#), in which we have

$$\left[\frac{D\rho}{Dt} \right]_{\text{ntrldiff}} = -\mathbf{J}^{(\Theta)} \cdot (\mathcal{T} \nabla p + \mathcal{C} \nabla \Theta), \quad (8.119)$$

thus enabling us to write the material time evolution of *in situ* density due to neutral diffusion

$$\left[\frac{D\rho}{Dt} \right]_{\text{ntrldiff}} = -\mathbf{J}^{(\Theta)} \cdot (\mathcal{T} \nabla p + \mathcal{C} \nabla \Theta). \quad (8.120)$$

EXERCISE 8.2: MISSING STEPS IN BUOYANCY FLUX DERIVATION

Fill in the missing steps needed to derive equation (8.79) for the buoyancy flux crossing the surface of the ocean.

EXERCISE 8.3: GLOBAL WARMING COMPARED TO ATOMIC BOMBS

To gauge the magnitude of a global warming of 1 W m^{-2} distributed over the ocean surface area, A , compare that to the enthalpy flux due to blasting an atomic bomb every second ($\Delta t = 1 \text{ s}$) and uniformly distributing the bomb's released energy, $\mathcal{E}_{\text{bomb}}$, over the ocean surface area every second. For this estimate, assume $\mathcal{E}_{\text{bomb}} \approx 6.3 \times 10^{13} \text{ J}$. How many bombs are needed to generate 1 W m^{-2} ?

EXERCISE 8.4: GLOBAL SEA LEVEL IN A BOUSSINESQ OCEAN

As seen in VOLUME 1 and VOLUME 2, the sea level for a Boussinesq ocean evolves according to the kinematic free surface equation

$$\partial_t \eta^{\text{bouss}} = -\nabla \cdot \mathbf{U} + Q_m / \rho_0, \quad (8.121)$$

where

$$\mathbf{U} = \int_{-H}^{\eta^{\text{bouss}}} \mathbf{u} dz \quad (8.122)$$

is the depth integrated horizontal velocity and ρ_0 is the Boussinesq reference density. Discuss the corresponding equation for the evolution of global mean sea level in this Boussinesq ocean. What is missing?

EXERCISE 8.5: TO MELT OR TO EXPAND?

Following [Trenberth \(2009\)](#) and [Griffies and Greatbatch \(2012\)](#), we ask where is heating most effective at raising global sea level? Is it more effective when used to melt land ice and allow the melt water to enter the ocean? Or should the heating go directly into warming the ocean, thus impacting a thermosteric sea level rise? The answer to this question is determined by fundamental properties of seawater. Discuss the answer.

EXERCISE 8.6: SEA LEVEL TENDENCY AND CONSERVATIVE TRACERS

Consider an arbitrary conservative tracer, C . The time tendency for the total amount of tracer in the global ocean is given by

$$\frac{d}{dt} \int_{\mathcal{R}} \rho C dV = \int_{\partial \mathcal{R}} Q_C dA, \quad (8.123)$$

where Q_C is the boundary flux of the tracer. Show that we can write the global mean sea level tendency as

$$\frac{d\bar{\eta}}{dt} = \frac{1}{\langle \rho C \rangle} \left[\bar{Q}_C - \frac{V}{A} \frac{d\langle \rho C \rangle}{dt} \right], \quad (8.124)$$

which is expresses the tendency in terms of changes in the density weighted concentration of the conservative tracer. Discuss this equation and contrast it to equation (8.93) based on the mass budget.

EXERCISE 8.7: THE VARIETIES OF LOCAL SEA LEVEL TENDENCIES

In this exercise we follow [Griffies and Greatbatch \(2012\)](#) to derive some equations for the time tendency of the sea level.

- (a) Starting from the seawater mass [continuity](#) equation

$$\frac{1}{\rho} \frac{D\rho}{Dt} = -\nabla \cdot \mathbf{v}, \quad (8.125)$$

and using the surface and bottom [kinematic boundary conditions](#), derive the following kinematic sea level equation

$$\frac{\partial \eta}{\partial t} = \frac{Q_m}{\rho(\eta)} - \nabla \cdot \mathbf{U} - \int_{\eta_b}^{\eta} \frac{1}{\rho} \frac{D\rho}{Dt} dz, \quad (8.126)$$

where we introduced the depth integrated horizontal velocity,

$$\mathbf{U} = \int_{\eta_b}^{\eta} \mathbf{u} dz. \quad (8.127)$$

Equation (8.126) decomposes the sea level tendency into a contribution from boundary mass fluxes, the convergence of the depth integrated flow, and the depth integrated non-Boussinesq steric effect. Note that for the Boussinesq ocean, the non-Boussinesq steric effect is missing ([Griffies and Greatbatch \(2012\)](#) offered a thorough study of this term).

- (b) Consider the mass budget for a column of fluid

$$\frac{\partial}{\partial t} \int_{\eta_b}^{\eta} \rho dz = Q_m - \nabla \cdot \mathbf{U}^\rho, \quad (8.128)$$

where we introduced the depth integrated density-weighted horizontal velocity,

$$\mathbf{U}^\rho = \int_{\eta_b}^{\eta} \rho \mathbf{u} dz. \quad (8.129)$$

Using these definitions, derive the following kinematic sea level equation

$$\frac{\partial \eta}{\partial t} = \frac{Q_m - \nabla \cdot \mathbf{U}^\rho}{\bar{\rho}^z} - \frac{H + \eta}{\bar{\rho}^z} \frac{\partial \bar{\rho}^z}{\partial t}, \quad (8.130)$$

where we introduced the depth averaged density,

$$\bar{\rho}^z = \frac{1}{H + \eta} \int_{\eta_b}^{\eta} \rho dz. \quad (8.131)$$

Equation (8.130) is directly related to equation (8.126), though each term is slightly different.

- (c) Consider an approximate hydrostatic fluid, in which the ocean bottom pressure, p_b , is given by

$$p_b - p_a = g \int_{\eta_b}^{\eta} \rho dz, \quad (8.132)$$

where p_a is the applied surface pressure. Use this equation, along with equation (8.130),

to derive the following expression for the time tendency of the sea level

$$\frac{\partial \eta}{\partial t} = \frac{g^{-1} \partial_t (p_b - p_a)}{\bar{\rho}^z} - \frac{H + \eta}{\bar{\rho}^z} \frac{\partial \bar{\rho}^z}{\partial t}. \quad (8.133)$$

- (d) Consider again the approximate hydrostatic fluid that satisfies equation (8.132). Derive the following sea level equation, which is a slight modification to equation (8.133)

$$\frac{\partial \eta}{\partial t} = \frac{g^{-1} \partial_t (p_b - p_a)}{\rho(\eta)} - \frac{1}{\rho(\eta)} \int_{\eta_b}^{\eta} \frac{\partial \rho}{\partial t} dz \quad (8.134)$$

- (e) Discuss why the global area mean of the local steric sealevel change

$$A^{-1} \int \left[\frac{\partial \eta}{\partial t} \right]_{\text{steric}} dA = -A^{-1} \int \left[\frac{1}{\rho(\eta)} \int_{\eta_b}^{\eta} \frac{\partial \rho}{\partial t} dz \right] dA \quad (8.135)$$

does not equal to the global steric change studied in Section 8.7.4,

$$A^{-1} \int \left[\frac{\partial \eta}{\partial t} \right]^{\text{steric}} dA \neq -\frac{V}{A \langle \rho \rangle} \frac{d \langle \rho \rangle}{dt}. \quad (8.136)$$



Chapter 9

WATER MASS TRANSFORMATION THEORY

In ocean physics, a [water mass](#) refers to a region of seawater characterized by a suite of physical properties. Water masses often originate through extremely large air-sea and ice-sea buoyancy fluxes at the high latitudes that form waters such as the Antarctic Bottom Water and North Atlantic Deep Water. As these waters enter the ocean interior they are transported over basin scales while they are eroded or transformed by irreversible mixing or sources. Water masses and their properties offer a conceptual means to partition or bin the fluid into distinct classes whose origin, movement, and transformation can be measured, modeled, and studied. Scalar properties generally used to classify water masses are simpler to measure than vector properties such as velocity. Hence, a water mass perspective offers the means to infer ocean circulation within the space of ocean properties without directly measuring vector fields. Such circulation inferences have been used since the early days of ocean circulation theory (e.g., [Sverdrup \(1947\)](#)).

In this chapter we develop the mathematical and physical basis for [water mass transformation](#) theory, which examines the budgets for fluid mass and tracer mass within layers or classes defined by properties such as buoyancy, Conservative Temperature, salinity, or biogeochemical tracers. Water mass transformation theory originates from the work of [Walin \(1977\)](#) and [Walin \(1982\)](#), and it has found many advances in both formalism and application since then (see [Groeskamp et al. \(2019\)](#) for a review). A water mass transformation perspective on circulation offers a valuable lens for describing and understanding how processes affect budgets and circulation as viewed in property space. This kinematic lens is distinct from the Eulerian and Lagrangian kinematics considered elsewhere in this book. It has proven to be particularly useful for examining questions where the irreversible transformation of properties plays a central role.

CHAPTER GUIDE

We make use of vector calculus (VOLUME 1), and mass and tracer budget kinematics (VOLUME 2). Additionally, we use basic results from [generalized vertical coordinates](#) in Part I of this volume. Finally, and perhaps most importantly, this chapter relies on our study of advection and diffusion from Chapters 4 and 5; aspects of parameterized tracer transport and mixing studied in Chapter 7; and buoyancy budgets in Chapter 8, including boundary conditions.

9.1 Conceptual framework	287
9.1.1 The distinct lens of water mass configuration space	287
9.1.2 Transformation and formation	288

9.2	Buoyancy transformation and formation	289
9.2.1	A three-layer thought experiment	289
9.2.2	How processes lead to transformations	290
9.3	Mathematical tools	292
9.3.1	Fluid mass in an infinitesimal cylinder	292
9.3.2	Fluid mass within a finite region	293
9.3.3	Fluid mass distribution function	293
9.3.4	Example regions	294
9.3.5	Integrals of arbitrary functions over regions	296
9.3.6	Moments of λ	297
9.3.7	Internal and external λ -moments	297
9.3.8	Further study	298
9.4	Water mass transformation across an internal λ-surface	298
9.4.1	Dia-surface flux and interior transformation	298
9.4.2	Dia-surface flux from diffusion and steady state balances	300
9.4.3	Transformation as the derivative of an integral	300
9.4.4	Kinematic and process methods of water mass transformation	301
9.4.5	General properties of interior transformation due to diffusion	303
9.4.6	Interior versus boundary water mass transformation	305
9.5	Budget for fluid mass in a $\Delta\lambda$-layer	306
9.5.1	Mass transport crossing interior open boundaries	306
9.5.2	Mass transport crossing the ocean surface	306
9.5.3	Mass budget and water mass formation	307
9.5.4	Mass budget and formation in terms of distribution functions	307
9.6	Mass budget for λ within a λ_∞-region	308
9.6.1	Processes affecting the mass of λ -stuff	308
9.6.2	Summary of the λ budget	311
9.6.3	Processes leading to water mass transformation	311
9.6.4	Water mass formation	313
9.6.5	Interior water mass transformation from diffusion	313
9.6.6	Surface water mass transformation	315
9.7	Buoyancy water mass transformation	316
9.7.1	Material time changes to S and Θ	316
9.7.2	Interior buoyancy water mass transformation	317
9.7.3	Surface non-advective flux for S and Θ	317
9.7.4	Surface buoyancy water mass transformation	317
9.8	Tracer water mass transformation within γ-layers	319
9.8.1	General form of the mass budget	319
9.8.2	Tracer processes	320
9.8.3	Transport across an interior layer interface	321
9.8.4	Transport across interior and surface boundaries	322
9.8.5	The layer tracer budget	323
9.8.6	Further study	323
9.9	Regions bounded by a tracer contour/surface	323
9.9.1	Closed region bounded by a tracer surface/contour	323
9.9.2	Region with $C \geq \tilde{C}$	325
9.9.3	Comments and further study	327
9.10	Exercises	327

9.1 Conceptual framework

Water mass transformation theory is a mathematical formalism that supports the study of budgets for fluid mass and tracer mass within layers or classes defined by properties such as Archimedean buoyancy (see VOLUME 2; shortened to **buoyancy** here), **Conservative Temperature**, **salinity**, or biogeochemical tracers. The theory is concerned with how processes affect the evolution of fluid within property space and in the characterization of circulation inferred from this evolution.

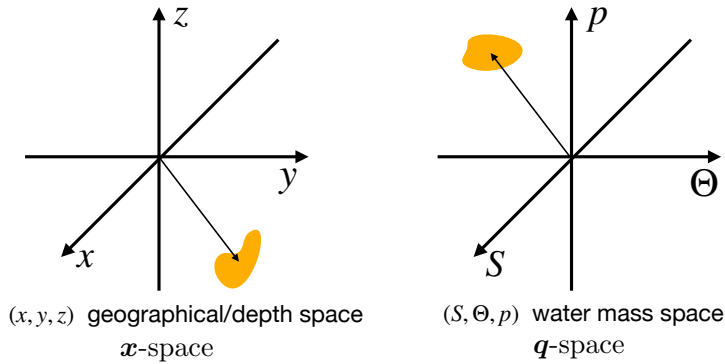


FIGURE 9.1: Left panel: a fluid element is positioned in geographical/depth \pmb{x} -space according to its horizontal (x, y) (longitude, latitude) position and its vertical geopotential, z . Right panel: the same fluid element is positioned in a particular water mass configuration space (\pmb{q} -space), here defined by $\pmb{q} = (S, \Theta, p)$ with salinity, S , Conservative Temperature, Θ , and pressure, p . Mapping between the two spaces is generally not 1-to-1. Namely, a point in \pmb{q} -space can be occupied by more than one point in \pmb{x} -space. The reason is that more than a single point in \pmb{x} -space can have the same values for (S, Θ, p) . Although the coordinate axes in \pmb{q} -space are depicted here as mutually orthogonal, there is no objective means to determine angles in \pmb{q} -space since it contains no metric. Rather, \pmb{q} -space, just like thermodynamic state space (see the chapters on thermodynamics in VOLUME 2), forms a **differentiable manifold** that has no metric.

9.1.1 The distinct lens of water mass configuration space

Water mass configuration space (denoted by \pmb{q} -space) is the space we work within to study water mass transformations.¹ This space has some or all of its coordinates set by properties other than geographic/depth coordinates. For example, in Figure 9.1 we present the three-dimensional \pmb{q} -space given by $\pmb{q} = (S, \Theta, p)$, where the position (or bin) for a fluid element is determined by its Conservative Temperature, Θ , salinity, S , and pressure, p . Operationally, we fill \pmb{q} -space by forming histograms that result in a \pmb{q} -space distribution of the fluid properties. For example, a one-dimensional \pmb{q} -space results from binning the ocean according to potential density, whereas retaining latitudinal information along with potential density renders a two-dimensional \pmb{q} -space. Typically \pmb{q} -space has three or fewer dimensions, given the three dimensionality of \pmb{x} -space. There is no implied constraint that any of the \pmb{q} -space coordinates are monotonic with respect to \pmb{x} -space. Indeed, there is no presumption that points in \pmb{q} -space maintain a 1-to-1 relation to points in \pmb{x} -space. For example, many points in \pmb{x} -space may fall into a single point (or bin) within \pmb{q} -space.

The lack of 1-to-1 mapping between water mass configuration space and geographic/depth space is a fundamental kinematic distinction from the 1-to-1 relation that holds between the

¹We prefer the term “configuration space” over the alternative “phase space”, since phase space in Hamiltonian dynamics specifically refers to position and momentum coordinates (see VOLUME 1). In contrast, configuration space, as used in our discussion of water masses, can be determined by almost any property or geographic position.

Eulerian reference frame and Lagrangian reference frame used for describing fluid motion (see the kinematics chapters in VOLUME 2). The lack of a 1-to-1 relation can be frustrating since circulation viewed in \mathbf{q} -space generally has incomplete \mathbf{x} -space information.² Even so, abandoning the 1-to-1 relation can be liberating since working within \mathbf{q} -space offers a framework to infer \mathbf{q} -space circulation even without measuring velocity of the fluid in geographical space. Correspondingly, ocean circulation when viewed through a water mass lens can offer understanding that complements traditional Eulerian or Lagrangian views.

Water mass configuration space generally has no metric, particularly when none of the chosen coordinates are geographical (latitude or longitude) or depth. Hence, there is generally no notion of distance or angles between points in water mass configuration space. For example, what does it mean to be orthogonal in temperature-salinity space or when studying the density-binned distribution of seawater? The absence of a metric is something we have already seen when studying thermodynamic configuration space in VOLUME 1. Mathematically, we say that both thermodynamic configuration space and water mass configuration space are [differentiable manifolds](#). Even so, one commonly sees a point in thermodynamic space depicted on a diagram with orthogonal axes (e.g., pressure-volume diagrams), or a position in water mass configuration space similarly depicted with orthogonal axes as in Figure 9.1. This depiction is arbitrary since these spaces contain none of the necessary geometric structure required to define a metric tensor. Hence, we have no objective means to determine angles or orthogonality. Depictions of property space using orthogonal axes satisfy a subjective desire for geometric structure when in fact there is none afforded to the underlying differentiable manifold.

9.1.2 Transformation and formation

Force imbalances lead to the motion of a fluid element through \mathbf{x} -space as captured by Newton's laws of motion. Likewise, [transformation](#) processes³ render motion in water mass configuration space (\mathbf{q} -space). That is, a fluid moves through \mathbf{q} -space if it is transformed in a manner that causes water to cross surfaces of constant \mathbf{q} . It follows that the convergence (local accumulation) or divergence (local depletion) of transformation leads to the [formation](#) of water mass classes, or its negative, being the destruction of water masses. Processes leading to transformation arise from mixing, solar radiation, and chemical reactions. Correspondingly, we measure zero motion along a \mathbf{q} -space coordinate axis when the property defining that axis remains materially unchanged. For example, adiabatic and isohaline processes such as linear waves can render nontrivial motion in geographical/depth space whereas they lead to no motion in (S, Θ) space.

Given the generally non-local and non-invertible relation between \mathbf{x} -space and \mathbf{q} -space, we find that \mathbf{q} -space is an unnatural kinematic venue to study forces and stresses acting between spatially adjacent fluid elements. Hence, the study of momentum and vorticity dynamics is more suitably handled via Eulerian or Lagrangian kinematics. Where water mass configuration space shines is by revealing the \mathbf{q} -space circulation effects from processes that affect material changes to fluid properties. For example, a water mass perspective has found use in framing key questions of primary interest in the Anthropocene, such as ocean buoyancy and its transformation through interior and boundary mixing, ocean heat uptake and transport, the hydrological cycle, steric

²Auxiliary methods such as the water tagging method of [Groeskamp et al. \(2014\)](#) can be used to recover some geographical information.

³In many parts of this book the word “transformation” refers to mathematical coordinate transformations, thus referring to a change of reference or change of description. Here, “transformation” refers to a physical process acting to change a property of a fluid element, thus acting to change one or more of the \mathbf{q} -space coordinates of a fluid element.

sea level rise, and irreversible changes to biogeochemical properties (see [Groeskamp et al. \(2019\)](#) for a review).

9.2 Buoyancy transformation and formation

Archimedean buoyancy is a common property used to partition or bin geophysical fluids into classes, with Archimedean buoyancy often approximated by potential density. In this section we introduce the notions of [transformation](#) and [formation](#) when partitioning the ocean according to density (γ) classes that locally measure buoyancy. The ideas presented here extend to any scalar property used to bin the ocean fluid.

Quantitatively, the transformation of fluid provides a measure of the mass per time that fluid moves across an isosurface of one of the \mathbf{q} -space coordinates. Hence, water mass transformation refers to the movement of water from one \mathbf{q} -space bin to another bin within the \mathbf{q} -space mass distribution. We here follow the convention whereby the transformation is positive if water moves to a larger value of a particular \mathbf{q} -space coordinate (e.g., higher density class), and negative if water moves to a smaller value for the \mathbf{q} -space coordinate (e.g., lower density class). Water mass [formation](#) refers to the difference in transformation across the surfaces bounding a layer, so that formation measures the change in seawater mass of the layer.

The formation is the layer integrated \mathbf{q} -space convergence of transformation, with both formation and transformation having dimensions of mass per time (or volume per time when considering a [Boussinesq ocean](#)). We typically measure transformation and formation using Sverdrup units:

$$1 \text{ Sv} = 10^6 \text{ m}^3 \text{ s}^{-1} \quad \text{volume-Sverdrup} \quad (9.1a)$$

$$1 \text{ Sv} = 10^9 \text{ kg s}^{-1} \quad \text{mass-Sverdrup.} \quad (9.1b)$$

The mass-Sverdrup can be routinely used for Boussinesq fluids merely by multiplying the volume-Sverdrup by the constant Boussinesq reference density, ρ_0 .

9.2.1 A three-layer thought experiment

To illustrate the concepts of transformation and formation, bin the World Ocean into density (γ) classes so that \mathbf{q} -space is just one dimensional. In performing the binning, we lose all information about latitude, longitude, and depth, while retaining information provided by γ -classes. Furthermore, partition the World Ocean into just three density classes (layers or bins) that are bounded by four density interfaces:

$$\text{light density layer} = [\gamma - \delta\gamma/2, \gamma + \delta\gamma/2] \quad (9.2a)$$

$$\text{middle density layer} = [\gamma + \delta\gamma/2, \gamma + 3\delta\gamma/2] \quad (9.2b)$$

$$\text{heavy density layer} = [\gamma + 3\delta\gamma/2, \gamma + 5\delta\gamma/2], \quad (9.2c)$$

where $\delta\gamma > 0$ is the size of the density bins. Figure 9.2 depicts a sample mass distribution; i.e., the mass census for seawater binned into these three density layers.⁴ Now consider a physical, chemical, or biological process that results in water leaving the middle density layer

⁴A realistic ocean is confronted with boundary forcing that causes the maximum and minimum density to be a function of time. It is thus common to fix the lower density limit to be well below the lightest water in the ocean and the upper density limit well above the maximum density, thus ensuring that all seawater is contained within the chosen binning. We introduce such “infinity” bounds in Section 9.3.3.

and entering both the light layer and the heavy layer.⁵ Let $G(\sigma)$ measure the mass per time that water crosses the density interface $\gamma = \sigma$; i.e., $G(\sigma)$ is the transformation. This particular thought experiment has the following transformations across the various layer interfaces

$$G(\sigma) = \begin{cases} 0 & \sigma = \gamma - \delta\gamma/2 \quad \text{closed boundary} \\ < 0 & \sigma = \gamma + \delta\gamma/2 \quad \text{mass moves to light density from middle density} \\ > 0 & \sigma = \gamma + 3\delta\gamma/2 \quad \text{mass moves from middle density to heavy density} \\ 0 & \sigma = \gamma + 5\delta\gamma/2 \quad \text{closed boundary.} \end{cases} \quad (9.3)$$

The difference in the transformation across the interface boundaries of a particular layer determines the formation/destruction of water in that layer. Here, the convergence of water into the light and heavy layers means that there is a positive formation of water in these two density layers. In contrast, the divergence of water from the middle density layer means there is a negative formation or a destruction of some of its water. We write these layer formations mathematically as follows

$$\text{light-formation} = -[G(\gamma + \delta\gamma/2) - G(\gamma - \delta\gamma/2)] > 0 \quad (9.4a)$$

$$\text{middle-formation} = -[G(\gamma + 3\delta\gamma/2) - G(\gamma + \delta\gamma/2)] < 0 \quad (9.4b)$$

$$\text{heavy-formation} = -[G(\gamma + 5\delta\gamma/2) - G(\gamma + 3\delta\gamma/2)] > 0. \quad (9.4c)$$

The minus sign out front emphasizes that the formation is the layer integrated convergence of the transformation.

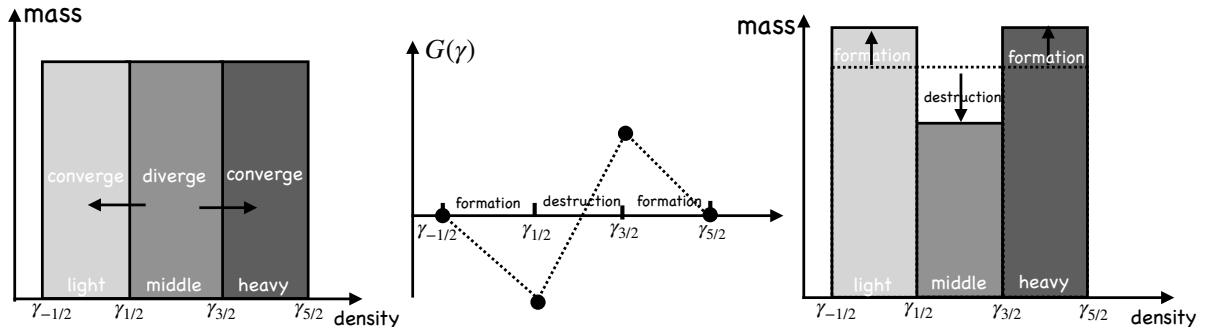


FIGURE 9.2: A sample mass distribution of the ocean binned into three density layers (light, middle, heavy) bounded by four density interfaces: $\gamma_{n/2} = \gamma + n\delta\gamma/2$ for $n = -1, 1, 3, 5$. The left panel depicts an ocean state with equal mass in each layer. Some process is then imagined to cause water to diverge from the middle layer and converge to the light and heavy layers. The right panel shows the mass distribution after the water has moved, so that the middle layer has experienced a negative formation (i.e., net loss or destruction of water mass) whereas the light and heavy layers have experienced a positive formation (i.e., net mass gain). The middle panel depicts the transformation, G , which measures the mass per time moving across the layer boundaries. By convention, $G > 0$ for water moving into a heavier density layer and $G < 0$ for water entering a lighter density layer. The addition of more layers refines the picture (e.g., by smoothing the plot of G) but it does not modify the basic ideas illustrated in this thought experiment.

9.2.2 How processes lead to transformations

Here we outline a few of the processes that affect circulation within water mass space, again focusing on buoyancy yet with easy generalization to any other property used to define a water

⁵Since the layer is the result of binning over the World Ocean, there can be some regions within a bin that experience processes that decrease the density, whereas other regions where density increases. In this manner, some water within the bin moves to a denser bin whereas other water moves to a lighter bin.

mass coordinate.

Interior transformation from mixing

Mixing moves water across layer boundaries in q -space, with q -space coordinates/properties materially modified in the presence of mixing (so long as there are spatial gradients in the property). For example, in our study of tracer kinematics in VOLUME 2, we consider how mixing causes tracers to move between fluid elements even as mixing does not alter the net mass of fluid elements, with the [barycentric velocity](#) playing a central role in that theory. Hence, in the presence of mixing, seawater fluid elements retain a fixed mass, and yet the mass is redistributed among layers defined by property isosurfaces since the isosurfaces move in the presence of mixing.

Surface mass fluxes

Precipitation, runoff, and evaporation alter the mass of the ocean. In turn, the layers where precipitation, runoff, and evaporation occur (layers that outcrop) have their mass altered through the surface mass fluxes. Additionally, if properties of the mass flux (e.g., temperature, salinity) differ from that of the ocean layer that it enters/leaves, then the properties of the ocean layer are modified upon mixing the ambient seawater with the water crossing the ocean surface boundary.

Surface and bottom boundary transformation

Surfaces of constant buoyancy that outcrop at the ocean surface or incrop at the ocean bottom are exposed to boundary fluxes that generally modify the buoyancy of the fluid within a layer. This modification causes the layer boundaries to move so that the mass distributed within the layers can be modified if the mass moves with a velocity distinct from the buoyancy surface. A particularly striking example occurs in the upper ocean boundary layer where surface boundary fluxes lead to the seasonal migration of density outcrops. The associated lateral movement of density layers causes water to entrain and detrain from a layer since the layer boundaries generally have a velocity distinct from fluid elements. In so doing, the seasonal cycle of surface buoyancy forcing can inflate or deflate a buoyancy layer by moving the layer boundaries so that the layer entrains or detrains mass. We return to this example when discussing Figure 9.14 when studying transformations due to surface boundary buoyancy fluxes.

Penetrative shortwave radiation provides another means to modify water masses, with penetrative radiation a function of the optical properties of the fluid. This radiation provides a heat source that can penetrate into the upper tens of meters in the ocean, and can impact on the temperature and density structure of the ocean layers affected by radiation.

Layers that intersect the ocean bottom are exposed to geothermal heating as well as enhanced mixing from turbulent bottom boundary layer processes. Each of these processes affects a transformation of the buoyancy, thus modifying the buoyancy layer interfaces and mass distribution within the layers.

Interior sources and sinks

When studying water masses defined by biogeochemical tracers (e.g., carbon, oxygen, nutrients), there are a variety of chemical reactions and biological processes that act to modify these properties. These processes generally cannot be represented mathematically as the convergence

of a flux, and so they are commonly referred to as a **non-conservative process**. They appear mathematically as a source/sink term in the tracer equation.

9.3 Mathematical tools

In this section we develop a suite of mathematical tools to quantify the conceptual ideas presented in Sections 9.1 and 9.2. In particular, we develop a formalism for integrating properties within a region bounded by isosurfaces of a scalar field, $\lambda = \lambda(\mathbf{x}, t)$. The formulation is given from a geometric perspective afforded by \mathbf{x} -space. It is also given from the complementary distributional perspective afforded by binning seawater mass according to λ -classes that define a one-dimensional \mathbf{q} -space (extensions to higher \mathbf{q} -space dimensions are straightforward).

In Section 9.2 we considered λ to be the buoyancy field, $\lambda = \gamma$, whereas here we assume it is a generic scalar field, $\lambda(\mathbf{x}, t)$. In contrast to the case of a **generalized vertical coordinate** (Part I), λ -isosurfaces are free to overturn or even to be situated in spatially disconnected regions. This freedom is motivated by the behavior of most ocean scalar properties, which commonly exhibit vertically unstratified or negatively stratified profiles, particularly within boundary layers. As mentioned in Section 9.1.1, this freedom comes at the cost of losing the 1-to-1 relation between \mathbf{x} -space and \mathbf{q} -space.

9.3.1 Fluid mass in an infinitesimal cylinder

Consider the calculation of fluid mass within an infinitesimal λ -layer bounded by two isosurfaces, $[\lambda - \delta\lambda/2, \lambda + \delta\lambda/2]$, as depicted in Figure 9.3. The mass within a tiny cylinder extending from one interface to the other is given by the fluid density, ρ , multiplied by the volume of the cylinder,⁶

$$\delta M = \rho \delta V = \rho \delta h \delta \mathcal{S}, \quad (9.5)$$

where $\delta \mathcal{S}$ is the cross-sectional area element and δh is the layer thickness. The geometric thickness, δh , is related to the differential λ -increment separating the two interfaces according to

$$\delta \lambda = \nabla \lambda \cdot \delta \mathbf{x} = |\nabla \lambda| \hat{\mathbf{n}} \cdot \delta \mathbf{x} = |\nabla \lambda| \delta h \quad \text{with} \quad \hat{\mathbf{n}} = \nabla \lambda |\nabla \lambda|^{-1}, \quad (9.6)$$

where $\delta \mathbf{x}$ is a position vector connecting points on the two interfaces. We thus see that the layer thickness is given by

$$\delta h = \frac{\delta \lambda}{|\nabla \lambda|}, \quad (9.7)$$

which connects a geometric property of the layer, $\delta h > 0$, to the λ -increment, $\delta \lambda > 0$. For a given λ -increment, the layer thickness is smaller with more tightly packed λ -isosurfaces as reflected by a larger $|\nabla \lambda|$. Furthermore, the geometric thickness is oriented according to the normal direction, $\hat{\mathbf{n}}$, so that δh measures the distance between the λ -interfaces in the direction of the normal. It follows that the fluid mass within the cylinder is given by

$$\delta M = \rho \delta V = \rho \delta h \delta \mathcal{S} = \frac{\rho \delta \lambda \delta \mathcal{S}}{|\nabla \lambda|}. \quad (9.8)$$

⁶Recall our notational convention is as follows: δ refers to an infinitesimal increment of a property measured within the fluid whereas d is a differential increment used for computing integrals.

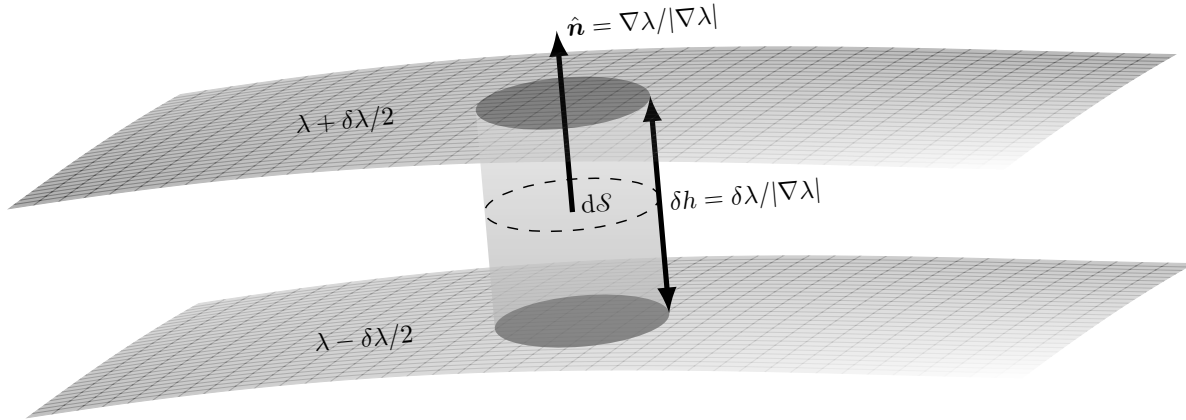


FIGURE 9.3: Depicting an infinitesimally thin λ -layer bounded by two interfaces $[\lambda - \delta\lambda/2, \lambda + \delta\lambda/2]$, with the λ -increment, $\delta\lambda > 0$. The cylinder extends between the two iso-surfaces and it has thickness, $\delta h = \delta\lambda/|\nabla\lambda|$, and cross-sectional area, δS . The cylinder is oriented according to the normal direction, $\hat{n} = |\nabla\lambda|^{-1} \nabla\lambda$, which points in the direction of increasing λ . We assume $|\nabla\lambda| \neq 0$, as required to define a normal direction. Indeed, if $\nabla\lambda = 0$ then we could not perform a binning according to λ classes, so the $|\nabla\lambda| \neq 0$ assumption is basic to the use of the scalar field, λ , for water mass analysis.

9.3.2 Fluid mass within a finite region

Making use of the infinitesimal cylinder mass (9.8) allows us to write the mass of fluid within the λ -region, $\lambda_1 \leq \lambda \leq \lambda_2$,

$$M(\lambda_1, \lambda_2) \equiv \int_{\Omega(\lambda_1 \leq \lambda \leq \lambda_2)} dM = \int_{\lambda_1}^{\lambda_2} \left[\int_{\partial\Omega(\lambda)} \frac{\rho dS}{|\nabla\lambda|} \right] d\lambda. \quad (9.9)$$

In this equation, $\Omega(\lambda_1 \leq \lambda \leq \lambda_2)$ is the region in space bounded by the λ_1 -interface and λ_2 -interface, and $\partial\Omega(\lambda)$ is the surface defined by a λ -isosurface. The $\partial\Omega(\lambda)$ integral is taken over the area of the λ -isosurface, which is then integrated over the range, $\lambda_1 \leq \lambda \leq \lambda_2$, to accumulate the layer mass.

9.3.3 Fluid mass distribution function

The region bounded by the layer interfaces can have any shape in \mathbf{x} -space and can even be spatially disconnected. This complexity motivates us to introduce the **mass distribution function** in water mass space by integrating the mass over the surface, $\partial\Omega(\lambda)$

$$m(\lambda) \equiv \frac{dM}{d\lambda} = \int_{\partial\Omega(\lambda)} \frac{\rho dS}{|\nabla\lambda|}. \quad (9.10)$$

Evidently, the mass distribution function is the mass density within λ space; i.e., the mass per λ . As defined, the mass distribution function serves the analog for \mathbf{q} -space that the *in situ* density, $\rho(\mathbf{x})$, does for \mathbf{x} -space:

$$dM = m(\lambda) d\lambda = \text{fluid mass within the infinitesimal } \lambda\text{-layer } [\lambda - d\lambda/2, \lambda + d\lambda/2], \quad (9.11)$$

with an illustration given by Figure 9.4. In practice, the mass distribution function is constructed through binning the ocean mass according to λ -classes, thus producing a histogram that approximates $m(\lambda)$. The mass distribution function then provides the means to compute the

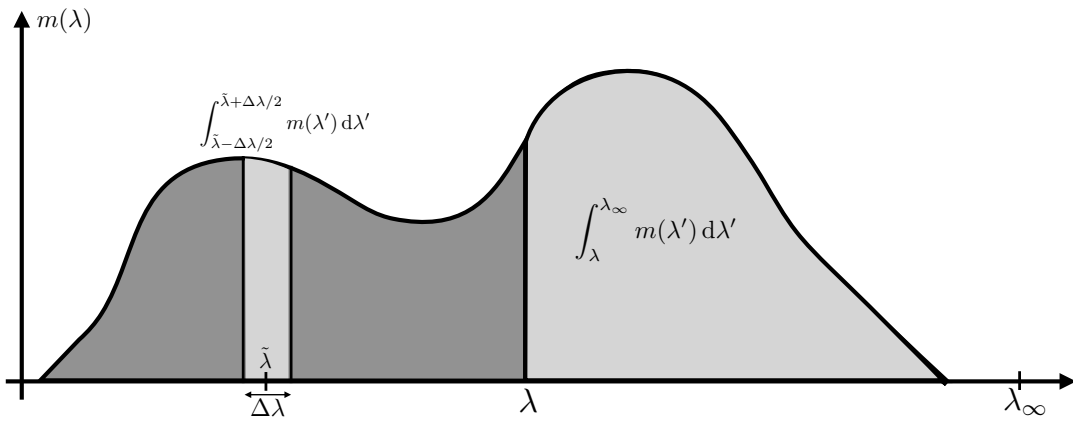


FIGURE 9.4: An example mass distribution function, $m(\lambda) = dM/d\lambda$, which measures the mass of fluid per λ -increment. Integration over a finite λ -region measures the fluid mass within that region. For example, the mass within a $\Delta\lambda$ -layer is given by $M(\tilde{\lambda} - \Delta\lambda/2, \tilde{\lambda} + \Delta\lambda/2) = \int_{\tilde{\lambda} - \Delta\lambda/2}^{\tilde{\lambda} + \Delta\lambda/2} m(\lambda') d\lambda'$ whereas the mass within the λ_∞ -region is $M(\lambda, \lambda_\infty) = \int_{\lambda}^{\lambda_\infty} m(\lambda') d\lambda'$, where we assume that λ_∞ is an arbitrary fixed value that is larger than any λ realized within the ocean.

fluid mass within a finite λ -region as in equation (9.9)

$$M(\lambda_1, \lambda_2) \equiv \int_{\Omega(\lambda_1 \leq \lambda \leq \lambda_2)} dM = \int_{\lambda_1}^{\lambda_2} m(\lambda) d\lambda. \quad (9.12)$$

Extensions to higher dimensional \mathbf{q} -space are straightforward, in which we consider, $m(\mathbf{q})$.

9.3.4 Example regions

To help ground the previous expressions for mass, we here consider some example regions commonly considered in water mass analysis.

$\Delta\lambda$ -layer defined by $[\lambda_1, \lambda_2] = [\lambda - \Delta\lambda/2, \lambda + \Delta\lambda/2]$

A $\Delta\lambda$ -layer is defined with the bounding interface values

$$\lambda_1 = \lambda - \Delta\lambda/2 \text{ and } \lambda_2 = \lambda + \Delta\lambda/2, \quad (9.13)$$

for some finite difference increment $\Delta\lambda > 0$. In this case the layer mass is

$$M(\lambda - \Delta\lambda/2, \lambda + \Delta\lambda/2) = \int_{\lambda - \Delta\lambda/2}^{\lambda + \Delta\lambda/2} \left[\int_{\partial\Omega(\lambda')} \frac{\rho d\mathcal{S}}{|\nabla \lambda'|} \right] d\lambda' = \int_{\lambda - \Delta\lambda/2}^{\lambda + \Delta\lambda/2} m(\lambda') d\lambda'. \quad (9.14)$$

λ_∞ -region defined by $[\lambda_1, \lambda_2] = [\lambda, \lambda_\infty]$

A λ_∞ -region is defined with

$$\lambda_1 = \lambda \text{ and } \lambda_2 = \lambda_\infty, \quad (9.15)$$

where λ_∞ is an arbitrary fixed constant that is larger than any value of λ realized in the ocean. The region mass is thus given by

$$M(\lambda, \lambda_\infty) = \int_{\Omega(\lambda \leq \lambda_\infty)} dM = \int_{\lambda}^{\lambda_\infty} \left[\int_{\partial\Omega(\lambda')} \frac{\rho d\mathcal{S}}{|\nabla \lambda'|} \right] d\lambda' = \int_{\lambda}^{\lambda_\infty} m(\lambda') d\lambda'. \quad (9.16)$$

An example λ_∞ -region is shown in Figure 9.5. The λ_∞ -region as so defined provides an expression for the differential mass increment

$$M(\lambda, \lambda_\infty) = \int_\lambda^{\lambda_\infty} m(\lambda') d\lambda' \implies dM(\lambda, \lambda_\infty) = -m(\lambda) d\lambda, \quad (9.17)$$

which follows since λ_∞ is a constant.

The value of the fixed constant, λ_∞ , is arbitrarily large, indeed it could be infinite. We can set it to an arbitrarily large and constant value since there is no contribution to the integral from regions with λ' outside the range realized within the ocean, merely since there is no ocean mass in that region. As an example, let $\lambda = \Theta$, the Conservative Temperature, in which the region $\Theta \leq \Theta_\infty$ encompasses the ocean region where the Conservative Temperature is larger (warmer) than Θ .

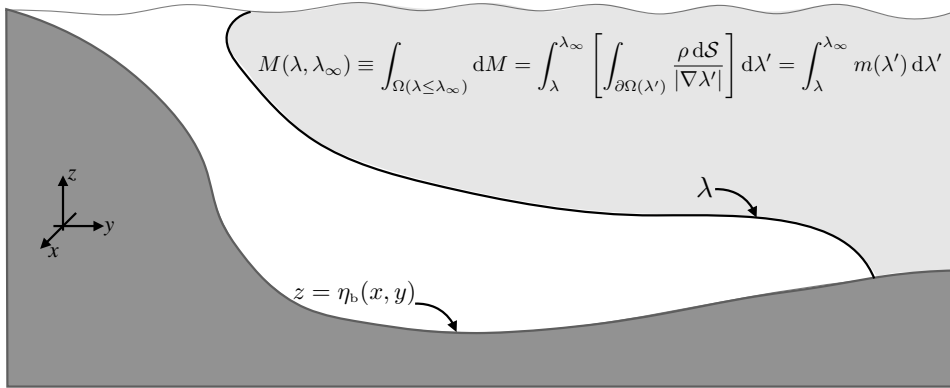


FIGURE 9.5: Depicting the mass of fluid within a λ_∞ -region, where $\lambda \leq \lambda_\infty$ with λ_∞ an arbitrary constant that is larger than any value of λ in the ocean domain. An example of such a region is for $\lambda = \Theta$, whereby warmer waters are typically shallower and towards the equator.

$\lambda_{-\infty}$ -region defined by $[\lambda_1, \lambda_2] = [\lambda_{-\infty}, \lambda]$

A $\lambda_{-\infty}$ -region is defined with

$$\lambda_1 = \lambda_{-\infty} \text{ and } \lambda = \lambda, \quad (9.18)$$

where $\lambda_{-\infty}$ is an arbitrary constant that is smaller than any value of λ realized in the ocean. The region mass is thus given by

$$M(\lambda_{-\infty}, \lambda) \equiv \int_{\Omega(\lambda_{-\infty} \leq \lambda)} dM = \int_{\lambda_{-\infty}}^\lambda \left[\int_{\partial\Omega(\lambda')} \frac{\rho dS}{|\nabla\lambda'|} \right] d\lambda' = \int_{\lambda_{-\infty}}^\lambda m(\lambda') d\lambda'. \quad (9.19)$$

This mass is the complement of that contained in the λ_∞ -region. The $\lambda_{-\infty}$ -region mass implies a corresponding differential mass increment via

$$M(\lambda_{-\infty}, \lambda) = \int_{\lambda_{-\infty}}^\lambda m(\lambda') d\lambda' \implies dM(\lambda_{-\infty}, \lambda) = m(\lambda) d\lambda. \quad (9.20)$$

$\lambda_{\pm\infty}$ -region defined by $[\lambda_1, \lambda_2] = [\lambda_{-\infty}, \lambda_\infty]$

The full ocean is contained in the $\lambda_{\pm\infty}$ -region

$$\lambda_1 = \lambda_{-\infty} \text{ and } \lambda_2 = \lambda_\infty, \quad (9.21)$$

so that the full ocean mass is written

$$M(\lambda_{-\infty}, \lambda_{\infty}) = \int_{\Omega(\lambda_{-\infty} \leq \lambda \leq \lambda_{\infty})} dM = \int_{\lambda_{-\infty}}^{\lambda_{\infty}} \left[\int_{\partial\Omega(\lambda)} \frac{\rho d\mathcal{S}}{|\nabla\lambda|} \right] d\lambda = \int_{\lambda_{-\infty}}^{\lambda_{\infty}} m(\lambda') d\lambda'. \quad (9.22)$$

Difference of mass between two λ_{∞} -regions

The difference in mass between two λ_{∞} -regions is given by

$$M(\lambda_1, \lambda_{\infty}) - M(\lambda_2, \lambda_{\infty}) = \int_{\lambda_1}^{\lambda_{\infty}} \left[\int_{\partial\Omega(\lambda)} \frac{\rho d\mathcal{S}}{|\nabla\lambda|} \right] d\lambda - \int_{\lambda_2}^{\lambda_{\infty}} \left[\int_{\partial\Omega(\lambda)} \frac{\rho d\mathcal{S}}{|\nabla\lambda|} \right] d\lambda. \quad (9.23)$$

The arbitrary constant, λ_{∞} , drops out when taking the difference so that we are left with the mass within the intersection of the two regions

$$M(\lambda_1, \lambda_2) = M(\lambda_1, \lambda_{\infty}) - M(\lambda_2, \lambda_{\infty}) = \int_{\lambda_1}^{\lambda_2} \left[\int_{\partial\Omega(\lambda)} \frac{\rho d\mathcal{S}}{|\nabla\lambda|} \right] d\lambda = \int_{\lambda_1}^{\lambda_2} m(\lambda') d\lambda'. \quad (9.24)$$

9.3.5 Integrals of arbitrary functions over regions

We can extend the above formalism to integrals of an arbitrary function, $F(\mathbf{x}, t)$, over a region defined by the λ_1 and λ_2 interfaces

$$\mathcal{I}_F(\lambda_1, \lambda_2) \equiv \int_{\Omega(\lambda_1 \leq \lambda \leq \lambda_2)} F dM = \int_{\lambda_1}^{\lambda_2} \left[\int_{\partial\Omega(\lambda)} \frac{F \rho d\mathcal{S}}{|\nabla\lambda|} \right] d\lambda. \quad (9.25)$$

Performing the area integral amounts to binning the function according to λ -increments, in which case we define the distribution function

$$m_F(\lambda) = \int_{\partial\Omega(\lambda)} \frac{F \rho d\mathcal{S}}{|\nabla\lambda|}, \quad (9.26)$$

so that an integral over the distribution is given by

$$\mathcal{I}_F(\lambda_1, \lambda_2) = \int_{\lambda_1}^{\lambda_2} m_F(\lambda) d\lambda. \quad (9.27)$$

In particular, consider the integral over a λ_{∞} -region

$$\mathcal{I}_F(\lambda, \lambda_{\infty}) = \int_{\lambda}^{\lambda_{\infty}} \left[\int_{\partial\Omega(\lambda')} \frac{F \rho d\mathcal{S}}{|\nabla\lambda'|} \right] d\lambda' = \int_{\lambda}^{\lambda_{\infty}} m_F(\lambda') d\lambda', \quad (9.28)$$

which has the derivative

$$\frac{\partial \mathcal{I}_F(\lambda, \lambda_{\infty})}{\partial \lambda} = - \int_{\partial\Omega(\lambda)} \frac{F \rho d\mathcal{S}}{|\nabla\lambda|} = -m_F(\lambda), \quad (9.29)$$

as follows from the fundamental theorem of calculus. Note how the derivative removes the arbitrary reference value, λ_{∞} . Analogously, the integral over a $\lambda_{-\infty}$ -region has the derivative

$$\frac{\partial \mathcal{I}_F(\lambda_{-\infty}, \lambda)}{\partial \lambda} = \int_{\partial\Omega(\lambda)} \frac{F \rho d\mathcal{S}}{|\nabla\lambda|} = m_F(\lambda). \quad (9.30)$$

9.3.6 Moments of λ

Setting $F = \lambda$ in the integral (9.25) renders

$$\Lambda(\lambda_1, \lambda_2) \equiv \int_{\Omega(\lambda_1 \leq \lambda \leq \lambda_2)} \lambda \, dM = \int_{\Omega(\lambda_1 \leq \lambda \leq \lambda_2)} \lambda \rho \, dV = \int_{\lambda_1}^{\lambda_2} \left[\int_{\partial\Omega(\lambda)} \frac{\lambda \rho \, dS}{|\nabla \lambda|} \right] \, d\lambda. \quad (9.31)$$

If λ is a tracer concentration (tracer mass per fluid mass), then $\Lambda(\lambda_1, \lambda_2)$ is the mass of tracer within the layer. Observe that λ can be pulled outside of the surface integral in equation (9.31) since λ is constant along $\partial\Omega(\lambda)$, thus rendering

$$\Lambda(\lambda_1, \lambda_2) = \int_{\lambda_1}^{\lambda_2} \left[\int_{\partial\Omega(\lambda)} \frac{\rho \, dS}{|\nabla \lambda|} \right] \lambda \, d\lambda = \int_{\lambda_1}^{\lambda_2} m(\lambda) \lambda \, d\lambda. \quad (9.32)$$

We can likewise define any higher powers as

$$\Lambda^{(n)}(\lambda_1, \lambda_2) \equiv \int_{\lambda_1}^{\lambda_2} \left[\int_{\partial\Omega(\lambda)} \frac{\rho \, dS}{|\nabla \lambda|} \right] \lambda^n \, d\lambda = \int_{\lambda_1}^{\lambda_2} m(\lambda) \lambda^n \, d\lambda = M(\lambda_1, \lambda_2) \langle \lambda^n \rangle. \quad (9.33)$$

The final equality introduced the mean value for the power

$$\langle \lambda^n \rangle = \frac{\int_{\lambda_1}^{\lambda_2} m(\lambda) \lambda^n \, d\lambda}{\int_{\lambda_1}^{\lambda_2} m(\lambda) \, d\lambda} \quad (9.34)$$

as defined over the $[\lambda_1, \lambda_2]$ region. We refer to $\langle \lambda^n \rangle$ as the n -moment of λ , with $n = 1$ yielding the mean.

9.3.7 Internal and external λ -moments

Now specify the region $[\lambda_1, \lambda_2] = [\tilde{\lambda}, \lambda_\infty]$ for the moment equation (9.33). Making use of the differential mass increment, $dM(\lambda, \lambda_\infty) = -m(\lambda) d\lambda$ as in equation (9.17) allows us to integrate the moment equation by parts

$$\Lambda^{(n)}(\tilde{\lambda}, \lambda_\infty) = \int_{\tilde{\lambda}}^{\lambda_\infty} \lambda^n m(\lambda) \, d\lambda \quad (9.35a)$$

$$= - \int_{\tilde{\lambda}}^{\lambda_\infty} \lambda^n \, dM \quad (9.35b)$$

$$= \int_{\tilde{\lambda}}^{\lambda_\infty} [-d(\lambda^n M) + n M \lambda^{n-1} \, d\lambda] \quad (9.35c)$$

$$= -\lambda_\infty^n M(\lambda_\infty, \lambda_\infty) + \tilde{\lambda}^n M(\tilde{\lambda}, \lambda_\infty) + n \int_{\tilde{\lambda}}^{\lambda_\infty} M(\lambda, \lambda_\infty) \lambda^{n-1} \, d\lambda \quad (9.35d)$$

$$= \tilde{\lambda}^n M(\tilde{\lambda}, \lambda_\infty) + n \int_{\tilde{\lambda}}^{\lambda_\infty} M(\lambda, \lambda_\infty) \lambda^{n-1} \, d\lambda, \quad (9.35e)$$

where the final equality follows since $M(\lambda_\infty, \lambda_\infty) = 0$. Making use of equation (9.33) thus leads to

$$M(\tilde{\lambda}, \lambda_\infty) \langle \lambda^n \rangle = \underbrace{M(\tilde{\lambda}, \lambda_\infty) \tilde{\lambda}^n}_{\text{external moment}} + \underbrace{n \int_{\tilde{\lambda}}^{\lambda_\infty} M(\lambda, \lambda_\infty) \lambda^{n-1} \, d\lambda}_{\text{internal moment}}. \quad (9.36)$$

We refer to the rightmost term as the *internal moment* since it is an integral over the region, whereas $M(\tilde{\lambda}, \lambda_\infty) \tilde{\lambda}^n$ is the *external moment*, which is the region mass times the boundary value, $\tilde{\lambda}^n$. We choose the moniker “external” since the external moment increases in direct proportion to the mass crossing the layer boundaries, including the external boundaries. In Section 9.6 we develop a budget for the $n = 1$ moment, in which the internal moment from equation (9.36) takes the form

$$M(\tilde{\lambda}, \lambda_\infty) [\langle \lambda \rangle - \tilde{\lambda}] = \int_{\tilde{\lambda}}^{\lambda_\infty} M(\lambda, \lambda_\infty) d\lambda. \quad (9.37)$$

We return to the notion of internal and external moments in Section 9.9.2.

9.3.8 Further study

The formulation given here in terms of mass distribution functions follows that of [Wal in \(1977\)](#) and [Wal in \(1982\)](#). In these two papers, Walin pioneered the formalism of water mass transformation analysis, which is sometimes referred to as [Wal in analysis](#) in his honor. The concept of internal and external tracer moments follows the internal and external heat introduced by [Holmes et al. \(2019b\)](#).

9.4 Water mass transformation across an internal λ -surface

We here develop the water mass transformation formalism to compute the transport of fluid crossing an interior λ -interface. This transport is referred to as the [water mass transformation](#) and is written as $G(\lambda)$. Figure 9.6 illustrates how this transformation appears in a mass budget for a $\Delta\lambda$ -layer, with details provided in this section.

9.4.1 Dia-surface flux and interior transformation

The object that measures the local water mass transformation is the dia-surface flux detailed in Section 2.4.8 and illustrated in Figure 9.7. This flux is given by the following equivalent expressions

$$w^{\text{dia}} = \hat{\mathbf{n}} \cdot (\mathbf{v} - \mathbf{v}^{(\lambda)}) = \frac{\dot{\lambda}}{|\nabla \lambda|} \quad \text{with} \quad \hat{\mathbf{n}} = \frac{\nabla \lambda}{|\nabla \lambda|} \quad \text{and} \quad \dot{\lambda} = \frac{D\lambda}{Dt}, \quad (9.38)$$

and with $w^{\text{dia}} > 0$ for water moving to regions of larger λ . It is computed as the projection of the relative velocity, $(\mathbf{v} - \mathbf{v}^{(\lambda)})$, onto the direction normal to the λ -surface, with the relative velocity being the difference between the fluid particle velocity, \mathbf{v} , and the velocity, $\mathbf{v}^{(\lambda)}$, of a point on the λ -surface. The velocity, $\mathbf{v}^{(\lambda)}$, satisfies the following kinematic constraint

$$(\partial_t + \mathbf{v}^{(\lambda)} \cdot \nabla) \lambda = 0. \quad (9.39)$$

This constraint is based on assuming that $\mathbf{v}^{(\lambda)}$ measures the velocity of a point that is fixed to the λ -surface. So by construction, the dia-surface flux, w^{dia} , locally measures the flux of fluid (volume per area per time) that penetrates a λ -surface in the direction of increasing λ .

The interior water mass transformation, $G(\lambda)$, is the area integral of ρw^{dia} over the full

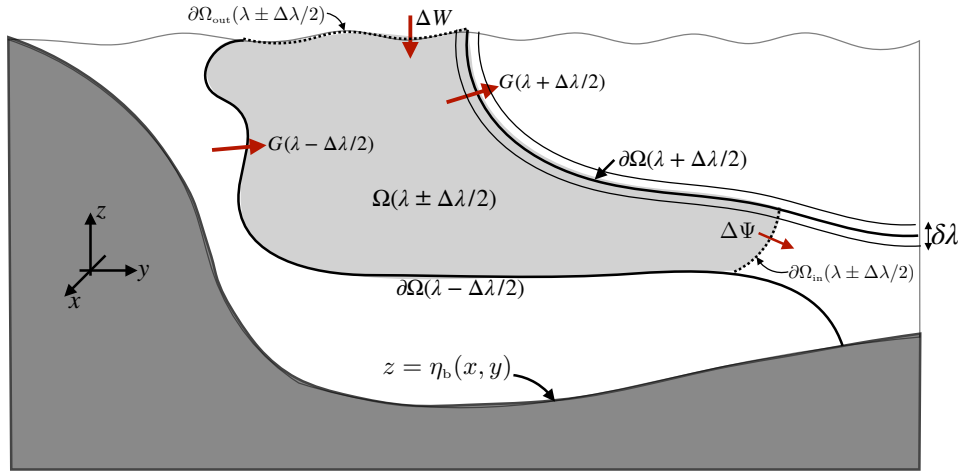


FIGURE 9.6: A layer of fluid with scalar property λ within the range $[\lambda - \Delta\lambda/2, \lambda + \Delta\lambda/2]$ (with $\Delta\lambda > 0$) and defined over a geographical domain $\Omega(\lambda \pm \Delta\lambda/2)$. In this example, λ increases to the right. The net fluid mass transport crossing the layer interfaces, $\partial\Omega(\lambda \pm \Delta\lambda/2)$, is $G(\lambda \pm \Delta\lambda/2)$, with our convention defining $G > 0$ for water moving to regions of larger λ , which orients the direction of the arrows. The fluid mass crossing the layer through the geographical bounds, $\partial\Omega_{in}(\lambda \pm \Delta\lambda/2)$, is written $\Delta\Psi = \Psi(\lambda \pm \Delta\lambda/2)$, with our convention setting $\Psi(\lambda \pm \Delta\lambda/2) > 0$ for water leaving $\Omega(\lambda \pm \Delta\lambda/2)$. The boundary $\partial\Omega_{in}(\lambda \pm \Delta\lambda/2)$ is absent when the domain extends across a basin or the global ocean (e.g., see Figure 9.11). The mass crossing the sea surface, $\partial\Omega_{out}(\lambda \pm \Delta\lambda/2)$, through precipitation, evaporation, melt, and river runoff is written $\Delta W(\lambda \pm \Delta\lambda/2)$, with $\Delta W(\lambda \pm \Delta\lambda/2) > 0$ for mass entering $\Omega(\lambda \pm \Delta\lambda/2)$. A layer interface can have an arbitrary stratification, such as the vertically non-monotonic profile depicted here for the $\lambda + \Delta\lambda/2$ interface. Additionally, the domain $\Omega(\lambda \pm \Delta\lambda/2)$ can generally be disconnected. The net domain boundaries are written $\partial\Omega_{in}(\lambda \pm \Delta\lambda/2) + \partial\Omega_{out}(\lambda \pm \Delta\lambda/2) + \partial\Omega(\lambda + \Delta\lambda/2) + \partial\Omega(\lambda - \Delta\lambda/2)$. The infinitesimal $\delta\lambda$ layer surrounding the $\partial\Omega(\lambda \pm \Delta\lambda/2)$ interface arises as part of the method detailed in Section 9.4.3 for computing $G(\lambda)$ according to the λ -derivative of a volume integral over the $\delta\lambda$ -layer.

extent of the λ -surface

$$G(\lambda) \equiv \int_{\partial\Omega(\lambda)} \rho w^{\text{dia}} dS = \int_{\partial\Omega(\lambda)} \rho \hat{\mathbf{n}} \cdot (\mathbf{v} - \mathbf{v}^{(\lambda)}) dS = \int_{\partial\Omega(\lambda)} \frac{\rho \dot{\lambda}}{|\nabla \lambda|} dS, \quad (9.40)$$

where $\partial\Omega(\lambda)$ is the surface occupied by the λ -interface (see Figure 9.6). Furthermore, the dimensions of $G(\lambda)$ are mass per time

$$G(\lambda) \quad [\equiv] \quad \text{M T}^{-1}, \quad (9.41)$$

thus measuring the mass per time crossing the λ -interface.

Based on the definition (9.40), we see that interior water mass transformation across a λ -interface occurs when there is a material change, $\dot{\lambda} \neq 0$, in the property defining the surface. If λ is a conservative tracer, then interior material changes arise from the mixing of λ , thus driving fluid to cross the moving λ -interface (we consider the case of tracer diffusion in Section 9.4.2). Material changes can also arise from sources and sinks, as when considering buoyancy surfaces in the presence of a nonlinear equation of state (Chapter 8). Sources and sinks also affect biogeochemical tracers.

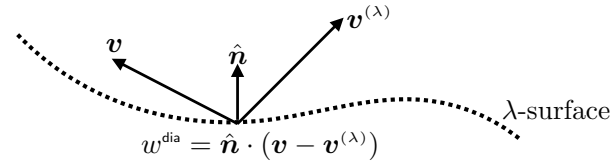


FIGURE 9.7: Schematic of the dia-surface flux, $w^{\text{dia}} = \hat{n} \cdot (\mathbf{v} - \mathbf{v}^{(\lambda)})$, as per equation (9.38), which measures the volume of fluid per time per area that crosses the λ -surface. The velocity of a fluid particle is \mathbf{v} , whereas $\mathbf{v}^{(\lambda)}$ is the velocity of a point fixed on the λ -surface. The normal direction, $\hat{n} = \nabla \lambda / |\nabla \lambda|$, points toward higher values of λ . If the normal projection of the fluid velocity is distinct from that of the surface velocity ($\hat{n} \cdot \mathbf{v} \neq \hat{n} \cdot \mathbf{v}^{(\lambda)}$), then fluid crosses the surface and w^{dia} is nonzero. As per equation (9.39), we see that $\mathbf{v}^{(\lambda)} \cdot \hat{n} = -|\nabla \lambda|^{-1} \partial_t \lambda$, so that for static surfaces, in which $\partial_t \lambda = 0$, then $w^{\text{dia}} = \hat{n} \cdot \mathbf{v}$. We depict the λ -surface with a dotted line to emphasize that it generally has fluid crossing it. The special case of a material surface arises when each point on the surface moves with the fluid velocity, \mathbf{v} , so that $\hat{n} \cdot \mathbf{v} = \hat{n} \cdot \mathbf{v}^{(\lambda)}$, in which case $w^{\text{dia}} = 0$.

9.4.2 Dia-surface flux from diffusion and steady state balances

In a fluid with interior transformation arising from tracer diffusion, the dia-surface flux across the λ -surface is

$$\rho w^{\text{dia}} = \hat{n} \cdot (\mathbf{v} - \mathbf{v}^{(\lambda)}) = \frac{\rho \dot{\lambda}}{|\nabla \lambda|} = \frac{\nabla \cdot (\rho \mathbf{K} \cdot \nabla \lambda)}{|\nabla \lambda|}, \quad (9.42)$$

where \mathbf{K} is the diffusion tensor (Section 4.8). As expected, there is more dia-surface flux crossing the λ -surface where there is more diffusion of λ .

Now assume the flow has reached a steady state so that $\partial_t \lambda = 0$, so $\hat{n} \cdot \mathbf{v}^{(\lambda)} = 0$. In this case advection of λ exactly balances its diffusion

$$\rho \mathbf{v} \cdot \nabla \lambda = \nabla \cdot (\rho \mathbf{K} \cdot \nabla \lambda), \quad (9.43)$$

where we used the steady mass continuity equation, $\partial_t \rho = -\nabla \cdot (\mathbf{v} \rho) = 0$, to write $\nabla \cdot (\rho \mathbf{v} \lambda) = \rho \mathbf{v} \cdot \nabla \lambda$. Hence, the dia-surface flux is given by the velocity projected onto the surface normal

$$\rho w^{\text{dia}} = \frac{\rho \dot{\lambda}}{|\nabla \lambda|} \stackrel{\text{diffusion}}{=} \frac{\nabla \cdot (\rho \mathbf{K} \cdot \nabla \lambda)}{|\nabla \lambda|} \stackrel{\text{steady}}{=} \frac{\rho \mathbf{v} \cdot \nabla \lambda}{|\nabla \lambda|} = \rho \mathbf{v} \cdot \hat{n}. \quad (9.44)$$

Notably, there is flow across the λ surfaces since diffusion drives $\mathbf{v} \cdot \hat{n} \neq 0$, thus indicating a nonzero water mass transformation. However, in a steady state this flow that crosses the surface is exactly balanced by diffusion of λ , as per equation (9.43). Consequently, there is no evolution of the fluid mass distribution within λ layers, even though there is a nonzero water mass transformation across the λ surfaces defining the layers. That is, with a steady state there can be nonzero water mass transformation across λ -surface, and yet there is no formation (or destruction) of water mass within λ -layers since there is no convergence (in λ -space) of the transformation. These are many words to express a rather simple result. Yet the meaning of these words are important to appreciate, particularly in the midst of manipulations with the water mass transformation equations arising in subsequent sections. We further pursue the case of diffusive transformation in Section 9.6.5.

9.4.3 Transformation as the derivative of an integral

The water mass transformation, $G(\lambda)$, given by equation (9.40) is an area integral over the λ surface. However, the integral is intractable in practice given the need to estimate an area integral over a surface that is a function of space and time. Here we derive a practical method that provides the means for estimating $G(\lambda)$ for all numerical realizations of water

mass transformation.

For this purpose, return to the discussion from Section 9.3.5 and set $F = \dot{\lambda}$ for the integral

$$\mathcal{I}_{\dot{\lambda}}(\lambda, \lambda_{\infty}) = \int_{\Omega(\lambda \leq \lambda_{\infty})} \dot{\lambda}' dM = \int_{\lambda}^{\lambda_{\infty}} \left[\int_{\partial\Omega(\lambda')} \frac{\rho \dot{\lambda}'}{|\nabla \lambda'|} d\mathcal{S} \right] d\lambda' = \int_{\lambda}^{\lambda_{\infty}} G(\lambda') d\lambda'. \quad (9.45)$$

Taking the functional derivative of this integral, and using the fundamental theorem of calculus, we arrive at an expression for the water mass transformation

$$G(\lambda) = -\frac{\partial \mathcal{I}_{\dot{\lambda}}(\lambda, \lambda_{\infty})}{\partial \lambda} \quad \text{fund. thm of calculus} \quad (9.46a)$$

$$= -\lim_{\delta\lambda \rightarrow 0} \frac{1}{\delta\lambda} \left[\int_{\lambda + \delta\lambda/2}^{\lambda_{\infty}} G(\lambda') d\lambda' - \int_{\lambda - \delta\lambda/2}^{\lambda_{\infty}} G(\lambda') d\lambda' \right] \quad \text{definition of derivative} \quad (9.46b)$$

$$= \lim_{\delta\lambda \rightarrow 0} \frac{1}{\delta\lambda} \int_{\lambda - \delta\lambda/2}^{\lambda + \delta\lambda/2} G(\lambda') d\lambda' \quad \text{combine integral limits} \quad (9.46c)$$

$$= \lim_{\delta\lambda \rightarrow 0} \frac{1}{\delta\lambda} \int_{\Omega(\lambda \pm \delta\lambda/2)} \dot{\lambda}' dM \quad \text{equation (9.45)} \quad (9.46d)$$

$$= \lim_{\delta\lambda \rightarrow 0} \frac{1}{\delta\lambda} \int_{\Omega(\lambda \pm \delta\lambda/2)} \dot{\lambda}' \rho dV \quad dM = \rho dV. \quad (9.46e)$$

We conclude that interior water mass transformation, $G(\lambda)$, across a λ -surface can be computed as a volume integral over an infinitesimal layer surrounding the λ -surface. The volume integral requires information about the material time change, $\dot{\lambda}$, a weighting of the time changes according to the mass, $dM = \rho dV$, and a binning of the full integrand, $\rho \dot{\lambda} dV$, according to λ -class $[\lambda - \delta\lambda/2, \lambda + \delta\lambda/2]$.⁷ We illustrate the identity (9.46e) in Figure 9.8, with this figure summarizing the practical method, based on binning, used in all calculations of water mass transformation.

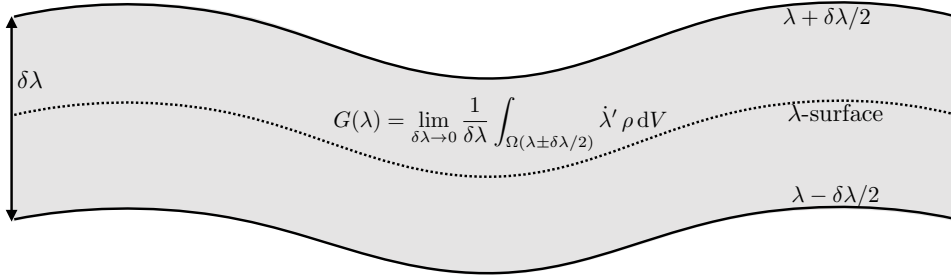


FIGURE 9.8: Illustrating equation (9.46e), in which we compute the interior water mass transformation, $G(\lambda)$, across a λ -surface as the volume integral over an infinitesimal region that surrounds the λ -surface. This figure summarizes the binning approach used in all calculations of interior water mass transformation, whereby processes contributing to the integrand, $\rho \dot{\lambda} dV$, are binned according to λ -classes as per the discussion in Section 9.4.4.

9.4.4 Kinematic and process methods of water mass transformation

There are two complementary means to view interior water mass transformation: the **process method** and the **kinematic method**. The two methods are mathematically identical and so

⁷The final expression in equation (9.46e) might appear to lead to a singularity given the limit $\delta\lambda \rightarrow 0$. However, as seen by the form in equation (9.46c), the integration volume also gets smaller as $\delta\lambda \rightarrow 0$ so that the limit is well defined.

they offer two means to compute the same transformation. The kinematic method tells us *how* transformation happens, whereas the process method helps to understand *why* transformation happens.

Kinematic method

The kinematic method focuses on the kinematic means for realizing dia-surface transport, thus providing information concerning how interior transformation occurs. It does so by binning processes contributing to the right hand side of

$$\rho \dot{\lambda} = \partial_t(\rho \lambda) + \nabla \cdot (\rho \lambda \mathbf{v}), \quad (9.47)$$

which arises from the local time tendency plus advection, so that

$$G(\lambda) = \lim_{\delta\lambda \rightarrow 0} \frac{1}{\delta\lambda} \int_{\Omega(\lambda \pm \delta\lambda/2)} [\partial_t(\rho \lambda) + \nabla \cdot (\rho \lambda \mathbf{v})] dV. \quad (9.48)$$

This method is operationally simpler than the process method since there are fewer terms to bin (i.e., just the local time tendency plus the divergence of the advective flux). However, it does not provide information about why there is transformation, with that information requiring us to bin tendencies arising from individual processes.

Process method

The **process method** focuses on physical (or biogeochemical) processes leading to movement of fluid across the λ -surface, thus providing information concerning *why* interior transformation occurs. It does so by binning processes contributing to the right hand side of the tracer equation

$$\rho \dot{\lambda} = -\nabla \cdot \mathbf{J} + \rho \dot{\Upsilon}, \quad (9.49)$$

where \mathbf{J} is a flux arising from non-advection processes such as diffusion, and $\dot{\Upsilon}$ is a source/sink term (dimensions of λ per time) that cannot be written as the convergence of a flux. With the tracer equation (9.49) inserted into the transformation equation (9.46e), we are led to

$$G(\lambda) = \lim_{\delta\lambda \rightarrow 0} \frac{1}{\delta\lambda} \int_{\Omega(\lambda \pm \delta\lambda/2)} (-\nabla \cdot \mathbf{J} + \rho \dot{\Upsilon}) dV \quad (9.50a)$$

$$= \lim_{\delta\lambda \rightarrow 0} \frac{1}{\delta\lambda} \oint_{\partial\Omega(\lambda \pm \delta\lambda/2)} (-\mathbf{J} \cdot \hat{\mathbf{n}}) d\mathcal{S} + \lim_{\delta\lambda \rightarrow 0} \frac{1}{\delta\lambda} \int_{\Omega(\lambda \pm \delta\lambda/2)} \rho \dot{\Upsilon} dV. \quad (9.50b)$$

The second equality made use of the divergence theorem to convert the volume integral into a surface integral, with $\hat{\mathbf{n}}$ the outward normal to the boundary, $\partial\Omega(\lambda \pm \delta\lambda/2)$. For tracer sources, we assume they do not modify the fluid mass at a point so that there is no source in the fluid mass equation.

For many purposes it is useful to decompose the non-advection flux divergence into contributions from interior processes, such as ocean mixing, along with boundary fluxes

$$\nabla \cdot \mathbf{J} = \nabla \cdot (\mathbf{J}^{\text{int}} + \mathbf{J}^{\text{out}} + \mathbf{J}^{\text{bot}}). \quad (9.51)$$

By definition,

$$\mathbf{J}^{\text{int}} \cdot \hat{\mathbf{n}} = 0 \quad \text{on } \partial\Omega_{\text{out}}(\lambda \pm \delta\lambda/2) \text{ and } \partial\Omega_{\text{bot}}(\lambda \pm \delta\lambda/2), \quad (9.52)$$

whereas $\mathbf{J}^{\text{int}} \cdot \hat{\mathbf{n}}$ is generally nonzero on interior layer boundaries. In contrast, the boundary fluxes, $\mathbf{J}^{\text{out}} \cdot \hat{\mathbf{n}}$ and $\mathbf{J}^{\text{bot}} \cdot \hat{\mathbf{n}}$, are identically zero everywhere except on their respective boundaries. Correspondingly, it is convenient to bin the volume weighted convergence, $-\nabla \cdot \mathbf{J}^{\text{int}} dV$, according to λ -classes, and to likewise bin the area weighted boundary fluxes, $\mathbf{J}^{\text{out}} \cdot \hat{\mathbf{n}} d\mathcal{S}$ and $\mathbf{J}^{\text{bot}} \cdot \hat{\mathbf{n}} d\mathcal{S}$. In this way we write the non-advection contribution to water mass transformation in the form

$$\begin{aligned}
 G(\lambda)_{\text{nonadv}} = & \underbrace{-\lim_{\delta\lambda \rightarrow 0} \frac{1}{\delta\lambda} \int_{\Omega(\lambda \pm \delta\lambda/2)} \nabla \cdot \mathbf{J}^{\text{int}} dV}_{\text{interior transformation} = \text{volume integral of convergence}} \\
 & \underbrace{-\lim_{\delta\lambda \rightarrow 0} \frac{1}{\delta\lambda} \int_{\partial\Omega_{\text{out}}(\lambda \pm \delta\lambda/2)} \mathbf{J}^{\text{out}} \cdot \hat{\mathbf{n}} d\mathcal{S}}_{\text{surface transformation} = \text{area integral of surface boundary fluxes}} \\
 & \underbrace{-\lim_{\delta\lambda \rightarrow 0} \frac{1}{\delta\lambda} \int_{\partial\Omega_{\text{bot}}(\lambda \pm \delta\lambda/2)} \mathbf{J}^{\text{bot}} \cdot \hat{\mathbf{n}} d\mathcal{S}}_{\text{bottom transformation} = \text{area integral of bottom boundary fluxes}}. \tag{9.53}
 \end{aligned}$$

Again, this expression decomposes the contribution from interior processes, here represented as the volume integral of the interior flux convergence, from the surface and bottom contributions, here represented as the area integral of the boundary fluxes. This decomposition is further examined in Sections 9.6.6 and 9.7.4 where we focus on the surface contribution to water mass transformation.

Since the boundary fluxes are, by definition, zero except on the boundaries, their divergence can be written in terms of a Dirac delta

$$\nabla \cdot [\mathbf{J}^{\text{out}} + \mathbf{J}^{\text{bot}}] = \mathbf{J}^{\text{out}} \cdot \hat{\mathbf{n}} \delta(z - \eta) + \mathbf{J}^{\text{bot}} \cdot \hat{\mathbf{n}} \delta(z - \eta_b). \tag{9.54}$$

This equation's use in the transformation equation (9.50a) leads to the expression (9.53). Furthermore, as detailed in our study of Neumann boundary conditions in VOLUME 1, we are afforded the ability to introduce Dirac deltas into the boundary conditions (9.54) since the boundary conditions are Neumann (flux) conditions. We made use of this approach for the surface buoyancy fluxes in Section 8.6.3, and it proves useful both conceptually and practically in decomposing contributions to water mass transformation.

Comments

As we saw, equality of the process method and kinematic method follows because the two provide expressions for the material time derivative. However, in the analysis of numerical model output, it can be nontrivial to realize this equivalence due to the extreme care required to diagnose the terms appearing in the scalar budget equation. See [Drake et al. \(2025\)](#) for a thorough discussion of the details as required for a particular finite volume numerical ocean model.

9.4.5 General properties of interior transformation due to diffusion

We here examine some general properties of water mass transformation arising just from interior processes such as diffusion.

A global integrated constraint on $G(\lambda)_{\text{int}}$

Consider the integrated water mass transformation given by equation (9.45), now integrated over the full ocean domain

$$\mathcal{I}_{\lambda}(\lambda_{-\infty}, \lambda_{\infty}) = \int_{\lambda_{-\infty}}^{\lambda_{\infty}} G(\lambda') d\lambda' = \int_{\Omega(\lambda_{-\infty}, \lambda_{\infty})} \rho \dot{\lambda}' dV. \quad (9.55)$$

This integral vanishes for water mass transformations arising from conservative interior processes (i.e., those processes determined by the convergence of a flux)

$$[\mathcal{I}_{\lambda}(\lambda_{-\infty}, \lambda_{\infty})]_{\text{int}} = \int_{\lambda_{-\infty}}^{\lambda_{\infty}} G(\lambda')_{\text{int}} d\lambda' \quad (9.56a)$$

$$= - \int_{\Omega(\lambda_{-\infty}, \lambda_{\infty})} \nabla \cdot \mathbf{J}^{\text{int}} dV \quad (9.56b)$$

$$= - \oint_{\partial\Omega(\lambda_{-\infty}, \lambda_{\infty})} \mathbf{J}^{\text{int}} \cdot \hat{\mathbf{n}} dS \quad (9.56c)$$

$$= 0, \quad (9.56d)$$

which follows since $\mathbf{J}^{\text{int}} \cdot \hat{\mathbf{n}} = 0$ on the ocean boundaries. Hence, there can be no net water mass transformation across a λ surface arising from conservative interior processes

$$\int_{\lambda_{-\infty}}^{\lambda_{\infty}} G(\lambda')_{\text{int}} d\lambda' = 0. \quad (9.57)$$

Instead, conservative interior processes only lead to rearrangement of water within the λ -bins. This result follows since these interior processes conserve the total content of λ within the global domain. Equation (9.57) provides a constraint that is useful to verify with any numerical realization of water mass transformation analysis.

Transformation across λ surfaces

We now focus on the transformation occurring along λ -surfaces as in Figure 9.9, in which case

$$G(\lambda)_{\text{int}} = - \lim_{\delta\lambda \rightarrow 0} \frac{1}{\delta\lambda} \int_{\Omega(\lambda \pm \delta\lambda/2)} \nabla \cdot \mathbf{J}^{\text{int}} dV \quad (9.58a)$$

$$= - \lim_{\delta\lambda \rightarrow 0} \frac{1}{\delta\lambda} \left[\int_{\Omega(\lambda + \delta\lambda/2)} \hat{\mathbf{n}} \cdot \mathbf{J}^{\text{int}} dS - \int_{\Omega(\lambda - \delta\lambda/2)} \hat{\mathbf{n}} \cdot \mathbf{J}^{\text{int}} dS \right]. \quad (9.58b)$$

Transformation occurs if there is an imbalance between the diffusive transport across the two bounding surfaces, $\Omega(\lambda + \delta\lambda/2)$ and $\Omega(\lambda - \delta\lambda/2)$.

We examine a special case that is not so much physically motivated but is instead motivated to help unravel the meaning of the mathematical symbols. In this case we assume the ocean surface is a constant λ surface with $\lambda = \lambda_{\text{top}}$ (see right panel of Figure 9.9). Along this surface we have $\hat{\mathbf{n}} \cdot \mathbf{J}^{\text{int}} = 0$, by construction since \mathbf{J}^{int} is nonzero only within the interior. Hence, the water mass transformation, $G(\lambda_{\text{top}} - \delta\lambda/2)_{\text{int}}$, has a contribution just from the flux crossing the $\Omega(\lambda_{\text{top}} - \delta\lambda)$ surface

$$\lim_{\delta\lambda \rightarrow 0} G(\lambda_{\text{top}} - \delta\lambda/2)_{\text{int}} = \lim_{\delta\lambda \rightarrow 0} \frac{1}{\delta\lambda} \int_{\Omega(\lambda_{\text{top}} - \delta\lambda)} \hat{\mathbf{n}} \cdot \mathbf{J}^{\text{int}} dS. \quad (9.59)$$

Likewise, along the top surface we have

$$G(\lambda_{\text{top}})_{\text{int}} = \lim_{\delta\lambda \rightarrow 0} \frac{1}{\delta\lambda} \int_{\Omega(\lambda_{\text{top}} - \delta\lambda/2)} \hat{\mathbf{n}} \cdot \mathbf{J}^{\text{int}} d\mathcal{S}, \quad (9.60)$$

where we set $\hat{\mathbf{n}} \cdot \mathbf{J}^{\text{int}} = 0$ for the surface $\Omega(\lambda_{\text{top}} + \delta\lambda/2)$, since this surface exists outside of the ocean.

The results (9.59) and (9.60) make it appear that $G(\lambda_{\text{top}} - \delta\lambda/2)_{\text{int}}$ and $G(\lambda_{\text{top}})_{\text{int}}$ are unbounded as $\delta\lambda \rightarrow 0$, so long as there is a nonzero diffusive transport through $\Omega(\lambda_{\text{top}} - \delta\lambda)$ or $\Omega(\lambda_{\text{top}} + \delta\lambda/2)$. However, this unbounded water mass transformation is not realized since the interior diffusive flux, $\hat{\mathbf{n}} \cdot \mathbf{J}^{\text{int}} = 0$, gets smaller in magnitude when approaching the ocean surface, and it does so in order to satisfy the no-flux surface boundary condition (9.52) satisfied by interior processes⁸

$$\hat{\mathbf{n}} \cdot \mathbf{J}^{\text{int}} = 0 \quad \text{at } z = \eta. \quad (9.61)$$

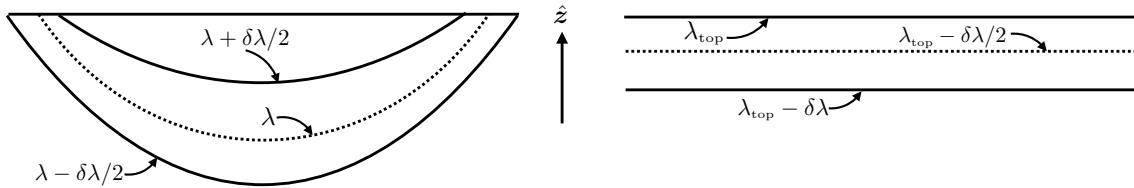


FIGURE 9.9: Example λ surfaces for studying interior transformation due to diffusion. The left panel shows λ surfaces that outcrop to the ocean surface, with the dotted surface the chosen λ surface across which we compute the water mass transformation, $G(\lambda)$. The right panel assumes the λ surfaces are flat and with $\lambda = \lambda_{\text{top}}$ the value along the surface boundary.

9.4.6 Interior versus boundary water mass transformation

Throughout this section we focused on transformation arising from interior processes such as diffusion. What about boundary processes? Indeed, where does interior become boundary? These questions are at the heart of boundary water mass transformation, both the ocean bottom and surface. Surface water mass transformation analysis, introduced in Sections 9.6.6 and 9.7.4, is the most common form of water mass transformation analysis in practice, given that it provides useful inferences based only on surface fluxes. Even so, it is important to note that the distinction between surface and boundary transformation is rather arbitrary for the following reasons.

Consider equation (9.46e) for the water mass transformation

$$G(\lambda) = \lim_{\delta\lambda \rightarrow 0} \frac{1}{\delta\lambda} \int_{\Omega(\lambda \pm \delta\lambda/2)} \dot{\lambda}' \rho dV. \quad (9.62)$$

When binning the integrand, we bin fluid everywhere in the domain, including next to boundaries where boundary fluxes directly contribute to $\dot{\lambda}$. Indeed, these fluxes are exposed when using the divergence theorem to convert the volume integral of $\rho \dot{\lambda} = -\nabla \cdot \mathbf{J}$ to a boundary area integral of $\mathbf{J} \cdot \hat{\mathbf{n}}$ (e.g., see Section 9.6.1). Another means to understand the role of boundary contributions follows [Nurser et al. \(1999\)](#), in which boundary fluxes act to inflate layers (including layers

⁸As discussed in Sections 8.5, and 9.7.3, when water is transported across the ocean surface the diffusive flux picks up a nonzero boundary contribution. That contribution is assumed to be part of the surface transformation in equation (9.53) so that the interior diffusive flux still satisfies the no-flux boundary condition (9.61). [Nurser and Griffies \(2019\)](#) discuss these ideas for the case of salinity.

that are otherwise vanished), or to deflate outcropped layers (including layers that end up vanishing). For these reasons, it is unnecessary in principle to distinguish between interior processes and boundary processes. Even so, for practical calculations, it is common to refer to surface transformation when making use just of surface boundary fluxes, which is how we consider surface transformation in Sections 9.6.6 and 9.7.4.

9.5 Budget for fluid mass in a $\Delta\lambda$ -layer

In this section we construct the fluid mass budget for a $\Delta\lambda$ -layer, making reference to Figure 9.6 for the notation. We write the budgets both in terms of extensive quantities (mass and mass transport) and intensive quantities (mass distribution and mass transport distribution). For mass, recall the definition (9.10) where layer mass is written in the equivalent manners

$$\Delta M \equiv M(\lambda - \Delta\lambda/2, \lambda + \Delta\lambda/2) = \int_{\Omega(\lambda \pm \Delta\lambda/2)} \rho dV = \int_{\lambda - \Delta\lambda/2}^{\lambda + \Delta\lambda/2} m(\lambda') d\lambda'. \quad (9.63)$$

We introduce analogous expressions for mass transports in the following.

9.5.1 Mass transport crossing interior open boundaries

As depicted in Figure 9.6, the layer region has an open boundary that is within the interior of the fluid. The mass transport leaving the layer through this interior open boundary is written

$$\Delta\Psi \equiv \Psi(\lambda - \Delta\lambda/2, \lambda + \Delta\lambda/2) = \int_{\partial\Omega_{in}(\lambda \pm \Delta\lambda/2)} \rho (\mathbf{v} - \mathbf{v}^{(b)}) \cdot \hat{\mathbf{n}} d\mathcal{S}, \quad (9.64)$$

where $\mathbf{v}^{(b)}$ is the velocity for a point on the boundary and $\hat{\mathbf{n}}$ is the outward normal along the boundary. One common example for an open interior boundary is when choosing a particular latitude, in which case $\mathbf{v}^{(b)} = 0$ and $\hat{\mathbf{n}} = \hat{\mathbf{y}}$ so that

$$\Psi(\lambda - \Delta\lambda/2, \lambda + \Delta\lambda/2) = \int_{\partial\Omega_{in}(\lambda \pm \Delta\lambda/2)} \rho v d\mathcal{S}. \quad (9.65)$$

In this case, $\partial\Omega_{in}(\lambda \pm \Delta\lambda/2)$ specifies the depth and longitude range for the layer at its intersection along the constant latitude boundary.

9.5.2 Mass transport crossing the ocean surface

The mass transport crossing the ocean free surface is written

$$W(\lambda - \Delta\lambda/2, \lambda + \Delta\lambda/2) = - \int_{\partial\Omega_{out}(\lambda \pm \Delta\lambda/2)} \rho (\mathbf{v} - \mathbf{v}^{(n)}) \cdot \hat{\mathbf{n}} d\mathcal{S} = \int_{\partial\Omega_{out}(\lambda \pm \Delta\lambda/2)} \mathcal{Q}_m d\mathcal{S}, \quad (9.66)$$

where $\mathcal{Q}_m d\mathcal{S}$ is the mass transport of water crossing the free surface ($\mathcal{Q}_m > 0$ for water entering the ocean), and where we made use of the surface **kinematic boundary condition** to write

$$\rho (\mathbf{v} - \mathbf{v}^{(b)}) \cdot \hat{\mathbf{n}} \equiv -\mathcal{Q}_m, \quad (9.67)$$

9.5.3 Mass budget and water mass formation

Bringing the above pieces together leads to the layer mass budget

$$\frac{d\Delta M}{dt} = -\Delta\Psi + \Delta W - [G(\lambda + \Delta\lambda/2) - G(\lambda - \Delta\lambda/2)], \quad (9.68)$$

where for brevity we dropped $\lambda \pm \Delta\lambda/2$ arguments for ΔM , $\Delta\Psi$, and ΔW . Although quite simple to state, this mass budget encapsulates a tremendous amount of details about the many processes leading to transport across layer boundaries.

In addition to a layer mass budget, we find it useful to define the water mass [formation](#) for the $\lambda \pm \Delta\lambda/2$ layer, $\mathcal{F}\Delta\lambda$, as

$$\mathcal{F}\Delta\lambda \equiv \underbrace{\frac{d\Delta M}{dt} + \Delta\Psi}_{\text{storage + outflow}} - \underbrace{\Delta W - \frac{[G(\lambda + \Delta\lambda/2) - G(\lambda - \Delta\lambda/2)]}{\Delta\lambda}}_{\text{formation into layer } \Omega_{(\lambda \pm \Delta\lambda/2)}} \Delta\lambda. \quad (9.69)$$

This equation defines the layer water mass formation, $\mathcal{F}\Delta\lambda$, is the product of the specific formation, \mathcal{F} , which is an intensive quantity (mass per time per λ -increment), and the layer width, $\Delta\lambda$,

$$\mathcal{F}\Delta\lambda = \text{mass/time of fluid forming within the interval } [\lambda - \Delta\lambda/2, \lambda + \Delta\lambda/2]. \quad (9.70)$$

The first equality in equation (9.69) defines the layer water mass formation, $\mathcal{F}\Delta\lambda$, as the time change of the mass within the layer (sometimes referred to as the [storage term](#)), plus the net mass leaving through the interior open boundary. Evidently, layer water mass formation is positive if the mass tendency is positive, $(dM/dt > 0)$. Additionally, formation is positive if mass leaves through the open boundary, $\Psi > 0$, which signals the transport of water to adjacent regions (still within the same layer) and so “forming” additional waters of this particular type. The second equality in equation (9.69) defines the layer water mass formation as the mass entering through the surface boundary outcrop region plus the integrated convergence of water mass transformation across interior layer interfaces.

We illustrate the water mass formation equation in Figure 9.10 for the case of a layer within the ocean interior, in which there is no contribution from W . Note that for the special case of a lower boundary set to the solid earth, then a steady state balance has

$$\Psi(\lambda_{-\infty}, \lambda) = -G(\lambda). \quad (9.71)$$

That is, the steady state transport through the inner boundary, $\partial\Omega_{\text{in}}(\lambda_{-\infty}, \lambda)$, extending from the bottom to the λ -surface is set by minus the water mass transformation, $-G(\lambda)$, across the λ -surface. Evidently, if there is no water mass transformation across the λ layer, $G(\lambda) = 0$, then a steady flow has no transport through the open boundary, $\Psi(\lambda_{-\infty}, \lambda) = 0$.

9.5.4 Mass budget and formation in terms of distribution functions

Following our use of a mass distribution function, $m(\lambda)$, in equation (9.63), and inspired by [Walsh \(1977\)](#) and [Walsh \(1982\)](#), we here introduce the mass distribution functions for the mass per time per λ -increment that is transported across the open boundary and upper ocean surface

$$\Psi(\lambda_0, \lambda) = \int_{\lambda_0}^{\lambda} \dot{m}_{\Psi}(\lambda') d\lambda' \quad \text{and} \quad W(\lambda_0, \lambda) = \int_{\lambda_0}^{\lambda} \dot{m}_W(\lambda') d\lambda', \quad (9.72)$$

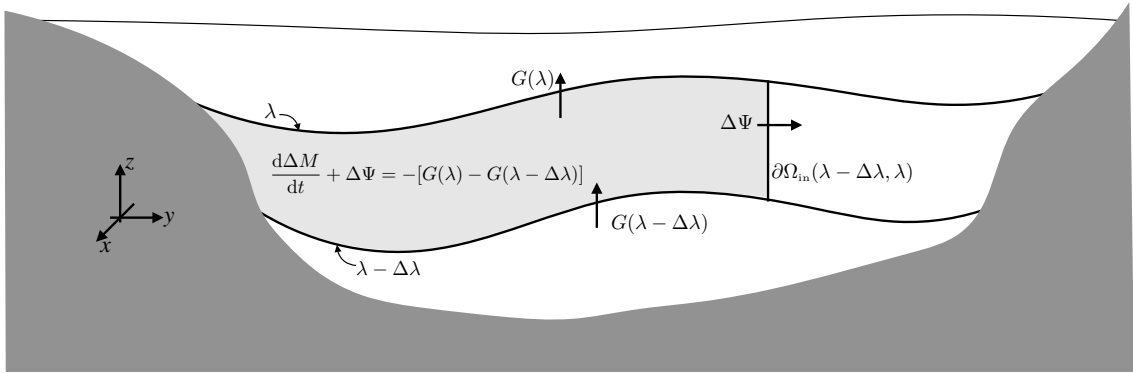


FIGURE 9.10: Water mass budget for the lightly shaded interior layer, $[\lambda - \Delta\lambda, \lambda]$ with $\Delta\lambda > 0$, and with one lateral boundary set to the rock and the other set to a vertical section (e.g., a constant latitude line). Assuming there is no flux of λ through the solid earth bottom, then the mass within the layer changes due to water mass transformation across the lower layer boundary, $G(\lambda - \Delta\lambda)$, water mass transformation across the upper layer boundary, $G(\lambda)$, and transport crossing the inner boundary, $\Psi(\lambda - \Delta\lambda, \lambda)$.

so that

$$d\Psi = \dot{m}_\Psi(\lambda) d\lambda = \text{mass/time of fluid crossing } \partial\Omega_{in} \text{ within } [\lambda - d\lambda/2, \lambda + d\lambda/2] \quad (9.73a)$$

$$dW = \dot{m}_W(\lambda) d\lambda = \text{mass/time of fluid crossing } \partial\Omega_{out} \text{ within } [\lambda - d\lambda/2, \lambda + d\lambda/2]. \quad (9.73b)$$

Use of these mass distribution functions leads to the intensive version of the mass budget equation (9.68)

$$\frac{dm}{dt} = -\dot{m}_\Psi + \dot{m}_W - \frac{\partial G}{\partial \lambda}, \quad (9.74)$$

and the corresponding intensive version of the water mass formation equation (9.69)

$$\mathcal{F} = \frac{dm}{dt} + \dot{m}_\Psi = \dot{m}_W - \frac{\partial G}{\partial \lambda}. \quad (9.75)$$

9.6 Mass budget for λ within a λ_∞ -region

We build from our understanding of the fluid mass budget in Section 9.5 to develop a budget for the mass of λ within the λ_∞ -region of Section 9.3.4 and as illustrated in Figure 9.11. Part of our aim is to further develop the formalism while also offering added insights into the causes for water mass transformation, $G(\lambda)$.

We here choose to be specific by considering λ to be an intensive property such as a material tracer concentration, in which case $\lambda \rho dV$ has dimensions of tracer mass. For non-material scalar fields, such as Conservative Temperature or buoyancy, the dimensions are modified accordingly, but the formalism is identical.

9.6.1 Processes affecting the mass of λ -stuff

Our starting point is the Leibniz-Reynolds transport theorem for a scalar field, here including the possibility of scalar sources

$$\frac{d}{dt} \left[\int_{\Omega(\lambda \leq \lambda_\infty)} \lambda \rho dV \right] = \int_{\Omega(\lambda \leq \lambda_\infty)} \rho \dot{\Upsilon} dV - \int_{\partial\Omega(\lambda \leq \lambda_\infty)} [\lambda \rho (\mathbf{v} - \mathbf{v}^{(b)}) + \mathbf{J}] \cdot \hat{\mathbf{n}} dS. \quad (9.76)$$

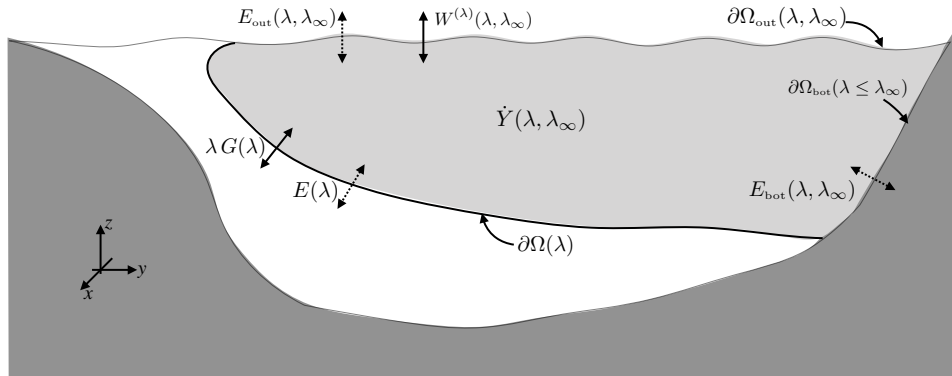


FIGURE 9.11: A λ_∞ -region for studying the λ budget, with the region bounded by the solid-earth bottom, $\partial\Omega_{\text{bot}}(\lambda \leq \lambda_\infty)$, the ocean surface boundary, $\partial\Omega_{\text{out}}(\lambda, \lambda_\infty)$, and the λ -interface, $\partial\Omega(\lambda)$. As drawn here, λ generally increases upward, as per Conservative Temperature, though that assumption is not necessary. In contrast to the $\Delta\lambda$ -region shown in Figure 9.6, the λ_∞ -region has no interior open boundary. Along the surface boundary, the λ budget is affected by the non-advection transport, $E_{\text{out}}(\lambda, \lambda_\infty)$, arising from processes such as diffusion, plus advective transport, $W^{(\lambda)}(\lambda, \lambda_\infty)$, arising from mass transported across the surface that can carry a non-zero amount of λ . Along the bottom, the λ budget is affected by non-advection transport, $E_{\text{bot}}(\lambda, \lambda_\infty)$, arising from processes such as geothermal heating. There is no corresponding advective transport along the bottom since we assume there is no mass crossing the ocean bottom. Along the interior boundary, $\partial\Omega(\lambda)$, the budget is affected by non-advection transport, $E(\lambda)$, arising from diffusion, as well as advective transport through $\lambda G(\lambda)$, with $G(\lambda)$ the interior water mass transformation from Section 9.4. Finally, there is the possibility for an interior volume source, $\dot{Y}(\lambda \leq \lambda_\infty)$, particularly for buoyancy in the presence of a nonlinear equation of state, and for biogeochemical tracers. Note that along $\partial\Omega(\lambda)$, the outward normal, $\hat{\mathbf{n}} = -\nabla\lambda/|\nabla\lambda|$, points to regions of smaller λ , which is the opposite convention used to define w^{dia} in equation (9.38). We encounter this minus sign in deriving equations (9.84) and (9.104).

The left hand side of this budget equation is the time tendency for the mass of λ -stuff within the domain. The right hand side can be decomposed into the following processes that are depicted in Figure 9.11.

Non-conservative sources and sinks

As noted in Section 9.4.4, the source term, $\rho \dot{Y}$, accounts for processes that cannot be represented as the convergence of a flux. We write its region integrated contribution using the shorthand

$$\dot{Y}(\lambda, \lambda_\infty) \equiv \int_{\Omega(\lambda \leq \lambda_\infty)} \rho \dot{Y} \, dV \equiv \int_\lambda^{\lambda_\infty} \dot{m}_Y(\lambda') \, d\lambda'. \quad (9.77)$$

The final equality introduced the mass distribution function for the source, in which

$$\dot{m}_Y(\lambda) \, d\lambda = \text{mass per time of } \lambda\text{-stuff created within } [\lambda - d\lambda/2, \lambda + d\lambda/2]. \quad (9.78)$$

Transport from non-advection processes

The contribution from boundary area integrated non-advection fluxes (e.g., diffusive fluxes and turbulent boundary fluxes) appears in the term

$$-\int_{\partial\Omega(\lambda \leq \lambda_\infty)} \mathbf{J} \cdot \hat{\mathbf{n}} \, d\mathcal{S} = -\int_{\partial\Omega_{\text{out}}(\lambda \leq \lambda_\infty)} \mathbf{J} \cdot \hat{\mathbf{n}} \, d\mathcal{S} - \int_{\partial\Omega_{\text{bot}}(\lambda \leq \lambda_\infty)} \mathbf{J} \cdot \hat{\mathbf{n}} \, d\mathcal{S} - \int_{\partial\Omega(\lambda)} \mathbf{J} \cdot \hat{\mathbf{n}} \, d\mathcal{S}. \quad (9.79)$$

Recall the minus signs arise since a non-advection flux increases the λ content of the region if the flux is oriented into the region, whereas $\hat{\mathbf{n}}$ is the region outward normal. The surface,

$\partial\Omega_{\text{out}}(\lambda \leq \lambda_\infty)$, extends along the upper ocean boundary and supports non-advectional surface boundary fluxes. Likewise, the boundary, $\partial\Omega_{\text{bot}}(\lambda \leq \lambda_\infty)$, intersects the ocean bottom and generally experiences bottom boundary fluxes, such as geothermal heating affecting the enthalpy budget. Finally, the surface, $\partial\Omega(\lambda)$, has non-advectional fluxes that cross the λ -interface, with diffusive fluxes the canonical example. Note that along the surface, $\partial\Omega(\lambda)$, the outward normal points toward regions of smaller λ (see Figure 9.11), so that

$$\hat{\mathbf{n}} = -\nabla\lambda/|\nabla\lambda| \quad \text{on } \partial\Omega(\lambda). \quad (9.80)$$

The sign here is opposite to that used to define the dia-surface flux, w^{dia} , in equation (9.38), where the normal direction is defined as $\nabla\lambda/|\nabla\lambda|$. We encounter this minus sign in deriving equations (9.84) and (9.104) in the following.

The boundary area integrated non-advectional fluxes give rise to non-advectional transports, with these transports having dimensions of mass of λ -stuff per time. We find it useful to write the transports using the shorthand

$$-\int_{\partial\Omega(\lambda \leq \lambda_\infty)} \mathbf{J} \cdot \hat{\mathbf{n}} \, d\mathcal{S} = E_{\text{out}}(\lambda, \lambda_\infty) + E_{\text{bot}}(\lambda, \lambda_\infty) + E(\lambda), \quad (9.81)$$

with a term having a positive value if it increases the λ mass of the region. We furthermore find it useful to introduce the mass distribution functions according to

$$E_{\text{out}}(\lambda, \lambda_\infty) + E_{\text{bot}}(\lambda, \lambda_\infty) = \int_\lambda^{\lambda_\infty} [\dot{m}_{\text{E}}^{\text{out}}(\lambda') + \dot{m}_{\text{E}}^{\text{bot}}(\lambda')] \, d\lambda', \quad (9.82)$$

where

$$\dot{m}_{\text{E}}^{\text{out}}(\lambda) \, d\lambda = \text{mass per time of } \lambda\text{-stuff from } \partial\Omega_{\text{out}} \text{ transport in } [\lambda - d\lambda/2, \lambda + d\lambda/2] \quad (9.83a)$$

$$\dot{m}_{\text{E}}^{\text{bot}}(\lambda) \, d\lambda = \text{mass per time of } \lambda\text{-stuff from } \partial\Omega_{\text{bot}} \text{ transport in } [\lambda - d\lambda/2, \lambda + d\lambda/2]. \quad (9.83b)$$

λ transported with interior mass fluxes

We next consider the contribution to the budget equation (9.76) arising from the transport of λ with mass that crosses the interior interface, $\partial\Omega(\lambda)$, whereby

$$-\int_{\partial\Omega(\lambda)} \lambda \rho (\mathbf{v} - \mathbf{v}^{(\lambda)}) \cdot \hat{\mathbf{n}} \, d\mathcal{S} = -\lambda \int_{\partial\Omega(\lambda)} \rho (\mathbf{v} - \mathbf{v}^{(\lambda)}) \cdot \hat{\mathbf{n}} \, d\mathcal{S} = \lambda G(\lambda), \quad (9.84)$$

To reach this result we noted that λ can be pulled outside of the $\partial\Omega(\lambda)$ integral since it is constant along this surface, thus allowing for the introduction of the water mass transformation, $G(\lambda)$, given by equation (9.40). Furthermore, we made note of the minus sign identified in equation (9.80) for the outward normal along $\partial\Omega(\lambda)$.

Surface boundary mass fluxes

The final term contributing to the right hand side of the λ budget equation (9.76) arises from the surface mass transport along the boundary, $\partial\Omega_{\text{out}}(\lambda \leq \lambda_\infty)$,

$$-\int_{\partial\Omega(\lambda \leq \lambda_\infty)} \lambda \rho (\mathbf{v} - \mathbf{v}^{(\text{b})}) \cdot \hat{\mathbf{n}} \, d\mathcal{S} = \int_{\partial\Omega_{\text{out}}(\lambda \leq \lambda_\infty)} \lambda Q_m \, d\mathcal{S} \equiv W^{(\lambda)}(\lambda, \lambda_\infty). \quad (9.85)$$

To reach the first equality we followed the steps in Section 9.5.2 by using the [kinematic boundary condition](#) to introduce the surface mass transport, $\mathcal{Q}_m d\mathcal{S}$. The final equality introduced a shorthand that corresponds to the $W(\lambda, \lambda_\infty)$ from Section 9.5.2. In the following, we find it useful to introduce the mass distribution function, $\dot{m}_w(\lambda)$, from equation (9.73b), thus rendering

$$W(\lambda, \lambda_\infty) = \int_\lambda^{\lambda_\infty} \dot{m}_w(\lambda') d\lambda' \quad \text{and} \quad W^{(\lambda)}(\lambda, \lambda_\infty) = \int_\lambda^{\lambda_\infty} \lambda \dot{m}_w(\lambda') d\lambda'. \quad (9.86)$$

Following the discussion in Sections 8.5.2, we have not assumed a relation between λ along the interface, $\partial\Omega_{\text{out}}(\lambda \leq \lambda_\infty)$, and the concentration, λ_m , contained in the entering mass. We prefer to keep the discussion general for now, providing a relation only when necessary.

9.6.2 Summary of the λ budget

Bringing terms together leads to the expanded version of the mass budget (9.76) for λ -stuff, now written as

$$\begin{aligned} \frac{d}{dt} \left[\int_{\Omega(\lambda \leq \lambda_\infty)} \lambda \rho dV \right] \\ = \dot{Y}(\lambda, \lambda_\infty) + E_{\text{out}}(\lambda, \lambda_\infty) + E_{\text{bot}}(\lambda, \lambda_\infty) + E(\lambda) + W^{(\lambda)}(\lambda, \lambda_\infty) + \lambda G(\lambda), \end{aligned} \quad (9.87)$$

which has the equivalent expression in terms of mass distribution functions

$$\begin{aligned} \frac{d}{dt} \int_\lambda^{\lambda_\infty} \lambda' m(\lambda') d\lambda' \\ = \int_\lambda^{\lambda_\infty} [\dot{m}_Y(\lambda') + \dot{m}_{\text{E}}^{\text{out}}(\lambda') + \dot{m}_{\text{E}}^{\text{bot}}(\lambda') + \lambda \dot{m}_w(\lambda')] d\lambda' + E(\lambda) + \lambda G(\lambda). \end{aligned} \quad (9.88)$$

These budget equations also include the budget for seawater mass within the $\Omega(\lambda \leq \lambda_\infty)$ region, as seen by dropping the diffusive contribution (since diffusion does not affect the mass of a fluid element), dropping the bottom boundary terms (no seawater mass through the solid-earth bottom), and dropping the interior source term (no interior seawater mass sources), thus revealing the seawater mass budget equation within the λ_∞ -region

$$\frac{d}{dt} \left[\int_{\Omega(\lambda \leq \lambda_\infty)} \rho dV \right] = W(\lambda, \lambda_\infty) + G(\lambda), \quad (9.89)$$

which takes on the following form in terms of mass distribution functions

$$\frac{d}{dt} \int_\lambda^{\lambda_\infty} m(\lambda') d\lambda' = \int_\lambda^{\lambda_\infty} \dot{m}_w(\lambda') d\lambda' + G(\lambda). \quad (9.90)$$

9.6.3 Processes leading to water mass transformation

We now massage the budget equations to explicitly identify processes leading to water mass transformation, $G(\lambda)$. For that purpose, make use of the moment equation (9.37) to write

$$\int_{\Omega(\lambda \leq \lambda_\infty)} \lambda \rho dV = M(\lambda, \lambda_\infty) \langle \lambda \rangle = M(\lambda, \lambda_\infty) \lambda + \int_\lambda^{\lambda_\infty} M(\lambda', \lambda_\infty) d\lambda', \quad (9.91)$$

which then leads to

$$\frac{d[M(\lambda, \lambda_\infty) \langle \lambda \rangle]}{dt} = \lambda \frac{dM(\lambda, \lambda_\infty)}{dt} + \int_\lambda^{\lambda_\infty} \frac{dM(\lambda', \lambda_\infty)}{dt} d\lambda'. \quad (9.92)$$

Note that there is no $d\lambda/dt$ term since λ in this equation is a fixed parameter, not a field.

Integrated water mass transformation over the λ_∞ -region

Use of the λ budget equation (9.87) for the left hand side of equation (9.92), and the mass budget equation (9.89) for the right hand side, yields

$$\begin{aligned} \dot{Y}(\lambda, \lambda_\infty) + E_{\text{out}}(\lambda, \lambda_\infty) + E_{\text{bot}}(\lambda, \lambda_\infty) + E(\lambda) + W^{(\lambda)}(\lambda, \lambda_\infty) + \lambda G(\lambda) \\ = \lambda [W(\lambda, \lambda_\infty) + G(\lambda)] + \int_\lambda^{\lambda_\infty} [W(\lambda', \lambda_\infty) + G(\lambda')] d\lambda'. \end{aligned} \quad (9.93)$$

Observe that the $\lambda G(\lambda)$ term cancels on both sides of this equation. The three contributions from the surface boundary mass fluxes also cancel, as revealed through the following identity

$$W^{(\lambda)}(\lambda, \lambda_\infty) - \lambda W(\lambda, \lambda_\infty) = \int_\lambda^{\lambda_\infty} (\lambda' - \lambda) \dot{m}_w(\lambda') d\lambda' \quad (9.94a)$$

$$= \int_\lambda^{\lambda_\infty} \left[\int_{\lambda'}^{\lambda_\infty} \dot{m}_w(\lambda'') d\lambda'' \right] d\lambda' \quad (9.94b)$$

$$= \int_\lambda^{\lambda_\infty} W(\lambda', \lambda_\infty) d\lambda', \quad (9.94c)$$

where the second equality follows from the double integral formula (9.164) derived in Exercise 9.5. To understand the physical reason we see no water mass transformation from surface mass fluxes, recall the discussion in Section 8.5.2. Namely, mixing and internal sources provide the only means for irreversible changes to water masses and thus to water mass transformation. In contrast, boundary mass transport contributes to transformation only if the mass participates in mixing. That is, the mass associated with boundary mass transport is incorporated into the ocean (or leaves the ocean) only in the presence of mixing. It is reassuring that the budget formalism leads to this same conclusion. Furthermore, this result is consistent with the expression (9.50b), whereby the water mass transformation is, again, determined solely in terms of the non-advection fluxes at the region boundaries, plus the interior source term.

Cancelling the mass transport terms thus leads to the integrated water mass transformation

$$\int_\lambda^{\lambda_\infty} G(\lambda') d\lambda' = \dot{Y}(\lambda, \lambda_\infty) + E_{\text{out}}(\lambda, \lambda_\infty) + E_{\text{bot}}(\lambda, \lambda_\infty) + E(\lambda). \quad (9.95)$$

Each term in this equation has dimensions mass of λ -stuff per time. This equation is an integrated version of the expression (9.50b) for the water mass transformation, here having exposed the processes contributing to transformation over the range $\lambda \leq \lambda_\infty$. Evidently, the accumulated effects from sources within the interior, plus non-advection fluxes along the surface and interior boundaries, lead to an integrated interior water mass transformation.

Water mass transformation across the λ -interface

An expression for the water mass transformation across the λ -interface is derived by taking $\partial/\partial\lambda$ of equation (9.95)

$$G(\lambda) = -\frac{\partial}{\partial\lambda} \left[\dot{Y}(\lambda, \lambda_\infty) + E_{\text{out}}(\lambda, \lambda_\infty) + E_{\text{bot}}(\lambda, \lambda_\infty) + E(\lambda) \right]. \quad (9.96)$$

This equation shows that water mass transformation across a λ -surface, $G(\lambda)$, is the λ -convergence of interior sources, boundary transport, and mixing processes. This equation takes on the following distributional form

$$G(\lambda) = \dot{m}_Y(\lambda) + \dot{m}_E^{\text{bot}}(\lambda) + \dot{m}_E^{\text{out}}(\lambda) - \frac{\partial E(\lambda)}{\partial\lambda}. \quad (9.97)$$

Again, this equation says that water mass transformation across a λ surface occurs if there are interior sources that modify the distribution through $\dot{m}_Y(\lambda)$; diffusive processes at the boundaries through $\dot{m}_E^{\text{bot}}(\lambda)$ and $\dot{m}_E^{\text{out}}(\lambda)$; and the convergence of diffusion across the interior layer interfaces through $-\partial E(\lambda)/\partial\lambda$.

9.6.4 Water mass formation

Recall from Section 9.5.4 that we derived equation (9.75) for water mass formation

$$\mathcal{F} = \dot{m}_W - \frac{\partial G}{\partial\lambda}. \quad (9.98)$$

Making use of equations (9.96) and (9.97) for the water mass transformation then leads to

$$\mathcal{F}(\lambda) = \dot{m}_W(\lambda) + \frac{\partial^2 E(\lambda)}{\partial\lambda^2} + \frac{\partial^2}{\partial\lambda^2} \left[\dot{Y}(\lambda, \lambda_\infty) + E_{\text{out}}(\lambda, \lambda_\infty) + E_{\text{bot}}(\lambda, \lambda_\infty) \right] \quad (9.99a)$$

$$= \dot{m}_W(\lambda) + \frac{\partial^2 E(\lambda)}{\partial\lambda^2} - \frac{\partial [\dot{m}_Y(\lambda) + \dot{m}_E^{\text{bot}}(\lambda) + \dot{m}_E^{\text{out}}(\lambda)]}{\partial\lambda}. \quad (9.99b)$$

The water mass formation equations (9.99a) and (9.99b) are dense with information. To help unpack some of that information, we consider the example in Figure 9.12. In this example, water experiences boundary forcing that increases the lowest value of λ while retaining the highest value unchanged. This forcing destroys waters with low λ and moves the distribution towards larger values. If $\lambda = \Theta$, we think of this example as the effects of surface heating on water masses.

9.6.5 Interior water mass transformation from diffusion

Equations (9.96) and (9.97) summarize the full suite of processes affecting water mass transformation across a chosen λ -surface. To help understand the interior term, follow the discussion from Section 9.4.2 by considering the interior transformation arising from diffusion

$$G_{\text{interior}}(\lambda) = -\frac{\partial E(\lambda)}{\partial\lambda} = \frac{\partial}{\partial\lambda} \left[\int_{\partial\Omega(\lambda)} \mathbf{J} \cdot \hat{\mathbf{n}} \, d\mathcal{S} \right] = \int_{\partial\Omega(\lambda)} \rho (\mathbf{v} - \mathbf{v}^{(\lambda)}) \cdot (\nabla\lambda/|\nabla\lambda|) \, d\mathcal{S}, \quad (9.100)$$

where the final equality used the definition (9.40) of interior water mass transformation according to the integrated dia-surface flux, $w^{\text{dia}} = \rho (\mathbf{v} - \mathbf{v}^{(\lambda)}) \cdot (\nabla\lambda/|\nabla\lambda|)$. Inserting the diffusive flux,

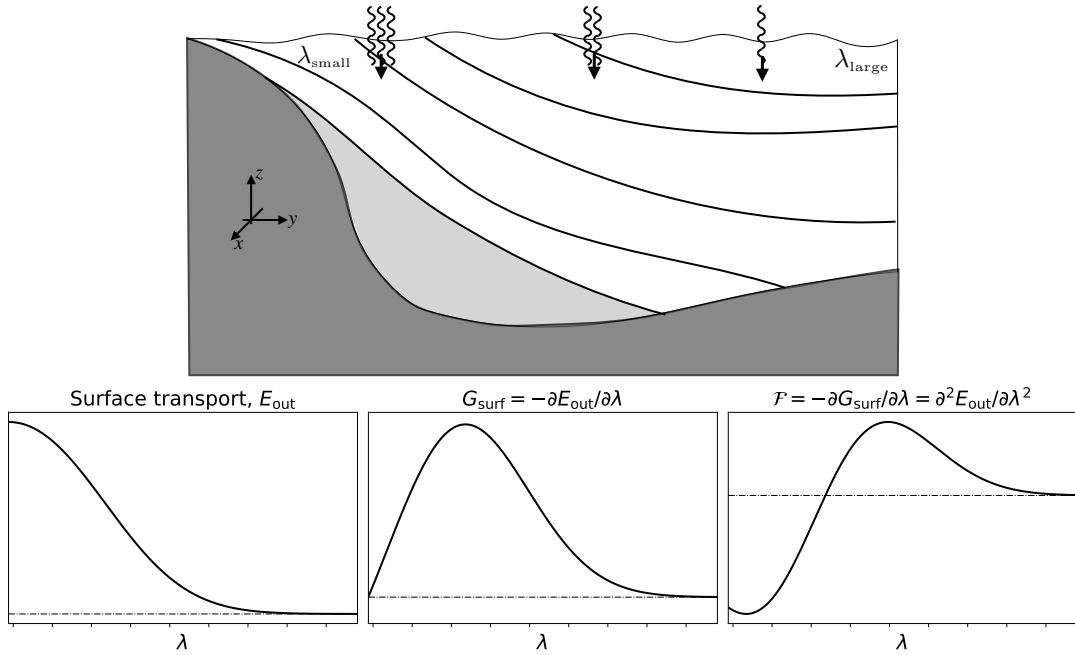


FIGURE 9.12: An example inspired from Figure 4 of [Nurser et al. \(1999\)](#). The top panel shows a section through the λ -field that outcrops with small λ values in the south ($\lambda = \Theta$ in the Southern Ocean is an example). The surface transport is all directed to increase the value of λ throughout the section so that $E_{\text{out}} > 0$ (e.g., surface heating), and with a stronger surface flux acting on the smaller values of λ (e.g., summertime warming in the high latitude Southern Ocean). There is a deep layer (the light gray layer) that does not outcrop in this section and whose values of λ are lower than any at the surface. The lower left panel shows the profile for the surface transport, E_{out} , binned according to λ . E_{out} approaches zero as λ approaches λ_{\max} , so that λ_{\max} remains the maximum value of λ . The middle lower panel shows the surface water mass transformation $G = -\partial E_{\text{out}}/\partial \lambda$, which is all positive, and with largest transformation at intermediate values of λ where the λ -derivative of E_{out} is largest in magnitude. The lower right panel shows the formation, $\mathcal{F} = -\partial G/\partial \lambda = \partial^2 E_{\text{out}}/\partial \lambda^2$. Under this surface forcing, waters with relatively small λ are destroyed ($\mathcal{F} < 0$) while waters with relatively large λ are formed ($\mathcal{F} > 0$). The three lower panels have the same horizontal λ axis, with λ increasing to the right along the horizontal axis. The dot-dash line is the zero line for each panel. All units are arbitrary, with zero the only physically relevant number for the lower three panels.

$\mathbf{J} = -\rho \mathbf{K} \cdot \nabla \lambda$ with \mathbf{K} the diffusion tensor, renders

$$E(\lambda) = - \int_{\partial\Omega(\lambda)} \mathbf{J} \cdot \hat{\mathbf{n}} \, d\mathcal{S} = \int_{\partial\Omega(\lambda)} \rho (\mathbf{K} \cdot \nabla \lambda) \cdot \hat{\mathbf{n}} \, d\mathcal{S}. \quad (9.101)$$

To go a bit further, let us make a couple of simplifying assumptions. First, just like in Section 9.4.2, assume a steady state so that the divergence of the advective flux balances the convergence of the diffusive flux

$$\nabla \cdot (\rho \mathbf{v} \lambda) = \nabla \cdot (\rho \mathbf{K} \cdot \nabla \lambda), \quad (9.102)$$

in which case

$$E(\lambda) = \int_{\partial\Omega(\lambda)} \lambda \rho \mathbf{v} \cdot \hat{\mathbf{n}} \, d\mathcal{S}. \quad (9.103)$$

Next, assume the only λ -dependence for the right hand side integral is with the explicit appearance of λ within the integrand. One example is if the flow is independent of λ and the region of interest has parallel λ surfaces that are equally spaced. In this case we can naively

take the functional derivative to find

$$-\frac{\partial E}{\partial \lambda} = - \int_{\partial\Omega(\lambda)} \rho \mathbf{v} \cdot \hat{\mathbf{n}} \, dS = \int_{\partial\Omega(\lambda)} \frac{\rho \mathbf{v} \cdot \nabla \lambda}{|\nabla \lambda|} \, dS. \quad (9.104)$$

This is the expected expression for a steady state version of $G_{\text{interior}}(\lambda)$, which results from setting $\mathbf{v}^{(\lambda)} = 0$ in equation (9.100).

9.6.6 Surface water mass transformation

Contributions to transformation from surface processes in the transformation equation (9.97) are given by

$$G_{\text{out}}(\lambda) \equiv -\frac{\partial E_{\text{out}}(\lambda, \lambda_\infty)}{\partial \lambda} = \dot{m}_{\text{E}}^{\text{out}}(\lambda) = -\lim_{\delta \lambda \rightarrow 0} \frac{1}{\delta \lambda} \int_{\partial\Omega_{\text{out}}(\lambda \pm \delta \lambda/2)} \mathbf{J} \cdot \hat{\mathbf{n}} \, dS, \quad (9.105)$$

where the final equality made use of equation (9.50b). Such surface transformation forms the focus of many studies of water mass transformation because it only requires surface boundary information, which is generally more accessible than information from interior ocean mixing processes or bottom geothermal processes. Furthermore, much of the transformation of water occurs in surface regions since this region is home to large contributions from surface boundary fluxes and associated ocean mixing. The basic equation we use is the non-advection flux equation (8.68), rewritten here for the scalar field λ

$$-\mathbf{J} \cdot \hat{\mathbf{n}} = \mathcal{Q}_\lambda - \lambda \mathcal{Q}_m = \mathcal{Q}_\lambda^{\text{nonadv}} + (\lambda_m - \lambda) \mathcal{Q}_m. \quad (9.106)$$

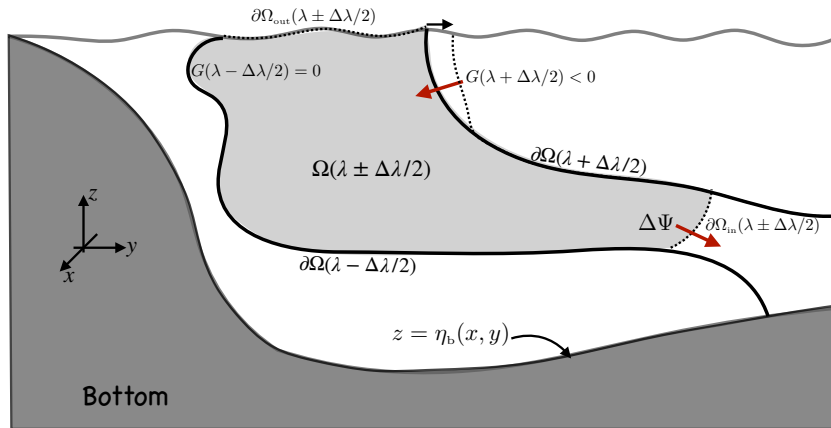


FIGURE 9.13: An example of surface transformation driven circulation oriented according to the Southern Ocean with Antarctica to the left. Here we depict a layer that is exposed to some form of air-sea interaction that causes the interface with $\lambda + \Delta\lambda/2$ to move meridionally. For example, if $\lambda = \Theta$ (Conservative Temperature), then a cold storm generally causes Θ outcrops to move meridionally, with cold isotherms moving northward (black arrow at ocean surface). Movement of the near-surface portion of the $\partial\Omega(\lambda + \Delta\lambda/2)$ interface causes fluid to entrain into the layer and thus contribute to the surface water mass transformation, $G(\lambda + \Delta\lambda/2) < 0$ (red arrow near the surface directed to the south; remember that $G(\lambda) > 0$ when water moves to the larger λ direction). In turn, the boundary, $\partial\Omega_{\text{in}}(\lambda \pm \Delta\lambda/2)$, expands as the near-surface portion of the interface, $\partial\Omega(\lambda + \Delta\lambda/2)$, moves to the north as a result of the entrained new water (black arrow moving to the north). If there is a net convergence of water mass into the layer (as determined by the net mass crossing both layer interfaces $\partial\Omega(\lambda + \Delta\lambda/2)$ and $\partial\Omega(\lambda - \Delta\lambda/2)$), then mass accumulates within the layer $[\lambda - \Delta\lambda/2, \lambda + \Delta\lambda/2]$.

Expressions for the water mass budget are based on integrations over finite regions bounded by λ -surfaces. Since the budgets are formulated over layers, the mass budget offers the means

to make very general inferences about the circulation within those layers, even without a direct measurement of the flow. This is a key power of water mass transformation theory, with surface transformation playing a central role. We depict an example in Figure 9.13 where the surface outcrop of a layer is exposed to air-sea interactions that lead to a meridional movement of the interface, $\lambda + \Delta\lambda/2$. This movement laterally entrains mass into the layer. If there is a net convergence of mass into the layer, then the layer mass increases.

9.7 Buoyancy water mass transformation

In Section 9.2 we considered the transformation of water masses as defined by buoyancy classes. For that analysis we set $\lambda = \gamma$, where γ is a density-like field whose isosurfaces approximate constant buoyancy surfaces and hence **neutral directions**. We here offer further details for such buoyancy water mass analysis. Neither buoyancy nor density are conservative scalars due to seawater's nonlinear **equation of state**. Hence, buoyancy water mass analysis must account for the source and sink terms that add to buoyancy evolution, in addition to diffusive transport processes affecting the conservative tracers, S and Θ .

9.7.1 Material time changes to S and Θ

The material time derivative of γ can be written as the sum of contributions from salinity, S , and Conservative Temperature, Θ ,

$$\rho \dot{\gamma} = \frac{\partial \gamma}{\partial S} \rho \dot{S} + \frac{\partial \gamma}{\partial \Theta} \rho \dot{\Theta}. \quad (9.107)$$

Following the decomposition of the water mass transformation in Section 9.4.4 for a general tracer, we here write the material time derivatives in the form

$$\rho \dot{S} = -\nabla \cdot \mathbf{J}_{\text{int}}^{(S)} - \mathbf{J}_{\text{out}}^{(S)} \cdot \hat{\mathbf{n}} \delta(z - \eta) - \mathbf{J}_{\text{bot}}^{(S)} \cdot \hat{\mathbf{n}} \delta(z - \eta_b) \quad (9.108a)$$

$$\rho \dot{\Theta} = -\nabla \cdot \mathbf{J}_{\text{int}}^{(\Theta)} - \mathbf{J}_{\text{out}}^{(\Theta)} \cdot \hat{\mathbf{n}} \delta(z - \eta) - \mathbf{J}_{\text{bot}}^{(\Theta)} \cdot \hat{\mathbf{n}} \delta(z - \eta_b), \quad (9.108b)$$

where we assumed there are no interior sources of S or Θ . The surface and bottom boundary contributions are weighted by the Dirac delta and projected into the normal direction along the two respective boundary surfaces. Following from the decomposition of water mass transformation given by equation (9.53), we are led to the following form for buoyancy transformation

$$G(\gamma) = \underbrace{- \lim_{\delta\gamma \rightarrow 0} \frac{1}{\delta\gamma} \int_{\Omega(\gamma \pm \delta\gamma/2)} \left(\frac{\partial \gamma}{\partial S} \nabla \cdot \mathbf{J}_{\text{int}}^{(S)} + \frac{\partial \gamma}{\partial \Theta} \nabla \cdot \mathbf{J}_{\text{int}}^{(\Theta)} \right) dV}_{\text{interior buoyancy transformation} = \text{volume integral of convergence}} \\ - \underbrace{\lim_{\delta\gamma \rightarrow 0} \frac{1}{\delta\gamma} \int_{\partial\Omega_{\text{out}}(\gamma \pm \delta\gamma/2)} \left(\frac{\partial \gamma}{\partial S} \mathbf{J}_{\text{out}}^{(S)} + \frac{\partial \gamma}{\partial \Theta} \mathbf{J}_{\text{out}}^{(\Theta)} \right) \cdot \hat{\mathbf{n}} d\mathcal{S}}_{\text{surface buoyancy transformation} = \text{area integral of surface boundary fluxes}} \\ - \underbrace{\lim_{\delta\gamma \rightarrow 0} \frac{1}{\delta\gamma} \int_{\partial\Omega_{\text{bot}}(\gamma \pm \delta\gamma/2)} \left(\frac{\partial \gamma}{\partial S} \mathbf{J}_{\text{bot}}^{(S)} + \frac{\partial \gamma}{\partial \Theta} \mathbf{J}_{\text{bot}}^{(\Theta)} \right) \cdot \hat{\mathbf{n}} d\mathcal{S}}_{\text{bottom buoyancy transformation} = \text{area integral of bottom boundary fluxes}}. \quad (9.109)$$

This expression is explored in the remainder of this section.

9.7.2 Interior buoyancy water mass transformation

Contributions from cabbeling, thermobaricity, and halobaricity (Section 8.3) arise from the interior transformation appearing in equation (9.109). Furthermore, in the special case of a linear equation of state, whereby $\nabla(\partial\gamma/\partial\Theta) = 0$ and $\nabla(\partial\gamma/\partial S) = 0$, then equation (9.57) means that the global integral of the interior transformation vanishes

$$\int_{\gamma_{-\infty}}^{\gamma_{\infty}} G_{\text{int}}(\gamma) d\gamma = \int_{\mathcal{R}} \left(\frac{\partial\gamma}{\partial S} \nabla \cdot \mathbf{J}_{\text{int}}^{(S)} + \frac{\partial\gamma}{\partial\Theta} \nabla \cdot \mathbf{J}_{\text{int}}^{(\Theta)} \right) dV = 0, \quad (9.110)$$

where \mathcal{R} is the global ocean domain. By inference, we conclude that any nonzero result for this integral is a global measure of the effects from the nonlinear equation of state

$$\text{contribution from nonlinear equation of state} = \int_{\gamma_{-\infty}}^{\gamma_{\infty}} G_{\text{int}}(\gamma) d\gamma. \quad (9.111)$$

9.7.3 Surface non-advective flux for S and Θ

We review a few of the distinct characteristics of surface non-advective fluxes of S and Θ as detailed in Section 8.5.2, here working with salinity, S , rather than salt concentration, $S = S/1000$.

Non-advective salt flux

The non-advective surface boundary flux for salt is given by equation (8.68), here written as

$$-\mathbf{J}^{(S)} \cdot \hat{\mathbf{n}} = \mathcal{Q}_S^{\text{non-adv}} + (S_m - S) \mathcal{Q}_m, \quad (9.112)$$

where $\mathcal{Q}_S^{\text{non-adv}}$ is a non-advective salt flux, such as might arise from parameterized turbulent transfer. For the salt concentration of water crossing the ocean surface, we generally take $S_m = 0$ for precipitation, evaporation, and river runoff, whereas $S_m \neq 0$ for sea ice melt and formation. Furthermore, the boundary term, $S = S(z = \eta)$, is commonly approximated by the bulk salt concentration in the upper few meters of the ocean.

Non-advective flux for Conservative Temperature

For Conservative Temperature we follow the discussion in Section 8.5.3, whereby the non-advective flux is given by equation

$$-\mathbf{J}^{(\Theta)} \cdot \hat{\mathbf{n}} = \mathcal{Q}_{\Theta}^{\text{non-adv}} + (\Theta_m - \Theta) \mathcal{Q}_m. \quad (9.113)$$

It is common to approximate the difference $\Theta_m - \Theta(z = \eta) = 0$, in which case the non-advective flux is just due to turbulent and radiative heat fluxes

$$-\mathbf{J}^{(\Theta)} \cdot \hat{\mathbf{n}} = \mathcal{Q}_{\Theta}^{\text{non-adv}} \quad \text{if } \Theta_m - \Theta(z = \eta) = 0. \quad (9.114)$$

9.7.4 Surface buoyancy water mass transformation

In Figure 9.14 we illustrate how a meridional gradient in the surface buoyancy loss causes entrainment into buoyancy layers. The calculation of this surface water mass transformation is

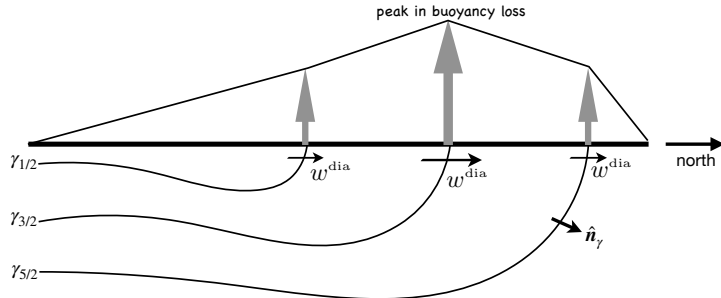


FIGURE 9.14: An example of surface water mass transformation, here illustrating the effects of transformation due to a meridional gradient in the surface buoyancy loss, with γ a density-like coordinate. The example is oriented for the northern hemisphere with increasing latitudes to the north/right. Buoyancy loss is denoted by the thick vertical arrows indicating the removal of buoyancy from the ocean, thus causing surface water to loose buoyancy and get more dense. The surface buoyancy loss causes γ interfaces to migrate to the south (denser water moves southward). This southward migration of the density outcrops causes dianeutral mass flux to move from lighter layers to denser layers, thus causing entrainment into the denser layers (black vectors pointed to the north, w^{dia}). With a peak in the buoyancy loss at a particular latitude, more entrainment is driven into the layer to the north of the peak (water converges to the layer $\gamma_{3/2} \leq \gamma \leq \gamma_{5/2}$) and less entrainment into the layer to the south (water diverges from the layer $\gamma_{1/2} \leq \gamma \leq \gamma_{3/2}$).

found by inserting the surface fluxes into equation (9.109) as per Section 9.7.3 to write

$$G(\gamma)^{\text{surf}} = \lim_{\delta\gamma \rightarrow 0} \frac{1}{\delta\gamma} \int_{\partial\Omega_{\text{out}}(\gamma \pm \delta\gamma/2)} (\gamma \beta [Q_S^{\text{nonadv}} + (S_m - S) Q_m] - \gamma \alpha [Q_\Theta^{\text{non-adv}} + (\Theta_m - \Theta) Q_m]) d\mathcal{S}, \quad (9.115)$$

where we introduced the thermal expansion and saline contraction coefficients, here defined according to⁹

$$\alpha = -\frac{1}{\gamma} \frac{\partial \gamma}{\partial \Theta} \quad \text{and} \quad \beta = \frac{1}{\gamma} \frac{\partial \gamma}{\partial S}. \quad (9.116)$$

Recall that $G(\gamma) > 0$ occurs when water is transformed into regions with larger γ . For example, net surface cooling in the presence of a positive thermal expansion coefficient ($\alpha > 0$) leads to $Q_\Theta^{\text{non-adv}} + (\Theta_m - \Theta) Q_m < 0$. Such cooling then leads to a positive contribution to $G(\gamma)^{\text{surf}}$ as water is transformed from light to heavy γ -classes. Likewise, a positive net salt transport into the upper ocean, $Q_S^{\text{nonadv}} + (S_m - S) Q_m > 0$, leads to a positive contribution to $G(\gamma)^{\text{surf}}$.

The integrand to equation (9.115) corresponds to minus the surface buoyancy flux derived in Section 8.6.3. The only difference is that we here make use of the surface element, $d\mathcal{S}$, and the corresponding fluxes $Q_\Theta^{\text{non-adv}}$, Q_S^{nonadv} , and Q_m . However, if the ocean surface has no overturns, we can write its vertical position as $z = \eta(x, y, t)$ and can also define the horizontal projection of the area element as

$$d\mathcal{S} = \sqrt{1 + |\nabla \eta|^2} dA. \quad (9.117)$$

In this case we can introduce the fluxes $Q_\Theta^{\text{non-adv}}$, $Q_S^{\text{non-adv}}$, and Q_m used in Section 8.6.3 via

$$Q_\Theta^{\text{non-adv}} d\mathcal{S} = Q_\Theta^{\text{non-adv}} dA \quad (9.118a)$$

$$Q_S^{\text{nonadv}} d\mathcal{S} = Q_S^{\text{non-adv}} dA \quad (9.118b)$$

$$Q_m d\mathcal{S} = Q_m dA, \quad (9.118c)$$

⁹For Boussinesq oceans, we replace the factor of γ^{-1} with ρ_0^{-1} on the right hand side of equation (9.116) with ρ_0 , the constant Boussinesq reference density.

to render

$$G(\gamma)^{\text{surf}} = \lim_{\delta\gamma \rightarrow 0} \frac{1}{\delta\gamma} \int_{\partial\Omega_{\text{out}}(\gamma \pm \delta\gamma/2)} (\gamma \beta [Q_s^{\text{non-adv}} + (S_m - S) Q_m] - \gamma \alpha [Q_\Theta^{\text{non-adv}} + (\Theta_m - \Theta) Q_m]) dA. \quad (9.119)$$

Integrating the surface transformation (9.119) over all γ -classes leads to the identity

$$\int_{\gamma=-\infty}^{\gamma=\infty} G(\gamma)^{\text{surf}} d\gamma = \int_{z=\eta} \left(\gamma \beta [Q_s^{\text{non-adv}} + (S_m - S) Q_m] - \gamma \alpha [Q_\Theta^{\text{non-adv}} + (\Theta_m - \Theta) Q_m] \right) dA. \quad (9.120)$$

This equality means that the diagnosed surface transformation, $G(\gamma)^{\text{surf}}$, which is obtained by binning surface fluxes into γ -classes, must properly add up to the area integrated surface fluxes as weighted by the surface value of γ . This equality is a useful check on the integrity of numerical binning code used to diagnose surface water mass transformation.

9.8 Tracer water mass transformation within γ -layers

In Sections 9.5 and 9.6 we developed the budgets for λ within layers defined λ . Here we extend that analysis to develop budgets for a tracer concentration, C , within a region within a layer of buoyancy, γ , as depicted in Figure 9.15. The upper panels to this figure illustrate a tracer patch in geographic/depth \mathbf{x} -space along with isolines of buoyancy, whereas the lower panels show the tracer distribution (histogram) binned within the buoyancy classes (\mathbf{q} -space). If the tracer is mixed within a layer, such as via the neutral diffusion process of Section 7.4, then the tracer patch is spread laterally within the buoyancy layer and yet the distribution (lower panel) is unchanged. In contrast, if the tracer is mixed across layer interfaces (dianeutral transport) then the tracer distribution is spread within buoyancy space.

Another means to alter the tracer distribution is to modify the buoyancy field. This situation is especially common for tracer near the surface, where boundary buoyancy forcing can act to move the layers thus causing tracer to move between layers even if the tracer patch is stationary in \mathbf{x} -space (e.g., see Figures 9.13 and 9.14). That is, if the tracer moves at a velocity that is distinct from the velocity of buoyancy surfaces, then that relative motion changes the tracer's distribution within buoyancy classes.

9.8.1 General form of the mass budget

As depicted in Figure 9.15 for buoyancy layers, and Figure 9.16 for generic layers, there are two general processes whereby a tracer distribution within layers can be modified: (i) the tracer can mix between layers and (ii) the layers can move relative to the tracer. These ideas transcend buoyancy and thus can be applied to any scalar field, λ , used to classify water masses. We quantify these two processes by writing the time change of tracer content within a λ -layer, which is arrived at by applying the Leibniz-Reynolds transport theorem to a λ -layer

$$\frac{d}{dt} \Delta M_C(\lambda \pm \Delta\lambda/2) = \int_{\Omega(\lambda \pm \Delta\lambda/2)} \rho \dot{C} dV - \oint_{\partial\Omega(\lambda \pm \Delta\lambda/2)} \rho C (\mathbf{v} - \mathbf{v}^{(b)}) \cdot \hat{\mathbf{n}} dS, \quad (9.121)$$

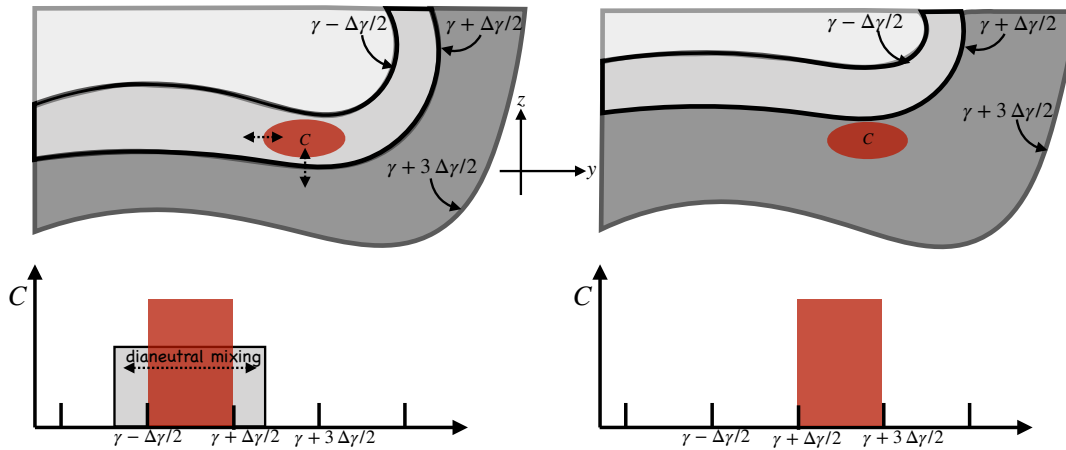


FIGURE 9.15: Depicting a tracer patch within the buoyancy layer bounded by the interface values $[\gamma - \Delta\gamma/2, \gamma + \Delta\gamma/2]$ (left panel) and $[\gamma + \Delta\gamma/2, \gamma + 3\Delta\gamma/2]$ (right panel). The upper panels show the tracer and buoyancy in geographic/depth x -space whereas the bottom panels show the tracer distribution (histogram) binned according to buoyancy (q -space). There are two general means to modify the distribution of tracer within the buoyancy classes. The first occurs via dianeutral mixing that spreads the tracer distribution to other buoyancy layers as depicted by the vertical arrow in the upper left panel and the horizontal arrows in the lower left panel. The lateral arrow in the upper left panel depicts neutral diffusion, which laterally spreads the tracer within a layer but does not alter the distribution across layers (see Section 7.4). The second means to alter the distribution occurs when the buoyancy surfaces move relative to the tracer. This scenario is depicted in the lower right panel whereby the tracer patch originally in buoyancy layer $[\gamma - \Delta\gamma/2, \gamma + \Delta\gamma/2]$ now finds itself in the layer $[\gamma + \Delta\gamma/2, \gamma + 3\Delta\gamma/2]$. This depiction is not realistic, since motion of interior buoyancy surfaces generally occurs along with mixing of tracer patches. Nonetheless, this example emphasizes that motion of the buoyancy surfaces need not precisely coincide with motion of the tracer patch.

where we wrote the mass of tracer C within the λ -layer

$$\Delta M_C(\lambda \pm \Delta\lambda/2) = \int_{\Omega(\lambda \pm \Delta\lambda/2)} \rho C \, dV. \quad (9.122)$$

The volume integral on the right hand side of equation (9.121) arises from material time changes to the tracer within the layer, whereas the surface integral arises from dia-surface transport across the layer boundary.

9.8.2 Tracer processes

We determine the material time changes for a conservative tracer according to the convergence of a flux

$$\rho \dot{C} = \rho \frac{DC}{Dt} = -\nabla \cdot \mathbf{J}. \quad (9.123)$$

Many biogeochemical tracers have additional source terms beyond the flux convergence considered here. As in Section 9.4.4, sources can be readily incorporated into the following by adding a source tendency term that acts throughout a layer.

The divergence theorem converts the convergence, $-\nabla \cdot \mathbf{J}$, into the area integral of fluxes over the layer boundaries, including interior layer interfaces as well as intersections with the surface and bottom boundaries. For the interior interfaces it is typically simpler in practice to bin the volume integrated material time changes within the λ -classes. In contrast, the surface and bottom boundary contributions are fed into the budget via Neumann boundary conditions applied to the flux \mathbf{J}

$$\mathbf{J} \cdot \hat{\mathbf{n}} \, dS = \text{boundary tracer transport}. \quad (9.124)$$

Note that when there is an advective/skew diffusive component to the subgrid scale flux (Chapters 6 and 7), then it adds to the resolved advective component to render a residual mean material time operator

$$\rho \frac{D^\dagger C}{Dt} = -\nabla \cdot \mathbf{J}^{\text{non-adv}}, \quad (9.125)$$

where

$$\frac{D^\dagger}{Dt} = \frac{\partial}{\partial t} + (\mathbf{v} + \mathbf{v}^*) \cdot \nabla, \quad (9.126)$$

with \mathbf{v}^* an eddy-induced velocity (see Section 7.1). For the purposes of water mass transformation analysis, we write

$$\dot{C} = \frac{D^\dagger C}{Dt}, \quad (9.127)$$

thus incorporating the eddy-induced advection into the kinematic expression for the material time derivative.

There are many interior and boundary processes that contribute to \dot{C} within a layer. We here write the following as a general expression for these contributions to the layer budget

$$\Delta E_c(\lambda \pm \Delta\lambda/2) = \int_{\Omega(\lambda \pm \Delta\lambda/2)} \rho \dot{C} dV = - \int_{\Omega(\lambda \pm \Delta\lambda/2)} \nabla \cdot \mathbf{J} dV, \quad (9.128)$$

which is sometimes usefully decomposed into interior and surface boundary processes

$$\Delta E_c^{\text{int}}(\lambda \pm \Delta\lambda/2) = \int_{\Omega(\lambda \pm \Delta\lambda/2)} \rho \dot{C}^{\text{int}} dV \quad (9.129a)$$

$$\Delta E_c^{\text{out}}(\lambda \pm \Delta\lambda/2) = - \int_{\partial\Omega_{\text{out}}(\lambda \pm \Delta\lambda/2)} \mathbf{J} \cdot \hat{\mathbf{n}} d\mathcal{S}. \quad (9.129b)$$

If the region boundary intersects the ocean bottom along $\partial\Omega_{\text{bot}}(\lambda \pm \Delta\lambda/2)$, then there is an additional bottom boundary contribution in the form

$$\Delta E_c^{\text{bot}}(\lambda \pm \Delta\lambda/2) = - \int_{\partial\Omega_{\text{bot}}(\lambda \pm \Delta\lambda/2)} \mathbf{J} \cdot \hat{\mathbf{n}} d\mathcal{S}. \quad (9.130)$$

9.8.3 Transport across an interior layer interface

The surface integral in the budget (9.121) involves transport across the layer interfaces, with this transport requiring motion of the interface relative to a fluid particle. The same formalism introduced earlier can be used to compute this transport. That is, we can generalize the transformation equation (9.46e) to write

$$G_c(\lambda) = \int_{\partial\Omega(\lambda)} \rho C (\mathbf{v} - \mathbf{v}^{(\text{b})}) \cdot \hat{\mathbf{n}} d\mathcal{S} = \frac{\partial}{\partial \lambda} \int_{\Omega(\lambda_0 \leq \lambda)} \rho \dot{\lambda} C dV. \quad (9.131)$$

As a check, note that for the special case where the tracer concentration is a constant along the layer interface, then $G_c(\lambda) = C G(\lambda)$. We consider this special case in Section 9.9 when studying budgets over regions bounded by a tracer isosurface.

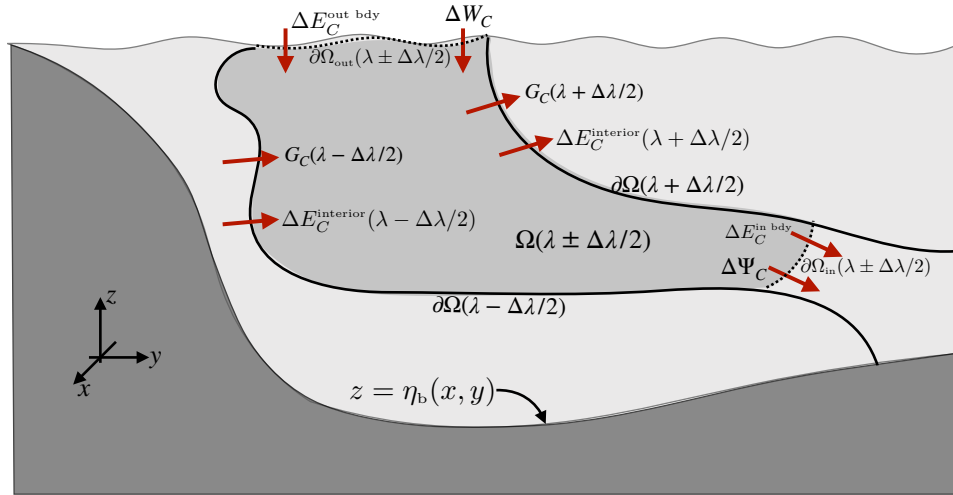


FIGURE 9.16: As for the schematic of a layer fluid mass budget depicted in Figure 9.6, we here illustrate the budget for a tracer, C , within a layer defined by the scalar property, λ , within the range $[\lambda - \Delta\lambda/2, \lambda + \Delta\lambda/2]$ and defined over a geographical/depth domain $\partial\Omega_{\text{in}}(\lambda \pm \Delta\lambda/2) + \partial\Omega_{\text{out}}(\lambda \pm \Delta\lambda/2) + \partial\Omega(\lambda + \Delta\lambda/2) + \partial\Omega(\lambda - \Delta\lambda/2)$. The budget for a tracer, C , over this layer is affected by the transport of tracer substance across the variety of layer boundaries. Transport processes include those determined by mixing and/or radiation across interior and surface boundaries, ΔE_C (equation (9.129b)). This term has no associated transfer of fluid mass and thus is absent from the water mass budget in Figure 9.6. Tracer budgets are also affected by processes that move fluid mass across layer boundaries: water mass transformation processes giving rise to $G_C(\lambda \pm \Delta\lambda/2)$ (equation (9.131)); transport across the surface domain boundary, ΔW_C , arising from precipitation, evaporation, runoff, and melt (equation (9.132)); and transport within the circulation crossing an interior domain boundary, $\Delta\Psi_C$ (equation (9.133)).

9.8.4 Transport across interior and surface boundaries

We now consider the impact on layer tracer mass budgets due to boundary transport. The budget contribution from mass fluxes crossing the ocean surface boundary is determined by making use of the surface [kinematic boundary condition](#)

$$\Delta W_C = \int_{\partial\Omega_{\text{out}}(\lambda \pm \Delta\lambda/2)} \rho C (\mathbf{v} - \mathbf{v}^{(\text{b})}) \cdot \hat{\mathbf{n}} \, d\mathcal{S} = \int_{\partial\Omega_{\text{out}}(\lambda \pm \Delta\lambda/2)} Q_m C_m \, dA, \quad (9.132)$$

where C_m is the tracer concentration within the mass transported across the boundary.¹⁰ As a check, note that in the special case of a constant tracer concentration in the mass transported across the boundary, then $\Delta W_C = C_m \Delta W$, where ΔW is the water mass transported across the ocean free surface as given by equation (9.66).

For the interior open boundary the contribution is written in the generic manner

$$\Delta\Psi_C = \int_{\partial\Omega_{\text{in}}(\lambda \pm \Delta\lambda/2)} C \rho (\mathbf{v} - \mathbf{v}^{(\text{b})}) \cdot \hat{\mathbf{n}} \, d\mathcal{S}. \quad (9.133)$$

Again, in the special case where the tracer concentration is a constant, C_b , along the interior boundary, then $\Delta\Psi_C = C_b \Delta\Psi$, where $\Delta\Psi$ is the fluid mass transport given by equation (9.64).

¹⁰Note that equation (26) in [Groeskamp et al. \(2019\)](#) incorrectly writes the integrand in equation (9.132) as $Q_m (C_m - C)$.

9.8.5 The layer tracer budget

Bringing all terms together leads to the layer tracer mass budget

$$\frac{d\Delta M_c}{dt} + \Delta\Psi_c = \Delta E_c + \Delta W_c - [G_c(\lambda + \Delta\lambda/2) - G_c(\lambda - \Delta\lambda/2)], \quad (9.134)$$

which is directly analogous to the fluid layer mass budget (9.68), with the added term ΔE_c arising from material tracer changes. As for the fluid mass budget discussed in Section 9.5.3, the layer tracer budget (9.134) provides the framework for rather general inferences about tracer transport within λ -classes.

9.8.6 Further study

Much in this section follows the treatment given by [Groeskamp et al. \(2019\)](#), which offers specific examples of tracer mass analysis.

9.9 Regions bounded by a tracer contour/surface

In Section 9.8 we developed layer tracer budget equations where the scalar field, λ , that defines the layer is generally distinct from the tracer, C , whose budget is examined. In this section we specialize to the case where $\lambda = C$ so that the region boundaries are determined by the tracer whose budget is under study. These budgets were introduced in Sections 9.5 and 9.6, and here we derive some further results.

As in Section 9.8, our starting point is the Leibniz-Reynolds transport theorem as applied to fluid mass and tracer mass computed over an arbitrary region, \mathcal{R} ,

$$\frac{d}{dt} \left[\int_{\mathcal{R}} \rho C \, dV \right] = - \int_{\partial\mathcal{R}} [\rho C (\mathbf{v} - \mathbf{v}^{(b)}) + \mathbf{J}] \cdot \hat{\mathbf{n}} \, d\mathcal{S} \quad (9.135a)$$

$$\frac{d}{dt} \left[\int_{\mathcal{R}} \rho \, dV \right] = - \int_{\partial\mathcal{R}} [\rho (\mathbf{v} - \mathbf{v}^{(b)})] \cdot \hat{\mathbf{n}} \, d\mathcal{S}. \quad (9.135b)$$

The region, \mathcal{R} , is arbitrary and can in general be disconnected. Throughout this section we make use of the following shorthand notation for region-integrated quantities

$$M = \int_{\mathcal{R}} \rho \, dV \quad \text{region fluid mass} \quad (9.136a)$$

$$M_c = \int_{\mathcal{R}} C \rho \, dV \quad \text{region tracer mass} \quad (9.136b)$$

$$\langle C \rangle = \frac{1}{M} \int_{\mathcal{R}} C \rho \, dV = \frac{M_c}{M} \quad \text{region averaged tracer concentration.} \quad (9.136c)$$

9.9.1 Closed region bounded by a tracer surface/contour

Consider a closed region, $\tilde{\mathcal{R}}$, bounded by a surface of constant tracer concentration, $C = \tilde{C}$, such as depicted in Figure 9.17. The tracer budget (9.135a) for this region is given by

$$\frac{d(M \langle C \rangle)}{dt} = -\tilde{C} \int_{\partial\tilde{\mathcal{R}}} \rho (\mathbf{v} - \mathbf{v}^{(b)}) \cdot \hat{\mathbf{n}} \, d\mathcal{S} - \int_{\partial\tilde{\mathcal{R}}} \mathbf{J} \cdot \hat{\mathbf{n}} \, d\mathcal{S}, \quad (9.137)$$

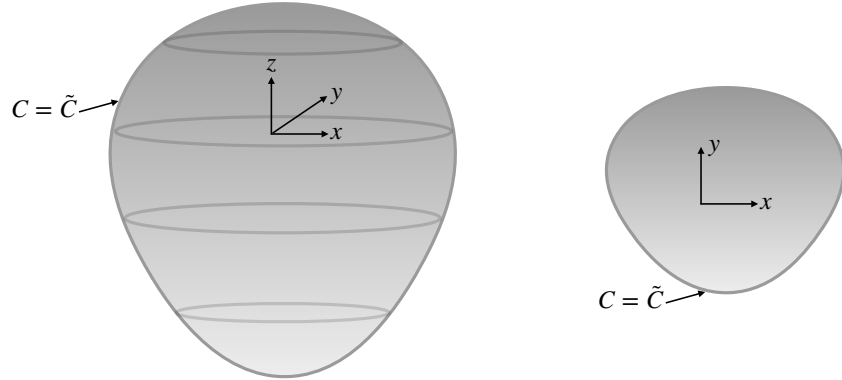


FIGURE 9.17: Left panel: a closed three-dimensional region, $\tilde{\mathcal{R}}$, with its boundary, $\partial\tilde{\mathcal{R}}$, defined by a surface of constant tracer concentration, $C = \tilde{C}$. Right panel: the analog closed two-dimensional region with its boundary defined by a contour of constant tracer concentration, $C = \tilde{C}$.

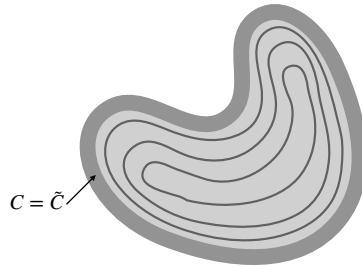


FIGURE 9.18: A two-dimensional region bounded by a finite-thick shell with constant tracer concentration, $C = \tilde{C}$. Inside the shell region the tracer concentration is not uniform.

where we pulled the tracer concentration outside of the surface integral since, by construction, it is constant on the boundary, $\partial\tilde{\mathcal{R}}$. Use of the mass budget (9.135b) then leads to the rather tidy result

$$\frac{d[M(\langle C \rangle - \tilde{C})]}{dt} = - \int_{\partial\tilde{\mathcal{R}}} \mathbf{J} \cdot \hat{\mathbf{n}} \, d\mathcal{S}. \quad (9.138)$$

The left hand side is the time change of the mass-weighted difference between the region averaged tracer concentration, $\langle C \rangle$, and the value of the tracer concentration defining the region boundary, \tilde{C} . These time changes are driven by a nonzero diffusive tracer transport bringing tracer mass across the region boundary. A nonzero diffusive flux on the region boundary arises only when there is a gradient of tracer concentration across that boundary. In the special case of a zero net diffusive tracer transport across the region boundary, the budget equation (9.138) reaches a steady state whereby

$$\frac{d}{dt} \left[M(\langle C \rangle - \tilde{C}) \right] = 0 \iff \int_{\partial\tilde{\mathcal{R}}} \mathbf{J} \cdot \hat{\mathbf{n}} \, d\mathcal{S} = 0. \quad (9.139)$$

A three-dimensional region bounded by a constant tracer concentration is not commonly encountered in large-scale stratified ocean and atmospheric fluids. In contrast, we often encounter quasi-two-dimensional regions as depicted in Figure 9.18, in which one may find two-dimensional surfaces bounded by a closed contour of constant tracer concentration. For example, in many parts of the ocean and atmosphere, transport occurs predominantly along two-dimensional surfaces defined by a constant buoyancy. We may thus find closed contours of tracer concentrations along constant buoyancy surfaces.

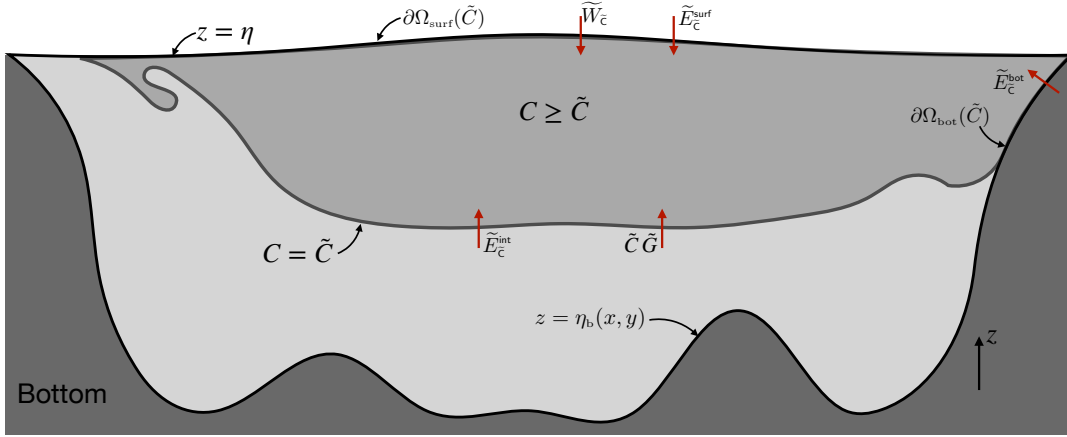


FIGURE 9.19: An ocean region where the tracer concentration is greater than a nominal value, $C \geq \tilde{C}$. A specific example is with $C = \Theta$, the Conservative Temperature, in which we are concerned with the ocean with temperature greater than Θ . Here we depict a case where the tracer concentration generally increases upward (as with $C = \Theta$), and yet with vertical stratification not everywhere monotonic, such as for $C = \Theta$ in the high latitudes where salinity effects on density stratification become dominant. Transport processes affecting the budget of C within this region arise from mixing at the interior boundary and surface boundary, \tilde{E}_C^{int} and \tilde{E}_C^{surf} , advection at the surface, $\tilde{W}_{\tilde{C}}$, and the tracer weighted water mass transformation across the interior layer boundary, $\tilde{C}\tilde{G}$. Arrows are oriented in which a positive value for the corresponding term adds tracer to the region.

To help illustrate a necessary condition to reach a steady state, consider the particular example depicted in Figure 9.18. In this figure, the tracer contour defining the region boundary is a thick shell defined by a uniform concentration $C = \tilde{C}$. The diffusive flux vanishes at each point within the boundary shell since the tracer concentration is uniform. Hence, the steady budget (9.139) leads to

$$(\langle C \rangle - \tilde{C}) \frac{dM}{dt} + M \frac{d\langle C \rangle}{dt} = 0. \quad (9.140)$$

If the total fluid mass within the region is constant, then the averaged tracer concentration is also constant, so that both terms in this steady budget vanish individually. Even so, this configuration does not reach a steady state at each point throughout the domain interior. The reason is that diffusion in the interior causes tracer to move from regions of high concentration to low concentration. Consequently, at any particular point within the domain there is an evolving tracer concentration. The only way for each point to reach a steady state within a region bounded by a tracer contour is for the tracer concentration to be a uniform constant throughout the region interior

$$C = \tilde{C} \quad \text{steady state tracer throughout a closed tracer region.} \quad (9.141)$$

Diffusion thus expels tracer gradients from steady state regions bounded by closed tracer contours, thus leaving a homogenous interior. We proved this same result from a different perspective in Section 5.8. It is satisfying to see this result follow from the present formalism based on Leibniz-Reynolds.

9.9.2 Region with $C \geq \tilde{C}$

As a second example, consider the tracer budget for a region where the tracer concentration is greater than or equal to a particular tracer value, such as depicted in Figure 9.19. In contrast

to the domain in Figure 9.16, here there is no inner boundary. To develop the fluid mass budget and the tracer mass budget, we introduce the fluid mass and tracer mass for the region with $C \geq \tilde{C}$

$$\tilde{M} = \int_{C \geq \tilde{C}} \rho \, dV \quad (9.142a)$$

$$\tilde{M}_{\bar{C}} = \int_{C \geq \tilde{C}} C \rho \, dV = \tilde{M} \langle C \rangle. \quad (9.142b)$$

We also make use of terms arising from water mass transformation across the \tilde{C} interface

$$\tilde{G} = - \int_{C=\tilde{C}} \rho (\mathbf{v} - \mathbf{v}^{(b)}) \cdot \hat{\mathbf{n}} \, d\mathcal{S} = - \int_{C=\tilde{C}} \rho w^{\text{dia}} \, d\mathcal{S} \quad (9.143a)$$

$$\tilde{G}_{\bar{C}} = - \int_{C=\tilde{C}} C \rho (\mathbf{v} - \mathbf{v}^{(b)}) \cdot \hat{\mathbf{n}} \, d\mathcal{S} = - \int_{C=\tilde{C}} C \rho w^{\text{dia}} \, d\mathcal{S}, \quad (9.143b)$$

as well as terms arising from ocean surface boundary mass transport

$$\tilde{W} = - \int_{\partial\Omega_{\text{surf}}(\tilde{C})} \rho (\mathbf{v} - \mathbf{v}^{(b)}) \cdot \hat{\mathbf{n}} \, d\mathcal{S} = \int_{\partial\Omega_{\text{surf}}(\tilde{C})} Q_m \, dA \quad (9.144a)$$

$$\tilde{W}_{\bar{C}} = - \int_{\partial\Omega_{\text{surf}}(\tilde{C})} C \rho (\mathbf{v} - \mathbf{v}^{(b)}) \cdot \hat{\mathbf{n}} \, d\mathcal{S} = \int_{\partial\Omega_{\text{surf}}(\tilde{C})} C Q_m \, dA. \quad (9.144b)$$

Finally, we need terms arising from subgrid scale transport across the \tilde{C} interface, ocean surface, and ocean bottom

$$\tilde{E}_{\bar{C}}^{\text{int}} = - \int_{C=\tilde{C}} \mathbf{J} \cdot \hat{\mathbf{n}} \, d\mathcal{S} \quad (9.145a)$$

$$\tilde{E}_{\bar{C}}^{\text{surf}} = - \int_{\partial\Omega_{\text{surf}}(\tilde{C})} \mathbf{J} \cdot \hat{\mathbf{n}} \, d\mathcal{S} \quad (9.145b)$$

$$\tilde{E}_{\bar{C}}^{\text{bot}} = - \int_{\partial\Omega_{\text{bot}}(\tilde{C})} \mathbf{J} \cdot \hat{\mathbf{n}} \, d\mathcal{S}. \quad (9.145c)$$

Recall that $\hat{\mathbf{n}}$ is the outward normal on a boundary so that positive values for the transports (9.145a)-(9.145c) increase the tracer mass within the region. For equations (9.143a) and (9.143b), we introduced the dia-surface transport velocity according to equation (9.38) for flow across the $C = \tilde{C}$ layer interface, with $\hat{\mathbf{n}} = \nabla C / |\nabla C|$ for these transports. Likewise, for equations (9.144a) and (9.144b) we made use of the surface kinematic boundary condition

$$\rho (\mathbf{v} - \mathbf{v}^{(s)}) \cdot \hat{\mathbf{n}} \, d\mathcal{S} = -Q_m \, dA, \quad (9.146)$$

where Q_m is the mass transport across the free surface, with $Q_m > 0$ adding mass to the ocean, and dA is the horizontal projection of the surface area element. By inspection of Figure 9.19, the fluid mass budget and tracer mass budget for this region are given by

$$\frac{d\tilde{M}}{dt} = \tilde{G} + \tilde{W} \quad (9.147a)$$

$$\frac{d[\tilde{M} \langle C \rangle]}{dt} = \tilde{C} \tilde{G} + \tilde{W}_{\bar{C}} + \tilde{E}_{\bar{C}}^{\text{surf}} + \tilde{E}_{\bar{C}}^{\text{bot}} + \tilde{E}_{\bar{C}}^{\text{int}}, \quad (9.147b)$$

where we assumed that no mass crosses through the solid earth. Furthermore, along the \tilde{C} -boundary we pulled the tracer concentration outside of the surface integral to write $\tilde{G}_{\bar{C}} = \tilde{C} \tilde{G}$.

Just as we did in Section 9.9.1, the tracer budget (9.147b) can be simplified by making use of the fluid mass budget (9.147a) to eliminate the water mass transformation contribution \tilde{G} , thus rendering

$$\frac{d\tilde{M}_{\bar{C}}}{dt} = [\tilde{W}_{\bar{C}} - \tilde{W} \tilde{C}] + \tilde{E}_{\bar{C}}^{\text{surf}} + \tilde{E}_{\bar{C}}^{\text{bot}} + \tilde{E}_{\bar{C}}^{\text{int}}. \quad (9.148)$$

In this equation we introduced the *internal tracer mass* according to

$$\tilde{M}_{\bar{C}} \equiv \tilde{M} (\langle C \rangle - \tilde{C}) = \int_{C \geq \tilde{C}} (C - \tilde{C}) \rho dV. \quad (9.149)$$

For completeness we express the internal tracer mass budget (9.148) in its integral form

$$\frac{d\tilde{M}_{\bar{C}}}{dt} = \int_{\partial\Omega_{\text{out}}} [Q_m (C - \tilde{C}) dA - \mathbf{J} \cdot \hat{\mathbf{n}} dS] - \int_{\partial\Omega_{\text{bot}}} \mathbf{J} \cdot \hat{\mathbf{n}} dS - \int_{C=\tilde{C}} \mathbf{J} \cdot \hat{\mathbf{n}} dS. \quad (9.150)$$

9.9.3 Comments and further study

Elimination of the water mass transformation, \tilde{G} , from the internal tracer mass budget equations (9.148) and (9.150) offers a practical advantage since \tilde{G} can be rather noisy in applications. Furthermore, for some applications (e.g., see [Holmes et al. \(2019b\)](#)) it is sufficient to consider the simpler budget (9.148) for internal tracer mass, rather than the budget (9.147b) for the total tracer mass.



9.10 Exercises

EXERCISE 9.1: TRANSFORMATION FROM DIFFUSION

We here express the equations for water mass transformation for a tracer, λ , satisfying

$$\rho \frac{D\lambda}{Dt} = -\nabla \cdot \mathbf{J}, \quad (9.151)$$

where \mathbf{J} is a downgradient diffusive flux

$$\mathbf{J} = -\rho \kappa \nabla \lambda, \quad (9.152)$$

with $\kappa > 0$ a kinematic diffusivity. Furthermore, assume $\lambda = \lambda(z, t)$ so that $\nabla \lambda = \partial_z \lambda \hat{z}$. Correspondingly, all λ surfaces are horizontal so that transformation across a λ surface is transformation across a constant z surface, which we write as $z = z(\lambda)$.

- Write the expression for the interior water mass transformation, $G(\lambda)$, arising from downgradient vertical diffusion. Write the form as a surface integral over the horizontal surface whose vertical position is $z = z(\lambda)$.
- Write the equivalent form for $G(\lambda)$ as a volume integral, following the methods from Section 9.4.3, and assume the volume integral is over a layer with thickness δz surrounding the $z = z(\lambda)$ horizontal surface.

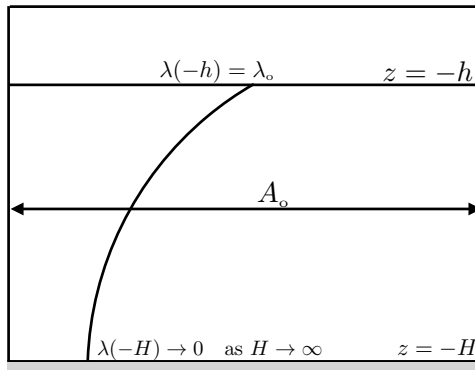


FIGURE 9.20: Depicting the setup for Exercise 9.2, in which we examine water mass transformation and formation for a tracer, λ , in steady state advection-diffusion balance. The tracer takes the boundary values, $\lambda(-h) = \lambda_0$ and $\lim_{H \rightarrow \infty} \lambda(-H) = 0$. The domain has vertical sidewalls with horizontal area A_0 , and it extends over the vertical range, $-H < z \leq h$, where $H \rightarrow \infty$.

- (c) Write the volume integral from the previous part as the difference of two surface integrals over constant z surfaces.
- (d) Assume a steady state and write the water mass transformation in terms of the vertical velocity as integrated over the $z = z(\lambda)$ horizontal surface.

EXERCISE 9.2: TRANSFORMATION AND FORMATION WITH STEADY ADVECTION-DIFFUSION

Consider a steady vertical advection-diffusion balance for a tracer, $0 \leq \lambda \leq \lambda_0$, in a Boussinesq ocean:

$$w \partial_z \lambda = \kappa \partial_{zz} \lambda, \quad (9.153)$$

where $\kappa > 0$ is a constant kinematic diffusivity and $w = w_0 > 0$ is an upwelling velocity that is constant throughout the domain. As in Figure 9.20, assume the vertical extent of the domain is $-H < z \leq -h$, with $h > 0$ a finite depth such as the base of the surface boundary layer, and with $H \gg h$ so that we can approximate $H \rightarrow \infty$. Furthermore, assume the domain has vertical sidewalls with a constant horizontal cross-sectional area, A_0 . Let $\lambda(z = -h) = \lambda_0$ and $\lim_{H \rightarrow \infty} \lambda(z = -H) = 0$. With a domain that is infinitely deep (in the limit with $H \rightarrow \infty$), there is an infinite reservoir of water that feeds the constant upwelling. To maintain volume conservation, we assume water leaves the domain through $z = -h$ at a rate equal to w_0 , thus entering the surface boundary layer where flow within the boundary layer is not of interest for this exercise.¹¹

- (a) Find the steady state solution, $\lambda(z)$, to equation (9.153) within the domain $-H < z \leq -h$ in the limit that $H \rightarrow \infty$, and that satisfies the stated boundary conditions.
- (b) What is the downgradient diffusive flux of λ ? What is its direction?
- (c) What is the advective flux of λ ? What is its direction?
- (d) What is the dia-surface flux, $w^{\text{dia}}(\lambda)$? What is its direction?
- (e) What is the water mass formation per unit λ increment, $\mathcal{F} = -\partial G / \partial \lambda$? Hint: assume

¹¹If we consider flow within the upper boundary layer, $-h \leq z$, then we might wish to set the boundary condition, $w(z = 0) = 0$, which is the rigid lid assumption, or to examine a nonzero transport across the ocean surface via precipitation, evaporation, or runoff. However, extending the domain to the ocean surface would make the exercise far more complicated. Namely, in that case w cannot be assumed to be a constant throughout the domain, nor can we assume u and v are zero. To avoid such complexities, and to allow us to focus on the water mass transformation equations, we restrict attention to the region below the boundary layer where we can maintain self-consistency with $w(z) = w_0$ and $\lambda = \lambda(z)$.

the cross-sectional area of the domain is given by¹²

$$A(z) = A_\circ [\lim_{H \rightarrow \infty} \mathcal{H}(z + H) - \mathcal{H}(z)], \quad (9.154)$$

where \mathcal{H} is the **Heaviside step function** given by

$$\mathcal{H}(z) = \begin{cases} 0 & \text{if } z < 0 \\ 1/2 & \text{if } z = 0 \\ 1 & \text{if } z > 0, \end{cases} \quad (9.155)$$

and whose derivative is the Dirac delta

$$d\mathcal{H}(z)/dz = \delta(z). \quad (9.156)$$

(f) What is the net water mass formation over the domain, $\int_0^{\lambda_\circ} \mathcal{F} d\lambda$?

EXERCISE 9.3: TRANSFORMATION AND FORMATION FROM DIFFUSION IN A STAGNANT FLUID
 In this exercise we examine how diffusion affects water mass transformation within a stagnant fluid ($\mathbf{v} = 0$) and with the tracer concentration a function of vertical position and time, $\lambda = \lambda(z, t)$ with $\partial_z \lambda > 0$. Assuming a Boussinesq ocean and with a constant kinematic diffusivity, $\kappa > 0$, we have the diffusion equation

$$\partial_t \lambda = \kappa \partial_{zz} \lambda. \quad (9.157)$$

As in Exercises 9.1 and 9.2, all λ surfaces are horizontal so that transformation across a λ surface is transformation across a constant z surface. Furthermore, as in Exercise 9.2, assume the domain has vertical sidewalls so that the horizontal cross-sectional area is

$$A(z) = A_\circ [\lim_{H \rightarrow \infty} \mathcal{H}(z + H) - \mathcal{H}(z)], \quad (9.158)$$

where \mathcal{H} is the Heaviside step function (9.155).

- (a) Write the expression for the water mass transformation, $G(\lambda)$, arising from downgradient diffusion. Write it as a surface integral over the horizontal $z = z(\lambda)$ surface.
- (b) Write the water mass transformation, $G(\lambda)$, for a tracer having an exponential vertical profile

$$\lambda = \lambda_\circ e^{z/d}, \quad (9.159)$$

where $\lambda_\circ = \lambda(z = 0)$ and $d > 0$ is a constant depth scale.

- (c) What is the velocity of a point fixed on a λ -surface, again assuming the exponential profile (9.159)? Hint: remember that the fluid is stagnant.
- (d) Write the water mass formation corresponding to the exponential tracer profile (9.159). Hint: this part is where we need to make use of the area expression (9.158).

EXERCISE 9.4: INTEGRATION BETWEEN TWO CLOSED TRACER CONTOURS

This exercise introduces some ideas of use for determining processes affecting the transport of matter across a tracer contour. Note that in general, the tracer concentration is a function of time. However, the present suite of questions concerns the instantaneous geometry of the tracer field, so that time dependence is not considered. Elements of this exercise follow from

¹²The expression (9.154) for the horizontal area can be considered the limit of a bowl domain becoming a vertical sidewall domain. For the bowl we have $\partial_z A \neq 0$, which has its generalization to the hypsometry of the ocean's bottom topography. See [de Lavergne et al. \(2016\)](#) for a discussion of its role in water mass processes.

the discussion from Section 9.3.1.

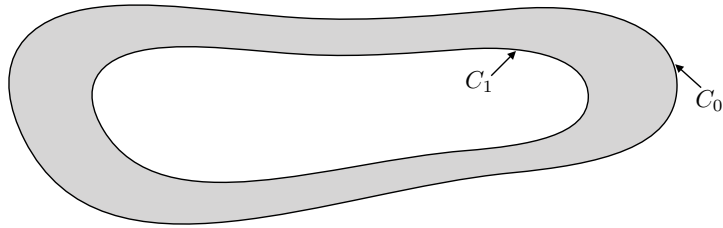


FIGURE 9.21: Illustrating the area contained between two closed tracer contours, $C_0 \leq C(x, y, t) \leq C_1$. Exercise 9.4 develops some mathematical expressions for integration within this area, with the resulting expressions of use for the analyses of tracer transport.

- (a) Consider a closed two-dimensional region bounded by two contours of tracer concentration, $C_0 \leq C(x, y, t) \leq C_1$, such as shown in Figure 9.21. Derive the following expression for the area enclosed by the two contours

$$\mathcal{A} = \int_{C_0}^{C_1} dC \oint \frac{dl}{|\nabla C|}. \quad (9.160)$$

In this expression, dl is the line element for a path taken in a counter-clockwise direction along a contour of constant C . We also assume the tracer concentration is not uniform in the region of interest so that $\nabla C \neq 0$.

- (b) As a corollary, show that for

$$\mathcal{A}(C) = \int_{C_0}^C dC' \oint \frac{dl}{|\nabla C'|} \quad (9.161)$$

we have the identity

$$\frac{\partial \mathcal{A}(C)}{\partial C} = \oint \frac{dl}{|\nabla C|}. \quad (9.162)$$

In words, this result means that the area between two tracer contours has a partial derivative, with respect to the tracer contour, equal to the line integral on the right hand side. The area per C is smaller in regions where the tracer gradient is larger; i.e., there is less area “concentration” in regions of strong tracer gradient.

- (c) Use the above two results to prove the following form of the Fundamental Theorem of Calculus

$$\frac{\partial}{\partial C} \left[\int \Phi(x) d\mathcal{A} \right] = \frac{\partial}{\partial C} \left[\int_{C_0}^C dC' \oint \frac{\Phi dl}{|\nabla C'|} \right] = \oint \frac{\Phi dl}{|\nabla C|}, \quad (9.163)$$

with Φ an arbitrary function. This identity is analogous to that derived in Section 9.3.5. It has many useful applications such as those discussed in [Marshall et al. \(2006\)](#).

EXERCISE 9.5: CAUCHY’S DOUBLE INTEGRAL FORMULA

In this exercise we derive the following double-integral identity, originally due to [Cauchy \(1823\)](#),

$$\int_{t_n}^{t_{n+1}} \left[\int_{t_n}^t \mathcal{B}(s) ds \right] dt = \int_{t_n}^{t_{n+1}} (t_{n+1} - t) \mathcal{B}(t) dt, \quad (9.164)$$

where we make reference to Figure 9.22 for the notation. To prove this identity, it is useful to

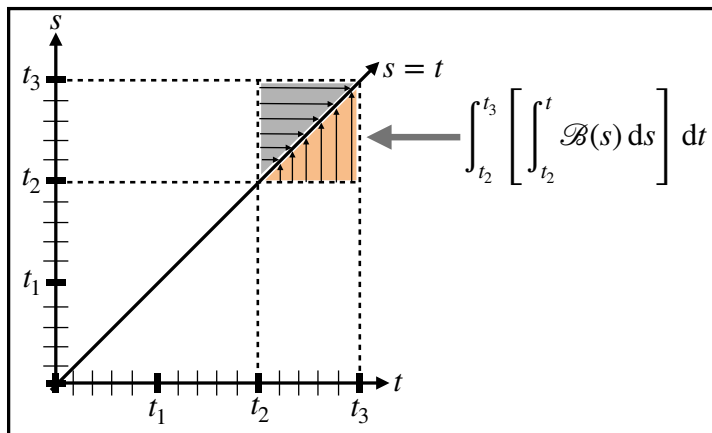


FIGURE 9.22: Gold region depicts the time integration domain used in one of the double integrals from equation (9.164) for the special case of $n = 2$. Note that the gray triangular region generally leads to a distinct integral.

make the substitution

$$A(s) = \int_{s_0}^s B(s') ds' \implies B(s) = dA/ds, \quad (9.165)$$

and then work separately on the two sides of equation (9.164) to show that they are the same.



Part III

Hamilton's principle for fluid mechanics

In this part of the book we add a new layer to the conceptual foundations of fluid mechanics, and we do so by making use of *Hamilton's variational principle* to develop the equations for continuum motion. To appreciate the various aspects of Hamilton's principle requires revisiting a number of foundational topics and making use of distinct mathematical methods. Hamilton's principle is applicable to conservative physical systems, so that we only consider perfect fluids in this part of the book (i.e., single-component fluids without diffusion, conduction, or friction). Even so, Hamilton's principle provides a satisfying means to unify across the variety of physical content within perfect fluid mechanics. On a practical side, it offers a useful framework to develop approximate theories. Namely, by developing approximations within the action, one is ensured that the associated Euler-Lagrange equations satisfy corresponding conservation laws. In a nutshell, this part of the book will appeal to those interested in understanding the whys of fluid mechanics as a complement to the hows.

The continuum expression of Hamilton's variational principle, and the associated continuum *Euler-Lagrange field equations*, are the foundations for both classical and quantum field theory. Among the most celebrated payoffs for developing the variational formalism, we are afforded the origin story for differential conservation laws (e.g., linear momentum, angular momentum, mechanical energy, potential vorticity) that is otherwise obscure using alternative approaches (i.e., by inspired manipulations of the dynamical equations). It does so by directly connecting continuous space-time symmetries of the action to differential conservation laws through use of the celebrated *Noether's theorem* ([Noether, 1918](#); [Noether and Tavel, 2018](#)). We used Noether's theorem in our study of analytical particle mechanics in **VOLUME 1**. Noether's original work concerned field theory, so our use of Noether's theorem for continuum mechanics is directly connected to her work.

HAMILTON'S PRINCIPLE AND LAGRANGIAN KINEMATICS

Many practitioners of fluid mechanics are neither aware of, nor concerned with, the use of Hamilton's variational principle for continuum mechanics. One reason for the intellectual distance arises from success of the Eulerian description of fluid mechanics, in which there is no concern for the flow map induced by the motion field, nor for the corresponding trajectories of fluid particles. Rather, the Eulerian approach focuses on the fluid velocity as a classical field, and the enumeration of forces acting on a fluid element that lead to accelerations via Newton's law. This approach offers a sufficient means to formulate the suite of fluid dynamical equations. Even so, there is more to the story that is revealed through the paired use of Hamilton's principle and Noether's theorem.

The absence of trajectories in Eulerian fluid mechanics distinguishes it from point particle mechanics and, it turns out, makes Hamilton's principle less transparent when formulated using Eulerian kinematics. In particular, Eulerian kinematics introduces nuances to Hamilton's principle related to the need to employ constraint fields not encountered with Lagrangian kinematics. These features of the Eulerian approach to Hamilton's principle have, whether fairly or unfairly, turned many practitioners away from Hamilton's principle. The nature of an Eulerian formulation of Hamilton's principle was clarified by [Salmon \(1988\)](#), who provided a systematic connection between Eulerian and Lagrangian formulations. Nonetheless, the direct connection between Lagrangian fluid kinematics to the kinematics of point particles offers a relatively straightforward extension (both conceptually and technically) of Hamilton's principle to fluid mechanics. It also more closely aligns to the methods used in continuum mechanics and quantum field theory. It is for these reasons that we embrace Lagrangian kinematics in our

study of Hamilton's principle in this part of the book.¹³

HARMONIC OSCILLATOR VERSUS THE MOTION FIELD

We start this part of the book in Chapter 10 by focusing on Hamilton's principle for a continuous scalar field, following approaches standard in the quantum field theory literature (e.g., [Quigg \(1983\)](#); [Ryder \(1985\)](#); [Ramond \(1990\)](#)). In this treatment, we establish the Euler-Lagrange field equations by taking the continuum limit of a discrete version of Hamilton's principle applied to coupled simple harmonic oscillators. As such, we are afforded a pedagogical introduction to Hamilton's principle for a continuum that builds from our work with discrete particles in VOLUME 1. This approach then lends the conceptual picture of the continuous field as representing small amplitude (linear) fluctuations relative to an equilibrium state.

In Chapter 11, we meld the classical field theory from Chapter 10 to the Lagrangian kinematics of continuum matter from VOLUME 2. Doing so offers a suitable framework to use Hamilton's principle for describing fluid flows. Notably, through the advent of the motion field, $\varphi(\mathbf{a}, T)$, appearing in Lagrangian kinematics, we appreciate that continuum mechanics is a fundamentally nonlinear field theory and thus it is not generally amenable to the harmonic oscillator paradigm that forms the foundation for much of classical and quantum field theory.¹⁴ That is, motion of continuum matter is not restricted to small fluctuations relative to an equilibrated state. So to examine the gamut of fluid motions, in Chapter 11 we apply Hamilton's principle to the fluid motion field, φ . We thus develop a field theory for the motion field as it appears in Lagrangian space-time. Even given this distinction between the scalar field theory from Chapter 10 to the Lagrangian space-time of the motion field, it is remarkable that the perfect fluid Euler-Lagrange equation (11.43a) is mathematically identical to equation (10.43) formulated for the continuous scalar field.

CONCERNING LOCAL FIELD THEORY

In our studies of continuum mechanics in general, or fluid mechanics in particular, we rely on *local fields* to formulate the equations describing motion of continuous matter. Namely, all fields (e.g., temperature, velocity, energy) depend locally on positions in Galilean space-time. Local field theories embody the inability for information to transfer at speeds faster than light or, for our studies that ignore electromagnetism, for signals to travel faster than acoustic waves. Furthermore, local field theories are ubiquitous in physics in part since they offer a robust conceptual and operational foundation that is simpler than non-local approaches.¹⁵ As noted on page 24 of [Ramond \(1990\)](#), local field theories are so well trusted that they are commonly used for describing non-local phenomena. For our study of fluid mechanics, we make use of both the Lagrangian and Eulerian reference frames. The Eulerian approach considers fields that are local in the Eulerian \mathbf{x} -space, whereas the Lagrangian approach considers fields that are local in the material \mathbf{a} -space.

These remarks about the relevance of local field theory might seem obvious, with action-at-a-distance phenomena absent from any fundamental processes in classical physics. Even so, there are approximate theories where we assume a wave speed to be infinite, thus transitioning

¹³It is notable that in solid mechanics, Hamilton's principle is more routinely used (e.g., see Chapter 2 of [Tromp \(2025\)](#)), presumably since Lagrangian kinematics is more routinely used in solid mechanics. Those interested in the Eulerian approach will find Chapter 8 of [Salmon \(1998\)](#) a valuable introduction.

¹⁴The study of linear waves in VOLUME 5 is one area where the harmonic oscillator paradigm is suited for fluid mechanics.

¹⁵Chapter 1 of [Morse and Feshbach \(1953\)](#) provides an insightful discussion of fields and their use in physics.

from a hyperbolic system to an elliptic system. The primary example occurs when assuming a non-divergent fluid flow, as in the Boussinesq ocean. For this case, the pressure is purely mechanical (i.e., it is not related to internal energy via a thermodynamic derivative), and it solves an elliptic boundary value problem to enforce the non-divergence nature of the flow. That is, for non-divergent flow, pressure is the Lagrange multiplier that ensure the constraint of $\nabla \cdot \mathbf{v} = 0$ is maintained at each point in space and time, with the acoustic wave speed assumed infinite. In general, if encountering a non-local process in classical physics, we must inquire about the corresponding unapproximated process in order to determine if the non-local theory is a physically sensible approximation to a local theory. If not, then the non-local theory is not a viable theory of classical continuum mechanics.

MATHEMATICS IN THIS PART

We rely extensively on the tensor analysis from VOLUME 1, including Cartesian tensors and general tensors. In particular, general tensors are needed for seamlessly moving between Eulerian and Lagrangian coordinates.

Chapter 10

SCALAR FIELD THEORY IN GALILEAN SPACE-TIME

In this chapter we study *classical scalar field theory* in Galilean space-time from the perspective of *Hamilton's principle* of stationary action. We motivate this study by considering the continuum limit of a system of coupled simple harmonic oscillators, which provides the canonical example of how to extend Lagrangian particle mechanics to Lagrangian continuum mechanics. We then develop the equations of motion within the continuum and make use of Noether's theorem to derive dynamical conservation laws connected to space-time symmetries.

CHAPTER GUIDE

This chapter relies on the formulation of Lagrangian mechanics and Hamilton's principle from VOLUME 1, as well as general tensor formalism, also from VOLUME 1. The use of general tensors here anticipates their use for the perfect fluid in Chapter 11. This chapter serves as the foundations for applying Hamilton's variational principle for perfect fluid mechanics in Chapter 11.

10.1	Loose threads	338
10.2	Continuum limit of coupled harmonic oscillators	338
10.2.1	Continuum limit	338
10.2.2	Continuum limit and the wave equation	339
10.2.3	Continuum limit of the Lagrangian	339
10.2.4	Further study	340
10.3	Hamilton's principle and the Euler-Lagrange equations	341
10.3.1	The action for a continuous field	341
10.3.2	Functional variation of the field	342
10.3.3	Variation of the action	342
10.3.4	Euler-Lagrange field equations	343
10.3.5	Example Lagrangian densities	344
10.4	Operational aspects of Hamilton's principle	345
10.4.1	Care with the partial derivative operations	345
10.4.2	Generalized spatial coordinates	346
10.4.3	Natural spatial boundary conditions	347
10.4.4	Galilean space-time notation	348
10.4.5	Mechanical equivalence of Lagrangians	349
10.4.6	The absence of second or higher derivatives in the Lagrangian	349
10.5	Space-time symmetry and stress-energy-momentum	350
10.5.1	Time symmetry and the Hamiltonian density	350
10.5.2	Stress-energy-momentum tensor	351

10.5.3	An auxiliary functional for deriving conservation laws	353
10.5.4	Summary of the cyclic coordinate method	353
10.6	Noether's theorem and symmetries of the action	355
10.6.1	Distinctions between Noether and Hamilton	355
10.6.2	Active transformations	355
10.6.3	Passive transformations	358
10.6.4	Total variation of the field	359
10.6.5	Variation of the action under an active transformation	359
10.6.6	Angular momentum and space isotropy	360
10.6.7	Comments	361
10.6.8	Further study	362

10.1 Loose threads

- Schrodinger equation: exercise 2.5 of *Hand and Finch* (1998)
- String using Hamilton's principle: exercise 2.13 of *Hand and Finch* (1998).
- Example Lagrangians from *Morse and Feshbach* (1953) chapter on variational methods.

10.2 Continuum limit of coupled harmonic oscillators

In this section we examine the continuum limit of the discrete oscillator system studied in VOLUME 1. The purpose of this study is to extend discrete Lagrangian mechanics and Hamilton's principle to the continuum, thus providing a direct connection to fluid mechanics and classical continuum field theory.

10.2.1 Continuum limit

We work in a classical physics universe, so that we have no concern for the quantum nature of matter. As such, the continuum limit is here considered as a mere mathematical transition from discrete classical matter to continuous classical matter. This approach is physically naive in the face of the molecular and atomic nature of matter as described by quantum mechanics. Even so, it provides a suitable mathematical framework for studying the classical mechanics of continuous media, and as such it serves the needs of this book.

The continuum limit for the coupled harmonic oscillator system is realized by the following:

$$\Delta \rightarrow dx \quad \text{equilibrium distance between particles becomes infinitesimal} \quad (10.1a)$$

$$N \rightarrow \infty \quad \text{infinite number of particles} \quad (10.1b)$$

$$(N+1)\Delta = \ell \quad \text{equilibrium length remains constant} \quad (10.1c)$$

$$m/\Delta = \sigma \quad \text{mass per length} \quad (10.1d)$$

$$\Gamma \Delta = \tau \quad \text{compressive/expansive force} \quad (10.1e)$$

$$n \Delta = x \quad \text{continuous coordinate for equilibrium position} \quad (10.1f)$$

$$\xi_n(t) \rightarrow \xi(x, t) \quad \text{displacement becomes function of space and time.} \quad (10.1g)$$

The displacement function, $\xi(x, t)$, measures the displacement of an infinitesimal piece of matter whose equilibrium position is x . As such, the coordinate x acts as a parameter that labels an

infinitesimal piece of matter whose equilibrium position is x and whose instantaneous position is $x + \xi(x, t)$.¹

We take the continuum limit starting from two different perspectives. First we focus on the equation of motion for the coupled oscillators, which is the topic of Section 10.2.2. Alternatively, we take the continuum limit of the Lagrangian and then derive the corresponding Euler-Lagrange equations, with this approach considered in Section 10.2.3. The second approach is aligned with the approach in classical field theory used in later sections.

10.2.2 Continuum limit and the wave equation

Introducing the notation from equations (10.1a)-(10.1g), yet without taking the continuum limit, brings the discrete coupled oscillator equation of motion from VOLUME 1 into the form

$$\ddot{\xi}_n = \frac{\Gamma}{m} (\xi_{n+1} - 2\xi_n + \xi_{n-1}) \quad (10.2a)$$

$$= \frac{\Gamma \Delta}{m/\Delta} \frac{\xi_{n+1} - 2\xi_n + \xi_{n-1}}{\Delta^2} \quad (10.2b)$$

$$= \frac{\tau}{\sigma} \left[\frac{\xi_{n+1} - 2\xi_n + \xi_{n-1}}{\Delta^2} \right]. \quad (10.2c)$$

To take the continuum limit, note that the finite difference on the right hand side approximates the second order spatial derivative operator, so that in the continuum limit we recover the one dimensional *wave equation*

$$(\partial_{tt} - c^2 \partial_{xx}) \xi = 0, \quad (10.3)$$

with the wave speed given by

$$c = (\tau/\sigma)^{1/2}. \quad (10.4)$$

We studied the mathematics of the wave equation (10.3) in VOLUME 1 in the context of *hyperbolic partial differential equations*. A general solution is given by

$$\xi(x, t) = A(x - ct) + B(x + ct), \quad (10.5)$$

where A and B are arbitrary smooth functions determined by the initial conditions and boundary conditions. The solution $A(x - ct)$ is a signal moving in the $+\hat{x}$ direction, whereas $B(x + ct)$ is a signal moving in the $-\hat{x}$ direction, both moving at speed c .

We have restricted attention to motion constrained to a line whereby the harmonic oscillators render a series of alternative rarefactions and compressions that lead to wave-like motions along that line. Upon taking the continuum limit, we find that each piece of the continuum oscillates about its equilibrium position, again with the oscillations in a direction aligned with the waves. Such motions are the defining characteristic of *longitudinal waves*. The longitudinal waves resulting from the continuum limit of coupled harmonic oscillators offers a prototype for the acoustic waves studied in VOLUME 5.

10.2.3 Continuum limit of the Lagrangian

Rather than taking the continuum limit of the equation of motion, we here consider the continuum limit of the Lagrangian and then derive the corresponding Euler-Lagrange equation

¹The displacement field, $\xi(x, t)$, is a one-dimensional version of the vector field, $\xi(\mathbf{x}, t)$, used for the *generalized Lagrangian mean* of Section 6.3.

of motion. This approach accords with the methods of classical field theory and it will serve many purposes in this book.

The following discrete Lagrangian was derived in VOLUME 1

$$L = \sum_{n=1}^{N+1} \left[\frac{m}{2} (\dot{\xi}_n)^2 - \frac{\Gamma}{2} (\xi_n - \xi_{n-1})^2 \right], \quad (10.6)$$

and it comprises the sum of the kinetic plus potential energy of the discrete oscillators. The continuum limit from Section 10.2.2 brings the kinetic energy to

$$\frac{m}{2} \sum_{n=1}^{N+1} (\dot{\xi}_n)^2 = \frac{\sigma}{2} \sum_{n=1}^{N+1} (\dot{\xi}_n)^2 \Delta \rightarrow \frac{\sigma}{2} \int_0^\ell (\partial_t \xi)^2 dx, \quad (10.7)$$

where we set $m = \sigma \Delta$ according to equation (10.1d), and made the correspondence

$$\sum_{n=1}^{N+1} \Delta \rightarrow \int_0^\ell dx. \quad (10.8)$$

Similarly, the continuum limit of the potential energy yields

$$\frac{\Gamma}{2} \sum_{n=1}^{N+1} (\xi_n - \xi_{n-1})^2 = \frac{\Gamma \Delta}{2} \sum_{n=1}^{N+1} \frac{(\xi_n - \xi_{n-1})^2}{\Delta^2} \Delta \rightarrow \frac{\tau}{2} \int_0^\ell (\partial_x \xi)^2 dx, \quad (10.9)$$

where we set $\Gamma \Delta = \tau$ according to equation (10.1e). As a result, the Lagrangian has the continuum limit

$$L = \sum_{n=1}^{N+1} \left[\frac{m}{2} (\dot{\xi}_n)^2 - \frac{\Gamma}{2} (\xi_n - \xi_{n-1})^2 \right] \rightarrow \frac{1}{2} \int_0^\ell [\sigma (\partial_t \xi)^2 - \tau (\partial_x \xi)^2] dx \equiv \int_0^\ell \mathcal{L} dx, \quad (10.10)$$

where we defined the *Lagrangian density*

$$\mathcal{L} = [\sigma (\partial_t \xi)^2 - \tau (\partial_x \xi)^2]/2. \quad (10.11)$$

Now observe that

$$\frac{\partial}{\partial t} \frac{\partial \mathcal{L}}{\partial (\partial_t \xi)} + \frac{\partial}{\partial x} \frac{\partial \mathcal{L}}{\partial (\partial_x \xi)} = \sigma \partial_{tt} \xi - \tau \partial_{xx} \xi = \sigma (\partial_{tt} \xi - c^2 \partial_{xx} \xi) = 0. \quad (10.12)$$

This result hints at a means to derive the Euler-Lagrange equation using a continuum version of Hamilton's principle, which is the topic of Section 10.3.

10.2.4 Further study

In transitioning from the discrete harmonic oscillators to the continuum field theory, we are inspired by treatments from [Fetter and Walecka \(2003\)](#) (chapters 4, 6, and 8), chapter 12 of [Goldstein \(1980\)](#), chapter 9 of [José and Saletan \(1998\)](#), and Chapter 2 of [Soper \(2008\)](#). Note that some of these treatments (e.g., Chapter 4 of [Fetter and Walecka \(2003\)](#)) works through the continuum limit of a string, which accords quite closely to the continuum limit of simple harmonic oscillators considered here.

10.3 Hamilton's principle and the Euler-Lagrange equations

The continuum limit considered in Section 10.2 suggests that we can study the mechanics of continuous media using the methods of Lagrangian mechanics and Hamilton's principle, and that we can pursue this approach without concern for the discrete nature of matter. In this section we explore the rudiments of the resulting field theory for scalar fields. For simplicity, we focus here on the case of one space dimension, along with time. Generalizations to higher space dimensions are straightforward, in which case the space-time domain, R , includes higher dimensional region of space, \mathcal{R} , along with a time interval.

10.3.1 The action for a continuous field

In VOLUME 1 we applied Hamilton's principle to the trajectories of discrete particles moving through space, with the spatial position specified by generalized coordinates and the position along a trajectory parameterized by time. Hamilton's principle states that the physically realized trajectory is that trajectory that makes the action stationary. Here we postulate that Hamilton's principle for point particles can be extended to continuous matter whose mechanics is described by space-time fields. Many steps in the derivation here are straightforward extensions of the discrete particle discussion.

Consider a 1+1 dimensional field, $\psi = \psi(x, t)$, that is a function of one Cartesian space coordinate, x , and time, t . For example, $\psi(x, t)$ can represent the displacement field, $\xi(x, t)$, introduced by the continuum limit of the oscillators studied in Section 10.2. In this manner, the continuum extension of the discrete particle from VOLUME 1 is here given by the space-time integral

$$S[t_A, x_A, t_B, x_B, \psi] = \int_{t_A}^{t_B} L dt = \int_{t_A}^{t_B} \left[\int_{x_A}^{x_B} \mathcal{L}(\psi, \partial_t \psi, \partial_x \psi, x, t) dx \right] dt, \quad (10.13)$$

where \mathcal{L} is the *Lagrangian density*² and the physical system lives on a space domain, $x \in [x_A, x_B]$, and evolves over the time range, $t \in [t_A, t_B]$. We refer to this space-time domain as

$$R \equiv x \in [x_A, x_B] \oplus t \in [t_A, t_B], \quad (10.14)$$

and its boundary is ∂R . On the left hand side of equation (10.13) we exposed the dependence of the action on the space and time endpoints, as well as the function, ψ . We generally omit such dependence for brevity in notation.

Note the presence of both space and time derivatives inside the action in equation (10.13), as per the use of both space and time as independent variables for the field, ψ . Evidently, the Lagrangian density, \mathcal{L} , is a functional³ of the field, ψ , and its derivatives, $\partial_t \psi$ and $\partial_x \psi$. Since ψ is a function of (x, t) , then the Lagrangian density, \mathcal{L} , is an implicit function of (x, t) through its dependence on $\psi(x, t)$, $\partial_t \psi(x, t)$, and $\partial_x \psi(x, t)$. Furthermore, we allow for \mathcal{L} to be an explicit function of (x, t) , which may arrive via other prescribed functions that contribute to the Lagrangian (e.g., a space-time dependent background field through which waves propagate, as studied in VOLUME 5). In Section 10.4.1 we emphasize the importance of being mindful of the variety of explicit and implicit dependencies of the Lagrangian density.

²We commonly refer to \mathcal{L} as the “Lagrangian”, thus omitting the “density” qualifier.

³A functional is a “function of a function”.

10.3.2 Functional variation of the field

In the action (10.13), it is the field, $\psi(x, t)$, that is the continuum extension of the generalized coordinates used in the discrete particle mechanics action from VOLUME 1. Correspondingly, it is the field that is varied when varying the continuum action. Let $\psi(x, t)$ be the physically realized field and introduce a virtual variation around that field according to

$$\psi(x, t|\epsilon) = \psi(x, t) + \epsilon \chi(x, t) = \psi(x, t) + \delta\psi(x, t). \quad (10.15)$$

The first equality introduced a non-dimensional parameter, ϵ , that scales the perturbation field, χ , thus defining a one-parameter family of functions, $\psi(x, t|\epsilon)$. The second equality in equation (10.15) introduced the δ notion commonly used for variations in VOLUME 1. We emphasize that it is the field that is varied, so that the field parameters, (x, t) , are the same across the two equalities in equation (10.15). Consequently, the δ operator commutes with space and time derivatives.

Figure 10.1 illustrates the field variation (10.15). There is a nonzero variation, $\delta\psi(x, t) = \epsilon \chi(x, t)$, for space-time points that are not on the space-time boundary, $(x, t) \notin \partial R$. In contrast, the field is specified along ∂R to be the physically realized field, so that on the space-time boundary there is no variation

$$\delta\psi(x, t) = 0 \quad \forall (x, t) \in \partial R \iff \frac{\partial \psi(x, t|\epsilon)}{\partial \epsilon} = 0 \quad \forall (x, t) \in \partial R. \quad (10.16)$$

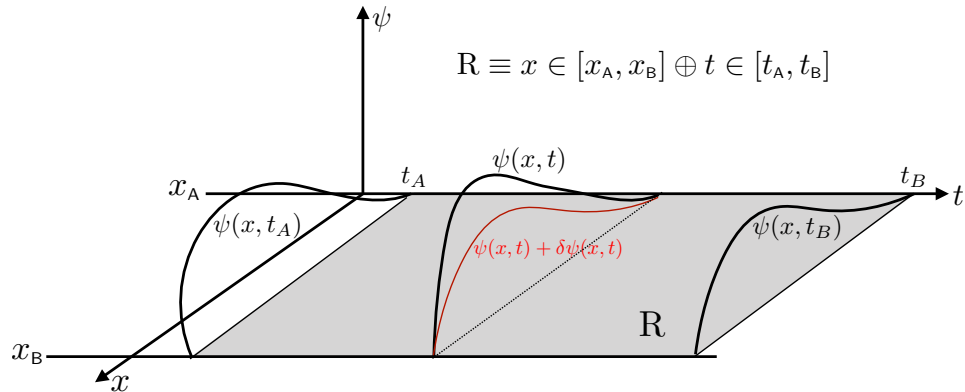


FIGURE 10.1: Illustrating the variation of a field for use in Hamilton's principle for continuous media. The field, $\psi(x, t)$, is specified along the space-time boundary of the domain, ∂R , where R is the space domain $x \in [x_A, x_B]$ plus a time domain $t \in [t_A, t_B]$. When not on ∂R , then there is a nonzero, $\delta\psi(x, t)$, whereas $\delta\psi = 0$ on the boundary, ∂R . This figure is inspired by Figure 25.3 of [Fetter and Walecka \(2003\)](#).

10.3.3 Variation of the action

Hamilton's principles says that the physically realized field, $\psi(x, t|\epsilon = 0)$, makes the action stationary, which is mathematically stated as

$$\text{Hamilton's principle} \implies \left[\frac{dS}{d\epsilon} \right]_{\epsilon=0} = \left[\frac{d}{d\epsilon} \int_R \mathcal{L} dx dt \right]_{\epsilon=0} = 0. \quad (10.17)$$

Making use of the δ shorthand leads to

$$\text{Hamilton's principle} \implies \delta S = \delta \left[\int_R \mathcal{L} dx dt \right] = 0 \quad \text{with} \quad \delta = [d/d\epsilon]_{\epsilon=0}. \quad (10.18)$$

In varying the action we only vary the field and its derivatives, with the space-time domain, R , unchanged. Hence, the variation operator commutes with the space-time integral

$$\delta S = \int_R \delta \mathcal{L} dx dt. \quad (10.19)$$

Variation of the Lagrangian density is computed according to the chain rule

$$\delta \mathcal{L} = \left[\frac{\partial \mathcal{L}}{\partial \psi} \right]_{\partial_t \psi, \partial_x \psi} \delta \psi + \left[\frac{\partial \mathcal{L}}{\partial (\partial_t \psi)} \right]_{\psi, \partial_x \psi} \delta (\partial_t \psi) + \left[\frac{\partial \mathcal{L}}{\partial (\partial_x \psi)} \right]_{\psi, \partial_t \psi} \delta (\partial_x \psi). \quad (10.20)$$

We exposed subscripts to denote which terms are held fixed during the partial functional derivative operation. This equation makes it clear that variation of the Lagrangian density occurs at a fixed space-time point, which explains why there are no $(\partial \mathcal{L} / \partial t) \delta t$ nor $(\partial \mathcal{L} / \partial x) \delta x$ terms. Correspondingly, under this variation we consider (x, t) as space-time parameters so that the ∂_x and ∂_t operators acting on ψ commute with the variation operator

$$\delta \mathcal{L} = \frac{\partial \mathcal{L}}{\partial \psi} \delta \psi + \frac{\partial \mathcal{L}}{\partial (\partial_t \psi)} \partial_t (\delta \psi) + \frac{\partial \mathcal{L}}{\partial (\partial_x \psi)} \partial_x (\delta \psi). \quad (10.21)$$

Further rearranging the space-time operators leads to the equivalent expression

$$\delta \mathcal{L} = \left[\frac{\partial \mathcal{L}}{\partial \psi} - \frac{\partial}{\partial t} \frac{\partial \mathcal{L}}{\partial (\partial_t \psi)} - \frac{\partial}{\partial x} \frac{\partial \mathcal{L}}{\partial (\partial_x \psi)} \right] \delta \psi + \frac{\partial}{\partial t} \left[\frac{\partial \mathcal{L}}{\partial (\partial_t \psi)} \delta \psi \right] + \frac{\partial}{\partial x} \left[\frac{\partial \mathcal{L}}{\partial (\partial_x \psi)} \delta \psi \right]. \quad (10.22)$$

10.3.4 Euler-Lagrange field equations

Plugging the result (10.22) into the action variation (10.19) leads to

$$\begin{aligned} \delta S = \int_R \delta \psi \left(\frac{\partial \mathcal{L}}{\partial \psi} - \frac{\partial}{\partial t} \frac{\partial \mathcal{L}}{\partial (\partial_t \psi)} - \frac{\partial}{\partial x} \frac{\partial \mathcal{L}}{\partial (\partial_x \psi)} \right) dx dt \\ + \int_R \left(\frac{\partial}{\partial t} \left[\frac{\partial \mathcal{L}}{\partial (\partial_t \psi)} \delta \psi \right] + \frac{\partial}{\partial x} \left[\frac{\partial \mathcal{L}}{\partial (\partial_x \psi)} \delta \psi \right] \right) dx dt. \end{aligned} \quad (10.23)$$

As noted earlier, we are assuming the field variation vanishes on the space-time boundary, so that $\delta \psi = 0$ for points on ∂R . Doing so eliminates the second integral since both terms integrate to boundary contributions. Furthermore, since $\delta \psi$ is an arbitrary variation of the field within the interior of the domain, a general satisfaction of Hamilton's principle, $\delta S = 0$, only holds if the integrand in the first integral vanishes for each space and time point, which thus leads to the continuum *Euler-Lagrange equations*

$$\delta S = 0 \implies \frac{\partial \mathcal{L}}{\partial \psi} - \frac{\partial}{\partial t} \left[\frac{\partial \mathcal{L}}{\partial (\partial_t \psi)} \right] - \frac{\partial}{\partial x} \left[\frac{\partial \mathcal{L}}{\partial (\partial_x \psi)} \right] = 0. \quad (10.24)$$

We emphasize here an important practical point related to computation of the partial derivatives. Namely, when performing the partial derivative on \mathcal{L} with respect to ψ and its derivatives, $\partial_t \psi$ and $\partial_x \psi$, each of the other variables in the Lagrangian density are held fixed. However, when

performing the space and time partial derivatives, ∂_x and ∂_t , we only maintain the complement space and time variable fixed, so that we need to employ the chain rule to extract all places where ∂_x and ∂_t affect. We offer details in Section 10.4.1 on these points about computing the partial derivatives.

10.3.5 Example Lagrangian densities

We have many opportunities in this book to use a Lagrangian density to derive the correspondingly Euler-Lagrange equations. Here we provide a few examples that lead to wave equations.

Acoustic wave equation

As studied in Section 10.2, the Lagrangian density

$$\mathcal{L} = [\sigma (\partial_t \psi)^2 - \tau (\partial_x \psi)^2]/2, \quad (10.25)$$

with σ and τ constants, renders the wave equation as the Euler-Lagrange equation

$$(\partial_{tt} - c^2 \partial_{xx}) \psi = 0, \quad (10.26)$$

where the wave speed is $c = \sqrt{\tau/\sigma}$ (equation (10.4)). Notice that the dimensions of \mathcal{L} are energy per length, which accords with this being a wave equation in a single spatial dimension. The Lagrangian (10.25) and wave equation (10.26) also hold for the more general case of a tension that is a function of time, $\tau = \tau(t)$, and a mass density that is a function of space, $\sigma = \sigma(x)$, in which case the wave speed is a function of space and time

$$c^2(x, t) = \tau(t)/\sigma(x). \quad (10.27)$$

We derived the Lagrangian density (10.25) in Section 10.2 by taking the continuum limit of coupled harmonic oscillators, where $\psi(x, t)$ represents the \hat{x} -displacement of a particle from its equilibrium position, so that linear fluctuations are *longitudinal waves* (wave motion in the same direction of the particle displacement). An analogous derivation leads to the same Lagrangian density for a tight string, with $\psi(x, t)$ now measuring the transverse displacements of the string from its equilibrium position (see Section 25 in [Fetter and Walecka \(2003\)](#)), and with linear oscillations leading to *transverse waves*.

Returning to the continuum harmonic oscillator, we note that it is directly related to the study of acoustic waves in a fluid. We pursue this study in VOLUME 5, thus encountering the Lagrangian density

$$\mathcal{L} = [c_s^{-2} (\partial_t p')^2 - (\nabla p')^2]/(2 \rho_e), \quad (10.28)$$

where ρ_e is the mass density of the background fluid state, c_s is the sound speed in the fluid, and p' is the perturbation pressure. In this case the Euler-Lagrange equation is the acoustic wave equation

$$\partial_t[(\rho_e c_s^2)^{-1} \partial_t p'] - \nabla \cdot (\rho_e^{-1} \nabla p') = 0, \quad (10.29)$$

which, in the special case of ρ_e and c_s independent of space and time, gives the wave equation

$$(\partial_{tt} - c_s^2 \nabla^2) p' = 0. \quad (10.30)$$

Note that the physical dimensions of the Lagrangian density (10.28) are not energy per volume,

so that the terms in the Lagrangian are thought of as pseudo-energy densities.

Sine-Gordon and Klein-Gordon wave equations

For another example, consider

$$\mathcal{L} = [\sigma (\partial_t \psi)^2 - \tau (\partial_x \psi)^2]/2 - \sigma \Gamma^2 (1 - \cos \psi), \quad (10.31)$$

where ψ is here a non-dimensional field. The corresponding Euler-Lagrange equation is known as the *sine-Gordon equation*

$$\partial_{tt} \psi - c^2 \partial_{xx} \psi + \Gamma^2 \sin \psi = 0. \quad (10.32)$$

As shown in Section 9.1.1 of [José and Saletan \(1998\)](#), the sine-Gordon equation is the continuum limit of a coupled pendulum-spring system, with Γ proportional to the gravitational acceleration. For small ψ , the sine-Gordon Lagrangian (10.31) and wave equation (10.32) reduce to the *Klein-Gordon* Lagrangian and Klein-Gordon equation

$$\mathcal{L} = [\sigma (\partial_t \psi)^2 - \tau (\partial_x \psi)^2]/2 + \sigma \Gamma^2 \psi^2 \quad \text{and} \quad (\partial_{tt} - c^2 \partial_{xx} + \Gamma^2) \psi = 0. \quad (10.33)$$

The Klein-Gordon equation forms the starting point for scalar quantum field theories (e.g., [Ryder \(1985\)](#)).

10.4 Operational aspects of Hamilton's principle

We here summarize a number of points about the formalism that are particularly relevant when performing the many operational steps with Hamilton's principle.

10.4.1 Care with the partial derivative operations

As noted in Section 10.3, the Lagrangian density, \mathcal{L} , is a functional of the field, ψ , as well as its space and time derivatives,

$$\frac{\partial \psi(x, t)}{\partial t} = \left[\frac{\partial \psi(x, t)}{\partial t} \right]_x \quad \text{and} \quad \frac{\partial \psi(x, t)}{\partial x} = \left[\frac{\partial \psi(x, t)}{\partial x} \right]_t, \quad (10.34)$$

where the subscripts on the right hand side of these equations indicate those variables held fixed while performing the partial derivative. We typically do not need this extra adornment for partial derivatives acting on functions of space and time. But the Lagrangian density is a rather loaded object, and so it is important to clarify what is meant by its derivatives.

With ψ and its derivatives explicit functions of (x, t) , then \mathcal{L} is an implicit function of (x, t) . There are additional physical systems where the Lagrangian density picks up an explicit space and time dependence, such as when waves move through a space and time dependent background media (VOLUME 5). Such added space and time dependence does not alter the derivation of the Euler-Lagrange field equation, since in that derivation we only vary the field and its derivatives. However, the distinction between implicit versus explicit functional dependence can easily lead to confusion when performing partial derivative manipulations involving ∂_t and ∂_x operations, such as when deriving the continuum conservation laws in Section 10.5. We thus find it useful to here write these derivatives for the record.

The partial time derivative of \mathcal{L} , computed at a fixed x position, is given by

$$\left[\frac{\partial \mathcal{L}}{\partial t} \right]_x = \left[\frac{\partial \mathcal{L}}{\partial \psi} \right]_{\partial_t \psi, \partial_x \psi} \frac{\partial \psi}{\partial t} + \left[\frac{\partial \mathcal{L}}{\partial (\partial_t \psi)} \right]_{\psi, \partial_x \psi} \frac{\partial^2 \psi}{\partial t^2} + \left[\frac{\partial \mathcal{L}}{\partial (\partial_x \psi)} \right]_{\psi, \partial_t \psi} \frac{\partial^2 \psi}{\partial x \partial t} + \left[\frac{\partial \mathcal{L}}{\partial t} \right]_{\psi, \partial_t \psi, \partial_x \psi, x}. \quad (10.35)$$

Exposing the subscripts on the \mathcal{L} partial derivatives helps to distinguish the time derivative on the left hand side from the time derivative appearing in the final term on the right hand side. Namely, the $(\partial \mathcal{L} / \partial t)_x$ on the left hand side only holds x fixed, whereas the $(\partial \mathcal{L} / \partial t)_{\psi, \partial_t \psi, \partial_x \psi, x}$ on the right hand side holds the full gamut, $\psi, \partial_t \psi, \partial_x \psi, x$, fixed while computing the time derivative. Distinguishing these two derivatives is the primary point of confusion, so that for it is commonly sufficient to abbreviate this equation with the more succinct expression

$$\frac{\partial \mathcal{L}}{\partial t} = \frac{\partial \mathcal{L}}{\partial \psi} \frac{\partial \psi}{\partial t} + \frac{\partial \mathcal{L}}{\partial (\partial_t \psi)} \frac{\partial^2 \psi}{\partial t^2} + \frac{\partial \mathcal{L}}{\partial (\partial_x \psi)} \frac{\partial^2 \psi}{\partial x \partial t} + \left[\frac{\partial \mathcal{L}}{\partial t} \right]_{\psi, \partial_t \psi, \partial_x \psi, x}. \quad (10.36)$$

A similar expression holds for the partial space derivative computed at a fixed time,

$$\left[\frac{\partial \mathcal{L}}{\partial x} \right]_t = \left[\frac{\partial \mathcal{L}}{\partial \psi} \right]_{\partial_t \psi, \partial_x \psi} \frac{\partial \psi}{\partial x} + \left[\frac{\partial \mathcal{L}}{\partial (\partial_t \psi)} \right]_{\psi, \partial_x \psi} \frac{\partial^2 \psi}{\partial t \partial x} + \left[\frac{\partial \mathcal{L}}{\partial (\partial_x \psi)} \right]_{\psi, \partial_t \psi} \frac{\partial^2 \psi}{\partial x^2} + \left[\frac{\partial \mathcal{L}}{\partial x} \right]_{\psi, \partial_t \psi, \partial_x \psi, t}, \quad (10.37)$$

which also has the succinct form⁴

$$\frac{\partial \mathcal{L}}{\partial x} = \frac{\partial \mathcal{L}}{\partial \psi} \frac{\partial \psi}{\partial x} + \frac{\partial \mathcal{L}}{\partial (\partial_t \psi)} \frac{\partial^2 \psi}{\partial t \partial x} + \frac{\partial \mathcal{L}}{\partial (\partial_x \psi)} \frac{\partial^2 \psi}{\partial x^2} + \left[\frac{\partial \mathcal{L}}{\partial x} \right]_{\psi, \partial_t \psi, \partial_x \psi, t}. \quad (10.38)$$

10.4.2 Generalized spatial coordinates

As when studying discrete particle mechanics, we often find that Cartesian space coordinates are less suited to symmetry of the physical configuration. This point is particularly relevant for Chapter 11 when working with the Lagrangian space-time field theory relevant to fluids, in which we coordinate lines are attached to fluid particles. We thus now allow for the spatial coordinates, $x^a (a = 1, 2, 3)$, to be arbitrary general coordinates rather than restricted to Cartesian. To do so requires results from general tensor analysis in VOLUME 1. In particular, we need the invariant volume element given by

$$dV = g d^3x, \quad (10.39)$$

where g is the square root of the spatial metric tensor's determinant as represented by the arbitrary spatial coordinates, and

$$d^3x = dx^1 dx^2 dx^3 \quad (10.40)$$

is a shorthand for the spatial coordinate element. Note that g can generally be a function of space and time.

⁴Note that some authors (e.g., chapter 12 of [Goldstein \(1980\)](#)), write d/dt and d/dx for the left hand side operators in equations (10.35) and (10.37), referring to these derivatives as “total time” and “total space” derivatives. We do not follow that nomenclature here.

We are thus led to a variation of the action⁵

$$\delta S = \int_R (\delta \mathcal{L}) g d^3x dt. \quad (10.41)$$

Generalizing the Cartesian coordinate derivation requires us now to keep track of g , so that

$$\int_R \delta \psi \left[\frac{\partial \mathcal{L}}{\partial \psi} - \frac{1}{g} \frac{\partial}{\partial t} \left[g \frac{\partial \mathcal{L}}{\partial (\partial_t \psi)} \right] - \frac{1}{g} \frac{\partial}{\partial x^a} \left[g \frac{\partial \mathcal{L}}{\partial (\partial_a \psi)} \right] \right] g d^3x dt. \quad (10.42)$$

Setting $\delta S = 0$ leads to the Euler-Lagrange equation

$$\frac{\partial \mathcal{L}}{\partial \psi} - \frac{1}{g} \frac{\partial}{\partial t} \left[g \frac{\partial \mathcal{L}}{\partial (\partial_t \psi)} \right] - \frac{1}{g} \frac{\partial}{\partial x^a} \left[g \frac{\partial \mathcal{L}}{\partial (\partial_a \psi)} \right] = 0. \quad (10.43)$$

From our study of the covariant divergence in VOLUME 1, we see that the covariant divergence of a vector naturally appears in this formulation. Namely, we have the covariant divergence

$$\nabla_a \left[\frac{\partial \mathcal{L}}{\partial (\partial_a \psi)} \right] = \frac{1}{g} \frac{\partial}{\partial x^a} \left[g \frac{\partial \mathcal{L}}{\partial (\partial_a \psi)} \right], \quad (10.44)$$

where ∇_a is the covariant derivative operator. For the remainder of this chapter we make use of general spatial coordinates since they are necessary for the study of fluids in Chapter 11 using Lagrangian space-time.

10.4.3 Natural spatial boundary conditions

As seen in Section 10.3.4, the Euler-Lagrange field equations arise by setting the field variation, $\delta \psi$, to zero on both the space and time boundaries. This assumption is typical of many treatments given that it offers a generalization of the discrete case in VOLUME 1, in which the variation vanishes at the initial and final times. It is also relevant for the case without boundaries, with all terms assumed to vanish at infinity. However, for geophysical fluid mechanics the question of spatial boundary conditions is often of primary importance. We thus investigate alternatives to setting $\delta \psi = 0$ on the spatial boundaries.⁶

In particular, consider a situation where the fluid is bounded by a static material boundary, $\partial \mathcal{R}$. All fields, whether the actual physical field or variations around this field, must satisfy the relevant kinematic boundary conditions. In terms of the Lagrangian density, the natural boundary condition is given by

$$\hat{\mathbf{n}} \cdot \frac{\partial \mathcal{L}}{\partial (\nabla \psi)} = \hat{n}_a \frac{\partial \mathcal{L}}{\partial (\partial_a \psi)} = 0 \quad \text{on } \partial \mathcal{R}, \quad (10.45)$$

where $\hat{\mathbf{n}}$ is the outward normal along the spatial boundary, $\partial \mathcal{R}$. The boundary condition (10.45) means that there is no generalized forces acting on the physical field at the boundaries. If this boundary condition is satisfied, then the Euler-Lagrange equation (10.24) follows even without specifying how $\delta \psi$ behaves on the spatial boundaries.

What if the boundary is dynamical and thus feels forces, such as occurs in free boundary problems? For example, the boundary could represent the material interface between the ocean

⁵The variation (10.41) only varies the field, ψ , which means there is no variation of the space-time element, $g d^3x dt$. In Section 10.6 we allow for coordinates to be varied, in which case we must consider variations of $g d^3x dt$.

⁶See Section 41 of [Fetter and Walecka \(2003\)](#) for similar considerations.

and atmosphere, in which forces are imparted at the boundary. In this case the boundary itself is dynamical and so it too must be incorporated into Hamilton's principle. This situation is more subtle than when the boundary is static, and we explore an example in VOLUME 5 when studying waves in potential flow in a homogeneous fluid layer with a dynamical free surface.

10.4.4 Galilean space-time notation

In certain places in the following, it proves useful to streamline the notation by making use of the space-time tensor notation from VOLUME 1. Here, we introduce the Greek index, $\alpha = 0, 1, 2, 3$ with $\alpha = 0$ corresponding to the time index and $\alpha = 1, 2, 3$ for space. In this manner the Euler-Lagrange field equation

$$\frac{\partial \mathcal{L}}{\partial \psi} - \frac{1}{g} \frac{\partial}{\partial t} \left[\frac{\partial \mathcal{L}}{\partial (\partial_t \psi)} \right] - \frac{1}{g} \frac{\partial}{\partial x^a} \left[\frac{\partial \mathcal{L}}{\partial (\partial_a \psi)} \right] = 0, \quad (10.46)$$

takes on the more compact form

$$\frac{\partial \mathcal{L}}{\partial \psi} - \frac{1}{g} \frac{\partial}{\partial x^\alpha} \left[\frac{\partial \mathcal{L}}{\partial (\partial_\alpha \psi)} \right] = 0, \quad (10.47)$$

or even more succinct by making use of the covariant space-time divergence

$$\frac{\partial \mathcal{L}}{\partial \psi} - \nabla_\alpha \left[\frac{\partial \mathcal{L}}{\partial (\partial_\alpha \psi)} \right] = 0. \quad (10.48)$$

Integrals over space and time take on the form

$$\int \int_{\mathcal{R}} g \, d^3x \, dt = \int_{\mathcal{R}} g \, d^4x, \quad (10.49)$$

so that the action is written

$$\mathcal{S} = \int_{\mathcal{R}} \mathcal{L}(\psi, \partial_\alpha \psi, x^\alpha) g \, d^4x. \quad (10.50)$$

Additionally, for brevity we sometimes write x rather than x^α when there is no need to expose the coordinate labels.

In the study of continuum conservation laws from Noether's theorem (Sections 10.5 and 10.6), we encounter continuity equations of the form

$$\nabla_\alpha J^\alpha = g^{-1} [\partial_t(g J^0) + \partial_a(g J^a)] = 0, \quad (10.51)$$

where J^α is a Galilean four-vector. Integration over the global spatial domain renders,

$$\int_{\mathcal{R}} \nabla_\alpha J^\alpha g \, d^3x = 0, \quad (10.52)$$

which for a time-independent domain yields the global conservation law

$$\frac{d}{dt} \int_{\mathcal{R}} J^0 g \, d^3x = - \int_{\partial \mathcal{R}} J^a \hat{n}_a g \, d\mathcal{S}. \quad (10.53)$$

If the boundary integral vanishes then we have a global constant of integration, which corresponds to a symmetry of the action.

10.4.5 Mechanical equivalence of Lagrangians

In VOLUME 1 we noted that the mechanic equations describing the motion of discrete particles are unchanged if the Lagrangian for a particle system is modified by a total time derivative of a function of the generalized coordinates. Analogously, the mechanics of a continuum field remains unchanged if the Lagrangian density is modified by a space and/or time derivative of functions that have zero variation along the boundaries. More specifically, consider the two Lagrangian densities and briefly return to Cartesian coordinates in 1+1 dimensions

$$\mathcal{L}^{\text{new}} = \mathcal{L}^{\text{old}} + \partial_t \Gamma(\psi, \partial_t \psi, \partial_x \psi, x, t) + \partial_x \Sigma(\psi, \partial_t \psi, \partial_x \psi, x, t), \quad (10.54)$$

where Γ and Σ are arbitrary functions of the field, ψ , its derivatives, $\partial_t \psi, \partial_x \psi$, as well as the space and time positions. To examine mechanical equivalence, consider a space-time domain $R = [x_A, x_B] \oplus [t_A, t_B]$, so that the action transforms into

$$\begin{aligned} \mathcal{S}^{\text{new}} = \mathcal{S}^{\text{old}} &+ \int_{x_A}^{x_B} (\Gamma[\psi(t_B), \partial_t \psi(t_B), \partial_x \psi(t_B), x, t_B] - \Gamma[\psi(t_A), \partial_t \psi(t_A), \partial_x \psi(t_A), x, t_A]) dx \\ &+ \int_{t_A}^{t_B} (\Sigma[\psi(x_B), \partial_t \psi(x_B), \partial_x \psi(x_B), x_B, t] - \Sigma[\psi(x_A), \partial_t \psi(x_A), \partial_x \psi(x_A), x_A, t]) dt. \end{aligned} \quad (10.55)$$

The added terms in the first integral are evaluated at the time boundaries, t_A and t_B , whereas the second integral is evaluated at the space boundaries, x_A and x_B . So mechanical equivalence depends arises if the field has zero variation along the space and time boundaries, in which case

$$\delta \mathcal{S}^{\text{new}} = \delta \mathcal{S}^{\text{old}}, \quad (10.56)$$

which then means that the associated Euler-Lagrange equation is unchanged.

A more general approach, allowing for arbitrary coordinates, is given by

$$\mathcal{L}^{\text{new}} = \mathcal{L}^{\text{old}} + \nabla_\alpha J^\alpha, \quad (10.57)$$

where $\nabla_\alpha J^\alpha$ is a Galilean space-time divergence of a four-vector, J^α . In this case the action changes by

$$\mathcal{S}^{\text{new}} = \mathcal{S}^{\text{old}} + \int_{\partial R} J^\alpha \hat{n}_\alpha d\mathcal{S}, \quad (10.58)$$

where we made use of the space-time form of the [divergence theorem](#), thus rendering a boundary integral of the flux projected onto the space-time boundary. Mechanical equivalence thus depends on how J^α behaves along the space-time boundaries. Details depend on specifics of the variation, in particular whether we are considering Hamilton's principle to derive the Euler-Lagrange equations, or whether we are probing symmetries of the dynamical system to determine conservation laws. We further pursue these points when studying symmetries in [Sections 10.5](#) and [10.6](#).

10.4.6 The absence of second or higher derivatives in the Lagrangian

It is notable that the Lagrangian in equation (10.13) is a functional of the field, ψ , and its first derivatives, $\partial_\alpha \psi$. We were originally motivated to consider just the field and its first derivatives based on the continuum limit of coupled oscillators from [Section 10.2](#), where the discrete Lagrangian (10.6) only includes the displacement field and its first time derivative.

But when moving away from the discrete limit, we might wish to include higher derivatives for continuum fields. Yet, as noted in Section 1.5 of [Ramond \(1990\)](#), higher derivatives in the Lagrangian can lead to non-causal behavior in the corresponding Euler-Lagrange field equations, with the Lorentz-Dirac equation of electrodynamics an example. Hearing Ramond's warning motivates us to also restrict Lagrangians to have no second or higher order derivatives.

10.5 Space-time symmetry and stress-energy-momentum

An experiment conducted on a mechanically closed and isolated physical system does not care about the origin of space or time. That is, an experiment conducted in London in the year 1900 yields the same results as when done in New York in the year 2000, assuming all relevant conditions are the same. This observation can be formalized by deriving conservation laws that arise from the absence of a dependence on the space-time origin. Operationally, we expose the equations describing the physical system to a coordinate variation, δx^α , that represents a bulk shift of every point within the physical system. *Noether's theorem* ([Noether, 1918](#); [Noether and Tavel, 2018](#)) provides the means to derive a corresponding conservation law.

In this section we derive conservation laws arising from symmetry in the space-time position. These conservation laws are maintained by the physically realized field, ψ , that satisfy the Euler-Lagrange equation. As noted in VOLUME 1 when studying classical point particles, to connect a symmetry to a conservation law it is sufficient to focus on the Lagrangian as it encapsulates the mechanics. In this section we identify cyclic coordinates in the Lagrangian density, with these coordinates then reflecting a symmetry of the physical system that leads to a corresponding conservation law. We consider an alternative approach in Section 10.6 that focuses on the action.

10.5.1 Time symmetry and the Hamiltonian density

Consider a physical system that respects time homogeneity. What does this symmetry imply about the dynamical fields? To answer this question, return to the partial time derivative in equation (10.36)

$$\frac{\partial \mathcal{L}}{\partial t} = \frac{\partial \mathcal{L}}{\partial \psi} \frac{\partial \psi}{\partial t} + \frac{\partial \mathcal{L}}{\partial(\partial_\alpha \psi)} \frac{\partial}{\partial x^\alpha} \frac{\partial \psi}{\partial t} + \left[\frac{\partial \mathcal{L}}{\partial t} \right]_{\psi, \partial_\alpha \psi, x^\alpha}. \quad (10.59)$$

Now make use of the Euler-Lagrange equation (10.48) to have

$$\frac{\partial \mathcal{L}}{\partial \psi} \frac{\partial \psi}{\partial t} = \nabla_\alpha \left[\frac{\partial \mathcal{L}}{\partial(\partial_\alpha \psi)} \right] \frac{\partial \psi}{\partial t} = g^{-1} \frac{\partial}{\partial x^\alpha} \left[g \frac{\partial \mathcal{L}}{\partial(\partial_\alpha \psi)} \right] \frac{\partial \psi}{\partial t}, \quad (10.60)$$

which then leads to

$$\frac{\partial \mathcal{L}}{\partial t} = g^{-1} \frac{\partial}{\partial x^\alpha} \left[g \frac{\partial \mathcal{L}}{\partial(\partial_\alpha \psi)} \frac{\partial \psi}{\partial t} \right] + \left[\frac{\partial \mathcal{L}}{\partial t} \right]_{\psi, \partial_t \psi, \partial_x \psi, x^\alpha}. \quad (10.61)$$

We now assume spatial coordinates whose representation of the metric tensor is time-independent so that

$$\partial_t g = 0. \quad (10.62)$$

This assumption holds for Eulerian coordinates and for Lagrangian coordinates used in fluid mechanics (with the time derivative taken holding the corresponding spatial coordinates fixed).⁷ With this assumption we have

$$\frac{\partial}{\partial t} \left[\frac{\partial \mathcal{L}}{\partial(\partial_t \psi)} \frac{\partial \psi}{\partial t} - \mathcal{L} \right] + \nabla_a \left[\frac{\partial \mathcal{L}}{\partial(\partial_a \psi)} \frac{\partial \psi}{\partial t} \right] = - \left[\frac{\partial \mathcal{L}}{\partial t} \right]_{\psi, \partial_t \psi, \partial_x \psi, \mathbf{x}}. \quad (10.63)$$

Following the discrete case discussed in VOLUME 1, introduce the *generalized (or canonical) momentum density*, \mathcal{P} , and the *Hamiltonian density*, \mathcal{H} , along with the energy flux, \mathcal{F} ,

$$\mathcal{P} \equiv \frac{\partial \mathcal{L}}{\partial(\partial_t \psi)} \quad \text{and} \quad \mathcal{H} = \mathcal{P} \partial_t \psi - \mathcal{L} \quad \text{and} \quad \mathcal{F}^a = \frac{\partial \mathcal{L}}{\partial(\partial_a \psi)} \frac{\partial \psi}{\partial t}. \quad (10.64)$$

These definitions bring equation (10.63) to the form of a budget equation for the Hamiltonian density

$$\partial_t \mathcal{H} + \nabla \cdot \mathcal{F} = - \left[\frac{\partial \mathcal{L}}{\partial t} \right]_{\psi, \partial_t \psi, \partial_x \psi, \mathbf{x}}. \quad (10.65)$$

Evidently, the Hamiltonian density at a point in space evolves according to the covariant convergence of the flux, \mathcal{F} , along with a source term due to any explicit time dependence of the Lagrangian density.

When the Lagrangian density has no explicit time dependence, so that

$$\mathcal{L} = \mathcal{L}(\psi, \partial_t \psi, \partial_a \psi, x^a), \quad (10.66)$$

then the budget equation (10.65) reduces to the *Hamiltonian density continuity equation*

$$\partial_t \mathcal{H} + \nabla \cdot \mathcal{F} = 0. \quad (10.67)$$

This equation is written in the form of a continuum conservation law, with such conservation laws encountered throughout this book. Evidently, for the special case of a time independent spatial domain, and with the flux, \mathcal{F} , having zero area integrated normal projection at the domain boundary, we are led to the conservation of the domain integrated Hamiltonian

$$\frac{dH}{dt} = 0 \quad \text{with} \quad H = \int_{\mathcal{R}} \mathcal{H} dV = \int_{\mathcal{R}} \mathcal{H} g d^3x, \quad (10.68)$$

where \mathcal{R} is the spatial domain. This result constitutes an expression of Noether's theorem arising from time symmetry.

10.5.2 Stress-energy-momentum tensor

The derivation in Section 10.5.1 can be generalized to yield a budget equation built from elements of the *stress-energy-momentum tensor*. The space-time derivative of the Lagrangian density is given by (again, being careful with partial derivatives as discussed in Section 10.4.1)

$$\frac{\partial \mathcal{L}}{\partial x^\beta} = \frac{\partial \mathcal{L}}{\partial \psi} \frac{\partial \psi}{\partial x^\beta} + \frac{\partial \mathcal{L}}{\partial(\partial_\alpha \psi)} \frac{\partial}{\partial x^\alpha} \frac{\partial \psi}{\partial x^\beta} + \left[\frac{\partial \mathcal{L}}{\partial x^\beta} \right]_{\psi, \partial_\alpha \psi, x^\alpha \neq \beta}. \quad (10.69)$$

⁷The metric tensor is generally time dependent when represented using generalized vertical coordinates considered in Part I of this book. We return to this point in Part I when formulating a Hamilton's principle with generalized vertical coordinates.

Use of the Euler-Lagrange equation (10.48) leads to

$$\frac{\partial \mathcal{L}}{\partial x^\beta} = g^{-1} \frac{\partial}{\partial x^\alpha} \left[g \frac{\partial \mathcal{L}}{\partial (\partial_\alpha \psi)} \frac{\partial \psi}{\partial x^\beta} \right] + \left[\frac{\partial \mathcal{L}}{\partial x^\beta} \right]_{\psi, \partial_\alpha \psi, x^\alpha \neq \beta}. \quad (10.70)$$

Now assume the metric determinant is independent of coordinate x^β so that

$$\partial g / \partial x^\beta = 0, \quad (10.71)$$

in which case we have

$$g^{-1} \frac{\partial}{\partial x^\alpha} \left[-g \delta^\alpha_\beta \mathcal{L} + g \frac{\partial \mathcal{L}}{\partial (\partial_\alpha \psi)} \frac{\partial \psi}{\partial x^\beta} \right] = - \left[\frac{\partial \mathcal{L}}{\partial x^\beta} \right]_{\psi, \partial_\alpha \psi, x^\alpha \neq \beta}. \quad (10.72)$$

Introducing the *stress-energy-momentum tensor*

$$T^\alpha_\beta = -\delta^\alpha_\beta \mathcal{L} + \frac{\partial \mathcal{L}}{\partial (\partial_\alpha \psi)} \frac{\partial \psi}{\partial x^\beta}, \quad (10.73)$$

brings equation (10.72) to the form

$$g^{-1} \partial_\alpha (g T^\alpha_\beta) = - \left[\frac{\partial \mathcal{L}}{\partial x^\beta} \right]_{\psi, \partial_\alpha \psi, x^\alpha \neq \beta}, \quad (10.74)$$

For each value of β , this equation says that the four-divergence of T^α_β is determined by the partial derivative of the Lagrangian with respect to x^β . Integrating over the global space domain, and assuming the domain is time-independent, leads to

$$\frac{d}{dt} \int_{\mathcal{R}} T^0_\beta g d^3x = - \int_{\partial \mathcal{R}} T^a_\beta \hat{n}_a d\mathcal{S} - \int_{\mathcal{R}} \left[\frac{\partial \mathcal{L}}{\partial x^\beta} \right]_{\psi, \partial_\alpha \psi, x^\alpha \neq \beta} g d^3x, \quad (10.75)$$

where we used the general coordinate version of the [divergence theorem](#) from VOLUME 1. If the Lagrangian is not an explicit function of x^β , and we have a vanishing boundary integral of the flux, T^a_β , projected onto the outward normal, then there is a global conserved quantity

$$\frac{d}{dt} \int_{\mathcal{R}} T^0_\beta g d^3x = 0 \iff x^\beta \text{ is a cyclic coordinate.} \quad (10.76)$$

In the study of analytical mechanics in VOLUME 1, we referred to x^β as a *cyclic* coordinate. Cyclic coordinates arise from a symmetry of the physical system, and the coordinates used to represent the system, along the direction defined by the cyclic coordinate. This symmetry then leads to a conservation law, as we just showed. This result represents an example implication of Noether's theorem: any symmetry gives rise to a conservation law. We offer more on Noether's theorem in Section 10.6. Note that when $\beta = 0$, the budget equation (10.74) includes equation (10.65) for Hamiltonian density

$$\mathcal{H} = T^0_0 = -\mathcal{L} + \frac{\partial \mathcal{L}}{\partial (\partial_t \psi)} \frac{\partial \psi}{\partial t} \quad \text{Hamiltonian density} \quad (10.77a)$$

$$\mathcal{F}^a = T^a_0 = \frac{\partial \mathcal{L}}{\partial (\partial_a \psi)} \frac{\partial \psi}{\partial t} \quad \text{Hamiltonian density flux,} \quad (10.77b)$$

and for $\beta = b > 0$ we define

$$T^0_b = \frac{\partial \mathcal{L}}{\partial t \psi} \frac{\partial \psi}{\partial x^b} \quad \text{momentum density} \quad (10.78a)$$

$$T^a_b = -\mathcal{L} \delta^a_b + \frac{\partial \mathcal{L}}{\partial_a \psi} \frac{\partial \psi}{\partial x^b} \quad \text{stress tensor.} \quad (10.78b)$$

10.5.3 An auxiliary functional for deriving conservation laws

[Hayes \(1970\)](#) introduced an alternative method for computing conservation laws, with particular application to the wave-action conservation law (see [VOLUME 5](#)). In this method we introduce the functional

$$\mathcal{E}(\psi, \Phi) = \frac{\partial \mathcal{L}}{\partial(\partial_\alpha \psi)} \frac{\partial \Phi}{\partial x^\alpha} + \frac{\partial \mathcal{L}}{\partial \psi} \Phi \quad (10.79a)$$

$$= \frac{\partial \mathcal{L}}{\partial(\partial_\alpha \psi)} \frac{\partial \Phi}{\partial x^\alpha} + g^{-1} \frac{\partial}{\partial x^\alpha} \left[g \frac{\partial \mathcal{L}}{\partial(\partial_\alpha \psi)} \right] \Phi \quad (10.79b)$$

$$= g^{-1} \frac{\partial}{\partial x^\alpha} \left[g \frac{\partial \mathcal{L}}{\partial(\partial_\alpha \psi)} \Phi \right] \quad (10.79c)$$

$$= \nabla_\alpha \left[\frac{\partial \mathcal{L}}{\partial(\partial_\alpha \psi)} \Phi \right], \quad (10.79d)$$

where we used the Euler-Lagrange equation (10.48) for ψ , and where $\Phi(\mathbf{x}, t)$ is an arbitrary function yet to be specified. As a four-divergence, the functional, \mathcal{E} , has a spatial domain integral depending on the boundary conditions.

Separating the space and time derivative terms, and introducing the canonical momentum from equation (10.64), leads to

$$\mathcal{E}(\psi, \Phi) = g^{-1} \partial_t (g \Phi \mathcal{P}) + g^{-1} \frac{\partial}{\partial x^a} \left[g \Phi \frac{\partial \mathcal{L}}{\partial(\partial_a \psi)} \right]. \quad (10.80)$$

Now we specify $\Phi = \partial \psi / \partial t$ to render

$$\mathcal{E} = g^{-1} \left[\frac{\partial [g(\mathcal{H} + \mathcal{L})]}{\partial t} \right]_{\mathbf{x}} + \nabla_a \mathcal{F}^a = \left[\frac{\partial \mathcal{L}}{\partial t} \right]_{\mathbf{x}} - \left[\frac{\partial \mathcal{L}}{\partial t} \right]_{\psi, \partial_t \psi, \partial_x \psi, \mathbf{x}}, \quad (10.81)$$

where \mathcal{F}^a are components to the energy flux (10.64), we introduced the Hamiltonian density, \mathcal{H} , also given by equation (10.64), and made use of equation (10.61) to introduce the partial time derivatives. If the metric is independent of time, then the $[\partial \mathcal{L} / \partial t]_{\mathbf{x}}$ term cancels on both sides, which then renders the Hamiltonian continuity equation (10.65). We can likewise derive the momentum conservation equations from Section 10.5.2 through setting $\Phi = \partial_a \psi$.

10.5.4 Summary of the cyclic coordinate method

A physical system has no dependence on cyclic coordinates, so there is an arbitrariness associated with the value of the coordinate. This arbitrariness then leads to a corresponding differential conservation law in the form of a continuity equation. We here summarize the cyclic coordinate method used in this section to construct conservation laws. Generalizing the discussion of *mechanical equivalence* from Section 10.4.5, we know that a space-time variation has no impact

on the physical system if the Lagrangian density changes only by a total divergence

$$\delta\mathcal{L} = \mathcal{L}[\psi(x'), \partial_\alpha\psi(x'), x'] - \mathcal{L}[\psi(x), \partial_\alpha\psi(x), x] = \delta x^\alpha \partial_\alpha\mathcal{L}. \quad (10.82)$$

If the Lagrangian has no explicit dependence on any of the space-time coordinates, x^α , then

$$\delta\mathcal{L} = \delta x^\alpha \partial_\alpha\mathcal{L} = \delta x^\alpha \left[\frac{\partial\mathcal{L}}{\partial\psi} \frac{\partial\psi}{\partial x^\alpha} + \frac{\partial\mathcal{L}}{\partial(\partial_\alpha\psi)} \frac{\partial}{\partial x^\beta} \frac{\partial\psi}{\partial x^\alpha} \right]. \quad (10.83)$$

Thus far we have not used the Euler-Lagrange equations, so that equation (10.83) results solely due to the absence of an explicit dependence of \mathcal{L} on the space-time coordinates, x^α . An alternative approach to computing the variation is found by writing

$$\delta\mathcal{L} = \frac{\partial\mathcal{L}}{\partial\psi} \delta\psi + \frac{\partial\mathcal{L}}{\partial(\partial_\alpha\psi)} \delta(\partial_\alpha\psi), \quad (10.84)$$

where we again assumed \mathcal{L} has no explicit dependence on any of the space-time coordinates, x^α . We now make use of the Euler-Lagrange equation (10.48) to bring equation (10.84) into the form

$$\delta\mathcal{L} = g^{-1} \frac{\partial}{\partial x^\alpha} \left[g \frac{\partial\mathcal{L}}{\partial(\partial_\alpha\psi)} \delta\psi \right] = g^{-1} \delta x^\beta \frac{\partial}{\partial x^\alpha} \left[g \frac{\partial\mathcal{L}}{\partial(\partial_\alpha\psi)} \frac{\partial\psi}{\partial x^\beta} \right], \quad (10.85)$$

where we made use of the variation of the field and its derivative

$$\delta\psi = \psi(x') - \psi(x) = \delta x^\beta \partial_\beta\psi(x) \quad (10.86a)$$

$$\delta(\partial_\alpha\psi) = \partial_\alpha[\psi(x') - \psi(x)] = \delta x^\beta \partial_\beta\partial_\alpha\psi(x), \quad (10.86b)$$

and remembered that δx^β is a constant. Setting $\delta\mathcal{L}$ from equation (10.83) equal to $\delta\mathcal{L}$ from equation (10.85) leads to

$$\delta x^\beta g^{-1} \partial_\alpha(g T^\alpha_\beta) = 0, \quad (10.87)$$

where we introduced the stress-energy-momentum tensor from equation (10.73)

$$T^\alpha_\beta = -\delta^\alpha_\beta \mathcal{L} + \frac{\partial\mathcal{L}}{\partial(\partial_\alpha\psi)} \frac{\partial\psi}{\partial x^\beta}. \quad (10.88)$$

We have thus established four conservation laws (one for each value of $\beta = 0, 1, 2, 3$) that correspond to the space-time shift symmetry

$$\nabla_\alpha T^\alpha_\beta = g^{-1} \partial_\alpha(g T^\alpha_\beta) = 0. \quad (10.89)$$

There is no conservation law for those coordinates that have an explicit appearance in the Lagrangian. For example, if the Lagrangian has an explicit time dependence, such as when considering astronomical tidal forcing on the ocean, then the total energy of the system (as measured by the globally integrated Hamiltonian density) is not a constant. Instead, the system's energy is affected by the astronomical forces whose dynamics is described by another Lagrangian density that sits outside of the ocean that serves to modify the gravitational force. That is, a non-constant energy is generally a consequence of a physical system being mechanically open. Similarly, if the Lagrangian is a function of one of the spatial coordinates, then that indicates the absence of spatial symmetry in that direction and so the absence of a global conservation law.

10.6 Noether's theorem and symmetries of the action

In Section 10.5 we derived dynamical conservation laws by identifying cyclic coordinates in the Lagrangian density. Here we further our understanding of how symmetries give rise to conservation laws by introducing a few more concepts and methods. Central to these concepts is the notion of a transformation, and we are only concerned with smooth and continuous transformations rather than discrete. To determine physical implications of a continuous transformation, it is sufficient to examine how the action varies under an infinitesimal transformation, which we refer to as a *variation*. This treatment is convenient since deriving the implications of infinitesimal variations is simpler mathematically than finite transformations. In effect, we only need to work to leading order in a Taylor expansion to deduce the differential conservation laws.

10.6.1 Distinctions between Noether and Hamilton

Recall from Section 10.3 that we derived the Euler-Lagrange equation of motion by examining how the action changes when confronted with a functional variation of the field, $\psi \rightarrow \psi + \delta\psi$, with $\delta\psi$ vanishing along the time boundary. Setting to zero the corresponding variation of the action, $\delta S = 0$, is the statement of Hamilton's principle that leads to the Euler-Lagrange equation (along with natural spatial boundary conditions) that are satisfied by the physically realized dynamical system. The variations are never physically realized. Hamilton's realized that by probing these unphysical realizations renders a novel perspective (relative to Newton) on the physically realized system.

To deduce conservation laws using Noether's theorem requires a conceptual approach that builds from that used for Hamilton's principle. For Hamilton's principle we postulate that variation of the action vanishes when considering a variation in the field in the interior of the space-time domain. For Noether's theorem we work exclusively with the physical system that satisfies the Euler-Lagrange equations that arise from invoking Hamilton's principle. Noether's theorem then exposes the differential conservation laws arising from symmetries, as probed by variations to the space-time, that leave the physically realized action unchanged (or mechanically equivalent).

10.6.2 Active transformations

There are two complementary perspectives we take when considering a transformation (and its infinitesimal version referred to as a *variation*): the *active transformation* (*active variation*) and the *passive transformation* (*passive variation*). Active transformations arise from moving the physical system through space-time, whereas a passive transformation modifies the space-time coordinates while keeping the physical system unchanged. We here discuss active transformations with Section 10.6.3 considering the passive.⁸ Notably, they lead to the same mathematical result, and yet conceptually it can be useful to take one or the other perspective when studying variations to physical systems.

Active transformations and Noether's first theorem

Operationally, an active transformation arises from confronting the action with a variation of the physical fields (to probe *internal symmetries*) and/or a variation of the space-time position

⁸Chapter 3 in [José and Saletan \(1998\)](#) provides a thorough discussion of active and passive transformations.

of the system (to probe space-time symmetries). With these variations considered in their active sense, we imagine the physical system to be transformed (e.g., moved or rotated) whereas the space-time coordinate system used to describe the physical system remain unchanged. Moving an experimental apparatus from one side of the laboratory to another is an example active transformation, as is rotating the apparatus by some angle. Those active transformations that leave the action unchanged are symmetries of the physical system that directly lead to differential conservation laws. This connection between active symmetries and conservation laws constitutes *Noether's first theorem*.

Active transformations leave the coordinate system unchanged

As note above, the coordinate system used to describe the physical system is unchanged when performing an active transformation. Instead, an active transformation results in the modification to the space-time position of a point within the physical system

$$x^\alpha \rightarrow x'^\alpha = x^\alpha + \delta x^\alpha, \quad (10.90)$$

where δx^α is a tiny coordinate variation so that the space-time point, x' , is very close to the point, x . Since the coordinate lines remain fixed under an active transformation, we do not introduce a new set of coordinates, which are typically expressed as $x^{\bar{\alpha}}$ in this book. Instead, we kept the same coordinates, and wrote x^α for the original space-time point and x'^α for the displaced space-time point.

Galilean space-time active transformations and Noether's first theorem

The space-time symmetries we focus on are taken from Galilean space-time, which is relevant for studies of geophysical fluid mechanics.⁹ In particular, we consider a uniform space-time translation plus a rigid rotation. For a space and time coordinate translation, the new point has a coordinate position relative to the original point according to the coordinate variation

$$\delta x^\alpha = h^\alpha, \quad (10.91)$$

where h^α is a constant coordinate variation that is scaled by a tiny non-dimensional number to ensure that δx^α is tiny. To investigate spatial rotations we examine the coordinate variation determined by a small spatial rotation of the physical system as given by

$$\delta x^a = \mathcal{R}^a_b x^b \quad \text{and} \quad \delta x^0 = 0. \quad (10.92)$$

Here we introduced the anti-symmetric rotation matrix

$$\mathcal{R}^a_b = \epsilon^a_{bc} \Omega^c, \quad (10.93)$$

with $\Omega = \hat{\Omega} |\Omega|$ a vector that orients the rotation and with $|\Omega| \ll 1$ a tiny angle. Bringing both the translation and rotation together into a single active variation leads to

$$x'^\alpha = x^\alpha + \delta x^\alpha = x^\alpha + h^\alpha + \mathcal{R}^\alpha_\beta x^\beta, \quad (10.94)$$

where $\mathcal{R}^\alpha_\beta = 0$ if either $\alpha = 0$ or $\beta = 0$.

⁹In other areas of physics, such as electrodynamics and quantum field theory, symmetries are examined within the Lorentzian space-time of special relativity.

Variations to the volume element under an active transformation

The spatial coordinate measure, d^3x , remains unchanged since the coordinate lines are fixed under an active transformation. However, since we are moving the physical system to a new space-time position and/or modifying its spatial orientation, the spatial metric tensor is generally modified. We here assume the metric is time independent, and consider the effects on the volume element under an active transformation. The volume element appearing within the action integral has a variation

$$\delta(g d^3x) = \delta(g) d^3x, \quad (10.95)$$

so we must determine a variation of the square root of the metric tensor determinant, g . It is a bit simpler to work with the determinant of the metric, g^2 , which is a function only of the metric tensor elements, g_{ab} , so that

$$\delta g^2 = \frac{\partial g^2}{\partial g_{ab}} \delta g_{ab} = g^2 g^{ab} \delta g_{ab}, \quad (10.96)$$

where the second equality follows from our study of determinants in VOLUME 1.¹⁰ We thus find that an active transformation leads to the variation of the spatial volume element

$$\delta(g d^3x) = (g d^3x) g^{ab} \delta g_{ab}/2 \iff \delta(dV) = dV g^{ab} \delta g_{ab}/2. \quad (10.97)$$

To determine the variation of the metric tensor components, we proceed much like in VOLUME 2, where we determined the material evolution of the [Cauchy-Green strain tensor](#), thus resulting in¹¹

$$g^{ab} \delta g_{ab} = 2 g^{ab} \nabla_a(\delta x_b) = 2 \nabla^b(\delta x_b) = 2 \nabla_a(\delta x^a), \quad (10.98)$$

so that

$$\delta(g d^3x) = (g d^3x) \nabla_a(\delta x^a) \iff \delta(dV) = dV \nabla_a(\delta x^a). \quad (10.99)$$

Evidently, under an active transformation, the relative variation of the volume element is determined by the covariant divergence of the coordinate variation, so that the active transformation is volume preserving if the covariant divergence vanishes

$$\nabla_a(\delta x^a) = 0 \implies \text{volume preserving active transformation.} \quad (10.100)$$

This result corresponds to that found using alternative methods in VOLUME 2, when studying how fluid flow divergence affects the volume of a fluid element. Indeed, we could have appealed to those earlier results to immediately write equation (10.99). Furthermore, we know that one physical way to alter the volume of a fluid region is to apply pressure work.

¹⁰In words, equation (10.96) says that the derivative of the determinant, with respect to one of its elements (here g_{ab}), equals to the determinant times the component of the inverse matrix corresponding to the element (here g^{ab}).

¹¹A more general approach makes use of *Lie derivatives* to compute the variation of the metric along the congruence of curves defined by the variation, δx^α . Here, we largely appeal to the intuition of the result (10.99). Section F.3 of [Tromp \(2025\)](#) provides a lucid discussion of Lie derivatives.

Variations to the mass element under an active transformation

In continuum mechanics we generally follow mass conserving parcels of matter. It is thus relevant to determine if the mass changes under an active transformation, in which we investigate

$$\delta(\rho dV) = \rho \delta(dV) + \delta\rho dV \quad (10.101a)$$

$$= dV (\rho \nabla_a (\delta x^a) + \delta x^a \partial_a \rho) \quad (10.101b)$$

$$= dV (g^{-1} \rho \partial_a (g \delta x^a) + \delta x^a \partial_a \rho) \quad (10.101c)$$

$$= dV \nabla_a (\rho \delta x^a). \quad (10.101d)$$

Evidently, the mass of a region of matter remains unchanged if the covariant divergence of the density weighted variation vanishes

$$\nabla_a (\rho \delta x^a) = 0 \implies \text{mass preserving active transformation.} \quad (10.102)$$

This sort of transformation requires the volume of the region to reduce while the density increases, and vice versa, thus keeping the mass unchanged. Conversely, a nonzero covariant divergence, $\nabla_a (\rho \delta x^a) \neq 0$, is the signal of a modification to the mass of an infinitesimal region.

10.6.3 Passive transformations

A *passive transformation* keeps the physical system untouched while it alters its coordinate representation. For example, the transformation between Cartesian coordinates and spherical coordinates is passive, as is the transformation between Eulerian and Lagrangian coordinates. Passive transformations have been discussed extensively in this book in the context of tensor analysis, whereby tensors are considered objective geometric objects whose coordinate representations leave a tensor unchanged whereas the tensor's representation is changed (see VOLUME 1). Equations written in a manner that remain form invariant under coordinate transformations are said to satisfy *coordinate covariance*. In the context of symmetry principles, if we can find a continuous transformation of the coordinates that leaves the physical action unchanged, then this passive transformation leads, through *Noether's second theorem*, to a local conservation law (sometimes referred to as a *Bianchi identity*). The particle relabeling symmetry detailed in Section 11.7 is an example of a passive transformation applied to fluid flow as represented using Lagrangian kinematics.

An infinitesimal passive transformation is a coordinate variation of the form

$$x^{\bar{\alpha}} = \delta^{\bar{\alpha}}_{\alpha} (x^{\alpha} + \delta x^{\alpha}), \quad (10.103)$$

which should be compared to the active variation in equation (10.90). The transformation matrix arising from the coordinate variation (10.103) is given by

$$\Lambda^{\bar{\alpha}}_{\beta} = \partial x^{\bar{\alpha}} / \partial x^{\beta} = \delta^{\bar{\alpha}}_{\alpha} [\delta^{\alpha}_{\beta} + \partial_{\beta}(\delta x^{\alpha})], \quad (10.104)$$

and its Jacobian determinant is, to leading order in variation, given by

$$\det(\Lambda^{\bar{\alpha}}_{\beta}) \approx 1 + \partial_{\alpha}(\delta x^{\alpha}). \quad (10.105)$$

Consequently, the space-time coordinate measure transforms according to

$$d^4 \bar{x} = \det(\Lambda^{\bar{\alpha}}_{\beta}) d^4 x = [1 + \partial_{\alpha}(\delta x^{\alpha})] d^4 x \implies \delta(d^4 x) = (\partial_{\alpha}(\delta x^{\alpha}) d^4 x). \quad (10.106)$$

Assuming the metric tensor is time independent, we find that the spatial volume element transforms as

$$\delta(dV) = \delta(g d^3x) = [g^{-1} \delta x^a \partial_a g + \partial_a(\delta x^a)] g d^3x = (\nabla_a \delta x^a) dV. \quad (10.107)$$

Hence, a volume conserving passive transformation arises from the same non-divergence condition (10.100) holding for the active transformation. In a similar manner, we find that the mass transforms under a passive transformation just as for the active transformation (10.101d), so that the mass is unchanged if $\nabla_a(\rho \delta x^a) = 0$.

10.6.4 Total variation of the field

In Section 10.3.2 we defined the functional variation of the field, $\delta\psi$. The functional variation affects a change just to the function, with the space-time point unchanged

$$\delta\psi(x^\alpha) = \psi'(x^\alpha) - \psi(x^\alpha), \quad (10.108)$$

where each term is evaluated at the same space-time point using the coordinate, x^α . This is the sort of variation considered for Hamilton's principle. Focusing here on active transformations, we find it useful to define the *total variation*, which considers both a functional change as well as a change to the space-time point, so that (dropping the α label on $\psi(x^\alpha)$ for brevity)

$$\Delta\psi(x) \equiv \psi'(x) - \psi(x) \quad (10.109a)$$

$$= [\psi'(x') - \psi(x')] + [\psi(x') - \psi(x)] \quad (10.109b)$$

$$\approx \delta\psi(x') + \delta x^\alpha \partial_\alpha \psi(x) \quad (10.109c)$$

$$\approx \delta\psi(x) + \delta x^\alpha \partial_\alpha \psi(x). \quad (10.109d)$$

For the final equality we set

$$\delta\psi(x') \approx \delta[\psi(x) + \delta x^\alpha \partial_\alpha \psi(x)] = \delta\psi(x) + \mathcal{O}(\delta^2), \quad (10.110)$$

with second order terms ignored. Evidently, to first order in δ , the total variation of the field is given by

$$\Delta\psi(x) = (\delta + \delta x^\alpha \partial_\alpha) \psi(x). \quad (10.111)$$

The first term on the right hand side is the functional variation, $\delta\psi$, and the second term is a transport term that arises from translation and/or rotation of the coordinates, $\delta x^\alpha \partial_\alpha \psi$. Note that when we are just probing space-time symmetries, then $\Delta\psi = 0$ so that $\delta\psi = -\delta x^\alpha \partial_\alpha \psi$.

10.6.5 Variation of the action under an active transformation

We here consider the variation of the action under an active transformation

$$\delta\mathcal{S} = \mathcal{S}' - \mathcal{S} = \int_R \mathcal{L}[\psi'(x'), \partial_\alpha \psi'(x'), x'^\alpha] g' d^4x' - \int_R \mathcal{L}[\psi(x), \partial_\alpha \psi(x), x^\alpha] g d^4x. \quad (10.112)$$

Making use of equation (10.107) for the volume element renders, to first order in variation,

$$\delta\mathcal{S} = \int_R [\delta + \nabla_\alpha(\delta x^\alpha)] \mathcal{L}[\psi(x), \partial_\alpha \psi(x), x^\alpha] g d^4x. \quad (10.113)$$

The chain rule yields the variation

$$\delta\mathcal{L} + \mathcal{L} \nabla_\alpha(\delta x^\alpha) = \frac{\partial\mathcal{L}}{\partial\psi} \delta\psi + \frac{\partial\mathcal{L}}{\partial(\partial_\alpha\psi)} \delta(\partial_\alpha\psi) + \frac{\partial\mathcal{L}}{\partial x^\alpha} \delta x^\alpha + g^{-1} \mathcal{L} \partial_\alpha(\delta x^\alpha) \quad (10.114a)$$

$$= \frac{\partial\mathcal{L}}{\partial\psi} \delta\psi + \frac{\partial\mathcal{L}}{\partial(\partial_\alpha\psi)} \delta(\partial_\alpha\psi) + \nabla_\alpha(\mathcal{L} \delta x^\alpha), \quad (10.114b)$$

with the Euler-Lagrange equation (10.47) substituted in for $\partial\mathcal{L}/\partial\psi$ rendering the very tidy result

$$\delta\mathcal{L} + \mathcal{L} \nabla_\alpha(\delta x^\alpha) = \nabla_\alpha \left[\frac{\partial\mathcal{L}}{\partial(\partial_\alpha\psi)} \delta\psi + \mathcal{L} \delta x^\alpha \right]. \quad (10.115)$$

Now introduce the total variation, $\Delta\psi$, from equation (10.109d), and the stress-energy-momentum tensor from equation (10.73) to find

$$\delta\mathcal{L} + \mathcal{L} \nabla_\alpha(\delta x^\alpha) = \nabla_\alpha \left[\frac{\partial\mathcal{L}}{\partial(\partial_\alpha\psi)} \Delta\psi - T^\alpha_\beta \delta x^\beta \right], \quad (10.116)$$

which then leads to the variation of the action under an active transformation

$$\delta\mathcal{S} = \int_R [\delta + \nabla_\alpha(\delta x^\alpha)] \mathcal{L} d^4x = \int_R \nabla_\alpha J^\alpha g d^4x = \int_{\partial R} J^\alpha \hat{n}_\alpha d\mathcal{S}, \quad (10.117)$$

where $\hat{n}_\alpha d\mathcal{S}$ is the oriented area element on the space-time boundary, and we introduced the space-time flux¹²

$$J^\alpha \equiv \frac{\partial\mathcal{L}}{\partial(\partial_\alpha\psi)} \Delta\psi - T^\alpha_\beta \delta x^\beta. \quad (10.118)$$

We conclude that if the total variation, $\Delta\psi$, reflects a symmetry of the physical system, then the action must have a zero variation, in which case we have the local conservation law (continuity equation)

$$\nabla_\alpha J^\alpha = 0, \quad (10.119)$$

where J^α is given by equation (10.118). This result constitutes Noether's first theorem.

10.6.6 Angular momentum and space isotropy

In Section 10.5 we considered the space-time symmetry associated with the absence of dependence on an origin, and we assumed the total field variation vanishes,

$$\Delta\psi = \psi'(x') - \psi(x) = 0 \implies \delta\psi = -\delta x^\alpha \partial_\alpha\psi. \quad (10.120)$$

In this case the conservation law reduces to a statement about the stress-energy-momentum tensor (see Section 10.5.2). Namely, if there is no special space or time origin, then linear momentum and mechanical energy are conserved. Here we display the angular momentum conservation law arising from the absence of a dependence on the orientation of the spatial coordinates. We also consider $\Delta\psi = 0$, but specify the spatial variation according to the rotation (10.93) so that the active variation is

$$\delta x^0 = 0 \quad \text{and} \quad \delta x^a = \mathcal{R}^a_b x^b = \epsilon^a_{bc} \Omega^c x^b, \quad (10.121)$$

¹²In the quantum field theory literature, J^α is referred to as a *current*, in analog to an electrical current. Here we refer to it as a flux to correspond to the nomenclature in fluid mechanics.

where Ω^c are the components to a spatial vector whose magnitude, $|\Omega|$, is small. The space-time flux, J^α , from equation (10.118) thus has the components

$$-J^\beta = T^\beta{}_\alpha \delta x^\alpha = T^\beta{}_a \epsilon^a{}_{bc} \Omega^c x^b. \quad (10.122)$$

At this point we assume Cartesian coordinates, so that the covariant derivative is a partial derivative, and the four-convergence of the flux is

$$-\partial_\beta J^\beta = \partial_\beta T^\beta{}_a \epsilon^a{}_{bc} \Omega^c x^b + T^\beta{}_a \epsilon^a{}_{\beta c} \Omega^c. \quad (10.123)$$

If the physical system has no concern for the origin of space, then we know from Section 10.5.4 that $\partial_\beta T^\beta{}_a = 0$ for each of the $a = 1, 2, 3$ spatial coordinates. If the physical system likewise has no concern for the orientation of space (i.e., it is spatially isotropic), then we must have rotational symmetry. For that property to manifest in a conservation law requires the stress-energy-momentum tensor to be symmetric so that

$$T^\beta{}_a \epsilon^a{}_{\beta c} = 0 \iff T^\beta{}_a = T_a{}^\beta = (T^\beta{}_a)^T. \quad (10.124)$$

We encountered this same condition in VOLUME 2 arising from similar considerations.¹³

10.6.7 Comments

The space-time symmetries considered in this section and Section 10.5 are generally broken in realistic physical systems. For example, in Chapter 11 we study the motion of a perfect fluid moving around a rotating and gravitating planet, with spatial symmetry reduced to axial symmetry around the rotation axis (assuming a smooth planet). When considering motion of a geophysical fluid on a realistic planet with non-smooth boundaries (i.e., mountains, land-sea boundaries), we have no spatial symmetry and so no momentum conservation. Even so, by examining the properties of closed fluid systems moving in spaces of particular symmetry, we reveal the conservation laws forming the foundation for the physical theory. Doing so provides a valuable conceptual and operational baseline for then examining how processes and boundary conditions break symmetry.

We have thus far only considered space-time symmetries, so that we assumed the total field variation vanishes,

$$\Delta\psi = \psi'(x') - \psi(x) = 0 \implies \delta\psi = -\delta x^\alpha \partial_\alpha \psi, \quad (10.125)$$

which means that the field is a scalar. But the formalism developed in this section also allows for probing symmetries in the space of fields, in which $\Delta\psi \neq 0$. If the action remains unchanged under a $\Delta\psi \neq 0$, then that reflects an *internal symmetry* that is not associated with space and time symmetries. Such internal symmetries are the basis for *gauge theories* of particle physics, as discussed in [Quigg \(1983\)](#), [Ryder \(1985\)](#), [Ramond \(1990\)](#), and many other texts.

¹³There are some Lagrangian densities that do not produce a symmetric stress-energy-momentum tensor when evaluating equation (10.73). However, we can add a term, $\partial_\lambda F^{\lambda\alpha}{}_\beta$, to $T^\alpha{}_\beta$ without affecting the conservation law (10.89), so long as $F^{\lambda\alpha}{}_\beta = -F^{\alpha\lambda}{}_\beta$. This gauge degree of freedom allows us to always work with a symmetrized stress-energy-momentum tensor. See Section E.1 of [Wald \(1984\)](#) or Section 3.2 of [Ryder \(1985\)](#) for more discussion on this point, which is of particular relevance to general relativity.

10.6.8 Further study

The treatment of Noether's theorem in this section was inspired by Chapter 2 of [Quigg \(1983\)](#), Section E.1 of [Wald \(1984\)](#), Section 3.2 of [Ryder \(1985\)](#), Section 1.5 of [Ramond \(1990\)](#), and Section 2.6 of [Tromp \(2025\)](#).



Chapter 11

HAMILTON'S PRINCIPLE FOR PERFECT FLUIDS

In this chapter we derive the momentum equation (Euler equation) for a single-component perfect fluid using *Hamilton's variational principle* rather than Newton's laws. To do so, we couple the field theory of Chapter 10 with the Lagrangian kinematics of the motion field, $\varphi(\mathbf{a}, T)$, thus deriving a field theory for φ in Lagrangian space-time. Hamilton's principle is concerned with conservative physical systems, such as a single component perfect fluid in a static gravitational field with each fluid parcel only experiencing reversible processes (i.e., no diffusion, friction, or conduction), which means that the fluid is contained within a materially and thermally closed domain. The fluid parcels feel conservative body forces from gravity, as well as, in a rotating terrestrial frame, the planetary Coriolis and planetary centrifugal forces are present. Interactions between the parcels are limited to mechanical contact forces from pressure, with pressure forces performing work on fluid parcels by modifying their volume (for non-Boussinesq fluids).

READER'S GUIDE FOR THIS CHAPTER

Mathematical elements of variational principles are presented in VOLUME 1, along with a suite of examples. We make use of arbitrary material coordinates (\mathbf{a} -space), thus requiring the general tensor analysis as detailed in VOLUME 1. We use general Eulerian (\mathbf{x} -space) coordinates up to the point of deriving the variation of the internal energy, at which point we assume Cartesian Eulerian coordinates. We make full use of the Lagrangian kinematics from VOLUME 2, and require a rudimentary understanding of thermodynamics also studied in VOLUME 2. Development and use of Hamilton's principle are provided in VOLUME 2 for discrete systems and in Chapter 10 for continuous fields.

Salmon (1988) is the canonical reference for Hamilton's principle in fluid mechanics (see also *Müller (1995)*, chapter 7 in *Salmon (1998)* and *Badin and Crisciani (2018)*). *Soper (2008)* provides a treatment based on the Lorentz space-time of special relativity, though with some non-relativistic limiting cases to connect with the Galilean space-time of terrestrial motion. *Jezierski and Kijowski (1990)* and *Sieniutycz (1994)* target a unification of thermodynamics with continuum mechanics using variational methods. Our presentation makes use of general tensor notation for working in Lagrangian space-time, and offers a particular emphasis on the motion field, $\varphi(\mathbf{a}, T)$, following from the treatment of continuum mechanics in Chapters 1 and 2 of *Tromp (2025)*.

11.1 Loose threads	364
11.2 Motion and velocity	364

11.2.1	The motion field, flow map, deformation matrix, and velocity	365
11.2.2	Including planetary rotation	366
11.3	Mass, density, and specific volume	366
11.3.1	Expressions for mass over a material region	366
11.3.2	Constant mass fluid parcels	367
11.3.3	Cartesian Eulerian for when varying internal energy	367
11.3.4	Concerning mass-labeling/unimodular coordinates	368
11.4	Energetics and entropy	368
11.4.1	Kinetic energy	368
11.4.2	Gravitational potential energy	369
11.4.3	Specific entropy is materially constant	369
11.4.4	Internal energy	369
11.5	Variation of the action and Euler-Lagrange equations	370
11.5.1	General expression for the Euler-Lagrange equation	371
11.5.2	Variation of the kinetic energy	372
11.5.3	Variation of the gravitational potential energy	373
11.5.4	Variation of the specific internal energy	373
11.5.5	How the pressure gradient appears	374
11.5.6	The perfect fluid Euler-Lagrange equation	376
11.5.7	Comments	376
11.6	Perfect fluid Hamiltonian continuity equation	377
11.6.1	Canonical momentum and Hamiltonian density	377
11.6.2	Energy flux and the covariant flux divergence	377
11.6.3	Lagrangian and Eulerian Hamiltonian continuity equations	378
11.7	Particle relabeling symmetry and potential vorticity	379
11.7.1	Passive transformation of Lagrangian space coordinates	379
11.7.2	Constraints from mass conservation	380
11.7.3	The motion field is a scalar	381
11.7.4	The specific internal energy is a scalar	382
11.7.5	Coordinate variation of the kinetic energy	382
11.7.6	Lagrangian expression for the potential vorticity	383
11.7.7	Eulerian expression for the potential vorticity	384
11.7.8	Global versus local conservation	385

11.1 Loose threads

- Referential flow and deviations from that flow
- Determine the forces of constraint arising from the no-normal flow boundary condition.
- Clean up notation and presentation, particularly in the particle relabeling Section 11.7.
- It would be nice not to need the Cartesian Eulerian assumption to compute the variation of the internal energy. Is there a simple way to generalize?

11.2 Motion and velocity

We here summarize salient points concerning the motion field studied in VOLUME 2.

11.2.1 The motion field, flow map, deformation matrix, and velocity

We conceive of fluid flow as the smooth movement through space of a matter continuum, with this movement measured by the three-component **motion field**, $\boldsymbol{\varphi}$. Mathematically, the motion field provides the **flow map** that takes the matter continuum from its reference state (e.g., some spatial configuration at time $T = t_R$) to the state at time $T > t_R$. Assuming \mathbf{x} is the position of a point in Euclidean space, the motion field provides a point transformation,

$$\mathbf{x} = \boldsymbol{\varphi}(\mathbf{a}, T) \quad \text{and} \quad t = T, \quad (11.1)$$

between the Eulerian (\mathbf{x} -position space) reference frame to the Lagrangian (\mathbf{a} -material space) reference frame. The motion field enables a 1-to-1 and invertible mapping (a *diffeomorphism*) between Eulerian and Lagrangian space-time. Transformation of tensors between Eulerian and Lagrangian space is provided by the **deformation matrix**, with components to this matrix given by the partial derivatives

$$F^i{}_I = \frac{\partial \varphi^i}{\partial a^I} = \partial_I \varphi^i, \quad (11.2)$$

where lowercase indices are reserved for Eulerian space coordinates, x^i , and upper case for Lagrangian coordinates, a^I . The components to the inverse of the deformation matrix are written $F^I{}_i$, so that

$$F^i{}_J F^J{}_j = \delta^i{}_j \quad \text{and} \quad F^I{}_i F^i{}_J = \delta^I{}_J. \quad (11.3)$$

We also have use for the determinant of the transformation matrix (the Jacobian of transformation), which is written

$$\det(F^i{}_I) = \frac{\partial \boldsymbol{\varphi}}{\partial \mathbf{a}} \quad (11.4)$$

Evaluating the motion field for a particular value for the material coordinate, \mathbf{a} , and allowing time to progress, provides the space-time trajectory, \mathbf{X} , of the fluid particle labeled by \mathbf{a}

$$\mathbf{X}(\mathbf{a}, T) = \boldsymbol{\varphi}(\mathbf{a}, T). \quad (11.5)$$

The velocity of a material fluid particle is determined by the material time derivative of the motion

$$\mathbf{v}^L(\mathbf{a}, T) = \partial_T \boldsymbol{\varphi}(\mathbf{a}, T) \iff (v^L)^i = \partial_T \varphi^i. \quad (11.6)$$

We include the L superscript to emphasize that \mathbf{v}^L is sampled on a fluid particle and so it is a function of (\mathbf{a}, T) . Consequently, we commonly refer to \mathbf{v}^L as the “Lagrangian velocity”. Even so, we see below (equation (11.8)) another candidate for this same name that is more precise from a tensor analysis perspective. The velocity \mathbf{v}^L has a dual Eulerian velocity, $\mathbf{v}(\mathbf{x}, t)$, that is equal to the Lagrangian velocity for the fluid particle that passes through \mathbf{x} at time t

$$\mathbf{v}(\mathbf{x}, t) = \mathbf{v}^L(\mathbf{a}, T) \quad \text{for } \mathbf{x} = \boldsymbol{\varphi}(\mathbf{a}, T) \text{ and } t = T. \quad (11.7)$$

This self-evident relation is reflected in all other properties of the continuum.

The Lagrangian velocity, $\mathbf{v}^L(\mathbf{a}, T)$, and Eulerian velocity, $\mathbf{v}(\mathbf{x}, t)$, are generally distinct functions of their respective coordinates, thus prompting use of the distinct symbols, \mathbf{v}^L versus \mathbf{v} . For example, we might choose one of the material coordinates to be the specific entropy since for a perfect fluid the specific entropy is constant on fluid particles. For this case it is clear that $\mathbf{v}^L(\mathbf{a}, T)$ and $\mathbf{v}(\mathbf{x}, t)$ are distinct mathematical functions. Even so, as tensors, both \mathbf{v}^L and \mathbf{v} carry Eulerian space-time indices, $(v^L)^i$ and v^i . A representation of the velocity that carries

Lagrangian space-time indices is realized through use of the inverse transformation matrix,

$$v^I = F^I_i (v^L)^i. \quad (11.8)$$

We encounter this *tensorially Lagrangian* representation of the velocity when studying the fluid particle relabeling symmetry in Section 11.7.

11.2.2 Including planetary rotation

As detailed in Section VOLUME 2, the inertial frame representation for the velocity of a fluid particle moving on the rotating planet is given by

$$\mathbf{v}_{\text{inertial}} = \mathbf{v} + \boldsymbol{\Omega} \times \mathbf{x}, \quad (11.9)$$

where \mathbf{v} is the particle velocity relative to the rotating planet, $\boldsymbol{\Omega}$ is the time-independent angular velocity of the rotating planet, \mathbf{x} is the position vector of the particle relative to an origin, and $\boldsymbol{\Omega} \times \mathbf{x}$ is the velocity arising from the rigid body rotation of the planetary reference frame. The corresponding Eulerian velocity field for fluid motion on a rotating planet is thus given by

$$\mathbf{v}_{\text{inertial}}(\mathbf{x}, t) = \mathbf{v}(\mathbf{x}, t) + \boldsymbol{\Omega} \times \mathbf{x}, \quad (11.10)$$

and the Lagrangian velocity is

$$\mathbf{v}_{\text{inertial}}^L(\mathbf{a}, T) = \partial_T \boldsymbol{\varphi}(\mathbf{a}, T) + \boldsymbol{\Omega} \times \boldsymbol{\varphi}(\mathbf{a}, T). \quad (11.11)$$

As studied in VOLUME 1, planetary rotation gives rise to the planetary Coriolis acceleration and planetary centrifugal acceleration when describing motion in the rotating terrestrial reference frame.

11.3 Mass, density, and specific volume

We here recall elements of fluid kinematics related to the mass and volume of infinitesimal material fluid parcels, and for finite sized spatial material domains denoted by \mathcal{R} . Since the region is material, it is time independent when expressed in terms of Lagrangian coordinates, $\mathcal{R}(\mathbf{a})$, whereas it is time dependent when expressed in terms of Eulerian coordinates, $\mathcal{R}(t)$.

11.3.1 Expressions for mass over a material region

From the discussion of mass conservation in VOLUME 2, the mass over a material region can be written in either the Eulerian or Lagrangian integral expressions

$$M = \int_{\mathcal{R}(t)} \rho(\mathbf{x}, t) g^E(\mathbf{x}) d^3x = \int_{\mathcal{R}(\mathbf{a})} \rho^L(\mathbf{a}, T) g^L(\mathbf{a}, T) d^3a. \quad (11.12)$$

The first expression for mass makes use of arbitrary Eulerian coordinates and thus represents the volume integral of mass density over the moving material region. The square root of the metric determinant, $g^E(\mathbf{x})$, is independent of Eulerian time, by construction of Eulerian coordinates, whereas the Lagrangian analog, $g^L(\mathbf{a}, T)$, is generally a function of the Lagrangian time. The second expression for mass in equation (11.12) makes use of Lagrangian coordinates,

with the material coordinate element given by

$$d^3a = da^1 da^2 da^3, \quad (11.13)$$

which has physical dimensions determined by those of the material coordinates, (a^1, a^2, a^3) . The products $g^E(x) d^3x$ and $g^L(a, T) d^3a$ have dimensions of volume (L^3), so that they are expressions for the same invariant volume element studied in VOLUME 1

$$dV = g^E(x) d^3x = g^L(a, T) d^3a. \quad (11.14)$$

This equation then leads to the identity for the Jacobian of transformation between Eulerian and Lagrangian coordinates

$$\frac{\partial x}{\partial a} = \frac{\partial \phi}{\partial a} = \det(F^i{}_I) = \frac{g^L}{g^E}. \quad (11.15)$$

11.3.2 Constant mass fluid parcels

From VOLUME 2, the mass of a fluid parcel remains constant when its center of mass follows a fluid particle trajectory, so that

$$dM = \rho^L(a, T) g^L(a, T) d^3a \quad (11.16)$$

is a material constant. The element, d^3a , measures the material coordinate volume and it is fixed within material space. Hence, mass conservation for material parcels means that $\rho^L(a, T) g^L(a, T)$ is independent of material time,

$$\partial_T[\rho^L(a, T) g^L(a, T)] = 0. \quad (11.17)$$

We can thus set its value at any convenient time instance, which we choose as the $T = t_R$ conditions and write

$$\dot{\rho}^L(a) \dot{g}^L(a) = \rho^L(a, T = t_R) g^L(a, T = t_R) = \rho^L(a, T) g^L(a, T), \quad (11.18)$$

with the corresponding mass of the material region

$$M = \int_{\mathcal{R}(a)} \dot{\rho}^L(a) \dot{g}^L(a) d^3a. \quad (11.19)$$

Evidently, $\dot{\rho}^L$, \dot{g}^L , and d^3a are each set at the initial time, and thus are unaltered when considering the variation of trajectories when varying the action for Hamilton's principle in Section 11.5. They can be changed, however, when varying coordinates as per the discussion of particle relabeling in Section 11.7.

11.3.3 Cartesian Eulerian for when varying internal energy

We need the specific volume for working with the internal energy in Section 11.4.4, which from equations (11.18) and (11.15) yield

$$\nu_s^L(a, T) = 1/\rho^L(a, T) = \frac{g^L(a, T)}{\dot{\rho}^L(a) \dot{g}^L(a)} = \frac{g^E(x)}{\dot{\rho}^L(a) \dot{g}^L(a)} \frac{\partial \phi(a, T)}{\partial a}. \quad (11.20)$$

When varying the internal energy, we find it convenient to choose Cartesian coordinates for describing Eulerian \mathbf{x} -space. For this case we have $\mathbf{g}^E = 1$ so that

$$\nu_s^L(\mathbf{a}, T) = \frac{1}{\dot{\rho}^L(\mathbf{a}) \dot{\mathbf{g}}^L(\mathbf{a})} \frac{\partial \Phi(\mathbf{a}, T)}{\partial \mathbf{a}} \Leftarrow \text{Cartesian Eulerian with } \mathbf{g}^E(\mathbf{x}) = 1 \quad (11.21a)$$

$$\frac{\partial \Phi(\mathbf{a}, T)}{\partial \mathbf{a}} = \mathbf{g}^L(\mathbf{a}, T) \Leftarrow \text{Cartesian Eulerian with } \mathbf{g}^E(\mathbf{x}) = 1. \quad (11.21b)$$

11.3.4 Concerning mass-labeling/unimodular coordinates

The material time independence of $\dot{\rho}^L \dot{\mathbf{g}}^L$ motivate some authors to assume the material coordinates are *unimodular*, which is also sometimes called *mass-labeling*. In this case, one sets

$$\dot{\rho}^L(\mathbf{a}) \dot{\mathbf{g}}^L(\mathbf{a}) = 1 \quad \text{mass-labeling (or unimodular) } \mathbf{a}\text{-space coordinates.} \quad (11.22)$$

These coordinates are used by, for example, [Salmon \(1988\)](#), [Jezierski and Kijowski \(1990\)](#), [Müller \(1995\)](#), and [Salmon \(1998\)](#). Furthermore, for \mathbf{a} -space mass-labeling coordinates and \mathbf{x} -space Cartesian coordinates, the specific volume from equation (11.21a) reduces to the Jacobian

$$\nu_s^L(\mathbf{a}, T) = \frac{\partial \Phi(\mathbf{a}, T)}{\partial \mathbf{a}} \quad \text{Cartesian } \mathbf{x}\text{-space and mass-labeling } \mathbf{a}\text{-space.} \quad (11.23)$$

Although rather convenient for many purposes, we do not choose mass-labeling \mathbf{a} -space coordinates for the following reasons. First, doing so makes it awkward to use dimensional analysis as a check on the equations.¹ Second, it hides the fundamentally non-Cartesian nature of material space coordinates by hiding $\dot{\mathbf{g}}^L$. This concern is mild, since one can readily assume the initial coordinate layout sets $\dot{\mathbf{g}}^L = 1$. Third, we wish to maintain a connection between the perfect fluid field theory of this chapter to the continuum mechanics of [Tromp \(2025\)](#), as well as the scalar field theory from Chapter 10, with unimodular coordinates obscuring that connection since it absorbs the density factor into the coordinates.

11.4 Energetics and entropy

In this section we develop equations for domain integrated kinetic energy, gravitational potential energy, and internal energy for a perfect fluid in a thermally and materially closed domain, \mathcal{R} , and as viewed from a rotating planetary reference frame.

11.4.1 Kinetic energy

Building on the two expressions for mass in equation (11.12) leads to the corresponding expressions for the kinetic energy within the material domain, first written using Cartesian Eulerian coordinates

$$E_{KE} = \frac{1}{2} \int_{\mathcal{R}(t)} (\mathbf{v} + \boldsymbol{\Omega} \times \mathbf{x}) \cdot (\mathbf{v} + \boldsymbol{\Omega} \times \mathbf{x}) \rho \mathbf{g}^E d^3x, \quad (11.24)$$

¹Throughout this book we exploit the dimensional nature of physical quantities to enable the use of dimensional analysis in debugging mathematical equations. Unimodular or mass-labeling coordinates make that process difficult.

and with the equivalent expression using arbitrary Lagrangian coordinates

$$E_{\text{KE}} = \frac{1}{2} \int_{\mathcal{R}(\mathbf{a})} (\partial_T \boldsymbol{\varphi} + \boldsymbol{\Omega} \times \boldsymbol{\varphi}) \cdot (\partial_T \boldsymbol{\varphi} + \boldsymbol{\Omega} \times \boldsymbol{\varphi}) \rho^L \dot{g}^L d^3a. \quad (11.25)$$

11.4.2 Gravitational potential energy

The gravitational potential, Φ_e , accounts for the potential energy per mass from the earth's gravity field. As such, its domain integral measures the total gravitational potential energy of the fluid

$$E_{\text{GPE}} = \int_{\mathcal{R}(t)} \Phi_e(\mathbf{x}, t) \rho g^E d^3x = \int_{\mathcal{R}(\mathbf{a})} \Phi_e(\boldsymbol{\varphi}, T) \dot{\rho}^L \dot{g}^L d^3a. \quad (11.26)$$

For most applications in this book, we assume the gravitational potential is time independent, which is required for a mechanically closed system as assumed here.²

11.4.3 Specific entropy is materially constant

As seen in our study of thermodynamics in VOLUME 2, the specific entropy is materially constant for a perfect fluid. Consequently, each fluid parcel has a specific entropy equal to the value at its initial condition

$$\mathcal{S}(\mathbf{a}, T) = \mathcal{S}(\mathbf{a}, T = t_A) = \dot{\mathcal{S}}(\mathbf{a}). \quad (11.27)$$

With the density satisfying equation (11.18), the constancy of specific entropy means that the entropy content of a fluid parcel can be written

$$\mathcal{S}(\mathbf{a}, T) \rho^L(\mathbf{a}, T) g^L(\mathbf{a}, T) d^3a = \dot{\mathcal{S}}(\mathbf{a}) \dot{\rho}^L(\mathbf{a}) \dot{g}^L(\mathbf{a}) d^3a. \quad (11.28)$$

When applying Hamilton's principle, the fluid particle trajectories are unaltered at their temporal boundaries. Hence, any field that is independent of time, such as the specific entropy, $\dot{\mathcal{S}}(\mathbf{a})$, has zero variation under changes to the fluid particle trajectories. However, when varying the material coordinates, such as when studying particle relabeling in Section 11.7, then we find a nonzero $\delta \dot{\mathcal{S}}(\mathbf{a})$.

11.4.4 Internal energy

As encountered in the study of thermodynamics in VOLUME 2, **internal energy** is that portion of the total energy for a region of the continuum that is not accounted for by the mechanical energy of macroscopic motion (**kinetic energy**) nor the mechanical energy arising from being in an external force field (gravitational potential energy). The fundamental thermodynamic relation for a single component fluid renders the natural functional dependency of specific internal energy (dimensions of energy per mass, which equals squared length per squared time)

$$\mathcal{I} = \mathcal{I}(\mathcal{S}, \nu_s) = \mathcal{I}(\dot{\mathcal{S}}(\mathbf{a}), \nu_s), \quad (11.29)$$

with \mathcal{S} the specific entropy and $\nu_s = 1/\rho$ the specific volume. We also made use of results from Section 11.4.3 by setting $\mathcal{S}(\mathbf{a}, T) = \dot{\mathcal{S}}(\mathbf{a})$ since the specific entropy remains materially constant. For the specific volume we make use of equation (11.21a), which assumes the Eulerian coordinates are Cartesian. In turn, it is just the Jacobian, $\partial \boldsymbol{\varphi}(\mathbf{a}, T)/\partial \mathbf{a}$, portion of the specific

²One exception concerns the study of a space-time dependent gravitational acceleration for tides.

volume that is affected by variations in the trajectories. Bringing the above results together renders the integrated internal energy for the material fluid domain

$$E_{\text{IE}} = \int_{\mathcal{R}(t)} \mathcal{I}(\mathbf{x}, t) \rho(\mathbf{x}, t) \mathbf{g}^E(\mathbf{x}) d^3x = \int_{\mathcal{R}(\mathbf{a})} \mathcal{I}[\dot{\mathcal{S}}(\mathbf{a}), \nu_s^L(\mathbf{a}, T)] \dot{\rho}^L(\mathbf{a}) \dot{\mathbf{g}}^L(\mathbf{a}) d^3a. \quad (11.30)$$

11.5 Variation of the action and Euler-Lagrange equations

The action for the perfect fluid is given by the space-time integral of the kinetic energy minus the gravitational energy and minus the internal energy³

$$\mathcal{S}^{\text{action}} = \int_{t_A}^{t_B} \int_{\mathcal{R}(\mathbf{a})} [\frac{1}{2} (\partial_T \boldsymbol{\varphi} + \boldsymbol{\Omega} \times \boldsymbol{\varphi}) \cdot (\partial_T \boldsymbol{\varphi} + \boldsymbol{\Omega} \times \boldsymbol{\varphi}) - \Phi_e - \mathcal{I}] \dot{\rho}^L \dot{\mathbf{g}}^L d^3a dT. \quad (11.31)$$

We here focus on the action written in terms of Lagrangian coordinates rather than the Eulerian coordinates, with functional dependencies given by

$$\boldsymbol{\varphi}(\mathbf{a}, T) \quad \text{and} \quad \Phi_e(\boldsymbol{\varphi}(\mathbf{a}, T), T) \quad \text{and} \quad \mathcal{I}(\dot{\mathcal{S}}(\mathbf{a}), \nu_s^L(\mathbf{a}, T)). \quad (11.32)$$

Making use of Lagrangian kinematics provides a direct link between Hamilton's principle applied here to continuum matter and Hamilton's principle applied to the discrete particle systems in VOLUME 1. Namely, we here examine a variation of the continuum motion field (i.e., trajectories) that vanishes at the temporal bounds (just like we did for particle mechanics)

$$\boldsymbol{\varphi}(\mathbf{a}, T) \rightarrow \boldsymbol{\varphi}(\mathbf{a}, T) + \delta \boldsymbol{\varphi}(\mathbf{a}, T) \quad \text{with} \quad \delta \boldsymbol{\varphi}(\mathbf{a}, t_A) = \delta \boldsymbol{\varphi}(\mathbf{a}, t_B) = 0. \quad (11.33)$$

Hamilton's principle says that when varying the action by varying the motion, the physically realized motion extremizes the action so that

$$\text{Hamilton's principle} \implies \delta \mathcal{S}^{\text{action}} = 0. \quad (11.34)$$

Extremizing the action leads to the *Euler-Lagrange* equation satisfied by the Lagrangian. As derived in this section, the Euler-Lagrange equation is a partial differential equation satisfied by each component, φ^i , of the motion field. That is, we derive a Lagrangian space-time field theory for the three component motion field, $\boldsymbol{\varphi}(\mathbf{a}, T)$.

We now summarize the operational task at hand to apply Hamilton's principle to the action (11.31). First, apply the variation operator, δ , to vary the motion field and compute the variation of the action. The variation operator acts solely on the motion field via equation (11.33). Hence, δ has no affect on space and time points, which means the variation operator commutes with (\mathbf{a}, T) and its differential operators.⁴ We organize the varied integrand to isolate $\delta \varphi^i$, and we do so via integrating by parts and setting $\delta \varphi^i$ to zero on the temporal boundaries. Invoking Hamilton's principle renders the Euler-Lagrange differential equations and natural boundary conditions on the material space boundaries.

³We write $\mathcal{S}^{\text{action}}$ for the action to distinguish it from the specific entropy, \mathcal{S} . Also note that the lower time bound for the action, t_A , is not necessarily the same as the time bound, t_R , used to define the base manifold.

⁴This commutation property holds when applying δ to the action for Hamilton's principle. However, as seen in Section 10.6, δ affects a variation of the space-time points when developing conservation laws using the methods of Noether's theorem. We emphasized these distinct variations in Section 10.6.1.

11.5.1 General expression for the Euler-Lagrange equation

We here directly follow the procedure used for the scalar field theory in Section 10.3. Here we have three fields for the three components to the motion field, with these fields living in Lagrangian space time. Following the approach in Section 10.3, we find it convenient to write the action (11.31) in the form

$$S^{\text{action}} = \int_{t_A}^{t_B} \int_{\mathcal{R}(\mathbf{a})} \mathcal{L} \dot{\mathbf{g}}^L d^3a dT \implies \delta S^{\text{action}} = \int_{t_A}^{t_B} \int_{\mathcal{R}(\mathbf{a})} (\delta \mathcal{L}) \dot{\mathbf{g}}^L d^3a dT, \quad (11.35)$$

where we defined the *Lagrangian density* (dimensions of energy per material coordinate volume, d^3a)

$$\mathcal{L}[\mathbf{\Phi}, \partial_T \mathbf{\Phi}, \partial_I \mathbf{\Phi}, \mathbf{a}, T] = \dot{\rho}^L \left[\frac{1}{2} (\partial_T \mathbf{\Phi} + \mathbf{\Omega} \times \mathbf{\Phi}) \cdot (\partial_T \mathbf{\Phi} + \mathbf{\Omega} \times \mathbf{\Phi}) - \Phi_e - \mathcal{I}(\dot{\mathcal{S}}, \nu_s^L) \right]. \quad (11.36)$$

Note that varying the trajectories has no affect on $\dot{\mathbf{g}}^L d^3a$ since these terms are fixed at $T = t_R$, and the same holds for $\dot{\rho}^L$.

Use of the chain rule renders a variation of the Lagrangian density⁵

$$\dot{\mathbf{g}}^L \delta \mathcal{L} = \dot{\mathbf{g}}^L \frac{\partial \mathcal{L}}{\partial \mathbf{\Phi}^i} \delta \mathbf{\Phi}^i + \dot{\mathbf{g}}^L \frac{\partial \mathcal{L}}{\partial (\partial_T \mathbf{\Phi}^i)} \delta (\partial_T \mathbf{\Phi}^i) + \dot{\mathbf{g}}^L \frac{\partial \mathcal{L}}{\partial (\partial_I \mathbf{\Phi}^i)} \delta (\partial_I \mathbf{\Phi}^i), \quad (11.37)$$

where the summation convention is followed for the motion field indices, so that repeated indices are summed over their range, $i = 1, 2, 3$. Since the variation operator, δ , commutes with (\mathbf{a}, T) derivative operators, we can write the equivalent expression

$$\dot{\mathbf{g}}^L \delta \mathcal{L} = \dot{\mathbf{g}}^L \frac{\partial \mathcal{L}}{\partial \mathbf{\Phi}^i} \delta \mathbf{\Phi}^i + \dot{\mathbf{g}}^L \frac{\partial \mathcal{L}}{\partial (\partial_T \mathbf{\Phi}^i)} \partial_T (\delta \mathbf{\Phi}^i) + \dot{\mathbf{g}}^L \frac{\partial \mathcal{L}}{\partial (\partial_I \mathbf{\Phi}^i)} \partial_I (\delta \mathbf{\Phi}^i). \quad (11.38)$$

We now bring the time and space derivative operators onto the full term and subtract the remainder. Doing so for the time derivative leads to

$$\dot{\mathbf{g}}^L \frac{\partial \mathcal{L}}{\partial (\partial_T \mathbf{\Phi}^i)} \frac{\partial (\delta \mathbf{\Phi}^i)}{\partial T} = \frac{\partial}{\partial T} \left[\dot{\mathbf{g}}^L \frac{\partial \mathcal{L}}{\partial (\partial_T \mathbf{\Phi}^i)} \delta \mathbf{\Phi}^i \right] - \frac{\partial}{\partial T} \left[\dot{\mathbf{g}}^L \frac{\partial \mathcal{L}}{\partial (\partial_T \mathbf{\Phi}^i)} \right] \delta \mathbf{\Phi}^i. \quad (11.39)$$

When plugging this term into the action variation (11.35), the total time derivative on the right hand side vanishes since we assume $\delta \mathbf{\Phi}^i$ vanishes at temporal boundaries as per equation (11.33). Similar manipulations lead to the material space derivative expression

$$\dot{\mathbf{g}}^L \frac{\partial \mathcal{L}}{\partial (\partial_I \mathbf{\Phi}^i)} \frac{\partial (\delta \mathbf{\Phi}^i)}{\partial a^I} = \frac{\partial}{\partial a^I} \left[\dot{\mathbf{g}}^L \frac{\partial \mathcal{L}}{\partial (\partial_I \mathbf{\Phi}^i)} \delta \mathbf{\Phi}^i \right] - \frac{\partial}{\partial a^I} \left[\dot{\mathbf{g}}^L \frac{\partial \mathcal{L}}{\partial (\partial_I \mathbf{\Phi}^i)} \right] \delta \mathbf{\Phi}^i. \quad (11.40)$$

When plugging this term into the action variation (11.35), the total space derivative term vanishes if we assume the following natural boundary condition

$$\frac{\partial \mathcal{L}}{\partial (\partial_I \mathbf{\Phi}^i)} \hat{n}_I = 0 \quad \text{at material boundaries}, \quad (11.41)$$

where \hat{n}_I are components to the outward normal one-form along the material boundary. We encountered a similar version of the natural boundary conditions in Section 10.4.3 when studying

⁵When integrating by parts, we must keep track of the metric tensor determinant, $\dot{\mathbf{g}}^L$, since it is a function of the material coordinates. We follow the approach in Section 10.4.2.

Hamilton's principle for a scalar field.

Bringing terms together leads to the variation of the action (11.35) taking the form

$$\delta S^{\text{action}} = \int_{t_A}^{t_B} \int_{\mathcal{R}(\mathbf{a})} \left(\frac{\partial \mathcal{L}}{\partial \varphi^i} - \frac{1}{\mathbf{\dot{g}}^L} \frac{\partial}{\partial T} \left[\mathbf{\dot{g}}^L \frac{\partial \mathcal{L}}{\partial (\partial_T \varphi^i)} \right] - \frac{1}{\mathbf{\dot{g}}^L} \frac{\partial}{\partial a^I} \left[\mathbf{\dot{g}}^L \frac{\partial \mathcal{L}}{\partial (\partial_I \varphi^i)} \right] \right) \delta \varphi^i \mathbf{\dot{g}}^L d^3 a dT, \quad (11.42)$$

Variation of the motion, $\delta \varphi^i$, is arbitrary everywhere except at the temporal boundaries. Setting the variation of the action to zero as per Hamilton's principle requires the Lagrangian density to satisfy the Euler-Lagrange equation as well as the natural kinematic boundary condition, with both satisfied by each of the $i = 1, 2, 3$ components of the motion field

$$\frac{\partial \mathcal{L}}{\partial \varphi^i} = \frac{1}{\mathbf{\dot{g}}^L} \frac{\partial}{\partial T} \left[\mathbf{\dot{g}}^L \frac{\partial \mathcal{L}}{\partial (\partial_T \varphi^i)} \right] + \frac{1}{\mathbf{\dot{g}}^L} \frac{\partial}{\partial a^I} \left[\mathbf{\dot{g}}^L \frac{\partial \mathcal{L}}{\partial (\partial_I \varphi^i)} \right] \quad (11.43a)$$

$$\frac{\partial \mathcal{L}}{\partial (\partial_I \varphi^i)} \hat{n}_I = 0 \quad \text{at material boundaries.} \quad (11.43b)$$

The presence of $1/\mathbf{\dot{g}}^L(\mathbf{a})$ on the outside of the derivatives, and $\mathbf{\dot{g}}^L(\mathbf{a})$ on the inside, allows us to identify a covariant divergence (based on $\mathbf{\dot{g}}^L$) on the right hand side of the Euler-Lagrange equation (11.43a). The $\mathbf{\dot{g}}^L(\mathbf{a})$ term cancels for the time derivative term, since $\mathbf{\dot{g}}^L(\mathbf{a})$ is independent of material time. However, it is an essential piece for the space derivative term given that Lagrangian space coordinates are not Cartesian.

The Euler-Lagrange equation (11.43a) and boundary conditions (11.43b) are identical to those derived in Section 10.3.4 when studying scalar field theory. The only operational difference is that here we have $i = 1, 2, 3$ fields whereas there we had a single scalar field. We also note that here the field theory is in Lagrangian space-time, (\mathbf{a}, T) , rather than Eulerian space-time, (\mathbf{x}, t) , and the dynamical field is the motion field, $\varphi(\mathbf{a}, T)$. As noted earlier in this section, the Lagrangian kinematic formulation of Hamilton's principle is directly connected to the discrete particle mechanics treatment of Hamilton's principle. In particular, by tracking the fluid motion field (i.e., fluid particle trajectories), we are afforded a straightforward means to constrain variations to vanish at the temporal boundaries. An Eulerian formulation does not follow fluid particles and requires Lagrange multipliers to constrain material coordinates to remain constant along trajectories (see Section 3 of [Salmon \(1988\)](#) for details).

In the remainder of this section we derive the Euler-Lagrange equations for the perfect fluid using the Lagrangian density (11.36). Rather than compute partial derivatives of the Lagrangian density as per the Euler-Lagrange equation (11.43a), we find it slightly more pedagogical to work directly from the action variation in equation (11.35).

11.5.2 Variation of the kinetic energy

Starting with the kinetic energy appearing in the Lagrangian density (11.36), we have

$$\begin{aligned} \frac{1}{2} (\partial_T \varphi + \boldsymbol{\Omega} \times \varphi) \cdot (\partial_T \varphi + \boldsymbol{\Omega} \times \varphi) \\ = \frac{1}{2} \partial_T \varphi \cdot \partial_T \varphi + \partial_T \varphi \cdot (\boldsymbol{\Omega} \times \varphi) + \frac{1}{2} (\boldsymbol{\Omega} \cdot \boldsymbol{\Omega}) (\varphi \cdot \varphi) - \frac{1}{2} (\boldsymbol{\Omega} \cdot \varphi)^2, \end{aligned} \quad (11.44)$$

which made use of the a standard vector identity from VOLUME 1. Use of the chain rule leads to the variation

$$\delta \left[\frac{1}{2} (\partial_T \varphi + \boldsymbol{\Omega} \times \varphi) \cdot (\partial_T \varphi + \boldsymbol{\Omega} \times \varphi) \right]$$

$$= \partial_T(\delta\varphi) \cdot (\partial_T\varphi + \Omega \times \varphi) + \partial_T\varphi \cdot (\Omega \times \delta\varphi) + \Omega^2 \varphi \cdot \delta\varphi - (\Omega \cdot \varphi)(\Omega \cdot \delta\varphi), \quad (11.45)$$

which can be rearranged to

$$\begin{aligned} \delta \left[\frac{1}{2} (\partial_T\varphi + \Omega \times \varphi) \cdot (\partial_T\varphi + \Omega \times \varphi) \right] \\ = \partial_T[(\partial_T\varphi + \Omega \times \varphi) \cdot \delta\varphi] - [\partial_{TT}\varphi + 2\Omega \times \partial_T\varphi - \Omega^2 \varphi + (\Omega \cdot \varphi)\Omega] \cdot \delta\varphi. \end{aligned} \quad (11.46)$$

Since the variations, $\delta\varphi$, vanish at the initial and final times, as per equation (11.33), the total time derivative in equation (11.46) drops out when integrated over time as part of the action. We are thus left with the kinetic energy variation

$$\begin{aligned} \frac{1}{2} \delta \int_{t_A}^{t_B} \int_{\mathcal{R}(\mathbf{a})} (\partial_T\varphi + \Omega \times \varphi) \cdot (\partial_T\varphi + \Omega \times \varphi) \dot{\rho}^L \dot{\mathbf{g}}^L d^3a dT \\ = - \int_{t_A}^{t_B} \int_{\mathcal{R}(\mathbf{a})} [\partial_{TT}\varphi + 2\Omega \times \partial_T\varphi + \Omega \times (\Omega \times \varphi)] \cdot \delta\varphi \dot{\rho}^L \dot{\mathbf{g}}^L d^3a dT, \end{aligned} \quad (11.47)$$

where we used the double vector product identity from VOLUME 1 to write

$$\Omega \times (\Omega \times \varphi) = -\Omega^2 \varphi + (\Omega \cdot \varphi)\Omega. \quad (11.48)$$

Variation of the kinetic energy in equation (11.47) reveals the material acceleration, $\partial_{TT}\varphi$, plus contributions from the planetary Coriolis and planetary centrifugal accelerations.

11.5.3 Variation of the gravitational potential energy

The gravitational potential energy (11.26) depends on the motion field, so that its variation follows from the chain rule

$$\delta\Phi_e = \frac{\partial\Phi_e}{\partial\varphi^i} \delta\varphi^i. \quad (11.49)$$

We thus have variation of the gravitational potential energy

$$\delta \int_{t_A}^{t_B} \int_{\mathcal{R}(\mathbf{a})} \Phi_e \dot{\rho}^L \dot{\mathbf{g}}^L d^3a dT = \int_{t_A}^{t_B} \int_{\mathcal{R}(\mathbf{a})} \frac{\partial\Phi_e}{\partial\varphi^i} \delta\varphi^i \dot{\rho}^L \dot{\mathbf{g}}^L d^3a dT. \quad (11.50)$$

11.5.4 Variation of the specific internal energy

As seen by equation (11.29), the specific internal energy is a function of the specific entropy and specific volume

$$\mathcal{I} = \mathcal{I}[\dot{\mathcal{S}}(\mathbf{a}), \nu_s^L(\mathbf{a}, T)], \quad (11.51)$$

where $\dot{\mathcal{S}}(\mathbf{a})$ is the specific entropy set by the initial conditions, and $\nu_s^L(\mathbf{a}, T)$ is related to the Jacobian of transformation between the Eulerian and Lagrangian coordinates, as given by equation (11.21a). It is through dependence on $\nu_s^L(\mathbf{a}, T)$ that the specific internal energy is a function of $\partial_I\varphi^i$, so that variation of the internal energy portion of the action is

$$\int_{t_A}^{t_B} \int_{\mathcal{R}(\mathbf{a})} \delta\mathcal{I} \dot{\rho}^L \dot{\mathbf{g}}^L d^3a dT = \int_{t_A}^{t_B} \int_{\mathcal{R}(\mathbf{a})} -p^L (\delta\nu_s^L) \dot{\rho}^L \dot{\mathbf{g}}^L d^3a dT, \quad (11.52)$$

where $p^L(\mathbf{a}, T)$ is the pressure written as a function of the Lagrangian space-time coordinates, and it is related to the specific internal energy via the thermodynamic identity from VOLUME 2

$$\delta \mathcal{J} = \left[\frac{\partial \mathcal{J}}{\partial \nu_s^L} \right]_s \delta \nu_s^L = -p^L \delta \nu_s^L. \quad (11.53)$$

From equation (11.21a) we have

$$\nu_s^L \dot{\rho}^L \dot{\mathbf{g}}^L = \partial \boldsymbol{\varphi} / \partial \mathbf{a} = \det(F^i{}_I) \quad (11.54)$$

so that

$$\dot{\rho}^L \dot{\mathbf{g}}^L \delta \nu_s^L = \delta(\dot{\rho}^L \dot{\mathbf{g}}^L \nu_s^L) = \delta(\partial \boldsymbol{\varphi} / \partial \mathbf{a}) = \delta \det(F^i{}_I). \quad (11.55)$$

We thus need to determine how the Jacobian varies when changing trajectories.

Since the Jacobian is only a function of the deformation matrix elements, $F^i{}_I = \partial_I \varphi^i$, the chain rule gives

$$\delta \det(F^i{}_I) = \frac{\partial \det(F^i{}_I)}{\partial F^l{}_L} \delta F^l{}_L = \frac{\partial \det(F^i{}_I)}{\partial F^l{}_L} \partial_L(\delta \varphi^l), \quad (11.56)$$

where the second equality noted that the trajectory variation operator commutes with the partial derivative operator. We now make use of an identity from VOLUME 1, thus enabling us to write the derivative of the Jacobian with respect to an element of the transformation matrix

$$\delta[\det(F^i{}_I)] = \det(F^i{}_I) F^L{}_l \partial_L(\delta \varphi^l) = \det(F^i{}_I) \partial_l(\delta \varphi^l), \quad (11.57)$$

where the final equality transformed from a Lagrangian partial derivative to an Eulerian partial derivative via

$$F^L{}_l \partial_L = \partial_l. \quad (11.58)$$

At the end of this chapter, we present an alternative derivation of equation (11.57), with this alternative more tedious than the one presented here, and yet it offers great experience with index gymnastics.

Equation (11.57) says that the relative variation of the Jacobian determinant is directly determined by the \mathbf{x} -space divergence of the motion field's variation. We can understand its kinematical content by observing that an \mathbf{x} -space divergence of $\delta \boldsymbol{\varphi}$ leads to a variation in the \mathbf{x} -space volume of a fluid parcel, and thus to a variation in the Jacobian. Making use of the variation (11.57) in equation (11.52) yields the internal energy variation

$$\int_{t_A}^{t_B} \int_{\mathcal{R}(\mathbf{a})} \delta \mathcal{J} \dot{\rho}^L \dot{\mathbf{g}}^L d^3 a dT = - \int_{t_A}^{t_B} \int_{\mathcal{R}(\mathbf{a})} p^L \frac{\partial(\delta \varphi^i)}{\partial x^i} \frac{\partial \boldsymbol{\varphi}}{\partial \mathbf{a}} d^3 a dT. \quad (11.59)$$

11.5.5 How the pressure gradient appears

We now present two related methods for how the pressure gradient appears within the integral (11.59).

Method I

Making use of the relations in Section 11.3 allows us to convert the right hand side of equation (11.59) to Cartesian Eulerian coordinates so that

$$\int_{\mathcal{R}(\mathbf{a})} p^L \frac{\partial(\delta\varphi^i)}{\partial x^i} \frac{\partial\mathbf{\Phi}}{\partial\mathbf{a}} d^3a = \int_{\mathcal{R}(t)} p \frac{\partial(\delta\varphi^i)}{\partial x^i} d^3x, \quad (11.60)$$

with integration by parts yielding

$$\int_{\mathcal{R}(t)} p \frac{\partial(\delta\varphi^i)}{\partial x^i} d^3x = \int_{\mathcal{R}(t)} \frac{\partial(p \delta\varphi^i)}{\partial x^i} d^3x - \int_{\mathcal{R}(t)} \frac{\partial p}{\partial x^i} \delta\varphi^i d^3x. \quad (11.61)$$

Assuming either zero mechanical forcing at the boundaries (e.g., free boundary with $p = 0$), or assuming $\delta\mathbf{\Phi} \cdot \hat{\mathbf{n}} = 0$ at the boundaries (i.e., rigid solid-earth boundary), allows us to drop the boundary term. We are thus left with the internal energy variation

$$\int_{\mathcal{R}(\mathbf{a})} \delta\mathcal{J} \dot{\rho}^L \dot{\mathbf{g}}^L d^3a = \int_{\mathcal{R}(t)} \frac{1}{\rho} \frac{\partial p}{\partial x^i} \delta\varphi^i \rho d^3x = \int_{\mathcal{R}(\mathbf{a})} \frac{1}{\rho^L} \frac{\partial p^L}{\partial \varphi^i} \delta\varphi^i \dot{\rho}^L \dot{\mathbf{g}}^L d^3a, \quad (11.62)$$

with the final equality converting back to Lagrangian coordinates and making use of equation (11.18) for the density, $\dot{\rho}^L \dot{\mathbf{g}}^L$.

Method II

Rather than convert to Cartesian Eulerian coordinates at the point done in equation (11.60), we write

$$p^L \frac{\partial(\delta\varphi^i)}{\partial x^i} \frac{\partial\mathbf{\Phi}}{\partial\mathbf{a}} = p^L \frac{\partial(\delta\varphi^i)}{\partial a^I} \frac{\partial a^I}{\partial x^i} \frac{\partial\mathbf{\Phi}}{\partial\mathbf{a}} = \frac{\partial}{\partial a^I} \left[p^L \delta\varphi^i \frac{\partial a^I}{\partial x^i} \frac{\partial\mathbf{\Phi}}{\partial\mathbf{a}} \right] - \delta\varphi^i \frac{\partial}{\partial a^I} \left[p^L \frac{\partial a^I}{\partial x^i} \frac{\partial\mathbf{\Phi}}{\partial\mathbf{a}} \right], \quad (11.63)$$

where the first equality made use of the chain rule and the second equality used the product rule. For the final term note that

$$\frac{\partial}{\partial a^I} \left[F^I_i \frac{\partial\mathbf{\Phi}}{\partial\mathbf{a}} \right] = \frac{\partial}{\partial a^I} \left[\frac{\partial a^I}{\partial x^i} \frac{\partial\mathbf{\Phi}}{\partial\mathbf{a}} \right] = 0, \quad (11.64)$$

which follows from the determinant identity (VOLUME 1), in which

$$\frac{\partial a^I}{\partial x^i} \frac{\partial\mathbf{\Phi}}{\partial\mathbf{a}} = \frac{1}{2} \epsilon^{IJK} \epsilon_{ijk} \frac{\partial\varphi^j}{\partial a^J} \frac{\partial\varphi^k}{\partial a^K}, \quad (11.65)$$

thus yielding equation (11.64) through anti-symmetry of ϵ^{IJK} and symmetry of the second partial derivatives ∂_{IK} and ∂_{IJ} . These results then bring equation (11.63) into the form

$$p^L \frac{\partial(\delta\varphi^i)}{\partial x^i} \frac{\partial\mathbf{\Phi}}{\partial\mathbf{a}} = \frac{\partial}{\partial a^I} \left[p^L \delta\varphi^i \frac{\partial a^I}{\partial x^i} \frac{\partial\mathbf{\Phi}}{\partial\mathbf{a}} \right] - \delta\varphi^i \frac{\partial p^L}{\partial a^I} \frac{\partial a^I}{\partial x^i} \frac{\partial\mathbf{\Phi}}{\partial\mathbf{a}}. \quad (11.66)$$

When integrated over the material domain, the ∂_I divergence term drops out due to the material boundary conditions. We are thus led to

$$\int_{\mathcal{R}(\mathbf{a})} \delta\mathcal{J} \dot{\rho}^L \dot{\mathbf{g}}^L d^3a = \int_{\mathcal{R}(\mathbf{a})} \frac{\partial p^L}{\partial a^I} \frac{\partial a^I}{\partial \varphi^i} \frac{\partial\mathbf{\Phi}}{\partial\mathbf{a}} \delta\varphi^i d^3a \quad \text{equations (11.59) and (11.66)} \quad (11.67a)$$

$$= \int_{\mathcal{R}(\mathbf{a})} \frac{1}{\rho^L} \frac{\partial p^L}{\partial x^i} \delta \varphi^i \dot{\rho}^L \dot{\mathbf{g}}^L d^3a \quad \text{chain rule and equation (11.54), (11.67b)}$$

which agrees with equation (11.62).

11.5.6 The perfect fluid Euler-Lagrange equation

Making use of the variation of the kinetic energy portion of the action (11.47), the gravitational potential energy portion (11.50), and the internal energy portion (11.62), leads us to the variation of the action under variations in the trajectories that are fixed at the temporal boundaries

$$\delta S^{\text{action}} = - \int_{t_A}^{t_B} \int_{\mathcal{R}(\mathbf{a})} \left[\partial_{TT} \varphi + 2 \boldsymbol{\Omega} \times \partial_T \varphi + \boldsymbol{\Omega} \times (\boldsymbol{\Omega} \times \varphi) + \frac{\partial \Phi_e}{\partial \varphi} + \frac{1}{\rho^L} \frac{\partial p^L}{\partial \varphi} \right] \cdot \delta \varphi \dot{\rho}^L \dot{\mathbf{g}}^L d^3a dT. \quad (11.68)$$

Hamilton's principle says that the physically realized action is stationary under variations to the motion, with that motion fixed at the temporal boundaries. Invoking this principle then leads to the Euler-Lagrange equation

$$\partial_{TT} \varphi + 2 \boldsymbol{\Omega} \times \partial_T \varphi = - \frac{1}{\rho^L} \frac{\partial p^L}{\partial \varphi} - \frac{\partial \Phi}{\partial \varphi} \iff \partial_T \mathbf{v}^L + 2 \boldsymbol{\Omega} \times \mathbf{v}^L = - \frac{1}{\rho^L} \frac{\partial p^L}{\partial \varphi} - \frac{\partial \Phi}{\partial \varphi}, \quad (11.69)$$

where we introduced the velocity in the rotating reference frame

$$\mathbf{v}^L = \partial_T \varphi, \quad (11.70)$$

and the geopotential

$$\Phi = \Phi_e - (\boldsymbol{\Omega} \times \varphi)^2 / 2, \quad (11.71)$$

which is the sum of the gravitational potential and the planetary centrifugal potential.

The Euler-Lagrange equation (11.69) is written with spatial derivatives taken with respect to the motion field, φ , and time derivatives with respect to Lagrangian time, T . Transforming this equation to an Eulerian perspective leads to the rotating perfect fluid Euler equation derived in VOLUME 2. It is particularly notable that this transformation is rather trivial, simply requiring a swap of the motion field for an Eulerian position, \mathbf{x} . This transformation to the Eulerian reference frame removes all remnants of the motion field from the equations. A key reason for this rather simple result arises from the form of the internal energy, whose dependence on trajectories arises only via the Jacobian, $\partial \varphi / \partial \mathbf{a}$. Different forms of the internal energy arise in other areas of continuum mechanics, thus making the translation to an Eulerian perspective less convenient than found here for the perfect fluid.

11.5.7 Comments

Based on our experience with particle mechanics in VOLUME 1, we expected to realize the same equations using Hamilton's principle as those found through Newton's laws. Even so, it is a remarkable result given the fundamentally distinct conceptual and operational perspectives. This agreement offers further confidence that the theoretical construct of continuum mechanics has a robust foundation beyond that afforded by the work of Euler and Cauchy in their applications of Newton's laws to the continuum.

11.6 Perfect fluid Hamiltonian continuity equation

As a means to illustrate the connection between symmetry and conservation within the perfect fluid, note that the Lagrangian density in equation (11.36) has no explicit dependence on time

$$\left[\frac{\partial \mathcal{L}}{\partial T} \right]_{\varphi^i, \partial_T \varphi^i, \partial_I \varphi^i, a^I} = 0, \quad (11.72)$$

where the subscripts on the derivative denote those terms that are held fixed in computing the partial derivative. According to the discussion of Noether's theorem in Sections 10.5 and 10.6, we know that the Hamiltonian density, \mathcal{H} , satisfies the Lagrangian space-time continuity equation (10.67)

$$\partial_T \mathcal{H} + \mathring{\nabla}_I \mathcal{F}^I = 0, \quad (11.73)$$

where

$$\mathring{\nabla}_I \mathcal{F}^I = (1/\mathring{g}^L) \partial_I (\mathring{g}^L \mathcal{F}^I) \quad (11.74)$$

is the covariant divergence as defined by the geometry of the reference manifold at $T = t_R$.

The canonical momentum, Hamiltonian density, and the energy flux are given in equation (10.64) for the scalar field are generalized to the φ^i field theory of a perfect fluid

$$\mathcal{P}_i \equiv \frac{\partial \mathcal{L}}{\partial (\partial_T \varphi^i)} \quad \text{and} \quad \mathcal{H} = \mathcal{P}_i \partial_T \varphi^i - \mathcal{L} \quad \text{and} \quad \mathcal{F}^I = \frac{\partial \mathcal{L}}{\partial (\partial_I \varphi^i)} \frac{\partial \varphi^i}{\partial T}, \quad (11.75)$$

where the implied summation over the i index is the only distinction from the scalar field in considered in Section 10.5. We now determine an expression of this continuity equation for the perfect fluid. Doing so provides useful experience with the variety of tensor manipulations arising from this formalism.

11.6.1 Canonical momentum and Hamiltonian density

Making use of the perfect fluid Lagrangian density (11.36) renders the canonical momentum

$$\mathcal{P}_j = \mathring{\rho}^L [\partial_T \varphi^i + (\boldsymbol{\Omega} \times \boldsymbol{\varphi})^i] \delta_{ij}, \quad (11.76)$$

so that the Hamiltonian density is

$$\mathcal{H} = \mathring{\rho}^L [\partial_T \varphi^i + (\boldsymbol{\Omega} \times \boldsymbol{\varphi})^i] \delta_{ij} \partial_T \varphi^j - \mathcal{L} = \mathring{\rho}^L (\partial_T \boldsymbol{\varphi} \cdot \partial_T \boldsymbol{\varphi} / 2 + \Phi + \mathcal{I}), \quad (11.77)$$

where we introduced the geopotential from equation (11.71). Evidently, the Hamiltonian density is the sum of the kinetic energy plus geopotential plus internal energy.

11.6.2 Energy flux and the covariant flux divergence

For the energy flux we need the derivative of the Lagrangian density with respect to the deformation matrix components, $F^i{}_I = \partial_I \varphi^i$, which appear only within the specific internal energy

$$\frac{\partial \mathcal{L}}{\partial F^i{}_I} = -\mathring{\rho}^L \frac{\partial \mathcal{I}}{\partial \nu_s} \frac{\partial \nu_s}{\partial F^i{}_I} \quad \text{chain rule with } \mathcal{I} = \mathcal{I}(\mathring{\mathcal{S}}, \nu_s) \text{ and } \mathring{\mathcal{S}} = \mathring{\mathcal{S}}(\mathbf{a}) \quad (11.78a)$$

$$= \mathring{\rho}^L p^L \frac{\partial \nu_s}{\partial F^i{}_I} \quad \text{thermodynamic identity (11.53)} \quad (11.78b)$$

$$= \frac{p^L}{\mathring{g}^L} \frac{\partial(\mathring{\rho}^L \mathring{g}^L \nu_s)}{\partial F^i_I} \quad \partial(\mathring{\rho}^L \mathring{g}^L) / \partial F^i_I = 0 \quad (11.78c)$$

$$= \frac{p^L}{\mathring{g}^L} \frac{\partial \det(F^i_I)}{\partial F^i_I} \quad \mathring{\rho}^L \mathring{g}^L \nu_s = \det(F^i_I) \text{ from equation (11.54)} \quad (11.78d)$$

$$= (p^L / \mathring{g}^L) \det(F^i_I) F^I_i \quad \text{determinant identity from VOLUME 1,} \quad (11.78e)$$

which yields the energy flux

$$\mathcal{F}^I = \frac{\partial \mathcal{L}}{\partial F^i_I} \frac{\partial \varphi^i}{\partial T} = (p^L / \mathring{g}^L) \det(F^i_I) F^I_i \partial_T \varphi^i. \quad (11.79)$$

Making use of the covariant divergence from VOLUME 1, we have the \mathbf{a} -space covariant flux divergence

$$\mathring{\nabla}_I [\det(F^i_I) F^I_i (p^L / \mathring{g}^L) \partial_T \varphi^i] = (1 / \mathring{g}^L) \partial_I [\det(F^i_I) F^I_i p^L \partial_T \varphi^i]. \quad (11.80)$$

The identity (11.64) says that $\partial_I [\det(F^i_I) F^I_i] = 0$, so that the covariant flux divergence is

$$\mathring{\nabla}_I [\det(F^i_I) F^I_i (p^L / \mathring{g}^L) \partial_T \varphi^i] = (1 / \mathring{g}^L) \det(F^i_I) F^I_i \partial_I (p^L \partial_T \varphi^i). \quad (11.81)$$

Finally, we convert the \mathbf{a} -space derivative to an \mathbf{x} -space derivative using the deformation matrix

$$F^I_i \partial_I = \partial_i, \quad (11.82)$$

so that

$$\mathring{\nabla}_I [\det(F^i_I) F^I_i (p^L / \mathring{g}^L) \partial_T \varphi^i] = (1 / \mathring{g}^L) \det(F^i_I) \partial_i (p^L \partial_T \varphi^i) = \mathring{\rho}^L \nu_s^L \partial_i (p^L \partial_T \varphi^i), \quad (11.83)$$

where the second equality used the determinant identity (11.21a) that says $\det(F^i_I) = \nu_s^L \mathring{\rho}^L \mathring{g}^L$.

11.6.3 Lagrangian and Eulerian Hamiltonian continuity equations

Bringing the pieces together leads the Hamiltonian density continuity equation (11.73) taking the following perfect fluid expression

$$\partial_T [\mathring{\rho}^L (\partial_T \varphi \cdot \partial_T \varphi / 2 + \Phi + \mathcal{J})] + \mathring{\rho}^L \nu_s^L \partial_i (p^L \partial_T \varphi^i) = 0. \quad (11.84)$$

The density $\mathring{\rho}^L = \mathring{\rho}^L(\mathbf{a})$ cancels from both terms, so that

$$\rho^L \partial_T (\partial_T \varphi \cdot \partial_T \varphi / 2 + \Phi + \mathcal{J}) + \partial_i (p^L \partial_T \varphi^i) = 0, \quad (11.85)$$

which has a corresponding Eulerian expression⁶

$$\rho \frac{D(\mathbf{v} \cdot \mathbf{v} / 2 + \Phi + \mathcal{J})}{Dt} + \nabla \cdot (p \mathbf{v}) = 0. \quad (11.86)$$

This equation accords with the perfect fluid total energy budget from VOLUME 2, which was derived using very different methods. This agreement lends further confidence to our use of Hamilton's principle with Lagrangian kinematics for the perfect fluid.

⁶Recall we are assuming Cartesian coordinates for \mathbf{x} -space.

11.7 Particle relabeling symmetry and potential vorticity

In this chapter we are working with a Lagrangian space-time field theory for the perfect fluid motion field, $\varphi(\mathbf{a}, T)$. Hence, as just seen in Section 11.6 for the Hamiltonian density, space-time symmetries leading to conservation laws in the perfect fluid arise from variations in the position within the Lagrangian space-time. For the usual momentum conservation laws corresponding to spatial symmetry, we take the material coordinates equal to the Cartesian coordinates at some reference time. For a perfect geophysical fluid in motion around a rotating and gravitating planet, we no longer have the full symmetry of empty space considered in Chapter 10. Instead, we have axial symmetry around the planetary rotational axis. As a result, perfect planetary fluid motion only realizes differential conservation laws for axial angular momentum conservation along with the energy conservation of Section 11.6.

For momentum conservation, the *active transformation* (Section 10.6.2) is realized by shifting the material spatial position of each fluid particle by the same constant, and for energy each fluid particle has its material time shifted by the same constant. Here we examine whether there is a nontrivial *passive transformation* that leaves the action invariant. Recall from our discussion in Section 10.6.3, a passive transformation only affects a variation to the coordinate representation of a physical system. *Noether's second theorem* says that each passive symmetry gives rise to a *Bianchi identity* that corresponds to a local conservation law. Here we consider *particle relabeling symmetry* and the corresponding local (in \mathbf{a} -space) conservation of potential vorticity. Our presentation is inspired by [Salmon \(1988\)](#), [Müller \(1995\)](#), [Padhye and Morrison \(1996\)](#), and Chapter 7 of [Salmon \(1998\)](#).

11.7.1 Passive transformation of Lagrangian space coordinates

Consider a time dependent coordinate transformation of the material spatial coordinates

$$\mathbf{a}' = \mathbf{a}'(\mathbf{a}, T), \quad (11.87)$$

with an infinitesimal version of this transformation

$$\mathbf{a}' = \mathbf{a} + \delta\mathbf{a}(\mathbf{a}, T). \quad (11.88)$$

In this manner, each fluid particle experiences a distinct variation of its material coordinate. The transformation is passive (only affects coordinates) and so the fluid particle trajectories are unchanged. We do not expect particle labels to affect our ability to describe the physically realized trajectories, and this expectation is given the name *particle relabeling symmetry* ([Salmon, 1988](#)).

We consider a particular form of coordinate transformation that is assumed to vanish at the material space and time bounds. Furthermore, we assume that the coordinate transformation respects the constraint of mass conservation holding for each fluid parcel. As shown in Sections 10.6.2 and 10.6.3, a mass conserving transformation, δa^I , as a zero density weighted covariant divergence. Since the material coordinates, a^I , are set at the reference time, $T = t_R$, the relevant density at that time is $\dot{\rho}^I = \rho^I(\mathbf{a}, T = t_R)$, as is the metric determinant, $\dot{g}^I(\mathbf{a}) = g^I(\mathbf{a}, T = t_R)$. Hence, the particular form of coordinate variation relevant to particle relabeling is given by

$$\delta\mathbf{a} = 0 \quad \text{at material space-time boundaries} \quad \text{and} \quad \dot{\nabla}_I(\dot{\rho}^I \delta a^I) = 0. \quad (11.89)$$

Since δa^I is time dependent, trajectories have their material coordinate modified at each point

that is not on the material space-time boundary, with the modification constrained by assuming that the mass of each fluid parcel is invariant.

To deduce the conservation resulting from particle relabeling symmetry, and to expose the key aspects of the derivation, it is sufficient to study flow in a non-rotating reference frame. Generalization to a rotating reference frame is straightforward. We thus consider the following perfect fluid action

$$S^{\text{action}} = \int_{t_A}^{t_B} \int_{\mathcal{R}(\mathbf{a})} \left(\frac{1}{2} \partial_T \boldsymbol{\varphi} \cdot \partial_T \boldsymbol{\varphi} - \Phi_e - \mathcal{J} \right) \dot{\rho}^L \dot{\mathbf{g}}^L d^3a dT. \quad (11.90)$$

11.7.2 Constraints from mass conservation

The spatial region where the fluid flows, \mathcal{R} , is material and each fluid parcel is material. Consequently, if particle relabeling is to render an equivalent description of the fluid, then the measurement of mass must remain unchanged using the new set of coordinates. Globally, mass conservation means that

$$\int_{\mathcal{R}(\mathbf{a})} \dot{\rho}^L \dot{\mathbf{g}}^L d^3a = \int_{\mathcal{R}'(\mathbf{a}')} \dot{\rho}'^L \dot{\mathbf{g}}'^L d^3a', \quad (11.91)$$

where $\mathcal{R}'(\mathbf{a}')$ is the functional expression for the domain when written in terms of the varied coordinates. Since the domain is not changed by the coordinate variation, we must have the functional expression for the domain when using coordinates \mathbf{a}' equal to the functional expression for the domain when using coordinates \mathbf{a} , which is succinctly expressed as

$$\mathcal{R}'(\mathbf{a}') = \mathcal{R}(\mathbf{a}). \quad (11.92)$$

Likewise, since the mass of a fluid parcel is unchanged we have

$$dM(\mathbf{a}) = dM'(\mathbf{a}') \implies \dot{\rho}^L(\mathbf{a}) \dot{\mathbf{g}}^L(\mathbf{a}) d^3a = \dot{\rho}'^L(\mathbf{a}') \dot{\mathbf{g}}'^L(\mathbf{a}') d^3a'. \quad (11.93)$$

This result then means that the Jacobian of transformation between the two material coordinates is given by the volume ratio

$$\frac{\partial \mathbf{a}'}{\partial \mathbf{a}} = \frac{\dot{\rho}^L(\mathbf{a}) \dot{\mathbf{g}}^L(\mathbf{a})}{\dot{\rho}'^L(\mathbf{a}') \dot{\mathbf{g}}'^L(\mathbf{a}')}, \quad (11.94)$$

which is a familiar result from coordinate transformations studied in VOLUME 1.

Specific volume is invariant

Making use of equation (11.21a) for the specific volume along with the mass conservation identity (11.94), we find

$$\nu_s^L(\mathbf{a}', T) = \frac{1}{\dot{\rho}'^L(\mathbf{a}') \dot{\mathbf{g}}'^L(\mathbf{a}')} \frac{\partial \boldsymbol{\varphi}}{\partial \mathbf{a}'} = \frac{1}{\dot{\rho}^L(\mathbf{a}) \dot{\mathbf{g}}^L(\mathbf{a})} \frac{\partial \mathbf{a}'}{\partial \mathbf{a}} \frac{\partial \boldsymbol{\varphi}}{\partial \mathbf{a}'} = \frac{1}{\dot{\rho}^L(\mathbf{a}) \dot{\mathbf{g}}^L(\mathbf{a})} \frac{\partial \boldsymbol{\varphi}}{\partial \mathbf{a}} = \nu_s^L(\mathbf{a}, T), \quad (11.95)$$

where the third equality made use of the chain rule identity in VOLUME 1 holding for determinants

$$\frac{\partial \mathbf{a}'}{\partial \mathbf{a}} \frac{\partial \boldsymbol{\varphi}}{\partial \mathbf{a}'} = \frac{\partial \boldsymbol{\varphi}}{\partial \mathbf{a}}. \quad (11.96)$$

Evidently, so long as the coordinate transformation from \mathbf{a} to \mathbf{a}' leaves the mass of a fluid parcel unchanged as per equation (11.93), then it also leaves its specific volume unchanged as per equation (11.95).

Zero covariant divergence of density weighted coordinate variation

So far we have only assumed the coordinate transformation is mass preserving. To determine a differential expression of that property, we make use of the discussion in Section 10.6.3 for infinitesimal coordinate transformations. Evidently, the mass conservation identity (11.93) means that, to second order in variation, the density weighted coordinate variation has a zero covariant divergence

$$\mathring{\nabla}_I(\mathring{\rho}^L \delta a^I) = (1/\mathring{g}^L) \partial_I(\mathring{g}^L \mathring{\rho}^L \delta a^I) = 0. \quad (11.97)$$

This constraint is satisfied by setting $\mathring{\rho}^L \delta \mathbf{a}$ equal to the covariant curl of an arbitrary vector

$$\mathring{\rho}^L \delta \mathbf{a} = \text{curl}(\mathbf{W}) \iff \mathring{\rho}^L \delta a^I = \mathring{\varepsilon}^{IJK} \partial_J W_K = (1/\mathring{g}^L) \epsilon^{IJK} \partial_J W_K, \quad (11.98)$$

where

$$\mathring{\varepsilon}^{IJK} = (1/\mathring{g}^L) \epsilon^{IJK} \quad (11.99)$$

is the coordinate covariant Levi-Civita tensor introduced in VOLUME 1, and $\mathbf{W} = \mathbf{W}(\mathbf{a}, T)$ is an arbitrary vector that parameterizes the coordinate variation.⁷

Summary from mass conservation

In summary, there are three conditions resulting from the constraint that mass remains invariant when performing a variation of the Lagrangian space coordinates: (1) we only need to vary the energy terms in the action, (2) the specific volume is invariant, and (3) the density weighted coordinate variation is a total curl

$$\delta S^{\text{action}} = \int_{t_A}^{t_B} \int_{\mathcal{R}(\mathbf{a})} \delta \left(\frac{1}{2} \partial_T \boldsymbol{\varphi} \cdot \partial_T \boldsymbol{\varphi} - \Phi_e - \mathcal{I} \right) \mathring{\rho}^L \mathring{g}^L d^3 a dT \quad (11.100a)$$

$$\delta \nu_s^L = 0 \quad (11.100b)$$

$$\mathring{\rho}^L \delta \mathbf{a} = \text{curl}(\mathbf{W}). \quad (11.100c)$$

11.7.3 The motion field is a scalar

The gravitational potential is a function of the spatial position as determined by the motion field

$$\Phi_e = \Phi_e(\boldsymbol{\varphi}), \quad (11.101)$$

so that the gravitational potential has a functional dependence

$$\Phi_e = \Phi_e[\boldsymbol{\varphi}(\mathbf{a}, T)]. \quad (11.102)$$

For the coordinate variation (11.88) to keep the geopotential invariant requires the motion field to satisfy⁸

$$\boldsymbol{\varphi}'(\mathbf{a}', T) = \boldsymbol{\varphi}(\mathbf{a}, T). \quad (11.103)$$

⁷Note that $W_K = \mathfrak{g}_{KL} W^L$, where $\mathfrak{g}_{KL} = F^k_K F^l_L g_{kl}$ is the Lagrangian representation of the metric tensor whereas g_{kl} is the Eulerian representation. Choosing Cartesian Eulerian coordinates so that $g_{kl} = \delta_{kl}$ means that \mathfrak{g}_{KL} is the Cauchy-Green strain tensor studied in VOLUME 2.

⁸The geopotential arising in a rotating reference frame is the sum of the gravitational potential plus the planetary centrifugal potential (see equation (11.69)) $\Phi(\boldsymbol{\varphi}) = \Phi_e(\boldsymbol{\varphi}) - (\boldsymbol{\Omega} \times \boldsymbol{\varphi})^2/2$. So if the motion field is a scalar under the coordinate variation as per equation (11.103), then so is the geopotential.

This equality means that the motion field, $\boldsymbol{\varphi}'(\mathbf{a}', T)$, points to the same fluid particle as the motion field, $\boldsymbol{\varphi}(\mathbf{a}, T)$. This condition is consistent with the concept of a passive transformation (i.e., a transformation of the coordinates so that the physical system remains unchanged). We conclude that each component of the motion field transforms as a scalar (zeroth order tensor) under the particle relabeling coordinate transformation, so that the total variation (see Section 10.6.4) of each component vanishes

$$\Delta \boldsymbol{\varphi} = \boldsymbol{\varphi}'(\mathbf{a}', T) - \boldsymbol{\varphi}(\mathbf{a}, T) = 0. \quad (11.104)$$

11.7.4 The specific internal energy is a scalar

To retain the same specific internal energy, \mathcal{I} , when affecting the passive variation requires \mathcal{I} to be a scalar under particle relabeling so that

$$\mathcal{I} = \mathcal{I}(\mathring{\mathcal{S}}(\mathbf{a}), \nu_s) = \mathcal{I}'(\mathring{\mathcal{S}}'(\mathbf{a}'), \nu'_s). \quad (11.105)$$

We already saw that mass conservation ensures that the specific volume remains a scalar under particle relabeling as per equation (11.100b). In order for relabeling to keep the specific entropy unchanged we must have

$$\mathring{\mathcal{S}}'(\mathbf{a}') = \mathring{\mathcal{S}}(\mathbf{a}). \quad (11.106)$$

To realize this symmetry requires the coordinate variation to be orthogonal to the \mathbf{a} -space gradient of the specific entropy

$$\delta \mathbf{a}^I \partial_I \mathring{\mathcal{S}} = \delta \mathbf{a} \cdot \nabla_{\mathbf{a}} \mathring{\mathcal{S}} = 0. \quad (11.107)$$

Namely, the relabeling must remain on a constant specific entropy surface. This condition reduces the coordinate variation to two degrees of freedom, and the constraint (11.107) can be readily realized by setting one of the material coordinates equal to the specific entropy. Alternatively, the constraint can be satisfied by writing the coordinate variation as

$$\dot{\rho}^L \delta \mathbf{a} = \text{curl}(\mathbf{W}) = \text{curl}(A \nabla_{\mathbf{a}} \mathring{\mathcal{S}}) \iff \dot{\rho}^L \delta a^I = \dot{\varepsilon}^{IJK} \partial_J W_K = \dot{\varepsilon}^{IJK} \partial_J (A \partial_K \mathring{\mathcal{S}}). \quad (11.108)$$

We have thus specified the particle relabeling variation up to an arbitrary function, $A(\mathbf{a}, T)$.

11.7.5 Coordinate variation of the kinetic energy

The coordinate variation of the kinetic energy per mass is

$$\delta(\partial_T \boldsymbol{\varphi} \cdot \partial_T \boldsymbol{\varphi} / 2) = \partial_T \boldsymbol{\varphi} \cdot \delta(\partial_T \boldsymbol{\varphi}), \quad (11.109)$$

where the variation of the velocity is given by

$$\delta(\partial_T \boldsymbol{\varphi}) = \frac{\partial \boldsymbol{\varphi}'(\mathbf{a}', T)}{\partial T} \Big|_{\mathbf{a}'} - \frac{\partial \boldsymbol{\varphi}(\mathbf{a}, T)}{\partial T} \Big|_{\mathbf{a}}. \quad (11.110)$$

Note the distinct time derivatives on the right hand side, as per the need to hold distinct space coordinates fixed while computing the time derivatives. This derivative, to first order in

variation, is given by

$$\frac{\partial \boldsymbol{\varphi}'(\mathbf{a}', T)}{\partial T} \Big|_{\mathbf{a}'} = \frac{\partial \boldsymbol{\varphi}(\mathbf{a}, T)}{\partial T} \Big|_{\mathbf{a}'} = \frac{\partial \boldsymbol{\varphi}(\mathbf{a}, T)}{\partial T} \Big|_{\mathbf{a}} + \frac{\partial a^I}{\partial T} \Big|_{\mathbf{a}'} \frac{\partial \boldsymbol{\varphi}(\mathbf{a}, T)}{\partial a^I}, \quad (11.111)$$

where the first equality follows from $\boldsymbol{\varphi}'(\mathbf{a}', T) = \boldsymbol{\varphi}(\mathbf{a}, T)$ as per equation (11.103), and the second equality follows from the chain rule. Next, make use of the coordinate variation (11.88) to write

$$\frac{\partial a^I}{\partial T} \Big|_{\mathbf{a}'} = \frac{\partial(a'^I - \delta a^I)}{\partial T} \Big|_{\mathbf{a}'} = - \frac{\partial(\delta a^I)}{\partial T} \Big|_{\mathbf{a}'} = - \frac{\partial(\delta a^I)}{\partial T} \Big|_{\mathbf{a}}, \quad (11.112)$$

where the second equality follows since the time derivative is computed with \mathbf{a}' fixed, and the third equality drops terms that are second order in the coordinate variation. This result thus brings the velocity variation in equation (11.111) to

$$\delta(\partial_T \boldsymbol{\varphi}) = \frac{\partial \boldsymbol{\varphi}'(\mathbf{a}', T)}{\partial T} \Big|_{\mathbf{a}'} - \frac{\partial \boldsymbol{\varphi}(\mathbf{a}, T)}{\partial T} \Big|_{\mathbf{a}} = - \frac{\partial(\delta a^I)}{\partial T} \Big|_{\mathbf{a}} \frac{\partial \boldsymbol{\varphi}}{\partial a^I}, \quad (11.113)$$

so that

$$\delta(\partial_T \boldsymbol{\varphi} \cdot \partial_T \boldsymbol{\varphi} / 2) = \partial_T \boldsymbol{\varphi} \cdot \delta(\partial_T \boldsymbol{\varphi}) = -\partial_T(\delta a^I) \partial_I \boldsymbol{\varphi} \cdot \partial_T \boldsymbol{\varphi} = -\partial_T(\delta a^I) v_I, \quad (11.114)$$

where every term is evaluated at the Lagrangian space-time point (\mathbf{a}, T) , and where we introduced the covariant expression for the Lagrangian velocity⁹

$$v_I = \partial_I \boldsymbol{\varphi} \cdot \partial_T \boldsymbol{\varphi} = F^i{}_I \delta_{ij} \partial_T \varphi^j = F^i{}_I v_i^L, \quad (11.115)$$

with Eulerian coordinates assumed Cartesian so that $\delta_{ij} (v^L)^j = v_i^L$.

11.7.6 Lagrangian expression for the potential vorticity

As this point, the action (11.90) has a variation given only through variations in the kinetic energy as per equation (11.114)

$$\delta \mathcal{S}^{\text{action}} = - \int_{t_A}^{t_B} \int_{\mathcal{R}(\mathbf{a})} \partial_T(\delta a^I) v_I \dot{\rho}^L \dot{g}^L d^3 a dT = \int_{t_A}^{t_B} \int_{\mathcal{R}(\mathbf{a})} \delta a^I (\partial_T v_I) \dot{\rho}^L \dot{g}^L d^3 a dT, \quad (11.116)$$

where we assumed the coordinate variation vanishes at the temporal bounds

$$\delta a^I = 0 \quad \text{for } T = t_A \text{ and } T = t_B. \quad (11.117)$$

We next introduce equation (11.108) for the non-divergent coordinate variation, and use equation (11.99) to relate the Levi-Civita tensor to the permutation symbol, so that

$$\dot{\rho}^L \dot{g}^L \delta a^I = \epsilon^{IJK} \partial_J W_K, \quad (11.118)$$

which brings the action variation to

$$\delta \mathcal{S}^{\text{action}} = \int_{t_A}^{t_B} \int_{\mathcal{R}(\mathbf{a})} \epsilon^{IJK} \partial_J W_K \partial_T v_I d^3 a dT. \quad (11.119)$$

⁹Recall that equation (11.8) introduced the contravariant Lagrangian representation of the velocity, $v^I = F^I{}_i (v^i)$.

Integrating by parts on the spatial derivative leads to

$$\delta S^{\text{action}} = - \int_{t_A}^{t_B} \int_{\mathcal{R}(\mathbf{a})} \epsilon^{IJK} W_K \partial_J \partial_T v_I d^3 a dT, \quad (11.120)$$

where we assumed the coordinate variation vanishes at the material boundaries

$$\delta a^I = 0 \quad \text{for } \mathbf{a} \in \partial \mathcal{R}(\mathbf{a}). \quad (11.121)$$

The time and space derivatives commute in equation (11.120), and the permutation symbol, ϵ^{IJK} , and specific entropy, $\dot{\mathcal{S}}$, are both independent of material time so that (with $W_K = A \partial_K \dot{\mathcal{S}}$)

$$\delta S^{\text{action}} = - \int_{t_A}^{t_B} \int_{\mathcal{R}(\mathbf{a})} W_K \partial_T (\epsilon^{IJK} \partial_J v_I) d^3 a dT \quad (11.122a)$$

$$= - \int_{t_A}^{t_B} \int_{\mathcal{R}(\mathbf{a})} A \partial_T (\partial_K \dot{\mathcal{S}} \epsilon^{IJK} \partial_J v_I) d^3 a dT. \quad (11.122b)$$

$$= - \int_{t_A}^{t_B} \int_{\mathcal{R}(\mathbf{a})} A \partial_T [(1/\dot{\rho}^L) \partial_K \dot{\mathcal{S}} \dot{\varepsilon}^{IJK} \partial_J v_I] \dot{\rho}^L \dot{g}^L d^3 a dT. \quad (11.122c)$$

At this point we assert that particle relabeling symmetry holds, so that the action has zero variation.¹⁰ For a zero variation to be realized with an arbitrary A requires the material time invariance of the Lagrangian expression of Ertel potential vorticity from VOLUME 3

$$Q \equiv \frac{\nabla_{\mathbf{a}} \dot{\mathcal{S}} \cdot \text{curl}(\mathbf{v})}{\dot{\rho}^L} = \frac{\partial_K \dot{\mathcal{S}} \dot{\varepsilon}^{IJK} \partial_J v_I}{\dot{\rho}^L} = \frac{\partial_K \dot{\mathcal{S}} \epsilon^{IJK} \partial_J v_I}{\dot{g}^L \dot{\rho}^L}. \quad (11.123)$$

11.7.7 Eulerian expression for the potential vorticity

Transforming the Lagrangian expression (11.7) of the potential vorticity into its Eulerian form offers useful experience with index gymnastics. First we transform the Lagrangian gradient of the specific entropy into its Eulerian gradient using the chain rule with the transformation matrix (11.2)

$$\partial_K \dot{\mathcal{S}} = F^k{}_K \partial_k \mathcal{S}, \quad (11.124)$$

where $\mathcal{S} = \mathcal{S}(\mathbf{x}, t)$ is the Eulerian expression for the specific entropy. Next, expand the Lagrangian expression of the relative vorticity according to (recall the Eulerian coordinates are Cartesian)

$$\epsilon^{IJK} \partial_J v_I = \epsilon^{IJK} \partial_J (F^i{}_I \partial_T \varphi^j \delta_{ij}) \quad (11.125a)$$

$$= \epsilon^{IJK} \partial_J (\partial_I \varphi^i \partial_T \varphi^j \delta_{ij}) \quad (11.125b)$$

$$= \epsilon^{IJK} \partial_I \varphi^i \partial_T \partial_J \varphi^j \delta_{ij} \quad (11.125c)$$

$$= \epsilon^{IJK} F^i{}_I \partial_T F^j{}_J \delta_{ij} \quad (11.125d)$$

$$= \epsilon^{IJK} F^i{}_I F^m{}_J \partial_m v^j \delta_{ij}, \quad (11.125e)$$

¹⁰A vanishing action variation is here not a result of invoking Hamilton's principle. Rather, it results from insisting that particle relabeling symmetry holds.

where we wrote the material time evolution of the transformation matrix in terms of the Eulerian expression for the velocity gradient tensor (VOLUME 2)

$$\partial_T F^j{}_J = F^m{}_J \partial_m v^j. \quad (11.126)$$

Now contract the relative vorticity (11.125e) with the gradient of the specific entropy

$$\partial_K \mathring{\mathcal{S}} \epsilon^{IJK} \partial_J v_I = \partial_k \mathcal{S} \epsilon^{IJK} F^i{}_I F^m{}_J F^k{}_K \partial_m v^j \delta_{ij}. \quad (11.127)$$

We can make this expression a bit more tidy through a coordinate transformation

$$\partial_K \mathring{\mathcal{S}} \epsilon^{IJK} \partial_J v_I = \partial_k \mathring{\mathcal{S}} \epsilon^{imk} \frac{\partial \Phi}{\partial a} \partial_m v^j \delta_{ij}. \quad (11.128)$$

Finally, using equation (11.21a) for the specific volume renders

$$\partial_K \mathring{\mathcal{S}} \epsilon^{IJK} \partial_J v_I = \partial_k \mathcal{S} \epsilon^{ijk} \partial_j (\delta_{im} v^m) = \mathring{g}^L \mathring{\rho}^L \frac{\nabla_x \mathcal{S} \cdot \text{curl}(\mathbf{v})}{\rho}, \quad (11.129)$$

which then leads us to the expected Eulerian expression for the potential vorticity, written entirely in terms of Eulerian quantities

$$Q = \frac{\nabla_x \mathcal{S} \cdot \text{curl}(\mathbf{v})}{\rho}. \quad (11.130)$$

11.7.8 Global versus local conservation

Space-time symmetries leading to the conservation of momentum and energy lead to differential conservation laws in the form of a continuity equation, such as equation (11.73) for the Hamiltonian density. A global spatial integration of the continuity equation leads to a constant of the motion (e.g., the globally integrated energy) in cases where the normal component of the corresponding fluxes vanish on the boundaries. Such differential conservation laws operationally arise when an active variation leads to a mechanically equivalent action, such as discussed in Section 10.5.4 for constant space-time shifts.

Rather than a mechanically equivalent Lagrangian, are there symmetries related to coordinate transformations (passive variations) that lead to unaltered actions? If so, then the corresponding Noether theorem conservation law does not appear as a continuity equation. Instead, it appears as a property that is a temporal constant everywhere in Lagrangian space-time. That is, it leads to a *local conservation law* rather than a *global conservation law*. As seen in this section, the material time independence of potential vorticity is just that local conservation law for a perfect fluid. That is, potential vorticity is constant for each point in the Lagrangian (material) space-time.



A more tedious calculation of the Jacobian variation (11.57)

To derive the variation of the Jacobian in equation (11.57), we made use of an identity from VOLUME 1 that expresses the derivative of the Jacobian with respect to an element of the matrix. Here, derive equation (11.57) without making use of that identity. The calculation is more tedious but it serves to further our experience with index gymnastics.

The first step makes use of the product rule

$$\delta \left[\frac{\partial \varphi^m}{\partial a^I} \frac{\partial \varphi^n}{\partial a^J} \frac{\partial \varphi^p}{\partial a^K} \right] = \frac{\partial(\delta \varphi^m)}{\partial a^I} \frac{\partial \varphi^n}{\partial a^J} \frac{\partial \varphi^p}{\partial a^K} + \frac{\partial(\delta \varphi^n)}{\partial a^J} \frac{\partial \varphi^m}{\partial a^I} \frac{\partial \varphi^p}{\partial a^K} + \frac{\partial(\delta \varphi^p)}{\partial a^K} \frac{\partial \varphi^m}{\partial a^I} \frac{\partial \varphi^n}{\partial a^J}. \quad (11.131)$$

We now introduce \mathbf{x} -space derivatives rather than sticking solely with \mathbf{a} -space derivatives, and for this purpose we make use of the chain rule to write

$$\frac{\partial(\delta \varphi^m)}{\partial a^I} = \frac{\partial(\delta \varphi^m)}{\partial x^q} \frac{\partial \varphi^q}{\partial a^I}, \quad \frac{\partial(\delta \varphi^n)}{\partial a^J} = \frac{\partial(\delta \varphi^n)}{\partial x^q} \frac{\partial \varphi^q}{\partial a^J}, \quad \frac{\partial(\delta \varphi^p)}{\partial a^K} = \frac{\partial(\delta \varphi^p)}{\partial x^q} \frac{\partial \varphi^q}{\partial a^K}, \quad (11.132)$$

where the \mathbf{x} -space derivatives of the variation, $\delta \varphi$, are computed at the point $\mathbf{x} = \boldsymbol{\varphi}(\mathbf{a}, T)$. Making use of equations (11.132) renders the variation

$$\begin{aligned} \delta \left[\frac{\partial \varphi^m}{\partial a^I} \frac{\partial \varphi^n}{\partial a^J} \frac{\partial \varphi^p}{\partial a^K} \right] \\ = \frac{\partial(\delta \varphi^m)}{\partial x^q} \frac{\partial \varphi^q}{\partial a^I} \frac{\partial \varphi^n}{\partial a^J} \frac{\partial \varphi^p}{\partial a^K} + \frac{\partial(\delta \varphi^n)}{\partial x^q} \frac{\partial \varphi^q}{\partial a^J} \frac{\partial \varphi^m}{\partial a^I} \frac{\partial \varphi^p}{\partial a^K} + \frac{\partial(\delta \varphi^p)}{\partial x^q} \frac{\partial \varphi^q}{\partial a^K} \frac{\partial \varphi^m}{\partial a^I} \frac{\partial \varphi^n}{\partial a^J}. \end{aligned} \quad (11.133)$$

Now reintroduce the permutation symbols to yield

$$\begin{aligned} \delta \left[\frac{1}{3!} \epsilon_{mnp} \epsilon^{IJK} \frac{\partial \varphi^m}{\partial a^I} \frac{\partial \varphi^n}{\partial a^J} \frac{\partial \varphi^p}{\partial a^K} \right] \\ = \frac{1}{3!} \epsilon_{mnp} \epsilon^{IJK} \frac{\partial(\delta \varphi^m)}{\partial x^q} \left(\frac{\partial \varphi^q}{\partial a^I} \frac{\partial \varphi^n}{\partial a^J} \frac{\partial \varphi^p}{\partial a^K} - \frac{\partial \varphi^q}{\partial a^J} \frac{\partial \varphi^n}{\partial a^I} \frac{\partial \varphi^p}{\partial a^K} - \frac{\partial \varphi^q}{\partial a^K} \frac{\partial \varphi^p}{\partial a^I} \frac{\partial \varphi^n}{\partial a^J} \right), \end{aligned} \quad (11.134)$$

which can be simplified to

$$\delta \left[\frac{1}{3!} \epsilon_{mnp} \epsilon^{IJK} \frac{\partial \varphi^m}{\partial a^I} \frac{\partial \varphi^n}{\partial a^J} \frac{\partial \varphi^p}{\partial a^K} \right] = \frac{1}{2} \epsilon_{mnp} \epsilon^{IJK} \frac{\partial(\delta \varphi^m)}{\partial x^q} \left(\frac{\partial \varphi^q}{\partial a^I} \frac{\partial \varphi^n}{\partial a^J} \frac{\partial \varphi^p}{\partial a^K} \right). \quad (11.135)$$

The right hand side vanishes unless $m = q$, which can be seen by expanding the terms. The case with $m = q = 1$ is given by

$$\begin{aligned} \frac{1}{2} \epsilon_{1np} \epsilon^{IJK} \frac{\partial(\delta \varphi^1)}{\partial x^1} \left(\frac{\partial \varphi^1}{\partial a^I} \frac{\partial \varphi^n}{\partial a^J} \frac{\partial \varphi^p}{\partial a^K} \right) \\ = \frac{1}{2} \epsilon_{123} \epsilon^{IJK} \frac{\partial(\delta \varphi^1)}{\partial x^1} \left(\frac{\partial \varphi^1}{\partial a^I} \frac{\partial \varphi^2}{\partial a^J} \frac{\partial \varphi^3}{\partial a^K} - \frac{\partial \varphi^1}{\partial a^I} \frac{\partial \varphi^3}{\partial a^J} \frac{\partial \varphi^2}{\partial a^K} \right), \end{aligned} \quad (11.136)$$

which can be simplified to

$$\frac{1}{2} \epsilon_{1np} \epsilon^{IJK} \frac{\partial(\delta \varphi^1)}{\partial x^1} \left(\frac{\partial \varphi^1}{\partial a^I} \frac{\partial \varphi^n}{\partial a^J} \frac{\partial \varphi^p}{\partial a^K} \right) = \epsilon^{IJK} \frac{\partial(\delta \varphi^1)}{\partial x^1} \left(\frac{\partial \varphi^1}{\partial a^I} \frac{\partial \varphi^2}{\partial a^J} \frac{\partial \varphi^3}{\partial a^K} \right). \quad (11.137)$$

The cases $m = 2$ and $m = 3$ lead to corresponding results, in which case we are led to

$$\delta \left[\frac{\partial \boldsymbol{\varphi}}{\partial \mathbf{a}} \right] = \frac{\partial(\delta \varphi^i)}{\partial x^i} \epsilon^{IJK} \left(\frac{\partial \varphi^1}{\partial a^I} \frac{\partial \varphi^2}{\partial a^J} \frac{\partial \varphi^3}{\partial a^K} \right) \quad (11.138a)$$

$$= \frac{\partial(\delta \varphi^i)}{\partial x^i} \frac{1}{3!} \epsilon_{mnp} \epsilon^{IJK} \frac{\partial \varphi^m}{\partial a^I} \frac{\partial \varphi^n}{\partial a^J} \frac{\partial \varphi^p}{\partial a^K} \quad (11.138b)$$

$$= \frac{\partial(\delta \varphi^i)}{\partial x^i} \frac{\partial \boldsymbol{\varphi}}{\partial \mathbf{a}}, \quad (11.138c)$$

which is equation (11.57).



Chapter 12

APPROXIMATE THEORIES FROM HAMILTON'S PRINCIPLE

In this chapter we derive some approximate theories for perfect fluids using *Hamilton's variational principle*.

READER'S GUIDE FOR THIS CHAPTER

This chapter is a direct follow-on from Chapter 11 that considered Hamilton's principle for a perfect fluid.

12.1	Loose threads	389
12.2	Boussinesq ocean	389
12.2.1	Unit Jacobian for non-divergent flow	389
12.2.2	Boussinesq energetics	390
12.2.3	Action for the Boussinesq ocean	390
12.2.4	Boussinesq Euler-Lagrange equation	391
12.2.5	Comments	392

12.1 Loose threads

- Adiabatic Boussinesq in buoyancy coordinates
- Quasi-geostrophy
- Semi-geostrophy
- shallow water

12.2 Boussinesq ocean

We studied the governing equations for a Boussinesq ocean in VOLUME 2. Here, we derive these via Hamilton's principle. There are some novel conceptual and technical points to raise here relative to the non-Boussinesq fluid considered in Chapter 11, thus warranting a full discussion of the Boussinesq case.

12.2.1 Unit Jacobian for non-divergent flow

Following the approach earlier in this chapter, we use Cartesian Eulerian coordinates so that $\mathbf{x} = \varphi(\mathbf{a}, T)$ provides the instantaneous Cartesian position of a fluid particle with material

label, \mathbf{a} , and material time, T . Additionally, we here assume material coordinates are given by the Cartesian initial positions of fluid particles, in which case the Jacobian is unity at the initial condition

$$\mathbf{a} = \dot{\mathbf{x}} \implies \frac{\partial \Phi}{\partial \dot{\mathbf{x}}} = 1 \quad \text{at } T = t_0. \quad (12.1)$$

With this choice for the Eulerian and material coordinates, the Jacobian of transformation is the ratio of the present fluid parcel volume to the initial parcel volume

$$\frac{\partial \Phi}{\partial \dot{\mathbf{x}}} = \frac{d^3 x}{d^3 \dot{x}}. \quad (12.2)$$

From our study of the kinematics of non-divergent flow in VOLUME 2, we know that non-divergent flows keep the volume of fluid parcels constant while following fluid particle trajectories, so that the Jacobian is a material constant

$$\partial_T (\partial \Phi / \partial \dot{\mathbf{x}}) = 0. \quad (12.3)$$

A unit initial value as per equation (12.1) along material constancy means that the Jacobian retains its unity value along each particle trajectory for all time

$$\partial \Phi / \partial \dot{\mathbf{x}} = 1 \quad \forall T. \quad (12.4)$$

12.2.2 Boussinesq energetics

As noted in our study of the [Boussinesq ocean](#) in VOLUME 2, the Boussinesq ocean does not respect the principle of equivalence, since the mass used for the kinetic energy (inertial mass) is based on a constant reference density, ρ_0 , whereas the mass used for the gravitational potential energy (gravitational mass) uses the *in situ* density, ρ . A constant reference density for kinetic energy means that the flow is non-divergent, whereas the *in situ* density for potential energy allows for buoyancy to affect motion via density gradients.

Now recall from Section 11.4.3 that the specific internal energy is a function of the specific entropy and specific volume. For the perfect fluid the specific entropy is a material constant. Equation (12.4) implies that the specific volume is also a material constant. Consequently, the specific internal energy for the Boussinesq ocean is a material constant. Evidently, there is a disconnect between pressure and internal energy for the Boussinesq ocean. Stated otherwise, we know that in the absence of flow divergence, there can be no pressure work on a fluid parcel. Hence, pressure in the Boussinesq ocean has no thermodynamic connection to internal energy. Pressure instead plays a purely mechanical role, which we see in Section 12.2.3 via its role as a Lagrange multiplier that constrains the flow to remain non-divergent. In VOLUME 2, we note that pressure is a constraint that maintains the non-divergent nature of the flow. The present discussion furthers that understanding through Hamilton's principle.

12.2.3 Action for the Boussinesq ocean

We follow the approach in VOLUME 1 by absorbing the centrifugal potential into the geopotential, thus writing

$$\Phi = g z. \quad (12.5)$$

In this manner we are led to the action for a Boussinesq ocean (recall that $\mathbf{a} = \dot{\mathbf{x}}$)

$$\begin{aligned} \mathcal{S}^{\text{action}} = & \int_{T_{\text{init}}}^{T_{\text{final}}} \int_{\mathcal{R}(\dot{\mathbf{x}})} \left[\frac{1}{2} \partial_T \boldsymbol{\varphi} \cdot \partial_T \boldsymbol{\varphi} + \partial_T \boldsymbol{\varphi} \cdot (\boldsymbol{\Omega} \times \boldsymbol{\varphi}) \right] \rho_0 d^3 \dot{\mathbf{x}} dT - \int_{T_{\text{init}}}^{T_{\text{final}}} \int_{\mathcal{R}(\dot{\mathbf{x}})} \Phi \dot{\rho} d^3 \dot{\mathbf{x}} dT \\ & + \int_{T_{\text{init}}}^{T_{\text{final}}} \int_{\mathcal{R}(\dot{\mathbf{x}})} p (\partial \boldsymbol{\varphi} / \partial \dot{\mathbf{x}} - 1) d^3 \dot{\mathbf{x}} dT, \end{aligned} \quad (12.6)$$

where p is a Lagrange multiplier that plays the role of mechanical pressure. Notice that we used the constant Boussinesq reference density, ρ_0 , for computing the kinetic energy, whereas the geopotential uses $\dot{\rho}$. The use of distinct densities arises since the Boussinesq ocean does not respect the principle of equivalence.

12.2.4 Boussinesq Euler-Lagrange equation

We now vary the Boussinesq action (12.6) by independently varying the trajectories as well as the Lagrange multiplier, p . Varying the Lagrange multiplier leads, as expected, to the non-divergence constraint (12.4)

$$\delta_p \mathcal{S}^{\text{act}} = 0 \implies \partial \boldsymbol{\varphi} / \partial \dot{\mathbf{x}} = 1. \quad (12.7)$$

We now detail results from varying the trajectories.

Kinetic energy variation arising from variation of the trajectories

Following the steps in Section 11.5.2, only now with density set to the constant reference density, ρ_0 , leads to variation of the kinetic energy contribution to the action

$$\begin{aligned} \delta \int_{T_{\text{init}}}^{T_{\text{final}}} \int_{\mathcal{R}(\dot{\mathbf{x}})} & \left[\frac{1}{2} \partial_T \boldsymbol{\varphi} \cdot \partial_T \boldsymbol{\varphi} + \partial_T \boldsymbol{\varphi} \cdot (\boldsymbol{\Omega} \times \boldsymbol{\varphi}) \right] \rho_0 d^3 \dot{\mathbf{x}} dT \\ & = - \int_{T_{\text{init}}}^{T_{\text{final}}} \int_{\mathcal{R}(\dot{\mathbf{x}})} [\partial_{TT} \boldsymbol{\varphi} + 2 \boldsymbol{\Omega} \times \partial_T \boldsymbol{\varphi}] \cdot \delta \boldsymbol{\varphi} \rho_0 d^3 \dot{\mathbf{x}} dT. \end{aligned} \quad (12.8)$$

Geopotential energy variation arising from variation of the trajectories

The chain rule leads to variation of the integrated geopotential

$$\delta \int_{\mathcal{R}(\dot{\mathbf{x}})} \Phi \dot{\rho} d^3 \dot{\mathbf{x}} = \int_{\mathcal{R}(\dot{\mathbf{x}})} \frac{\partial \Phi}{\partial \varphi^i} \delta \varphi^i \dot{\rho} d^3 \dot{\mathbf{x}} = \int_{\mathcal{R}(\dot{\mathbf{x}})} \frac{\partial \Phi}{\partial \varphi^i} \delta \varphi^i \rho^L d^3 \dot{\mathbf{x}}, \quad (12.9)$$

where the final equality made use of the identity (11.18) with a unit Jacobian

$$\dot{\rho} = \rho^L \partial \boldsymbol{\varphi} / \partial \dot{\mathbf{x}} = \rho^L. \quad (12.10)$$

Constraint variation arising from variation of the trajectories

Varying the trajectories leads to variation of the constraint

$$\int_{\mathcal{R}(\dot{\mathbf{x}})} p \delta (\partial \boldsymbol{\varphi} / \partial \dot{\mathbf{x}}) d^3 \dot{\mathbf{x}} = \int_{\mathcal{R}(\dot{\mathbf{x}})} p \frac{\partial (\delta \varphi^i)}{\partial x^i} d^3 \dot{\mathbf{x}} = - \int_{\mathcal{R}(\dot{\mathbf{x}})} \frac{\partial p}{\partial x^i} \delta \varphi^i d^3 \dot{\mathbf{x}}, \quad (12.11)$$

where we used equation (11.138c) for the Jacobian variation in the presence of a unit Jacobian

$$\delta \left[\frac{\partial \boldsymbol{\varphi}}{\partial \dot{\boldsymbol{x}}} \right] = \frac{\partial(\delta \varphi^i)}{\partial x^i} \frac{\partial \boldsymbol{\varphi}}{\partial \dot{\boldsymbol{x}}} = \frac{\partial(\delta \varphi^i)}{\partial x^i}, \quad (12.12)$$

and assumed zero mechanical forcing at the domain boundaries.

The Euler-Lagrange equation for the Boussinesq ocean

Bringing terms together leads to the action variation under variation of the trajectories

$$\begin{aligned} \delta_{\boldsymbol{\varphi}} \mathcal{S}^{\text{act}} = & - \int_{T_{\text{init}}}^{T_{\text{final}}} \int_{\mathcal{R}(\dot{\boldsymbol{x}})} [\partial_{TT} \boldsymbol{\varphi} + 2 \boldsymbol{\Omega} \times \partial_T \boldsymbol{\varphi}] \cdot \delta \boldsymbol{\varphi} \rho_0 d^3 \dot{\boldsymbol{x}} dT \\ & - \int_{T_{\text{init}}}^{T_{\text{final}}} \int_{\mathcal{R}(\dot{\boldsymbol{x}})} \frac{\partial \Phi}{\partial \varphi^i} \delta \varphi^i \rho^L d^3 \dot{\boldsymbol{x}} dT - \int_{T_{\text{init}}}^{T_{\text{final}}} \int_{\mathcal{R}(\dot{\boldsymbol{x}})} \frac{\partial p}{\partial x^i} \delta \varphi^i d^3 \dot{\boldsymbol{x}} dT. \end{aligned} \quad (12.13)$$

Setting the variation to zero leads to the Boussinesq Euler-Lagrange equations

$$\partial_T \boldsymbol{v}^L + 2 \boldsymbol{\Omega} \times \boldsymbol{v}^L = - \frac{1}{\rho_0} \frac{\partial p}{\partial \boldsymbol{\varphi}} - \frac{\rho^L}{\rho_0} \frac{\partial \Phi}{\partial \boldsymbol{\varphi}}, \quad (12.14)$$

which agrees with the perfect fluid Boussinesq ocean equations derived in VOLUME 2 using Newtonian methods.

12.2.5 Comments

Absence of an equivalence principle for the Boussinesq ocean prompts a careful treatment of the density factors. Furthermore, note how the pressure, here appearing as a Lagrange multiplier, corresponds directly to the thermodynamic pressure for the non-Boussinesq fluid in Section 11.5. That correspondence is not a coincidence, with the sign of the constraint as written in equation (12.6) chosen to facilitate the agreement.



Part IV

End matter

Appendix A

GLOSSARY OF CONCEPTS AND TERMS

action The action is the time integral of the Lagrangian density. Hamilton's principle states that the functional variation of the action is stationary for physically realized time evolution. xi, 137

active tracer An active tracer affects the flow. Consequently, the tracer equation for active tracers is nonlinear. Temperature and matter concentration are two active tracers, in which these two tracers impact on the density, with density then modifying pressure that then modifies the flow. 165, 255

advection equation The advection equation, $(\partial_t + \mathbf{v} \cdot \nabla) C = 0$, is the canonical transport equation that arises from an Eulerian perspective on the evolution of a scalar field in the presence of fluid flow. We encounter the advection equation throughout this book. 143, 146

advective tracer flux The advective tracer flux, $\rho C \mathbf{v}$, is the mass of tracer per area per time that transported with the fluid flow. The convergence of this flux affects a time change to the mass of tracer per volume. 151

ageostrophic Ageostrophic flow is any part of the flow field that is not in balance through geostrophy. In the context of Ekman mechanics, the ageostrophic flow is that flow directly affected by friction. In general, the ageostrophic flow has a nonzero horizontal divergence, which contrasts to the non-divergent horizontal flow for f -plane geostrophic flows. 231

anomalous diffusion Brownian motion as formulated by [Einstein \(1905a\)](#) leads to the mean squared spread of a cloud of Brownian particles evolving according to $d\bar{x^2}/dt = 2\kappa$, so that for a constant diffusivity the spread grows as $\bar{x^2} = 2\kappa t$. Anomalous diffusion arises when $\bar{x^2} \propto t^\xi$ for $\xi \neq 1$. Section 3 of [Young \(1999\)](#) provides a summary of anomalous diffusion in geophysical flows. 116

anti-symmetric tensor An anti-symmetric (also skew-symmetric) tensor equals to minus its transpose, $\mathbf{A} = -\mathbf{A}^T$. 225

Archimedean buoyancy The Archimedean buoyancy is the buoyancy acting on a test fluid element computed relative to a reference buoyancy. We consider both a globally referenced density, thus leading to the globally referenced Archimedean buoyancy, $b = -g(\rho - \rho_0)/\rho_0$, as well as a locally referenced density, used to compute neutral directions. The Archimedean buoyancy of a test fluid element makes use of perhaps the most ancient of physical concepts in fluid mechanics. 106, 226, 287, 289

baroclinicity Baroclinicity is the miss-alignment between density and pressure that renders a source for vorticity, $\mathbf{B} = -\nabla \times (\rho^{-1} \nabla p) = (\nabla \rho \times \nabla p)/\rho^2$. In a Boussinesq ocean, the baroclinicity vector arises just from horizontal gradients in the buoyancy, $\mathbf{B} = \nabla b \times \hat{\mathbf{z}}$. 65, 77

barycentric velocity The barycentric velocity is the center of mass velocity for a fluid element. The barycentric velocity plays the same role for multi-component fluids as the fluid parcel velocity does for single-component fluids. Differences between the barycentric velocity and the velocity of a specific fluid constituent can lead to the exchange of matter constituents across the boundary of the fluid element, with that exchange typically represented as diffusion. 38, 58, 146, 155, 157, 265, 266, 291

barystatic sealevel When freshwater enters the ocean, such as from melting continental ice sheets, it adds to the ocean mass and in turn increases global mean sea level. This change is referred to as **barystatic sealevel** change according to the sea level terminology paper from *Gregory et al. (2019)*. Although ocean salinity changes upon changing the freshwater content, the net effect on global mean sea level is almost entirely barystatic since the global halosteric effect is negligible. We can understand why the global halosteric effect is so tiny by recognizing that freshwater entering the ocean sees its salinity increase whilst the ambient seawater is itself freshened. These compensating salinity changes (which are often mistakenly ignored) have corresponding compensating sea level changes, thus bringing the global halosteric effect to near zero. 277, 280, 396

Batchelor scale The Batchelor scale sets the smallest spatial scale of scalar (e.g., temperature or salinity) fluctuations in a flow with both turbulent advection and molecular diffusion. It is the dissipation scale for scalars, below which molecular diffusion dominates over advective stirring. 221

Bernoulli potential The Bernoulli potential is the sum of the mechanical energy per mass plus the enthalpy per mass, $\mathcal{B} = \mathcal{M} + \mathcal{H} = \mathcal{K} + \Phi + \mathcal{I} + p/\rho$. For the Boussinesq ocean, the Bernoulli potential is $\mathcal{B} = \mathcal{K} + P^b + \varphi$. 76

biharmonic operator The biharmonic operator is the squared Laplacian operator, $\nabla^4 = \nabla^2 \nabla^2$. Biharmonic operators arise in elasticity theory as well as for Stokes flow in fluid mechanics. For geophysical fluid mechanics, biharmonic operators are commonly used for numerical reasons to enhance the scale-selectivity of dissipation. 253

body forces A body force acts throughout the extent of a fluid element, and it is synonymous with external force. Examples include the gravitational force, as well as the Coriolis and centrifugal forces arising from the rotating planetary reference frame. These forces are also known as long range forces. xix

bolus velocity The bolus velocity is a horizontal velocity that arises from the correlation between layer thickness and layer velocity when performing an eddy-mean decomposition in isopycnal coordinates or in a stacked shallow water model. 212, 218

boundary propagator The boundary propagator is the boundary Green's function for the diffusion and advection-diffusion problem, which incorporate time dependence along with space dependence. 181

Boussinesq ocean The Boussinesq ocean equations serve as a useful framework to study aspects of the ocean circulation, both large-scale and small-scale. The Boussinesq ocean's prognostic velocity is non-divergent, thus representing an incompressible flow, and yet the Boussinesq ocean fluid admits density variations, as for a compressible fluid. That is, the study of a Boussinesq ocean concerns the incompressible flow of a compressible fluid, thus exemplifying the important distinction between a fluid property versus a flow property. Since the flow is non-divergent, the pressure in the Boussinesq ocean is not the thermodynamic pressure found in the compressible non-Boussinesq fluid. Rather, Boussinesq pressure serves a purely mechanical role by acting as the Lagrange multiplier to constrain the Boussinesq flow to be non-divergent. The Boussinesq ocean has an inertial mass based on a constant reference density, ρ_0 , whereas the gravitational mass is based on the *in situ* density, ρ . Hence, the Boussinesq ocean does not respect the principle of equivalance, thus making it necessary to exercise special care when studying energetics of the Boussinesq ocean. 35, 55, 141, 183, 289, 389, 390

Brownian motion Brownian motion is the process whereby a relatively large particle (e.g., piece of dust) is transported by the random motion of molecules within the fluid. [Einstein \(1905a\)](#) provided a theory for Brownian motion, which provided clear evidence for the molecular nature of matter. Brownian motion was also used as an inspiration for [Taylor \(1922\)](#) in his theory of turbulent diffusion. 109, 112, 223

budget equations Much of this book is concerned with deriving and understanding equations that describe the evolution of fluid properties, with such equations (differential or integral) derived from physical principles such as Newton's laws of motion, Hamilton's principle of stationary action, Noether's theorem, thermodynamic laws, mass conservation, and vorticity mechanics. These are the budget equations that form the theoretical foundation of continuum mechanics. ix

buoyancy Buoyancy, or more precisely the Archimedean buoyancy, is the vertical force, acting on a region, \mathcal{R} , immersed in a fluid, with the forces those static forces from gravity and hydrostatic pressure. If the density of the displaced fluid is greater than the density of the matter within the region, $\rho^{\text{fluid}} > \rho^{\mathcal{R}}$, then the buoyancy force is in the $+\hat{z}$ direction, thus leading to a rising motion of the region. The converse happens if $\rho^{\text{fluid}} < \rho^{\mathcal{R}}$, in which case the region experiences a negative buoyancy force so that it sinks. If $\rho^{\text{fluid}} = \rho^{\mathcal{R}}$, then the region experiences zero buoyancy force so that the region is neutrally buoyant and it floats. When considering buoyancy of fluid elements, then we find a net positive or negative buoyancy arises only for a fluid environment with density inhomogeneities, so that the buoyancy of a fluid element vanishes in a fluid with a homogeneous density. 269, 287

buoyancy frequency The buoyancy frequency, N , provides a measure of the vertical stratification of denisty. It also provides a measure of the angular frequency for buoyancy oscillations. We compute the squared buoyancy frequency for the ocean via $N^2 = g(\alpha \partial_z \Theta - \beta \partial_z S)$, whereas the atmosphere typically computes it according to the vertical derivative of the potential temperature. If $N^2 < 0$ then the vertical column is gravitationally unstable. 35, 227

cabbeling Consider the mixing of two seawater elements. Let the fluid elements separately have distinct Conservative Temperature and/or salinity, but equal locally referenced

potential density. For a linear equation of state, whereby density is a linear function of Θ and S , then the resulting mixed fluid element has the same density as the unmixed separate elements. However, for a nonlinear equation of state, the mixed element generally has a different density. Furthermore, a property of seawater is that the density of the mixed element is greater than the unmixed elements. This densification upon mixing is a physical process known as cabbeling (McDougall, 1987b). 260–263, 280

Cauchy-Green strain tensor The Cauchy-Green strain tensor is the metric for Euclidean space represented using Lagrangian (material) coordinates, g_{IJ} . Furthermore, it is the representation when the Eulerian version of the metric tensor makes use of Cartesian coordinates, so that $g_{IJ} = F^i_I F^j_J \delta_{ij}$. Note that in Section 1.6 of Tromp (2025), g_{IJ} is referred to as the *right Cauchy-Green deformation rate tensor*, which is the term also used in ?. We use the term “strain” rather than “deformation” to help reduce confusion with the deformation matrix, F^i_I . 357, 381

Chapman-Kolmogorov The Chapman-Kolmogorov composition principle states that for a Markov process, the probability of going from a state A to a state C later in time can be found by summing over all possible intermediate states B. Namely, it is all possible paths through the middle, added up, thus expressing how multi-step transitions are built from one-step transitions. 113

compatibility Compatibility refers to the mathematical compatibility between the equations for tracer conservation and mass conservation. Compatibility manifests by the continuity equation for tracers reducing to the mass continuity equation when the tracer concentration is a uniform constant. Compatibility requires the non-advection tracer fluxes to vanish when the tracer concentration is uniform, and for tracer boundary conditions to reduce to those for the fluid mass. 149

Conservative Temperature Conservative Temperature, Θ , is the potential enthalpy of a fluid element divided by a standard heat capacity. Conservative Temperature is far more conservative than potential temperature, θ . Hence, Θ is the preferred variable for measuring changes in heat within the ocean. 141, 165, 255, 256, 269, 287

conservative tracer Conservative tracers evolve via the convergence of advective and diffusive fluxes within the fluid interior, along with boundary conditions. Conservative tracers have no interior sources or sinks, so the net content of a conservative tracer over any finite volume domain is affected only through transport across boundaries. 106, 127, 141, 143, 255

contact force A contact force acts on the boundary of a fluid element, with examples including stresses from pressure and from friction. Contact forces are local forces. Contact forces are sometimes referred to as internal forces, since they arise from local interactions internal to the fluid, as distinct from body forces that arise from long range external forces that act throughout the body of a fluid element. Contact forces are also called tractions in some areas of continuum mechanics. Contact forces are molecular in origin, though we are unconcerned in this book with details of the molecular dynamics leading to these forces. Contact forces act on a region of a continuous media through the area integrated stresses acting on the boundary enclosing the region. xix, 82

continuity equation A continuity equation is a flux-form differential conservation law for intensive fluid properties that are typically expressed using the Eulerian kinematic perspective.

Examples include the mass continuity equation for all constituents within a fluid sample, $\partial_t \rho + \nabla \cdot (\rho \mathbf{v}) = 0$, and the tracer continuity equation holding for individual matter constituents, $\partial_t (\rho C) + \nabla \cdot (\rho \mathbf{v} C + \mathbf{J}) = 0$. [49](#), [141](#), [146](#), [282](#)

continuum approximation The continuum approximation assumes that mathematical limits for fluid volumes tending to zero are reached on length and time scales very large compared to molecular space and time scales. The temporal realization of the continuum approximation is based on recognizing that macroscopic motion associated with fluid flows (e.g., advection, waves, and mixing) evolves with time scales far longer than the time scales of molecular motions. Hence, from a macroscopic perspective, the continuum approximation leads us to assume that all fluid motions are continuous in both space and time. [109](#)

Coulomb gauge The Coulomb gauge is commonly used in electrostatics (e.g., [Jackson \(1975\)](#)). For the eddy-induced velocity, with $\rho \mathbf{v}^* = \nabla \times (\rho \Psi^*)$, the Coulomb gauge is defined by setting $\nabla \cdot (\rho \Psi^*) = 0$. [154](#)

Coulomb-Ampere solution The Coulomb-Ampere solution is for a non-divergent vector field in the absence of boundaries, and it is written as the convolution of the source with the free-space Green's function. [154](#)

covariance Covariance means that the physical equations are form invariant under a chosen symmetry operation. The fundamental equations of geophysical fluid mechanics are respect Galilean covariance, and they do so using any arbitrary coordinate system. [27](#)

covariant derivative The covariant derivative is the generalization of the partial derivative operator that transforms as a $(0, 1)$ tensor with arbitrary coordinates. [129](#)

deformation matrix Motion of the matter continuum provides a flow map that continuously and smoothly reshapes the continuum as time evolves. Deformation refers to this reshaping of the continuum, with deformation quantified through the deformation matrix computed from material space derivatives of the flow map. Mathematically, the deformation matrix is the transformation matrix moving between \mathbf{a} -space (Lagrangian) and \mathbf{x} -space (Eulerian) coordinates. [365](#)

dia-surface transport The dia-surface transport refers to the transport of mass (mass per time) crossing a surface. If the surface is moving, then the dia-surface transport must take into account motion of the surface. The dia-surface transport is a fundamental kinematic object for stratified flows, and it plays a particularly central role in the fluid mechanical equations using generalized vertical coordinates. [166](#)

diabatic A diabatic process in a fluid occurs with the exchange of heat between fluid elements. In this manner, physical systems experiencing diabatic processes are said to be thermally open. [143](#)

diagnostic equation A diagnostic equation determines the value of a field at a particular time instance. An example is the non-divergence condition, $\nabla \cdot \mathbf{v} = 0$, satisfied by velocity in a Boussinesq ocean. There are generally no time derivatives appearing in diagnostic equations, though this property is generally a function of the chosen coordinate system. [xi](#)

dianeutral diffusion Dianeutral diffusion refers to irreversible ocean mixing processes that are parameterized by diffusive fluxes that are oriented perpendicular to the local neutral direction. Dianeutral diffusion is often also called diapycnal diffusion. Furthermore, it is commonly approximated as vertical diffusion given that in much of the ocean interior has neutral directions close to horizontal. This mixing is important for ocean stratification, transformation of water mass properties, and changes to potential energy. 227

dianeutral direction The dianeutral direction points orthogonal to the neutral direction, with the dianeutral direction given by $\hat{\gamma} = (-\alpha \nabla \Theta + \beta \nabla S) / | -\alpha \nabla \Theta + \beta \nabla S |$. 226

differentiable manifold A differentiable manifold is locally Euclidean and possess smoothness and continuous properties that allow one to perform differential calculus. A differentiable manifold is not necessarily equipped with a metric. For example, Gibbs' thermodynamic configuration space is a differentiable manifold that has no *a priori* metric structure. 287, 288

diffusion Diffusion is the physical process by which a field, such as a tracer, spreads in space over time due to random motion, either from molecular chaos (molecular diffusion) or turbulent flows (turbulent diffusion). The net flux moves from regions of higher concentration to regions of lower concentration, thus moving down the concentration gradient. The mathematical equation describing diffusion is the canonical parabolic partial differential equation. 109, 143

diffusion dissipation functional The diffusion dissipation functional is the domain integral of $\mathbf{J} \cdot \nabla C / 2$, where \mathbf{J} is the diffusive flux. The functional derivative (Fréchet derivative) of this functional equals to the diffusion operator. 135

diffusion tensor The diffusion tensor is a second order symmetric and positive-definite tensor with dimensions of squared length per time. It is used to parameterize the downgradient eddy diffusive fluxes of tracers arising from turbulent motions. 131, 268

diffusive flux The diffusion of tracer is derived by computing the convergence of the tracer diffusive flux, which is a flux that is directed down the tracer gradient and its strength is mediated by a diffusion tensor. 124

diffusivity The diffusivity is the physical parameter that measures how fast a substance spreads out by diffusion. It sets the proportionality between the gradient of a quantity and the resulting diffusive flux. We generally work with the kinematic diffusivity, whose physical dimensions are $L^2 T^{-1}$. The diffusivity for molecular diffusion is a scalar, whereas for turbulent diffusion it is a second order tensor. 122

Dirac delta The Dirac delta provides an idealization of a point source, $\delta(\mathbf{x})$, and it is formally infinite when evaluated at $\mathbf{x} = 0$ whereas it vanishes at all other points. The Dirac delta plays a central role in the theory of Green's functions. When multiplied by mass, it provides the mass density for a point particle. In mathematics, the Dirac delta is known as a generalized function or a distribution. 126, 136, 272

Dirac delta sheet The Dirac delta sheet refers to the ability to absorb the Neumann boundary condition into a modified interior source. By doing so, the boundary value problem has a modified interior source that is proportional to a Dirac delta (hence the term Dirac delta sheet), but it now has a homogeneous boundary condition. This reformulation of the

Neumann boundary condition is commonly pursued in the geophysical fluids literature, such as when studying potential vorticity and for water mass analysis. 272

Dirichlet boundary condition The Dirichlet boundary condition prescribes the value of a function along the boundary. 141, 172

divergence theorem The divergence theorem, also known as Gauss's divergence theorem, provides a relation between the volume integral of the divergence of a vector to the boundary integral of the vector projected onto the outward normal: $\int_{\mathcal{R}} \nabla \cdot \mathbf{F} dV = \oint_{\partial\mathcal{R}} \mathbf{F} \cdot \hat{\mathbf{n}} dS$. There are many corollaries to this theorem that we use in this book, one that says for Cartesian tensors that $\int_{\mathcal{R}} \nabla \phi dV = \oint_{\partial\mathcal{R}} \phi \hat{\mathbf{n}} dS$, which we use in formulating the effects from pressure in a weak formulation of the equations of motion. 23, 60, 349, 352

double diffusive processes Double diffusive processes refer to a class of small-scale mixing processes that occur when temperature and salinity gradients act together to produce density stratification. Because heat diffuses about 100 times faster than salt in seawater, a stratification that is stable in density can nonetheless become unstable dynamically, leading to distinctive mixing patterns such as salt fingering or diffusive convection. 223, 261

downscale cascade The downscale cascade refers to the transfer of a conserved (or approximately conserved) quantity, such as typically kinetic energy, enstrophy, tracer or buoyancy variance, from larger spatial scales to progressively smaller scales through nonlinear interactions, without direct forcing or dissipation at the intermediate scales. Imagine a turbulent ocean flow in which mechanical energy is injected at some large scale, for example, by winds, tides, or instabilities. The nonlinear advection terms in the equations of motion redistribute this energy across scales. A downscale cascade occurs when this redistribution is predominantly from large to small scales, eventually reaching scales where dissipation (e.g., viscosity, mixing) can act. It manifests through filamentation, front sharpening, submesoscale generation, and turbulent mixing, and is diagnosed through spectral fluxes in numerical models and observations. The downscale cascade is in contrast to an upscale cascade, where kinetic energy or other invariants flow from smaller to larger scales (e.g., barotropic kinetic energy in 2D turbulence). 221

dual form stress The dual form stress, $-\eta \nabla p$, differs by a gradient from the form stress, $+p \nabla \eta$. Even though both have dimensions of a pressure, the dual form stress does not act to accelerate a fluid element. When integrated over a region where one can drop the gradient term, the integrated effects from the dual form stress equal to that from the form stress. However, it is not possible to make a local identification between the form stress and the dual form stress. 95

Dufour effect The Dufour effect is a flux of heat that arises from matter concentration gradients and pressure gradients. 111, 257

dynamic diffusivity The dynamic diffusivity equals to the kinematic diffusivity times the density of the fluid. When referring to "diffusivity" in this book, we generally mean the kinematic diffusivity rather than the dynamic diffusivity. 122, 123

eddy An eddy refers to any flow feature that is a departure from a subjectively chosen mean. 189

eddy diffusivity An eddy diffusivity is an emergent property of the flow that aims to capture the essential features of turbulent motion to irreversible mixing of tracers. Eddy diffusivities are typically far larger than molecular diffusivities, given the far more efficient nature of turbulent transport than molecular transport. 139, 251

eddy-induced velocity An eddy-induced velocity is an emergent property of the flow that aims to capture the advective transport features of turbulent motion. Eddy-induced velocities are akin to Stokes' drifts, and they play an important role in parameterizations of geostrophic eddies. 156, 225, 252, 258, 261

elements pillar The elements pillar of geophysical fluid mechanics comprises the physical and mathematical formulation of conceptual models used to garner insight into rotating and stratified fluid motion. This pillar is concerned with setting the stage by deductively and descriptively exposing how physical concepts are mathematically expressed to describe geophysical fluid flows. ix

elliptic partial differential equation An elliptic partial differential equation (PDE) is a second order PDE whose coefficients satisfy certain positivity conditions that ensure it behaves like Laplace's equation. The solutions are smooth and non-propagating, thus commonly found when studying static or equilibrium phenomena. 154

emergent phenomena pillar The emergent phenomena pillar of geophysical fluid mechanics studies solutions to equations that describe phenomena, such as waves, instabilities, turbulence, and general circulation, all of which emerge from the fundamental equations based on first principles. These phenomena can emerge in manners that are far from simple to understand deductively, particularly when considering nonlinear behavior such as turbulence. ix

emergent scale There are two general types of dimensional scales that we use to non-dimensionalize a mathematical physics equation. One is the emergent scale, which emerges from the flow itself. Emergent scales, such as the length scale and velocity scale of the flow, are specified by the subjective interest of the theorist though these scales are not under direct control. That is, we choose to focus on flows with a particular scale for purposes of examining the corresponding equations that describe that flow regime. A key example concerns our study of planetary geostrophy and quasi-geostrophy, where we choose to focus on flows of a particular scale where the Coriolis acceleration is of leading order importance. xii

ensemble mean The ensemble mean is based on averaging over a suite of identically prepared flow realizations that differ in a controlled manner such as through the initial conditions. For many purposes this is the most analytically convenient mean operator, though it is often difficult to realize in practice. 87, 192

epineutral Epineutral refers to processes that are oriented parallel to the local neutral direction, which are directions on which a fluid parcel can be displaced without experiencing a buoyancy force. 229

epineutral diffusion Epineutral (also neutral) diffusion is based on a diffusion tensor that yields diffusive fluxes oriented along neutral directions. It is also known as neutral diffusion. It parameterizes irreversible mixing of tracers along local neutral directions. Epineutral diffusion is a refinement of isopycnal diffusion, motivated by the fact that potential density

surfaces are not exactly neutral in a compressible, thermally expanding, and saline fluid like seawater. 238

equation of state An equation of state expresses a constraint satisfied by thermodynamic variables in thermodynamic equilibrium. In geophysical fluid mechanics, we typically refer to the equation of state as an equation specifying the mass density of a fluid element in terms of thermodynamic state properties, such as temperature, tracer concentration, and pressure. The equation of state for the atmosphere is well approximated by the ideal gas equation, whereas the ocean has a nonlinear equation of state whose coefficients are fixed by empirical measurements. 77, 316

Euler-Lagrange equation The Euler-Lagrange equation is a differential equation that results from Hamilton's principle of stationary action. In classical mechanics, the Euler-Lagrange equation is the same as Newton's equation of motion. 137

Eulerian mean An Eulerian mean refers to any averaging operation taking place at a fixed point in space so that it is computed within the Eulerian reference frame. 191

Eulerian reference frame An Eulerian reference frame describes fluid motion relative to a fixed position (x -space), commonly referred to as the laboratory frame. This kinematic description measures fluid properties as the fluid streams by a fixed observer. It is not concerned with determining trajectories. Instead, Eulerian kinematics focuses on fluid properties as continuous fields that are functions of the space position, x , and time, t . 288

evolution equation An evolution equation determines the time tendency (Eulerian evolution) of a quantity such as the temperature or velocity. Terms in the prognostic equation are referred to as time tendencies. Evolution equations are also referred to as prognostic equations. x

external scale There are two general types of dimensional scales that we use to non-dimensionalize a mathematical physics equation. One is the external scale, with examples in this book being the gravitational acceleration, Coriolis parameter, and specified background or reference state. External scales are set by the geophysical parameter regime in which the flow occurs, and as such they are under direct control of the theorist or experimentalist. The other scale is emergent, and is a property of the flow. xii

f-plane The f -plane is a tangent plane approximation (tangent to the geoid) that makes use of Cartesian coordinates for studying geophysical fluid motion local to a point on the rotating planet and using a constant Coriolis parameter. Since motion is assumed to be on a constant geopotential, the f -plane makes use of the effective gravitational acceleration that includes both central gravity acceleration plus the planetary centrifugal acceleration. 183

Fick's law of diffusion Fick's law of diffusion says that the diffusive flux of tracer concentration is given by a kinematic diffusivity times minus the gradient of the concentration, so that the flux is directed down the tracer concentration gradient. 111, 122, 125

fine scale mixing Fine-scale mixing refers to the mixing of seawater properties (e.g., heat, salt, momentum, tracers) that occurs at spatial scales just above the molecular dissipation range, typically meters to tens of meters, driven by the interaction between larger-scale internal

waves or mesoscale motions and small-scale shear or stratification. It is the intermediate regime between large-scale stirring (hundreds of meters to kilometers, e.g., eddies and fronts) and microscale turbulent mixing (millimeters and below, at the Kolmogorov and Batchelor scales). 223

flat representation The flat representation refers to the $(0, 2)$ representation of second order tensors. For example, the flat representation of the diffusion tensor is $\mathbf{K} = K_{mn} \mathbf{e}^n \otimes \mathbf{e}^m$. The flat representation follows the musical nomenclature for second order tensors, where we have sharp, flat, and natural representations. 129

flow map The flow map smoothly and continuously deforms the matter continuum through space as the fluid moves, and it is written as $\boldsymbol{\varphi}(\mathbf{a}, T)$. The flow map provides the trajectory for the fluid particle specified by the material coordinate, \mathbf{a} . So in this sense we can consider the flow map as the accumulation of all fluid particle pathlines, and with its time derivative, $\partial_T \boldsymbol{\varphi}(\mathbf{a}, T)$, providing the velocity of the fluid particle, $\partial_T \boldsymbol{\varphi}(\mathbf{a}, T) = \mathbf{v}[\mathbf{x} = \boldsymbol{\varphi}(\mathbf{a}, T), t = T] = \mathbf{v}^l(\mathbf{a}, T)$. The motion field is the reason there is a flow map, so that the nomenclature “motion field” and “flow map” are used interchangeably in this book since they both refer to movement of the continuum. 193, 365

fluid parcel Fluid parcel are infinitesimal deformable regions of a perfect fluid that maintain a fixed matter content and fixed thermodynamic properties, so that they have fixed mass and fixed enthalpy. 205

flux-form conservation law A flux-form conservation law is a partial differential equation written in the form of a local time tendency of an intensive quantity that equals to (is driven by) the convergence of a flux. Such equations are generally written from an Eulerian perspective. Examples include the mass conservation equations, which are referred to as continuity equations, such as for the mass of all constituents within a fluid sample and for tracer continuity equations for individual matter constituents. 146

form stress Form stress is the contribution from pressure acting to give a horizontal acceleration. For a surface defined by $z = \eta(x, y, t)$, the form stress is given by $p \nabla_h \eta$ when acting on the top side of the surface, and $-p \nabla_h \eta$ on the bottom side. The name arises since the stress depends on the form, or shape, of the surface on which pressure acts. 61, 63, 77

formation In the context of water mass analysis, fluid moves through water mass configuration space (\mathbf{q} -space) if it is transformed in a manner that causes water to cross surfaces of constant \mathbf{q} . It follows that the convergence (local accumulation) or divergence (local depletion) of transformation leads to the formation of water mass classes, or its negative, being the destruction of water masses. More precisely, formation is the layer integrated \mathbf{q} -space convergence of transformation, with both formation and transformation having dimensions of mass per time. 288–290, 307

Fourier’s law of conduction Fourier’s law expresses the conductive flux of heat as proportional to a conductivity times the gradient of temperature, with the flux directed down the temperature gradient. The time changes to the temperature are given by the convergence of the downgradient flux. 111, 123

Fréchet derivative The Fréchet derivative provides a generalization of an ordinary derivative. It measures how a functional (a mapping from functions to numbers) changes when the

input function is varied. We make use of such derivatives when working with variational calculus. It is effectively the same as the functional derivative. 136

functional derivative The functional derivative (effectively the same as the Fréchet derivative) provides a generalization of an ordinary derivative. It measures how a functional (a mapping from functions to numbers) changes when the input function is varied. We make use of such derivatives when working with variational calculus. 136

gauge function A gauge function is a physically unspecified function that is associated with a gauge symmetry. The simplest gauge function we encounter in this book is the arbitrary constant associated with streamfunctions for two-dimensional non-divergent flows. For three-dimensional non-divergent flows, gauge symmetry allows for an arbitrary gradient to be added to the vector streamfunction. We also encounter gauge functions when studying fluxes in flux-form Eulerian conservation laws. In these cases, is only the convergence of a flux that is physically relevant, so that the flux is arbitrary up to the curl of a vector function. 154

gauge symmetry A gauge symmetry arises from a redundancy in the mathematical description of a physical system. In fluid mechanics, there is a gauge symmetry associated with the ability to add a constant to the streamfunction in a horizontally non-divergent flow, with the constant not affecting the velocity field. For three dimensional non-divergent flow, the vector streamfunction is arbitrary up to the gradient of a scalar, with the details of this scalar irrelevant to the physics of the fluid flow. We also encounter gauge symmetries when defining the flux of a scalar field. Since the convergence of the flux affects time changes to the scalar, the flux is arbitrary up to the curl of a scalar. The presence of gauge symmetries affords us some freedom to choose a particular gauge to suite our subjective needs, with the choice not altering the objective physics. A standard reference for gauge symmetry, in the context of electromagnetism, is given in Section 27-4 in Volume II of ?. 150

generalized Lagrangian mean The generalized Lagrangian mean refers to a kinematic method used to decompose the flow into a Lagrangian mean plus a fluctuation relative to the mean. It is a hybrid Eulerian/Lagrangian method that introduces an Eulerian disturbance field to measure the position of a fluid particle relative to its mean position. 189, 191, 193, 194, 206

generalized vertical coordinate A generalized vertical coordinate, σ , has a one-to-one invertible relation with the geopotential vertical coordinate, z , so that $\sigma = \sigma(x, y, z, t)$, and yet this coordinate is typically not orthogonal to the horizontal Cartesian coordinates. Generalized vertical coordinates are commonly used as the basis for numerical ocean and atmosphere models, and frequently used for theoretical formulations. 128, 129, 218, 243, 285, 292

Gent-McWilliams effect The general tendency for baroclinic eddies to extract potential energy from the flow and to thus relax fronts towards the horizontal. This effect from used by *Gent and McWilliams (1990)* and *Gent et al. (1995)* as the basis for the parameterization of the stirring effects from ocean geostrophic eddies. 230, 231

geophysical fluid dynamics Geophysical fluid dynamics is a branch of fluid mechanics concerned with natural fluid motion on a rotating and gravitating body such as a planet or star. ix

geophysical fluid mechanics Geophysical fluid mechanics is a branch of theoretical physics concerned with natural fluid motion on a rotating and gravitating body such as a planet or star, making use of concepts and methods from classical continuum mechanics and thermodynamics. [vii](#)

geostrophic balance The geostrophic balance is a diagnostic balance between the pressure gradient acceleration and the Coriolis acceleration. It is well maintained for the large-scale and low frequency middle to high latitude motions in the atmosphere and ocean. Geostrophic balance does not hold near the equator, since the Coriolis parameter vanishes there. [xi](#), [98](#), [183](#)

global instabilities Global fluid instabilities arise from the constructive interference of waves and so involve the solution of an eigenvalue problem to determine properties of unstable waves. At most, a necessary condition can be derived to determine whether a global instability exists. Global instabilities are also referred to as wave instabilities. [xxi](#)

Green's function The Green's function is the formal inverse of a linear differential operator. Knowledge of the Green's function allows one to write the solution to a linear differential equation as an integral, with the Green's function acting as a kernel. [131](#), [154](#), [170](#)

H-theorem Boltzmann's H-theorem is a foundational result in kinetic theory that explains how a gas evolves irreversibly toward thermodynamic equilibrium starting from time-reversible microscopic dynamics. The gas evolves irreversibly toward a state of maximum entropy, even though the underlying microscopic dynamics are time-reversible. [139](#)

haline contraction coefficient The haline expansion coefficient is a response function that measures the relative change in density as the salinity is altered while holding the pressure and temperature. It is typically positive, so that density increases as salinity increases. [257](#)

Hamilton's principle Hamilton's principle of stationary action is a variational method used to derive the equations of motion for a non-dissipative dynamical system, with the corresponding differential equations of motion known as the Euler-Lagrange equations. In classical mechanics, Hamilton's principle results in the same equations as Newton's second law. However, Hamilton's principle has widespread use beyond classical mechanics, making it part of most theories of physics. [137](#)

Heaviside step function The Heaviside step function, $\mathcal{H}(x)$, also known as the unit step function, is a discontinuous non-dimensional mathematical function that outputs 0 for negative input values and unity for positive input values. It takes values $\mathcal{H}(\tau) = 0$ for $\tau < 0$ and $\mathcal{H}(\tau) = 1$ for $\tau > 0$. The derivative of a Heaviside step function is the Dirac delta: $d\mathcal{H}/dx = \delta(x)$. Note that we do not define the Heaviside at $x = 0$, though some authors give it a value of $\mathcal{H}(0) = 1/2$. For our purposes, the properties of the Heaviside step function remain unchanged whether it is defined at $x = 0$ or not. See footnote on page 20 of [?](#) for more details. [329](#)

horizontal diffusion Horizontal diffusion is based on a diffusion tensor that yields diffusive fluxes oriented along geopotential (horizontal) surfaces. [132](#)

hydrodynamics A branch of fluid mechanics concerned with the flow of a homogeneous (constant density) incompressible fluid. [vii](#)

hydrostatic balance The hydrostatic balance is a diagnostic balance between the vertical pressure gradient force and the weight of fluid. The exact hydrostatic balance holds for a static fluid in a gravity field. The approximate hydrostatic balance holds quite well for moving fluids with scales of motion such that the vertical scales are far smaller than the horizontal scales. [xi](#)

hyperbolic partial differential equation A hyperbolic partial differential equation a second order PDE whose solutions have finite propagation speed, can exhibit oscillations, and typically require initial conditions in time. Disturbances propagate with finite speed along characteristic curves (or surfaces). [339](#)

ideal impermeability theorem In the context of potential vorticity, the impermeability theorem is a kinematic result that says that the potential vorticity flux does not penetrate the isosurface of the scalar field used to define the potential vorticity. For example, if potential vorticity is defined by buoyancy, then the potential vorticity flux does not penetrate a buoyancy surface. This result holds even in the presence of irreversible processes, and it follows from kinematics. [81](#)

impulse response function The impulse response function is the response of a dynamical system to unit impulse. If the dynamical system is linear, then the impulse response function equals to the Green's function for the initial value problem. [182](#)

information entropy Information entropy is used in statistical physics as a measure of the order/disorder of a probability distribution. It is proportional to the expectation value of the $\ln p$, where p is the probability density. It was originally introduced by [Boltzmann \(1966\)](#) in his proof of the H-theorem for kinetic theory of gases, and then by [?](#) for information theory and [?](#) for statistical mechanics. [139](#)

integral curve An integral curve is defined so that a given vector field is tangent to each point along the curve. For example, fluid particle trajectories are integral curves for the fluid velocity field. [193](#), [195](#)

internal energy Internal energy refers to the energy of microscopic (molecular) degrees of freedom that are not explicitly resolved when working within the continuum approximation. Internal energy is not readily accessed nor harnessed, which contrasts to the mechanical energy of macroscopic motion. [369](#)

irreversible process A physical process that results in the increase of entropy. Processes that increase the entropy of a fluid particle include the mixing of momentum such as through viscous friction; the mixing of matter such as through the diffusion of constituents in a multi-component fluid; and the mixing of enthalpy (diffusion of heat) in a fluid with variable temperature. [vii](#)

isopycnal An isopycnal is a surface of constant potential density, which serves also as a surface of constant globally referenced Archimedean buoyancy. [189](#)

kinematic boundary condition The kinematic boundary conditions arise from the kinematic constraints on fluid motion when encountering a boundary. The simplest kinematic boundary condition is the no-normal flow, in which $\mathbf{n} \cdot \mathbf{v} = 0$ for flow encountering a static and material boundary, such as the solid-earth, with $\hat{\mathbf{n}}$ the outward normal. When

the boundary is material and yet moves, then $\mathbf{n} \cdot (\mathbf{v} - \mathbf{v}^{(b)}) = 0$, where $\mathbf{v}^{(b)}$ is the velocity of a point attached to the moving boundary. When the surface allows for fluid to cross, then the kinematic boundary condition is written $\rho(\mathbf{v} - \mathbf{v}^{(b)}) \cdot \hat{\mathbf{n}} = -Q_m$, where Q_m is the mass per time per area crossing the surface. If the boundary is the ocean surface, and the boundary is a monotonic function of vertical, then we can write the surface ocean kinematic boundary condition as $w + \rho^{-1} Q_m = (\partial_t + \mathbf{u} \cdot \nabla) \eta$, where $z = \eta(x, y, t)$ is the vertical position of the ocean free surface, and Q_m is the mass per time per horizontal area of fluid crossing the boundary. 31, 33, 57, 266, 282, 306, 311, 322, 326

kinematic method In water mass transformation theory, there are two complementary means to view interior water mass transformation: the *process method* and the *kinematic method*. The two methods are mathematically identical and so they offer two means to compute the same transformation. The kinematic method tells us *how* transformation happens, whereas we make use of the process to help understand *why* transformation happens. 301

kinetic energy Kinetic energy of a fluid is a dynamical property arising from the macroscopic motion of the fluid. The kinetic energy for a fluid element of mass $\rho \delta V$ is given by $\frac{1}{2} \mathbf{v} \cdot \mathbf{v} \rho \delta V$, where \mathbf{v} is the fluid velocity. 369

kinetic stress tensor The kinetic stress tensor is a stress acting on an Eulerian region due to the transport of momentum across the boundary of that region, $\mathbb{T}^{\text{kinetic}} = -\rho \mathbf{v} \otimes \mathbf{v}$. In components, we have $(\mathbf{v} \otimes \mathbf{v})^{ab} = v^a v^b$. 91

Kronecker delta The Kronecker delta symbol, δ_{ab} , equals to unity if the indices $a = b$ and zero otherwise. The Kronecker delta is the Cartesian coordinate representation of the metric for Euclidean space using Cartesian coordinates. 128

Lagrangian mean A Lagrangian mean refers to any averaging operation taking place at a fixed point in material space so that it is computed within the Lagrangian reference frame. 191

Lagrangian reference frame A Lagrangian reference frame is defined by motion of material fluid particles; i.e., it is a reference frame that is comoving with the continuum of fluid particles (*a*-space). The mechanical description aims to determine the continuum of trajectories, with each trajectory delineated by a continuous material coordinate that labels each fluid particle. The Lagrangian reference frame is non-inertial since fluid particles generally experience accelerations via changes to their speed and/or direction. 288

Langevin equation The Langevin equation is a stochastic differential equation that describes the position of a Brownian particle. The two forces acting on the particle are the viscous damping from the liquid, and the random noise forcing from molecular impulses. 116

Laplace-Beltrami operator The Laplace-Beltrami operator is the Laplacian written using arbitrary coordinates. It is written $\}^{-1} \partial_{\overline{m}} (\} g^{\overline{m}\overline{n}} \partial_{\overline{n}} C$, where $\}$ is the square root of the determinant of the metric tensor written using the $\xi^{\overline{m}}$ coordinates. 131

Leibniz-Reynolds transport theorem The Leibniz-Reynolds transport theorem provides the means to take the time derivative of an integrated fluid property, thus providing the basis for all finite-volume budgets within fluid mechanics. It serves to link the weak form (integral budgets) and strong form (differential budgets) of fluid mechanics. 157, 308, 319, 323

local instabilities Local fluid instabilities are afforded a local necessary and sufficient condition to determine whether the fluid base state is unstable to perturbations. Gravitational instability provides the canonical example, along with centrifugal and symmetric instabilities. Local instabilities are also referred to as parcel instabilities. [xxi](#)

local steric sealevel change The local steric sea level change refers to the depth integral of a local time derivative of the *in situ* density, thus providing a means to determine how local changes to density affect changes to sea level. There are a variety of expressions for the local steric change, with details provided by [Griffies and Greatbatch \(2012\)](#), [Griffies et al. \(2014\)](#). A common expression is given by $(\partial\eta/\partial t)_{\text{steric}} = -\rho(\eta)^{-1} \int_{\eta_b}^{\eta} \partial\rho/\partial t \, dz \approx -\rho_0^{-1} \int_{\eta_b}^{\eta} \partial\rho/\partial t \, dz$. [283](#)

locally referenced potential density The locally referenced potential density is numerically equal to the *in situ* density at each point in the fluid. However, when computing spatial gradients, we hold the pressure fixed so that the gradient only probes changes in salinity and temperature. The locally referenced potential density is used for computing gravitational stability and neutral directions. [263](#)

Markov processes A discrete time stochastic process is Markov if its future depends on the present state but not on the past. Diffusion is the continuum limit of a discrete Markov process. [112](#)

mass distribution function In the context of water mass transformation theory, the mass distribution function refers to the distribution of fluid mass as a function of water mass coordinates. [293](#)

material coordinate A material coordinate (also Lagrangian coordinate) provides continuum of markers that distinguish fluid particles. These coordinates are used in the Lagrangian or material reference frame. There is a one-to-one relation between material coordinates and Eulerian coordinates, thus providing an invertible mapping between the Eulerian and Lagrangian reference frames. [195](#)

material invariant The Lagrangian (material) time derivative vanishes for a property that is a material invariant. [146](#)

material tracers Fluids generally contain multiple matter constituents, and we refer to such matter constituents as material tracers, with examples being salinity and freshwater in the ocean, oxygen, nitrogen, and water vapor in the atmosphere. We measure the concentration of matter within a fluid element as the ratio of the mass of matter constituent to the mass of all constituents within the sample. The tracer concentration satisfies the tracer equation. [141](#)

metric A metric tensor is a symmetric second order tensor that provides the means to measure the distance between two points in space. The Kronecker delta is the Cartesian coordinate representation of the Euclidean space metric tensor. When working with alternative coordinates (e.g., spherical, generalized vertical coordinates), the coordinate representation becomes less trivial. [128](#)

mixing Mixing is the process whereby fluid elements irreversibly exchange properties. Mixing in geophysical fluids is affected by molecular diffusion, and its efficiency is enhanced

through turbulent processes such as breaking waves and stirring by large scale eddies. Mixing is commonly parameterized by downgradient diffusion with an eddy diffusivity, though not all mixing processes are downgradient. 143, 146

mixing length The mixing length is a notion introduced by ? that estimates the length scale associated with turbulent diffusive transport. It is generally much larger than the molecular mean free path. Determination of turbulent length and velocity scales is subject to large uncertainties and variations given the multiple regimes of turbulence exhibited by geophysical flows. 122

modified mean The modified mean refers to the generalized Lagrangian mean of a field, with the particle displacement tracking only the vertical position. The modified mean appears in the study of isopycnal averaging used to describe turbulent motions in a perfect stratified fluid. 207

molecular diffusion Diffusion is the physical process by which a field, such as a tracer, spreads in space over time due to random motion. Molecular diffusion arises from molecular chaos. The net flux moves from regions of higher concentration to regions of lower. 109, 111, 146, 223

momentum based viewpoint Determining the forces, either directly or indirectly, provides physical insight into the cause of fluid flow and its changes. This approach is referred to a momentum based viewpoint since it is based on working directly with the momentum equation (i.e., Newton's second law of motion). This viewpoint is distinct from a vorticity viewpoint whereby the primary concern is with terms contributing to the evolution of vorticity. x

Montgomery potential The Montgomery potential, $M = \varphi - bz$, satisfies the buoyancy coordinate form of the hydrostatic balance. The Montgomery potential plays a role for isopycnal coordinates that is directly analogous to pressure in geopotential coordinates. Correspondingly, the Montgomery potential is the geostrophic streamfunction in buoyancy coordinates. 72

motion field The motion field, φ , is the mathematical object (or a “machine” using the language of ?) that generates a nonlinear time dependent and invertible flow map that continuously and smoothly reshapes the continuum as it moves through Euclidean space as time evolves. The motion field is the reason there is a flow map, so that the nomenclature “motion field” and “flow map” are used interchangeably in this book. Both refer to movement of the continuum as time progresses. 193, 365

musical nomenclature The musical nomenclature is sometimes used for distinguishing the representation of second order tensors. The natural representation of a second order tensor occurs with one tensor index upstairs and the other downstairs. The natural representation is sometimes denoted by (1, 1), to indicate the number of indices up and down. The sharp representation, or (2, 0) representation, is when the tensor is represented with both indices upstairs. Finally, the flat representation or (0, 2) representation is where both indices are downstairs. 129

natural boundary condition Natural boundary conditions arise in the context of formulating the diffusion operator as the functional derivative of the dissipation functional, in which case the natural boundary condition is the Neumann (flux) boundary condition. 136

natural representation The natural representation refers to the $(1, 1)$ representation of second order tensors. For example, the natural representation of the diffusion tensor is $\mathbf{K} = K^m{}_n \mathbf{e}^n \otimes \mathbf{e}_m$. [129](#)

Neumann boundary condition The Neumann boundary condition prescribes the normal derivative of a function along the boundary. For tracers, the Neumann boundary condition is often referred to as the flux boundary condition since by prescribing the normal derivative we prescribe the flux. [136](#), [141](#), [172](#)

neutral diffusion Neutral (also epineutral) diffusion is based on a diffusion tensor that yields diffusive fluxes oriented along neutral directions. It is also known as neutral diffusion. It parameterizes irreversible mixing of tracers along local neutral directions. Neutral diffusion is a refinement of isopycnal diffusion, motivated by the fact that potential density surfaces are not exactly neutral in a compressible, thermally expanding, and saline fluid like seawater. [132](#), [225](#), [238](#), [258](#), [260](#), [261](#)

neutral directions A neutral direction is a direction along which movement of a test fluid element leaves its local Archimedean buoyancy zero (i.e., where the test fluid element retains the same *in situ* density as the local environment), are directions where the fluid element remains neutrally buoyant. These directions are referred to as neutral directions. In effect, the test fluid element floats along a neutral direction. [223](#), [226](#), [238](#), [316](#)

neutral tangent plane A neutral tangent plane is a plane that sits tangent to a neutral direction at each point in the ocean. [238](#)

neutrality condition The neutrality refers to the property of neutral directions that the α and β weighted gradients of Θ and S are exactly balanced when aligned along a neutral direction. So when considering neutral directions from the perspective of the mixed test fluid element, the mixing-induced changes in Θ precisely compensate mixing-induced changes in S as per the neutrality condition, $\alpha \hat{\mathbf{t}}^\gamma \cdot \nabla \Theta = \beta \hat{\mathbf{t}}^\gamma \cdot \nabla S$, where $\hat{\mathbf{t}}^\gamma$ is the unit direction pointing along the neutral displacement. [242](#)

Newton's law of viscous friction Newton's law of viscous friction is a phenomenological constitutive relation that proposes that viscous friction within a fluid follows that for a Newtonian fluid, whereby there is a linear relationship between frictional stress and strain as realized by a constant molecular viscosity. Turbulent eddy viscosities are not constant in space and time, though they generally follow the same stress-strain mathematical form as for molecular diffusion. [111](#), [124](#)

Noether's theorem Noether's theorem states that for any symmetry of a physical system, there is a corresponding dynamical conservation law. For example, a classical particle system that exhibits Galilean symmetry maintains a constant linear momentum, constant mechanical energy, and constant angular momentum. A conservation law provides a dynamical constraint on the motion. The deduction of dynamical constraints is naturally arrived at using the methods of analytical mechanics, particularly through Hamilton's principle of stationary action. Noether's theorem is one of the most important foundational elements in 20th century mathematical physics. [334](#)

non-advection flux A non-advection flux is any flux of a scalar field that is not advective, with the canonical example being a diffusive flux. [266](#), [270](#)

non-conservative process A non-conservative process is a process that cannot be written as the convergence of a flux, but is instead written in the form of a source or sink in the budget equation for a property. 292

non-dimensionalization Non-dimensionalization is the process of removing all physical dimensions from an equation of motion, and in turn to identify a set of non-dimensional numbers that characterize a particular flow regime. xii

parabolic partial differential equation A parabolic partial differential equation a second order PDE that describes diffusive processes, in which disturbances smooth out over time but do not propagate as waves. The spatial portion of the parabolic operator is typically elliptical, so that a time independent parabolic equation reduces to an elliptic equation. 110, 131, 141

parcel instabilities Parcel instabilities are afforded a local necessary and sufficient condition to determine whether the fluid base state is unstable to perturbations. Gravitational instability provides the canonical example, along with centrifugal and symmetric instabilities. Parcel instabilities are also referred to as local instabilities. xxi

passive tracer A passive tracer is a scalar field that satisfies the tracer equation, but it has zero impact on the velocity and is thus dynamically passive. Hence, a passive tracer provides a means to probe the advective-diffusive features of the flow without modifying it. 106, 111, 131, 141, 170, 269

Peclet number The Peclet number is a non-dimensional number that measures the strength of advective transport to diffusive transport: $\text{Pe} = U L / \kappa$, where U is a characteristic velocity scale, L is a length scale, and κ is a kinematic diffusivity. 144

perfect fluid A fluid that flows in the absence of irreversible processes so that the motion is reversible and the specific entropy remains constant following a fluid particle. A perfect fluid is a continuum of infinitesimal material fluid parcels. Some authors use the term *ideal fluid*, but we eschew that term to avoid confusion with *ideal gas*. vii, 146

phase average A phase average refers to an average of a field computed over the phase of the field. This choice for an averaging operation is particularly relevant when the fluctuating field involves quasi-linear waves. 192

Phillip's layering instability The Phillip's layer instability arises from the spatial dependence of the eddy diffusivity. It explains how a vertically sheared turbulence in a stably stratified fluid can organize into horizontal layers separated by sharp density interfaces. 123, 139

planetary vorticity Planetary vorticity refers to the vorticity imparted to every fluid due to its existence in a rotating planetary reference frame. xix

Poisson's equation Poisson's equation, $\nabla^2 \Psi = \sigma$, is a linear elliptic partial differential equation where the Laplacian of a scalar function, Ψ , equals to a source term, σ . This equation arises in many contexts within geophysical fluid mechanics. 154

polarized A wave field is polarized if it has a preferred sense of rotation. 204

potential density Potential density is the density of a fluid element moved to a reference pressure, p_R , while maintaining fixed specific entropy and fixed tracer concentration. For seawater, this movement is equivalent to fixed Conservative Temperature and fixed salinity, so that $\varrho(S, \Theta) = \rho(S, \Theta, p_R)$. 289

potential enthalpy Potential enthalpy is the enthalpy of a fluid element moved to a reference pressure, p_R , while maintaining fixed specific entropy and fixed tracer concentration: $\mathcal{H}^{\text{pot}}(S, C) = \mathcal{H}(S, p_R, C)$. It is used to define the Conservative Temperature, $c_p^{\text{ref}} \Theta \equiv \mathcal{H}^{\text{pot}}(S, C) = \mathcal{H}(S, p_R, C)$. 141, 256

potential temperature Potential temperature, θ , is the temperature that a fluid element reaches after performing an adiabatic and constant concentration translation to a standard pressure. For the ocean and atmosphere, the standard pressure is generally taken as the standard surface pressure. 255, 269

potential vorticity Potential vorticity is a strategically chosen component of the vorticity vector that melds mechanics (vorticity) to thermodynamics (stratification). Material conservation properties of potential vorticity render important constraints on fluid motion, thus promoting it as a primary field in the study of geophysical fluid mechanics. xix, 269, 384

Prandtl number The Prandtl number is the ratio of the kinematic viscosity to the kinematic diffusivity. 124

process method In water mass transformation theory, the process method refers to an analysis of interior fluid processes that lead to the transformation of water across surfaces of constant water mass coordinates. Example processes for buoyancy-based water mass analysis include mixing and internal sources. In general, there are two complementary means to view interior water mass transformation: the *process method* and the *kinematic method*. The process method focuses on physical processes leading to movement of fluid across the water mass coordinate surface. The kinematic and process methods are mathematically identical and so they offer two means to compute the same transformation. The kinematic method tells us *how* transformation happens, whereas we make use of the process to help understand *why* transformation happens. 301, 302

prognostic equation A prognostic equation determines the time tendency (Eulerian evolution) of a quantity such as the temperature or velocity. Terms in the prognostic equation are referred to as time tendencies. A prognostic equation is also referred to as an evolution equation. x, xi

quasi-Stokes transport The quasi-Stokes transport refers to the eddy-driven transport arising from use of the TRM kinematic framework. 210, 218, 229

real fluid A fluid whose flow is affected by irreversible processes arising from momentum mixing (nonzero viscous friction); enthalpy mixing (nonzero diffusivity for temperature); matter mixing (nonzero diffusivity of matter constituents); and through sources such as radiation and chemical reactions. The specific entropy increases following a fluid particle moving in a real fluid. vii

reciprocity condition The reciprocity condition refers to properties of Green's functions according to their behavior when the source and field points are swapped. Green's functions for self adjoint operators, such as the Laplacian, have full symmetry under such swaps. For parabolic operators, such as the diffusion equation, reciprocity involves the adjoint Green's function and more care is needed. 171, 174

rectification Rectification occurs if oscillatory or turbulent motions produce a mean flow or other slowly varying effect through nonlinear terms in the governing equations. 83, 189

residual mean velocity The residual mean velocity is the sum of the Eulerian mean plus the eddy-induced velocity, $\mathbf{v}^\dagger = \mathbf{v} + \mathbf{v}^*$. The residual mean provides the net advective effect on tracers from eddy advection plus mean advection. 151, 226, 258

Reynolds decomposition A Reynolds decomposition is a method to decompose the flow field, Ψ , into a mean, $\bar{\Psi}$, plus a departure from the mean (an eddy), Ψ' . This decomposition satisfies the following three properties: (i) $\bar{\Psi}' = 0$ (mean of eddy vanishes); (ii) $\bar{\Psi} = \bar{\bar{\Psi}}$ (mean of mean equals mean); (iii) $\bar{A\Psi} = A\bar{\Psi}$ (mean of constant equals the constant).. 192

Reynolds stress tensor The turbulent contribution to the kinetic stress tensor is known as the Reynolds stress tensor. 91

Reynolds transport theorem The Reynolds transport theorem is the Leibniz-Reynolds transport theorem applied to a Lagrangian region. 133, 184

Robin boundary condition The Robin or mixed boundary condition combines aspects of the Neumann and Dirichlet boundary conditions by specifying the sum of the normal derivative along the boundary (like the Neumann condition), as well as the value along the boundary (like the Dirichlet condition). 172

salinity Salinity is 1000 times the mass concentration of salt within a sample of seawater. More precisely, the salinity, S , is the *Absolute Salinity*. Absolute Salinity is distinct from the *practical salinity* determined by conductivity measurements. IOC et al. (2010) provides a full accounting of the theory and practice of ocean salinity, with ? providing a summary of their interpretation within ocean models. 255, 256, 264, 287

scalar mechanics Scalar fields provide a number at each point in space and time. Scalar mechanics is the study of scalar fields, such as tracers, density, and other thermodynamical tracers. Mathematically, the advection-diffusion equation is the most prominent equation arising in scalar mechanics. 106

scale selective Scale selective refers to the property of a differential operator to act preferentially on a particular scale relative to another. This term is used most commonly in reference to Laplacian-like operators used to model molecular or turbulent diffusion, whereby small scales in the concentration field are dissipated more rapidly than large scales. 125

secondary circulation Secondary circulation is a relatively weak, typically cross-stream (transverse) circulation that accompanies a dominant primary flow, often arising from imbalances (e.g., ageostrophic flow), friction, or nonlinearities. It consists of motions in the plane perpendicular to the main flow direction. While usually much smaller in magnitude,

secondary circulations play an outsized role in transporting mass, momentum, tracers, and vorticity across flow structures. 231

self-adjoint A self-adjoint operator is a linear operator that equals to its adjoint, where adjoint is defined relative to a chosen inner product. For real matrices, the adjoint is the transpose, so that a symmetric matrix is a self-adjoint matrix. For complex operators, self-adjoint refers to Hermitian operators (such as considered in quantum mechanics). For partial differential equations, self-adjointness is determined by properties of the differential operator, the boundary conditions, and the inner product. The eigenfunctions of self-adjoint operators form a complete set over the space of functions that satisfy the same boundary conditions as the eigenfunctions. We make particular use of this property when performing an eigenfunction expansion of Green's functions. 135

sharp representation The sharp representation refers to the $(2, 0)$ representation of second order tensors. For example, the sharp representation of the diffusion tensor is $\mathbf{K} = K^{mn} \mathbf{e}_n \otimes \mathbf{e}_m$. The sharp representation follows the musical nomenclature for second order tensors, where we have sharp, flat, and natural representations. 129

sifting property The sifting property is a basic property of the Dirac delta, whereby the integral of the Dirac delta times another function yields the function evaluated at the point where the Dirac delta is singular. In one dimension, this property reads $\int_{-\infty}^{\infty} \delta(x) f(x) dx = f(0)$. 176

skew diffusion Skew diffusion is the process of transporting tracers through the convergence of skew tracer fluxes. Skew tracer fluxes result from contracting the tracer concentration gradient with the anti-symmetric skew diffusion tensor, and they differ by a total curl from the advective tracer fluxes. Hence, skew fluxes and advective fluxes have the same convergence, so that the skew diffusion process and the advection process affect the same time tendency on a tracer. 152, 225, 261

skew tracer flux The skew tracer flux, $-\nabla C \times \rho \Psi^*$, has a convergence equal to that of the advective tracer flux, $\rho C \mathbf{v}$, with $\mathbf{v} = \nabla \times \Psi^*$. The skew tracer flux is neither upgradient nor downgradient. Rather, it is oriented parallel to isosurfaces of tracer concentration. In some contexts, such as when studying the effects from mesoscale eddies, it can be more convenient to focus on the skew flux than the advective flux. 151, 152

skew-symmetric tensor A skew-symmetric (also anti-symmetric) tensor equals to minus its transpose, $\mathbf{A} = -\mathbf{A}^T$. 225

skewson Skewson is any process that leads to tracer transport via skew fluxes, with skew diffusion a particular example. It is a stylized name that emphasizes its connection to advection. 153

Soret effect The Soret effect is the diffusion of matter due to a temperature gradient. 111, 257

specific thickness The specific thickness is the partial derivative, $\partial s / \partial z$, of the generalized vertical coordinate, $s(x, y, z, t)$, with respect to the vertical. It provides the Jacobian of transformation between z -coordinates and generalized vertical coordinates. 208

steric Steric effects generally refer to properties of a substance associated with the space occupied by atoms. In the sea level context, steric effects refer to changes in sea level

associated with density changes, with changes in density associated with changes in the volume occupied by seawater molecules. Changes in global mean sea level arising from changes in the global mean density are called global steric sealevel changes. 275

steric sea level The steric sea level is the thickness of a fluid layer bounded below by an isobar and above by the sea surface. It is commonly used for ocean circulation studies to map geostrophic flows. The dynamic topography is also referred to as the ocean dynamic topography. 275

stirring Stirring is the tracer transport process affected by advection. Stirring generally acts to reversibly rearrange fluid elements and to increase tracer gradients, particularly when the flow is turbulent. By increasing gradients, and thus increasing the surface area of tracer contours, stirring enhances the ability of molecular diffusion to affect irreversible mixing that acts to dissipate gradients. 143

Stokes drift The Stokes drift refers to the Stokes mean velocity, which is the difference between the Lagrangian mean velocity and the Eulerian mean velocity. 83, 193, 198

Stokes mean The Lagrangian mean (mean computed on fluid elements) minus the Eulerian mean (mean computed at a fixed point) defines the Stokes mean. Note that the literature sometimes refers to the Stokes mean as the “Stokes correction”. We avoid that terminology in order to avoid the spurious notion that one type of mean operator is more correct than the other. Instead, a mean operator is subjectively chosen based on its suitability to a particular question. 193

Stokes' theorem The vector calculus form of Stokes' theorem says that for a simply connected surface, $\oint_{\partial\Omega} \mathbf{A} \cdot d\mathbf{x} = \int_{\Omega} (\nabla \times \mathbf{A}) \cdot \hat{\mathbf{n}} dS$, where \mathbf{A} is a vector, Ω is a simply connected surface with boundary $\partial\Omega$, $d\mathbf{x}$ is a line increment around the boundary, and $\hat{\mathbf{n}}$ is an outward normal to the surface and which defines the orientation. 27

storage term In the analysis of budgets, we sometimes refer to time tendency terms as the storage term, which contrasts to fluxes crossing boundaries of the budget region. 307

strain rate tensor The strain rate tensor, \mathbf{S} , is the symmetric portion of the velocity gradient tensor. The strain rate tensor measures the ability of fluid flow to deform fluid elements through stretching, straining, and dilation. 150

stress tensor The stress tensor is a second order tensor that organizes the stresses acting within a fluid. The stress tensor components have dimension of force per unit area, and each component is oriented by both the direction of the stress and the outward normal of the surface on which the stress acts. 124

subgrid scale Subgrid scale (SGS) refers to processes happening at scales smaller than the grid (length) scale of either a numerical model or field measurement. The parameterization of subgrid scale process remains an active area of ocean and atmospheric physics, given the importance of such processes for the large scale circulation. 221, 258

surface transformation That portion of water mass transformation theory concerned with how surface boundary fluxes contribute to water mass transformation. Surface transformation theory forms the focus of many studies of water mass transformation because it only requires surface boundary information, which is generally more accessible than information

from interior ocean mixing processes or bottom geothermal processes. Furthermore, much of the transformation of water occurs in surface regions since this region is home to large contributions from surface boundary fluxes and associated ocean mixing. 315

Sverdrup balance The Sverdrup balance is a diagnostic balance between vertically integrated meridional transport and the wind stress curl. In particular, a positive wind stress curl leads to northward vertically integrated flow. This balance helps to explain the steady equatorward ocean circulation appearing in the eastern portion of middle latitude gyres. xi

thermal expansion coefficient The thermal expansion coefficient is a response function that measures minus the relative change in density as the temperature is altered while holding the pressure and matter concentration fixed. It is typically positive, so that density decreases as temperature increases. Freshwater near its freezing point is an important counterexample, where the negative thermal expansion coefficient allows for solid ice to float on liquid water. 257

thermobaricity Thermobaricity is a physical process that results in density changes due to the pressure dependence of the ratio of the thermal expansion coefficient to the haline contraction coefficient. 260–263, 280

thermodynamic equilibrium In our study of equilibrium thermodynamics, we are concerned with macroscopic fluid systems whose evolution tends toward states whose properties are determined by intrinsic factors rather than depending on memory of previous external influences. These particular macrostates are known as thermodynamic equilibria. At a basic level, a system in thermodynamic equilibrium could remain in that state for all time, with details of the equilibrium dependent on the constraints imposed on the system. When constraints are removed, then a system generally transitions to another thermodynamic equilibria. Note that “for all time” is a loaded term. More precisely, we mean “for a time extremely long compared to any time scale relevant to the physical system under consideration”. 109

thermosteric The temperature component of steric sea level change is referred to as the thermosteric sea level. For global mean sea level, thermosteric effects dominate over halosteric effects, with global halosteric effects negligible. Locally, however, thermosteric and halosteric effects can be sizable. 275

thickness weighted averaging Thickness weighted averaging refers to the use of a layer thickness when performing a low pass filter average for dynamical fields. It is commonly used for shallow water models and isentropic vertical coordinate models. 3, 69, 81, 208

time tendency Those terms in a prognostic Eulerian equation that contribute to the time evolution are referred to as time tendencies. For prognostic equations, knowledge of the processes contributing to the net time tendency enables a prediction of flow properties. x

tracer equation The tracer equation is a partial differential equation describing the evolution of tracer fields, such as material tracers and thermodynamic tracers (potential enthalpy). Tracers are intensive scalar fluid properties that evolve through advection (in an Eulerian description), diffusion, and source/sinks. 54

traditional approximation The traditional approximation comprises three approximations that come as a package in order to maintain physical consistency. (A) It sets to zero the Coriolis terms in the horizontal momentum equations that involve the vertical velocity, thus retaining only the local vertical component of the earth's angular rotation vector. (B) It drops the metric terms, uw/r and vw/r , associated with the vertical velocity as they appear in the horizontal momentum equations. (C) The shallow fluid approximation and both parts of the traditional approximation must be taken together in order to maintain a consistent energy and angular momentum conservation principle for the resulting equations. 60

transformation In the context of water mass analysis, transformation refers to the process of moving water across surfaces defined by water mass coordinates. For example, with water mass configuration space defined by surfaces of constant Conservative Temperature, Θ , then when water moves across Θ surfaces we say that the water has been transformed. Processes leading to transformation arise from mixing, solar radiation, and chemical reactions. Correspondingly, we measure zero motion along a water mass coordinate axis when the property defining that axis remains materially unchanged. For example, adiabatic and isohaline processes such as linear waves can render nontrivial motion in geographical/depth space whereas they lead to no motion in (S, Θ) space. 288–290

transformed residual mean The transformed residual mean is the Eulerian mean field that when evaluated at the mean vertical position of an isopycnal is equal to the isopycnal thickness weighted average of the field. 209

turbulence closure When we measure fluid motions in the laboratory or field, we generally do not measure the motions at scales on the order of $L_{\text{macro}} \approx 10^{-4}$ m. That is, our measurement devices generally have a spatial resolution coarser than L_{macro} , so that $L_{\text{measure}} \gg L_{\text{macro}}$. Likewise, numerical simulations are generally designed using discrete grids with length scales $L_{\text{numerical}} \gg L_{\text{macro}}$. The equations describing motions at the measurement/simulation length scales involve effects from fluctuations occurring at the smaller (unmeasured) scales. The reason for this coupling is that the fluid equations are nonlinear, and with the nonlinearities leading to an interaction across spatial scales. These fluctuations, generally associated with turbulent or chaotic motions, have statistical correlations that can play a role, sometimes a dominant role, in the evolution of flow features at the measured/simulated scales. The parameterization of these correlations in terms of measured/simulated motions constitutes the turbulence closure problem. 194

turbulent diffusion Diffusion is the physical process by which a field, such as a tracer, spreads in space over time due to random motion. Turbulent diffusion arises from random motion within a turbulent flow. The net flux moves from regions of higher concentration to regions of lower. The efficiency for diffusive transport in a turbulent fluid is many orders higher than that from molecular diffusion. Chapter 13 in [Vallis \(2017\)](#) provides a pedagogical discussion of turbulent diffusion in geophysical flows. 119

turbulent flow Turbulent flow is characterized by a quasi-random fluid flow that supports an enhanced amount of mixing and transport of fluid properties. Geophysical fluid flows are predominantly turbulent across multiple scales. 119

turbulent velocity scale The turbulent velocity scale is a measure of the velocity of random turbulent motion that leads to turbulent diffusion. The turbulent velocity scale is much

smaller than molecular speeds. Determination of turbulent length and velocity scales is subject to large uncertainties and variations given the multiple regimes of turbulence exhibited by geophysical flows. As a result, tracer transport by turbulent flows has remained a topic of much research since the early 20th century. [123](#)

vector invariant The vector-invariant form of the velocity equation is based on replacing the material time derivative with the vorticity and kinetic energy, through use of the identity $(\mathbf{v} \cdot \nabla)\mathbf{v} = \boldsymbol{\omega} \times \mathbf{v} + \nabla(\mathbf{v} \cdot \mathbf{v})/2$, where $\boldsymbol{\omega} = \nabla \times \mathbf{v}$. [59](#)

velocity gradient tensor The velocity gradient tensor, \mathbf{G} , is the Eulerian means to quantify flow deformation. Its elements are the spatial derivatives of the velocity field. It is commonly decomposed into the symmetric strain rate tensor (also known as the deformation rate tensor) plus the anti-symmetric rotation tensor. [149](#)

vertical gauge The vertical gauge refers to the choice to set to zero the third component of the vector streamfunction, whose curl yields a non-divergent transport velocity. The vertical gauge is commonly used for parameterized eddy-induced velocities. [155](#)

vorticity Vorticity is the curl of the velocity, $\boldsymbol{\omega} = \nabla \times \mathbf{v}$. It plays a leading role in the study of geophysical fluid flows, where it is important to distinguish the relative vorticity, $\boldsymbol{\omega} = \nabla \times \mathbf{v}$, from the planetary vorticity, $2\boldsymbol{\Omega}$. [xix](#), [25](#)

vorticity based viewpoint A variety of vorticity constraints offer the means to deduce flow properties without determining forces, thus prompting the **vorticity based viewpoint** that is distinct from the momentum-based approach, thus prompting the importance of vortex mechanics in geophysical fluid mechanics. [x](#), [419](#)

Walin analysis Walin analysis is another name for water mass transformation theory, which focuses on mass distribution functions and follows the methods introduced by [Walin \(1977\)](#) and [Walin \(1982\)](#). [298](#)

water mass In ocean physics, a water mass refers to a region of seawater characterized by a suite of physical properties. Water masses often originate through extremely large buoyancy fluxes at the high latitudes that form waters such as the Antarctic Bottom Water and North Atlantic Deep Water. As these waters enter the ocean interior they are transported over basin scales while they are eroded or transformed by irreversible mixing or sources. Water masses and their properties offer a conceptual means to partition or bin the fluid into distinct classes whose origin, movement, and transformation can be measured, modeled, and studied. Scalar properties generally used to classify water masses are simpler to measure than vector properties such as velocity. Hence, a water mass perspective offers the means to infer ocean circulation within the space of ocean properties without directly measuring vector fields. [285](#)

water mass configuration space Water mass configuration space (denoted by \mathbf{q} -space) is the space we work within to study water mass transformations. This space has some or all of its coordinates set by properties other than geographic/depth coordinates. Operationally, we fill \mathbf{q} -space by forming histograms that result in a \mathbf{q} -space distribution of the fluid properties. For example, a one-dimensional \mathbf{q} -space results from binning the ocean according to potential density, whereas retaining latitudinal information along with

potential density renders a two-dimensional \mathbf{q} -space. Typically \mathbf{q} -space has three or fewer dimensions, given the three dimensionality of \mathbf{x} -space. There is no implied constraint that any of the \mathbf{q} -space coordinates are monotonic with respect to \mathbf{x} -space. Indeed, there is no presumption that points in \mathbf{q} -space maintain a 1-to-1 relation to points in \mathbf{x} -space. For example, many points in \mathbf{x} -space may fall into a single point (or bin) within \mathbf{q} -space. 287

water mass transformation Water mass transformation theory examines the budgets for fluid mass and tracer mass within layers or classes defined by properties such as Archimedean buoyancy, Conservative Temperature, salinity, or biogeochemical tracers. The theory is concerned with how processes affect the evolution of fluid within property space and in the characterization of circulation inferred from this evolution. This kinematic lens is distinct from the Eulerian and Lagrangian kinematics, with particular use for examining questions where the irreversible transformation of properties plays a central role. The theory originates from the work of [Walin \(1977\)](#) and [Walin \(1982\)](#), and it has found many advances in both formalism and application since then (see [Groeskamp et al. \(2019\)](#) for a review). 285, 287, 298

wave instabilities Wave instabilities arise from the constructive interference of waves and so involve the solution of an eigenvalue problem to determine properties of unstable waves. At most, a necessary condition can be derived to determine whether a wave instability exists. Wave instabilities are also referred to as global instabilities. xxi

zonal mean The zonal mean refers to a spatial averaging operation computed by a line integral of a field over the full longitudinal extent of the domain, and then a division by the zonal length of the domain. The zonal mean is particularly relevant for regions that are zonally periodic, such as the atmosphere and the ocean in the latitudes around the Drake Passage. Notably, the resulting zonally averaged field is independent of longitude. 192

Appendix B

LIST OF ACRONYMS

AI artificial intelligence xvii

GFD geophysical fluid dynamics ix

GFM geophysical fluid mechanics vii, 190

GLM generalized Lagrangian mean 189, 193, 194

GVC generalized vertical coordinate xx, 2, 5–7, 10–12, 14, 16, 21–23, 28, 31, 36

TRM transformed residual mean 209

TWA thickness weighted average 3, 69, 70, 81–83, 86, 89–92, 97, 98, 100, 208

Appendix C

LIST OF SYMBOLS

Many symbols encountered in this book are defined local to their usage and are not used far outside of that location. Many other symbols appear in a variety of places and are included in the tables given below. Additionally, we generally aim to respect the following conventions.

- Many symbols are adorned with extra labels. One usage exposes tensor indices, with tensor indices written using the slanted math font, such as F^i for the component i of the vector \mathbf{F} . Another usage expresses part of the name for the symbol, with the label written with the upright sans serif. Examples include the “ b ” in η_b for the position of the bottom solid boundary of a fluid domain, and the “ h ” in ∇_h for the horizontal gradient operator.
- We strive for unique symbols to represent distinct mathematical and/or physical objects. Yet that goal must confront the multitude of mathematical expressions appearing in this book. We have chosen, on rare occasions, to allow some symbols to carry multiple meanings. In such cases we emphasize the particular meaning of the symbol to help avoid confusion with its alternative meaning.

NON-DIMENSIONAL NUMBERS

SYMBOL	NAME	MEANING
Bu	Burger	$Bu = (\text{deformation radius}/\text{horizontal length scale of flow})^2 = (L_d/L)^2$
Db	Deborah	$Db = \text{relaxation time}/\text{observation time}$
Ek	Ekman	$Ek = \text{vertical frictional acceleration}/\text{planetary Coriolis acceleration}$
Fr	Froude	$Fr = \text{fluid particle speed}/\text{fluid wave speed} = U/c$
Ge	Geostrophic	$Ge = \text{horizontal accelerations from Coriolis}/\text{pressure acceleration} = f U L \rho_a/p$
Kn	Knudsen	$Kn = \text{molecular mean free path}/\text{macroscopic length scale}$
Ma	Mach	$Ma = \text{fluid particle speed}/\text{sound wave speed} = U/c_s$
Pr	Prandtl	$Pr = \text{viscosity}/\text{diffusivity} = \mu/\kappa$
Pe	Peclet	$Pe = \text{advective transport}/\text{diffusive transport} = U L/\kappa$
Re	Reynolds	$Re = \text{inertial acceleration}/\text{frictional acceleration} = U L/\nu$
Ri	Richardson	$Ri = \text{squared buoyancy frequency}/\text{squared vertical shear}$
Ro	Rossby	$Ro = \text{horizontal inertial acceleration}/\text{planetary Coriolis acceleration} = U/(f L)$

SYMBOL	MEANING
\mathcal{A}	wave action
$A^L(\mathbf{a}, T)$	Lagrangian representation of a fluid property as a function of material coordinates and time
\mathbf{a}	coordinate position for a fluid particle using arbitrary material/Lagrangian coordinates
\mathbf{A}, \mathbf{A}	second order skew symmetric tensor with elements satisfying $A^{mn} = -A^{nm}$
A^v	Avogadro's number: $A^v = 6.0222 \times 10^{23}$ mole $^{-1}$
\mathbf{B}	baroclinicity vector: $\mathbf{B} = \nabla \rho \times (-\rho^{-1} \nabla p) = (\nabla \rho \times \nabla p)/\rho^2$
\mathcal{B}	base (or reference) manifold for describing the space of continuum matter
b	Archimidean buoyancy with $b > 0$ for relatively light fluid: $b = -g(\rho - \rho_0)/\rho$
C	tracer concentration = mass of tracer per mass of fluid = tracer mass fraction
C_d	dimensionless bottom drag coefficient: $C_d > 0$
\mathcal{C}	circulation of velocity around the boundary of a surface $\mathcal{C} \equiv \oint_{\partial \mathcal{S}} \mathbf{v} \cdot d\mathbf{r}$
c_{grav}	shallow water gravity wave speed: $c_{\text{grav}} = \sqrt{g H}$
\mathbf{c}_g	wave group velocity, given by wavevector gradient of dispersion relation: $\mathbf{c}_g = \nabla_{\mathbf{k}} \varpi(\mathbf{k})$
c_p	wave phase velocity: $\mathbf{c}_p = C_p \hat{\mathbf{k}}$
C_p	wave phase speed
c_s	sound speed: $c_s^{-2} = [\partial \rho / \partial p]_{\Theta, S}$
c_p	heat capacity at constant pressure: $c_p = [\partial \mathcal{H} / \partial T]_{p, C}$
\mathbf{E}, \mathbf{E}	second order eddy transport tensor for tracers, and with elements E^{mn}
$\mathbb{E}^1, \mathbb{E}^2, \mathbb{E}^3$	one (line), two (plane), and three dimensional Euclidean space
\mathcal{E}	total energy per mass of a fluid element = sum of internal plus mechanical energies
\mathbf{e}_a	basis vectors for a chosen coordinate system, with index $a = 1, 2, 3$ for 3-dimensional space
e^a	basis one-forms for a chosen coordinate system, with index $a = 1, 2, 3$ for 3-dimensional space
f	Coriolis parameter, also the planetary vorticity: $f = 2\Omega \sin \phi$
f_0	Coriolis parameter at a particular latitude: $f_0 = 2\Omega \sin \phi_0$
\mathbf{F}	frictional acceleration vector
$F^i{}_I$	deformation matrix, which transforms between \mathbf{x} -space (Eulerian) and \mathbf{a} -space (Lagrangian)
G	water mass transformation, with dimensions of mass per time
$G = G^{\text{grav}}$	Newton's gravitational constant: $G = 6.674 \times 10^{-11} \text{ N m}^2 \text{ kg}^{-2} = 6.674 \times 10^{-11} \text{ m}^3 \text{ kg}^{-1} \text{ s}^{-2}$
$G(\mathbf{x} \mathbf{x}_0)$	Green's function with \mathbf{x} the observation point (or field point) and \mathbf{x}_0 the source point
$\tilde{G}(\mathbf{x} \mathbf{x}_0)$	modified Green's function for Laplace's operator with Neumann boundary conditions
$G^\ddagger(\mathbf{x} \mathbf{x}_0)$	adjoint Green's function for non-self adjoint operators such as the diffusion operator
$\mathcal{G}(\mathbf{x} \mathbf{x}_0)$	free space Green's function; i.e., the Green's function without boundaries
\mathbf{G}	velocity gradient tensor with elements $G^i{}_j$
\mathcal{G}	Gibbs potential per mass of a fluid element
g_e	gravitational acceleration from central gravity due to just the mass of the planet
g	effective gravitational acceleration from central gravity + planetary centrifugal as evaluated at the Earth's surface: $g \approx 9.8 \text{ m s}^{-2}$

SYMBOL	MEANING
g'	reduced gravity defined between two shallow water layers: $g'_{k+1/2} = g(\rho_{k+1} - \rho_k)/\rho_{\text{ref}} \ll g$
\mathfrak{g}	metric tensor (symmetric positive definite second order tensor) with components \mathfrak{g}_{ab}
\mathfrak{g}	square root of the metric tensor determinant: $\mathfrak{g} = \sqrt{\det(\mathfrak{g}_{mn})}$
\mathfrak{g}^E	square root of the metric tensor determinant using Eulerian coordinates: $\mathfrak{g}^E = \sqrt{\det(\mathfrak{g}(\mathbf{x}))}$
\mathfrak{g}^L	square root of the metric tensor determinant using Lagrangian coordinates: $\mathfrak{g}^L = \sqrt{\det(\mathfrak{g}(\mathbf{a}, T))}$
h_k	layer thickness for a shallow water fluid: $h_k = \eta_{k-1/2} - \eta_{k+1/2} = \delta_k \eta_{k-1/2}$
h	layer thickness for a continuously stratified fluid: $h = \bar{h} \delta\sigma$
\mathfrak{h}	specific thickness for a generalized vertical coordinate: $\mathfrak{h} = \partial z / \partial \sigma = 1 / (\partial \sigma / \partial z)$
$\mathcal{H}(x)$	Heaviside step function: $\mathcal{H}(x) = 0$ for $x < 0$ whereas $\mathcal{H}(x) = 1$ for $x > 0$
H	vertical length scale of the flow under consideration
H	sometimes used as depth of the ocean bottom: $z = -H(x, y) = \eta_b(x, y)$
H	Hamiltonian energy function
\mathcal{H}	Hamiltonian density used in field theory; dimensions energy per volume (when in 3d space)
\mathcal{H}	enthalpy per mass of a fluid element
\mathbf{I}	unit tensor or Kronecker tensor: $\mathbf{I} = \delta^{ab} \mathbf{e}_a \otimes \mathbf{e}_b = \delta^a_b \mathbf{e}_a \otimes \mathbf{e}^b = \delta_a^b \mathbf{e}^a \otimes \mathbf{e}_b = \delta_{ab} \mathbf{e}^a \otimes \mathbf{e}^b$
\mathfrak{J}	internal energy per mass of a fluid element
i	$i = \sqrt{-1}$ used for imaginary numbers
i, j, k	tensor indices/labels for Eulerian coordinates
I, J, K	tensor indices/labels for Lagrangian coordinates
$\text{Im}[\cdot]$	imaginary part of a complex number; e.g., $\text{Im}[e^{-i\omega t}] = -\sin(\omega t)$
\mathbf{J}	tracer flux; for material tracers the dimensions are mass per time per area
\mathbf{k}	wavevector (dimensions inverse length) for a wave of wavelength $\Lambda = 2\pi/ \mathbf{k} $
$\hat{\mathbf{k}}$	unit vector in the direction of a wave: $\mathbf{k} = \hat{\mathbf{k}} \mathbf{k} $ (as distinct from the vertical unit vector, \hat{z})
$ \mathbf{k} $	wavenumber: $ \mathbf{k} = 2\pi/\Lambda$
K	kinetic energy for a particle of mass m : $K = m \mathbf{V} \cdot \mathbf{V}/2$
K	kinetic energy for a system of N particles, $\sum_{n=1}^N m^n \mathbf{V}^n \cdot \mathbf{V}^n$
\mathcal{K}	kinetic energy per mass of a fluid element arising from macroscopic motion: $\mathcal{K} = \mathbf{v} \cdot \mathbf{v}/2$
\mathcal{K}^{hyd}	kinetic energy per mass for an approximate hydrostatic flow: $\mathcal{K}^{\text{hyd}} = \mathbf{u} \cdot \mathbf{u}/2$
\mathcal{K}^{sw}	kinetic energy per horizontal area for a shallow water layer: $\mathcal{K}^{\text{sw}} = \rho h \mathbf{u} \cdot \mathbf{u}/2$
\mathbf{K}, \mathbf{K}	positive and symmetric second order tensor parameterizing diffusive mixing
k	integer index to label a layer in a shallow water model with $k = 1, N$ layers ($k = 1$ is top layer)
k_B	Boltzmann constant: $k_B = 1.3806 \times 10^{-23} \text{ m}^2 \text{ kg s}^{-2} \text{ K}^{-1} = R^* / A^v$
k_R	Rossby height/depth: $k_R = \mathbf{k} N / f_0$ with horizontal wavenumber $ \mathbf{k} = \sqrt{k_x^2 + k_y^2}$
L	Lagrangian used in Lagrangian mechanics: kinetic minus potential energies: $L = K - P$
L	length scale for a particular physical feature and commonly used in scale analysis

SYMBOL	MEANING
\mathcal{L}	Lagrangian density used in field theory; dimensions energy per volume (when in 3d space)
L_d	deformation radius: (a) shallow water $L_d = \sqrt{g H}/f$; (b) continuous internal $L_d = H N/f$
\mathcal{M}	mechanical energy per mass of a fluid element arising from macroscopic motion
\mathcal{M}^{sw}	mechanical energy per area of a shallow water fluid column: $\mathcal{M}^{sw} = \mathcal{K}^{sw} + \mathcal{P}^{sw}$
\mathbf{M}	moment of inertia tensor
\mathbf{M}	potential momentum vector: $\mathbf{M} = \mathbf{u} + 2\boldsymbol{\Omega} \times \mathbf{X}$
M	Montgomery potential for continuously stratified fluid $M = \varphi - bz$
M	mass, as in the mass of a fluid region, $M = \int_{\mathcal{R}} \rho dV$
M_k^{dyn}	Montgomery potential for a shallow water layer: $M_k^{dyn} = \sum_{j=0}^{k-1} g_{j+1/2}^r \eta_{j+1/2}$
M^{air}	mass per mole of air: $M^{air} = 28.8 \times 10^{-3} \text{ kg mole}^{-1}$
N	buoyancy frequency
\mathcal{O}	order of magnitude
P	potential energy of a physical system, with corresponding force $\mathbf{F} = -\nabla P$
\mathcal{P}_k^{sw}	potential energy per horizontal area for a shallow water fluid: $\mathcal{P}_k^{sw} = g \rho_k \int_{\eta_{k+1/2}}^{\eta_{k-1/2}} z dz$
\mathcal{P}	phase of a wave
\mathcal{P}_σ	generalized momentum for discrete particle system: $\mathcal{P}_\sigma = \partial L / \partial \dot{\xi}^\sigma$
\mathcal{P}	generalized momentum density for continuous media: $\mathcal{P} = \partial \mathcal{L} / \partial (\partial_t \psi)$
\mathbf{P}	linear momentum of a physical system
p	pressure at a point in the fluid
p_a	pressure applied to the ocean surface from the atmosphere or cryosphere
p_b	pressure at the bottom of a fluid column, at the fluid-solid earth interface
p_{slp}	sea level pressure with an area average, $\langle p_{slp} \rangle = 101.325 \times 10^3 \text{ N m}^{-2}$
$p_{k-1/2}$	hydrostatic pressure at the layer interface with vertical position $z = \eta_{k-1/2}$
p_k^{dyn}	dynamic pressure in a shallow water layer: $p_k^{dyn} = \rho_{ref} \sum_{j=0}^{k-1} g_{j+1/2}^r \eta_{j+1/2}$
P_k	pressure integrated over a shallow water layer: $P_k \equiv \int_{\eta_{k+1/2}}^{\eta_{k-1/2}} p_k(z) dz = h_k (g \rho_k h_k / 2 + p_{k-1/2})$
Q	potential vorticity for continuously stratified (Ertel PV) or shallow water (Rossby PV)
q	quasi-geostrophic potential vorticity either for a continuous fluid or shallow water fluid
Q_m	mass flux (mass per horizontal area per time) across ocean surface: $Q_m > 0 \text{ enters ocean}$
\mathcal{Q}_m	mass flux (mass per surface area per time) across ocean surface: $\mathcal{Q}_m dS = Q_m dA$
Q_c	turbulent tracer flux (tracer per horiz area per time) across ocean surface: $Q_c > 0 \text{ enters ocean}$
\mathcal{Q}_c	turbulent tracer flux (tracer per surface area per time) across ocean surface: $QCcal dS = Q_c dA$
r	radial distance of a point relative to an origin
\mathbf{R}	rotation tensor: $2 R^m{}_n = \partial_n v^m - \partial^m v_n = -2 R_n{}^m$
\mathbb{R}^1	real number line
\mathbb{R}^2	two-dimensional space of real numbers
\mathbb{R}^3	three-dimensional space of real numbers
R	radius of a sphere

SYMBOL	MEANING
R_e	radius of sphere whose volume approximates that of the earth: $R_e = 6.371 \times 10^6 \text{ m}$
R^g	universal gas constant: $R^g = 8.314 \text{ J mole}^{-1} \text{ K}^{-1} = 8.314 \text{ kg m}^2 \text{ s}^{-2} \text{ mole}^{-1} \text{ K}^{-1}$
R^{air}	specific gas constant for air: $R^{\text{air}} = R^g/M^{\text{air}} = 2.938 \times 10^2 \text{ m}^2 \text{ s}^{-2} \text{ K}^{-1}$
\mathcal{R}	arbitrary region or manifold
$\mathcal{R}^a{}_b$	orthogonal rotation matrix
$\text{Re}[\cdot]$	real part of a complex number; e.g., $\text{Re}[e^{-i\omega t}] = \cos(\omega t)$
\mathcal{S}	spatial manifold
\mathcal{S}	entropy per mass of a fluid element
$\mathcal{S} = \mathcal{S}^{\text{action}}$	action: time integral of the Lagrangian: $\mathcal{S} = \int_{t_A}^{t_B} L \, dt$
\mathbf{S}	strain rate tensor: $2\mathbf{S} = \nabla \mathbf{v} + (\nabla \mathbf{v})^T$
\mathbf{S}^{dev}	deviatoric strain rate tensor: $\mathbf{S}^{\text{dev}} = \mathbf{S} - S^q_q/3$
S	salt concentration = mass of salt in a fluid element per mass of seawater
S	Absolute Salinity, generically referred to as salinity: $S = 1000 \mathcal{S}$
s	expression for a generic surface: $s = s(x, y, z, t)$.
s	arc-length along a curve $\mathbf{x}(s)$ with infinitesimal increment $ds = \sqrt{d\mathbf{x} \cdot d\mathbf{x}}$
$\hat{\mathbf{s}}$	unit tangent to a curve, also written as $\hat{\mathbf{s}} = \hat{\mathbf{t}}$ (see below)
sgn	sign function related to Heaviside step function via $\text{sgn}(x) = 2\mathcal{H}(x) - 1$
T	absolute thermodynamic <i>in situ</i> temperature (Kelvin if in a thermodynamic equation)
T	time scale for a particular physical process and commonly used in scale analysis
T	time (universal Newtonian time) measured in the Lagrangian reference frame
t	time (universal Newtonian time) measured in the Eulerian reference frame
τ	general symbol for time as considered in the tensor analysis chapters
\mathbf{T}	stress tensor with natural elements $T^m{}_n$
$\mathbb{T}^{\text{kinetic}}$	kinetic stress tensor: $\mathbb{T}^{\text{kinetic}} = -\rho \mathbf{v} \otimes \mathbf{v}$
$\mathbb{T}^{\text{sw kinetic}}$	kinetic stress tensor for shallow water fluid: $\mathbb{T}^{\text{sw kinetic}} = -\rho \mathbf{u} \otimes \mathbf{u}$
$\hat{\mathbf{t}}$	unit tangent to a curve: $\hat{\mathbf{t}} = d\mathbf{x}/ds$, where s is the arc-length so that $ds = \sqrt{d\mathbf{x} \cdot d\mathbf{x}}$
\mathbf{u}	horizontal velocity of a fluid particle, with Cartesian representation: $\mathbf{u} = \hat{\mathbf{x}} u + \hat{\mathbf{y}} v$
U	horizontal velocity scale of the flow under consideration
\mathbf{U}	depth integrated horizontal velocity: $\mathbf{U} = \int_{\eta_b}^{\eta} \mathbf{u} \, dz$
V	volume, as in the volume of a fluid region, $V = \int_{\mathcal{R}} dV$
\mathbf{v}	velocity of a fluid particle: $\mathbf{v} = D\mathbf{x}/Dt$, with Cartesian components $\mathbf{v} = \hat{\mathbf{x}} u + \hat{\mathbf{y}} v + \hat{\mathbf{z}} w$
\mathbf{v}^*	eddy-induced velocity
\mathbf{v}^\dagger	residual velocity of a fluid particle: $\mathbf{v}^\dagger = \mathbf{v} + \mathbf{v}^*$
$\mathbf{v}^{(b)}$	velocity of a point on a region boundary
$\mathbf{v}^L(\mathbf{a}, T)$	Lagrangian velocity of a fluid particle so that $\mathbf{v}^L(\mathbf{a}, T) = \mathbf{v}[\mathbf{x} = \boldsymbol{\varphi}(\mathbf{a}, T), t = T]$
\mathbf{v}_I	velocity of a fluid particle measured in the inertial/absolute reference frame: $\mathbf{v}_I = \mathbf{v} + \boldsymbol{\Omega} \times \mathbf{x}$
W	vertical velocity scale of the flow under consideration
\mathcal{W}	on-shell action
w	vertical component to the velocity: $w = Dz/Dt$
w^{dia}	dia-surface flux = volume per surface area per time crossing a σ -surface: $w^{\text{dia}} = (1/ \nabla \sigma) \dot{\sigma}$
$w^{(\dot{\sigma})}$	dia-surface velocity = volume per <i>horizontal area</i> per time crossing σ -surface: $w^{(\dot{\sigma})} = \dot{\sigma} \partial z/\partial \sigma$

LATIN SYMBOLS AND THEIR MEANING

SYMBOL	MEANING
(x, y, z)	triplet of Cartesian coordinates
\mathbf{x}	spatial position as a line segment with an arrow pointing from an origin to the position of a particle
x	spatial position represented by either general coordinates or Cartesian coordinates
$\hat{\mathbf{x}}$	initial position for a fluid particle using arbitrary coordinates
$(\hat{\mathbf{x}}, \hat{\mathbf{y}}, \hat{\mathbf{z}})$	triplet of Cartesian unit vectors oriented in a righthand sense
$\mathbf{X}(t)$	position for a point particle defining a trajectory through space-time
$\mathbf{X}(\mathbf{a}, T)$	position of a material fluid particle expressed using material coordinates
z_σ	specific thickness for a generalized vertical coordinate: $z_\sigma = \partial z / \partial \sigma = h$

GREEK SYMBOLS AND THEIR MEANING

SYMBOL	MEANING
α	thermal expansion: $\alpha = -\rho^{-1} \partial \rho / \partial \theta$ or $\alpha = -\rho^{-1} \partial \rho / \partial \Theta$ or $\alpha = -\rho^{-1} \partial \rho / \partial T$
α_T	thermal expansion in terms of <i>in situ</i> temp: $\alpha = -\rho^{-1} \partial \rho / \partial T$
$\alpha^{(\Theta)}$	thermal expansion in terms of Conservative Temperature: $\alpha^{(\Theta)} = -\rho^{-1} \partial \rho / \partial \Theta$
α_{aspect}	aspect ratio; ratio of vertical to horizontal scales of the flow: $\alpha_{\text{aspect}} = H/L$
$\beta, \beta^{(S)}$	haline (saline) contraction coefficient: $\beta = \beta^{(S)} = \rho^{-1} \partial \rho / \partial S$
β	meridional derivative of planetary vorticity: $\beta = \partial_y f$
$\hat{\gamma}$	dianeutral unit direction perpendicular to the neutral tangent plane
δ_{ab}	Kronecker delta, which is the metric for Euclidean space with Cartesian coordinates
δ_b^a	components to the Kronecker tensor in arbitrary coordinates
ϵ	kinetic energy dissipation from viscosity (energy per time per mass)
ϵ_{ab}	components to the permutation symbol in two space dimensions
ϵ_{abc}	components to the permutation symbol in three space dimensions
ε_{abc}	components to the Levi-Civita symbol in three space dimensions: $\varepsilon_{abc} = \sqrt{\det(g_{ab})} \epsilon_{abc}$
ζ	vertical component to the relative vorticity; e.g., $\zeta = \partial_x v - \partial_y u$
ζ_a	vertical component to the absolute vorticity; e.g., $\zeta_a = f + \zeta$
η	vertical position of the free upper surface of a fluid domain: $z = \eta(x, y, t)$
η	vertical position of a generalized vertical coordinate surface: $z = \eta(x, y, \sigma, t)$, with σ the generalized vertical coordinate
$\eta_{k-1/2}$	vertical position of the top interface of the k shallow water layer
$\eta_{k+1/2}$	vertical position of the lower interface of the k shallow water layer
$\eta_b = -H$	vertical position of static solid-earth boundary: $z = \eta_b(x, y) = -H(x, y)$
θ	potential temperature
Θ	Conservative Temperature
κ	molecular kinematic diffusivity
κ_T	molecular diffusivity for <i>in situ</i> temperature in water: $\kappa_T = 1.4 \times 10^{-7} \text{ m}^2 \text{ s}^{-1}$
κ_S	molecular diffusivity for salt in water: $\kappa_S = 1.5 \times 10^{-9} \text{ m}^2 \text{ s}^{-1}$
κ_{eddy}	kinematic eddy diffusivity: $\kappa_{\text{eddy}} \gg \kappa$
Λ	wavelength of a wave: $\Lambda = 2\pi/ \mathbf{k} $, where \mathbf{k} is the wavevector and $ \mathbf{k} $ the wavenumber.
λ	reduced wavelength of a wave: $\lambda = \Lambda/(2\pi) = 1/ \mathbf{k} $.
λ	longitude on the sphere: $0 \leq \lambda \leq 2\pi$
μ_n	chemical potential for constituent n within a fluid (energy per mass)
$\tilde{\mu}_n$	chemical potential for constituent n within a fluid (energy per mole number)
μ	relative chemical potential for a binary fluid
μ_{vsc}	chemical potential for seawater: $\mu = \mu_{\text{salt}} - \mu_{\text{water}}$
ν_{vsc}	dynamic viscosity = $\rho \nu$
ν_s	specific volume: $\nu_s = \rho^{-1}$
ν	molecular kinematic viscosity
ν_{air}	molecular kinematic viscosity of air: $\nu_{\text{air}} \approx 1.3 \times 10^{-5} \text{ m}^2 \text{ s}^{-1}$
ν_{water}	molecular kinematic viscosity of fresh water: $\nu_{\text{water}} \approx 10^{-6} \text{ m}^2 \text{ s}^{-1}$
ν_{eddy}	eddy viscosity: $\nu_{\text{eddy}} \gg \nu$
ξ^a	a'th component to a generalized coordinate
Π	Exner function
Π	Boussinesq dynamic enthalpy

GREEK SYMBOLS AND THEIR MEANING

SYMBOL	MEANING
ρ	Eulerian <i>in situ</i> density (mass per volume) of a fluid element: $\rho = \rho(\mathbf{x}, t)$
ρ^L	mass density following a fluid particle trajectory (Lagrangian mass density): $\rho^L = \rho^L(\mathbf{a}, T)$
$\dot{\rho}^L$	initial mass density in Lagrangian space-time: $\dot{\rho}^L = \rho^L(\mathbf{a}, T = t_0)$
ρ_0	constant reference density used for the Boussinesq ocean
ρ_{ref}	constant reference density used for the shallow water fluid
ϱ	potential density referenced to a specified pressure
σ	generalized vertical coordinate, $\sigma = \sigma(x, y, z, t)$
τ	stress vector such as from winds or bottom stresses acting on the ocean
\mathbb{T}	frictional stress tensor
φ	pressure divided by the Boussinesq reference density: $\varphi = p/\rho_0$
φ	sometimes used as the variable for parameterizing a curve
ϕ	latitude on the sphere: $-\pi/2 \leq \phi \leq \phi/2$
Φ_e	gravitational potential from a spherical and homogeneous earth
Φ	geopotential from central gravity plus planetary centrifugal; also, potential energy per mass
Φ	inverse flow map that generates an inverse mapping of the fluid continuum: $\mathbf{a} = \Phi(\mathbf{x}, t)$
φ	motion field that maps the fluid continuum as time evolves: $\mathbf{x} = \varphi(\mathbf{a}, T)$
ψ	streamfunction for two-dimensional non-divergent flow: $\mathbf{u} = \hat{\mathbf{z}} \times \nabla \psi$
Ψ	vector streamfunction for three-dimensional non-divergent flow: $\mathbf{v} = \nabla \times \Psi$
ω	relative vorticity: $\omega = \nabla \times \mathbf{v}$
ω	angular frequency for a wave so that the wave period is $2\pi/ \omega $
ϖ	dispersion relation for linear waves, relating angular frequency to the wavevector: $\omega = \varpi(\mathbf{k})$
Ω	angular velocity for a rotating reference frame
Ω	earth's angular velocity oriented through the north pole: $ \Omega = 7.2921 \times 10^{-5} \text{ s}^{-1}$

SYMBOL	MEANING
$[\equiv]$	“has dimensions” for use in referring to the physical dimensions
\times	vector cross product
∇	covariant derivative operator, which acts on a (p, q) tensor to produce a $(p, q + 1)$ tensor.
∇	gradient operator
∇_h	horizontal gradient operator on constant z surface: $\nabla_h = \hat{\mathbf{x}} (\partial/\partial x)_z + \hat{\mathbf{y}} (\partial/\partial y)_z = \hat{\mathbf{x}} \partial_x + \hat{\mathbf{y}} \partial_y$
$\nabla \cdot$	divergence operator that acts on a vector to produce a scalar
$\nabla \times$	curl operator
∇_σ	horizontal gradient on constant σ -surface: $\nabla_\sigma = \hat{\mathbf{x}} (\partial/\partial x)_\sigma + \hat{\mathbf{y}} (\partial/\partial y)_\sigma$
$\partial/\partial\sigma$	vertical partial derivative with general vertical coordinate: $\partial_\sigma = \partial/\partial\sigma = \partial/\partial\sigma = (\partial z/\partial\sigma) \partial/\partial z$
$\partial/\partial t$	Eulerian time derivative acting at a fixed spatial position, \mathbf{x} , also written as ∂_t
$[\partial/\partial t]_\sigma$	time derivative computed on constant σ -surface
D/Dt	material, Lagrangian, or substantial time derivative following a fluid particle
D_r/Dt	time derivative following a ray (integral lines of the group velocity): $D_r/Dt = \partial/\partial t + \mathbf{c}_g \cdot \nabla$
D_g/Dt	time derivative following the horizontal geostrophic flow $D_g/Dt = \partial/\partial t + \mathbf{u}_g \cdot \nabla$
$\ddot{}$	inexact differential operator commonly found in thermodynamics
δ	virtual displacement (also the variation) for Lagrangian mechanics and Hamilton’s principle
δ	differential increment that signals an object following the fluid flow
$\delta(x)$	one-dimensional Dirac delta with dimensions of inverse length
$\delta^{(2)}(\mathbf{x})$	two-dimensional Dirac delta with dimensions of inverse area
$\delta(\mathbf{x})$	three-dimensional Dirac delta with dimensions of inverse volume
$\delta(t)$	temporal Dirac delta with dimensions of inverse time
Δ	finite difference increment in space: $\Delta_x, \Delta_y, \Delta_z, \Delta_\sigma$
dA	infinitesimal horizontal area element: $dA = dx dy$
d^3a	infinitesimal region of material space: $d^3a = da db dc$
$d\mathcal{S}$	infinitesimal area element on a surface
dV	infinitesimal volume element, sometimes written $dV = d\mathbf{x}$
$d\mathbf{x}$	infinitesimal volume element, with Cartesian expression $d\mathbf{x} = dV = dx dy dz$
δV	infinitesimal volume for a region moving with the fluid (Lagrangian region)
$\int_{\mathcal{R}} dV$	volume integral over an arbitrary region, \mathcal{R}
$\int_{\mathcal{R}(\mathbf{v})} dV$	volume integral over a region following the fluid flow (Lagrangian integral)
$\int_{\mathcal{S}} d\mathcal{S}$	surface integral over an arbitrary surface \mathcal{S}
$\oint_{\partial\mathcal{R}} d\mathcal{S}$	surface integral over a closed surface $\partial\mathcal{R}$ that bounds the volume \mathcal{R}
$\oint d\ell$	closed line integral over a periodic domain
$\oint_{\partial\mathcal{S}} d\ell$	counter-clockwise closed line integral over the boundary of a surface, $\partial\mathcal{S}$
\sim	“similar to” or “scales as”
\approx	approximately equal to
$\dot{\Psi}$	time derivative following a trajectory; for fluid particle trajectories then, $\dot{\Psi} = D\Psi/Dt$

BIBLIOGRAPHY

- Abernathay, R., D. Ferreira, and A. Klocker, Diagnostics of isopycnal mixing in a circumpolar channel, *Ocean Modelling*, 72(0), 1 – 16, doi:10.1016/j.ocemod.2013.07.004, 2013. 223, 236, 243
- Adcroft, A., and J.-M. Campin, Rescaled height coordinates for accurate representation of free-surface flows in ocean circulation models, *Ocean Modelling*, 7, 269–284, doi:10.1016/j.ocemod.2003.09.003, 2004. 9
- Adcroft, A., R. Hallberg, and M. Harrison, A finite volume discretization of the pressure gradient force using analytic integration, *Ocean Modelling*, 22, 106–113, doi:10.1016/j.ocemod.2008.02.001, 2008. 60, 61, 64, 72
- Aiki, H., T. Jacobson, and T. Yamagata, Parameterizing ocean eddy transports from surface to bottom, *Journal of Geophysical Research*, 31, L19 302, doi:10.1029/2004GL020703, 2004. 232, 237
- Anderson, P. W., More is different, *Science*, 177, 393–396, doi:10.1126/science.177.4047.39, 1972. ix
- Andrews, D. G., and M. E. McIntyre, An exact theory of nonlinear waves on a Lagrangian-mean flow, *Journal of Fluid Mechanics*, 89, 609–646, doi:10.1017/S0022112078002773, 1978a. 189, 201
- Andrews, D. G., and M. E. McIntyre, On wave action and its relatives, *Journal of Fluid Mechanics*, 89, 647–664, doi:10.1017/S0022112078002785, 1978b. 189, 201
- Badin, G., and F. Crisciani, *Variational formulation of fluid and geophysical fluid dynamics*, Springer International Publishing, Switzerland, 218 pages, 2018. xii, 363
- Balwada, D., Q. Xiao, K. S. Smith, R. Abernathey, and A. R. Gray, Vertical fluxes conditioned on vorticity and strain reveal submesoscale ventilation, *Journal of Physical Oceanography*, 51(9), 2883–2901, doi:10.1175/JPO-D-21-0016.1, 2021. 150
- Batchelor, G. K., On steady laminar flow with closed streamlines at large Reynolds number, *Journal of Fluid Mechanics*, 1, 177–190, doi:10.1017/S0022112056000123, 1956. 170
- Beckers, J.-M., H. Burchard, J.-M. Campin, E. Deleersnijder, and P. P. Mathieu, Another reason why simple discretizations of rotated diffusion operators cause problems in ocean models: Comments on isoneutral diffusion in a z -coordinate ocean model, *Journal of Physical*

- Oceanography*, 28, 1552–1559, doi:10.1175/1520-0485(1998)028<1552:ARWSDO>2.0.CO;2, 1998. 241
- Beckers, J.-M., H. Burchard, E. Deleersnijder, and P. P. Mathieu, Numerical discretization of rotated diffusion operators in ocean models, *Monthly Weather Review*, 128, 2711–2733, doi:10.1175/1520-0493(2000)128<2711:NDORDO>2.0.CO;2, 2000. 242
- Black, T. L., The new NMC mesoscale eta model: description and forecast examples, *Weather and Forecasting*, 9, 265–278, 1994. 9
- Bleck, R., Finite difference equations in generalized vertical coordinates. Part I: Total energy conservation, *Contributions to Atmospheric Physics*, 51, 360–372, 1978. 2
- Boltzmann, L., Further studies on the thermal equilibrium of gas molecules, in *Kinetic Theory, Vol. 2: Irreversible Processes*, edited by S. G. Brush, pp. 88–175, Pergamon Press, Oxford, english translation of Boltzmann (1872), “Weitere Studien über das Wärmegleichgewicht unter Gasmolekülen”, 1966. 139, 407
- Böning, C. W., W. R. Holland, F. O. Bryan, G. Danabasoglu, and J. C. McWilliams, An overlooked problem in model simulations of the thermohaline circulation and heat transport in the Atlantic Ocean, *Journal of Physical Oceanography*, 8, 515–523, doi:10.1175/1520-0442(1995)008<0515:AOPIMS>2.0.CO;2, 1995. 238
- Bradshaw, P., Possible origin of prandt's mixing-length theory, *Nature*, 249, 135–136, doi:10.1038/249135b0, 1974. 122
- Bühler, O., *Waves and mean flows*, 2nd ed., Cambridge University Press, Cambridge, UK, doi:10.1017/CBO9781107478701, 2014a. 189, 195, 201
- Bühler, O., A gentle stroll through EP flux theory, *European Journal of Mechanics B*, 47, 12–15, doi:10.1016/j.euromechflu.2014.01.010, 2014b. 82
- Buzzicotti, M., B. A. Storer, H. Khatri, S. M. Griffies, and H. Aluie, Spatio-temporal coarse-graining decomposition of the global ocean geostrophic kinetic energy, *Journal of Advances in Modeling Earth Systems*, 15, doi:10.1029/2023MS003693, 2023. 192
- Callies, J., Restratification of abyssal mixing layers by submesoscale baroclinic eddies, *Journal of Physical Oceanography*, 48, 1995–2010, doi:10.1175/JPO-D-18-0082.1, 2018. 2, 29
- Callies, J., and R. Ferrari, Dynamics of an abyssal circulation driven by bottom-intensified mixing on slopes, *Journal of Physical Oceanography*, 48, 1257–1282, doi:10.1175/JPO-D-17-0125.1, 2018. 28
- Carslaw, H. S., and J. C. Jaeger, *Conduction of Heat in Solids*, Oxford University Press, 1959. 106
- Cauchy, A.-L., *Résumé des leçons données à l'école royale polytechnique sur le calcul infinitésimal*, Imprimerie royale, 1823. 330
- Cole, S. T., C. Wortham, E. Kunze, and W. B. Owens, Eddy stirring and horizontal diffusivity from argo float observations: Geographic and depth variability, *Geophysical Research Letters*, 42(10), 3989–3997, doi:10.1002/2015GL063827, 2015GL063827, 2015. 223

- Courant, R., and D. Hilbert, *Methods of Mathematical Physics Volume I*, Wiley-Interscience, New York, 1953. 135, 137
- Courant, R., and D. Hilbert, *Methods of Mathematical Physics Volume II: Partial Differential Equations*, Wiley-Interscience, 1962. 135, 137
- Cox, M., and K. Bryan, A numerical model of the ventilated thermocline, *Journal of Physical Oceanography*, 14, 674–687, 1984. 238
- Cox, M. D., Isopycnal diffusion in a z -coordinate ocean model, *Ocean Modelling*, 74, 1–5, 1987. 240, 241, 242, 253
- Crank, J., *The Mathematics of Diffusion*, Oxford University Press, 1956. 106
- Csanady, G. T., *Turbulent Diffusion in the Environment*, D. Reidel Publishing Company, 1973. 121, 124
- Danabasoglu, G., R. Ferrari, and J. McWilliams, Sensitivity of an ocean general circulation model to a parameterization of near-surface eddy fluxes, *Journal of Climate*, 21, 1192–1208, doi:10.1175/2007JCLI1508.1, 2008. 223, 243
- de Lavergne, C., G. Madec, Julien Le Sommer, A. J. G. Nurser, and A. C. Naveira Garabato, On the consumption of Antarctic Bottom Water in the abyssal ocean, *Journal of Physical Oceanography*, 46, 635–661, doi:10.1175/JPO-D-14-0201.1, 2016. 329
- DeSzeke, R. A., and A. F. Bennett, Microstructure fluxes across density surfaces, *Journal of Physical Oceanography*, 23, 2254–2264, 1993. 215
- Drake, H. F., S. Bailey, R. Dussin, S. M. Griffies, J. Krasting, G. MacGilchrist, G. Stanley, J.-E. Tesdal, and J. D. Zika, Water mass transformation budgets in finite-volume generalized vertical coordinate ocean models, *Journal of Advances in Modeling Earth Systems (JAMES)*, 17, doi:10.1029/2024MS004383, 2025. 303
- Dukowicz, J. K., and R. D. Smith, Stochastic theory of compressible turbulent fluid transport, *Physics of Fluids*, 9, 3523–3529, doi:10.1063/1.869460, 1997. 243
- Eckart, C., An analysis of the stirring and mixing processes in incompressible fluids, *Journal of Marine Research*, 7, 265–275, 1948. 143, 144, 205, 221, 223
- Einstein, A., Über die von der molekularkinetischen theorie der wärme geforderte bewegung von in ruhenden flüssigkeiten suspendierten teilchen [on the motion of small particles suspended in liquids at rest as required by the molecular-kinetic theory of heat], *Annalen der Physik*, 17, 549–560, doi:10.1002/andp.19053220806, 1905a. 109, 112, 118, 119, 395, 397
- Einstein, A., Über einen die erzeugung und verwandlung des lichtes betreffenden heuristischen gesichtspunkt [on a heuristic viewpoint concerning the production and transformation of light], *Annalen der Physik*, 17, 132–148, doi:10.1002/andp.19053220607, 1905b. 109
- Einstein, A., Zur elektrodynamik bewegter körper [on the electrodynamics of moving bodies], *Annalen der Physik*, 17, 891–921, doi:10.1002/andp.19053221004, 1905c. 109
- Eliassen, A., and E. Palm, On the transfer of energy in stationary mountain waves, *Geofysiske Publikasjoner*, 22(1–23), 1960. 82

- Ferrari, R., J. C. McWilliams, V. M. Canuto, and M. Dubovikov, Parameterization of eddy fluxes near oceanic boundaries, *Journal of Climate*, 21, 2770–2789, doi:10.1175/2007JCLI1510.1, 2008. [223](#), [237](#), [243](#)
- Ferrari, R., S. M. Griffies, A. J. G. Nurser, and G. K. Vallis, A boundary-value problem for the parameterized mesoscale eddy transport, *Ocean Modelling*, 32, 143–156, doi:10.1016/j.ocemod.2010.01.004, 2010. [237](#), [238](#), [243](#)
- Ferreira, D., and J. Marshall, Formulation and implementation of a residual-mean ocean circulation model, *Ocean Modelling*, 13, 86–107, 2006. [233](#)
- Fetter, A. L., and J. D. Walecka, *Theoretical Mechanics of Particles and Continua*, Dover Publications, Mineola, New York, 570 pp, 2003. [340](#), [342](#), [344](#), [347](#)
- Feynman, R. P., R. B. Leighton, and M. L. Sands, *The Feynman lectures on physics*, Addison-Wesley Publishing Company, Reading, Mass, 1963.
- Fox-Kemper, B., R. Lumpkin, and F. O. Bryan, Lateral transport in the ocean interior, in *Ocean Circulation and Climate, 2nd Edition: A 21st Century Perspective, International Geophysics Series*, vol. 103, edited by G. Siedler, S. M. Griffies, J. Gould, and J. Church, pp. 185–209, Academic Press, 2013. [245](#)
- Gardiner, C. W., *Handbook of stochastic methods for physics, chemistry and the natural sciences*, 2nd ed., 442 pp., Springer-Verlag, Berlin, Heidelberg, New York, 1985. [119](#)
- Garrett, C., Turbulent dispersion in the ocean, *Progress in Oceanography*, 70, 113–125, 2006. [145](#), [204](#), [205](#)
- Garrett, C., P. MacCready, and P. Rhines, Boundary mixing and arrested ekman layers: Rotating stratified flow near a sloping boundary, *Annual Review of Fluid Mechanics*, 25, 291–323, doi:10.1146/annurev.fl.25.010193.001451, 1993. [2](#), [29](#)
- Gebbie, G., Cancelation of deglacial thermosteric sea level rise by a barosteric effect, *Journal of Physical Oceanography*, 50, 3623–3639, doi:10.1175/JPO-D-20-0173.1, 2020. [277](#), [278](#), [279](#), [280](#)
- Gent, P. R., and J. C. McWilliams, Isopycnal mixing in ocean circulation models, *Journal of Physical Oceanography*, 20, 150–155, doi:10.1175/1520-0485(1990)020<0150:IMIOCM>2.0.CO;2, 1990. [225](#), [241](#), [242](#), [405](#)
- Gent, P. R., J. Willebrand, T. J. McDougall, and J. C. McWilliams, Parameterizing eddy-induced tracer transports in ocean circulation models, *Journal of Physical Oceanography*, 25, 463–474, doi:10.1175/1520-0485(1995)025<0463:PEITTI>2.0.CO;2, 1995. [156](#), [215](#), [225](#), [229](#), [230](#), [231](#), [232](#), [233](#), [234](#), [236](#), [237](#), [238](#), [252](#), [253](#), [254](#), [405](#)
- Gilbert, A. D., and J. Vanneste, Geometric approaches to Lagrangian averaging, *Annual Review of Fluid Mechanics*, 57, 117–140, doi:10.1146/annurev-fluid-030524-095913, 2025. [189](#), [190](#), [201](#)
- Gill, A., *Atmosphere-Ocean Dynamics*, International Geophysics Series, vol. 30, Academic Press, London, 662 + xv pp, 1982. [223](#)

- Gnanadesikan, A., A global model of silicon cycling: Sensitivity to eddy parameterization and dissolution, *Global Biogeochemical Cycles*, 13, 199–220, 1999. 242
- Goldstein, H., *Classical Mechanics*, Addison-Wesley Publishing, Reading, MA, 1980. 340, 346
- Graham, F., and T. McDougall, Quantifying the nonconservative production of Conservative Temperature, potential temperature, and entropy, *Journal of Physical Oceanography*, 43, 838–862, doi:10.1175/JPO-D-11-0188.1, 2013. 224
- Greatbatch, R. J., Exploring the relationship between eddy-induced transport velocity, vertical momentum transfer, and the isopycnal flux of potential vorticity, *Journal of Physical Oceanography*, 28, 422–432, doi:10.1175/1520-0485(1998)028<0422:ETRBEI>2.0.CO;2, 1998. 99, 100
- Greatbatch, R. J., and K. G. Lamb, On parameterizing vertical mixing of momentum in non-eddy resolving ocean models, *Journal of Physical Oceanography*, 20, 1634–1637, doi:10.1175/1520-0485(1990)020<1634:OPVMOM>2.0.CO;2, 1990. 99, 233, 234
- Gregory, J., S. M. Griffies, C. Hughes, J. Lowe, J. Church, I. Fukimori, N. Gomez, R. Kopp, F. Landerer, R. Ponte, D. Stammer, M. Tamisiea, and R. van den Wal, Concepts and terminology for sea level—mean, variability and change, both local and global, *Surveys in Geophysics*, 40, 1251–1289, doi:10.1007/s10712-019-09555-7, 2019. 277, 278, 396
- Griffies, S. M., The Gent-McWilliams skew-flux, *Journal of Physical Oceanography*, 28, 831–841, doi:10.1175/1520-0485(1998)028<0831:TGMSF>2.0.CO;2, 1998. 153, 231
- Griffies, S. M., *Fundamentals of Ocean Climate Models*, Princeton University Press, Princeton, USA, 518+xxxiv pages, 2004. 61, 135, 137, 153, 190, 215, 237, 238, 245
- Griffies, S. M., and R. J. Greatbatch, Physical processes that impact the evolution of global mean sea level in ocean climate models, *Ocean Modelling*, 51, 37–72, doi:10.1016/j.ocemod.2012.04.003, 2012. 190, 226, 229, 264, 280, 281, 282, 409
- Griffies, S. M., and R. Hallberg, Biharmonic friction with a Smagorinsky-like viscosity for use in large-scale eddy-permitting ocean models, *Monthly Weather Review*, 128, 2935–2946, doi:10.1175/1520-0493(2000)128<2935:BFWASL>2.0.CO;2, 2000. 137
- Griffies, S. M., A. Gnanadesikan, R. C. Pacanowski, V. Larichev, J. K. Dukowicz, and R. D. Smith, Isoneutral diffusion in a z -coordinate ocean model, *Journal of Physical Oceanography*, 28, 805–830, doi:10.1175/1520-0485(1998)028<0805:IDIAZC>2.0.CO;2, 1998. 135, 137, 241, 242
- Griffies, S. M., C. W. Böning, F. O. Bryan, E. P. Chassignet, R. Gerdes, H. Hasumi, A. Hirst, A.-M. Treguier, and D. Webb, Developments in ocean climate modelling, *Ocean Modelling*, 2, 123–192, doi:10.1016/S1463-5003(00)00014-7, 2000. 61, 236
- Griffies, S. M., J. Yin, P. J. Durack, P. Goddard, S. Bates, E. Behrens, M. Bentsen, D. Bi, A. Biastoch, C. W. Böning, A. Bozec, C. Cassou, E. Chassignet, G. Danabasoglu, S. Danilov, C. Domingues, H. Drange, R. Farneti, E. Fernandez, R. J. Greatbatch, D. M. Holland, M. Ilicak, J. Lu, S. J. Marsland, A. Mishra, W. G. Large, K. Lorbacher, A. G. Nurser, D. Salas y Mélia, J. B. Palter, B. L. Samuels, J. Schröter, F. U. Schwarzkopf, D. Sidorenko, A.-M. Treguier, Y. Tseng, H. Tsujino, P. Uotila, S. Valcke, A. Voldoire, Q. Wang, M. Winton,

- and Z. Zhang, An assessment of global and regional sea level for years 1993–2007 in a suite of interannual CORE-II simulations, *Ocean Modelling*, 78, 35–89, doi:10.1016/j.ocemod.2014.03.004, 2014. 279, 280, 409
- Griffies, S. M., A. Adcroft, and R. W. Hallberg, A primer on the vertical lagrangian-remap method in ocean models based on finite volume generalized vertical coordinates, *Journal of Advances in Modeling Earth Systems*, 12, doi:10.1029/2019MS001954, 2020. 2, 50, 60, 67, 99, 243, 248
- Griffiths, D. J., *Introduction to Electrodynamics*, Prentice-Hall, Englewood Cliffs, New Jersey, USA, 479 pp, 1981. 154
- Groeskamp, S., J. Zika, T. McDougall, B. Sloyan, and F. Laliberté, The representation of ocean circulation and variability in thermodynamic coordinates, *Journal of Physical Oceanography*, 44, 1735–1750, doi:10.1175/JPO-D-13-0213.1, 2014. 288
- Groeskamp, S., R. P. Abernathey, and A. Klocker, Water mass transformation by cabbeling and thermobaricity, *Geophysical Research Letters*, doi:10.1002/2016GL070860, 2016. 264
- Groeskamp, S., S. M. Griffies, D. Iudicone, R. Marsh, A. G. Nurser, and J. D. Zika, The water mass transformation framework for ocean physics and biogeochemistry, *Annual Review of Marine Science*, 11, 1–35, doi:10.1146/annurev-marine-010318-095421, 2019. 264, 285, 289, 322, 323, 420
- Haine, T. W. N., S. M. Griffies, G. Gebbie, and W. Jiang, A review of Green's function methods for tracer timescales and pathways in ocean models, *Journal of Advances in Modeling Earth Systems (JAMES)*, 17, doi:10.1029/2024MS004637, 2025. 141, 183
- Hallberg, R., A thermobaric instability in Lagrangian vertical coordinate ocean models, *Ocean Modelling*, 8, 227–300, 2005. 72
- Hand, L. N., and J. D. Finch, *Analytical Mechanics*, 1st ed., Cambridge Press, 1998. 338
- Haney, R. L., On the pressure gradient force over steep topography in sigma-coordinate ocean models, *Journal of Physical Oceanography*, 21, 610–619, 1991. 61
- Hayes, W. D., Conservation of action and modal wave action, *Proceedings of the Royal Society of London. Series A Mathematical and Physical Sciences*, 320, 187–206, doi:www.jstor.org/stable/77799, 1970. 353
- Holloway, G., Eddy transport of thickness and momentum in layer and level models, *Journal of Physical Oceanography*, 27, 1153–1157, 1997. 236
- Holmes, R. M., C. De Lavergne, and T. J. McDougall, Tracer transports within abyssal mixing layers, *Journal of Physical Oceanography*, 49, 2669–2695, doi:10.1175/JPO-D-19-0006.1, 2019a. 2, 29, 32
- Holmes, R. M., J. Zika, and M. H. England, Diathermal heat transport in a global ocean model, *Journal of Physical Oceanography*, 49, 141–161, doi:10.1175/JPO-D-18-0098.1, 2019b. 298, 327
- Huang, K., *Statistical Mechanics*, John Wiley and Sons, New York, 493 pp, 1987. 111

Huw Davies, J., Global map of solid Earth surface heat flow, *Geochemistry, Geophysics, Geosystems*, 14, 4608–4622, doi:10.1002/ggge.20271, 2013. 276

IOC, SCOR, and IAPSO, *The international thermodynamic equation of seawater-2010: calculation and use of thermodynamic properties*, Intergovernmental Oceanographic Commission, Manuals and Guides No. 56, UNESCO, doi:10.25607/OBP-1338, 196pp, 2010. 224, 256, 257, 264, 265, 414

Jackson, J. D., *Classical Electrodynamics*, John Wiley and Sons, New York, USA, 848 pp, 1975. 154, 399

Jansen, M., A. Adcroft, S. M. Griffies, and I. Grooms, The averaged hydrostatic Boussinesq equations in generalized vertical coordinates, *Journal of Advances in Modeling Earth Systems (JAMES)*, 16, doi:10.1029/2024MS004506, 2024. 81, 190, 215, 218, 233

Jaynes, E. T., Information theory and statistical mechanics, *Physical Review*, 106(4), 620–630, doi:10.1103/PhysRev.106.620, 1957.

Jeziorski, J., and J. Kijowski, Thermo-hydrodynamics as a field theory, in *Nonequilibrium Theory and Extremum Principles, Advances in Thermodynamics*, vol. 3, edited by S. Sieniutycz and P. Salaman, pp. 282–317, Taylor & Francis, 1990. 363, 368

José, J. V., and E. J. Saletan, *Classical Dynamics: A Contemporary Approach*, Cambridge Press, 670 pp., 1998. 340, 345, 355

Kantha, L. H., and C. A. Clayson, *Small Scale Processes in Geophysical Fluid Flows*, Academic Press, New York, USA, 883 pp, 2000. 223

Killworth, P. D., On the parameterization of eddy transfer Part I: Theory, *Journal of Marine Research*, 55, 1171–1197, 1997. 236

Klocker, A., and R. Abernathey, Global patterns of mesoscale eddy properties and diffusivities, *Journal of Physical Oceanography*, 44, 1030–1046, 2014. 223

Klocker, A., and T. J. McDougall, Influence of the nonlinear equation of state on global estimates of dianeutral advection and diffusion, *Journal of Physical Oceanography*, 40, 1690–1709, doi:10.1175/2010JPO4303.1, 2010. 264

Kundu, P., I. Cohen, and D. Dowling, *Fluid Mechanics*, Academic Press, 921 + xxiv pp, 2016. 121

Kushner, P. J., and I. M. Held, Potential vorticity thickness fluxes and wave-mean flow interaction, *Journal of Atmospheric Sciences*, 56, 948–958, 1999. 215

Langevin, P., Sur la théorie du mouvement brownien [on the theory of brownian motion], *Comptes Rendus Hebdomadaires des Séances de l'Académie des Sciences*, 146, 530–533, 1908. 116, 119

Lapeyre, G., P. Klein, and B. L. Hua, Does the tracer gradient vector align with the strain eigenvectors in 2d turbulence?, *Physics of Fluids*, 11(12), 3729–3737, doi:10.1063/1.870234, 1999. 150

- Large, W., J. McWilliams, and S. Doney, Oceanic vertical mixing: a review and a model with a nonlocal boundary layer parameterization, *Reviews of Geophysics*, 32, 363–403, doi:10.1029/94RG01872, 1994. 223, 273
- Larson, V. E., The relationship between the transilient matrix and the Green's function for the advection-diffusion equation, *Journal of Atmospheric Sciences*, 56(14), 2447–2453, doi:10.1175/1520-0469(1999)056<2447:trbtmm>2.0.co;2, 1999. 172
- Le Sommer, J., F. d'Ovidio, and G. Madec, Parameterization of subgrid stirring in eddy resolving ocean models. part 1: Theory and diagnostics, *Ocean Modelling*, 39(1-2), 154–169, doi:10.1016/j.ocemod.2011.03.007, 2011. 245
- Lee, M.-M., D. Marshall, and R. Williams, On the eddy transfer of tracers: advective or diffusive?, *Journal of Marine Research*, 55, 483–505, 1997. 83
- Lemarié, F., L. Debreu, A. F. Shchepetkin, and J. C. McWilliams, On the stability and accuracy of the harmonic and biharmonic isoneutral mixing operators in ocean models, *Ocean Modelling*, 52-53, 9–35, doi:10.1016/j.ocemod.2012.04.007, 2012. 241, 242
- Lemons, D. S., and A. Gythiel, Paul Langevin's 1908 paper "on the theory of brownian motion", *American Journal of Physics*, 65(11), 1079–1081, doi:10.1119/1.18725, includes English translation of Langevin (1908): *Sur la théorie du mouvement brownien*, C. R. Acad. Sci. (Paris) 146, 530–533, 1997. 116
- Lin, S. J., A finite volume integration method for computing pressure gradient force in general vertical coordinates, *Quarterly Journal of the Royal Meteorological Society*, 123, 1749–1762, doi:10.1002/qj.49712354214, 1997. 60, 61, 64
- Loose, N., S. Bachman, I. Grooms, and M. Jansen, Diagnosing scale-dependent energy cycles in a high-resolution isopycnal ocean model, *Journal of Physical Oceanography*, doi:10.1175/JPO-D-22-0083.1, 2022. 70, 81
- Loose, N., G. M. Marques, A. Adcroft, S. Bachman, S. M. Griffies, I. Grooms, R. W. Hallberg, and M. Jansen, Comparing two parameterizations for the restratification effect of mesoscale eddies in an isopycnal ocean model, *Journal of Advances in Modeling Earth Systems (JAMES)*, 15, doi:10.1029/2022MS003518, 2023. 70, 81, 233, 234
- Lorbacher, K., S. J. Marsland, J. A. Church, S. M. Griffies, and D. Stammer, Rapid barotropic sea-level rise from ice-sheet melting scenarios, *Journal of Geophysical Research*, 117, C06003, doi:10.1029/2011JC007733, 2012. 280
- Lowe, J. A., and J. M. Gregory, Understanding projections of sea level rise in a hadley centre coupled climate model, *Journal of Geophysical Research: Oceans*, 111(C11), doi:10.1029/2005JC003421, 2006. 277
- MacKinnon, J., Louis St. Laurent, and A. C. Naveira Garabato, Diapycnal mixing processes in the ocean interior, in *Ocean Circulation and Climate, 2nd Edition: A 21st century perspective, International Geophysics Series*, vol. 103, edited by G. Siedler, S. M. Griffies, J. Gould, and J. Church, pp. 159–183, Academic Press, doi:10.1016/B978-0-12-391851-2.00007-6, 2013. 223, 224
- Maddison, J., and D. Marshall, The Eliassen-Palm flux tensor, *Journal of Fluid Mechanics*, 729, 69–102, doi:10.1017/jfm.2013.259, 2013. 81, 96

Malvern, L. E., *Introduction to the Mechanics of a Continuous Media*, Prentice-Hall, Englewood Cliffs, USA, 713pp, 1969.

Marion, J. B., and S. T. Thornton, *Classical Dynamics of Particles and Systems*, Harcourt Brace Jovanovich, San Diego, USA, 602 pp, 1988. [x](#)

Marques, G. M., N. Loose, E. Yankovsky, J. M. Steinberg, C.-Y. Chang, N. Bhamidipati, A. Adcroft, B. Fox-Kemper, S. M. Griffies, R. W. Hallberg, M. F. Jansen, H. Khatri, and L. Zanna, NeverWorld2: An idealized model hierarchy to investigate ocean mesoscale eddies across resolutions, *Geoscientific Model Development*, 15, 6567–6579, doi:10.5194/gmd-15-6567-2022, 2022. [81](#)

Marshall, J. C., E. Shuckburgh, H. Jones, and C. Hill, Estimates and implications of surface eddy diffusivity in the Southern Ocean derived from tracer transport, *Journal of Physical Oceanography*, 36, 1806–1821, 2006. [330](#)

McComb, W., *The Physics of Fluid Turbulence*, 1st ed., Oxford University Press, Oxford, 602pp, 1990. [120](#), [121](#)

McDougall, T. J., Neutral surfaces, *Journal of Physical Oceanography*, 17, 1950–1967, doi: 10.1175/1520-0485(1987)017<1950:NS>2.0.CO;2, 1987a. [223](#), [227](#)

McDougall, T. J., Thermobaricity, cabbeling, and water-mass conversion, *Journal of Geophysical Research*, 92, 5448–5464, doi:10.1029/JC092iC05p05448, 1987b. [223](#), [260](#), [261](#), [262](#), [263](#), [280](#), [398](#)

McDougall, T. J., Potential enthalpy: a conservative oceanic variable for evaluating heat content and heat fluxes, *Journal of Physical Oceanography*, 33, 945–963, doi:10.1175/1520-0485(2003)033<0945:PEACOV>2.0.CO;2, 2003. [256](#)

McDougall, T. J., Thermodynamic concepts used in physical oceanography, *EGUspHERE [preprint]*, doi:10.5194/egusphere-2025-4556, 2025. [264](#)

McDougall, T. J., and P. C. McIntosh, The temporal-residual-mean velocity. Part II: isopycnal interpretation and the tracer and momentum equations, *Journal of Physical Oceanography*, 31, 1222–1246, doi:10.1175/1520-0485(2001)031<1222:TTRMVP>2.0.CO;2, 2001. [163](#), [190](#), [207](#), [209](#), [215](#), [218](#), [230](#)

McDougall, T. J., and Y. You, Implications of the nonlinear equation of state for upwelling in the ocean interior, *Journal of Geophysical Research*, 95, 13,263—13,276, 1990. [264](#)

McDougall, T. J., S. Groeskamp, and S. M. Griffies, On geometric aspects of interior ocean mixing, *Journal of Physical Oceanography*, 44, 2164–2175, doi:10.1175/JPO-D-13-0270.1, 2014. [223](#), [225](#), [227](#), [229](#), [239](#), [261](#)

McDougall, T. J., P. M. Barker, R. M. Holmes, R. Pawlowicz, S. M. Griffies, and P. J. Durack, The interpretation of temperature and salinity variables in numerical ocean model output, and the calculation of heat fluxes and heat content, *Geoscientific Model Development*, 14, 6445–6466, doi:10.5194/gmd-14-6445-2021, 2021.

McIntosh, P. C., and T. J. McDougall, Isopycnal averaging and the residual mean circulation., *Journal of Physical Oceanography*, 26, 1655–1660, 1996. [215](#), [230](#)

- Mellor, G. L., and T. Yamada, Development of a turbulent closure model for geophysical fluid problems, *Reviews of Geophysics*, 20, 851–875, 1982. [223](#)
- Mellor, G. L., L.-Y. Oey, and T. Ezer, Sigma coordinate pressure gradient errors and the seamount problem, *Journal of Atmospheric and Oceanic Technology*, 15, 1122–1131, 1998. [61](#)
- Mermin, N. D., What's wrong with these equations?, *Physics Today*, 42, 9–11, doi:10.1063/1.2811173, 1989. [viii](#)
- Middleton, J. F., and J. W. Loder, Skew fluxes in polarized wave fields, *Journal of Physical Oceanography*, 19, 68–76, doi:10.1175/1520-0485(1989)019<0068:SFIPWF>2.0.CO;2, 1989. [153](#), [189](#), [204](#), [205](#), [238](#)
- Misner, C., K. Thorne, and J. Wheeler, *Gravitation*, W.H. Freeman and Co., 1279 pages, 1973.
- Moffatt, H., Transport effects associated with turbulence with particular attention to the influence of helicity, *Reports on Progress in Physics*, 46, 621–664, doi:10.1088/0034-4885/46/5/002, 1983. [153](#), [205](#)
- Montgomery, R. B., Circulation in upper layers of southern North Atlantic, *Papers in Physical Oceanography*, 6, 55, 1938. [238](#)
- Morse, P. M., and H. Feshbach, *Methods of Theoretical Physics Part I and II*, McGraw-Hill Book Company, New York, 1953. [335](#), [338](#)
- Müller, P., Ertel's potential vorticity theorem in physical oceanography, *Reviews of Geophysics*, 33, 67–97, doi:10.1029/94RG03215, 1995. [363](#), [368](#), [379](#)
- Müller, P., and C. Garrett, From stirring to mixing in a stratified ocean, *Oceanography*, 15, 12–19, 2002. [145](#), [223](#)
- Nakamura, N., A new look at eddy diffusivity as a mixing diagnostic, *Journal of the Atmospheric Sciences*, 58(24), 3685–3701, doi:10.1175/1520-0469(2001)058<3685:ANLAED>2.0.CO;2, 2001. [223](#)
- Noether, E., Invariante variationsprobleme, *Nachrichten von der Gesellschaft der Wissenschaften zu Göttingen, Math-phys. Klasse*, pp. 235–257, 1918. [334](#), [350](#)
- Noether, E., and M. Tavel, Invariant variational problems, *arXiv:physics/0503066 [physics.hist-ph]*, 2018. [334](#), [350](#)
- Nurser, A. G., and S. M. Griffies, Relating diffusive surface salinity fluxes to boundary freshwater and salt fluxes, *Journal of Physical Oceanography*, 49, 2365–2376, doi:10.1175/JPO-D-19-0037.1, 2019. [180](#), [269](#), [305](#)
- Nurser, A. G., and M.-M. Lee, Isopycnal averaging at constant height. Part I: The formulation and a case study, *Journal of Physical Oceanography*, 34, 2721–2739, 2004a. [215](#)
- Nurser, A. G., and M.-M. Lee, Isopycnal averaging at constant height. Part II: Relating to the residual streamfunction in Eulerian space, *Journal of Physical Oceanography*, 34, 2740–2755, 2004b. [215](#)

Nurser, A. G., R. Marsh, and R. Williams, Diagnosing water mass formation from air-sea fluxes and surface mixing, *Journal of Physical Oceanography*, 29, 1468–1487, doi:10.1175/1520-0485(1999)029<1468:DWMFFA>2.0.CO;2, 1999. 305, 314

Okubo, A., Horizontal dispersion of floatable particles in the vicinity of velocity singularities such as convergences, *Deep-Sea Research and Oceanographic Abstracts*, 17, 445–454, doi:10.1016/0011-7471(70)90059-8, 1970. 150

Olbers, D. J., J. Willebrand, and C. Eden, *Ocean Dynamics*, 1st ed., Springer, Berlin, Germany, 704 pages, 2012. xii, 224

Otto, A., F. Otto, O. Boucher, J. Church, G. Hegerl, P. Forster, N. Gillett, J. Gregory, G. Johnson, R. Knutti, N. Lewis, U. Lohmann, J. Marotzke, G. Myhre, D. Shindell, B. Stevens, and M. Allen, Energy budget constraints on climate response, *Nature Geosciences*, 6, 415–416, doi:10.1038/ngeo1836, 2013. 277

Padhye, N., and P. J. Morrison, Fluid element particle relabeling, *Physics Letters A*, 219, 287–292, doi:10.1016/0375-9601(96)00472-0, 1996. 379

Perrin, J., Mouvement brownien et réalité moléculaire [brownian motion and molecular reality], *Annales de Chimie et de Physique (8ème série)*, 18, 5–114, no DOI assigned; see also English translation reviewed in *Nature* (1910)., 1909. 119

Peterson, H. G., and J. Callies, Rapid spin up and spin down of flow along slopes, *Journal of Physical Oceanography*, doi:10.1175/JPO-D-21-0173.1, 2022. 2, 10, 67

Peterson, K. A., and R. J. Greatbatch, Vorticity fluxes in shallow water ocean models, *Atmosphere-Ocean*, 39, 1–14, doi:10.1080/07055900.2001.9649662, 2001. 100

Phillips, N. A., A coordinate system having some special advantages for numerical forecasting, *Journal of Meteorology*, 14, 184–185, doi:10.1175/1520-0469(1957)014<0184:ACSHSS>2.0.CO;2, 1957. 9

Phillips, O. M., On flows induced by diffusion in a stably stratified fluid, *Deep-Sea Research: Oceanography Abstracts*, 17, 435–440, doi:10.1016/0011-7471(70)90058-6, 1970. 2, 29

Plumb, R. A., Eddy fluxes of conserved quantities by small-amplitude waves, *Journal of Atmospheric Sciences*, 36, 1699–1704, 1979. 205

Polzin, K. L., J. M. Toole, J. R. Ledwell, and R. W. Schmitt, Spatial variability of turbulent mixing in the abyssal ocean, *Science*, 276, 93–96, 1997. 223

Prandtl, L., Bericht über untersuchungen zur ausgebildeten turbulenz, *Zeitschrift für Angewandte Mathematik und Mechanik*, 5, 136–139, doi:10.1002/zamm.19250050212, 1925a.

Prandtl, L., Bericht über untersuchungen zur ausgebildeten turbulenz [report on investigations of fully developed turbulence], *Zeitschrift für Angewandte Mathematik und Mechanik (ZAMM)*, 5(2), 136–139, doi:10.1002/zamm.19250050212, 1925b. 122

Prandtl, L., Report on investigation of developed turbulence, *Tech. Rep. Technical Memorandum 1231*, National Advisory Committee for Aeronautics (NACA), english translation of Prandtl (1925), ZAMM 5(2):136–139, 1949. 122

- Pudig, M. P., W. Zhang, K. S. Smith, and L. Zhang, Parameterizing isopycnal mixing via kinetic energy backscattering in an eddy-permitting ocean model, *Journal of Advances in Modeling Earth Systems, in review*, 2026. 70, 191
- Quigg, C., *Gauge Theories of the Strong, Weak, and Electromagnetic Interactions*, Benjamin Cummings: Frontiers in Physics, Menlo Park, California, 1983. 335, 361, 362
- Ramond, P., *Field Theory: A Modern Primer*, Addison-Wesley Frontiers in Physics, 1990. 335, 350, 361, 362
- Redi, M. H., Oceanic isopycnal mixing by coordinate rotation, *Journal of Physical Oceanography*, 12, 1154–1158, doi:10.1175/1520-0485(1982)012<1154:OIMBCR>2.0.CO;2, 1982. 238, 240, 242
- Reif, F., *Fundamentals of Statistical and Thermal Physics*, McGraw-Hill, New York, 1965. 111
- Rhines, P. B., Basic dynamics of the large-scale geostrophic circulation, in *WHOI 1982 Summer Study Program*, Woods Hole Oceanographic Institute, 1982. 84, 212
- Rhines, P. B., and W. R. Holland, A theoretical discussion of eddy-driven mean flows, *Dynamics Of Atmospheres And Oceans*, 3, 289–325, doi:10.1016/0377-0265(79)90015-0, 1979. 186
- Rhines, P. B., and W. R. Young, Homogenization of potential vorticity in planetary gyres, *Journal of Fluid Mechanics*, 122, 347–367, 1982. 167, 170
- Roberts, M. J., and D. Marshall, Do we require adiabatic dissipation schemes in eddy-resolving ocean models?, *Journal of Physical Oceanography*, 28, 2050–2063, doi:10.1175/1520-0485(1998)028<2050:DWRADS>2.0.CO;2, 1998. 254
- Rooth, C., Hydrology and the ocean circulation, *Progress in Oceanography*, 11, 131–149, doi:10.1016/0079-6611(82)90006-4, 1982. 238
- Roquet, F., G. Madec, L. Brodeau, and J. Nycander, Defining a simplified yet realistic equation of state for seawater, *Journal of Physical Oceanography*, 45, 2464–2579, doi:10.1175/JPO-D-15-0080.1, 2015. 279
- Ruan, X., and R. Ferrari, Diagnosing diapycnal mixing from passive tracers, *Journal of Physical Oceanography*, 51, 757–767, doi:10.1175/JPO-D-20-0194.1, 2021. 186
- Ryder, L. H., *Quantum Field Theory*, Cambridge University Press, 443 pp., 1985. 335, 345, 361, 362
- Salmon, R., Hamiltonian fluid mechanics, *Annual Review of Fluid Mechanics*, 20, 225–256, doi:10.1146/annurev.fl.20.010188.001301, 1988. 334, 363, 368, 372, 379
- Salmon, R., *Lectures on Geophysical Fluid Dynamics*, Oxford University Press, Oxford, England, 378 + xiii pp., 1998. xii, 335, 363, 368, 379
- Schmitt, R. W., Double diffusion in oceanography, *Annual Review of Fluid Mechanics*, 26, 255–285, 1994. 223, 261
- Shannon, C. E., A mathematical theory of communication, *Bell System Technical Journal*, 27(3), 379–423, doi:10.1002/j.1538-7305.1948.tb01338.x, reprinted with corrections in Bell Syst. Tech. J., 27, 623–656 (1948)., 1948.

- Shao, A., A. Adcroft, R. W. Hallberg, and S. M. Griffies, A general-coordinate, nonlocal neutral diffusion operator, *Journal of Advances in Modeling Earth Systems*, 12, doi:10.1029/2019MS001992, 2020. 242, 248
- Shchepetkin, A., and J. McWilliams, A method for computing horizontal pressure-gradient force in an ocean model with a non-aligned vertical coordinate, *Journal of Geophysical Research*, 108, 35.1–35.34, 2002. 61
- Sieniutycz, S., *Conservation Laws in Variational Thermo-Hydrodynamics*, Kluwer Academic Publications, 1994. 363
- Smith, K. S., and J. Marshall, Evidence for enhanced eddy mixing at middepth in the southern ocean, *Journal of Physical Oceanography*, 39, 50–69, 2009. 236, 243
- Smith, K. S., and G. K. Vallis, The scales and equilibration of midocean eddies: forced-dissipative flow, *Journal of Physical Oceanography*, 32, 1699–1721, 2002. 236
- Smith, R. D., The primitive equations in the stochastic theory of adiabatic stratified turbulence, *Journal of Physical Oceanography*, 29, 1865–1880, doi:10.1175/1520-0485(1999)029<1865:TPEITS>2.0.CO;2, 1999. 218
- Smith, R. D., and P. R. Gent, Anisotropic Gent-McWilliams parameterization for ocean models, *Journal of Physical Oceanography*, 34, 2541–2564, 2004. 245, 246, 248, 249, 250
- Smyth, W. D., and J. R. Carpenter, *Instability in Geophysical Flows*, Cambridge University Press, Cambridge, UK, 327 pp, 2019. 139, 140
- Solomon, H., On the representation of isentropic mixing in ocean models, *Journal of Physical Oceanography*, 1, 233–234, doi:10.1175/1520-0485(1971)001<0233:OTROIM>2.0.CO;2, 1971. 238
- Soper, D. E., *Classical Field Theory*, Dover Publications, 2008. 340, 363
- Stakgold, I., *Boundary value problems of mathematical physics, volume I*, SIAM, Philadelphia, 340 pp, 2000.
- Starr, V. P., A quasi-Lagrangian system of hydrodynamical equations, *Journal of Meteorology*, 2, 227–237, doi:10.1175/1520-0469(1945)002<0227:AQLSOH>2.0.CO;2, 1945. 2
- Sun, S., R. Bleck, C. Rooth, J. Dukowicz, E. Chassignet, and P. D. Killworth, Inclusion of thermobaricity in isopycnic-coordinate ocean models, *Journal of Physical Oceanography*, 29, 2719–2729, 1999. 72
- Sverdrup, H., Wind-driven currents in a baroclinic ocean: with application to the equatorial currents of the eastern Pacific, *Proc. Natl. Acad. Sci. USA*, 33, 318–326, 1947. 285
- Symon, K., *Mechanics*, Addison-Wesley Publishing Co., Reading, MA, USA, 639 pp, 1971. x
- Taylor, G. I., Diffusion by continuous movements, *Proceedings of the London Mathematical Society*, 20(1), 196–212, doi:10.1112/plms/s2-20.1.196, read June 10, 1920, 1922. 109, 119, 121, 223, 397
- Thorpe, S., *The Turbulent Ocean*, 439 pp., Cambridge University Press, Cambridge, UK, 2005. 223

- Tracy, E. R., A. J. Brizard, A. S. Richardson, and A. N. Kaufman, *Ray Tracing and Beyond: Phase Space Methods in Plasma Wave Theory*, Cambridge University Press, 2014. [xv](#)
- Treguier, A. M., I. M. Held, and V. D. Lariehev, On the parameterization of quasi-geostrophic eddies in primitive equation ocean models, *Journal of Physical Oceanography*, 27, 567–580, doi:10.1175/1520-0485(1997)027<0567:POQEIP>2.0.CO;2, 1997. [223](#), [236](#), [243](#)
- Trenberth, K. E., An imperative for climate change planning: Tracking earth's global energy, *Current Opinion in Environmental Sustainability*, 1(1), 19–27, doi:10.1016/j.cosust.2009.06.001, 2009. [281](#)
- Tromp, J., *Theoretical and Computational Seismology*, Princeton University Press, Princeton, USA, 2025. [xv](#), [335](#), [357](#), [362](#), [363](#), [368](#), [398](#)
- Vallis, G. K., *Atmospheric and Oceanic Fluid Dynamics: Fundamentals and Large-scale Circulation*, 2nd ed., Cambridge University Press, Cambridge, 946 + xxv pp, 2017. [120](#), [121](#), [137](#), [153](#), [167](#), [221](#), [225](#), [418](#)
- Van Roekel, L., A. Adcroft, G. Danabasoglu, S. M. Griffies, B. Kauffman, W. Large, M. Levy, B. Reichl, T. Ringler, and M. Schmidt, The KPP boundary layer scheme for the ocean: revisiting its formulation and benchmarking one-dimensional simulations relative to LES, *Journal of Advances in Modeling Earth Systems*, 10, 2647–2685, doi:10.1029/2018ms001336, 2018. [273](#)
- Veronis, G., The role of models in tracer studies, in *Numerical Models of Ocean Circulation*, pp. 133–146, National Academy of Sciences, 1975. [238](#)
- Wald, R. M., *General Relativity*, University of Chicago Press, Chicago, USA, 1984. [361](#), [362](#)
- Waln, G., A theoretical framework for the description of estuaries, *Tellus*, 29(2), 128–136, doi:10.1111/j.2153-3490.1977.tb00716.x, 1977. [285](#), [298](#), [307](#), [419](#), [420](#)
- Waln, G., On the relation between sea-surface heat flow and thermal circulation in the ocean, *Tellus*, 34, 187–195, doi:10.1111/j.2153-3490.1982.tb01806.x, 1982. [285](#), [298](#), [307](#), [419](#), [420](#)
- Waterhouse, A. F., J. A. MacKinnon, J. D. Nash, M. H. Alford, E. Kunze, H. L. Simmons, K. L. Polzin, L. C. St. Laurent, O. M. Sun, R. Pinkel, L. D. Talley, C. B. Whalen, T. N. Huussen, G. S. Carter, I. Fer, S. Waterman, A. C. Naveira Garabato, T. B. Sanford, and C. M. Lee, Global Patterns of Diapycnal Mixing from Measurements of the Turbulent Dissipation Rate., *Journal of Physical Oceanography*, 44(7), 1854–1872, doi:10.1175/JPO-D-13-0104.1, 2014. [223](#)
- Weiss, J., The dynamics of enstrophy transfer in two-dimensional hydrodynamics, *Physica D: Nonlinear Phenomena*, 48, 273–294, doi:10.1016/0167-2789(91)90088-Q, 1991. [150](#)
- Wenegrat, J. O., and L. N. Thomas, Centrifugal and symmetric instability during ekman adjustment of the bottom boundary layer, *Journal of Physical Oceanography*, 50, 1793–1812, doi:10.1175/JPO-D-20-0027.1, 2020. [29](#)
- Whalen, C. B., L. D. Talley, and J. A. MacKinnon, Spatial and temporal variability of global ocean mixing inferred from argo profiles, *Geophysical Research Letters*, 39(18), n/a–n/a, doi:10.1029/2012GL053196, 2012. [223](#)

- Wolfe, C., Approximations to the ocean's residual circulation in arbitrary tracer coordinates, *Ocean Modelling*, 75, 20–35, doi:10.1016/j.ocemod.2013.12.004, 2014. 215
- Wunsch, C., On oceanic boundary mixing, *Deep-Sea Research*, 17, 291–307, doi:10.1016/0011-7471(70)90022-7, 1970. 2
- Young, W. R., Stirring and mixing, in *WHOI 1999 Summer Study Program in Geophysical Fluid Dynamics*, Woods Hole Oceanographic Institute, 1999. 119, 121, 145, 149, 395
- Young, W. R., An exact thickness-weighted average formulation of the Boussinesq equations, *Journal of Physical Oceanography*, 42, 692–707, doi:10.1175/JPO-D-11-0102.1, 2012. 81, 88, 89, 90, 91, 100, 190, 215, 218, 233
- Zeitlin, V., *Geophysical Fluid Dynamics: Understanding (almost) everything with rotating shallow water models*, Oxford University Press, 2018. xix
- Zhao, R., and G. K. Vallis, Parameterizing mesoscale eddies with residual and Eulerian schemes, and a comparison with eddy-permitting models, *Ocean Modelling*, 23, 1–12, doi:10.1016/j.ocemod.2008.02.005, 2008. 233
- Zinnser, W., *Writing to Learn*, Harper Perennial, 1993. xiv

INDEX

velocity
 Eulerian, 365

AABW, 285

acoustic waves, 344

action, [xi](#)
 variation, 359

active tracer, 165

active transformation, 355, 379

adiabatic flow, 166

advection, 153
 maths, 149

advection equation, 146
 geometric, 147

advection-diffusion equation, 170

advective boundary transport, 270

advective flux, 265, 266

advective tracer flux, 151, 229

anisotropic Gent-McWilliams, 249

anisotropic neutral diffusion, 245

association versus causation, [xi](#)

atomic bomb, 281

available potential energy, 231

averaging, 86
 Reynolds, 87
 thickness equation, 89
 thickness weighted, 88
 thickness weighted tracer, 90

balances, [xi](#)

baroclinicity
 generalized vertical coordinates, 65

barotropic model, 101

barycentric velocity, 146, 265

Batchelor scale, 221

Bernoulli

potential, 75

Bianchi identities, 379

Bianchi identity, 358

body forces, [xix](#)

bolus velocity, 83, 86, 90, 92, 212

bottom
 following coordinates, 10
 water mass transformation, 302

boundary
 conditions, 171
 propagator, 181
 water mass transformation, 308

boundary condition
 natural, 135
 Neumann, 135

Boussinesq ocean
 Hamilton, 389

Brownian motion, 112, 223

budget analysis, [ix](#)

buoyancy, 255, 269
 boundary condition, 269
 coordinates, 10
 surface ocean budget, 271

cabbeling, 260, 261, 263

cabbeling parameter, 262, 280

canonical momentum density, 350

causal relations, [ix](#)

center of mass velocity, 265, 266

classical field theory, 337, 341

coarse graining, 192

compatibility
 total mass + tracer mass, 149

composition property
 Green's function, 177

conservation

- global, 385
local, 385
Conservative Temperature, 255
conservative tracers, 106, 127, 141, 143
contact forces, xix
continuum limit, 338
coordinate covariance, 358
Coulomb gauge, 154
covariance, 379
 coordinate, 358
covariant divergence, 129
cross-diffusion, 224
current, 359
cyclic coordinates, 352
- deformation matrix, 365
density
 evolution, 224, 256
dia-surface flow, 165
dia-surface transport, 31, 36
 non-divergent, 40
dia-surface velocity, 39
 compared to vertical, 43
diabatic process, 166
diagnostic equation, xi
dianeutral direction, 226
diapycnal velocity component, 73
diffeomorphism, 365
differentiable manifold, 288
diffusion, 111, 258, 265
 dissipation functional, 135
 Fick's law, 121
 fine scale, 224
 horizontal, 132
 isotropic, 132
 molecular, 111, 224
 momentum, 124
 neutral, 132, 137, 260
 operator, 125, 131, 135
 skew, 152
 temperature, 123
 tensor, 131
 tracer moments, 133, 134
 tracer powers, 138
 tracer variance, 133
 turbulent, 119
diffusion operator, 239
diffusion tensor, 225, 265
- diffusion tensor transformation, 246
diffusivity, 265
 air, 122
 dynamic, 121
 kinematic, 121
 molecular, 121
 temperature, 123
 turbulent, 121
dimensional analysis, xii
Dirac delta, 136, 302, 316
Dirichlet boundary condition, 172
double integral identity, 330
downscale cascade, 221
dual pressure form stress, 95
- eddy tracer fluxes, 201
eddy-induced
 mass flux, 150
 mass streamfunction, 150
 velocity, 150, 225, 252
Eliassen-Palm
 flux, 82, 96, 97
 flux tensor, 96, 97
emergent scales, xii
ensemble average, 87
ensemble averaging
 ensemble, 87
ensemble mean, 192
epineutral diffusion, 238
equation of state, 260
Ertel potential vorticity, 384
Euler-Lagrange equations, 343, 370
 continuum, 339
Euler-Lagrange field equations, 334, 337
Eulerian
 mean, 193
Eulerian mean, 191
Eulerian velocity, 365
exterior moment of λ , 297
external
 moment, 297
 tracer mass, 325
external scales, xii
- Fick's law, 121
field theory, 341
 local, 335
fine scale mixing, 223, 224

- flow map, 365
fluid
dynamics, xviii
kinematics, xviii
mass distribution, 293
form stress, 62, 233
Fourier's law, 123
Fréchet derivative, 136
freshwater
boundary condition, 266, 267
velocity, 265
functional derivative, 136
functional variations, 135
gauge
invariance, 153
symmetry, 150
gauge theory, 361
Gauss's divergence theorem, 60
general vertical coordinates
basis one-forms, 11
basis vectors, 10
circulation, 27
common confusion, 7
contravariant velocity, 17
covariant velocity, 17
diffusion operator, 24
divergence, 23
divergence theorem, 23
examples, 33
Jacobian, 19
layer integrated diffusion, 25
Levi-Civita tensor, 20
material time derivative, 23
metric tensor, 18
partial derivatives, 21
position vector, 14
related to Cartesian, 6
specific thickness, 19
triple product identity, 13
vector, 16
vector cross product, 28
velocity, 16
volume element, 20
vorticity, 25
generalized Lagrangian mean, 189, 196
kinematics, 193
tracers, 200
generalized momentum density, 350
generalized vertical coordinates, 2
Gent-McWilliams
anisotropic, 249
available potential energy, 231
boundary value problems, 237
effect, 230
form stress, 233
parameterization, 228
secondary circulation, 230
thickness diffusion, 234, 236
geostrophic
balance, xi
contours, 167, 186
geostrophic streamfunction, 75
geostrophy
isopycnal models, 75
global conservation, 385
global instability, xxi
global mean sea level, 273
gradient
generalized vertical, 22
gradient operator
Cartesian, 21
general vertical coordinate, 21
gravitational potential energy, 369
Green's function
advection-diffusion equation, 173
composition, 177
non-closed reciprocity, 176
passive tracers, 170
reciprocity, 174
halosteric sea level, 277
Hamilton's Principle, 334
fluid mechanics, 334
Hamilton's principle, xi, 337, 363, 368, 389
continuum, 341
Hamiltonian continuity equation, 351
Hamiltonian density, 350
hydrodynamics, vii
impulse response function, 182
information entropy, 139
instability
global, xxi
wave, xxi
integration in λ -space, 292

- interfacial form stress, 92
interior moment of λ , 297
interior water mass transformation, 302
internal
 moment, 297
 tracer mass, 325
internal energy, 369
internal symmetry, 355, 361
irreversible process, vii
isopycnal
 coordinates, 10
 ensemble, 205
 layer transport, 205
 mean, 207
 primitive equations, 71
- Jacobian
 on a curve, 186
 operator, 186
- kinematic
 water mass transformation, 299
- kinematic boundary condition, 266
- kinematics
 motion field, 365
- kinetic energy, 368
- kinetic stress, 91
- Klein Gordon equation, 345
- Kronecker delta, 128
- Lagrangian
 density, 371
 mean, 194
- Lagrangian density, 339, 341, 371
- Lagrangian mean, 191
- Lagrangian mechanics
 continuum, 341
- Lagrangian velocity, 365
- Langevin equation, 116
- Laplace-Beltrami operator, 130
- layer mass continuity, 50
 compressible, 50
 pressure coordinates, 52
- local conservation, 385
- longitudinal waves, 339, 344
- longwave radiation, 270
- mass
 λ -layer, 292
- mass budget
 λ -layer, 307
- mass continuity
 generalized vertical coordinates, 48
 layer integrated, 50
- mass distribution function, 293
- mass equation
 general vertical coordinates, 58
- mass-labeling coordinates, 368
- mass-Sverdrup, 289
- material time derivative
 general vertical coordinates, 42
 isopycnal models, 73
- material tracers, 141
- mean free path, 122
- mean tracer equation, 215
- mechanical equivalence, 349, 353
- meridional
 overturning circulation, 55
 overturning transport, 253
- mesoscale eddies, 221, 225
- mesoscale eddy mixing, 223
- metric tensor, 128
- mixed boundary condition, 172
- mixing, 225
 surface boundary, 267
 tensor, 225
- mixing length, 122
- modified mean, 207
- modified mean density, 206
- molecular
 diffusion, 223, 224
- moments of λ , 297
- momentum equation
 flux form, 59
 general vertical coordinates, 58
 horizontal, 58
 vertical, 58
- momentum-based, x
- Montgomery potential, 72
- motion field, 365
- NADW, 285
- natural boundary condition, 135
- natural boundary conditions, 347, 371
- Neumann boundary condition, 135, 172
- neutral
 anisotropic neutral diffusion, 245

- density, 289
diffusion, 238
directions, 238
slope, 226
tangent plane, 238
tangent plane coordinates, 246
neutral diffusion, 137, 260
neutrality condition, 242, 247
Newtonian friction, 124
Noether's first theorem, 355, 379
Noether's second theorem, 358, 379
Noether's theorem, 334, 337, 350, 351, 379
non-advection
 flux, 265, 266
 transport, 270
non-dimensionalization, xii
non-divergent
 barotropic model, 101
notation
 slanted, 127
 upright, 127
obduction, 47
ocean
 buoyancy, 255
 free surface, 33
 mixed layer base, 34
 mixing processes, 223
one-forms, 11
overturning streamfunction, 55
parameterizations, 221
particle displacement, 202
particle relabeling, 379
passive
 tracer, 141, 170
 tracer source, 172
passive transformation, 355, 358, 379
perfect fluid, vii, 146
phase
 averaging, 192
Phillip's layering instability, 139
planetary
 vorticity, xix
potential energy
 shallow water layer, 95
potential vorticity, 26
Boussinesq, 66
Ertel, 384
generalized vertical coordinates, 64
isopycnal coordinates, 77
thickness weighted average, 99
Prandtl number, 124
pressure
 contact force, 62
 contact stress, 60
 coordinates, 8
 gradient force, 60
 Lagrange multiplier, x, 390
 time derivative, 257
pressure form stress
 interfacial stress, 63
pressure form stress
 dual, 95
principle of equivalence, 389
process water mass transformation, 299
prognostic equation, x
quasi-Stokes transport, 210, 214, 215
real fluid, vii
reciprocity, 174
rectification, 83, 189
reductio ad absurdum, 167
rescaled geopotential coordinate, 53
residual mean
 transport, 226
 velocity, 226
Reynolds
 average, 87
 stress, 91
Reynolds transport theorem, 133
Robin boundary condition, 172
rotation matrix, 246
rotational
 fluxes, 203
 tracer flux, 151, 229
salinity, 255
salt
 boundary condition, 266, 267
 concentration, 264
 velocity, 265
scalar
 mechanics, 106
scale analysis, xii

- scale selectivity, 125
scales
 emergent, xii
 external, xii
sea level, 273
 Boussinesq ocean, 281
 budget, 274
 steric, 275
 thermosteric, 275, 276
self-adjoint operator, 135, 175
shortwave radiation, 270
sine-Gordon equation, 345
skew
 diffusion, 152, 225, 258
 diffusion tensor, 152
 skew diffusion and skewson, 153
 symmetric tracer fluxes, 202
 tracer flux, 151, 229
space-time symmetry, 360
specific
 thickness, 34, 208, 211
specific thickness, 19
stirring, 225
Stokes
 drift, 83, 84, 193, 198, 199
 mean, 193, 198
storage, 307
streamfunction
 meridional- σ , 55
stress-energy-momentum tensor, 351
subduction, 47
subgrid scales, 221
surface water mass transformation, 302, 313,
 315
 buoyancy, 316
 circulation, 315
Sverdrup, 289
Sverdrup balance, xi
symmetric
 tracer fluxes, 202
symmetry
 condition, 242
 internal, 361
 particle relabeling, 379
 space-time, 360
Taylor-Bretherton identity, 82, 99
tensor
 (1, 1) representation, 128
 (2, 0) representation, 128
 0, 2) representation, 128
 flat representation, 128
 musical nomenclature, 128
 natural representation, 128
 sharp representation, 128
 terrain following coordinates, 8
thermobaricity, 260, 261, 263
thermobaricity parameter, 262, 280
thermosteric sea level, 279
thickness, 211
 equation, 53
 isopycnal thickness equation, 73
 specific, 34
 specific thickness, 73
 weighted average, 88, 215
 weighted velocity, 75
 weighting, 208
thickness weighted averaging, 81
time
 mean, 191
 tendency, x
tracer
 active, 165
 material, 141
 mechanics, xx
 parameterization, 221
 passive, 141
 transport tensor, 216
 variance, 133
tracer equation
 general vertical coordinates, 58
 layer integrated, 54
 mean, 215
tracer fluxes
 rotational, 203
 skew symmetric, 202
 symmetric, 202
tracer mass
 external, 325
 internal, 325
tracer mass analysis, 285, 319
 external, 325
 internal, 325
 special cases, 323
tracer moments, 133, 187

- tracers
 conservative, 106, 127, 141, 143
- trajectory
 fluid particle, 365
- generalized vertical coordinates, 45
- transformation
 active, 355, 379
- passive, 355, 358, 379
- transformation matrix
 general vertical coordinates, 6
- transformed residual mean, 208
- velocity, 210
- transverse waves, 344
- turbulent transport, 225, 270
- two-dimensional
 flow, 101
- unimodular coordinates, 368
- vanishing layers, 77
- variation
 action, 342
- field, 342
- total, 359
- velocity
 Lagrangian, 365
- tensorially Lagrangian, 365
- velocity equation
 vector-invariant, 59, 75
- velocity vector
 generalized vertical coordinates, 45
- vertical
 gauge, 154
- vertical velocity, 43, 90
- decomposed, 43
- viscosity, 124
- molecular, 124
- volume-Sverdrup, 289
- vorticity
 general vertical coordinate, 59, 64
- isopycnal coordinates, 78, 102
- isopycnal models, 75
- relative, 59
- thickness weighted average, 99
- water mass, 285
- water mass analysis
 mathematics, 292
- tracers, 319
- water mass configuration space, 287
- water mass formation, 288, 307
- buoyancy, 289
- water mass transformation, 285, 287, 288, 298
- boundary, 308
- buoyancy, 289, 316
- dia-surface flux, 298
- interior, 298
- kinematic, 299
- kinematic method, 301, 302
- process, 299
- process method, 301, 302
- processes, 290, 311
- surface, 313, 315
- wave
 longitudinal, 339
- wave equation, 339
- wave instability, xxi
- waves
 polarized, 203
- zonal
 mean, 192